Jack O. Haller
Thomas L. Slovis
Aparna Joshi

Pediatric Radiology

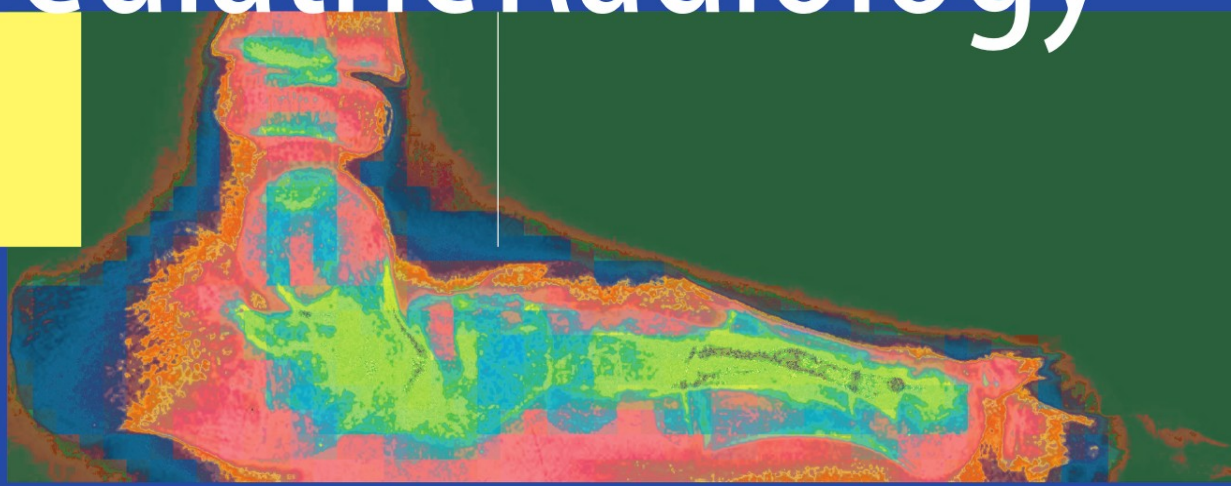

3rd Edition

Springer

Jack O. Haller · Thomas L. Slovis · Aparna Joshi
Pediatric Radiology
3rd Edition

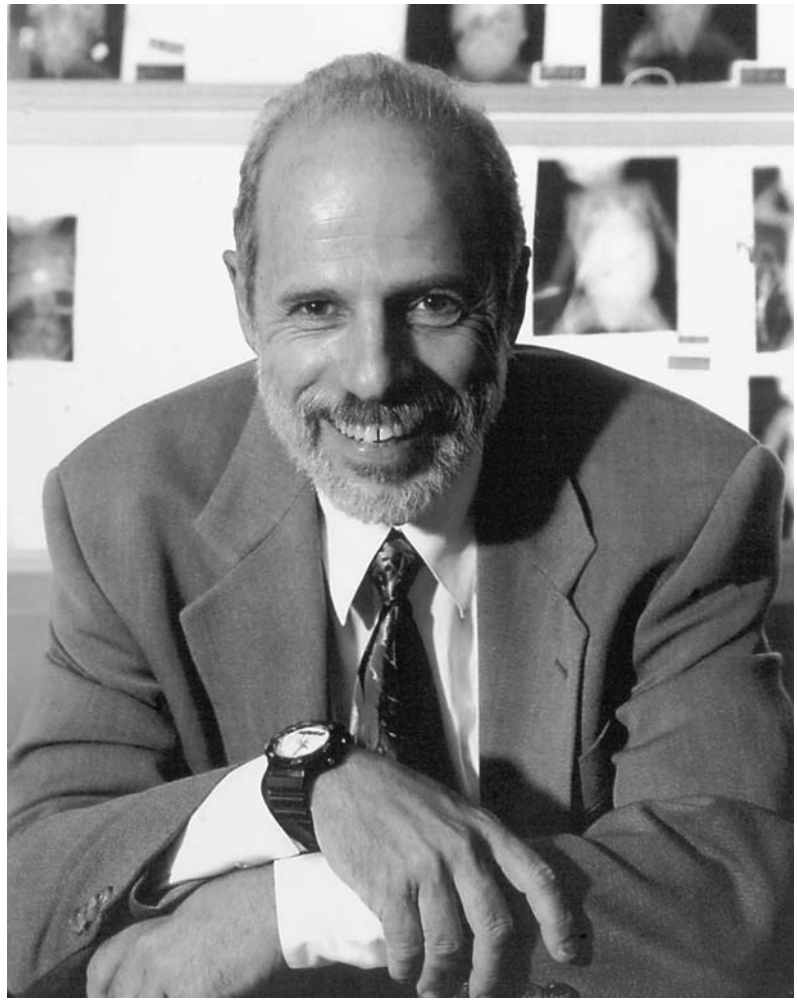

Jack O. Haller (February 9, 1944–June 15, 2004)
Teacher, Colleague, Friend

To Jack: A Farewell to a Friend

Suddenly
A dawn
The world is not the same anymore
The days always follow one another
Endlessly
No beginning, no end
I accepted it.

Suddenly
The world seems suspended
Time halted in mid sentence
A day broke the sequence
The clocks marking time
Stopped.

Suddenly
We are suspended without him
In mid sentence
His presence, a gift
A gift to those who knew him
We paid no attention to the clocks
He was there.

I know
The days will start to follow each other
Again
But there will be different days
The clocks will start again
But never the same clocks.

John C. Leonidas, June 2004

Jack O. Haller
Thomas L. Slovis
Aparna Joshi

Pediatric Radiology

Third Edition

With 286 Figures in 818 Separate Illustrations
and 28 Tables

Springer

Jack O. Haller, MD
Professor of Radiology
Kings County Hospital, Downstate Medical Center
Health Science Center at Brooklyn, State University of New York
Brooklyn, NY, USA

Thomas L. Slovis, M.D.
Professor of Radiology and Pediatrics
Pediatric Imaging Department, Children's Hospital of Michigan
3901 Beaubien Boulevard, Detroit, MI 48201, USA

Aparna Joshi, MD
Assistant Professor of Radiology
Pediatric Imaging Department, Children's Hospital of Michigan
3901 Beaubien Boulevard, Detroit, MI 48201, USA

Title of the First Edition:
Haller/Slovis, Introduction to Radiology in Clinical Pediatrics
© 1984 by Year Book Medical Publishers, Inc. Chicago, London

Library of Congress Controll Number: 2004111250

ISBN 3-540-21354-6 Springer Berlin Heidelberg New York

ISBN 3-540-59059-5 2nd ed. Springer-Verlag Berlin Heidelberg New York

This work is subject to copyright. All rights are reserved, whether the whole or part of the material is concerned, specifically the rights of translation, reprinting, reuse of illustrations, recitation, broadcasting, reproduction on microfilm or in any other way, and storage in data banks. Duplication of this publication or parts thereof is permitted only under the provision of the German Copyright Law of September 9, 1965, in its current version, and permission for use must always be obtained from Springer-Verlag. Violations are liable to prosecution under the German Copyright Law.

Springer is a part of Springer Science+Business Media
springeronline.com
© Springer-Verlag Berlin Heidelberg 1995, 2005
Printed in Germany

The use of designations, trademarks, etc. in this publication does not imply, even in the absence of a specific statement, that such names are exempt from the relevant protective laws and regulations and therefore free for general use.

Product liability: The publisher can not guarantee the accuracy of any information about dosage and application contained in this book. In every individual case the user must check such information by consulting the relevant literature.

Editor: Dr. Ute Heilmann, Heidelberg, Germany
Desk editor: Dörthe Mennecke-Bühler, Heidelberg, Germany
Production editor: Ingrid Haas, Heidelberg, Germany

Cover-Design: Frido Stein-Broo, Pau, Spain
Reproduction and Typesetting: AM-productions GmbH, Wiesloch, Germany
Printing and bookbinding: Stürtz AG, Würzburg, Germany

Printed on acid-free paper. 21/3150 ih - 5 4 3 2 1 0

Dedication: First Edition

To Adolf and Frieda Haller, my mentors, my inspiration, my parents.
J.O.H.

To Ellie, Michael, Debbie, Andy, and Lisa, my family, without whose love, patience, and inspiration this project could not have been completed.
T.L.S.

Dedication: Second Edition

To Walter E. Berdon, Jerome M. Levine, David H. Baker, and Joseph O. Reed, whose teaching and counsel molded our careers, and whose integrity and dedication to excellence in their craft had a profound influence on our lives.
J.O.H.
T.L.S.

Dedication: Third Edition

To my coauthor Tom Slovis, who for more than 30 years has been the epitome of true friendship. His loyalty, care, camaraderie, and brotherhood have been the mainstays of my career and personal support. He and his wife Ellie have provided me and my family with love, kindness, respect, and devotion, and I am grateful that I am blessed to have him as my friend.
J.O.H.

To the medical students and residents who have stimulated this edition. Their constant questions, suggestions, and enthusiasm encouraged me to improve and update this work. I hope that the transfer of this knowledge continues to improve our care of children.
T.L.S.

To my parents, Asha and Sharadchandra Joshi, whose patience, guidance, and love have shaped my life.
A.J.

Preface to Third Edition

The third edition follows 20 years after our initial offering. It updates the technology of pediatric imaging. It is designed for medical students and residents in both pediatrics and radiology, nurse practitioners, physician assistants, and all who take care of children.

This edition gets us back to basics with a new chapter on the effects of radiation in children. It deals more with what to order and why. The proliferation of imaging techniques is not a good thing if imaging replaces superb history taking, good physical examination, and excellent clinical judgment.

We continue the socratic approach of asking questions to stimulate the reader's interest. There are 30% more new pictures and more quiz cases.

We have attempted to write this book at several levels – the text for the medical student and nonradiologist, the figures with images of various complex diseases and findings to further stimulate the radiology resident, and the further reading lists to encourage those who want to know more.

We hope you enjoy this "quick read."

The Authors

Preface to First Edition

The idea for this book grew out of our experience in teaching pediatric radiology to clinicians and students. Clearly, there is a strong desire on the part of those taking care of children to familiarize themselves with the rudiments of the pediatric radiograph. While radiologists have primary responsibility for the interpretation of films, clinicians bring valuable insight and information. Often they present additional important data or ask searching questions that prompt a re-evaluation of the films so that a more appropriate diagnosis may be obtained.

While primers are available in adult radiology, comparable editions in pediatrics are lacking. We have therefore adapted the teaching sessions of Joseph O. Reed, Director of Radiology at Children's Hospital of Michigan and Professor of Radiology at Wayne State University School of Medicine, as the framework for our text. In addition, Rosalind H. Troupin has generously allowed us to use some of her ideas for this book, which is an elementary guide to common pediatric radiographic examinations and problems. It is our intent to provide an approach to these examinations to help the clinician discern the normal from the abnormal. A second goal is to help the pediatrician, house officer, and medical student learn the indications for various procedures, as well as to recognize some of the more common abnormalities. This text is by no means meant to provide an in-depth discussion of various disease entities, nor is it intended to catalog the various subtle radiographic findings in these entities.

The radiographs in this volume are often reproduced to enhance a single finding under discussion, often at the expense of other portions of the film. Also, arrows and letters have been kept to a minimum so as not to obscure the radiographs.

It is our hope that, by providing this primer for pediatric radiology, we will stimulate clinicians to visit the X-ray department, share in the interpretation of their patients' films, and continue to stimulate us so that together we can provide optimal care for children.

Jack O. Haller · Thomas L. Slovis

Preface to Second Edition

Why did we write a 2nd edition? There were several reasons. First, the popularity of the first edition demanded a repeat. Students, housestaff, clinicians, and directors of radiology, pediatric radiology, and pediatric programs across the nation were continually calling us to ask where they could obtain more copies. The first addition was simply sold out; there were no copies left.

Second, in our capacities as directors of pediatric radiology departments, we also ran out of copies; we found the first edition so helpful in acclimating our radiology and pediatric staffs to pediatric radiology, that we needed new copies for ourselves.

Third, in the ten years since publication of the first edition there have been major changes in the field of radiology. Therefore, we really needed to update it; hence, the added information on ultrasound, CT, and MRI. While it is hard to cover such complex fields in a book such as this, we have tried to give the reader at least a working practical introduction to the topics as they relate to pediatrics.

We know, based on our experience with the first edition, that this volume will be helpful to clinicians and housestaff from both radiology and pediatric departments. But we have also found that family practice and emergency physicians, nurse practitioners, and physicians' assistants profit from reading the first edition; we have also geared our new text towards these groups as well. Enjoy!

Jack O. Haller · Thomas L. Slovis

Acknowledgments: Third Edition

The third edition was produced at Children's Hospital of Michigan through the efforts of the audiovisual department, particularly Amanda Oberlee. She took all the photographs, collated them, and performed the labeling and computer refinement of the images. Jennifer Handley typed the entire manuscript multiple times until all of us "had enough." Michele Klein-Fedyshin once again reviewed the text "as a student" and as the copy editor. She also did the index. Drs. David Bloom, Swati Mody, and John Crowley read our work and made helpful suggestions.

Dr. Alex Cacciarelli, a superb medical artist, contributed all the new drawings. They are a wonderful addition.

We thank all the individuals for their fine work and dedication.

Acknowledgments: First Edition

We wish to acknowledge a number of individuals without whom this work would not have been completed. Drs. Ronald L. Poland, John K. Kelly, Harvey I. Wilner, and Alfredo Lazo offered helpful criticisms of early drafts. Drs. Alkis Zingas, Alfredo Lazo, and Lawrence R. Kuhns were kind enough to lend us computerized tomographic images and the nuclear medicine images found within the text. Virginia Newman did yeoman work in typing and retyping numerous revisions of this manuscript over a two-year period. Without her hard work, the task would have been impossible.

Albert Paglialunga and Shelley Eshelman provided the reproductions of the radiographs and the schematic diagrams, respectively. They were patient and responsive.

Dr. Joshua A. Becker, a chairman and friend, has continued to provide support and encouragement for academic pursuits and sustains a gratifying working milieu.

Drs. George B. Comerci, Lewis A. Barness, and C. Henry Kempe stimulated our interest in pediatrics and urged close rapport with our pediatric colleagues. Dr. R. Parker Allen has been responsible for first "turning on" many of his students to radiology.

Drs. David H. Baker and Walter E. Berdon, our mentors, godfathers, and friends, have always encouraged us and continue to serve as models of excellence in pediatric radiology.

Dr. Joseph O. Reed (whose Reed's Rules appear throughout this book) has helped with his guidance, teaching, and critical appraisal of the manuscript. He has provided this stimulus by emphasizing basic principles as a means to learning radiology and, in fact, medicine itself.

Acknowledgments: Second Edition

We are grateful for the efforts of many individuals who helped make this second edition possible. Particularly, we would like to thank Jennifer Handley for typing the entire manuscript with endless corrections and modifications. Michele Klein reviewed the manuscript both as a teaching tool and also as a proofreader. Her suggestions and contributions were invaluable. Cliff Roberts prepared all of the photographs in this text. He worked tirelessly to make the images perfect, and without his efforts the book would not have been possible. Lastly, we would like to thank all of those who read, corrected, or contributed to the many chapters. These include Joshua A. Becker for his continued encouragement, members of the faculty at Children's Hospital of Michigan (Gary Amundson, Cristie Becker, David Corbett, John Crowley, Daniel Eggleston, Sam Kottamasu, John Pereira, and Susan Roubal), and to the authors who allowed us to use pictures from other articles and text in this edition.

Contents

1 Diagnostic Medical Imaging: How, Why, and When

Introduction

Diagnostic medical imaging can be accomplished in many ways using various physical tools. X-rays (gamma rays) create the images seen on plain films and in fluoroscopy, angiography, and computed tomography. A tomogram is an image of a thin section, a small slice of the whole body, demonstrated with increased resolution and detail. Gamma rays are also used in nuclear medicine and positron emission tomography (PET). Sound waves create the information necessary to make an ultrasound image, while magnetic fields provide the data for an image in a magnetic resonance (MR) examination. The proliferation of imaging modalities for diagnostic evaluation is predicated on the emergence of the computer. It is the vital cog for acquisition and processing of the data and the manipulation after processing (postprocessing). Reconstruction of images in many planes and three-dimensional rendering of the anatomy are among the most valuable options offered by postprocessing (Fig. 1.1). Use of computers for storing and moving images is rapidly evolving. Picture archiving communication systems (PACS) now permit images to be seen in real time on imaging monitors throughout the hospital, on the Internet via web servers in the hospital, and in remote locations such as physicians' offices and homes.

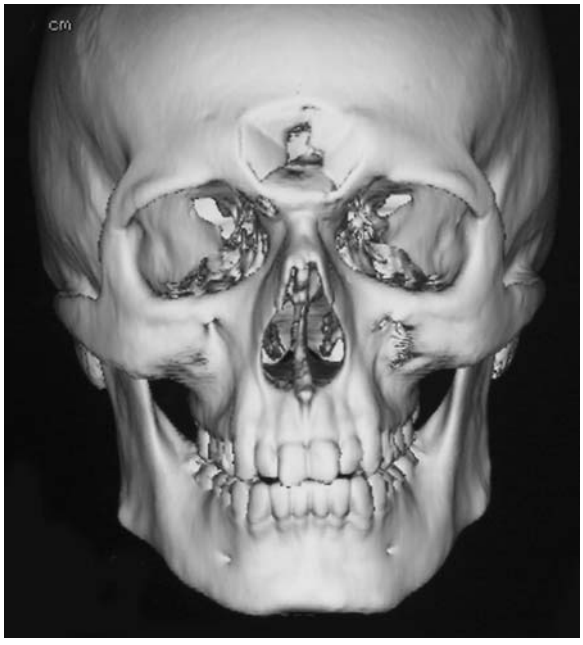

Fig. 1.1. Frontal three-dimensional computed tomographic image of a teenager who was hit in the forehead by a hammer. Note the exquisite detail of the shattered bone

Nature of Radiographs

X-rays are short electromagnetic radiations produced by energy conversion when fast-moving electrons from the filament of the X-ray tube interact with the tungsten anode (target) (Fig. 1.2). When an X-ray beam is directed toward a part of the body, X-rays are absorbed by the more dense tissue (e.g., bone), causing ionization within the body. X-rays that *pass through* the entire body interact with the recording medium, forming an image. The recording medium may be X-ray film but more commonly is an activated cassette (computed radiography, CR) or a directly digitized image which is then immediately placed on the PACS system. The resultant image is a recording of internal body structures in which the black areas represent regions that have allowed the X-rays to pass through and the white areas the regions that have absorbed all X-rays. Thus, the least dense body structures (i.e., lungs) appear *black,* and the more dense structures (i.e., bone), which have absorbed the X-rays, appear *white* (Fig. 1.3). The ability to postprocess digital images has caused a "disconnect" and makes all images look good. We can no longer tell by looking at the image whether the dose of radiation used for the exposure is appropriate. This is called the "uncoupling effect," where the final product is uncoupled from the amount of radiation utilized.

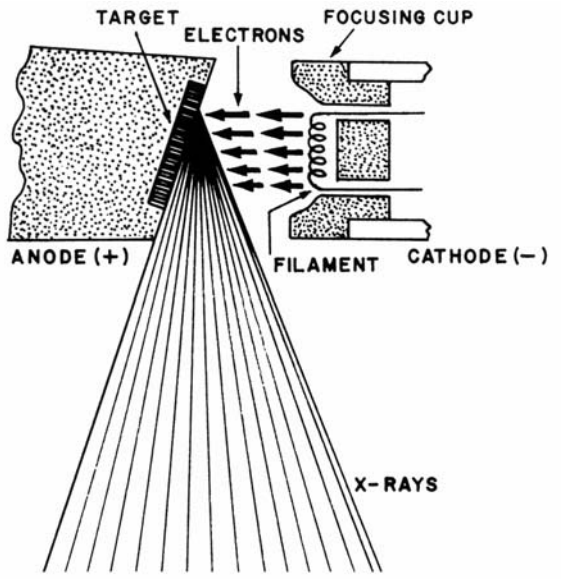

Fig. 1.2. Production of X-rays

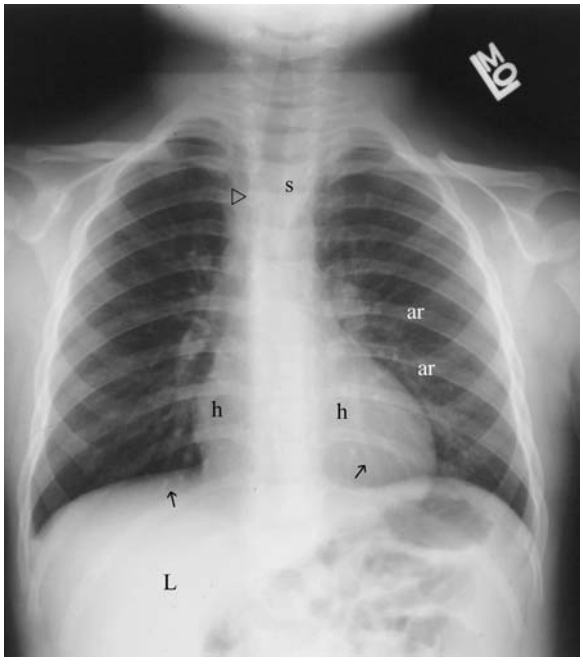

Fig. 1.3. Frontal chest examination of a child
The normal lungs are air-filled and are black. The heart (*h*) has absorbed some radiation and is gray. It is similar to the liver (*L*). The bones have absorbed the most radiation. Note the spine (*s*) and the anterior rib margins (*ar*). The heart and liver are transparent organs and you can see the pulmonary vascularity (*arrows*) through them. The *arrowhead* is on the pedicle of the spine

In addition to static radiography, there are many diagnostic X-ray methods which let us see images in "real time." *Fluoroscopy* allows us to study internal body functions, for example, respiratory motion, cardiac motion, or peristalsis of bowel. In fluoroscopy the image is portrayed through an intensifier onto a television monitor. Individual static radiographs can also be taken during this procedure. *Cineradiography* is the recording of successive fluoroscopic images on videotape or DVD. Since a major reason for fluoroscopy is visualization of motion, detailed resolution of the image may not be crucial. By using an intermittent rather than constant X-ray beam – pulsed fluoroscopy – the radiation dose can be diminished without loss of diagnostic information (see Chap. 2).

Some X-ray studies involve the use of contrast media. These substances are used to enhance and emphasize visualization of structures of the body. They can be injected, swallowed, or given as enemas. Examples of contrast media are air, barium sulfate, iodine-containing solutions, and gadolinium. Barium and iodine are quite dense and absorb the X-ray beam – thus appearing white – hence their usefulness in demonstrating internal structures (Fig. 1.4).

Angiography is the study of blood vessels after contrast medium has been injected. The contrast medium flowing through the blood vessels of selected organs or masses reveals minute vascular detail (see Chap. 9). Computed tomographic angiography (CTA) utilizes contrast medium but avoids more invasive catheterization, while magnetic resonance angiography (MRA) images the blood vessels with or without contrast medium with the use of computer manipulation (see below).

Radionuclide imaging – nuclear medicine and PET – utilizes a radioisotope. It is combined with a compound that normally goes to a specific organ or organs of the body, for example, bone or liver. When injected, it accumulates in these tissues, where it emits gamma rays that can be recorded on film or on a computer. Because of specific organ-tissue binding or excretion, nuclear medicine can give functional (physiological) information. The tomographic (thin-section) equivalent in nuclear medicine is single-photon emission computed tomography (SPECT). Tomographic studies have increased resolution compared to routine nuclear studies.

PET is also a tomographic nuclear medicine study. In this instance, however, specially created positron-emitting radioisotopes (made by a cyclotron) of high energy and very short half-life are incorporated into metabolically relevant compounds and used to bind

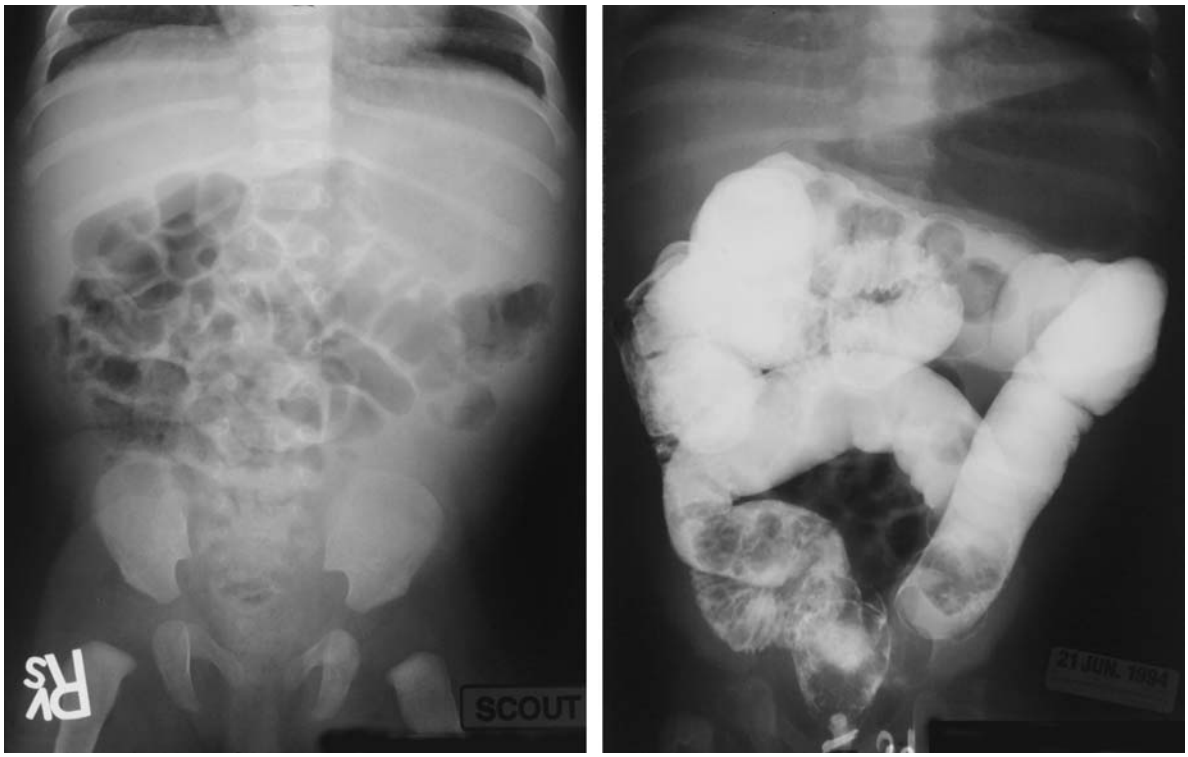

a b

Fig. 1.4. Use of contrast
a Supine film of the abdomen shows air in the bowel (black), but it is uncertain which is small or large bowel
b Barium, a contrast agent, was placed in the colon. Stool (dark, circular objects) within the colon is outlined by the barium. The X-ray beams are absorbed by the barium, and thus the colon appears white and allows delineation of the air-filled upper gastrointestinal tract (black)

to a specific organ/receptor. Most often for body imaging in oncology, 18-fluoro-deoxyglucose (FDG) is the agent selected. This isotope has a half-life of 100.9 min.

The ability to merge images from different imaging studies has led to the development of PET-CT. This fusion of both anatomical and physiological data allows for more sophisticated diagnoses. By being able to detect "viable" tumor, the correct therapy can be given. The next step is the development of a "delivery package" (a way to bind the therapeutic agent to a compound which delivers it specifically to the tumor) via molecular tracers.

Remember that X-rays pass through the body to hit a detector. Those X-rays stopped by the body are immediately absorbed and are seen as white (i.e., bone). On the other hand, the child who is injected with a radioisotope *emits* radiation, which is detected and made into an image. The isotope emits radiation until it decays – a matter of the half-life of the isotope and physiological excretion. When technetium-99m is used (half-life of 6 h), a child with normal urinary excretion will lose 50% of the radiation in the first 6 h.

Computed tomography (CT) utilizes an X-ray beam in a rotating carriage to scan a narrow cross-section of the body. In conventional CT the X-ray beam and detectors rotate about the patient, while in the newer spiral (helical) scanners there is continuous movement of the patient through the gantry as the radiographic tube and detector system rotate about the patient (continuous acquisition). When intravenous contrast medium is used, spiral CT can also produce angiographic images (CTA). A computer within the CT unit synthesizes the data generated by either of these processes and reconstructs them into images that can be displayed. The radiologist has a choice of various software programs (algorithms), each of which highlights specified densities and contrast (bone, soft tissue, etc.). The portion of gray scale pertinent to the anatomy is achieved through window and level selections on the console. Table 1.1

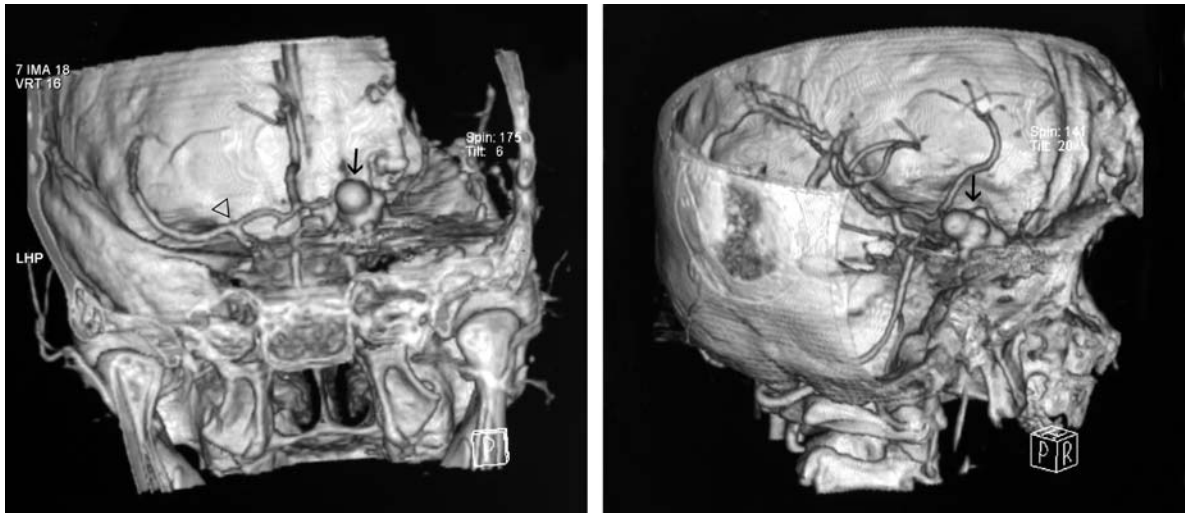

a b

Fig. 1.5. CTA in three-dimensional reconstructional format
a Posterior view shows a large aneurysm (*arrow*) at the bifurcation of the internal carotid artery on the patient's right. You are viewing this patient from behind. The *arrowhead* on the other side shows the normal bifurcation
b Lateral view shows the large multilobulated aneurysm (*arrow*)

Table 1.1. Density and Hounsfield units as noted on CT

Substance	Color	HU (CT units)
Bone	Most white	750–1000
Contrast	White	75–300
Soft tissue	Gray	40–60
Water	Dark gray-black	–10 to +10
Fat	Black	–100
Air	Most black	–500

shows the appearance of the various densities on CT. Density is measured in Hounsfield units (CT units).

There are now multidetector CT scanners (MDCT) with 4, 8, 16, 32, and, on the horizon, 64 detector units. These are exquisitely fast and present highly detailed images and reconstructions. The reconstruction shows much more than we can see on the axial images alone. With these new units, CTA rivals conventional angiography in detail while being much less invasive (Fig. 1.5). The MDCTs give a higher radiation dose (see Chap. 2) than the single-detector units.

Other Imaging Modalities Without Radiation

High-frequency sound (>20,000 cycles per second) is called ultrasound and may be produced by a piezoelectric crystal. The crystal is the most important component of the ultrasound transducer (Fig. 1.6).

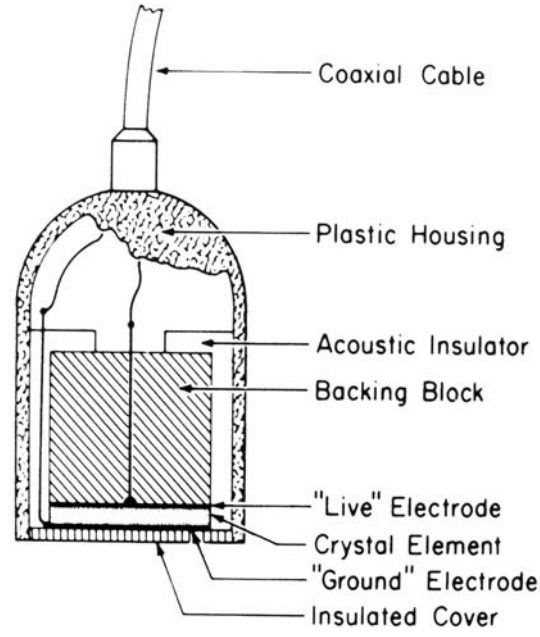

Fig. 1.6. Ultrasound transducer. (From [1] with permission)

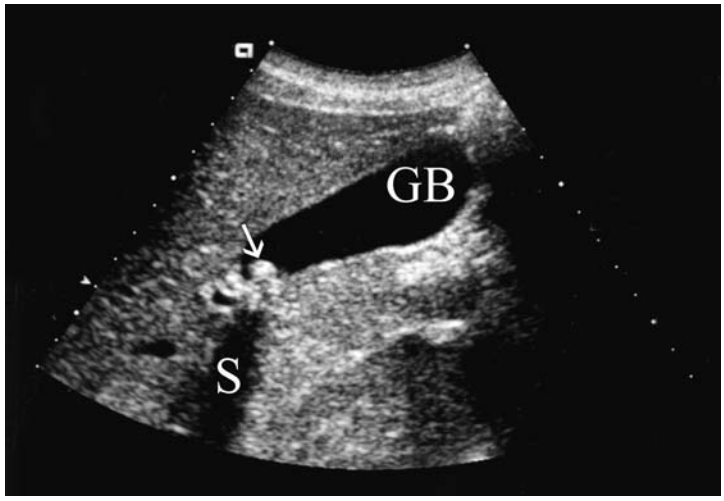

Fig. 1.7. Ultrasound of the gallbladder with gallstones
The gallbladder (*GB*) appears black and the *arrow* points to an echogenic (white) stone. The stone blocks the echoes from passing posteriorly and creates a black shadow (*S*). Note the liver which is echogenic (gray) directly anterior and to the left of the gallbladder

The transducer converts an electrical signal into ultrasonic energy (sound) that can be transmitted into tissues. The echoes returning from the patient are then converted back into an electrical signal and recorded on film or on PACS. Color-flow Doppler imaging allows us to examine the nature of vascular flow (patency, waveform, etc.). Diagnostic ultrasound causes no known significant biological adverse effect at the frequencies that we use. The ultrasonic appearance of normal body tissue is as follows:

- Without echoes: anechoic; these appear black
  - Cystic regions or fluid-filled viscera (e.g., gallbladder)
  - Blood vessels: flowing blood
- With echoes: shades of gray and white
  - Viscera (e.g., liver, spleen, brain)
  - Air: artifact behind it
  - Calcium and bone: the whitest; blocks echoes behind it (shadowing) (Fig. 1.7).

Doppler ultrasound allows us to visualize vascular flow. It can be pulsed Doppler showing merely waveforms or imaging Doppler showing color flow within a vessel or in organs (Fig. 1.8). Ultrasonic contrast agents consist of microbubbles which, when injected intravenously or within a fluid-filled structure, are easily visualized as turbulence and enhance the conspicuity of blood or fluid flow. The usefulness of these contrast agents is the subject of future research.

MR captures the rotational motion of the electrical charge on protons in the nucleus of cells of our body as they respond to a magnetic field. There is no ionizing radiation and no significant biological effects at the magnetic strengths in clinical use. As with other forms of imaging, computer manipulation of the data allows the production of images in multiple planes. A pulse sequence is a combination of imaging parameters which the physician selects to produce images of predictable tissue contrast. The spin-echo concept of MR uses two basic pulse sequences, called TI and T2 based on tissue relaxation time. T1 is the anatomical sequence while T2 is the pathological sequence showing most pathology as white (Fig. 1.9). We use the different appearances of specific tissues on T1 and T2 to diagnose the nature of these entities (Table 1.2).

Table 1.2. Spin echo appearance on MR imaging

Tissue	T1	T2	Clues
Fat	White	Gray	Fat fades
Flowing blood	Black	Black	Blood is black
Water (fluid)	Black	White	Water whitens
Bone	Black	Black	Bone is black

From the basic T1-weighted and T2-weighted concept have evolved multiple sequences developed to emphasize specific body parts, vessels, or pathology (Table 1.3). It may be important to eliminate the signal of fat (fat-suppressed images) so that the pathology can be better appreciated.

MR examinations were initially quite slow. With higher-field-strength magnets, echo planar single shot and volumetric techniques have allowed pro-

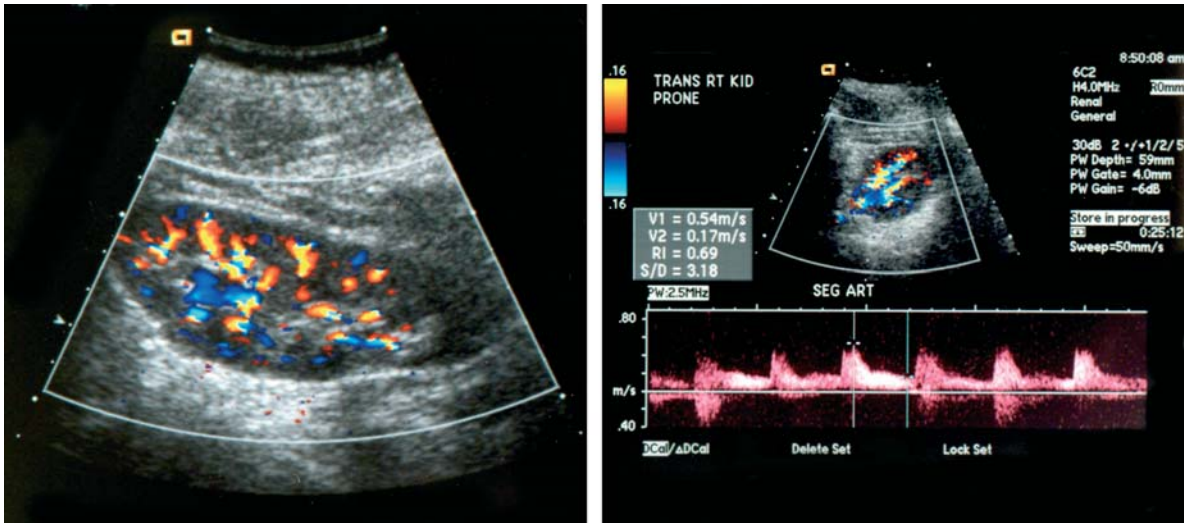

Fig. 1.8. Doppler ultrasound
a The kidney is seen with color-flow Doppler in the vessels throughout the kidney. The flow towards the transducer is shown as *red, orange,* and *yellow* while that away from the transducer is shown as *dark blue* to *light blue*. The greatest velocities are the lightest colors
b Utilization of both the image and the Doppler wave form shows systole as a vertical upsweep and diastole as the lower, more horizontal region. This is Doppler ultrasound of the same kidney seen in **a**

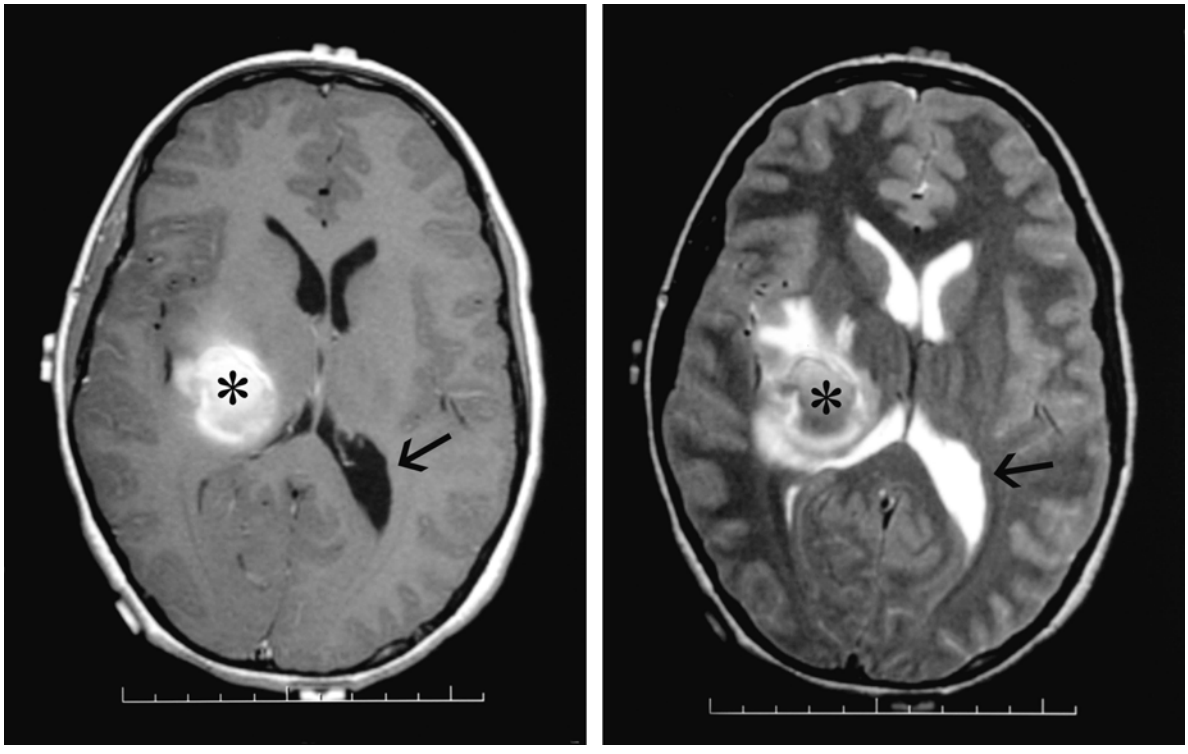

Fig. 1.9. MR imaging of the brain
a T1 sequence shows the cerebrospinal fluid (CSF) in black. The *arrow* points to the left occipital horn. Note the large white area (*asterisk*) on the right effacing the right occipital horn
b T2 image of the same region shows the CSF in the lateral ventricles as white (*arrow*). The pathological lesion in the right thalamus represents a hemorrhagic tumor. Note that its consistency on T2 differs from that on T1

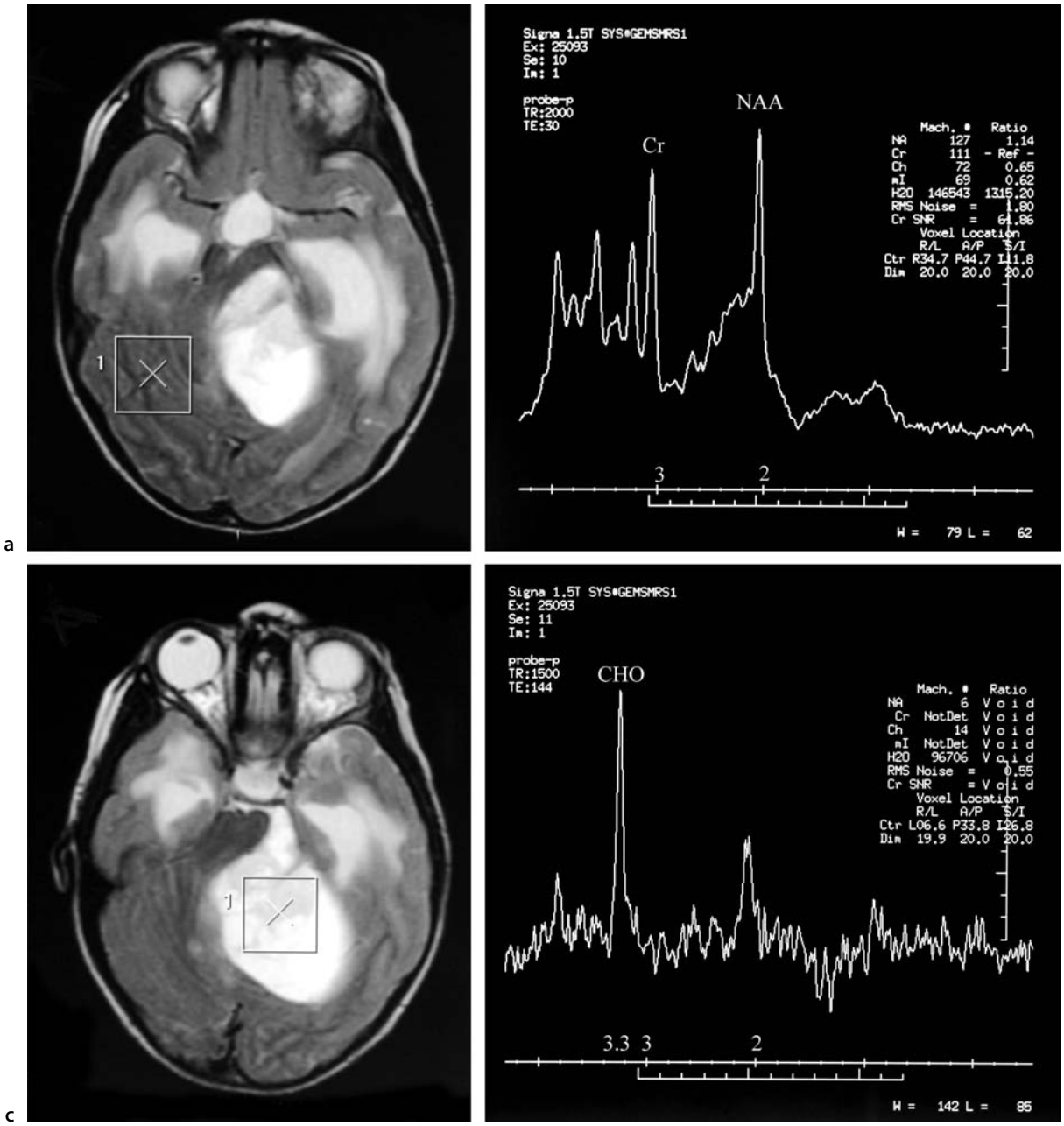

Fig. 1.10. Magnetic resonance spectroscopy (MRS)
a A T2-weighted MR image with the voxel (the *box* with the ×) in normal tissue
b MRS done with the long point-resolved spatially localized spectroscopy (PRESS technique) is normal. The horizontal axis is parts per million (ppm). The tallest peak occurs at 2 ppm and represents *N*-acetyl aspartate (*NAA*). The scale is positive to the viewer's left and negative to the right. The second largest peak, at 3 ppm, is creatine (*Cr*)
c The same image as in **a** but now with the voxel on a large tumor in the posterior fossa
d Spectroscopy here shows absence of the NAA and Cr peaks. There is a large peak at 3.3 ppm which represents choline (*CHO*). This is markedly elevated in tumors

Table 1.3. Pulse sequences

1. Spin echo – the gold standard
   a) Conventional
   b) Fast spin echo (FSE)
   Both conventional and FSE can give T1 or T2 images depending on the parameters utilized. T1 shows anatomy while T2 shows pathology since pathology has increased water (edema) or vascular component. FSE is used for MR urography, cholangiopancreatography, and myelography.
2. Inversion recovery (IR)
   Enhances tissue contrast. Can be T1 (IR in central nervous system for showing myelination in infants) or T2 (FLAIR in central nervous system for diminishing (blackening) spinal fluid signal to show paraventricular pathology). Used extensively in musculoskeletal imaging STIR (short tau inversion recovery) to eliminate fat signal.
3. Gradient echo (GRE)
   a) Conventional
   b) Three-dimensional
   Both conventional and three-dimensional GRE lowers resolution but enhances contrast. Conventional gradient echo can be used to show hemosiderin while three-dimensional allows for angiographic studies (MRA and MRV).
4. Echoplanar imaging (a form of ultrafast imaging)
   Allows for functional imaging, diffusion weighted imaging, and cardiac imaging.
5. Ultrafast sequences
   MR fluoroscopy

duction of multiple images in a matter of seconds to minutes. This has permitted the development of diffusion (earliest imaging of acute cerebral infarct), perfusion (relative cerebral blood flow), and fetal imaging. Cardiac anatomy and flow imaging is routinely performed.

MRA is accomplished through computer manipulation to "show" only blood vessels and to "suppress" everything else; vascular structures are beautifully visualized (see Chap. 9).

Magnetic resonance spectroscopy (MRS) is a biochemical evaluation of the brain. It is used to identify and quantify metabolites and by its spectrum separate pathology from normal tissue (Fig. 1.10).

Proper Utilization of Imaging

An imaging test should be obtained when the value of the result is greater than the cost (risk) of the test. Costs are defined in many ways – monetary, radiation, morbidity (sedation or contrast medium), anxiety of the patient and the parents, time, and inconvenience. In the current health-care environment less is clearly better for the system but not necessarily for the patient. It is our job to make sure that every patient gets the appropriate imaging suited for his/her particular clinical need.

Once the decision is made to image, the radiologist considers the differential diagnosis and the appropriate questions asked by the pediatrician. The answers to the questions posed before ordering a test enables a proper examination. If a functional question is asked (e.g., about the percentage of renal function), a nuclear study is optimal, while an anatomical study, such as ultrasound, is not (Table 1.4). The imaging study chosen should give results leading to the proper diagnosis; even a negative result may provide useful information and lead to appropriate advice or counseling.

The major problem of utilization remains *overutilization,* e.g., the ordering of skull films for insignificant trauma, or "routine" chest films, or repeating films already obtained. Proper utilization also involves choosing the correct modality to answer the question. Lack of knowledge on a clinician's part of the capabilities and limitations of an imaging procedure, overdependence on imaging rather than the clinical evaluation, and the use of imaging as a screening procedure all lead to many unnecessary examinations.

The pediatric radiologist influences utilization practices and helps obtain the optimal study. Conversant with all the modalities and their pitfalls, the radiologist can reduce the number of films/examinations to decrease radiation dose and can teach the

Table 1.4. Comparison of modalities

Modality	Physical agent	Strength	Weakness	Comment
Plain film	X-ray	Global view of anatomy	Does not reveal fine detail of organs	Least expensive
Ultrasound	Sound waves	Good organ detail, anatomical	Operator-dependent; air and/or bone may prevent visualization of organs	No radiation, no sedation; less invasive; relatively cheap
CT	X-ray	Good organ detail, quick, anatomical	May need sedation and/or contrast	Moderately expensive, radiation
MR	Electromagnetic waves	Great tissue contrast, multiple planes; anatomical; new inroads to functional imaging	Relatively slow, needs sedation in younger children; may need contrast	Most expensive; no radiation
Nuclear	Gamma rays	Physiological (functional)	Organ-specific; poor on anatomic detail	Moderately expensive

technologist the various ways to avoid repeat films or to lower the dose, for example, in CT examination, using a lower milliamperage (see Chap. 2).

The imager who examines children has a multifaceted role: (a) as a consultant determining the appropriate examination(s) and the number of films necessary, (b) as a member of the health care team interpreting films and conserving resources, and (c) as a teacher of his/her clinical colleagues.

The role as a consultant is vital for improved patient care. In the past, most clinical groups made regular rounds in the radiology department. As use of PACS and web server access to images increases, the clinician may never come to the radiology department but can see the image *without* a report and *without* ever discussing the findings or the correct next imaging procedure with a radiologist. Immediate and concurrent transmission of the report (voice recognition dictation) with the image would allow the expert (pediatric radiologist) to provide a useful interpretation. This step is evolving rapidly. However, it is still important in many instances that the radiologist discuss the case with referring clinicians. Timely and effective communication between the clinician and radiologist becomes a challenge of the new technology.

References and Further Reading

1. Curry TS III, Dowdey JE, Murry RC Jr (1990) Christensen's physics of diagnostic radiology, 4th edn. Lea and Febiger, Philadelphia
2. Bushberg JT, Seibert JA, Leidholdt EM Jr, Boone JM (2002) The essential physics of medical imaging, 2nd edn. Lippincott Williams and Wilkins, Philadelphia, pp 97–144
3. Huda W, Slone RM, Aaland MT (2002) Review of radiological physics, 2nd edn. Lippincott Williams and Wilkins, Philadelphia
4. National Council on Radiation Protection and Measurements (1981) Radiation protection in pediatric radiology. National Council on Radiation Protection and Measurements, Washington (NCRP report 68)
5. National Council on Radiation Protection and Measurements (1983) Biological effects of ultrasound: mechanisms and clinical implications. National Council on Radiation Protection and Measurements, Washington (NCRP report 74)

2 Understanding Radiation and Its Effect on Children

Every day each of us receives 1 millirad of radiation from environmental sources. The biggest contribution to environmental radiation comes from radon gas, which is a decay product in the uranium series. However, the largest source of radiation exposure resulting from human activity is diagnostic X-rays. Using this as a reference point, Table 2.1 shows the various ways of expressing radiation. The unit of absorbed dose is the gray, while the unit of absorbed dose equivalent and effective dose – quantities used in radiation protection – is the sievert. In today's medical imaging compendium, CT accounts for perhaps 70% of the effective radiation dose. The doses expressed in Table 2.2 are in fact those of the multidetector CTs. These doses are much higher than with the older single-detector systems.

Since radiation is ubiquitous in our environment, why are we concerned about medical radiation? Firstly, the background dose is much lower than that of CT. There have never been proven deleterious effects secondary to "normal" background radiation. The biological effects of radiation result primarily from damage to DNA, but not all damaged DNA causes ill effects. Single-strand breaks of DNA are readily repaired and there appear to be no measurable effects. On the other hand, breaks in both DNA strands are more difficult to repair. It is this sort of damage that causes genetic mutations, carcinogenesis, and cell death. Some effects of radiation are purely related to dose–*deterministic effects*. As an example, for a given radiation dose to the eye, a cataract will form in the lens. Since we know these doses, and they are large, deterministic effects should be easy to avoid. *Stochastic effects* are much more insidious. In this instance, *any* radiation may cause DNA damage. The effect depends on what portion of the DNA is injured. Since this effect occurs at random, there is a probability of DNA injury at any dose and therefore no safe threshold. This leads to the concept of *linear no-threshold*. This principle states that no level of radiation exposure can be assumed to be absolutely safe.

Of those effects caused by radiation (genetic mutations, carcinogenesis, and cell death), the one we are most concerned about is carcinogenesis. There are a lot of data for radiation-induced cancer, both incidence and mortality. The incidence of cancer is 2–2.5 times greater than the mortality. The biological

Table 2.1. Units of radiation[a]

Units of radiation absorbed dose: rad (rad), gray (Gy)
1 Gy = 100 rad
1 cGy = 1 rad
1 cGy = 1000 mrad
Unit of absorbed dose equivalent or effective dose, terms used for radiation protection only:
sievert (Sv), rem (*r*oentgen-*e*quivalent-*m*an)
1 Sv = 100 rem
10 mSv = 1 rem
Rem = rad×quality factor. For X-rays and gamma rays the quality factor = 1
Unit of exposure: roentgen

[a] Background radiation is approximately 1 millirad/day.
mrad = millirad = 1/1000 of a rad.
mSv = millisievert = 1/1000 of a sievert.

Table 2.2. Relative dose by imaging test[a]

Chest examination, 2 views	10–20 mrad
Abdominal examination, 1 view	50–100 mrad
Fluoroscopy	
Nonpulsed	300–500 mrad/min
Pulsed	100–150 mrad/min
CT[b]	
Head	6 rad (2–3 rad)
Abdomen	3 rad (1 rad)

[a] Background radiation approximately 1 mrad/day (really 300 mrad/year).
[b] Scan dose expressed as CT dose index. The first dose is CT with "adult" factors.
The dose in parentheses is the dose when CT parameters are adjusted for children.

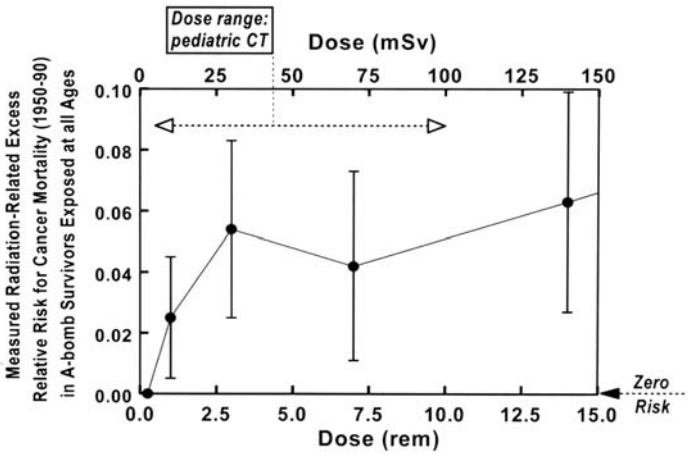

Fig. 2.1. CT radiation and data from atomic bomb survivors.
Relevant dose range for pediatric CT: 6–100 mSv (0.006 = 0.1 Sv). "There is direct, statistically significant evidence for risk in the dose range from 0 to 0.1 Sv." (From [5] with permission)

effects of radiation are greatest on the faster-growing organisms – the fetus, infant, and young child. The thyroid gland, breast tissue, and gonads are organs with increased sensitivity in growing children. Work originally published in 1958 by Alice Stewart [1], substantiated in 1977 by Bithell and Stewart [2], and confirmed in 1997 by Doll and Wakeford [3] shows that the excess risk of cancer (above the spontaneous level) in fetuses whose mother was irradiated in the third trimester is increased by 40 % (if the baseline is 1/1000, then risk is 1.4/1000 of a particular cancer). It is obvious that the first factor in children's vulnerability to radiation carcinogenesis is the age at exposure.

A second factor in children's vulnerability to radiation carcinogenesis is the life-long *cumulative effect of radiation*. The younger the patient and the more times he/she is exposed to radiation, the higher the probability of cancer. This is why we want appropriate usage of all radiation-producing tests (CR, CT, etc.). The third factor which explains why children are at the greatest risk of radiation carcinogenesis is the fact that it takes a long time to develop a cancer and that children have the longest life span remaining after exposure.

Until 2000 there were only theoretical reasons why low-dose radiation (between 0.5 and 120 mSv) caused increased carcinogenesis. Pierce and Preston studied the data from the atomic bomb survivors who had received doses in this range and found 35,000 survivors with a 50-year follow-up [4]. They knew the age at exposure and they found that the solid cancer risks persist over 50 years. There was a 10 % increase over the expected cancer rate. The kinds of cancers observed in the survivors were the same cancers seen in older people but occurred at a somewhat younger age. The youngest children were 10 times more sensitive than middle-aged adults. The cost of this study was over a half a billion dollars and there was a suitable control. There has never been a more careful study of the effects of radiation.

Brenner showed that our current CT doses overlap those doses from which excessive cancers were occurring in the atomic bomb survivors (Fig. 2.1) [5]. He estimated that a small but significant risk of excess cancers would occur in children exposed to these CT doses. It is a small individual risk, but since the use of CT in children is increasing rapidly, it becomes a significant public health problem.

Radiation-producing modalities and specifically CT are some of the most valuable tests in diagnostic imaging. CT use is increasing for "routine" diseases such as kidney stones, appendicitis, and bowel obstruction, to mention just a few. It is helping us make rapid diagnosis and improving outcome. It is appropriate to use CT when the benefits outweigh the risks. Therefore it is the responsibility of the referring physician as well as the pediatric imager to make sure we are dealing with the most appropriate test for a specific problem. MR and ultrasound frequently can replace a radiation-producing test.

Once the pediatric imager has screened the request for the appropriateness of the examinations ordered, it is then important to give the least radiation necessary to obtain a diagnostic image during the examination. This occurs when one pays specific attention to detail. In CT this means attention to the milliamperage (mA) multiplied by time of exposure in

seconds (mAs). Milliamperage seconds is linearly related to dose. The kilovoltage (kV) utilized is important as small increases in kV result in greater increases of dose. We must also determine how many phases of the exam we do, i. e., do we do the examination first without contrast and then with contrast? With a two-phased examination there is double the radiation dose. The general concept of ALARA – as low as reasonably achievable – should always be utilized. We must obtain diagnostic images but must also be aware of the cost in radiation for that image.

References and Further Reading

1. Stewart A (1958) A survey of childhood malignancies. Br Med J 28:1495–1508
2. Bithell JF, Stewart AM (1977) Pre-natal irradiation and childhood malignancy: a review of British data from the Oxford Survey. Br J Cancer 1975 31:271–287
3. Doll T, Wakeford R (1997) Risk of childhood cancer from fetal irradiation. Br J Radiol 70:130–139
4. Pierce DA, Preston DL (2000) Radiation-related cancer risks at low doses among atomic bomb survivors. Radiat Res 154:178–186
5. Brenner DJ (2002) Estimating cancer risks from pediatric CT: going from the qualitative to the quantitative. Pediatr Radiol 32:228–231
6. National Council on Radiation Protection and Measurements (2001) Evaluation of the linear-nonthreshold dose-response model for ionizing radiation. National Council on Radiation Protection and Measurements, Washington (NCRP report 136)
7. Hall EJ (ed) (2000) Radiobiology for the radiologist, 5th edn. Lippincott Williams and Wilkins, Philadelphia
8. Brenner DJ, Elliston CD, Hall EJ, Berdon WE (2001) Estimated risks of radiation-induced fatal cancer from pediatric CT. AJR Am J Roentgenol 176:289–296
9. Hall EJ (2002) Neuhauser Lecture. Lessons we have learned from our children: cancer risks from diagnostic radiology. Pediatr Radiol 32:700–706
10. Slovis TL (ed) (2002) Conference on the ALARA (as low as reasonably achievable) concept in pediatric CT intelligent dose reduction. Pediatr Radiol 32:217–317
11. The Society for Pediatric Radiology (2002) 2002 SPR Seminar in radiation dose reduction. Pediatr Radiol 32:707–754
12. National Cancer Institute, The Society for Pediatric Radiology (2002) Radiation risks and pediatric computed tomography. A guide for health care providers. National Cancer Institute, Rockville, Md (brochure, also available from www.cancer.gov; www.pedrad.org)
13. Frush DP, Donnelly LF, Rosen NS (2003) Computed tomography and radiation risks: what pediatric health care providers should know. Pediatrics 112:951–957
14. Wakeford R, Little MP (2003) Risk coefficients for childhood cancer after intrauterine irradiation: a review. Int J Radiat Biol 79:293:309

3 Chest Examinations in Children

The chest film is the most frequently ordered pediatric radiographic examination. However, because one looks at so many chest radiographs, familiarity may create a false sense of security rather than expertise. A thorough, detailed, systematic approach to the radiographic evaluation is crucial for anyone dealing with children. In this chapter we discuss the general diagnostic principles and approach; the specifics of chest examinations for neonates and infants are reviewed in Chap. 4. This chapter also stresses those areas where the approach to the pediatric chest radiograph differs from the adult film [the 3 T's: technical factors, tubes, and traps – i.e., anatomical structures unique to kids; thanks to Dr. Moira Cooper, pediatric radiologist, (British Columbia Children's Hospital, Vancouver, Canada)]. We present common pathological conditions as a foil to the normal chest film (Fig. 3.1).

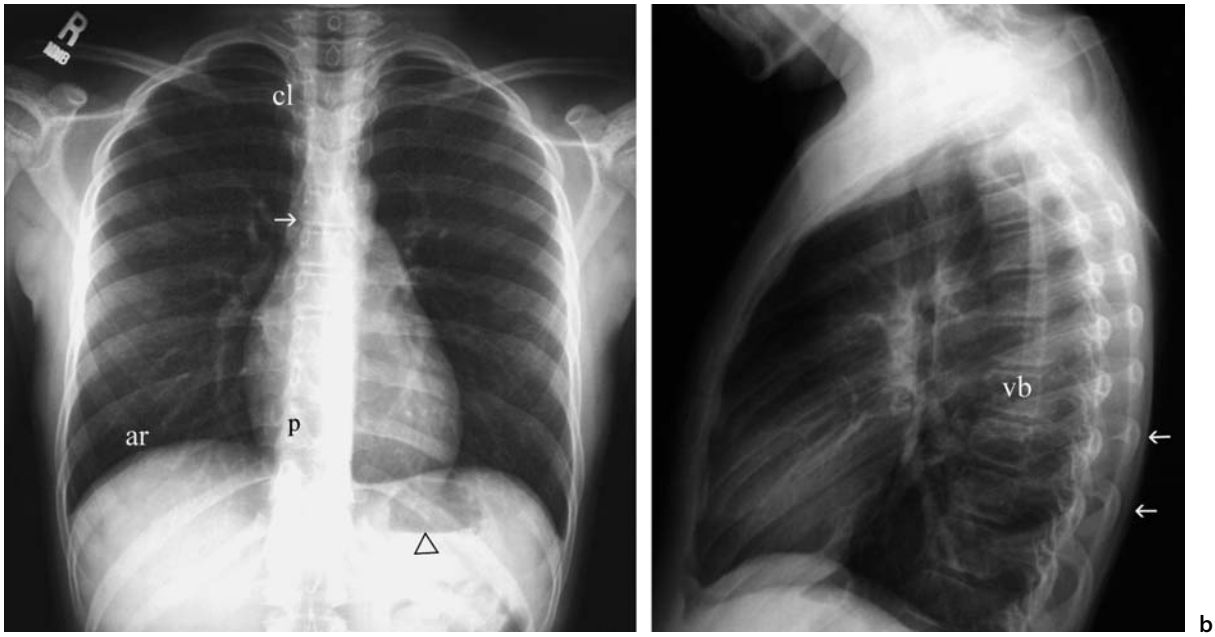

a b

Fig. 3.1. Normal inspiratory chest
a Frontal examination reveals a normal lung volume. The criteria for a normal lung volume are: (a) less than one-third of the heart is projected below the hemidiaphragm; (b) the diaphragm is rounded, and the sixth or seventh anterior rib (*ar*) intersects the diaphragm; and (c) the lungs are air-filled (black). This is a properly positioned, nonrotated film as evidenced by (1) comparative anterior ribs equidistant from the pedicles (*p*), (2) medial aspects of the clavicles (*cl*) symmetrically positioned, (3) the carina approximates the right pedicles (*arrow*), and (4) no difference in aeration between the two sides. The film was taken with the patient erect, as shown by the air–fluid level in the stomach (*arrowhead*)
b Lateral examination confirms normal aeration of the lungs. Note that the vertebral bodies (*vb*) get blacker as we go from superior to inferior. The patient is slightly rotated as you can see the ribs on each side (*arrows*)

Technical Factors

Technical problems in pediatric radiology are caused largely by uncooperative children. The young patients are not feeling well, the environment is strange, and they may as a result be quite frightened. Preliminary evaluation of the chest radiograph should assess these technical factors:

- The degree of inspiration: lung volume
- The position of the patient: extent of rotation and posture of the patient
- How the film was obtained
- Adequacy of the exposure

Lung Volume

The radiographic examination of the chest begins with frontal and lateral roentgenographs taken after deep inspiration. The degree of inspiration, i.e., the lung volume, generally determines what is seen on the film. The answers to the questions in Table 3.1 determine whether or not adequate lung volume is obtained.

If the child has taken a shallow breath, the heart may appear enlarged, the vessels may coalesce to give a false impression of an opacity, especially in the region of the bases and hila, and sometimes the radiograph has a hazy quality due to the influx of blood and lack of aerated lung.

Hyperexpansion of the lungs – pathological increase in lung volume or air trapping – is involuntary. The changes of hyperexpansion listed in Table 3.1 should be visible on both frontal and lateral films. Figures 3.1–3.3 demonstrate the differences between the normal radiograph and those in which inspiration is either pathologically increased or suboptimal. Can you pick out the optimal radiograph?

Position of the Patient

The position of the patient is determined by rotation and posture (lying, sitting, or standing).

The child's posture is important. When the patient is supine, the vascular supply to the upper and lower lobes is equal since gravity has no effect. When the child is sitting or standing, gravity plays a significant role, and the upper-lobe vessels are less distended than the lower-lobe vessels (one-third to two-thirds size). One can determine an erect film by looking at the air–fluid level in the stomach and at changes in the pulmonary vasculature.

Rotation of a child is determined by the answers to the questions in Table 3.2. Figure 3.4 shows the parameters that determine rotation, while Fig. 3.5 exemplifies the posture of the patient, showing supine and erect films. Compare these figures with Fig. 3.1. To which side is the child rotated in Fig. 3.4b and e? See Appendix 2.

Table 3.1. Determining lung volume: questions and answers (Figs. 3.1–3.3)

Question	Answer
How much of the heart projects below the dome of the diaphragm on the frontal view?	More than 1/3: expiratory effort; not enough air in lungs Less than 1/3: good inspiratory effort; normal amount of air None: may be hyperexpanded; too much air
On the frontal view, are the domes of the diaphragm flat?	No, very domed: expiratory examination No, rounded: good inspiratory effort Yes, flat: good or may be too great a lung volume
Are the hemidiaphragms flat or vertically oriented on the lateral film?	No, horizontally oriented: expiratory effort Yes, vertically oriented: good or possibly increased lung volume
Which anterior rib crosses the diaphragm on the frontal film? (Remember that the anterior ribs move more than the posterior ribs on good inspiration)	3rd or 4th: expiratory effort 5th or 6th: inspiratory effort 7th or lower: good or possibly too great a lung volume
On the lateral view, is there a triangle of air behind the heart?	No: expiratory effort (except if large heart) Yes: inspiratory effort
Are the lungs black or white on the frontal film?	Black: air-filled, inspiratory White or gray: not air-filled, expiratory

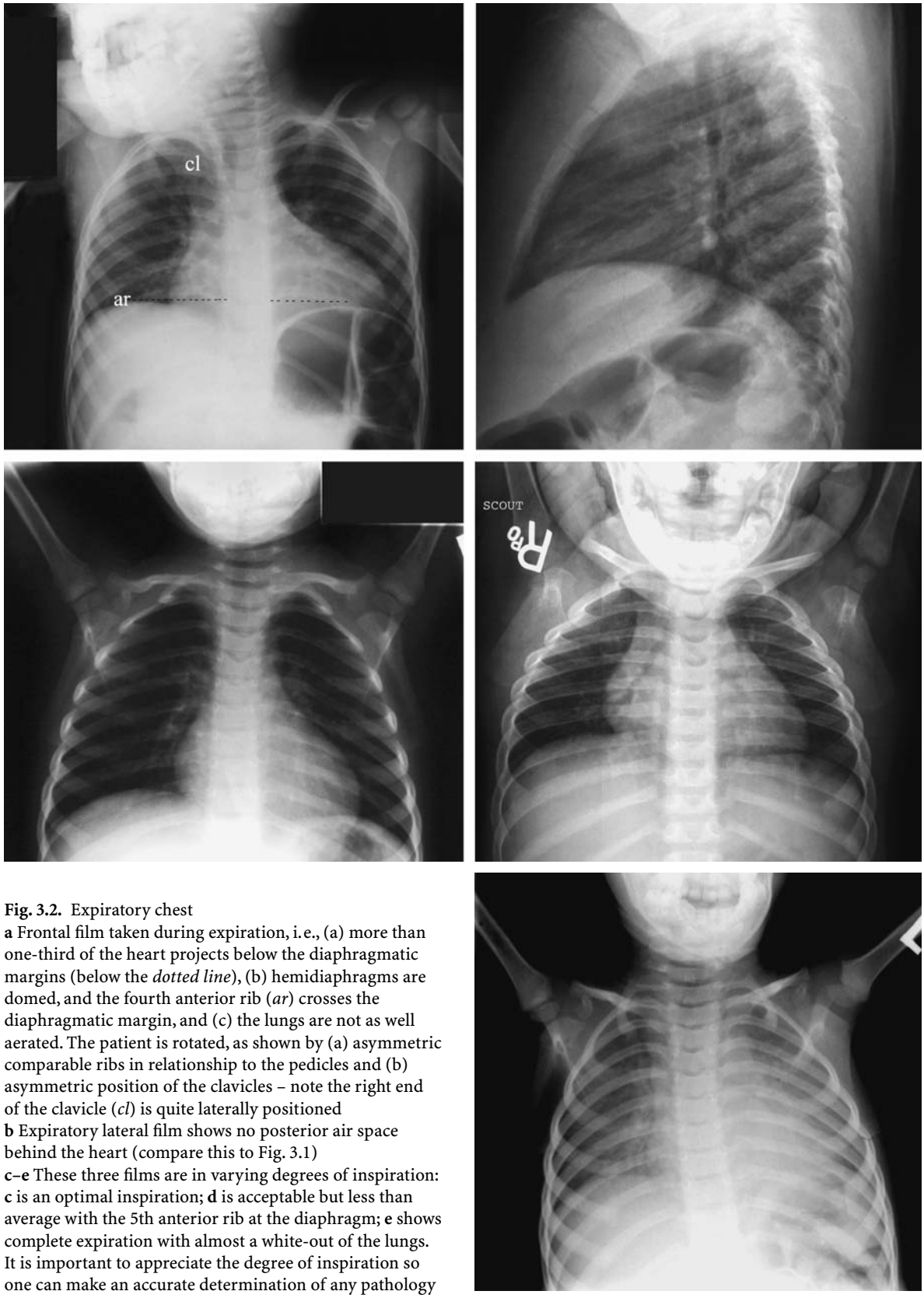

Fig. 3.2. Expiratory chest
a Frontal film taken during expiration, i. e., (a) more than one-third of the heart projects below the diaphragmatic margins (below the *dotted line*), (b) hemidiaphragms are domed, and the fourth anterior rib (*ar*) crosses the diaphragmatic margin, and (c) the lungs are not as well aerated. The patient is rotated, as shown by (a) asymmetric comparable ribs in relationship to the pedicles and (b) asymmetric position of the clavicles – note the right end of the clavicle (*cl*) is quite laterally positioned
b Expiratory lateral film shows no posterior air space behind the heart (compare this to Fig. 3.1)
c–e These three films are in varying degrees of inspiration: **c** is an optimal inspiration; **d** is acceptable but less than average with the 5th anterior rib at the diaphragm; **e** shows complete expiration with almost a white-out of the lungs. It is important to appreciate the degree of inspiration so one can make an accurate determination of any pathology

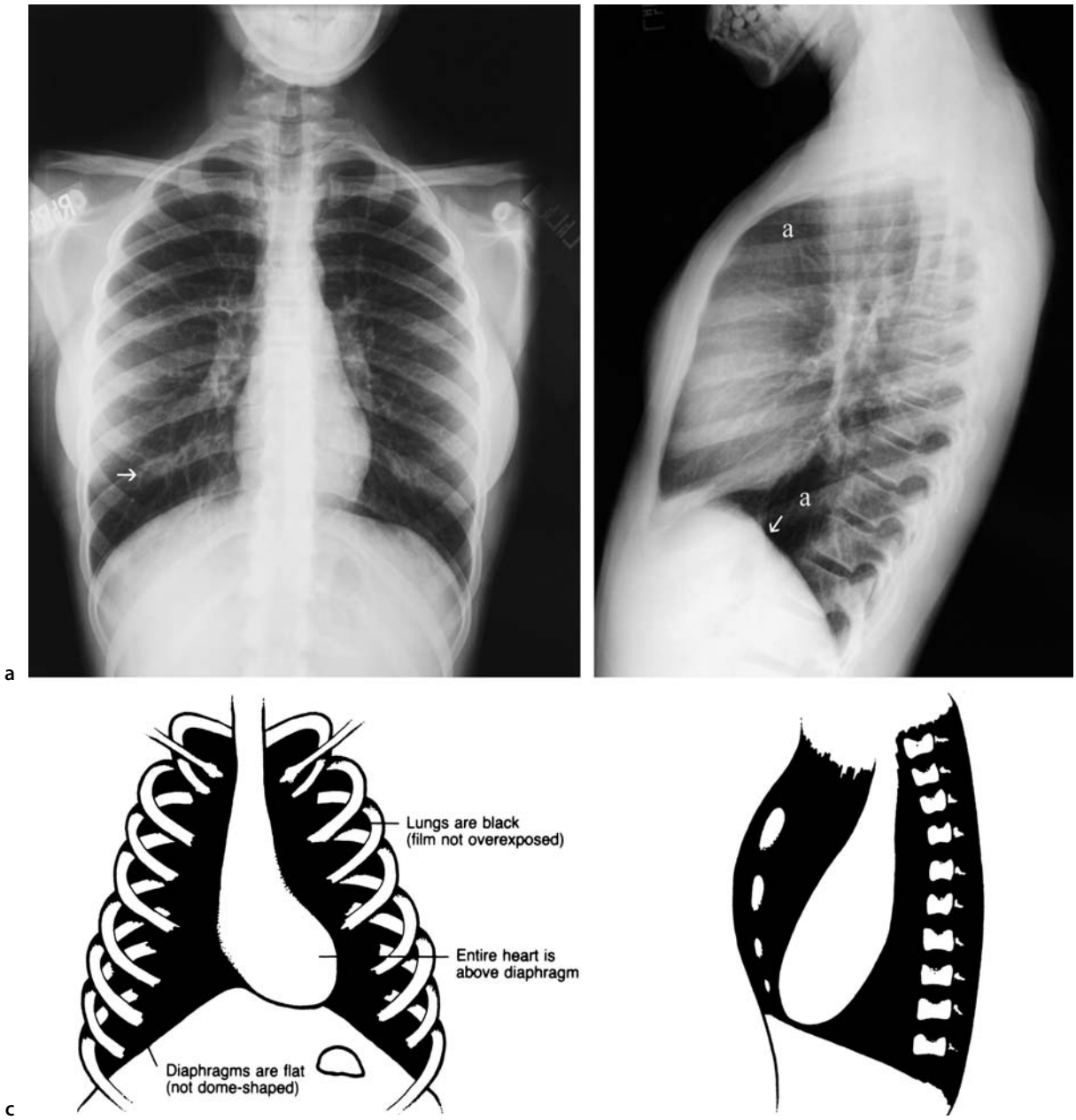

Fig. 3.3. Hyperexpanded chest radiograph
a Frontal view. The entire heart is projected above the diaphragm, the hemidiaphragms are flattened, and the lungs are quite black – yet the film is not overexposed. You know this because you can see the pedicles of the spine behind the heart and the peripheral vasculature (*arrow*)
b Lateral view. The hemidiaphragms are obliquely oriented (*arrow*), and there is a large air space (*a*) both behind and in front of the heart. Remember: hyperexpansion is involuntary and is caused by air trapping. It must be seen on both frontal and lateral projections
c, d Comparable drawings of the hyperexpanded lungs

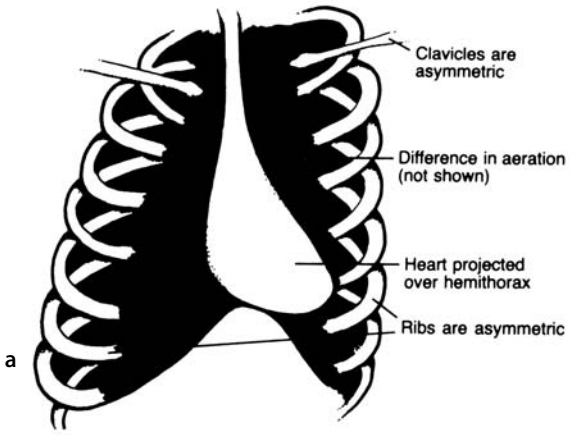

a

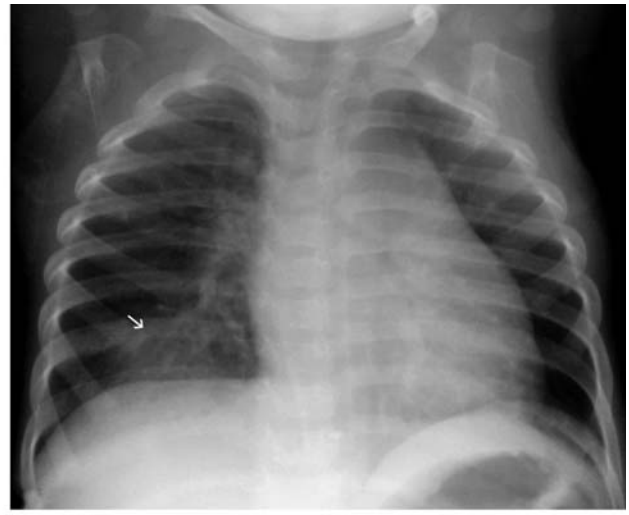

b

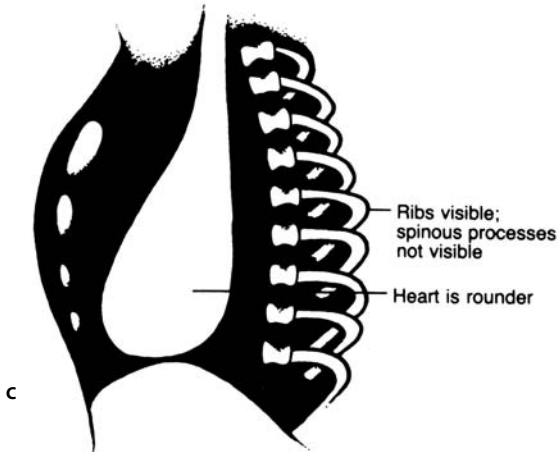

c

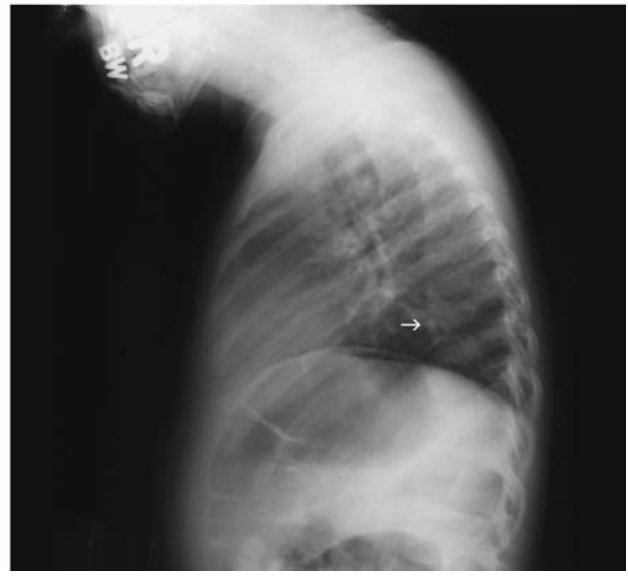

d

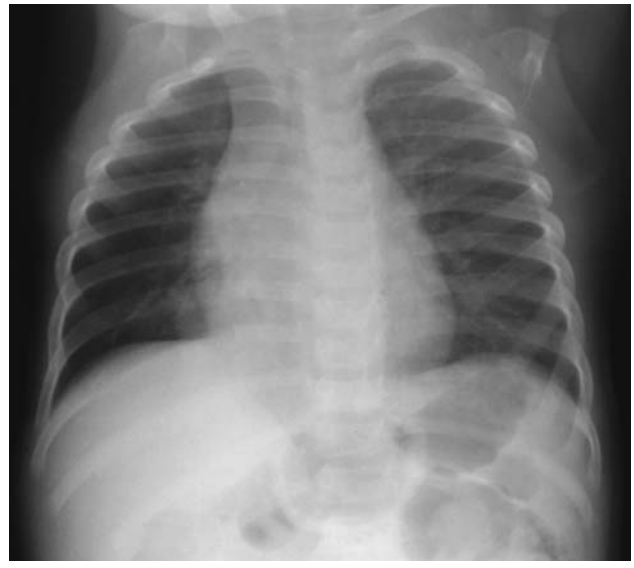

e

Fig. 3.4. The rotated chest
a Schematic drawing demonstrates the signs of rotation – asymmetric clavicles, differences in aeration (not shown), heart projected over one hemithorax and not the other, asymmetric ribs when relating the anterior rib to the pedicle
b Rotated chest as in **a**. Note the child has an opacity (*arrow*) in the lower right lung field. To which side is the child rotated? (Answer in Appendix 2)
c Schematic drawing of the rotated lateral film. The ribs are visible and not the spinous process
d Lateral radiograph of child in **b**, showing these findings and the posterior opacity (*arrow*)
e Another rotated child with all of the abnormalities described above. To which side is this child rotated? (Answer in Appendix 2).

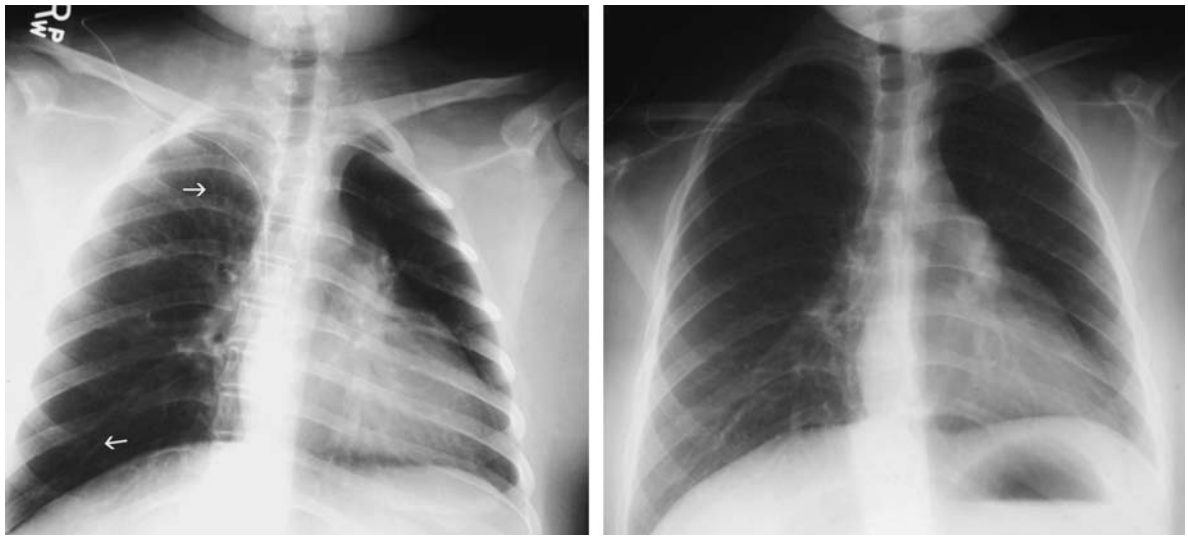

Fig. 3.5. Effect of patient position and the tube target distance
a Patient in supine position, with approximately 46 in. (ca 1.2 m) between the X-ray tube and the film. Upper-lobe vessels (*arrow*) are equal in size to those of the lower lobe (*arrow*). The heart is magnified. There is a central venous catheter in place
b Patient is erect and 6 ft (ca 1.8 m) from the X-ray tube. It is difficult to see the upper lobe vessels, but the lower lobe vessels are easily seen

Table 3.2. Determining rotation: answers and questions

Question	Answer
On the frontal film, are the anterior ribs equidistant from ipsilateral pedicles?	No: rotated patient Yes: straight patient
Are the medial aspects of the clavicles symmetrical in relation to the midline on the frontal view?	No: rotated patient Yes: straight patient
What is the position of the carina in relation to the right pedicles on the frontal film?	To the left of the right pedicles: patient is rotated, or another abnormality is present Approximates the right pedicles: patient is straight
Is one lung blacker than the other on the frontal view?	Yes: patient is rotated, or abnormality is causing localized difference in aeration No: straight patient
On the lateral view, are the ribs seen posteriorly?	Yes: rotated patient No: straight patient

How the Film Was Obtained

The third major technical factor to keep in mind is how the film was obtained. Greater magnification occurs when structures, such as the heart, are farther from the film. When the X-ray beam passes through the patient from back to front [a posterior–anterior (PA) projection], the heart is closer to the film and is less magnified. Conversely, if the X-ray beam enters the front of the patient's chest, passes through the back and onto the film [an anterior–posterior (AP) projection], the magnified heart and great vessels may give the impression of cardiomegaly. This is a common problem with portable chest films, which are taken in the AP direction.

Another important factor in magnification is the distance of the X-ray tube from the film. Routinely, portable films are exposed 40 in. (ca. 1 m) from the tube, adding to the magnification. Figure 3.6 shows the principles of magnification and the criteria for recognizing how a film was obtained.

Adequacy of Exposure

Be sure that the film is properly exposed or the digital image is windowed and leveled properly (Figs. 3.7, 3.8). You can tell this on the frontal film by examining the vertebral column *behind the heart*. If you can see the detailed spine and pedicle through the heart and can also see the pulmonary vessels in the peripheral lung, the exposure is correct. If you see *only* the spine but not the pulmonary vessels, the film is too dark (overexposed). On digital images, the exposure will usually be correct as one can window and level the picture. However, on digital images, one cannot tell much about radiation dose (Chap. 2).

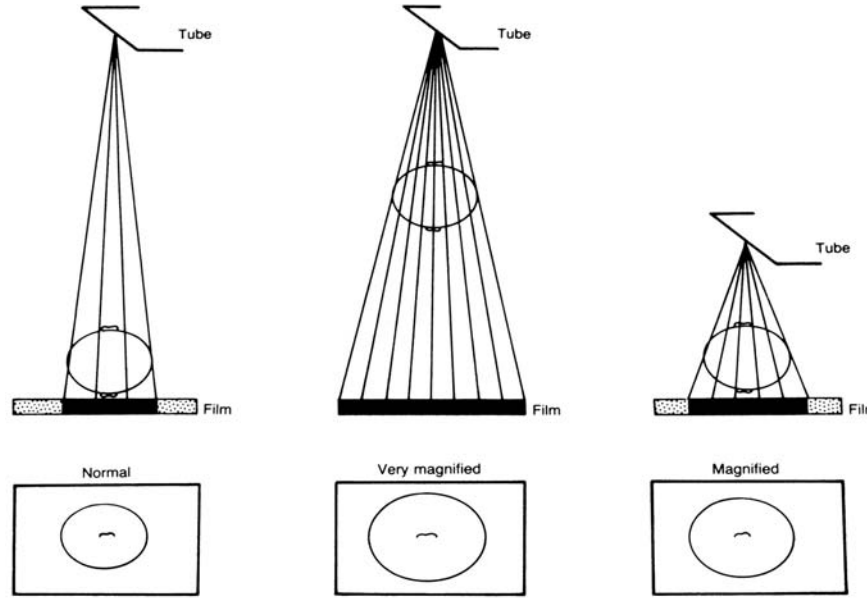

Fig. 3.6. Tube–film distance and magnification

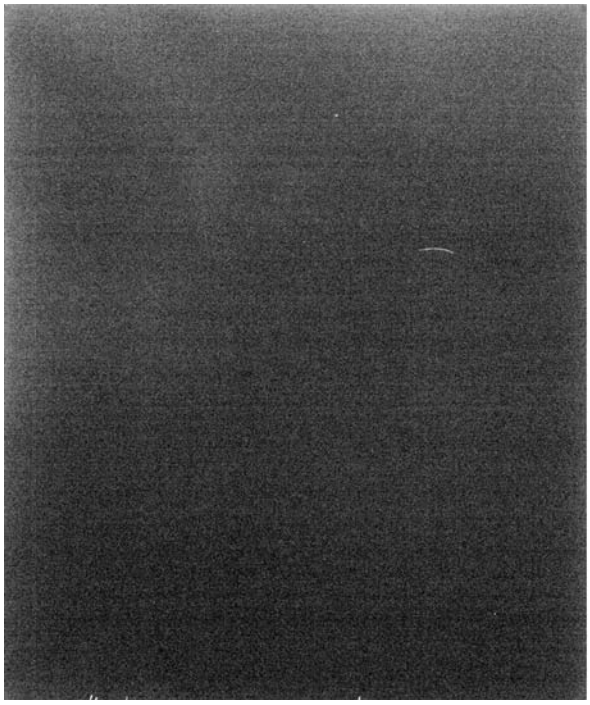

a

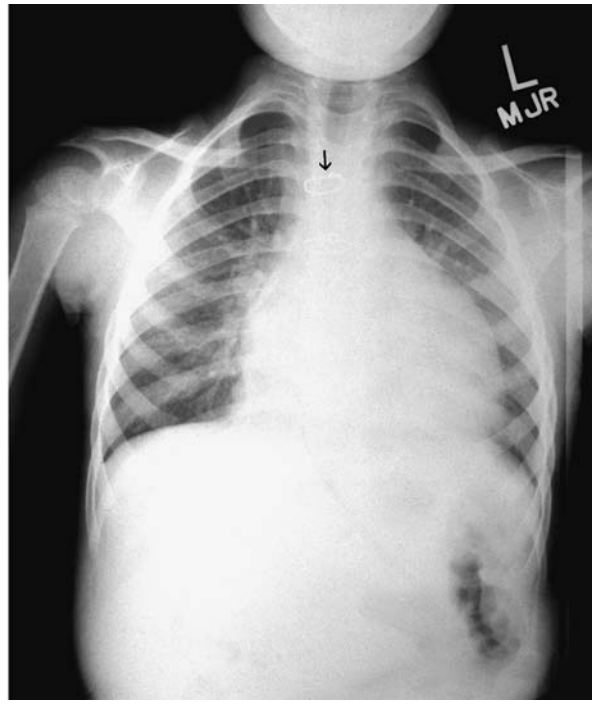

b

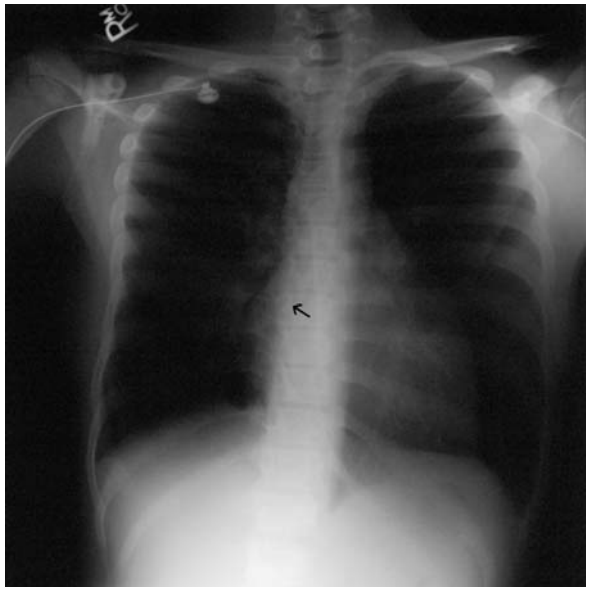

c

Fig. 3.7. Adequacy of exposure
a This is an entirely black film, showing that there has been too much exposure (overexposure) and all of the X-ray beams have passed through the patient to hit the cassette or film and none were absorbed by the patient
b This is an underexposed examination. The film is white, and you can barely see the surgical sutures (*arrow)* in the sternum and cannot see the spine at all
c This is a (overexposed) frontal examination; a properly exposed examination is seen in Fig. 3.1. Note how on the poorly exposed film the pedicles can be seen (*arrow*), but you cannot see peripheral lung markings

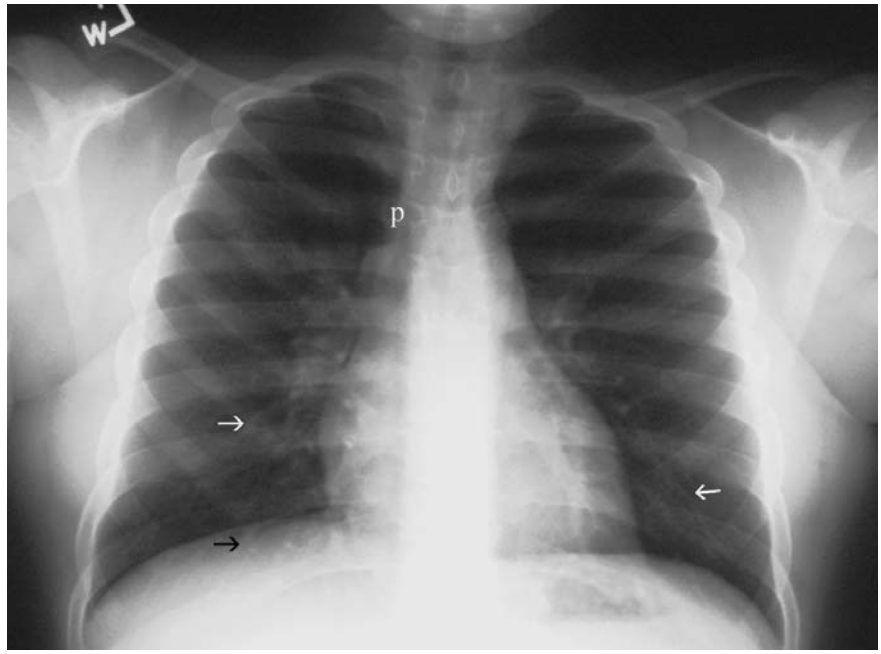

Fig. 3.8. On the properly exposed films, you can see both the pedicles (*p*) and the peripheral lung markings (*arrow*). Is the film up correctly? (See Appendix 2)

Traps: Unique Anatomical Normal Variants and Positions of Tubes

The chest radiograph accounts for a least 50% of all pediatric imaging, and therefore you must be aware of the normal variants. The thymus may dominate the mediastinal silhouette (see below). Normal skin folds are frequently seen in young infants and must be differentiated from pneumothoraces (the presence of pulmonary vessels extend into the "black area" when there is a skin fold; there are no markings when there is a pneumothorax (see Chap. 4).

The central cleft of the two posterior neural arches which have not fused is often noted (Fig. 3.9). These spinous processes of the spine usually fuse between the ages of 3 and 5 years.

Occasionally one will see calcific densities overlying the right or left thorax on infant chest radiographs. These are the sternal centers in a slightly rotated film (Fig. 3.10).

It is important to note the position of the tubes, clips, sutures, and monitoring devices. If the child who is intubated is having unexplained respiratory distress, two views (frontal and lateral) may help define tube position (Fig. 3.11).

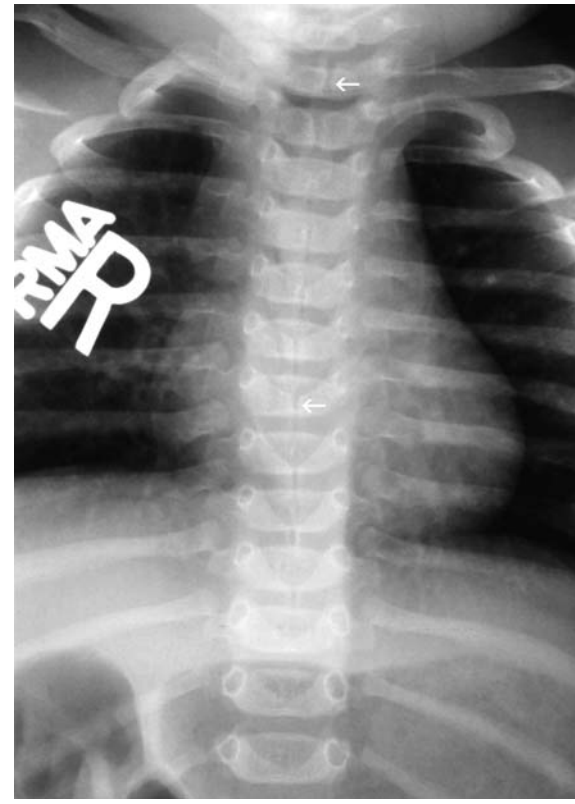

Fig. 3.9. Traps
Nonfusion of spinous process. On this supine film of a 6-month-old infant, the spinous processes (*arrow*) of the thoracic vertebrae are not fused at multiple levels

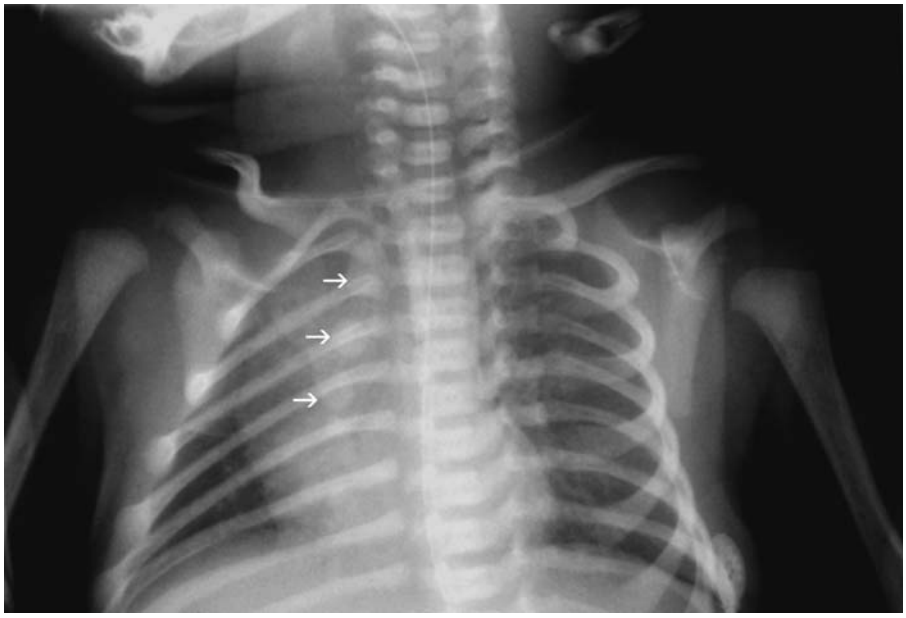

Fig. 3.10. Sternal ossification centers
As you can tell by the ribs, this patient is quite rotated. There is a nasogastric tube in the esophagus. You should note multiple rounded bony structures projecting over the heart in the right hemithorax (*arrows*). These are the sternal ossification centers, which because of rotation are clearly visible

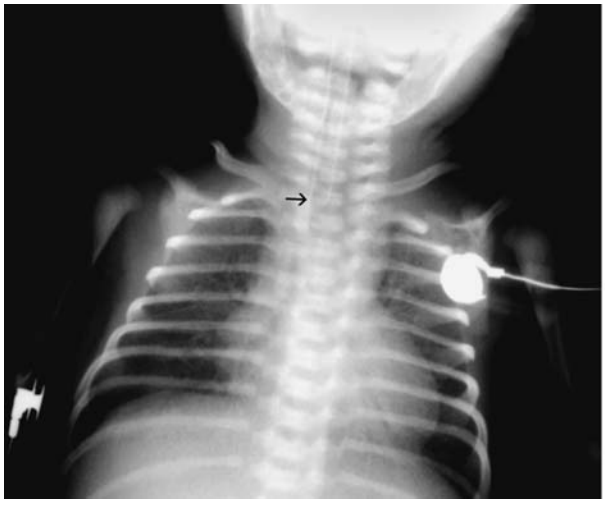

a

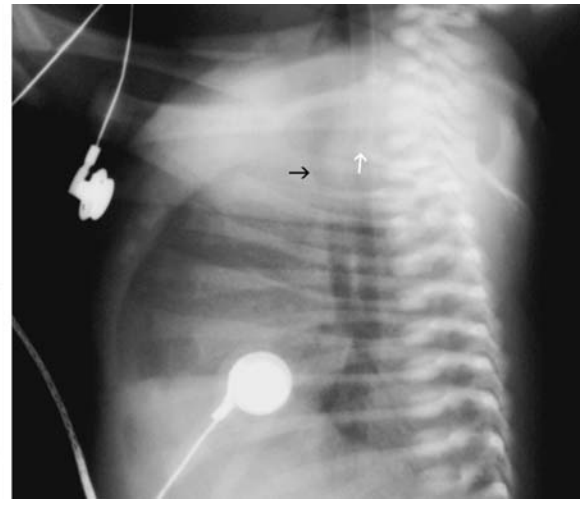

b

Fig. 3.11. This neonate has respiratory distress
a Frontal radiograph shows the endotracheal tube in the appropriate position (*arrow*). However, see the lateral film
b On this lateral radiograph, the endotracheal tube is in the esophagus (*white arrow*); the airway (*black arrow*) is anterior. Whenever there is a question of unexplained respiratory distress, a lateral film may be helpful, particularly in an intubated patient

Interpreting the Film: The Radiologist's Circle

Anyone can glance at a pediatric chest film, and with very little training identify obvious abnormalities – right? Wrong! It takes most radiologists years to get into the habit of reading a chest radiograph properly. Let's face it: anyone ordering a chest film is going to look at the heart and lungs, but radiologists look first at the nonpulmonary areas, i.e., the abdomen, bones, soft tissues, and airway, to be sure that they do not miss any abnormality (see Appendix 1: "Rules for Reading Pediatric X-Rays"). Only then does one progress to the mediastinum, and observes the lungs last.

A good habit to develop is to make an imaginary circle on the film so as to dispense with all the noncardiopulmonary areas. Begin at the corners and/or where the patient information is. Be sure when imaging on PACS that all the patient information and technical factors are displayed (there are options to remove technical data). Check the name, date, and especially the left or right marker. Nothing is more embarrassing than missing dextrocardia with abdominal situs inversus because one did not look for the marker and therefore put the film up wrong. An easy way to complete the circle is to go from the name tag to the markers to the ABCS of the film: *A*=abdomen, *B*=bones, *C*=chest (airway, mediastinum, lungs, and diaphragm), *S*=soft tissues.

Abdomen

► ***Rule No. 1:*** On every chest film, read the abdominal portion as you would read an abdominal film.*

Evaluate the abdomen (regardless of how little of it can be seen) on every chest film, and note whether the stomach bubble is on the left and the liver on the right. Look specifically for calcifications, such as gallstones or pancreatic stones. Is the bowel distended? Are there air–fluid levels? Is this an erect film? Can you see free intraperitoneal air or fluid? Now look at Fig. 3.12 with these clues in mind; on every chest film, look at the abdomen as if you were reading an abdominal film.

Bones and Soft Tissues

One can often see portions of the arms, shoulders, ribs, sternum, and mandible, as well as cervical, thoracic, and lumbar vertebrae. Be alert for fractures, congenital abnormalities, bone destruction, or other signs of disease. It is very embarrassing to miss absent clavicles on a chest film because the bones were not viewed systematically. This is also a good time to examine the soft tissues of the neck, thorax, and abdomen to detect any swelling, foreign body, calcifications, etc. The soft tissues may reveal multiple artifacts, such as hair braids, buttons, bandages, or redundant skin folds. Soft tissue swelling or subcutaneous calcifications can be clues to systemic disease. By now you have returned, via your imaginary circle, to the cervical area, and you are ready to inspect the vertebrae. What abnormalities do you see in Figs. 3.13–3.17? Look at the films and then go to Appendix 2.

* These rules were adopted from Joseph O. Reed, M.D., chief of pediatric imaging at Children's Hospital of Michigan from 1957 through 1987. Throughout this text we include these fundamental concepts, which were used daily in his teaching sessions. (See Appendix 1)

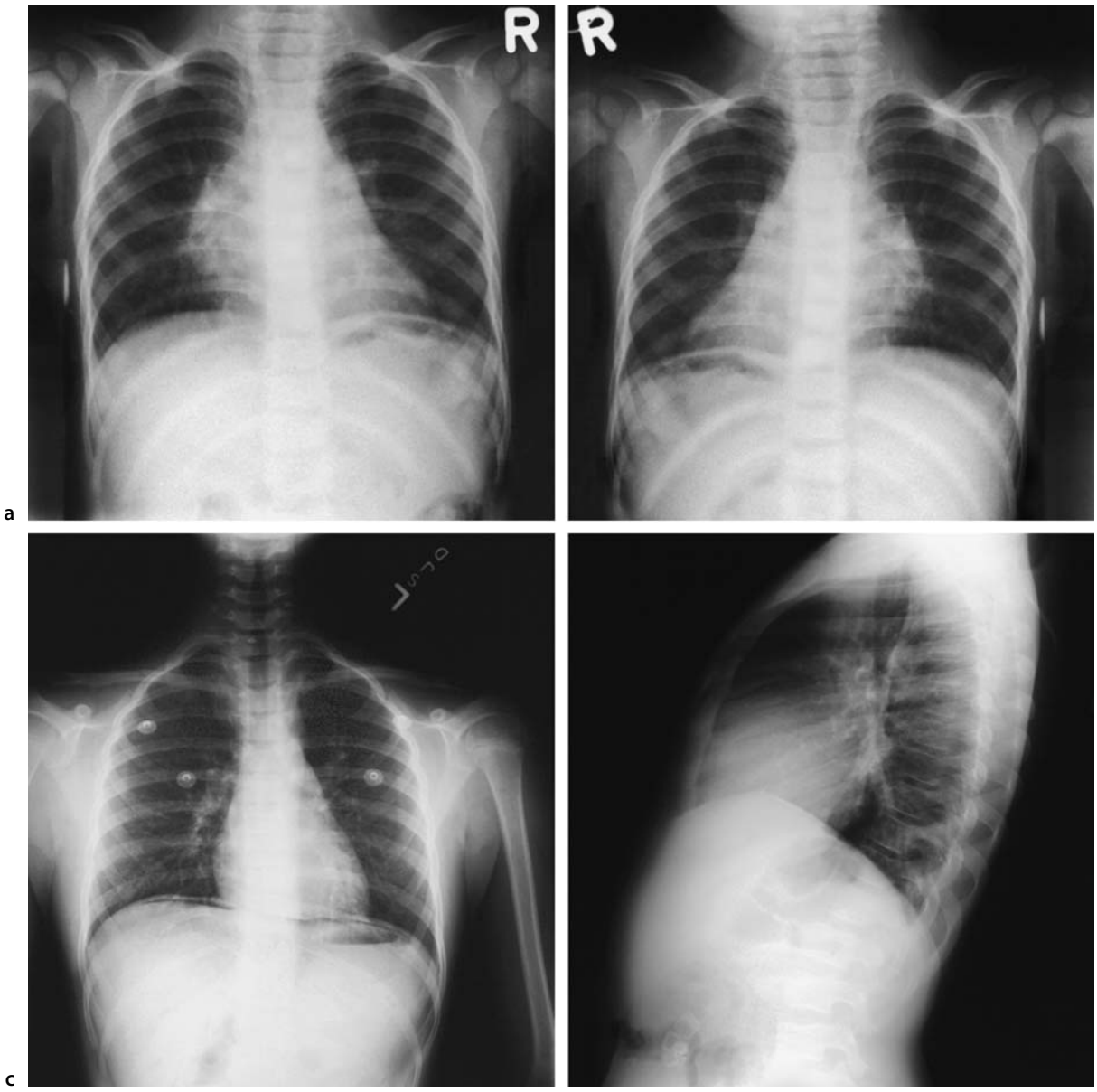

Fig. 3.12. Can you find the abnormality? (Look at the films; then read on)
a Film of a 12-month-old boy. No, the film is not labeled incorrectly. The patient has dextrocardia and abdominal situs inversus
b Correct position of the film
c An 11-year-old girl with blunt abdominal trauma. Free air is seen below the diaphragm. The "diaphragm" extends across the midline – an impossibility. This is the "continuous diaphragm sign." Note how you can see both sides of the diaphragm. The patient was in a motor vehicle accident and had a perforated bowel
d A lateral radiograph of a sickle cell patient with a large heart. Most importantly, did you see the gallstones?

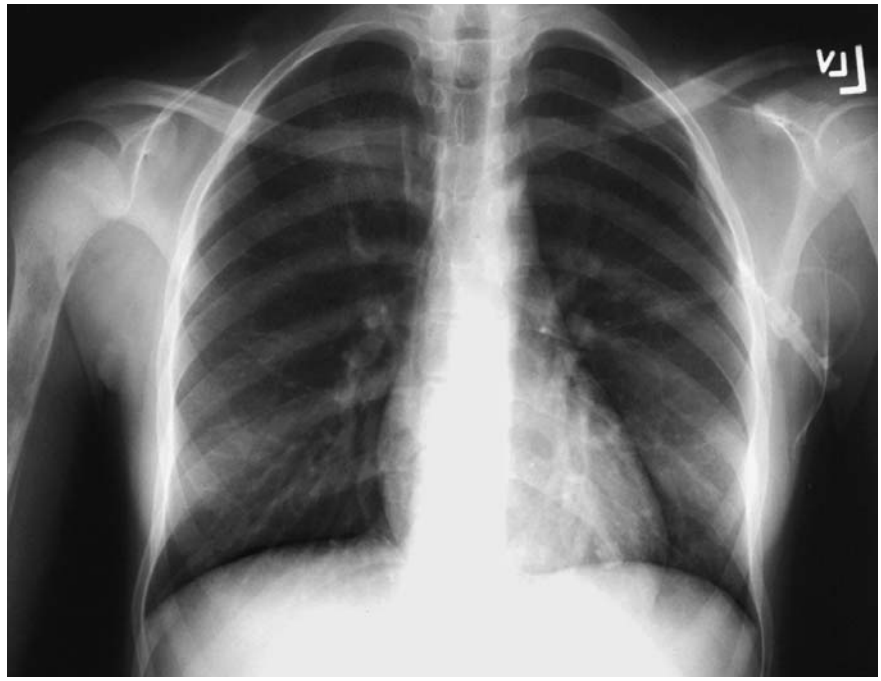

Fig. 3.13. This 13-year-old girl presented with fever and pain

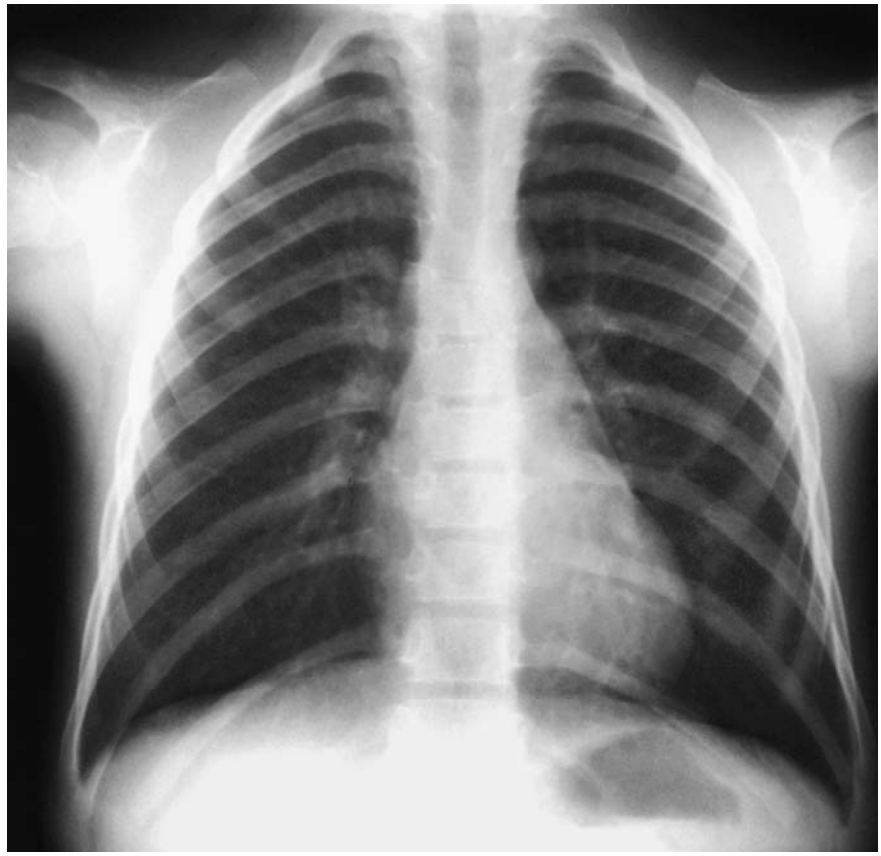

Fig. 3.14. A 9-year-old boy with a cough

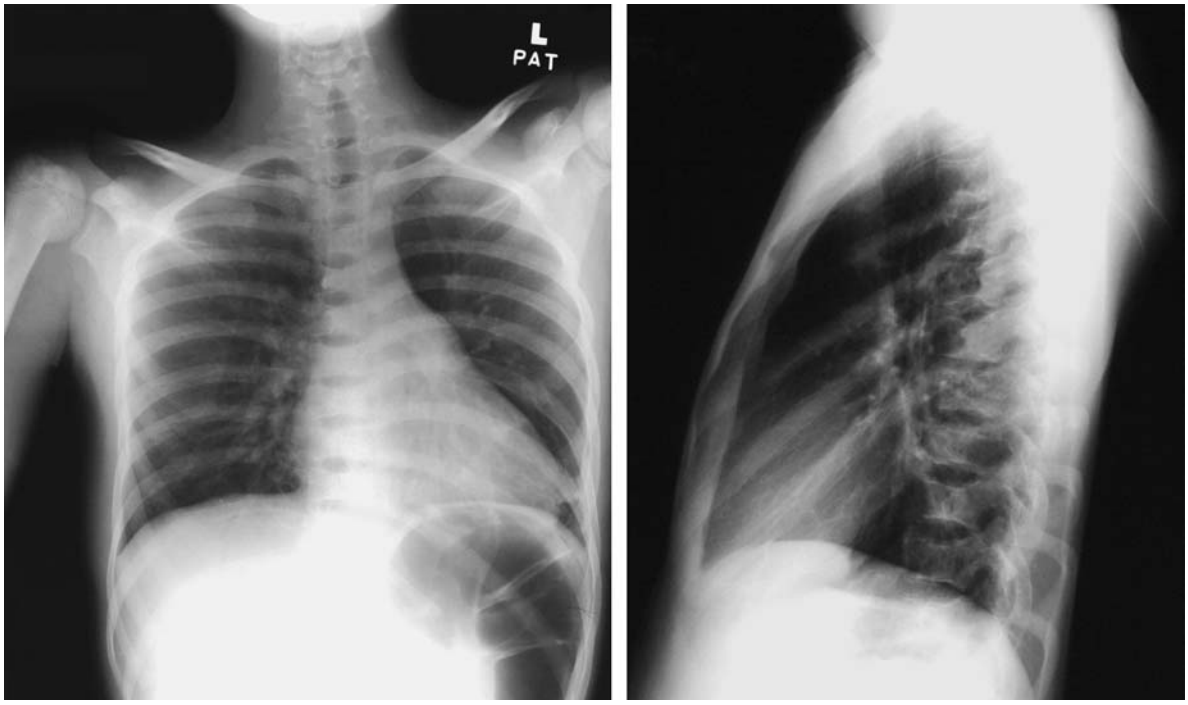

Fig. 3.15. A 17-year-old boy with a cough

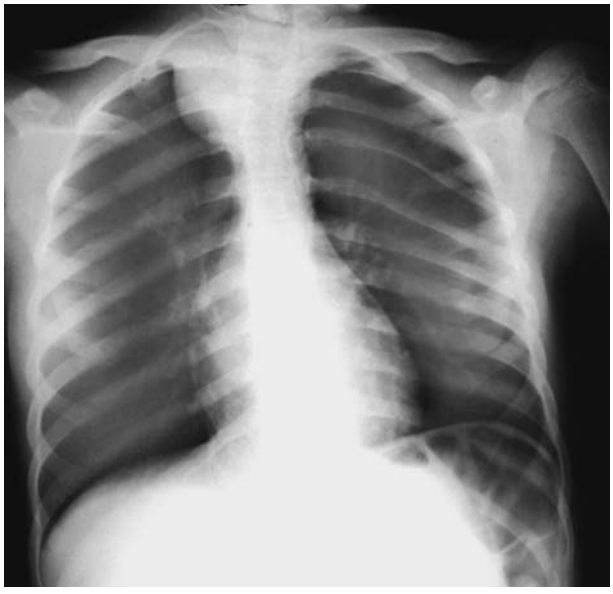

Fig. 3.16. This 12-year-old presented with café au lait spots and scoliosis

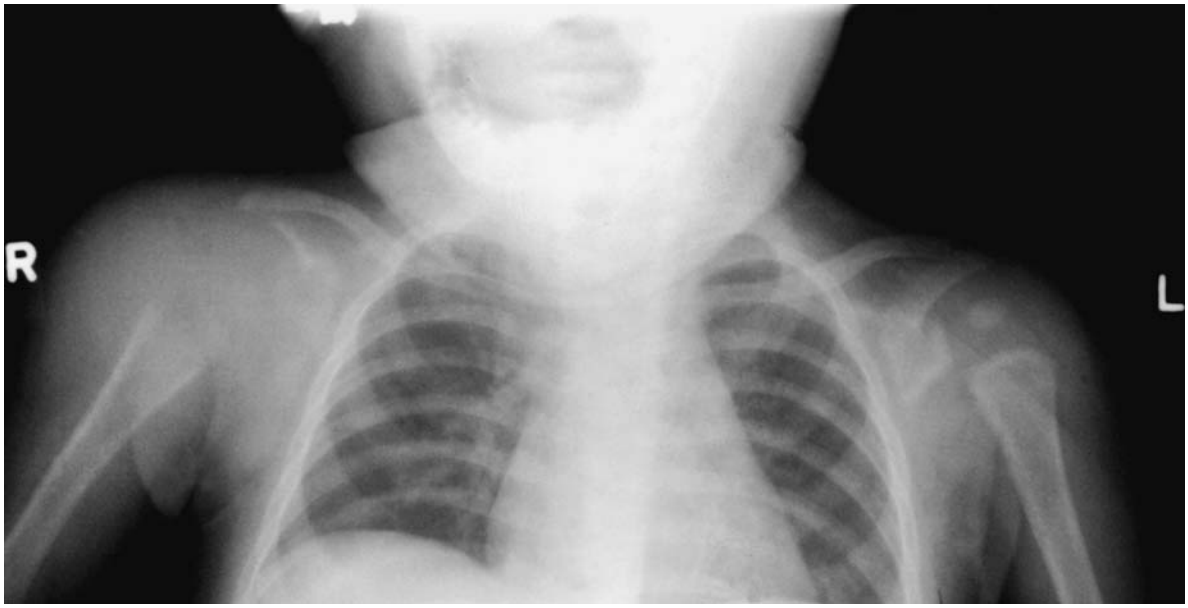

Fig. 3.17. A 6-month-old infant with fever of unknown origin

Chest (Airway, Mediastinum, Diaphragm, Lungs)

► ***Rule No. 2:*** Knowledge of anatomy is the key to the correct radiographic diagnosis.

Airway

The cephalic-most portion of the airway is the nose and choanal air space. These structures are seen best on CT (Fig. 3.18), but the rest of the airway is best and most conveniently seen on the plain film.

The lateral view of the neck is optimal for evaluating the supraglottic (*supra*, above; *glottis*, vocal cords) airway (Figs. 3.19, 3.20). A proper study is obtained by aligning the top of the film with the top of the patient's ear. The cephalic-most portion of the airway is the nasopharynx, which communicates anteriorly with the nares and merges posteriorly to form the hypopharynx. For all practical purposes, the lower border of the nasopharynx is the hard palate, soft palate, and the uvula. The oropharynx (below the hard and soft palate) leads to the air spaces at the base of the tongue, which are the valleculae. Immediately behind the valleculae is the epiglottis. The hyoid bone is inferior and anterior to the valleculae. The oropharynx also merges posteriorly with the nasopharynx to form the hypopharynx. One can see the palatine tonsils in the lateral walls of the hypopharynx. Anteriorly, the hypopharynx leads to the larynx and becomes the esophagus inferiorly and medially. The pyriform sinuses are the most lateral and inferior aspects of the hypopharynx; their inferior margins provide a handy landmark for the level of the vocal cords. It is important when obtaining a lateral neck examination to slightly hyperextend the patient's head and neck. This flattens the redundant soft tissues in the retropharyngeal area against the cervical spine. The child must be straight lateral and have air in the hypopharynx.

The frontal radiograph is best for viewing the subglottic airway. The true vocal cords are at the same level as the tip of the pyriform sinuses. Immediately below the glottis is the subglottic region, which is only several millimeters long and merges inferiorly into the proximal trachea (Figs. 3.21, 3.22). Note that the airway is a dynamic system and changes in caliber and position so that an isolated, single film may be quite misleading. Nonetheless, an abnormal configuration of the airway should be pursued in the light of the clinical history.

Magnification high-kilovoltage radiography is a noninvasive, useful procedure to delineate the upper airway, trachea, and major bronchi. This technique is most useful for children with stridor, choking, suspected foreign body, vascular ring, and intratracheal

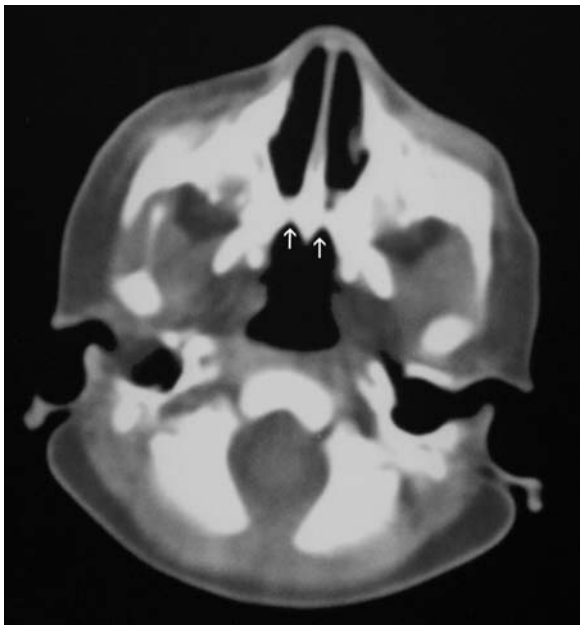

Fig. 3.18. Choanal atresia. In this newborn baby there is bony connection between the vomer and the lateral palatine bone. All these bones have fused and this is bony choanal atresia (*arrows*)

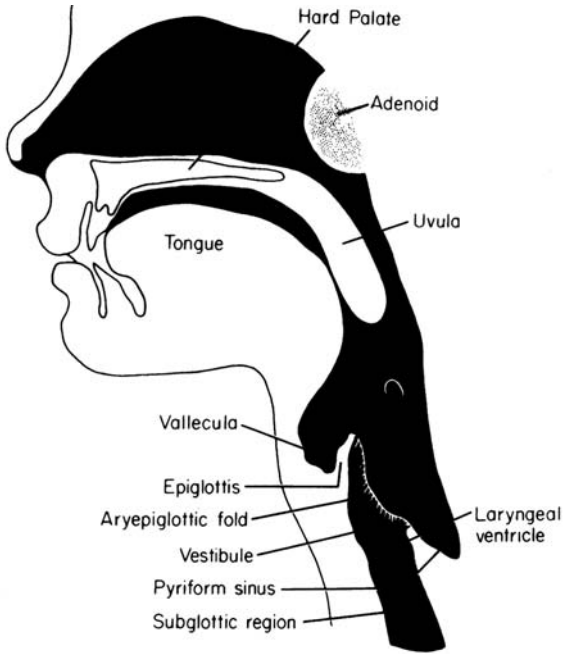

Fig. 3.19. The normal airway, lateral view. (From [1] with permission)

mass. It is obtained at fluoroscopy so airway changes in caliber can be noted. An exquisite view is obtained by using a Thoreaus filter to selectively screen out low-kilovoltage radiation, increasing the exposure kV and magnifying the child's airway (Fig. 3.23). This technique has, for the most part, obviated the more invasive tracheogram, where contrast was instilled into the trachea and pictures obtained. The magnification high-kilovoltage technique can be used without sedation and with relatively little radiation.

► ***Rule No. 3:*** The airway should be visible on all normal chest films.

Figure 3.24 depicts several pathological states of the airway diagnosed by radiographs of the chest or neck. What are the abnormalities, and what are the diseases? See Appendix 2.

The parameters to evaluate the airway, be it extra- or intrathoracic, are *patency, position,* and *size*. One should see the entire airway, from the oral and nasal pharynges to the right and left main-stem bronchi. The walls should be parallel and smooth. However, buckling of the trachea to the right in the lower neck and upper thorax is normal in an infant. The intrathoracic airway is not a midline structure (the carina overlies the right pedicles). What abnormality can you detect in Fig. 3.25?

Mediastinum

The mediastinum is composed of the thymus, trachea, heart, great vessels, esophagus, lymph nodes, and neural elements. It can be separated into the anterior, middle, and posterior compartments (Fig. 3.26). In examining the mediastinum, remember:

► ***Rule No. 2:*** Knowledge of anatomy is the key to correct radiographic diagnosis.

In the mediastinum, look for *position, size*, and *contour* of the individual components. The initial examination of the mediastinum is best accomplished by the plain film. However, for most abnormalities or questions of abnormality, MR or CT is utilized. Therefore in this discussion of the mediastinum plain film findings are followed by cross-sectional imaging.

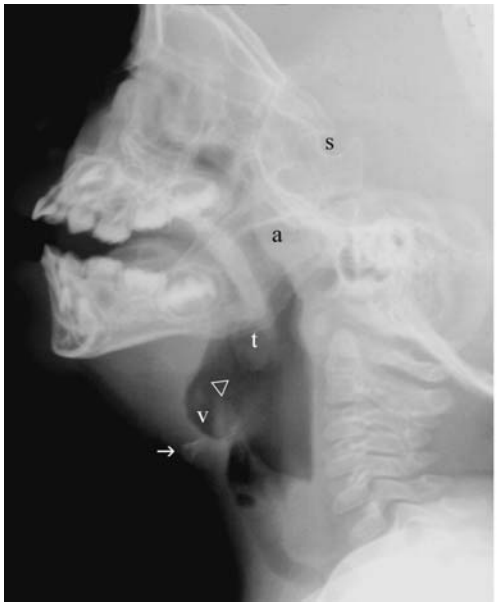

a

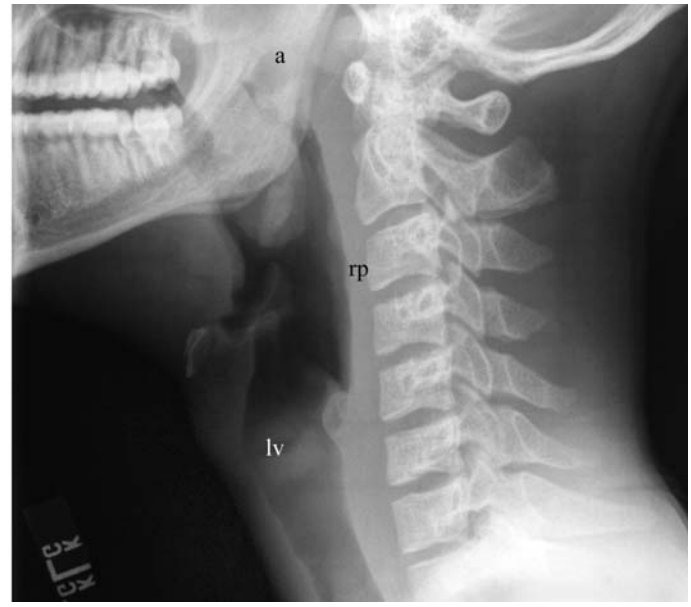

b

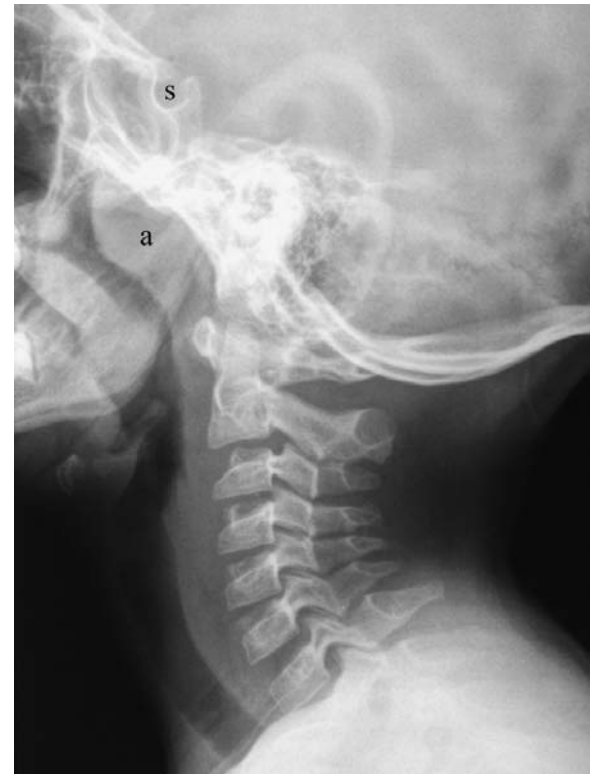

c

Fig. 3.20. Normal (and almost normal) lateral neck examinations in a 2-year-old, an 8-year-old, and a 10-year-old
a This 2-year-old is in the neutral position. Using our basic concept of looking at the entire film, we note that the sella turcica (*s*) is normal. The patient has adenoid tissue (*a*), which should be present by 6 months of age, and also palatine tonsils (*t*). The patient has abundant air in the hypopharynx and one can see the retropharyngeal soft tissue space (behind the hypopharynx and in front of the spine) is quite normal. The vallecula at the base of the tongue (*v*), hyoid bone (*arrow*), epiglottis (*arrowhead*), and the laryngeal ventricle are normal. There is buckling of the proximal trachea as expected in this age group
b A 9-year-old child in which we see similar anatomy, perhaps better defined. The adenoid tissue (*a*) is somewhat larger and is encroaching upon the nasal air passage. *rp*, retropharyngeal space; *lv*, laryngeal ventricle. The palatine tonsils are also large
c A 10-year-old child. The sella (*s*) is normal. The adenoids (*a*) do not narrow the nasal air passage (normal)

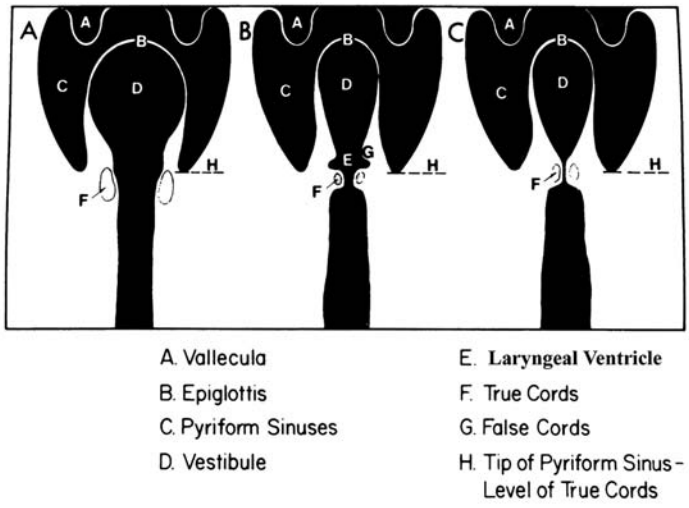

Fig. 3.21. Schematic drawings of the frontal airway during various phases of respiration and phonation
A, quiet breathing; *B*, phonation; *C*, closed glottis. (From [1] with permission)

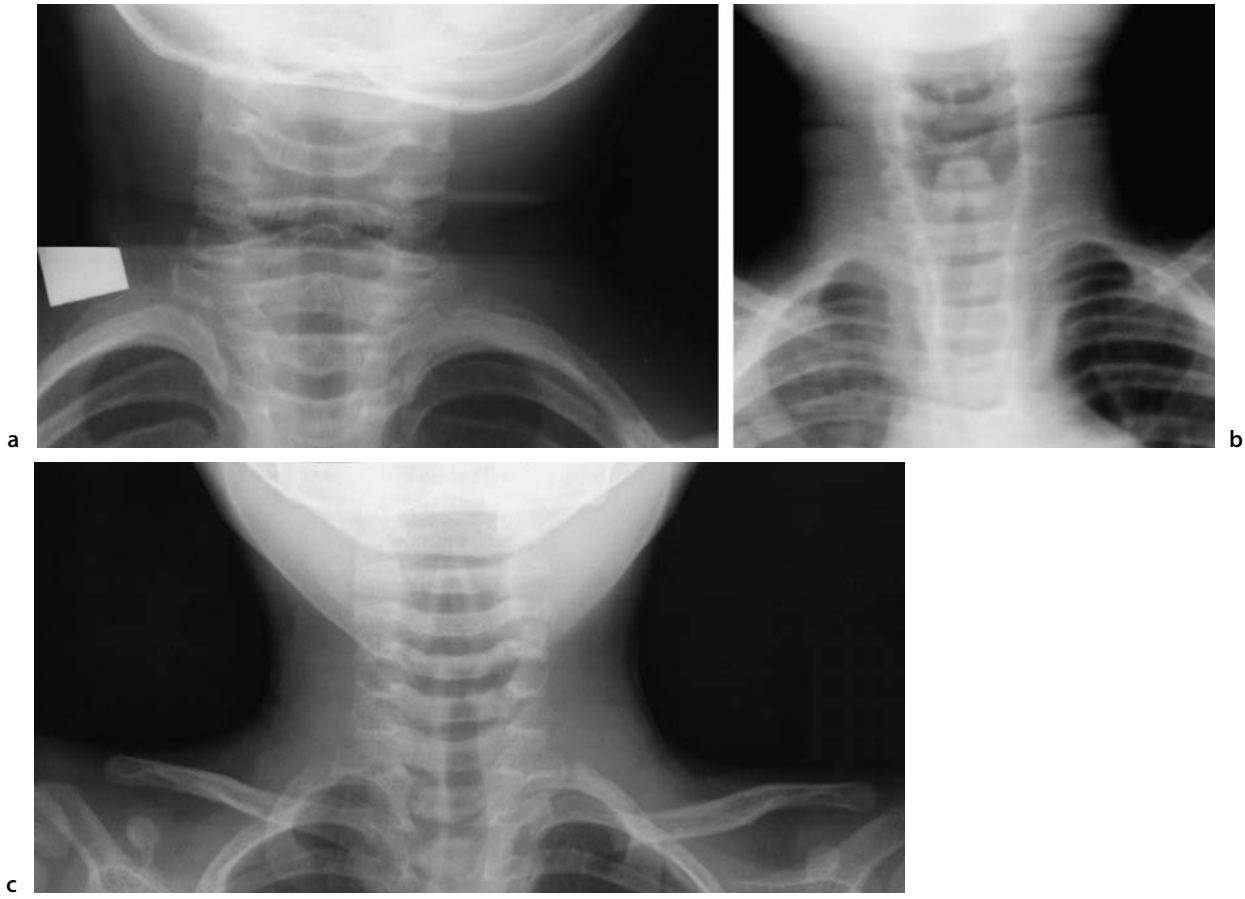

Fig. 3.22. Three frontal radiographs (**a–c**) corresponding to the schematic view in Fig. 3.21:
a quiet breathing,
b phonation,
c closed glottis

Fig. 3.23 a – e. Legend see p. 34

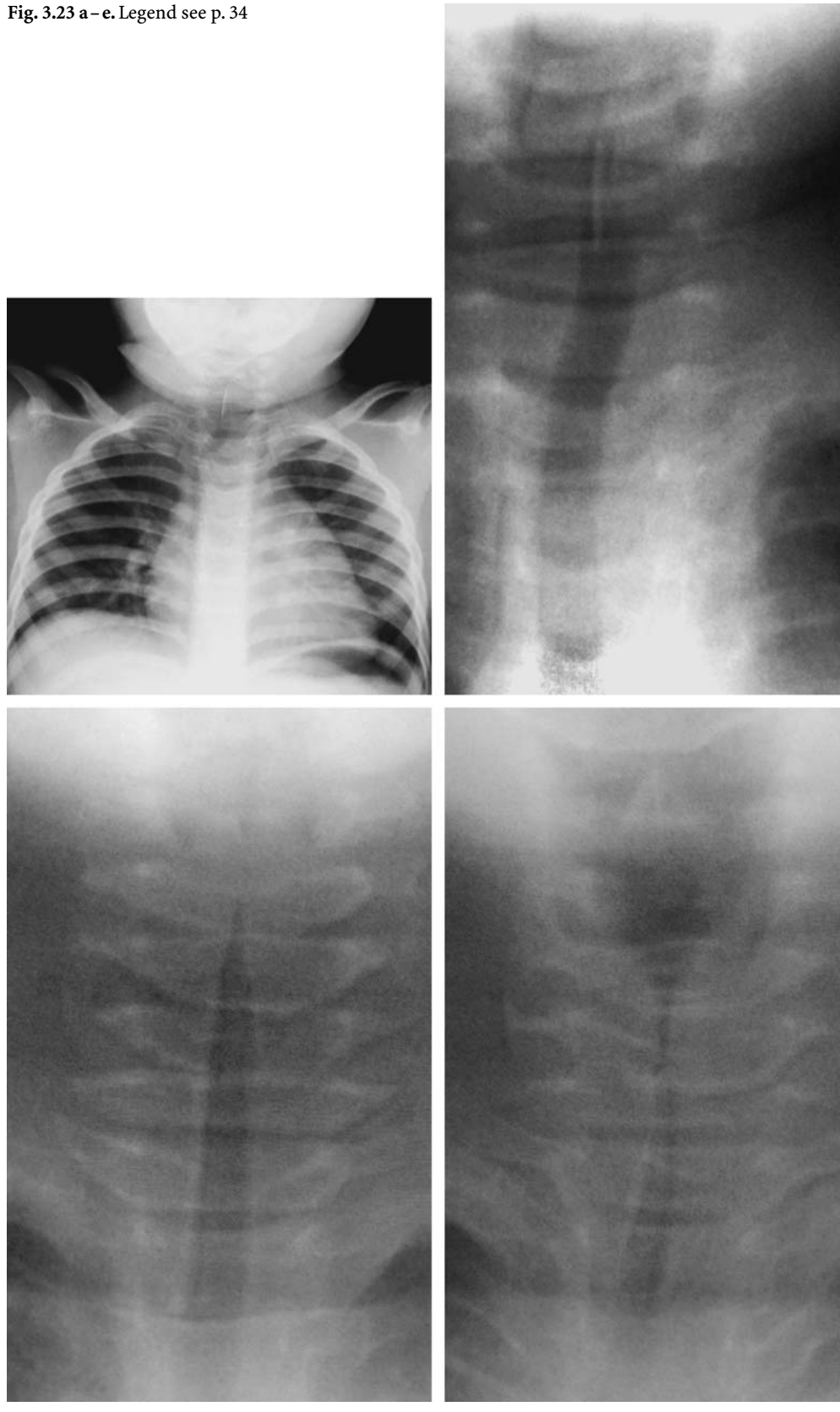

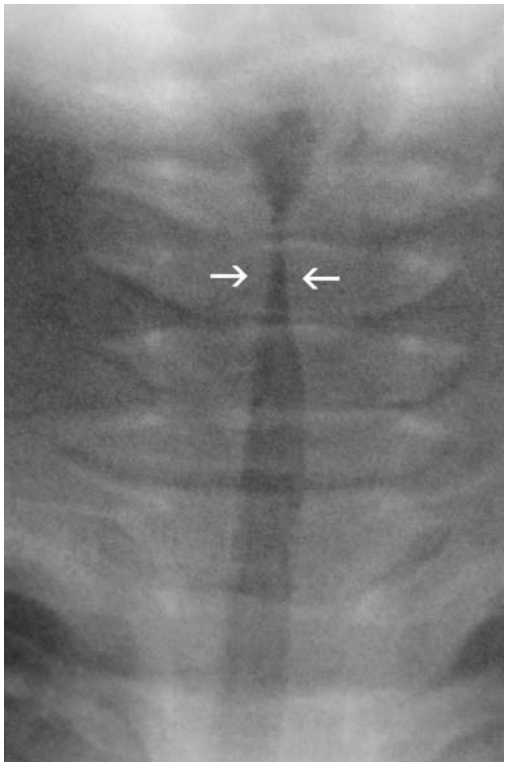

e

Fig. 3.23. A 1-year-old boy with stridor
a Frontal radiograph shows the lungs to be of normal volume and the heart of normal size. The thoracic airway is clearly demonstrated, but there is a linear opacity within the airway in the cervical region
b Magnification high-kV film showing the foreign body. A piece of eggshell was later removed. (From [2] with permission)
c–e Three views of a magnification high-kV technique in a 1-year-old with stridor. There is narrowing and penciling of the airway (*arrow*) on all films. This was a fixed change, but on clinical follow-up several weeks later the patient was not longer stridorous and the airway appeared normal. This represents inflammatory changes (laryngotracheobronchitis – croup)

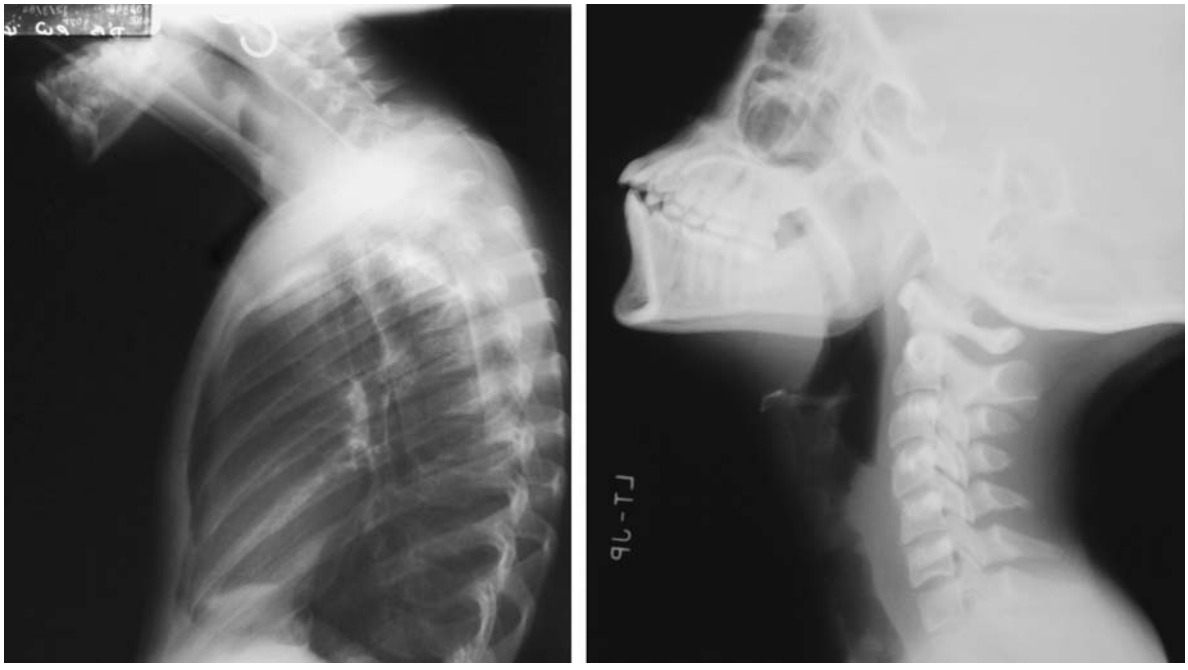

a b

Fig. 3.24. What anatomical abnormality can you see in these two separate examinations –
a a lateral chest film and
b a lateral neck film in another child? (Answer in Appendix 2)

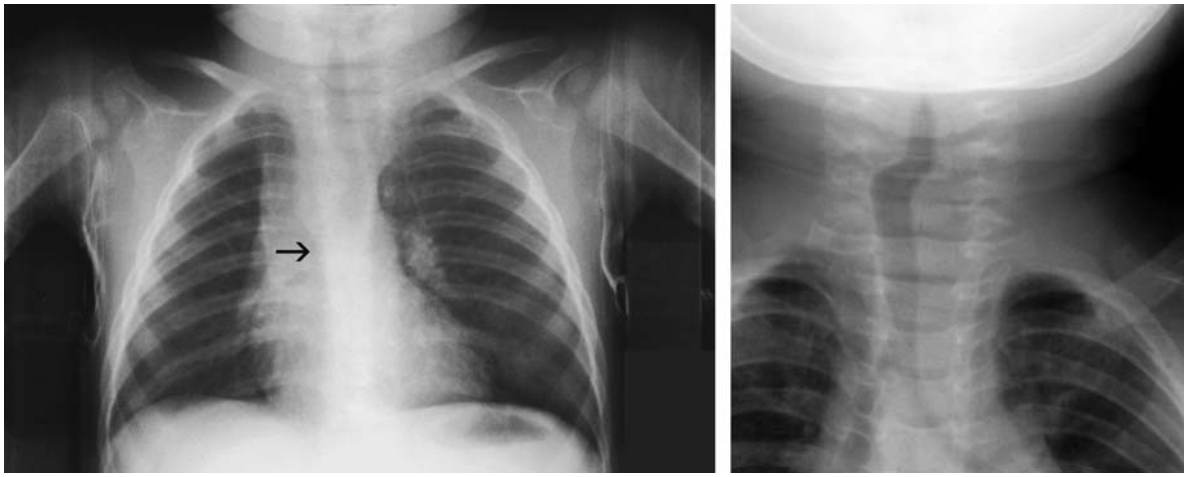

a b

Fig. 3.25. A 6-month-old infant with cough
a Frontal radiograph shows the carina pushed to the left. There is a bulge on the right side of the airway. Can you see a normal aortic arch on the left? This is a right aortic arch to the right of the trachea with a right descending aorta (*arrow*) to the right of the spine. This child has congenital heart disease, tetralogy of Fallot. Many children (approximately one-third) with this disease have a right aortic arch
b Normal buckling of the airway in an infant

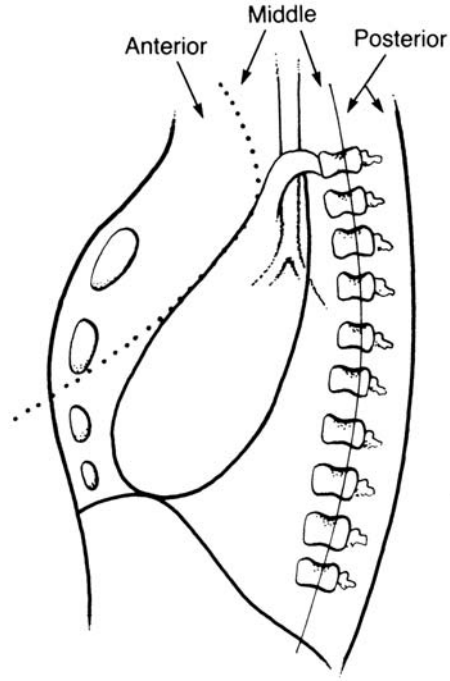

Fig. 3.26. Mediastinum
Anterior, the space in front of the heart and great vessels; *middle*, the space between the anterior and posterior mediastinal components, including heart, airway, esophagus, and lymph nodes; *posterior*, everything *behind* a line connecting the midportion aspects of the vertebrae, including the vertebrae, neural elements, and paraspinal lymph tissue. (See "Masses and Pseudomasses" for masses typical of these areas.) Some definitions begin the posterior mediastinum with the anterior aspect of the vertebral body

Thymus

One of the major factors that makes pediatric chest X-rays difficult to evaluate is the thymus. It is said that he who masters the thymus has mastered 90 % of pediatric chest films, because this gland can simulate cardiac enlargement, lobar collapse, pulmonary infiltrates, and mediastinal masses. The thymus is prominent in some children until 4–5 years of age. It starts to become a problem when it is still prominent in children over the age of 5.

The thymus is always anterior in position, which is why it is difficult to diagnose right heart enlargement in a younger child based on fullness of the anterior mediastinum. Since it is such an anterior structure, it is subject to wide variations in shape and size on the frontal chest radiograph; even with the slightest degree of rotation, the thymus may obscure almost the entire right or left lung. To avoid errors in interpretation, check the degree of inspiration and the position of the patient before deciding about unusual densities (Fig. 3.27) (see "Technical Factors," above).

Thymic size is a major area of concern. The thymus may occupy the entire anterior thorax, extending down to the diaphragm and out to the lateral thoracic wall. It usually appears smaller as the child gets older, but the thymus weighs most in an adolescent. Thymic remnants can remain even into adulthood. It is a unique organ which also shrinks during periods of stress. The contour of the thymus is "wavy" because it insinuates itself between anterior ribs. It is a "soft" organ and does not push other mediastinal structures. Occasionally, fluoroscopy or ultrasound is necessary to decide whether the contour of a "mediastinal mass" is indeed wavy and anterior, consistent with a thymus.

More often, however, if an abnormality is suspected in the mediastinum, cross-sectional imaging (MR or CT) is performed. Both tests require the young patient to be sedated. CT, of course, entails radiation exposure, and the patient also receives an intravenous contrast agent, but it has the advantage of showing calcium and, if pertinent, the lung parenchyma (see below). For proper evaluation of the mediastinum with CT, contrast media is essential. With contrast media, the vessels and heart "light up" (turn white – "enhance"). Thus, anything not enhanced must be explained by normal anatomical structures or else it is abnormal. MR has the advantage of presenting images in multiple planes (coronal, sagittal, axial, and oblique) and most precisely shows extension of tumor into the spinal canal. MR differentiates tissue characteristics to a greater extent than CT, but it is poor for calcium and lung parenchyma.

Since either test may be better depending on the pathology, images of both modalities are presented (Figs. 3.28, 3.29). These images help define masses, lymph nodes, and aberrant vessels between and around normal structures.

An important finding in the mediastinum and soft tissue is adventitious air – it occurs in pneumomediastinum or can descend down from above as in hypopharyngeal perforation (Fig. 3.30).

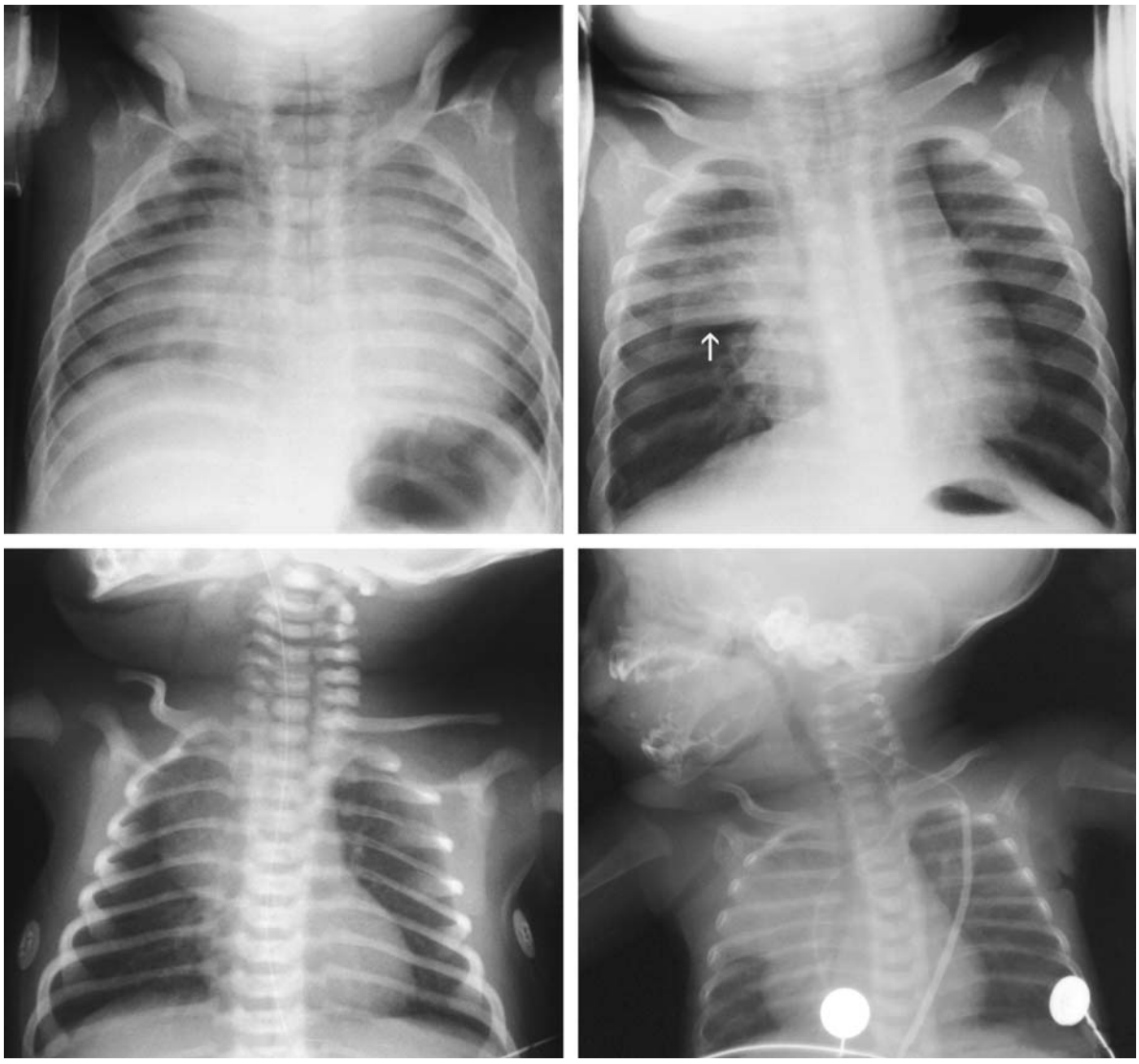

Fig. 3.27. Thymus
a Frontal radiograph shows all the parameters of a film taken during expiration. If you are not acquainted with these criteria, you may interpret this film as showing an infiltrate in both lungs. (See Table 3.1 and Fig. 3.2 for criteria establishing that the film is taken during expiration.) Note that the spinous processes are not fused
b With a good inspiratory effort, same child shows that the "infiltrate" is really thymus which is quite prominent on the right. Notice the thymic sail sign (*arrow*).
c In this rotated film, one can see the effect of the thymus in the right upper thorax. A nasogastric tube is in the stomach
d A more rotated film shows again how the thymus can masquerade as a parenchymal opacity. This patient has a central vascular line in the right atrium

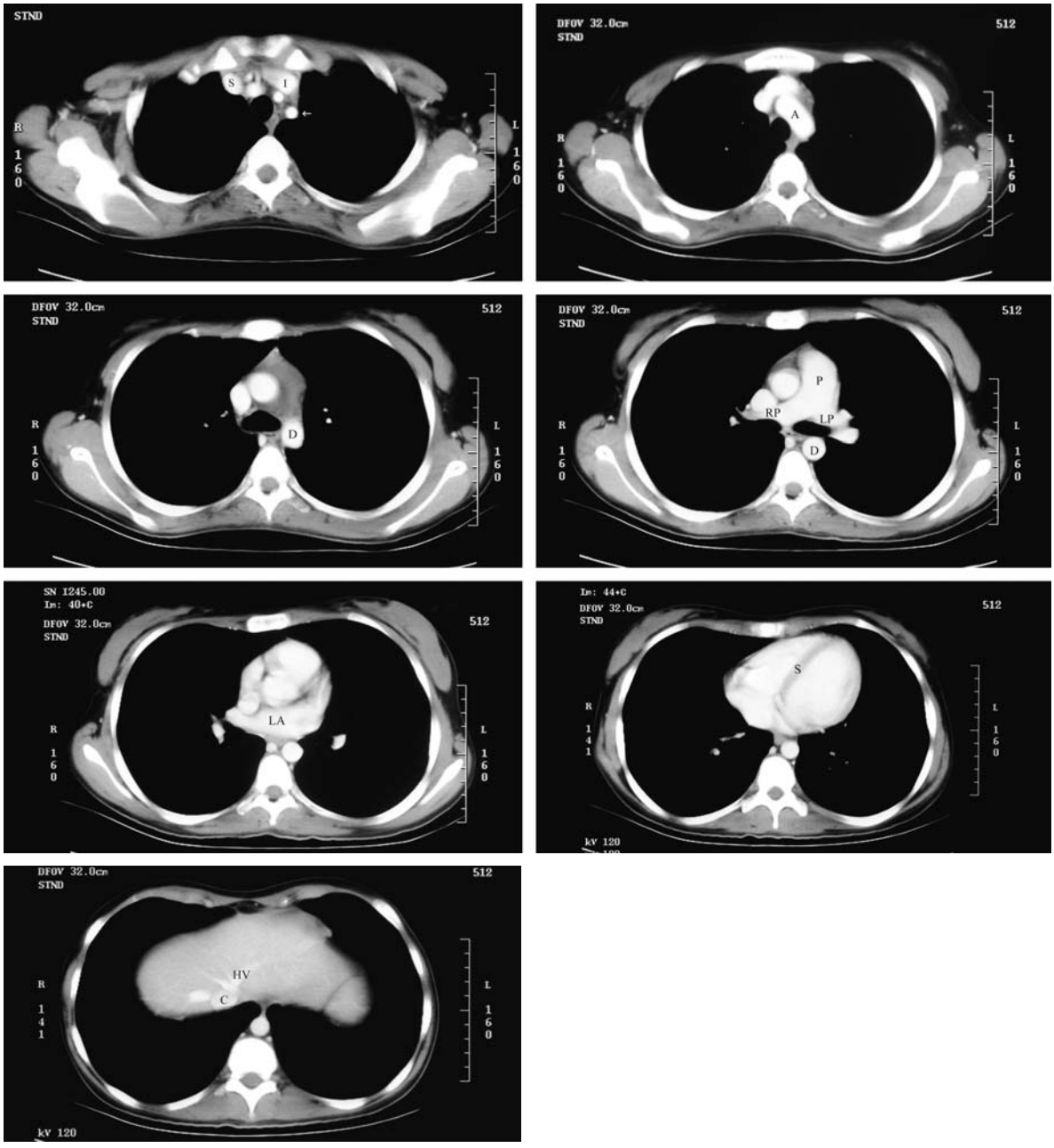

Fig. 3.28. Normal contrast-enhanced CT of the mediastinum (axial projection). Remember the vessels in the heart "light up"
a Most cephalic section reveals the sternum anteriorly. The superior vena cava (*S*) and innominate vein (*I*) are clearly visible. The left subclavian artery is seen (*arrow*)
b A next lower section shows the aortic arch on the left side (*A*)
c Proceeding inferiorly, the descending aorta (*D*) is noted. Note the nonenhanced thymus of triangular shape anteriorly. This occurs in children over 5 years of age. Before 5 years of age, the thymus is rectangular
d A section through the main pulmonary artery (*P*) and its right (*RP*) and left (*LP*) branches. This section is just below the carina and the left main-stem bronchus is seen above the descending aorta (*D*)
e This section is at the level of the left atrium (*LA*)
f A section showing the ventricular septum (*S*) and both ventricles
g The most cephalic section of the liver showing the joining of the hepatic veins (*HV*) to the interior vena cava (*C*)

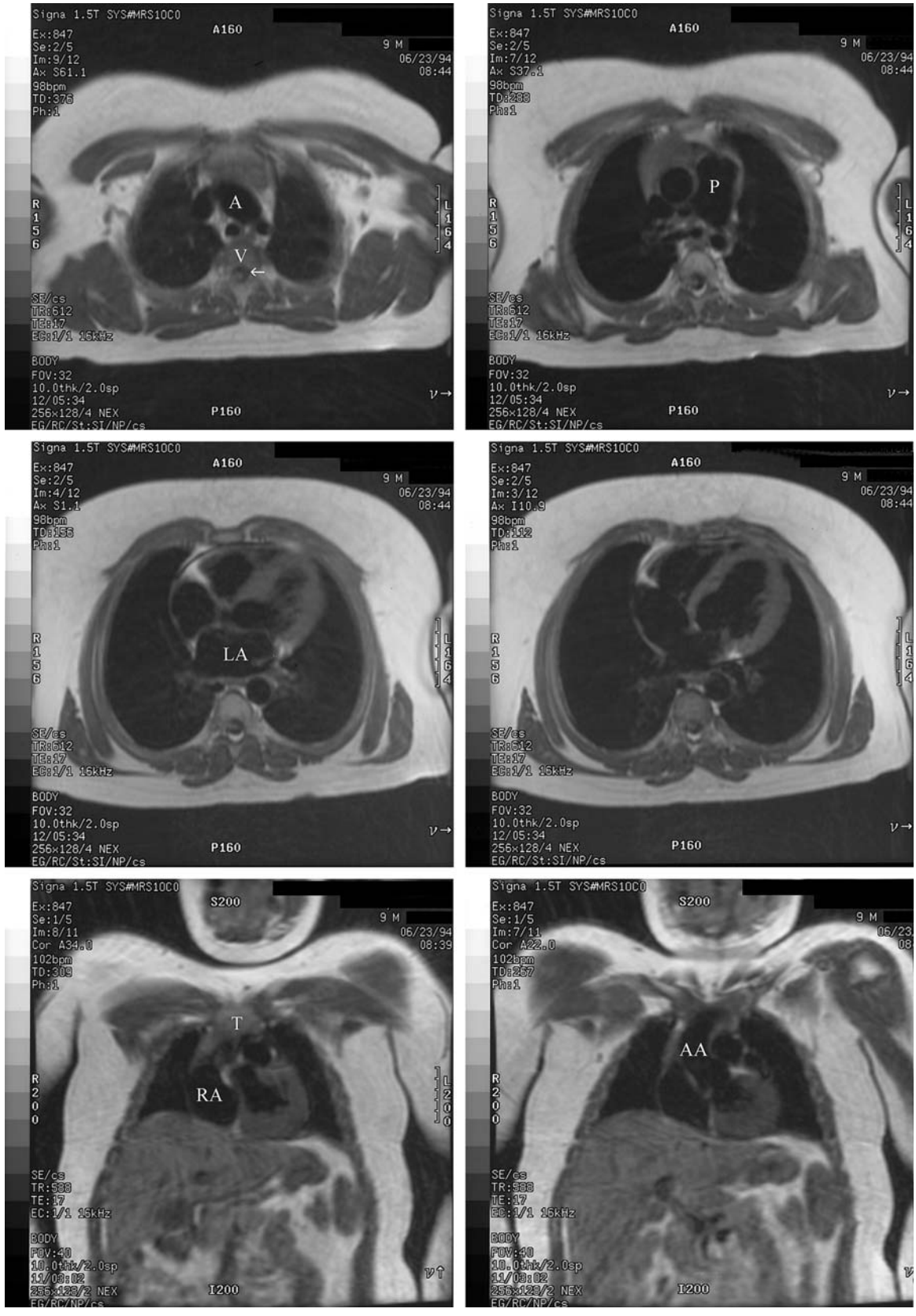

Fig. 3.29 a – k. Legend see p. 40

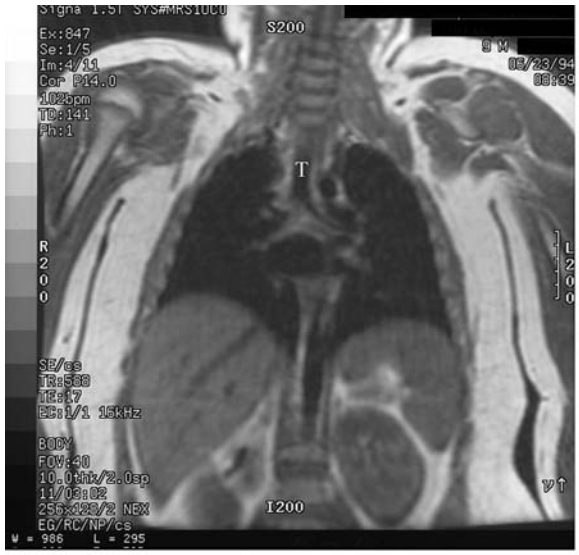

g

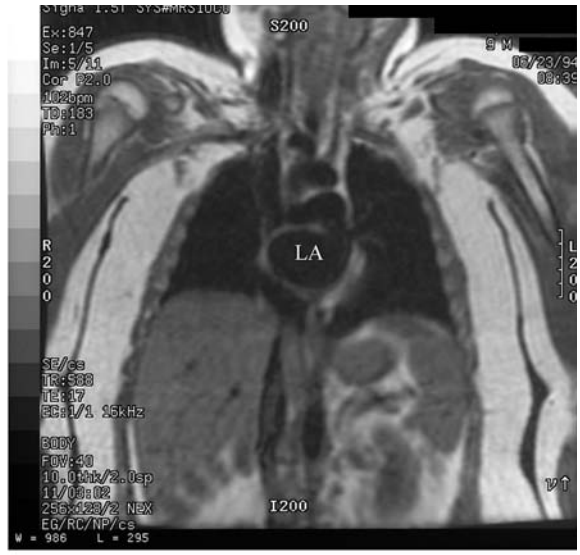

h

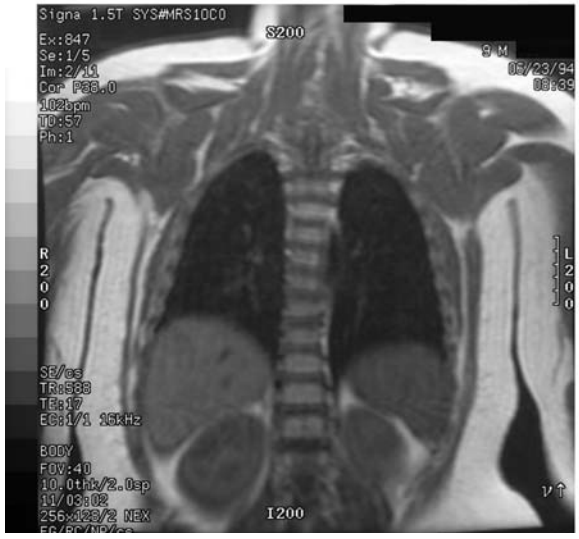

i

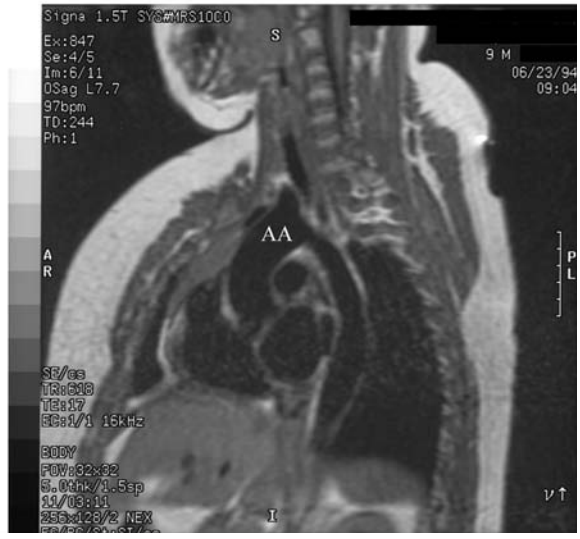

j

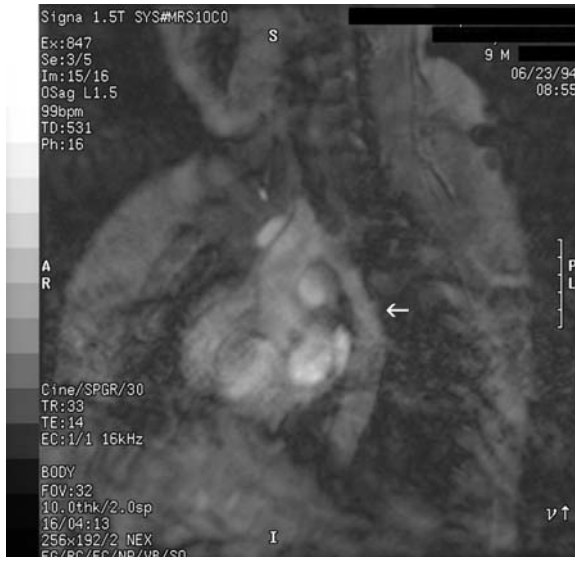

k

Fig. 3.29. MR of the mediastinum (axial, coronal, and sagittal sections). Remember: black is flowing blood
a The cephalic-most section reveals the rectangular, homogeneous thymus anteriorly beneath the sternum and in front of the aortic arch (*A*). The vertebral body (*V*) and dural sac (*arrow*) are seen posteriorly on all the sections
b The next section is at the level of the main pulmonary artery (*P*). This patient has coarctation of the aorta. Note the small descending aorta
c The next caudad plane is at the level of the left atrium (*LA*)
d Section through four chambers of the heart
e Most anterior coronal section showing thymus (*T*) and right atrium (*RA*)
f Next posterior section through the ascending aorta (*AA*)
g, h Section through the trachea (*T*) and left atrium (*LA*)
i Posterior section showing the vertebral bodies
j Oblique midline sagittal section showing the aortic arch (*AA*). See the discrepancy between the aortic arch and proximal descending aorta
k Static sagittal scan of a cine MR imaging with the computer-enhanced blood appearing white. Note the descending aorta (*arrow*)

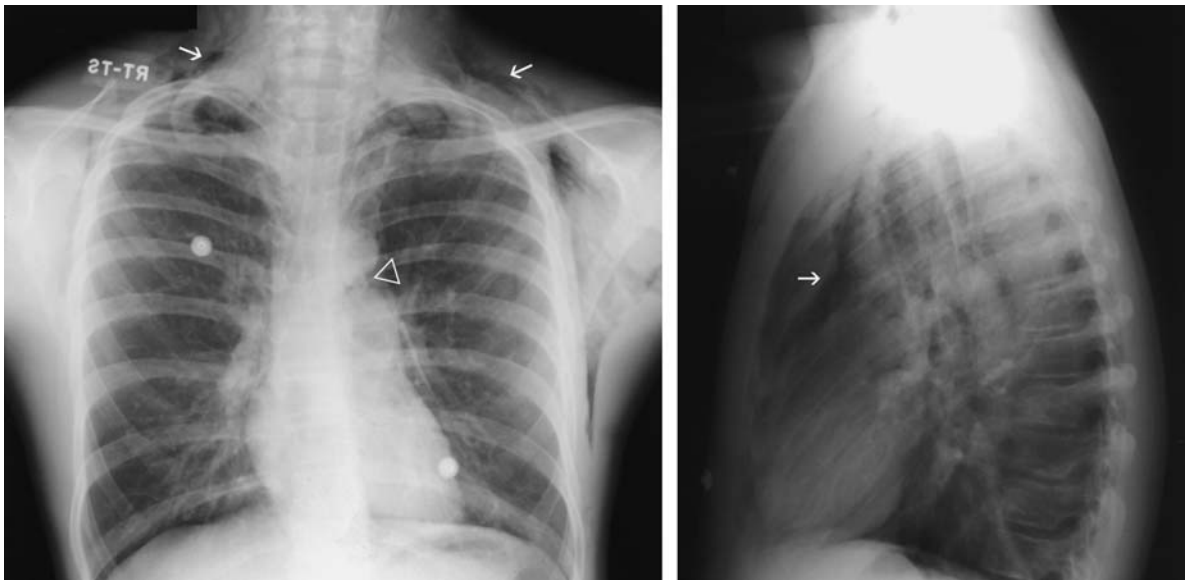

Fig. 3.30. Mediastinal and pericardial air
a Frontal examination shows air (black) in both shoulders (*arrows*), axilla, chest wall, and in the mediastinum. There is separation of the aortic knob from the pulmonary artery (*arrowhead*). In this instance, there is both air in the mediastinum, as seen in the shoulders, and air in the pericardium, as seen by the separation of the pulmonary artery and aorta
b Lateral view shows air (*arrow*) anterior to the heart and in the mediastinum

Heart

The heart must also be evaluated for *position, size*, and *contour*. Its position is normally in the left hemithorax with a small right thoracic border. The appearance of the heart on the frontal film depends greatly on the degree of inspiration and on the size of the thymus. For these reasons the lateral roentgenograph is important as the air space behind the heart and the position of the anterior margin of the trachea play a major diagnostic role.

There are two methods for using the lateral film to evaluate heart size. In the first, a perpendicular line drawn from the carina to the diaphragm should not intersect the heart. A second method is to extend a line paralleling the anterior wall of the trachea inferiorly to the diaphragm. In this instance, the line should not intersect the heart nor should the line be pushed back to "hit" the spine above the diaphragm. Both methods work best on nonrotated lateral films. Remember, an enlarged heart pushes the trachea back, as do other mediastinal abnormalities. Therefore if a frontal film shows questionable cardiac enlargement, look at the lateral! If the lateral film is normal, the heart size is normal (Fig. 3.31).

- ***Rule No. 4:*** A mass must be seen in two planes. If the heart is really large, it must appear large in two planes, both frontal and lateral.

The *contour* of the heart on plain films, in our experience, is not helpful in determining the *specific* nature of congenital anomalies. Echocardiography, MR, and cardiac catheterization are more accurate methods of diagnosing congenital defects. Nonetheless, evaluating the contour of the heart in an older child where the thymus is smaller can be valuable. In young children the left atrial appendage is not a prominent bulge on the left side because it is usually obscured by even a small thymus. The pulmonary artery, however, may be prominent normally in adolescents (especially girls).

Pulmonary vascular changes, on the other hand, may give a clue to the exact nature of the cardiac disease. Normally one sees pulmonary vessels in the hila and the middle third of the lungs but not in the more peripheral portion. Signs of increased arterial flow include: (a) enlarged central vessels, (b) enlarged vessels in the medial third of the lung, and (c) on the erect film, equalization of vessel size between upper and lower lobes. Venous congestion associated with clinical findings of congestive heart failure can

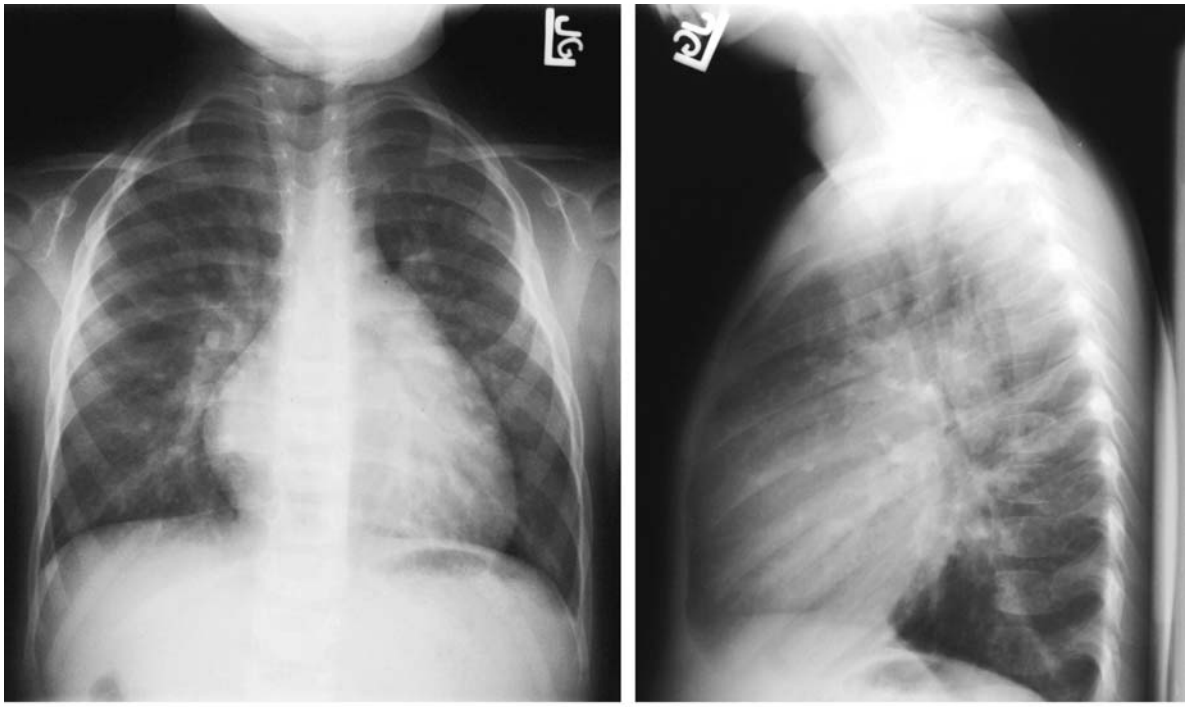

a b

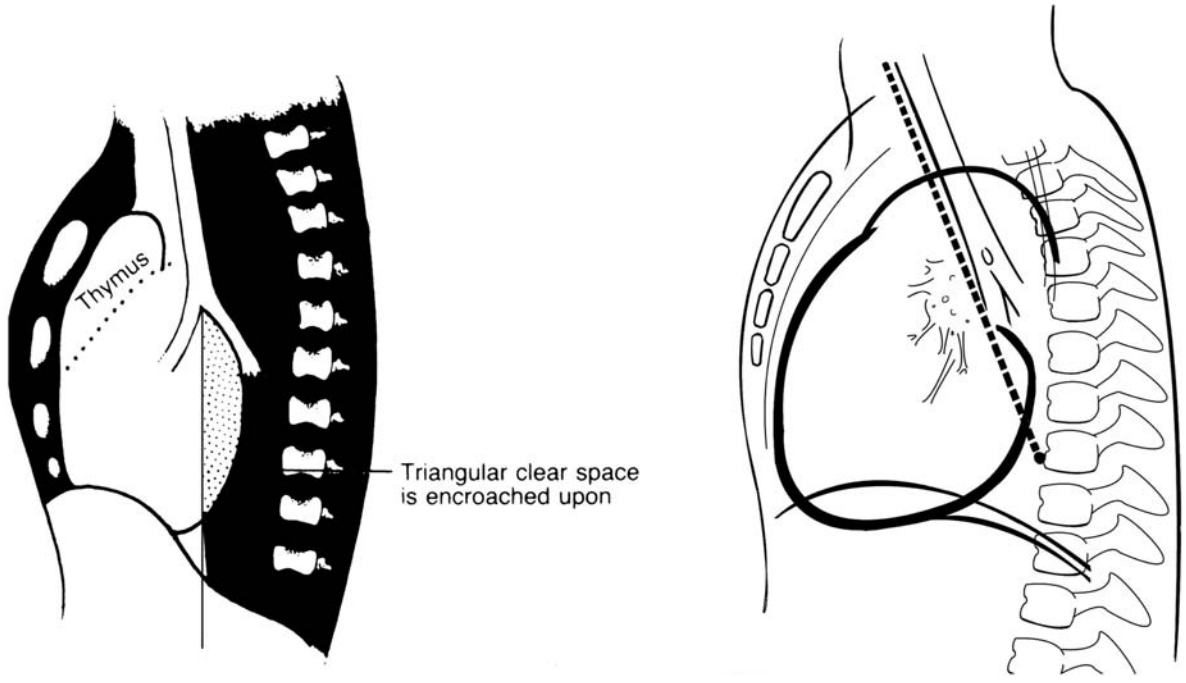

c d

Fig. 3.31. Evaluation of cardiac enlargement on lateral film
a Frontal view of the chest shows the heart to be enlarged. There are indistinct vessels. These two findings suggest congestive heart failure
b The trachea and carina are easily seen on the lateral film
c, d Using the carinal line (**c**) or the anterior tracheal line (**d**) demonstrates cardiomegaly. In this instance, both parameters are seen – the heart extends behind the imaginary line and the line hits the spine above the diaphragm
e see p. 43

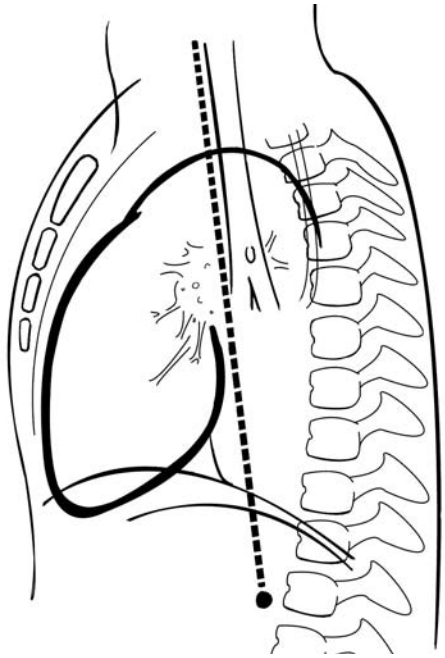

e

Fig. 3.31 (*continued*)
e Normal anterior tracheal line

be indicated by: (a) loss of distinct vessels at the bases (interstitial edema), (b) alveolar filling (pulmonary edema), or (c) right-sided pleural effusion. Remember: language here is important! Overcirculation, increased arterial flow, and increased vascularity all suggest left-to-right shunt. Congestion and pulmonary venous distension suggest congestive heart failure.

It is much more difficult to detect *decreased* pulmonary vascularity. Correlating pulmonary vascularity with heart size and the clinical status of the patient (cyanotic vs acyanotic) is frequently helpful in determining specifics of congenital heart disease. *Note:* Overcirculation is usually associated with cardiomegaly. If you suspect overcirculation but the heart appears normal, something is usually wrong with your observations.

Cardiac MR is becoming an extremely important imaging modality. Aside from precise anatomy, it offers functional information about pulmonary vein and myocardial blood flow and myocardial ischemia.

Great Vessels

The great vessels that are easily identified are the inferior vena cava (on the lateral view) and the aorta (on the frontal film). The position of the trachea is the key to locating the aortic arch (see Fig. 3.25). A right aortic arch is often associated with congenital heart disease or vascular ring which presses on both the airway and the esophagus. For this reason, pay special attention to the tracheal air column and the bulges along either side. The right and left pulmonary arteries are easily identified, and the main pulmonary artery is one of the moguls (bumps) of the left heart border (Fig. 3.32).

What is the unusual dilatation above the right main-stem bronchus in Fig. 3.33? MR is superb for defining the side of the arch as well as abnormalities of the great vessels (Fig. 3.34). See Appendix 2.

Esophagus

The esophagus is another structure seen in the mediastinum. It is posterior to the trachea and may contain air in younger children. An air–fluid level in the esophagus, however, is always abnormal. Since esophageal problems may manifest as respiratory symptoms, the barium swallow is a valuable diagnostic examination in cases of unexplained respiratory disease (Fig. 3.35).

► ***Rule No. 5:*** An esophagram must be performed on any child with unexplained respiratory disease.

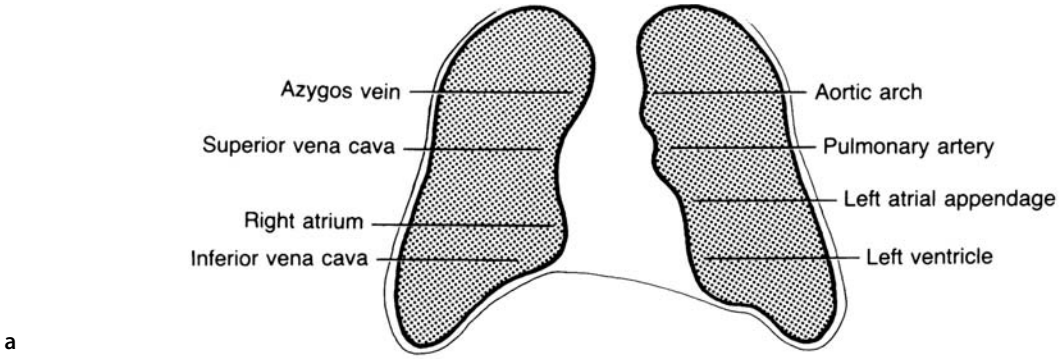

a

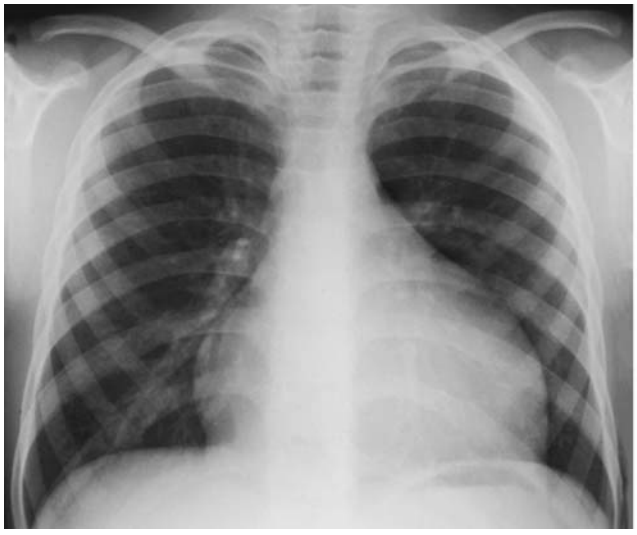

b

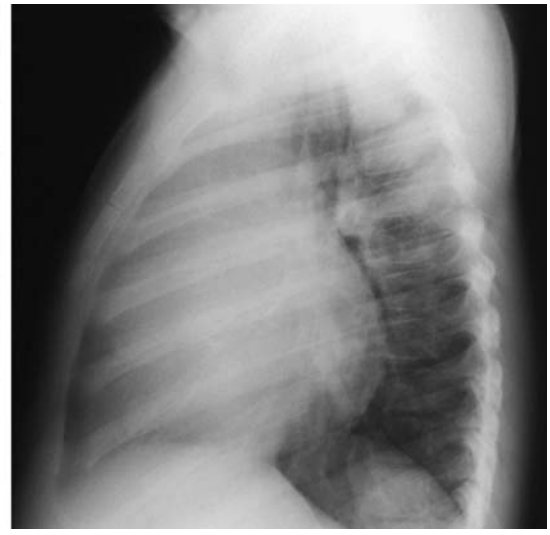

c

Fig. 3.32. Moguls (bumps along heart border)
a Schematic drawing of the impression of various vascular and cardiac structures in the mediastinal silhouette
b, c A young child with pericardial effusion. This was diagnosed by echocardiography. The plain film, however, is revealing in that the cardiac silhouette is large but none of the normal moguls are seen. Note how far back the cardiac silhouette is on the lateral view

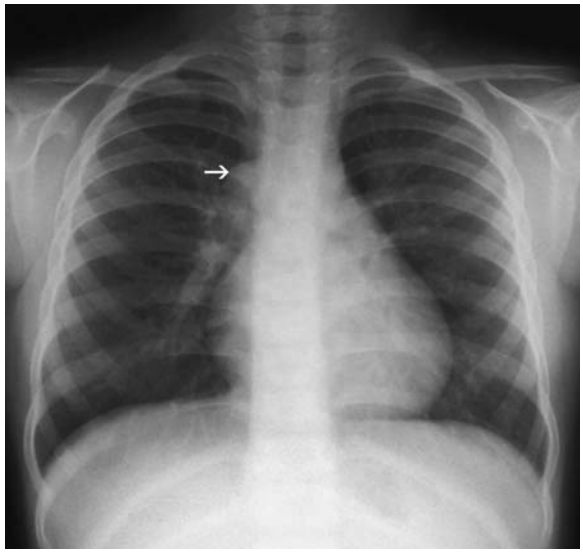

Fig. 3.33. What is the unusual dilatation (*arrow*) above the right main-stem bronchus?

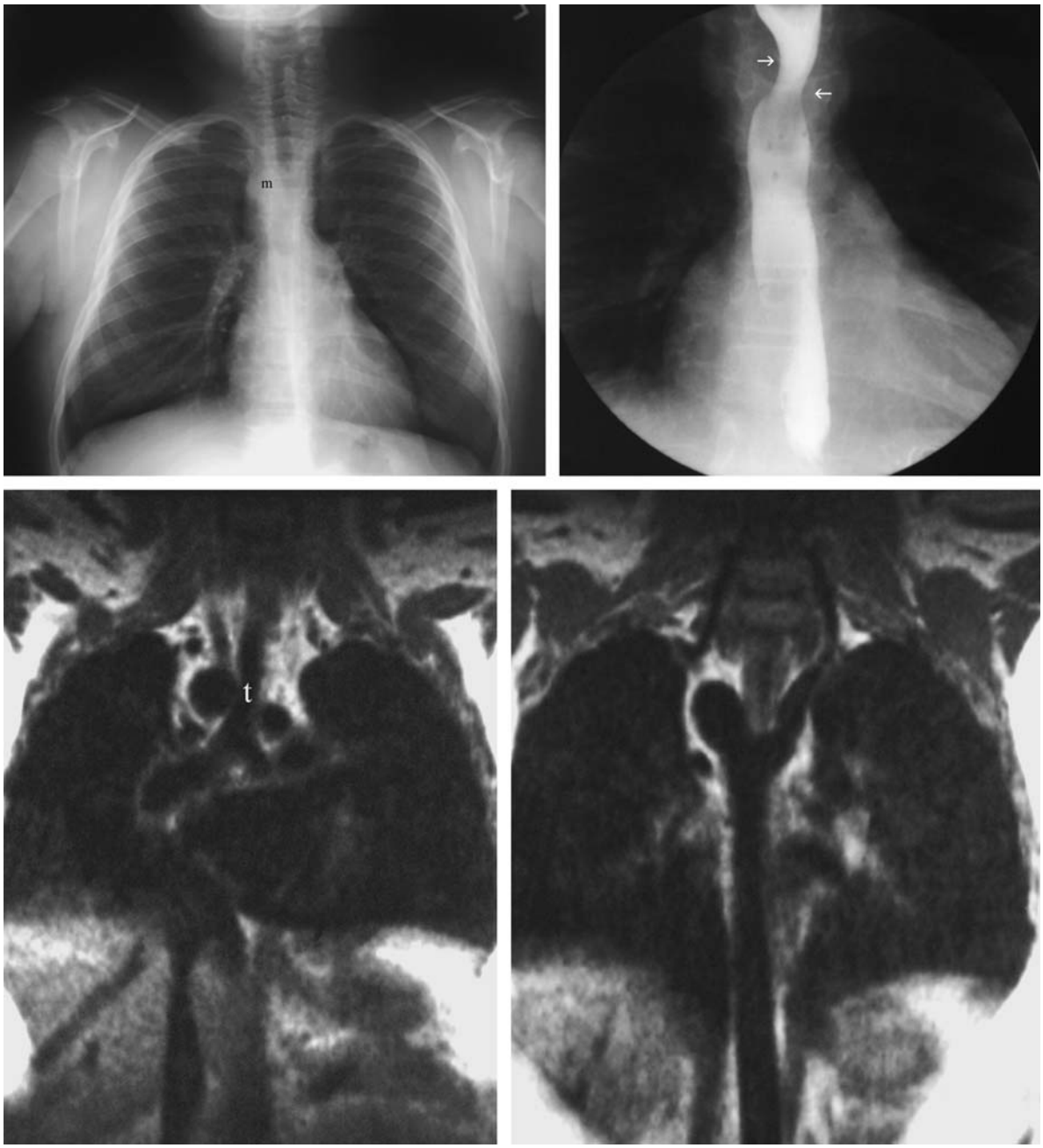

Fig. 3.34. Vascular ring
a Plain film examination shows a mass (*m*) to the right of the airway with the carina to the left of midline
b Barium swallow in the frontal projections shows the impression on the right and left side of the esophagus (*arrows*)
c Coronal MR reveals two circles, one to the right and one to the left of the trachea (*t*). These circular impressions are the right and left arches
d A more posterior coronal MR section shows the two arches joining and descending. This is a double aortic arch
e–g see p. 46

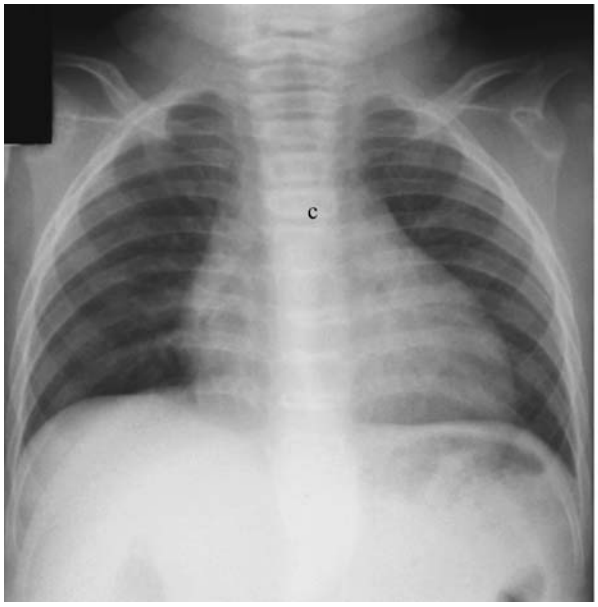

e

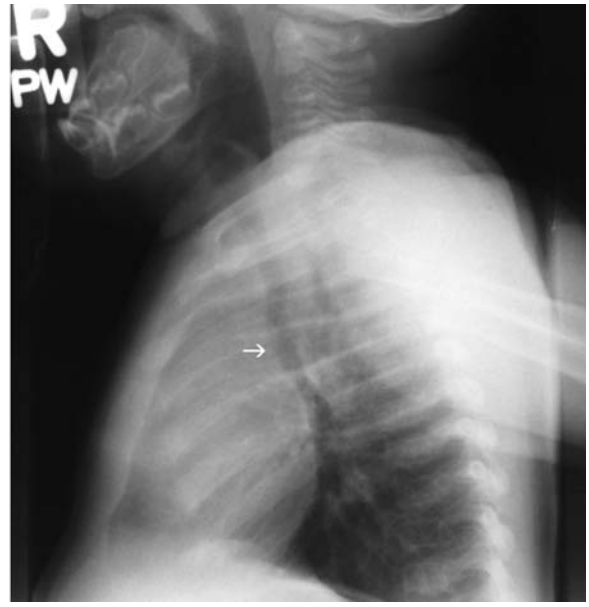

f

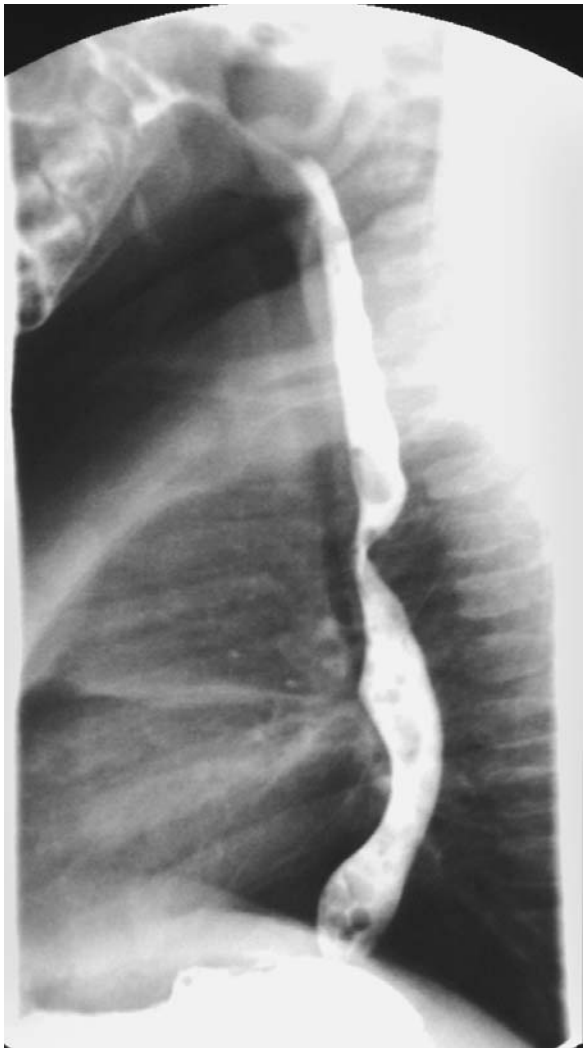

g

Fig. 3.34 e – g (*continued*)
e Another child with a double aortic arch. The carina (*c*) is over the left pedicles
f The lateral film shows anterior bowing of the trachea (*arrow*)
g Lateral film of a barium swallow in this child showing the mass impression behind the esophagus and causing slight bowing and narrowing of the airway

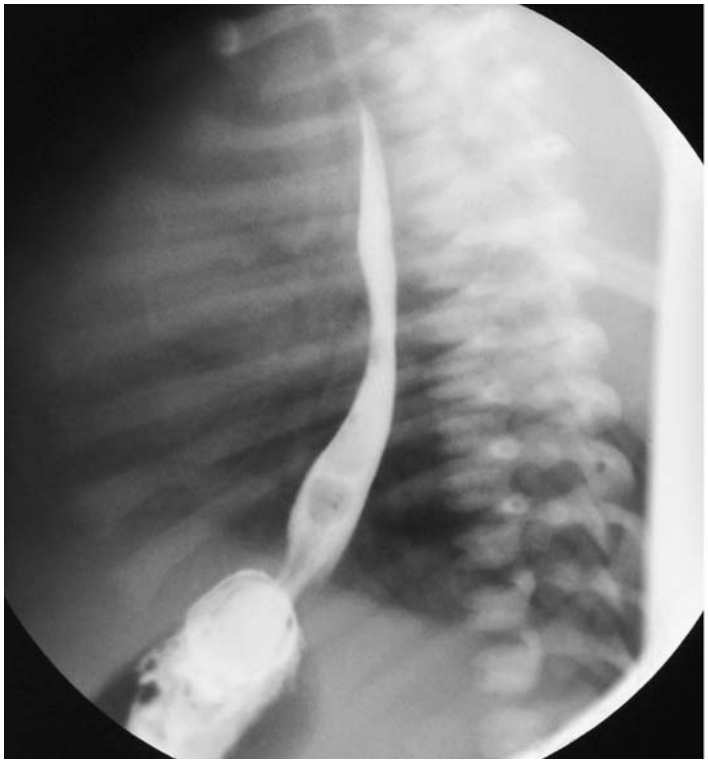

a

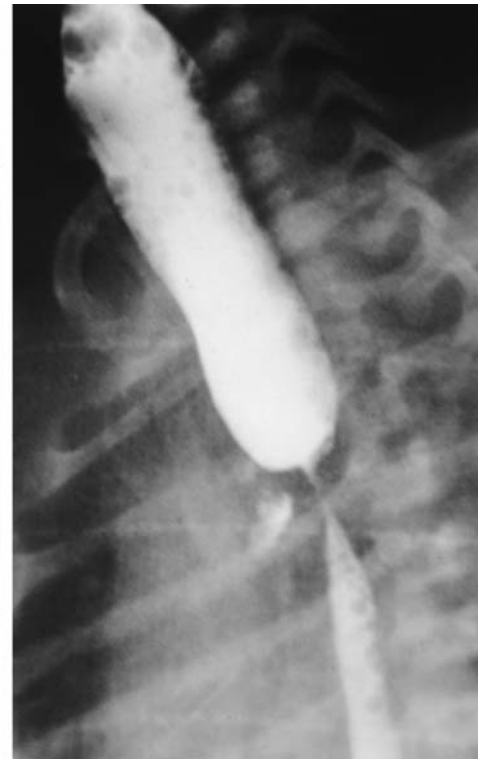

b

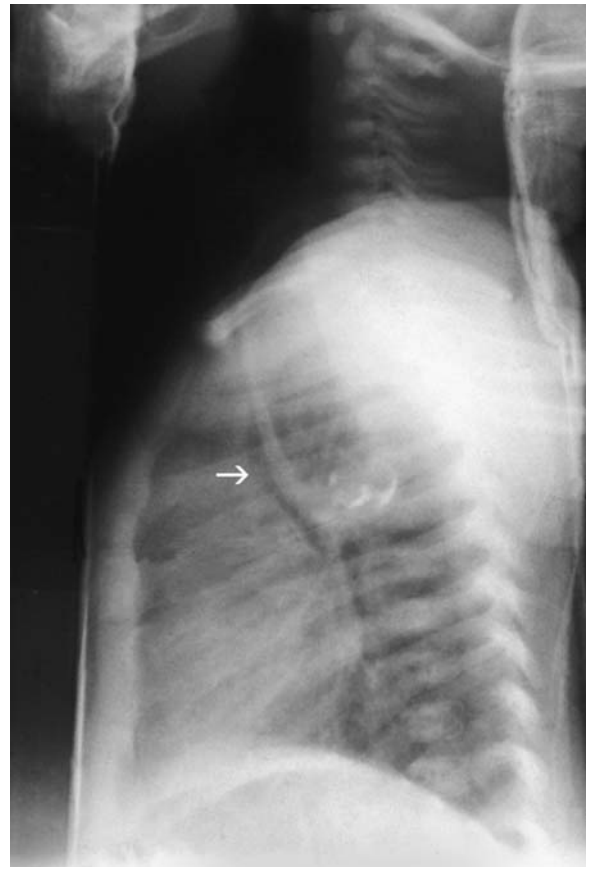

c

Fig. 3.35. Relationship between the esophagus and the trachea
a Normal lateral esophagram. Note the trachea and esophagus and their relationship
b Lateral view of a child with esophageal stricture
c Lateral view after most of the barium has passed into the stomach. Note how the dilated esophagus (now filled with air) bows and compresses the trachea (*arrow*)

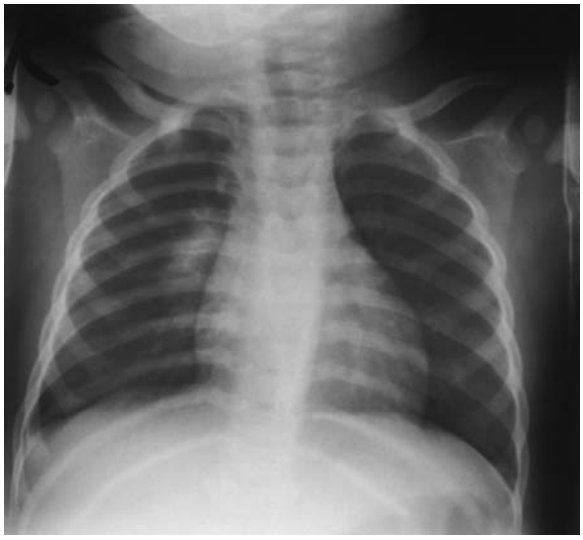

Fig. 3.36. Enlarged mediastinal and hilar nodes
This 8-month-old had tuberculosis. There is enlargement of the right hilum and the right bronchus is narrowed by multiple mediastinal nodes

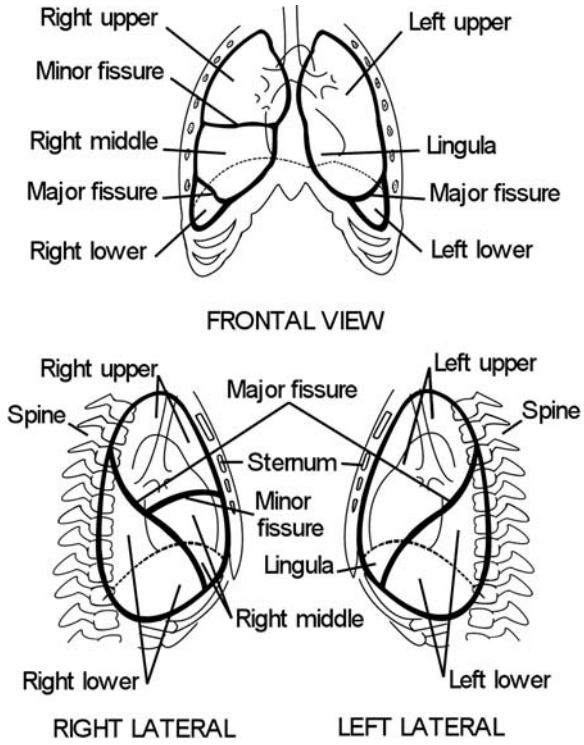

Fig. 3.37. Lobar and fissure anatomy

Lymph Nodes

Mediastinal lymph nodes are not visible on plain films unless they are enlarged (Fig. 3.36). Lymph nodes are well seen on CT and MR.

Lungs

Let's review the anatomy of the lungs (Fig. 3.37). The upper and middle right lobes are separated by the minor fissure frequently seen in a normal chest radiograph. The major fissure separates the right lower lobe from the right middle lobe and upper lobe. The left major fissure is more vertical and posterior. These can often be seen on the lateral film. The pulmonary vessels are easily seen branching in the inner two-thirds of the lung. Most of the time the right hilum is lower than the left; it is never higher. The major bronchi are seen centrally because of the opacity of the mediastinum surrounding these air-filled tubes; they cannot be seen peripherally. There are few visible lung markings in the peripheral third of the lung, especially in young children. Normally the pleura is not visible. The hemidiaphragms change contour with respiration but are nicely dome-shaped on both frontal and lateral films.

Because the lungs are air-filled, they offer sharp contrast to the soft tissue opacity of the heart and diaphragm, whose margins are quite sharp (see Fig. 3.1). If the margins are fuzzy or obliterated, the lung adjacent to these margins is abnormal (the silhouette sign).

Fine detail of lung anatomy is seen best with CT (Fig. 3.38). Routine CT is performed at 5- to 10-mm intervals and reconstructed with bone and standard algorithms. High-resolution CT is performed at thin sections (1- to 2-mm) and with bone algorithm. We view both with lung windows. High-resolution CT demonstrates the lung detail of the secondary lobules with their concomitant vessels and bronchioles. The bronchioles and arteries are central with the interlobular septum composed of connective tissue and pulmonary veins peripherally placed (Fig. 3.39). High-resolution CT facilitates diagnosis of bronchiectasis, diffuse lung disease, defining the full extent of pulmonary disease as well as explaining worrisome findings on the plain film. It is used for detection of pulmonary metastatic disease when standard CT is equivocal.

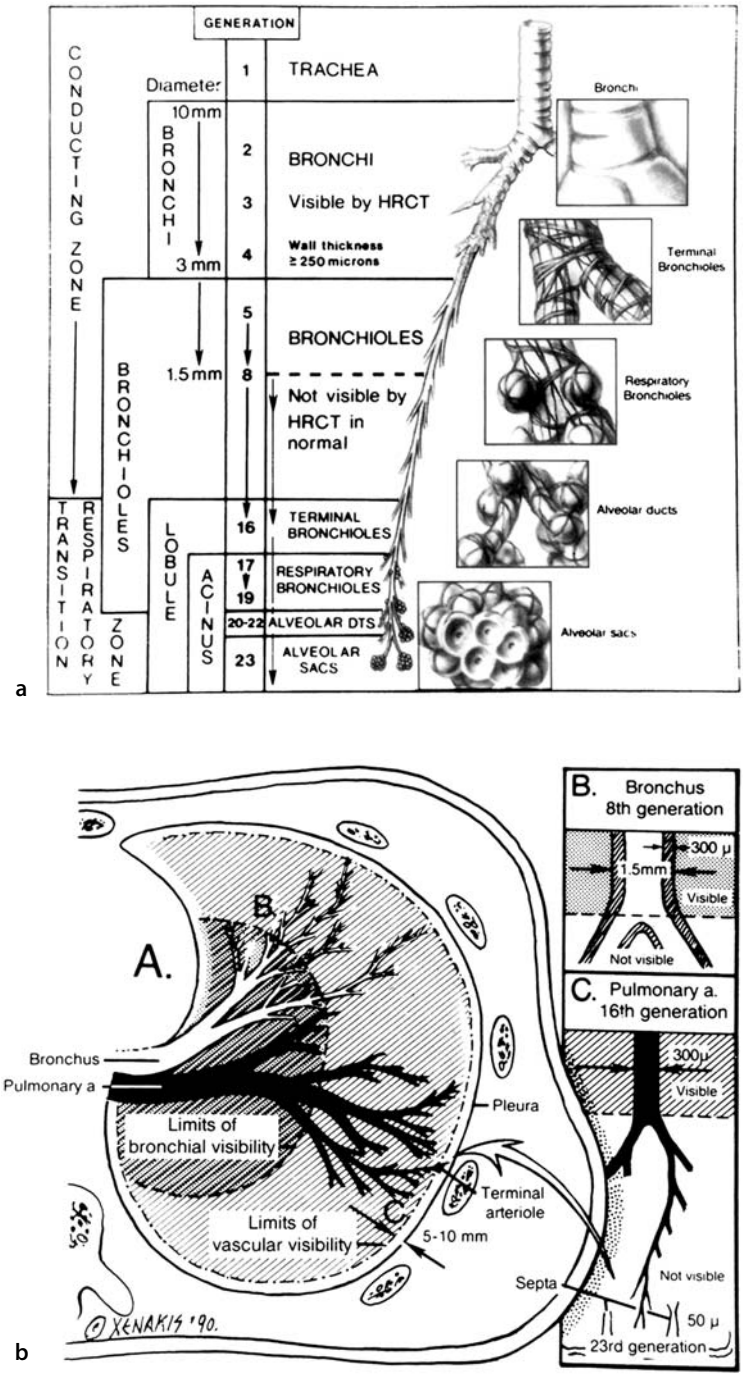

Fig. 3.38. Anatomy as seen on high-resolution CT
This shows the ability of CT to visualize small structures within the lung. (From [2] with permission)

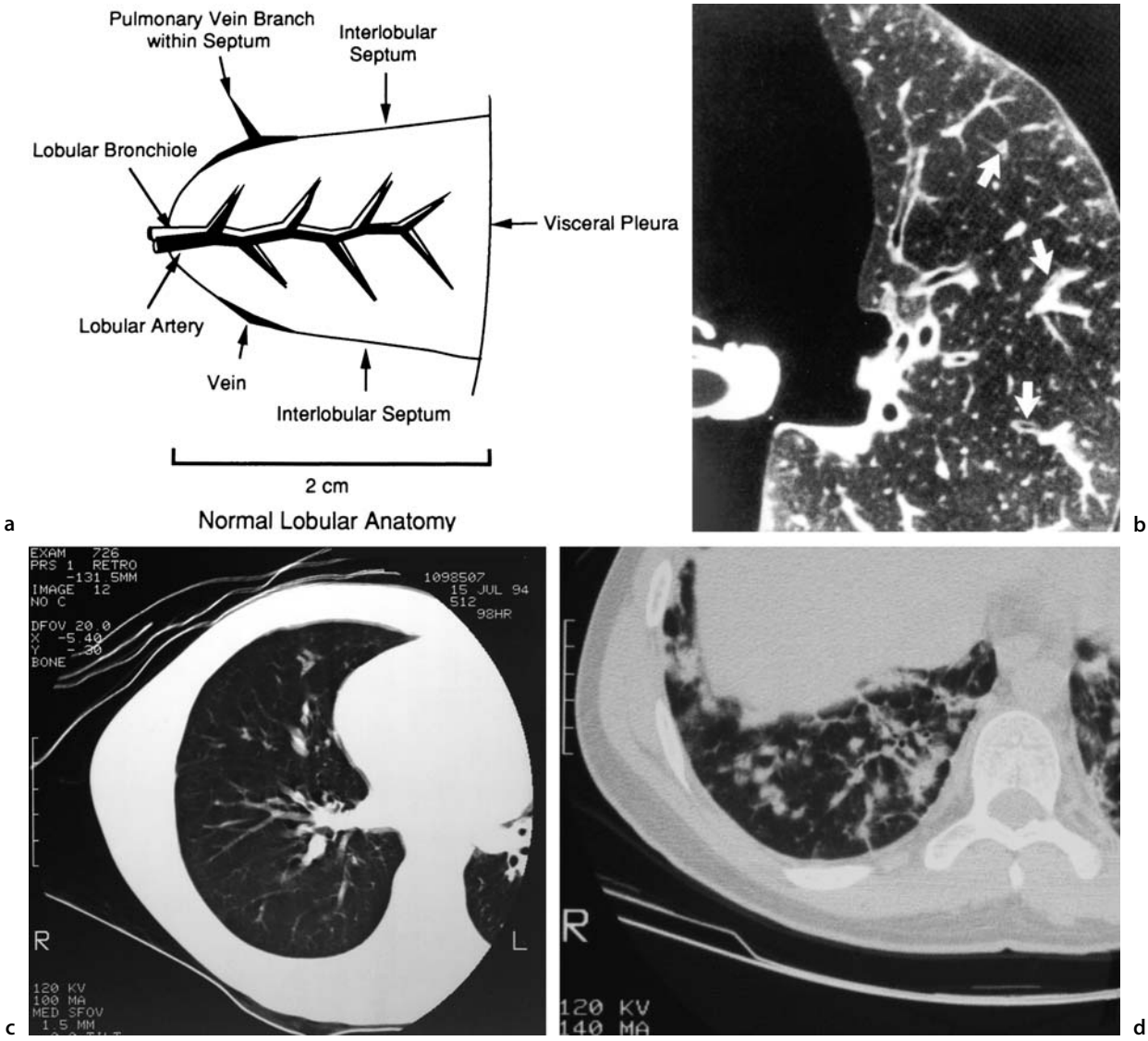

Fig. 3.39. High-resolution CT. This is the anatomy of the secondary pulmonary lobule
a Anatomy of the secondary pulmonary lobule
b Normal appearance in an isolated lung preparation (*arrows*, pointing to small bronchus). (**a, b** from [3] with permission)
c Normal appearance in a 10-year-old child
d High-resolution CT in a teenager with hypogammaglobulinemia and lymphoid interstitial pneumonitis. Note the effects on the secondary lobule

Common Pathological Conditions

Hyperexpansion

Hyperexpansion of the lungs results from "air trapping," i.e., the air cannot exit as rapidly as it enters. This may be caused by any functional or organic airway obstruction. Logically, hyperexpansion is manifested by flattening or inversion of the diaphragm, widening of the rib interspaces, and larger clear spaces in front and in back of the heart. The heart itself may be compressed and reduced in transverse diameter. The lungs may appear darker than normal, but check that the film was not overexposed (see Fig. 3.3). In general, it looks as if the child took a very deep breath when he clearly seems too young to have

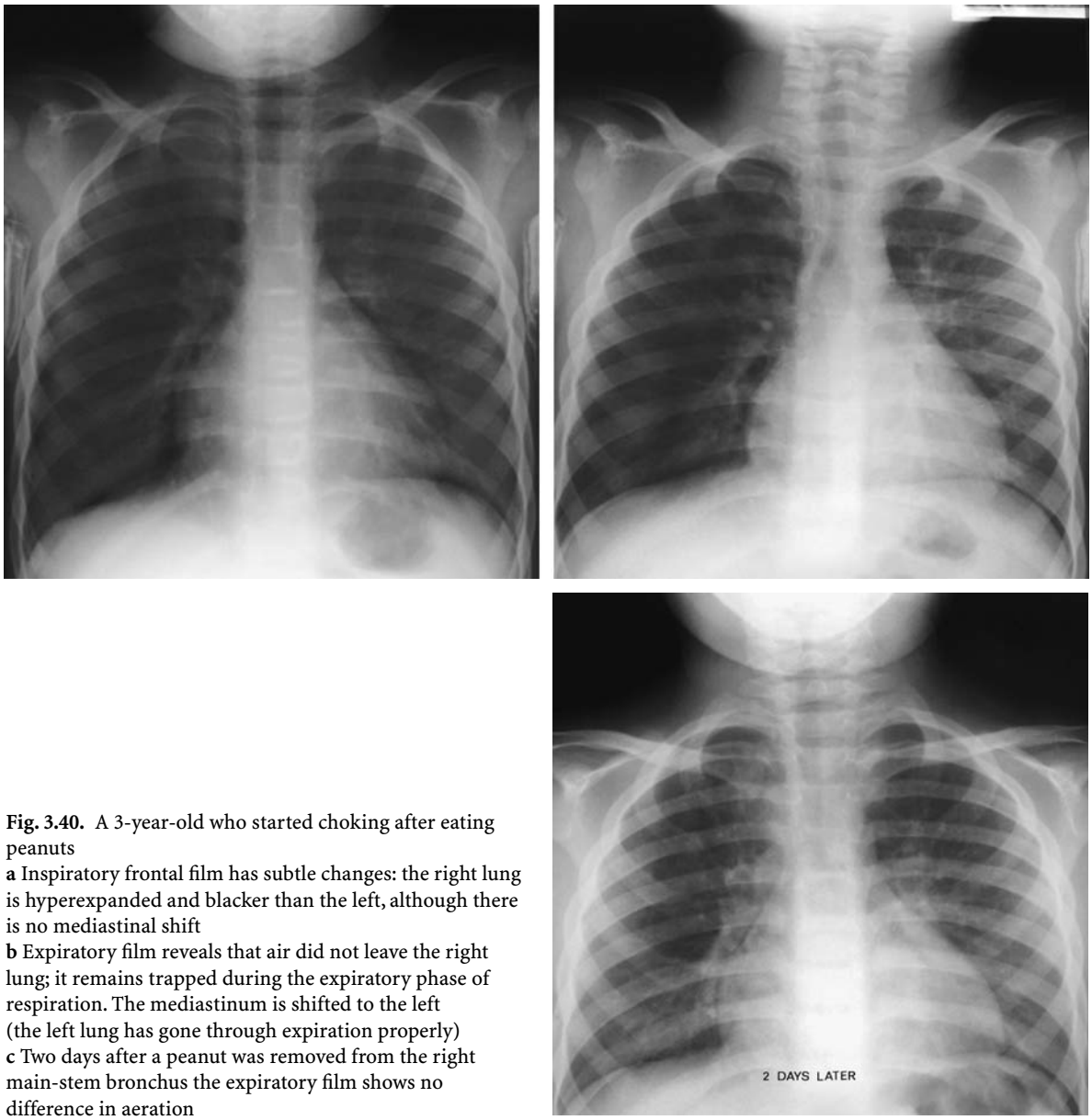

Fig. 3.40. A 3-year-old who started choking after eating peanuts
a Inspiratory frontal film has subtle changes: the right lung is hyperexpanded and blacker than the left, although there is no mediastinal shift
b Expiratory film reveals that air did not leave the right lung; it remains trapped during the expiratory phase of respiration. The mediastinum is shifted to the left (the left lung has gone through expiration properly)
c Two days after a peanut was removed from the right main-stem bronchus the expiratory film shows no difference in aeration

followed the technician's instructions. The air trapping is involuntary and must be seen on both frontal and lateral views to be sure this finding is real.

When hyperexpansion occurs chronically, cor pulmonale may result. Hyperexpansion may be unilateral or bilateral. Common causes of *bilateral* hyperexpansion are (a) asthma, (b) bronchiolitis, and (c) cystic fibrosis. Isolated hyperexpansion of one or two lobes *unilaterally* is commonly found in children who have aspirated a foreign body or have hilar nodes compressing the bronchus (Fig. 3.40). Because of unilateral hyperexpansion, the mediastinum may be shifted. In addition, unilateral hyperexpansion may result from atelectasis or collapse of the contralateral segment of lung. Recognizing unilateral hyperexpansion of the lung is extremely important in pediatrics because children frequently aspirate foreign material.

► ***Rule No. 6:*** In unilateral hyperexpansion of the lungs, you must see how the air moves. Air must move in and out of each lung. Mediastinal position is critical to this determination.

The movement of air within a lung can be visualized by various procedures, such as (a) inspiratory and expiratory radiographs (look for shift of mediastinal position), (b) fluoroscopy of the chest (look for shift of mediastinal position and appropriateness of diaphragmatic motion), and (c) decubitus films (the down side is the "expiratory" side of the radiograph). With these maneuvers one should be able to see which side is abnormal, i.e., air in the abnormal side does not move appropriately (see Fig. 3.40).

If there is too much air in one hemithorax, be sure there are lung markings within the area; one may be overlooking a pneumothorax. It is mandatory to identify the visceral–pleural margin.

Lobar Collapse

It is often helpful to think of the lobes of the lungs as being attached at the hila as if they were a fan. When these lobes collapse, they still retain their hilar attachment, and the other lobes often expand to compensate. The patterns of the lobar collapse are identified in two ways: by seeing the collapsed lobe in a recognizable pattern, and by noticing subtle shifts of intrathoracic structures such as the fissures between lobes of the lung and loss of normal roentgenological borders (silhouette sign) (Figs. 3.41, 3.42). Five questions should be asked when an opacity is seen that appears to be a lobar collapse:

- To which side is the mediastinum shifted?
- In what directions are the major and minor fissures deviated?
- What normal structures are silhouetted?
- Is the hilum shifted up or down?
- Is the diaphragm elevated (see Figs. 3.41, 3.42)?

A common cause of lobar collapse in children is mucus plugging in postoperative and asthmatic patients. Always look for foreign bodies by carefully examining the right and left main-stem bronchi. Masses such as lymph nodes (due to tuberculosis, other infections, or lymphoma), or extrinsic masses such as bronchogenic cysts, can also cause lobar collapse.

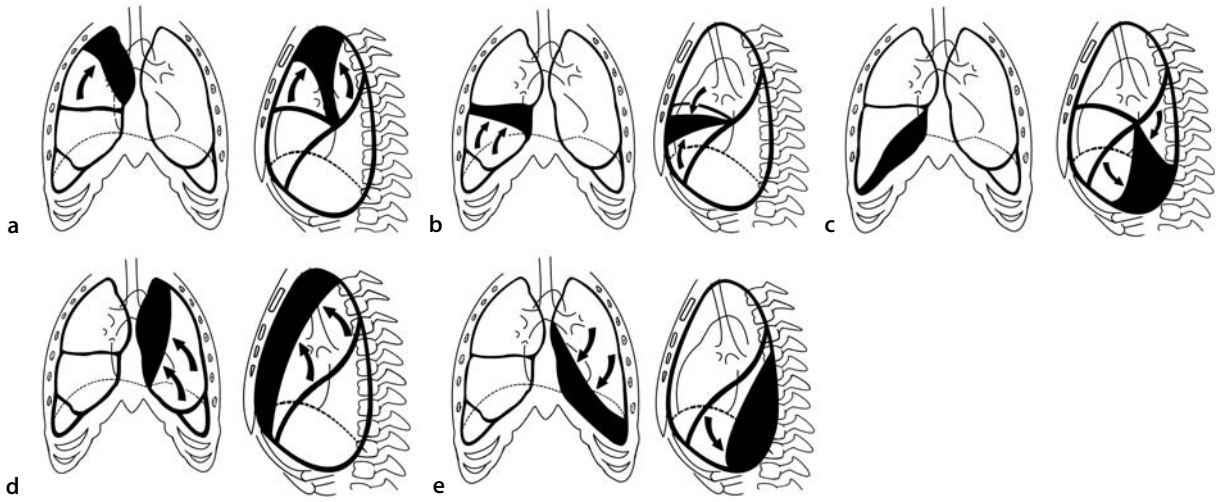

Fig. 3.41. Lobar collapse. Note the shifts of the various fissures. The *blackened area* and *arrows* denote the position of collapse as opposed to the standard position seen in Fig. 3.37
a Right upper lobe collapse
b Right middle lobe collapse. The heart margin is obliterated
c Right lower lobe collapse
d Left upper lobe collapse. The major fissure moves anteriorly
e Left lower lobe collapse

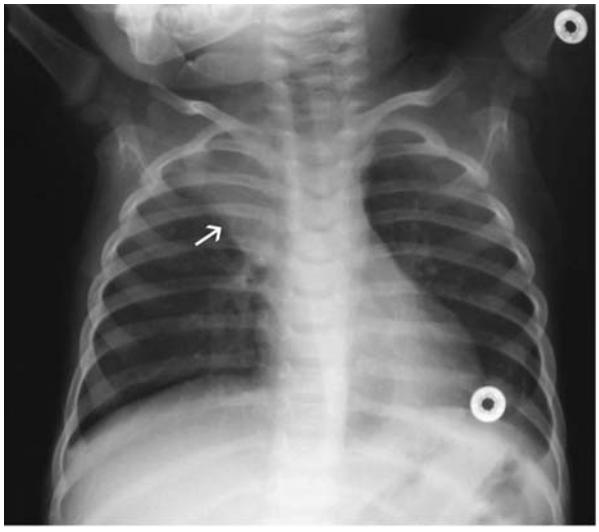

a

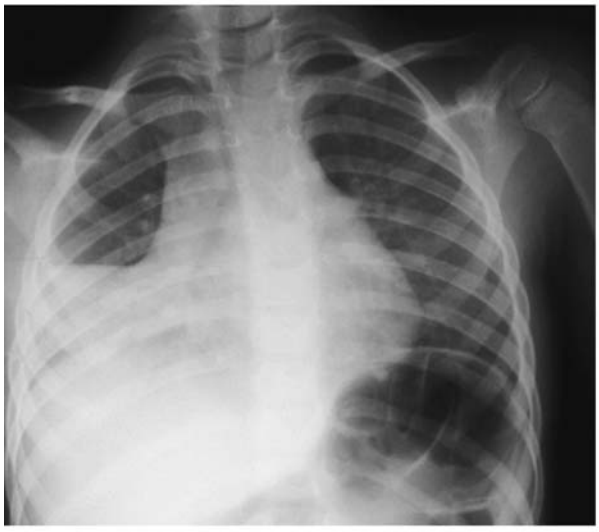

b

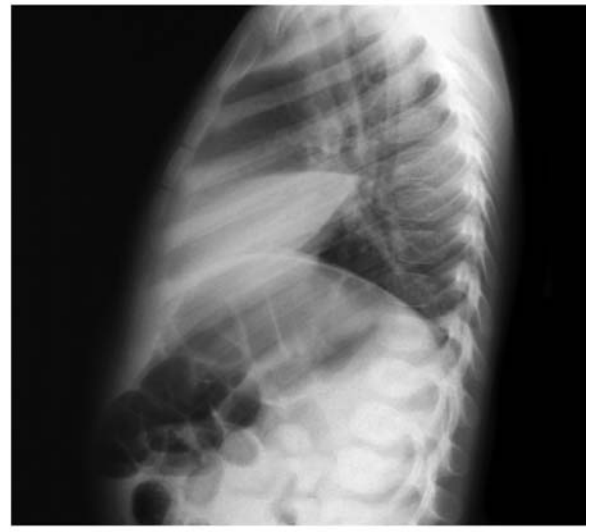

c

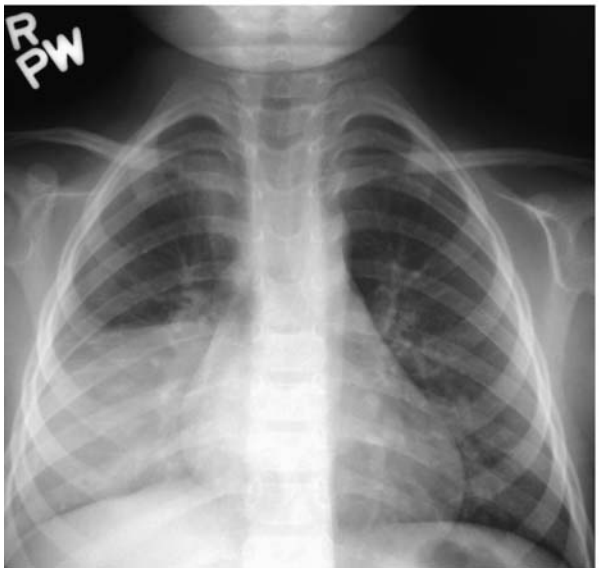

d

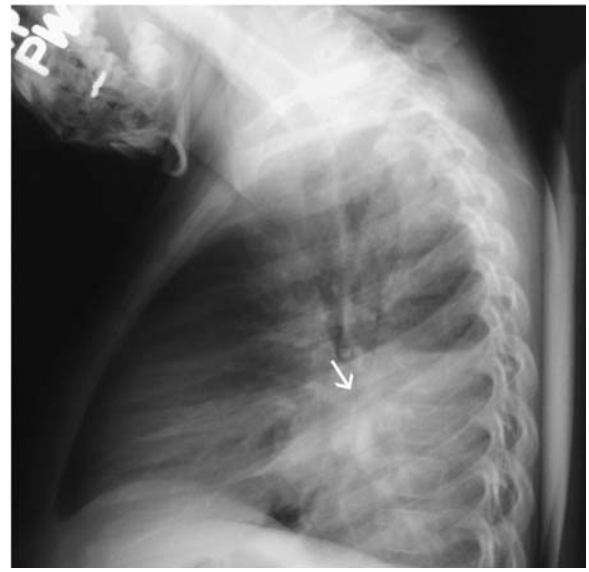

e

Fig. 3.42. Examples of lobar collapse
a Frontal film showing right upper lobe collapse with elevation of the minor fissure (*arrow*)
b, c Frontal radiograph showing obscuration of the right heart border, collapse of the middle lobe, and shift of the mediastinum toward the right. The lateral film shows the wedge-shaped collapse overlying the heart
d, e Right lower lobe collapse. The right heart border is maintained but, as seen on the lateral film, the opacity is posterior and the major fissure is depressed posteriorly (*arrow*). The heart margin is normal
f–h see p. 54

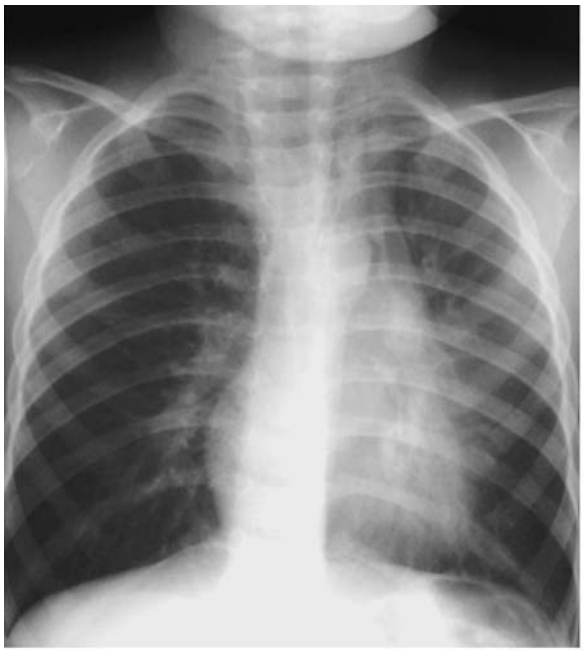

f

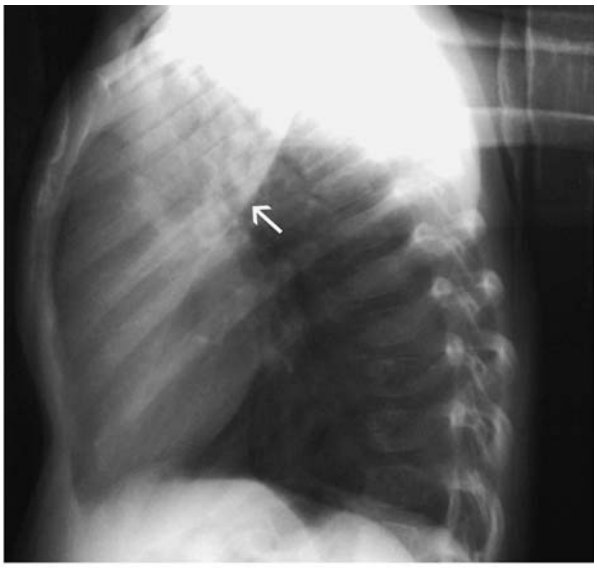

g

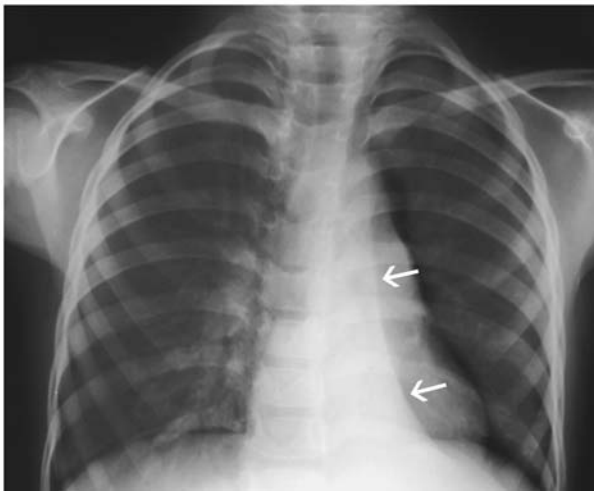

h

Fig. 3.42 (*continued*)
f, g Left upper lobe collapse. Note that the heart margin is quite irregular and not well seen. The major fissure (*arrow*) is anteriorly displaced and there is opacity anteriorly
h Left lower lobe collapse. The heart is no longer transparent and the major fissure is shifted medially and denotes an area of opacity from the spine to visualization of the fissure (*arrows*)

Change in Pulmonary Densities

An opacity is represented by the image appearing too white, and a lucency by its appearing too black. An opacity in the lung may be caused by (a) pneumonic consolidation, (b) atelectasis, (c) neoplasm, or (d) a localized collection of fluid. Sometimes the causes of opacities are indistinguishable. In fact, two processes often are coexistent. When discussing this problem with colleagues, beware of the word "infiltrate." This has come to mean a pneumonic process, but some radiologists understand it to mean atelectasis or edema.

The heart and liver are transparent organs, i.e., you can see through them and visualize the normal branching pulmonary vessels (Fig. 3.1). If you cannot see this phenomenon, there is opacity present (Fig. 3.43).

- ***Rule No. 7:*** The heart and liver are transparent organs.

Opacities within the alveolar space frequently show air bronchograms. These occur when air within the bronchi is seen against a background of airless lung or fluid-filled alveoli. Most alveolar opacities are confluent and larger than individual vessels. Any material, such as pneumonic consolidation or fluid from congestive heart failure, may be manifest by alveolar air-space opacity. In diseases such as viral pneumonia opaque discrete linear streaks are found. These "increased interstitial markings" represent peribronchial thickening and atelectasis: what is commonly termed "the radiological dirty lung," a common finding in patients with asthma. Remember, the dirty lung is a sign, not a specific disease!

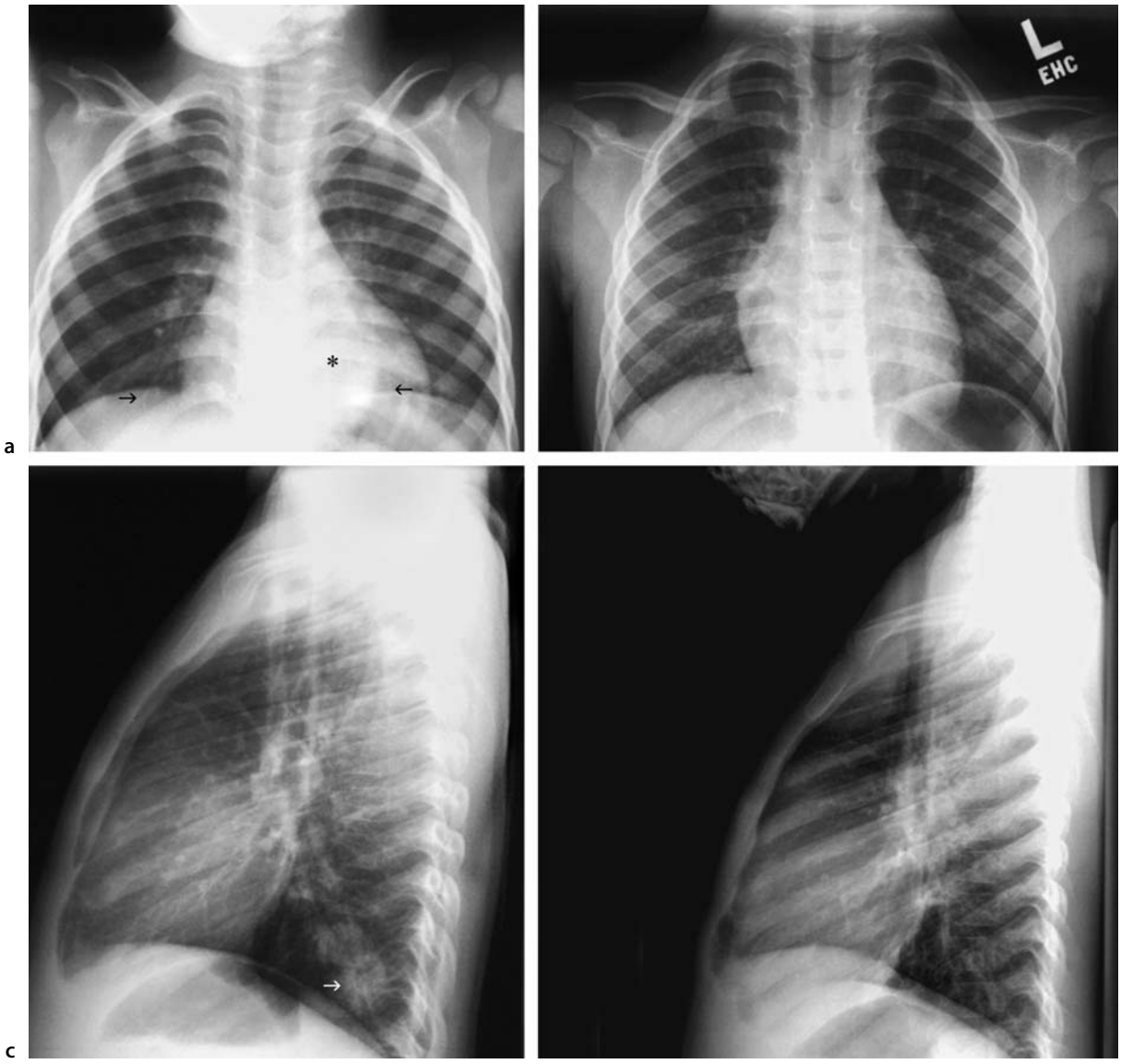

Fig. 3.43. The heart and liver are transparent organs
a A 2-year-old with fever and cough. One can see vessels through the liver and through the most left lateral contour of the heart (*arrows*). However, medially, there is a large opacity consistent with a left lower lobe pneumonia (*asterisk*)
b, c A 3-year-old with fever and tachypnea. There is a subtle opacity behind the left heart on the frontal film. The lateral film, however, shows a large opacity (*arrow*) posteriorly making the vertebral body look whiter than the ones above. This is a good sign on the lateral that there is opacity
d The same child at follow-up examination: note how black the vertebrae appear without the lower lobe opacity

Lobar pneumonia can silhouette the mediastinum, mimicking lobar collapse (Fig. 3.43). However, there is no mediastinal shift of the same magnitude, nor is there a significant loss of lung volume associated with change of position of the fissures.

The most overdiagnosed (nonexistent) pneumonias are: "right lower lobe pneumonia" at the medial lung base, often caused by pulmonary arterial branches seen on a film taken with a poor inspiration, making the hilar vessels stand out. Be careful before diagnosing a perihilar infiltrate on a rotated film! Be leery of opacities in the perihilar regions and the right lower lobe. A clue is that if upon close inspection of the film it appears that the opacity in the right lower lobe is really individual white lines, it probably is *not* pneumonia. The most *overlooked*

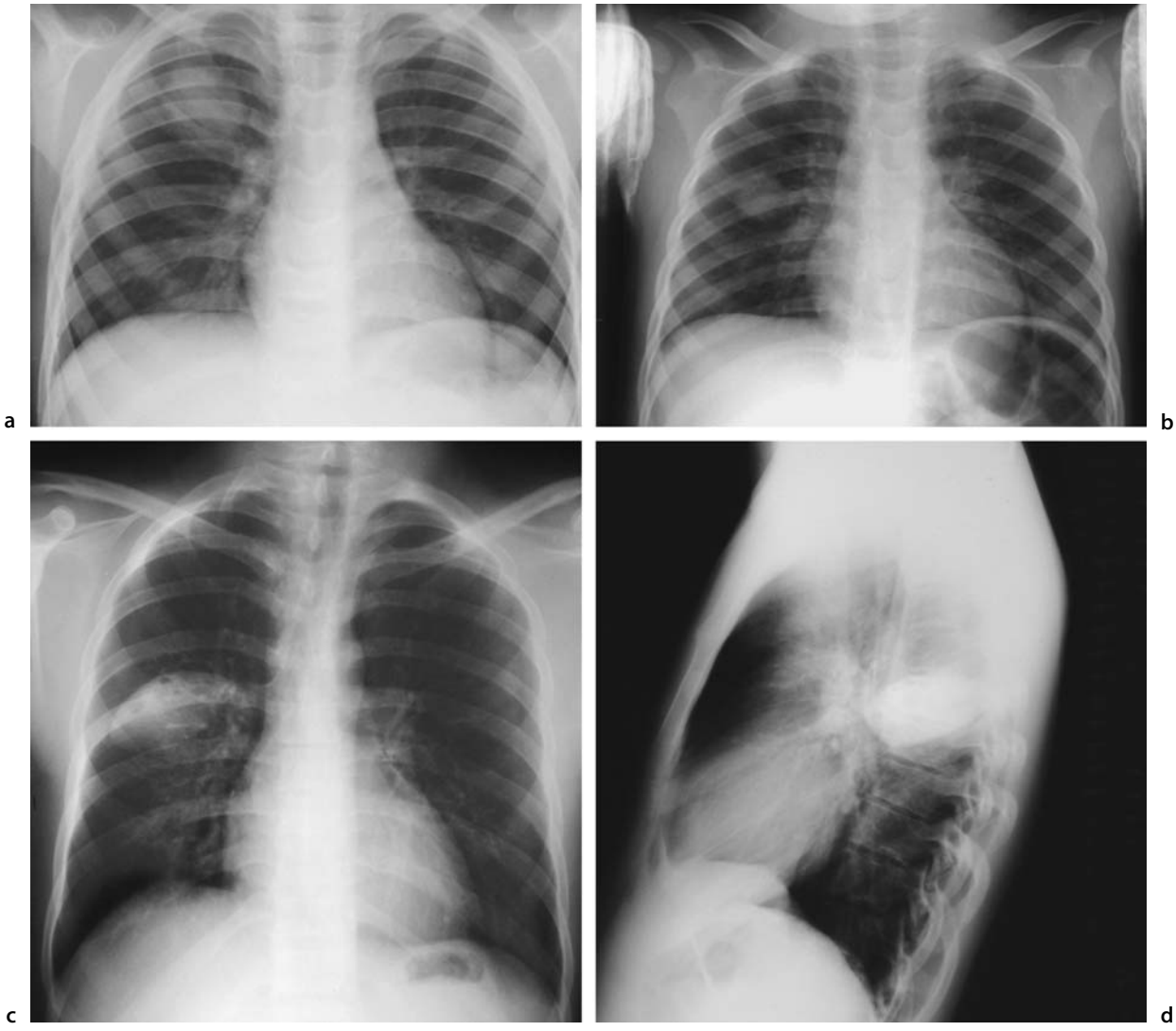

Fig. 3.44. Unusual pulmonary opacities
a Round pneumonia. The frontal chest film shows a right upper lobe rounded opacity that might, at first glance, be mistaken for a tumor or metastasis. Antibiotic therapy resulted in a subsequent normal examination
b Another child with a right lung round opacity. This too proved to be a round pneumonia. Most round pneumonias are caused by streptococcal organisms
c Loculated pleural fluid. This child had unexplained fever and cough for 2 weeks after antibiotic therapy for pneumonia. Chest films show an elliptical density on the right. Note how it conforms to the position of the minor fissure. This is characteristic of a loculated effusion (in this case, infected fluid) in the fissure
d Lateral film of another child with loculated pleural fluid in the posterior portion of the major fissure

pneumonia is that found in the left lower lobe (see Fig. 3.43). This is easily recognized when you remember that the heart should have the same density throughout. It is transparent. *Be aware of changes in opacity and density!* Loss of pulmonary artery visibility or a sudden change from gray to white in any portion of the heart should make you suspicious of retrocardiac pneumonia. When reading a chest film, train yourself to *look through things*, i.e., the heart and liver. Also, keep your eye on the left hemidiaphragm; it should be seen as clearly as the right. Any disruption may mean adjacent pneumonia or atelectasis (silhouette sign).

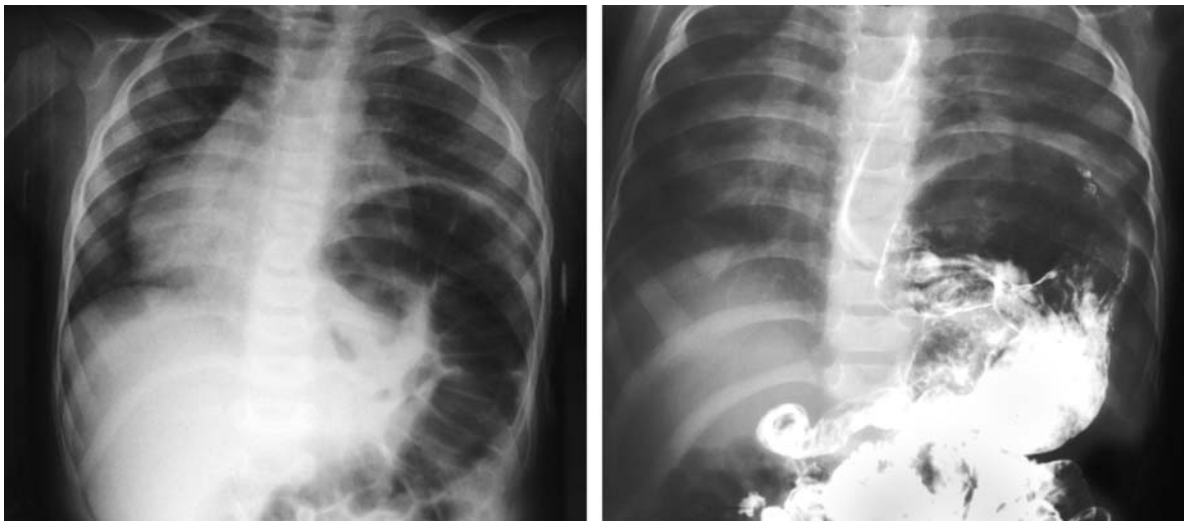

a b

Fig. 3.45. A 16-month-old with cough
a Frontal chest radiograph shows the mediastinum shift to the right and bowel loops compressing the left lower lung
b Barium was given, confirming the intrathoracic location of the stomach and small bowel. At surgery there was an intact diaphragm, but it was very thin, consistent with a large eventration. When the eventration is this large, it acts as a mass causing the same symptoms as a diaphragmatic hernia

Masses and Pseudomasses

Commonly a "mass" in the lungs of children is in fact a pseudomass caused by the "round" pneumonia (Fig. 3.44). This type of opacity is sometimes so perfectly round that it simulates a neoplasm. Appropriate treatment is given, and follow-up films are obtained after 15 days to document whether the mass disappears. Another pseudomass is caused by loculated fluid in the fissure. Often this fluid has a teardrop shape and conforms to the anatomy of the fissure; the opacity is often sharply demarcated for one-half to three-quarters of its borders (see Fig. 3.44).

A common juxtadiaphragmatic pseudomass is due to partial eventration – thinning of the muscles of the diaphragm; it is most often seen on the right as a "bump" on the diaphragmatic surface. Such a phenomenon is *usually asymptomatic and does not require therapy*, but a large eventration can act as a diaphragmatic hernia, causing mediastinal shifts (Fig 3.45).

True primary lung neoplasms are uncommon in children. The most common ones are extensions of mediastinal structures or are caused by defects of the diaphragm and are in fact extrapulmonary (Fig. 3.46). It is appropriate, then, to discuss mediastinal masses in this category. These masses arise in any of the three components of the mediastinum. The most common posterior mediastinal mass is a neurogenic tumor such as a neuroblastoma, ganglioneuroma, or neurofibroma. The hemidiaphragm inserts posteriorly at the L1–2 level; therefore, a posterior basilar intrathoracic mediastinal mass may masquerade as an abdominal mass. Remember the normal inferior extent of the thoracic cavity. If the ribs are separated, the posterior mediastinal mass is in the thorax.

Middle mediastinal masses are most commonly of lymphoid origin (e.g., lymphoma), but lesions of any of the other structures of the middle mediastinum – such as esophageal duplication – may occur. The most common anterior mediastinal masses are "terrible" lymphomas, teratomas, and thymomas (in children aged over 10 years). True parenchymal masses are frequently due to metastasis such as that from Wilms' tumor (Fig. 3.47). Congenital masses found in the neonate are discussed in the next chapter (Chap. 4).

The outline below is a useful summary of the etiology of mediastinal masses:

- Anterior mediastinum (the four T's and a C)
  - Thyroid (ectopic thyroid is often mentioned, never seen!)
  - "Terrible" lymph node enlargement by either infection or malignancy
  - Teratoma
  - Thymoma
  - Cystic hygroma

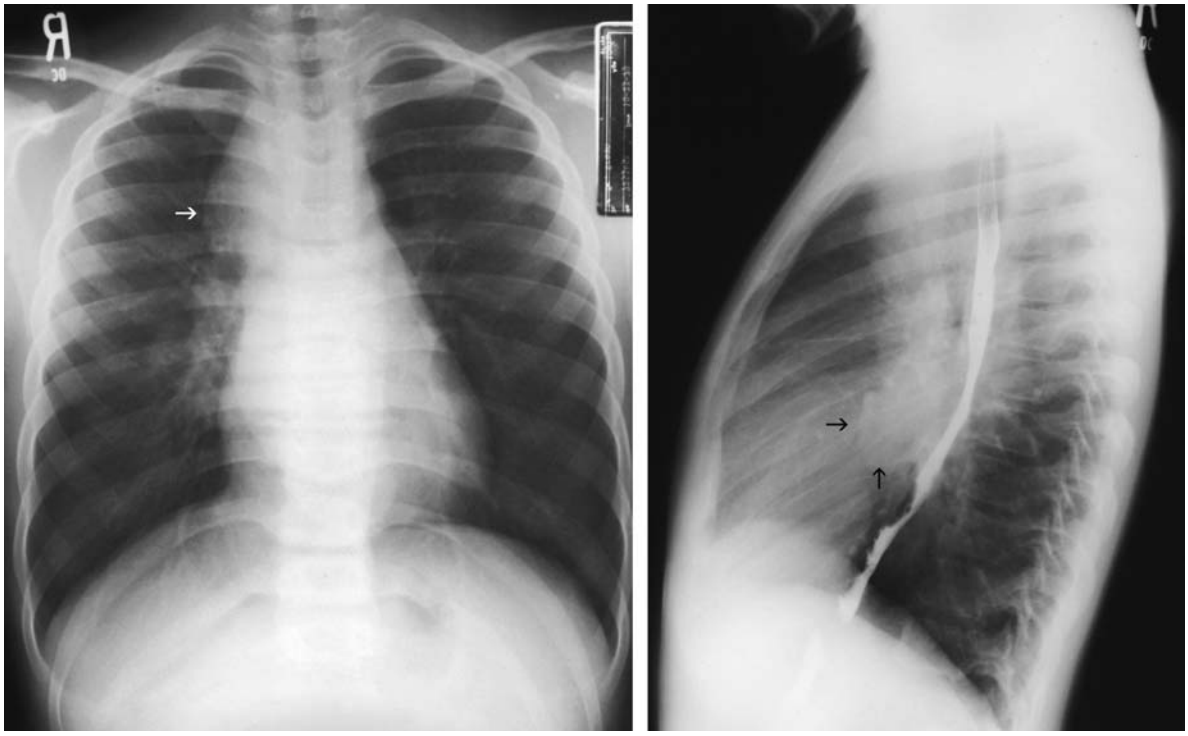

Fig. 3.46. Mediastinal mass
a This 10-year-old has a widened mediastinum. He is too old to have a large thymus and, in fact, has an enlarged right hilum with paratracheal adenopathy (*arrow*). The subcarinal region is also "too white" when compared to the rest of the heart
b Lateral roentgenograph opacity the density in the middle mediastinum – a common presentation for a lymphoma (*arrows*). There is contrast material in the esophagus

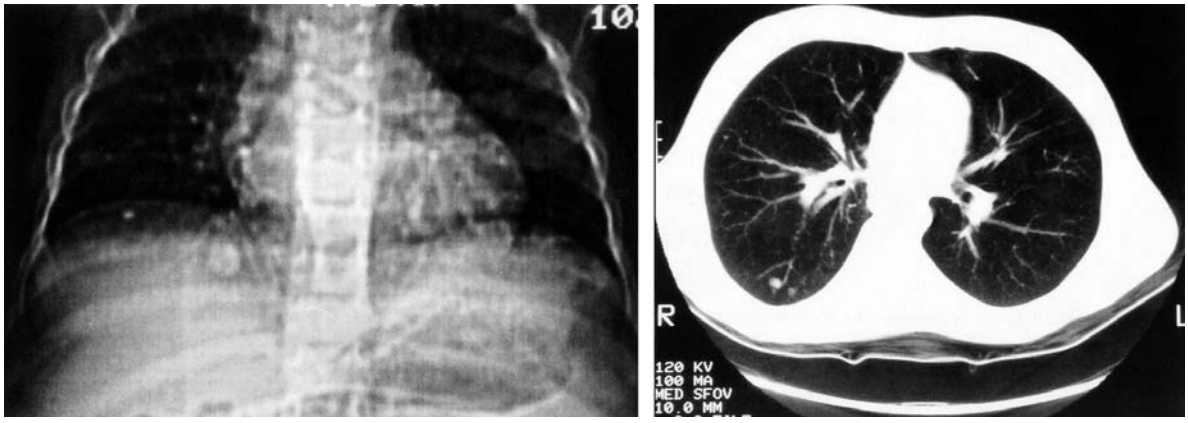

Fig. 3.47. Metastatic lung disease
a Scout film prior to CT in this 3-year-old who had a Wilms' tumor removed 7 months previously. There are multiple rounded opacities in the chest
b CT reveals multiple lung metastases

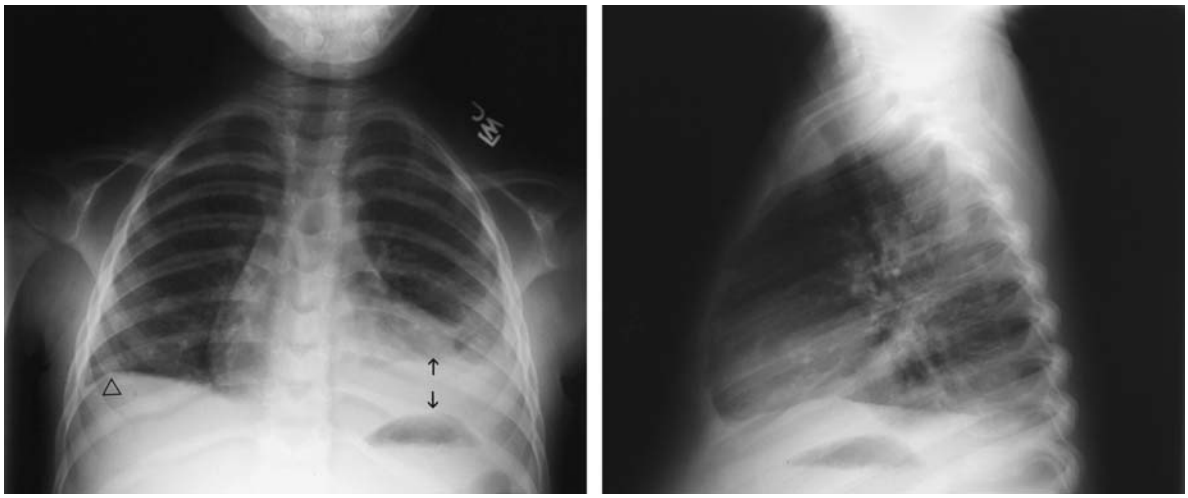

Fig. 3.48. Pleural effusion
a, b Erect frontal (**a**) and lateral (**b**) view of a patient with nephrotic syndrome who is 5 years old. The silhouette sign is present as the left heart margin is obscured. Note the distance between the stomach and the apparent diaphragm on the left side (*arrows*). The diaphragm should be closely applied to the stomach and therefore this could not be diaphragm but is fluid beneath the lung and above the diaphragm – a subpulmonic effusion. There is another cardinal sign of subpulmonic effusion on the right side. The highest point of the diaphragm is quite lateral (*arrowhead*). This is the shape of the bottom of the lung and there is fluid below the lung and above the hemidiaphragm. On neither side do we really see the diaphragm. It is important to note that the usual pleural reaction is an opacity tracking along the lateral chest wall. There is a very small lateral component on the right side and a much larger lateral component on the left side. The lateral view shows separation of the stomach and diaphragm as well as opacity posteriorly

- Middle mediastinum (an abnormality for each organ)
  - Esophagus: duplication cysts
  - Great vessels: aneurysmal dilatation
  - Hila: enlarged lymph nodes (leukemia, lymphoma, tuberculosis, etc.)
  - Trachea: bronchogenic cysts
  - Pericardium: cyst
- Posterior mediastinum (T, E, N)
  - Tuberculosis (Pott's disease) or any spinal infection
  - Extramedullary hematopoiesis (almost always in adults)
  - Neural tumors: neuroblastoma, ganglioneuroma, neurofibroma, neurenteric cyst
- Tips when viewing mediastinal masses include:
  - Middle mediastinal masses silhouette the heart border and aorta.
  - Posterior mediastinal masses may spread ribs or cause vertebral changes.

Pleura

Pleural reaction (effusion or thickening) is best indicated by an opacity between the aerated lung and rib border (Fig. 3.48). Thickened pleura, loculated pleural fluid, and empyema appear similar radiographically and may not be differentiated by normal radiographic techniques. Decubitus films demonstrate free-flowing fluid but may not show movement of loculated pleural fluid, viscous empyema, or thickened pleura. An excellent way to detect small amounts of fluid or limited pleural thickening not visible on the frontal film is to look carefully at the posterior lung sulci on the lateral film. Then check the thickness of the pleural line in relationship to each rib; it should be snug against the rib. Fluid can also accumulate beneath the inferior surface of the lung and can simulate an elevated hemidiaphragm. Such collections are called subpulmonic effusions and are recognized by the laterally shifted "diaphragmatic dome" (see Fig. 3.48).

The most common cause of pleural effusion in children is infection, and almost any infection can cause a small pleural effusion. Pleural effusions are also frequently seen in patients with congestive heart failure (if unilateral, always on the right) and chronic renal disease. In difficult cases enhanced CT can differentiate pleural disease from effusion or parenchymal disease (Fig. 3.49). Ultrasound can often be used as well to find fluid for diagnostic taps.

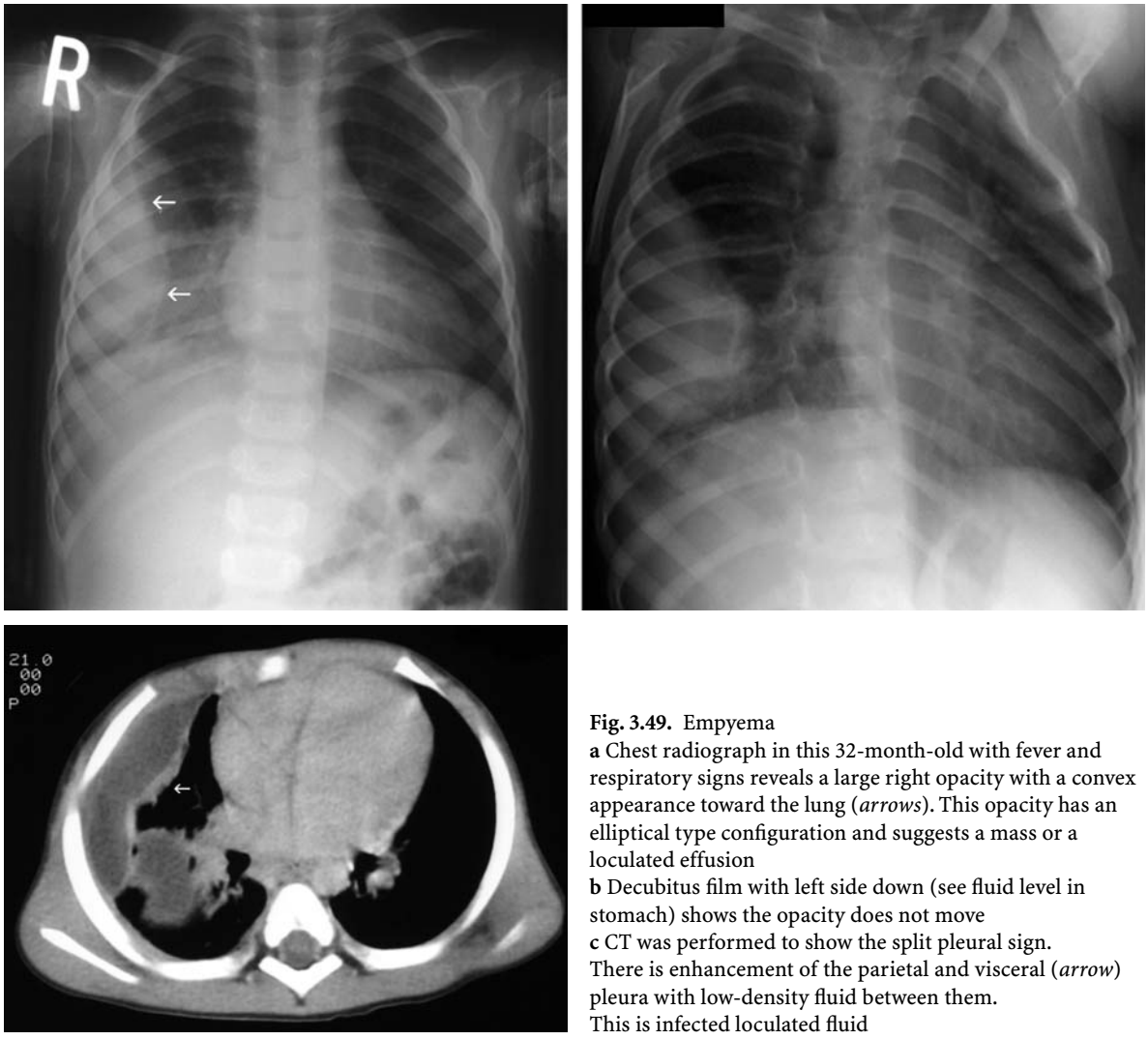

Fig. 3.49. Empyema
a Chest radiograph in this 32-month-old with fever and respiratory signs reveals a large right opacity with a convex appearance toward the lung (*arrows*). This opacity has an elliptical type configuration and suggests a mass or a loculated effusion
b Decubitus film with left side down (see fluid level in stomach) shows the opacity does not move
c CT was performed to show the split pleural sign. There is enhancement of the parietal and visceral (*arrow*) pleura with low-density fluid between them. This is infected loculated fluid

Summary

A thorough radiographic work-up should include the following, in order of priority:

- Good erect, nonrotated inspiratory frontal and lateral chest films
- Inspiratory and expiratory films (if foreign body is suspected, there is persistent hyperexpansion or atelectasis) and/or fluoroscopy of the chest to observe mediastinal shift and diaphragmatic excursion (decubitus films may help)
- Specialized magnification high-kV films of the airway, if the air passage itself needs evaluation
- An esophagram in any unexplained airway disease
- MR or CT for mediastinal masses
- High-resolution CT for complete work-up of unusual or questionable pulmonary parenchymal abnormalities

Remember, the chest radiograph can be a very tricky thing. It is easy to get "seduced" by obvious pathology such as a mass opacity, a large heart, or a large pleural effusion. You must resist the temptation to describe the obvious abnormality and force yourself to do a routine, orderly scan of the entire chest film and not be "seduced" by the obvious lesion. This method will help train you to spot more subtle findings, such as a rib fracture. A convenient

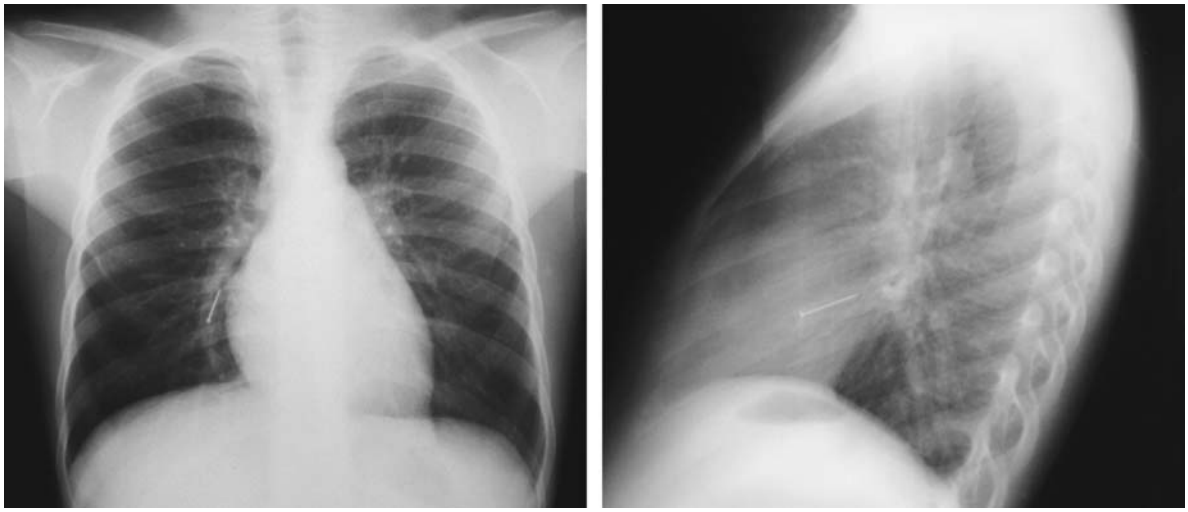

a b

Fig. 3.50. A child with acute onset of respiratory distress. (See Appendix 2)

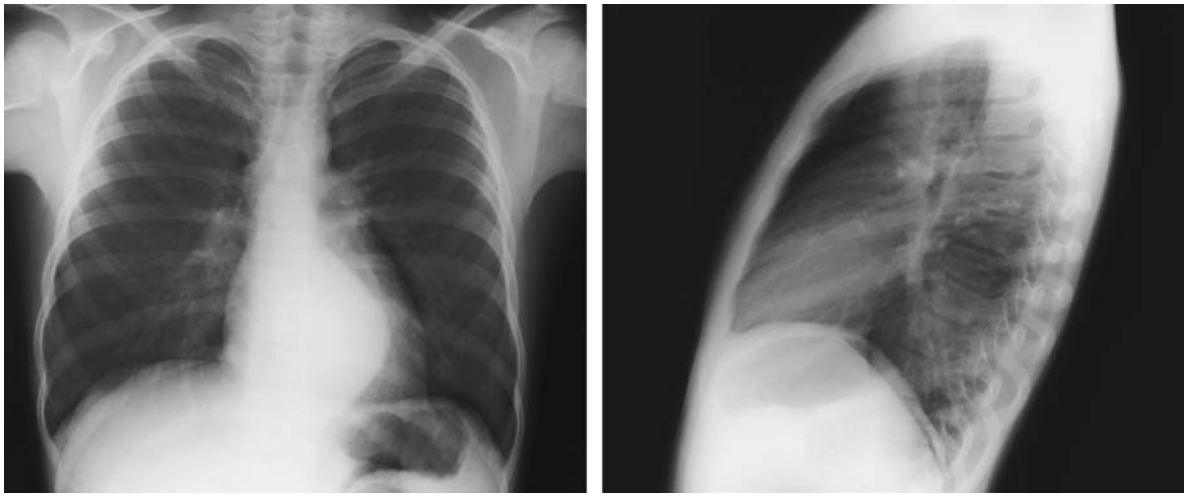

a b

Fig. 3.51. Chronic lung disease. (See Appendix 2)

way to read systematically is to evaluate the technical factors of lung volume, patient position, and the way the film was exposed. Use the radiologist's circle and ABCS: *A*=abdomen, *B*=bones, *S*=soft tissue, and *C*=chest (airway, mediastinum, lungs, and diaphragm). Now evaluate Figs. 3.50–3.52. Approach each one systematically and describe the abnormalities you see. The answers are in the Appendix 2.

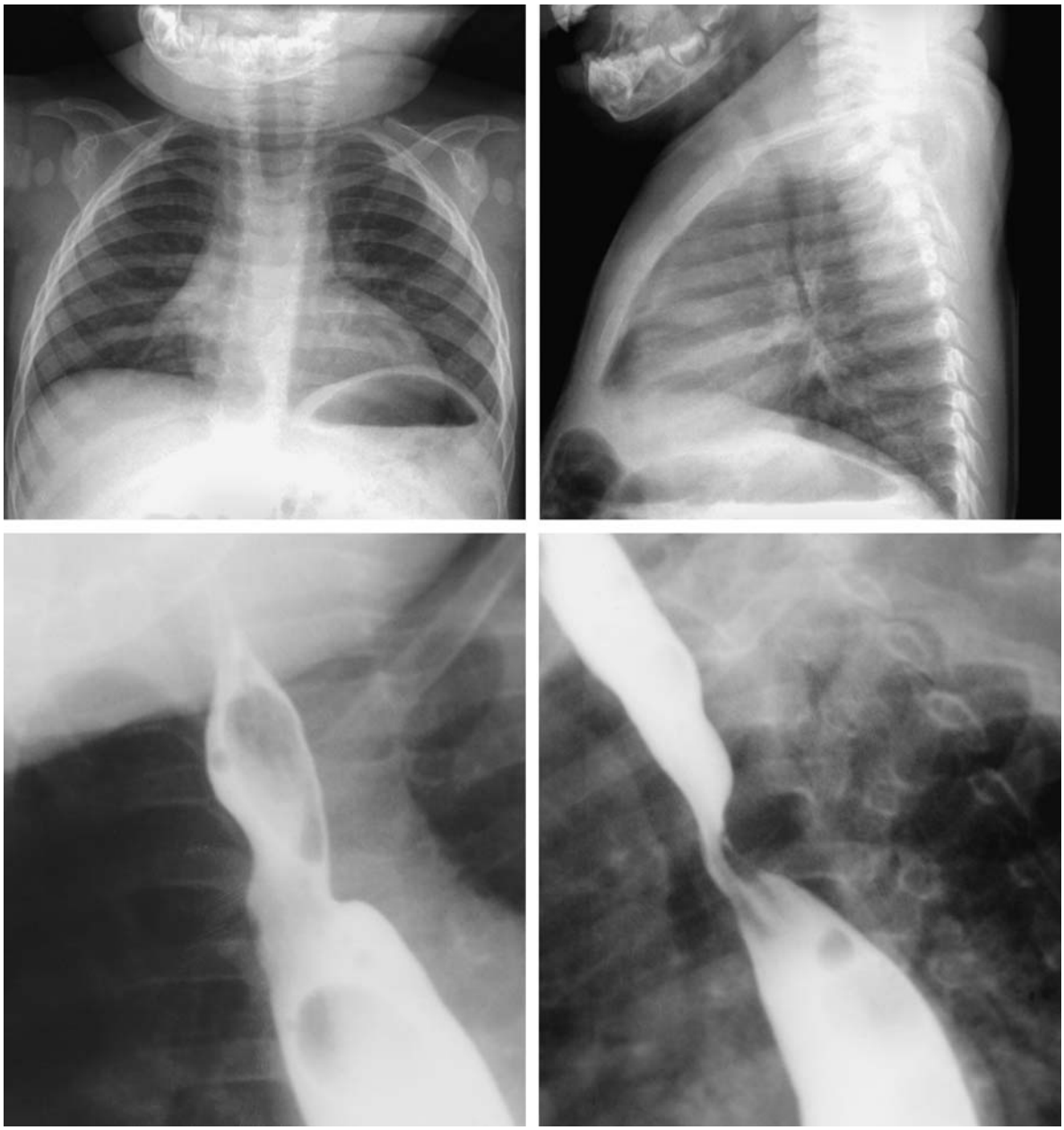

Fig. 3.52. A child with wheezing. (See Appendix 2)

References and Further Reading

1. Slovis TL, Haller JO, Berdon WE, Baker DH, Joseph PM (1979) Noninvasive visualization of the pediatric airway. Curr Probl Diagn Radiol 8:1–67
2. Naidich DP, Webb WR, Mueller NL, Krinsky G, Zerhouni EA, Siegelman SS (1998) Computed tomography and magnetic resonance of the thorax, 3rd edn. Lippincott-Raven, New York
3. Webb WR, Mueller NL, Naidich DP (1996) High-resolution CT of the lung, 2nd edn. Lippincott-Raven, New York
4. Kuhn JP, Slovis TL, Haller JO (eds) (2003) Caffey's pediatric diagnostic imaging, 10th edn. Mosby, Philadelphia
5. Newman B (ed) (1999) Imaging of medical disease in the newborn lung. Radiol Clin North Am 37:1049–1065
6. Boiselle PM (ed) (2003) Multislice helical CT of the thorax. Radiol Clin North Am 41:617–626
7. Slovis TL (1977) Noninvasive evaluation of the pediatric airway: a recent advance. Pediatrics 59:872

4 The Chest in the Neonate and Young Infant

Rapid physiological changes occur in the first minutes and hours of a newborn's life. The fluid-filled lungs empty of surfactant-rich fluid and fill with air. The circulatory system is dramatically changed when the ductus arteriosus closes. The lungs now receive a major influx of blood, and gaseous exchange occurs. During the subsequent days to weeks, the pulmonary artery pressures fall from near systemic values. This drop in pulmonary vascular resistance permits clinical recognition of left-to-right shunts, such as ventricular septal defects and atrial septal defects.

The newborn infant breathes and cries. Both of these processes fill the lungs and the gastrointestinal tract with air. The lungs fill with air during the first breath. The gastrointestinal tract fills more slowly, and it may take up to 24 h for gas to reach the rectum (although it occurs by 12 h in most healthy infants).

The sequence and timing of these expected physiological and anatomical changes allow the radiologist to detect the infant making an abnormal transition to extrauterine life.

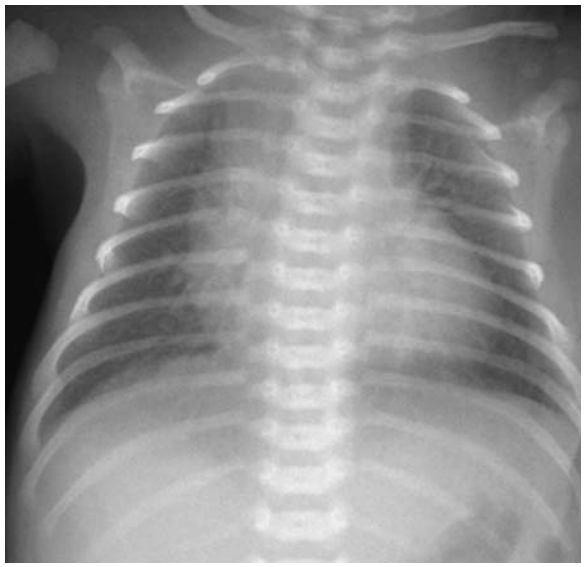

Fig. 4.1. Transitional chest
The frontal examination in this near-term infant shows mild hyperexpansion during the transition period. The mediastinum is wide because of the thymus and magnification of this supine technique. There are some increased strand-like opacities which probably represent a small amount of retained fetal fluid. The lateral margin of the right heart is obscured by the thymus

Technical Factors

The method for taking chest films in a neonate differs from that in older children (Chap. 3). The baby remains supine, the film (which is under the baby) is exposed with the X-ray tube above for the AP projection. The tube–film distance is 36–40 in. (91–102 cm) because the equipment must be fixed within the restraints of the isolette and life-support systems (Fig. 4.1). A lateral film may be taken by turning the baby onto its side. It may also be taken as a "cross-table lateral," i.e., with the baby supine and the beam directed through the baby's side. The cross-table lateral technique is particularly important when there is a possibility of free air (pneumothorax or pneumomediastinum). Since the child is supine, and air rises, air can be seen under the sternum. The single-view neonatal chest radiograph exposes the patient to 3–5 mrad (Fig. 4.2)

On all supine portable films there is inherent magnification of mediastinal structures and absence of the effect of gravity on both the pulmonary vascularity and on fluid within the bowel. Why is this important? (Answers in Appendix 2.)

Newborns are unique in other ways: (a) a normal neonate breathes at a rate of 30–50 times per minute, and it is therefore more difficult to get a "good inspiratory film"; (b) the trachea in the neonate and young infant is "too long" for the contracted chest in expiration and therefore buckles; and (c) normal neonates have a large anterior mediastinal mass – the thymus – which is accentuated by the AP projection (Fig. 4.3).

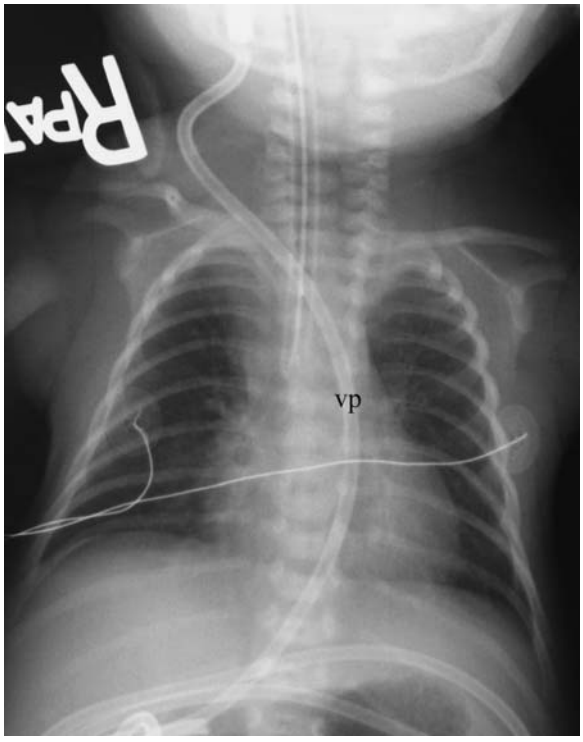

Fig. 4.2. Chest radiograph in a newborn with respiratory distress
The patient has a ventricular peritoneal catheter (*vp*) and an endotracheal tube. What is wrong with the endotracheal tube? The tip is in the right main-stem bronchus

How then does one determine the normal film? What criteria should be used? The approach is the same as that outlined in Chap. 3; lung volume and patient position, i.e., rotation, must be evaluated first (review "Technical Factors" in Chap. 3). The radiologist's circle must be followed, and since there are multiple films on the sick neonate, strict attention must be paid to the name, date, and time of examination. The ABC'S approach is important in evaluating the neonatal chest as well.

► ***Rule No. 1:*** On every chest film, read the abdominal portion as you would read an abdominal film.

Interpreting the Film

Abdomen

The neonate frequently has an orogastric or nasogastric tube for decompression of a distended stomach or for feeding. Its position must be noted, as it may be in the esophagus (a good situation for aspiration), deep within the small bowel or, worse, extraluminal (Fig. 4.4). Venous catheters may be either in an umbilical vein, within the portal venous system, in the inferior vena cava, or in the heart. These venous catheters are seen anteriorly as they pass into the left

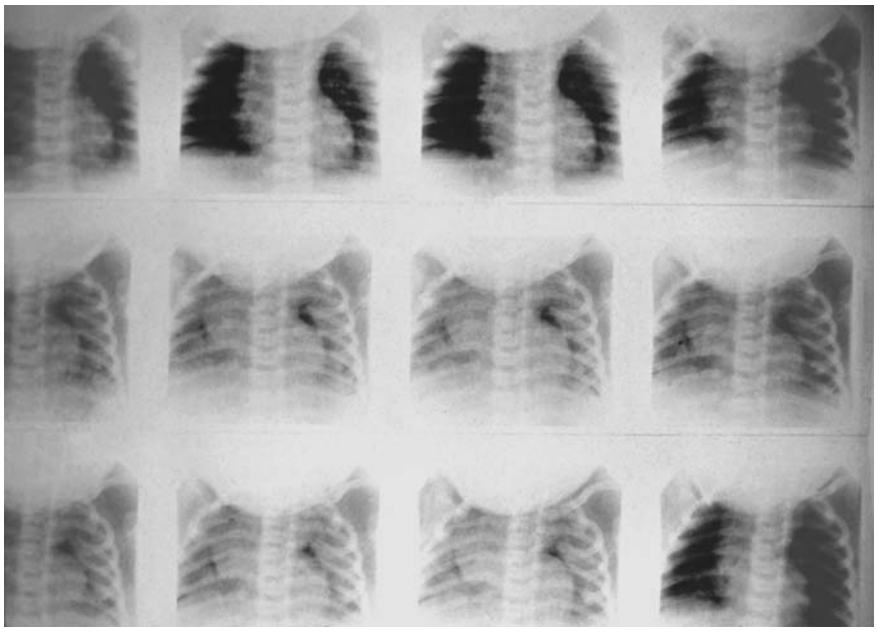

Fig. 4.3. Phases of respiration
Multiple films were obtained at 1 film per second. This infant has a pneumomediastinum and was crying. *Top row,* the heart size is normal, and the lungs are well aerated. *Middle row,* during expiration, the lungs are becoming opaque and filling with blood. The hemidiaphragms are elevated, and a pneumomediastinum outlines the heart. *Bottom row,* by the last film the patient is again in the inspiratory phase of respiration. (Courtesy of Walter E. Berdon, MD, and David H. Baker, Babies' and Children's Hospital, New York)

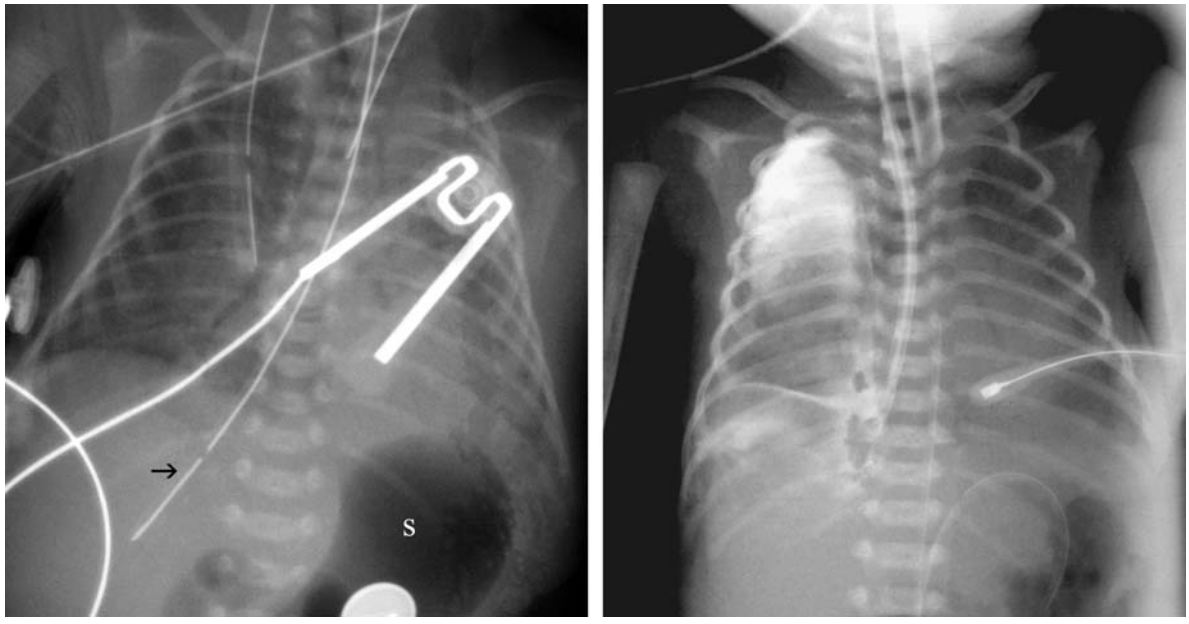

a b

Fig. 4.4. Perforation of esophagus by a nasogastric tube
a Frontal film shows the tip of the nasogastric tube (*arrow*) in the right side of the posterior thorax or upper right abdomen. *s*, stomach
b Contrast medium injected into the nasogastric tube spills into the pleural space

Fig. 4.5 a – d.
Legend see p. 66

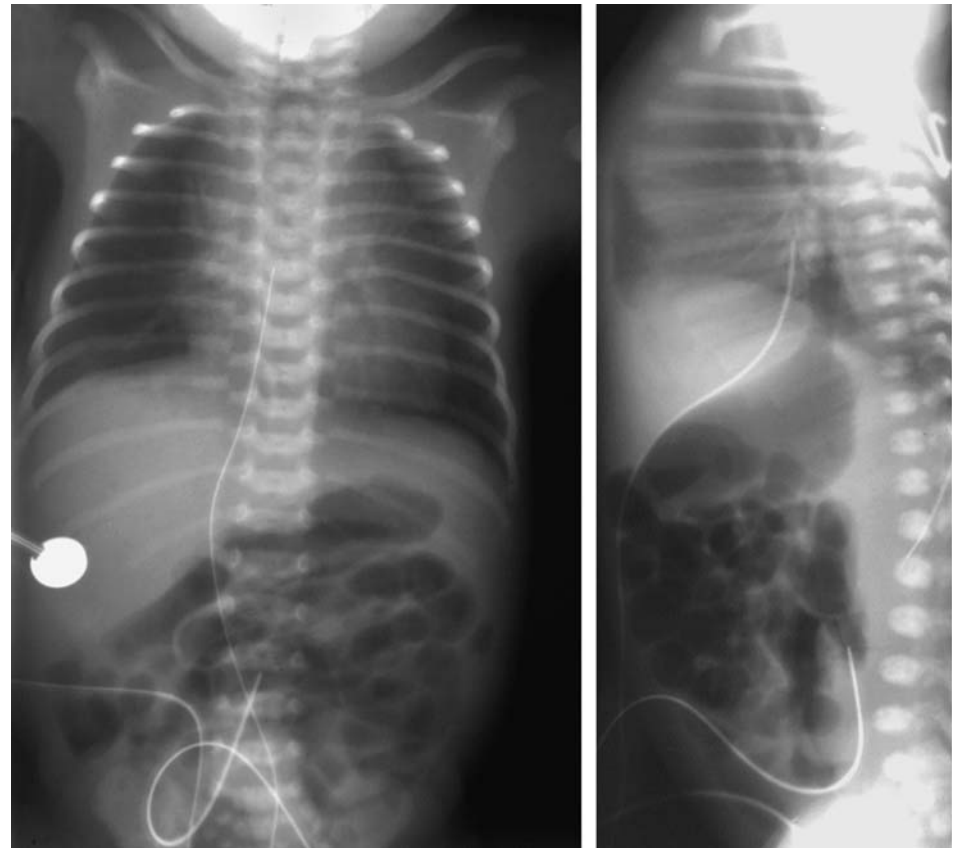

a b

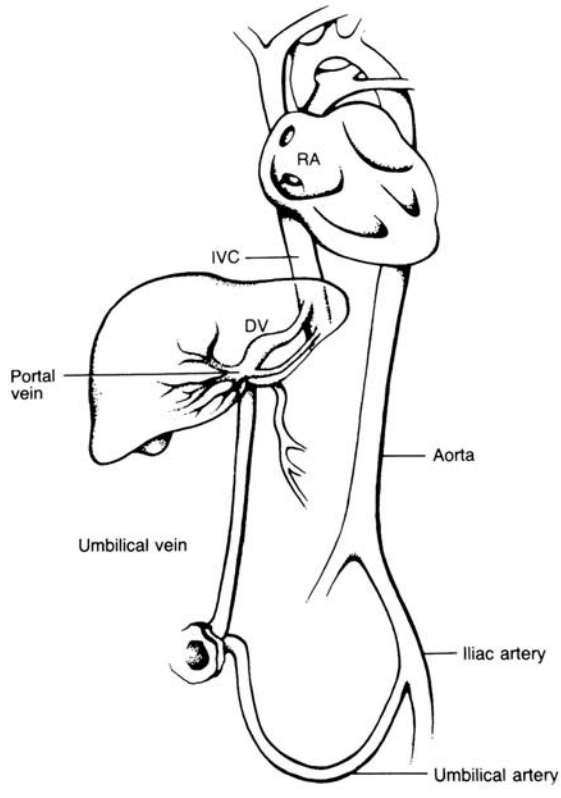

c

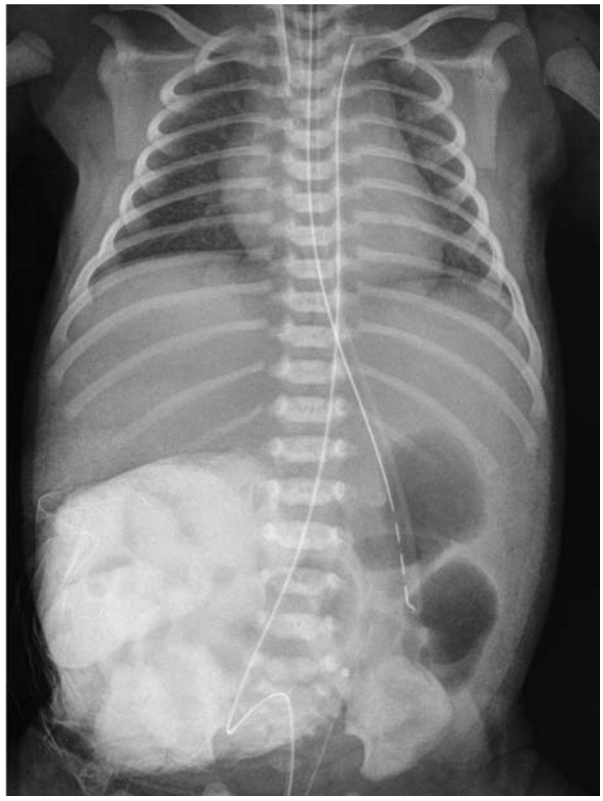

d

Fig. 4.5. Catheters and tubes
a Frontal radiographs of the chest and abdomen. Two tubes can be seen: one whose tip ends in a vessel within the abdomen, and one in a vessel within the chest
b The lateral film confirms which tube is arterial and which is venous. The anterior catheter starts in the umbilical vein and extends to the liver into the inferior vena cava, via the ductus venosus and into the right atrium. The arterial line dips inferiorly in the iliac artery and then rises posteriorly in the abdominal aorta
c Anatomy of the umbilical vessels. A catheter in the umbilical vein crosses the portal vein and enters the ductus venosus on its way to the right atrium. The umbilical artery dips down to join the internal iliac artery then the main aorta. *IVC*, inferior vena cava; *DV,* ductus venosus; *RA*, right atrium. The ideal location for the tip of the umbilical venous line is in the right atrium. The umbilical arterial line tip may be at L4–5 (bifurcation of the aorta) or at T8 above the diaphragm
d This is a neonate with an abdominal wall defect (abdominal opacity). The arterial line has mistakenly been placed in the left subclavian artery

portal vein, through the ductus venosus, and into the inferior vena cava, while the umbilical artery catheter is posterior (Fig. 4.5). The arterial catheter enters through the umbilical artery, proceeds caudad in the iliac vessels, and then ascends through the abdominal aorta. The catheter course is to the left of midline.

What abnormalities do you find in the two premature infants in Fig. 4.6? The answer is in Appendix 2.

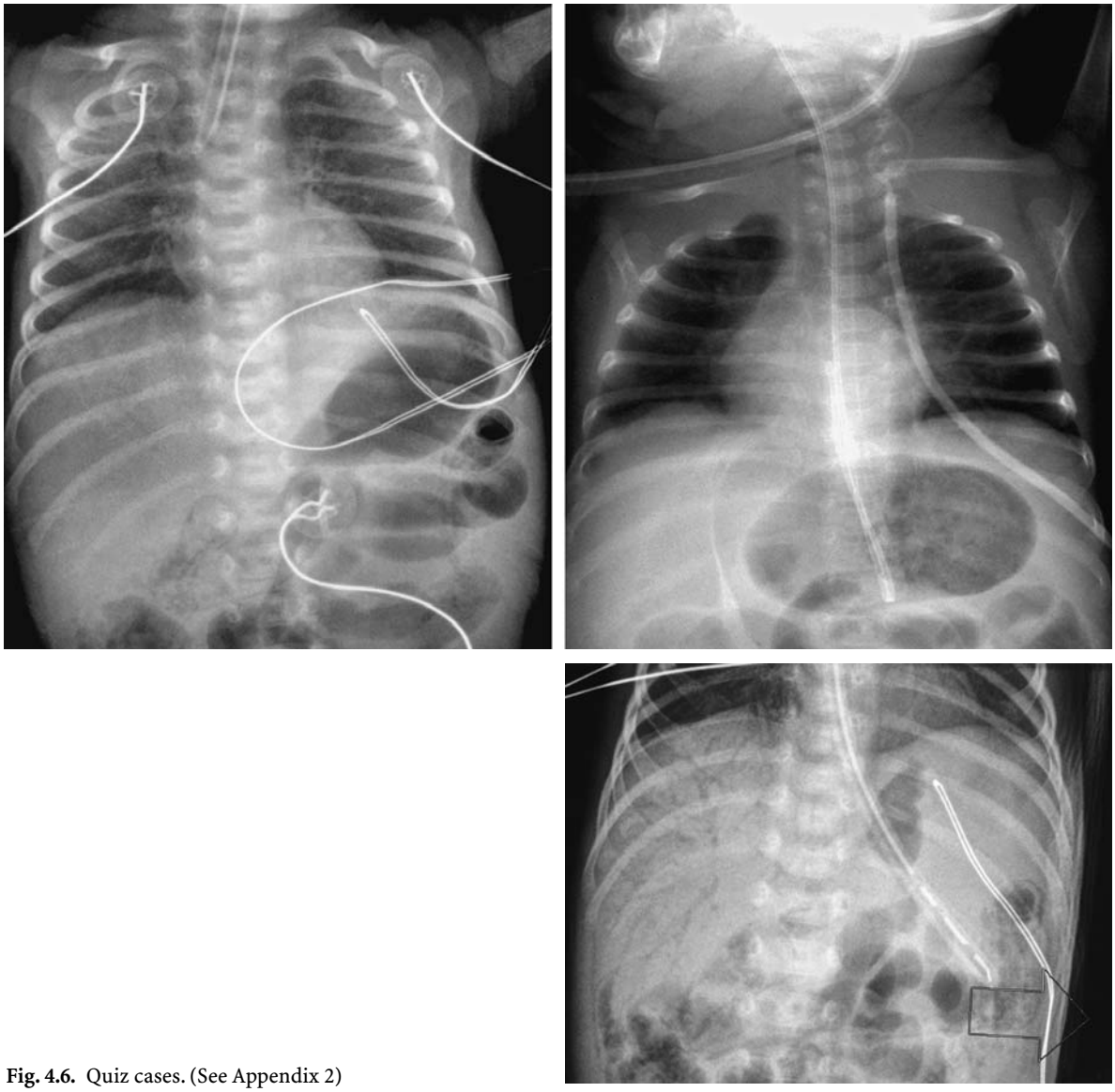

Fig. 4.6. Quiz cases. (See Appendix 2)

Bones and Soft Tissues

As one continues in the imaginary circle around the periphery of the film, the bones and soft tissues should be considered as important clues to the well-being of a baby. There is little subcutaneous fat in normal neonates but abundance of fat in infants of diabetic mothers. Usually the soft tissues are quite inconspicuous. However, edema (anasarca) is found in neonates with hydrops fetalis or hypoproteinemia. A rather common soft tissue density is an umbilical clamp on the residual umbilical cord. It may project as a "mass" in the midabdomen.

Because the neonatal radiograph is the first opportunity for detecting congenital abnormalities, be sure to check the bones for such abnormalities as hemivertebrae, absence of the clavicles, and fractures secondary to trauma of the birth process. The bones also provide a clue to a possible congenital infection (TORCHS infections: toxoplasmosis, rubella, cytomegalic inclusion disease, herpes, and syphilis).

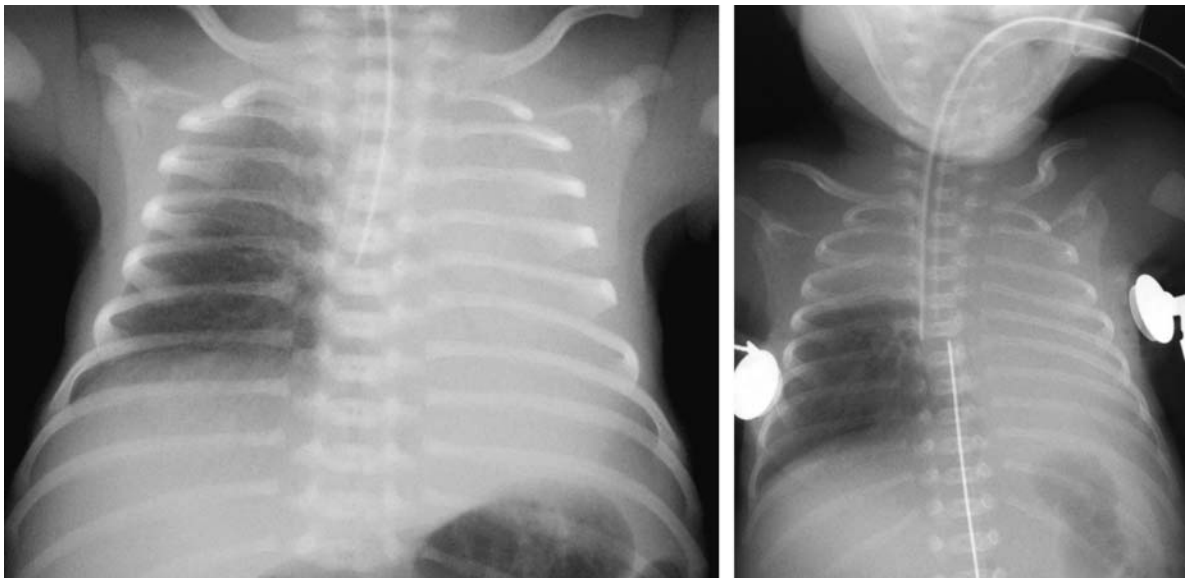

Fig. 4.7. Endotracheal tube position
a This is a neonate with a tube in the right main-stem bronchus. The left lung is atelectatic
b The endotracheal tube in this neonate is in the same position as in **a.** He has both right upper lobe atelectasis and left lung collapse. The airway is so small that a tube plus normal secretions can cause obstruction or ball valve effect in almost any lobe

Chest

Airway

The parameters used to evaluate the extrathoracic and intrathoracic airway are patency, position, and size.

► ***Rule No. 3:*** The airway should be visible on all chest films. To examine the airway in detail, it is frequently useful to use your finger as a pointer so that each structure receives your undivided attention.

In assessing *patency* one should see the airway from the oropharynx and nasopharynx to the right and left main-stem bronchi. The neonate with an obstructed nasal passage presents with severe respiratory distress because the newborn is an obligate nose breather. The only part of the airway not seen on the plain film is the nasal airway. This is best seen with CT. The CT demonstrates not only the various sites of nasal obstruction but also the kind of obstruction – bony or membranous (see Chap. 3).

Regarding *position,* remember that the trachea is *not* a midline structure (the carina projects adjacent to the right pedicles). Buckling of the trachea is normal.

Airway size is difficult to ascertain, as it is a dynamic structure that changes in caliber. However, if on all views the airway is persistently small, further investigation is necessary. It is *normal* for neonates and young infants to occasionally have some air in the esophagus (not so in older children).

Sick neonates often require an endotracheal tube. It is crucial to tell the clinician about the relationship of the tube to the carina because these tubes can move. If they slip into the main-stem bronchus on either side (more frequently on the right, as it is a straighter drop), obstructive emphysema on one side with atelectasis on the other may occur (Fig. 4.7). The ideal position of the endotracheal tube is at the level of the inferior margins of the clavicles.

Mediastinum

The heart and mediastinal structures demand attention as to *position*, *size,* and *contour.*

The *position* is easily determined on a nonrotated film. The aortic arch frequently cannot be seen in a neonate, and its position must be inferred from the position of the carina. On a normal study the carina overlies the right pedicles, and the aortic arch is therefore positioned on the left. Similarly, a right-sided aor-

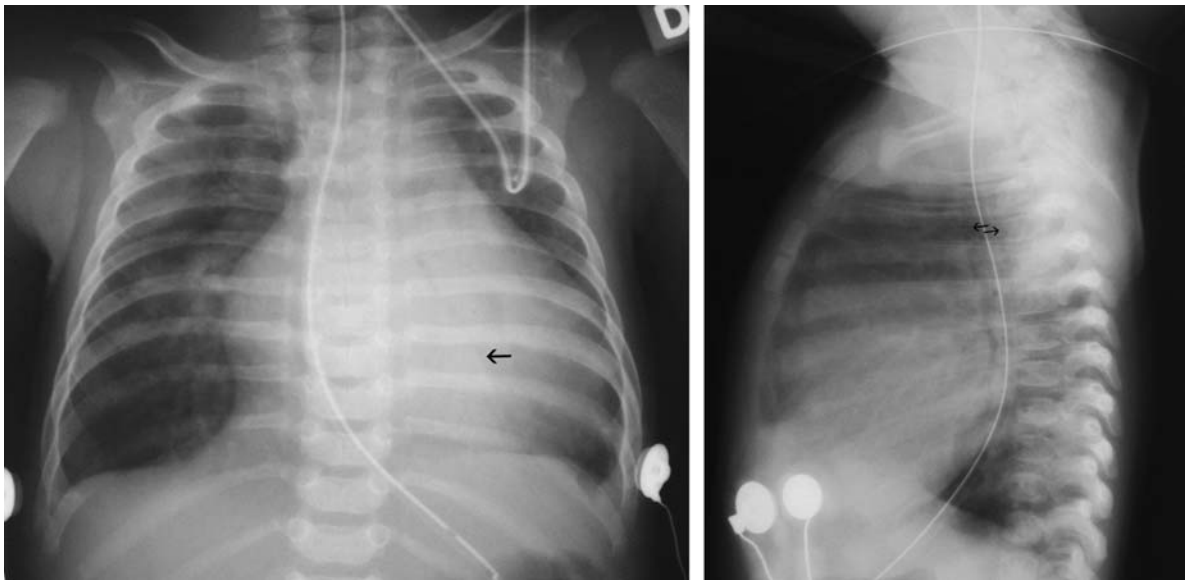

Fig. 4.8. Cardiac enlargement
a Frontal radiograph reveals a nasogastric tube in the stomach. The heart occupies some of the right hemithorax and extends to the left lateral chest wall. The density behind the heart (*arrow*) is atelectasis secondary to impingement on the left mainstem bronchus by the large heart
b On the lateral film, see how the heart extends posterior behind the airway, almost reaching the spine. The airway is pulled backward toward the spine (*arrows* to show the distance between airway and spine)

tic arch may be inferred if the position of the carina is midline or to the left. A right aortic arch should alert the physician to the possibility of congenital heart disease and/or a vascular ring. The thymus constitutes the major portion of the mediastinal silhouette in a normal newborn (see Fig. 4.1; see also Chap. 3). It may extend from the lung apex to the diaphragmatic surfaces, be insinuated into the minor fissure on the right (giving a "sail sign"), and may be bilaterally symmetrical or predominantly one-sided. The normal thymus is situated in the anterior mediastinum and never "pushes" on the airway or any other intrathoracic structure. Because the thymus is so ubiquitous and large, evaluating cardiac size becomes more difficult in the neonate and young infant (the thymus may be seen in some children up to the age of 4–5 years).

Size is the second parameter used in evaluating the mediastinal silhouette.

- ***Rule No. 4:*** A mass must be seen in two planes; i.e., if the heart is really large, it must appear large in two planes.

If the heart is large, it should appear so in both *frontal* and *lateral views.* Since the thymus is in the anterior mediastinum, it is difficult to evaluate heart size on the frontal film. The lateral roentgenograph is most valuable in this regard (Fig. 4.8). The retrocardiac air space should be seen, and one of two lines described in Chap. 3 should not intersect the heart (see Chap. 3, Fig. 3.31).

The *contour* of the heart, the third parameter, is considered to be helpful in determining the specific nature of congenital heart defects. A narrow cardiac base is described in transposition of the great vessels and a "boot-shaped" heart in tetralogy of Fallot. Clinically these signs may not be very important as echocardiography most often can give a specific diagnosis. However, in infants as in older children, pulmonary vascular changes may give the clue to the general category of the cardiac disease, for example, a left-to-right shunt. In contrast to the older child, the pulmonary vessels of a newborn can be seen at the hila and only in the medial third of the lungs. Vessels should be hard to find in the lateral two-thirds of the normal lung. When there is vascular congestion secondary to congestive heart failure or over-circulation from a left-to-right shunt, the vascularity becomes much easier to see in the lateral two-thirds of the lung. It is much more difficult, however, to detect decreased pulmonary vascularity (as found in severe pulmonic stenosis or atresia).

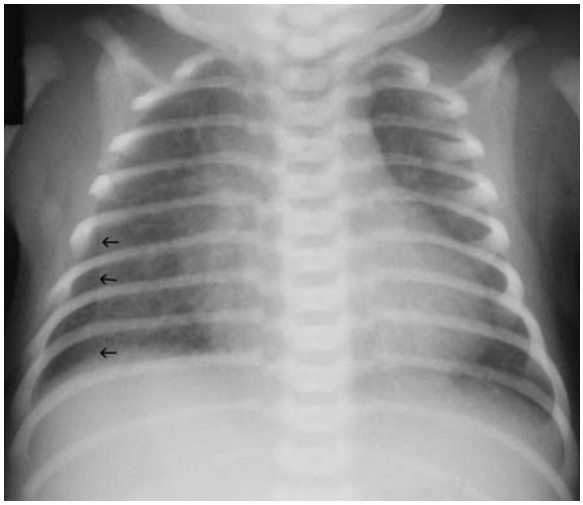

Fig. 4.9. Skin fold.
The apparent pneumothorax on the right is actually a skin fold (*arrows*), easily determined when the margin does not conform to that of a collapsed lobe or lung. If uncertain, repeat the film after moving the baby to a different position, for example, decubitus view. There are lung markings lateral to the skin fold

Deceptive Shadows

One of the most common mistakes in diagnosing a pneumothorax is confusing it with a skin fold (Fig. 4.9). This error can be avoided by realizing that the border of the fold does not conform to the position that a collapsed lobe or lung would assume. In addition, the skin fold is frequently seen extending off into the axilla. If you are uncertain, a repeat film with the baby in another position is helpful, or perform a cross-table lateral.

Another important finding on a neonatal chest film is the "ductus bump," seen best on the frontal view at the level of the pulmonary artery (Fig. 4.10). This is formed by the superimposition of the main and left pulmonary artery on the patent ductus arteriosus, and it usually is not visible by day 3. It cannot be seen on the lateral film. The scapula, however, may create a pseudomass in this region.

The following summarizes the assessment of the neonatal chest and also lists questions to ask oneself about each film and specific parameters for evaluating the airway, mediastinal silhouette, and lungs. Remember the ABCS and Rule No. 1. General considerations are:

- Lung volume: Are the lungs hyperinflated?
- Position of patient: Is the patient rotated? Why?

Table 4.1. Differential diagnosis of respiratory distress in the newborn

Systemic diseases
Sepsis
Profound anemia
Hypothermia
Hypovolemic – shock
Electrolyte imbalance
Adrenal insufficiency
Severe acidosis
Extrathoracic causes
Central nervous system
Hemorrhage
Vein of Galen malformation
Tumor
Trauma (include cord laceration)
Increased pressure including hydrocephalus
Extrathoracic airway obstruction
Neuromuscular
Werdnig-Hoffmann disease
Skeletal abnormalities
Osteogenesis imperfecta
Thanatophoric dwarfism
Asphyxiating thoracic dystrophy of Jeune
Abdominal
Perforation
Necrotizing enterocolitis
Obstruction
Mass or visceromegaly
Ascites
Intrathoracic causes
Surgical (or potentially surgical)
Congenital heart anomalies
Diaphragmatic hernia
Congenital cystic adenomatoid malformation
Congenital lobar emphysema
Esophageal atresia +/– fistula
Pleural effusions
Chyle
Blood
Pus
Complication of airblock
Pneumothorax
Pneumomediastinum
Progressive pulmonary interstitial emphysema
Patent ductus arteriosus
Medical
Transient tachypnea of newborn (retained fetal fluid)
Aspiration syndromes including meconium aspiration
Persistent pulmonary hypertension
Congenital pneumonia
Hyaline membrane disease
Bronchopulmonary dysplasia
Pulmonary hemorrhage

With permission modified from [1].

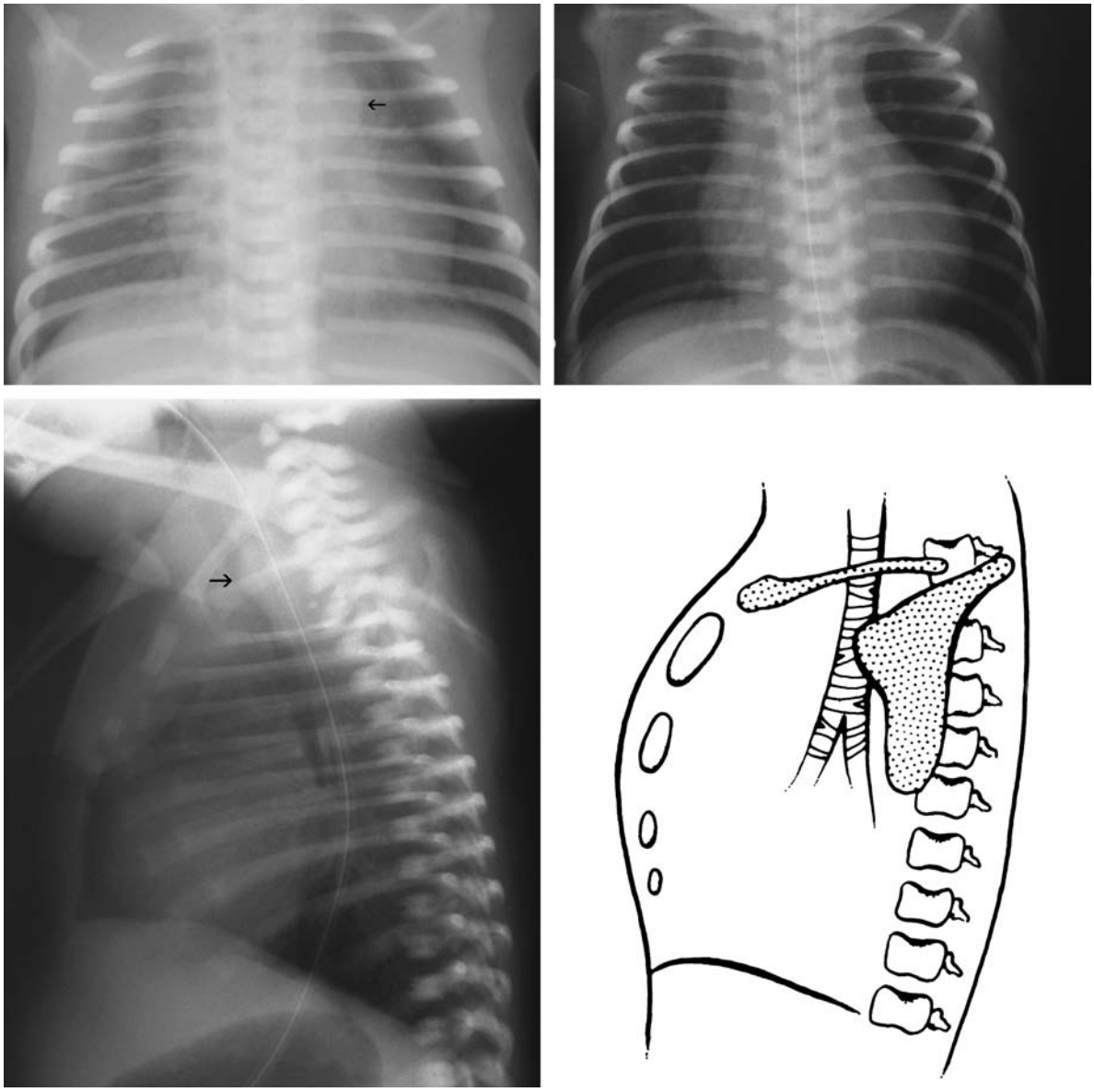

Fig. 4.10. Pseudomasses
a, b "Ductus bump." Frontal views of the chest in an infant 1 day (**a**) and 3 days old (**b**). The "bump" (*arrow*) in the upper mediastinum on **a** is no longer visible on **b**. It was caused by the superimposition of the main pulmonary artery, left pulmonary artery, and ductus arteriosus. The latter gradually retracts, and the mass disappears
c This lateral film shows another pseudomass. The trachea looks as if it is being compressed posteriorly by a mass (*arrow*)
d In fact, the "mass" is caused by superimposition of the scapula over the airway

- Exposure: Is the film properly exposed? How do you know?
  Specific factors include:
- Airway
  - Patency
  - Position
  - Size
- Mediastinal silhouette
  - Position
  - Size
  - Contour
- Lungs (see Table 4.1)
  - Volume
  - Pulmonary density
  - Vascularity

Table 4.2. Differential diagnosis of lung pathology based on lung volume and type of density

Lung volume	Type of density	Disease considerations
Increased (generalized)	None	Aspiration syndromes Congenital heart disease
Increased (first days)	Multiple course areas (Strand-like densities following bronchovascular patterns)	Meconium aspiration Retained fetal fluid (TTN)
	Localized	Pneumonia
Increased (generalized)	Increased pulmonary vascularity Fine, lacelike, strand-like lines or cysts	Congenital heart disease Pulmonary interstitial emphysema Bronchopulmonary dysplasia
Increased >1st week–months	None	Chronic aspiration, cystic fibrosis, congenital heart disease
Normal or decreased	Homogeneous fine granular (ground-glass) density with air bronchograms	Hyaline membrane disease (RDS and HMD) Group B β-hemolytic streptococcal pneumonia
Variable	Variable	Persistent pulmonary hypertension Group B β-hemolytic streptococcal infection
Localized increase in volume	Air-filled	Lobar emphysema
	Fluid-filled	Bronchial obstruction (lobar emphysema initially, congenital cyst, bronchogenic cyst)
	Air and/or fluid filled	Cystic adenomatoid malformation

With permission from [1].
TTN=transient tachypnea of the newborn; RDS=respiratory distrea syndrome.

An Approach to Common Neonatal Abnormalities

Respiratory distress is a symptom, not a disease. The symptom complex includes tachypnea, retractions, nasoflaring, grunting, and cyanosis. It can be caused by many systemic and extrathoracic causes as well as intrathoracic causes (both medical and surgical) (Table 4.1).

Correlation of the generalized lung volume (increased, decreased, normal) with type of pulmonary opacity leads to the differential diagnoses of neonatal lung disease (Table 4.2). Since the lung volume has already been assessed, differentiating the various forms of pulmonary opacity is the next task. You should ask yourself the following questions:

- What is the gestational age of the patient (Table 4.3)?
- Are the opacities uniform and homogeneous (Fig. 4.11)?
- Do the opacities correspond to the distribution of blood vessels or bronchi (Fig. 4.12)?
- Do they involve the whole lung or a portion of the lung (Fig. 4.13)?

Table 4.3. Diseases correlate with gestational age

Premature (24–34 weeks)
Immature lung
Hyaline membrane disease
Persistent pulmonary hypertension
Near term (34–37 weeks) and term (38–42 weeks)
Retained fetal fluid
Aspiration syndromes including meconium aspiration
Persistent pulmonary hypertension

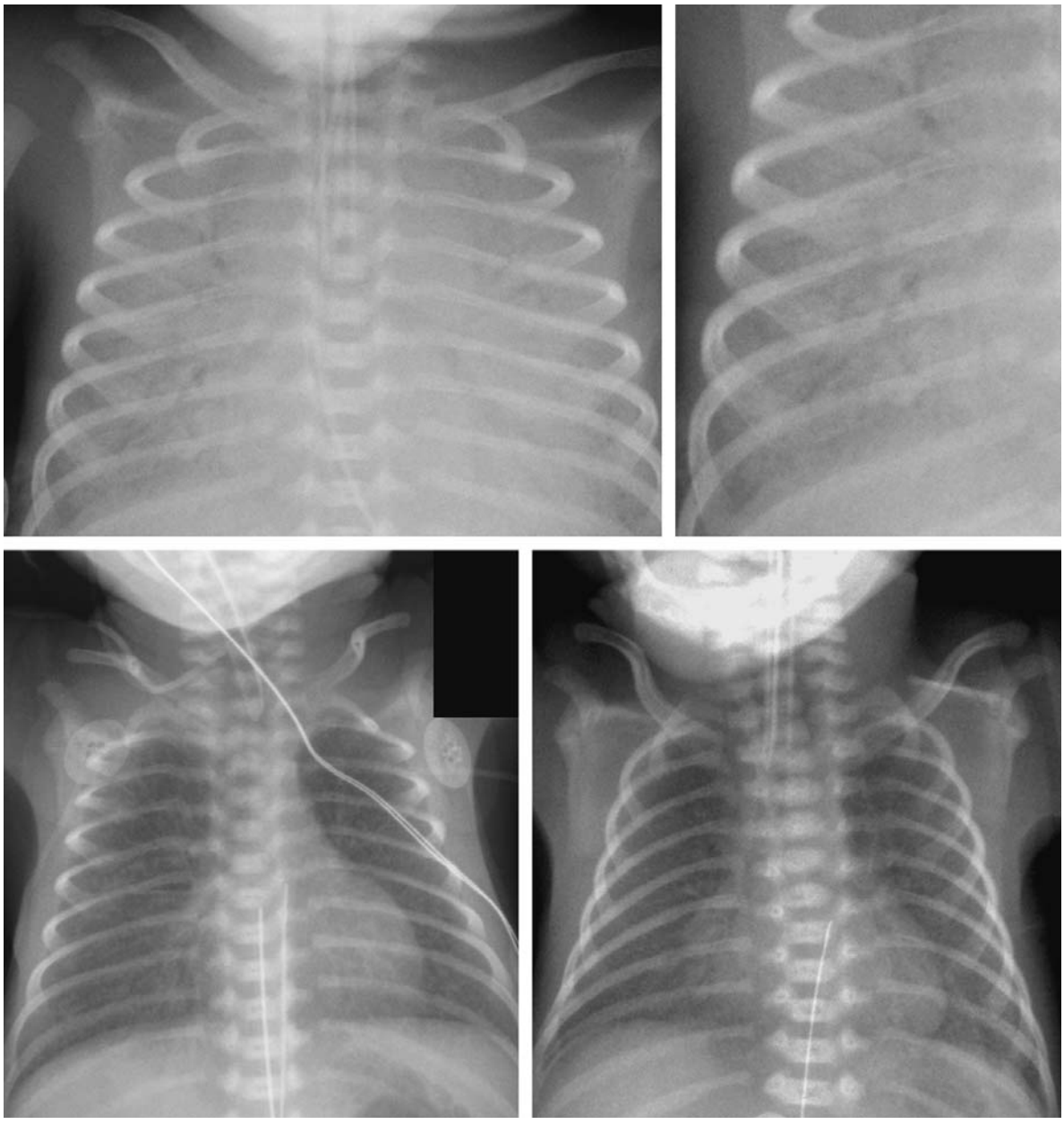

Fig. 4.11. Hyaline membrane disease
a Frontal radiograph of a premature infant demonstrates "ground-glass" appearance of both lungs with a normal volume. The endotracheal tube is at the carina
b Frontal magnified view of the granular appearance caused by the atelectatic surfactant-deficient alveoli (terminal air sacs)
c, d Two premature neonates with hyaline membrane disease already treated with surfactant delivered through the endotracheal tube. The disease has been modified from **a** and **b**. The improvement of the lungs is random as various amounts of surfactant go into each lung

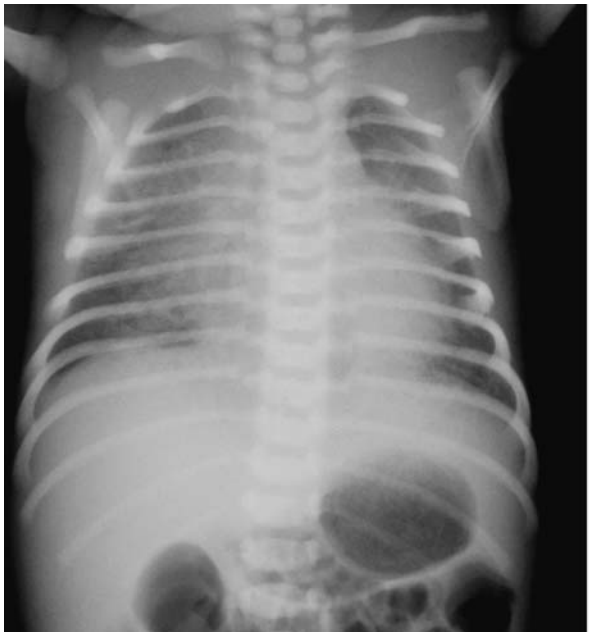

a

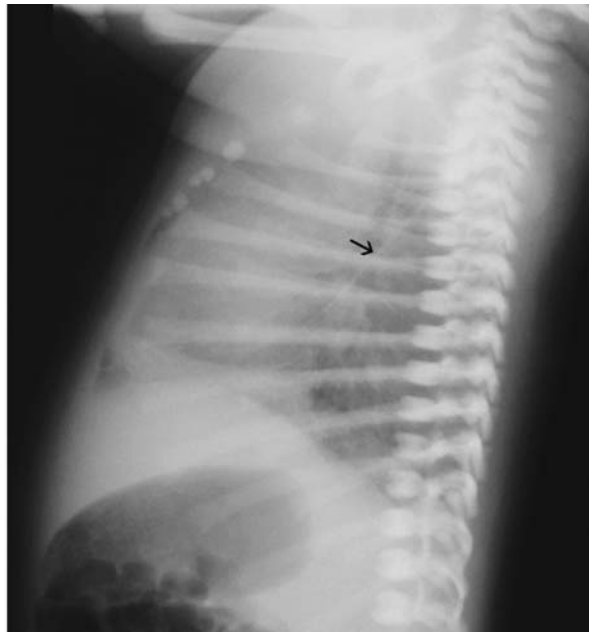

b

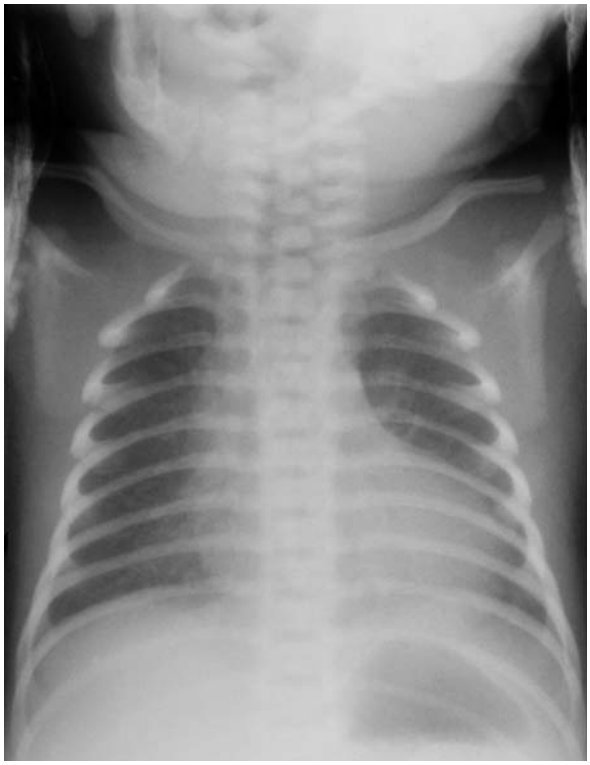

c

Fig. 4.12. Transient tachypnea of the newborn (retained fetal fluid)
a This frontal film of a newborn infant born by cesarean section reveals strand-like densities extending from the hila throughout both lungs. The heart is not enlarged. Lung volume is increased
b Lateral film shows fluid in the major fissure (*arrow*)
c Frontal radiographs of the same child 2 days later. Chest is normal

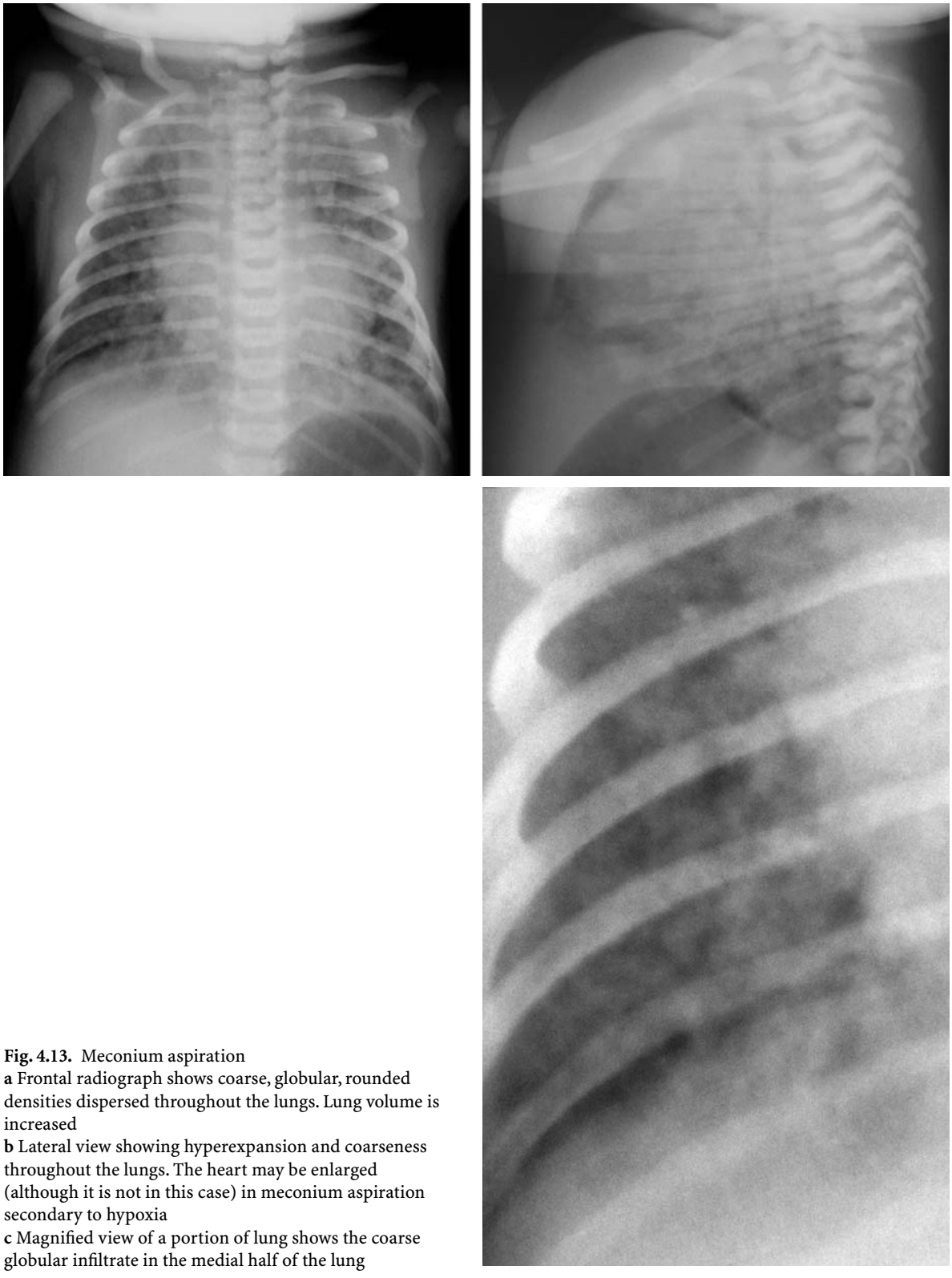

Fig. 4.13. Meconium aspiration
a Frontal radiograph shows coarse, globular, rounded densities dispersed throughout the lungs. Lung volume is increased
b Lateral view showing hyperexpansion and coarseness throughout the lungs. The heart may be enlarged (although it is not in this case) in meconium aspiration secondary to hypoxia
c Magnified view of a portion of lung shows the coarse globular infiltrate in the medial half of the lung

Diseases with Generalized Increase in Lung Volume

Increased lung volume may be the first and only clue to significant parenchymal or cardiovascular abnormalities in the neonate. From a teleological point of view, the lungs are hyperexpanded as the infant tries desperately to adapt to its new environment and cannot oxygenate optimally (Fig. 4.1). Any of the aspiration syndromes (discussed below), pneumonias, or congenital heart diseases may present with relatively clear lungs and hyperexpansion. However, there are frequently opacities within the lung parenchyma or other clues, such as pulmonary vascularity and cardiac size (see above), that point to the correct diagnosis.

Two conditions can be readily anticipated from changes the fetus undergoes from intrauterine to extrauterine life. First, the neonate may not be able to clear all the fetal fluid from its lungs (see Fig. 4.12). Since one-third of the fluid exits through the tracheobronchial tree and is expelled when the thorax is compressed in the birth canal, tracheobronchial obstruction or a cesarean section (in which the infant's chest is not compressed) may lead to retained fetal fluid – the wet lung syndrome – radiographically. These babies have increased lung volume and strand-like opacities emanating from the hila that follow the course of the tracheobronchial tree (with the vessels and lymphatics). Pleural fluid may also be present; it outlines the lung fissures. Retained fetal fluid usually clears within 24–48 h (transient tachypnea of the newborn is another name for this entity).

The second abnormality that can result from the birth sequence is aspiration (see Fig. 4.13). The most serious kind is meconium aspiration. A fetus passes meconium in utero because of some perinatal stress. At the first breath this viscous material may be inhaled. The radiograph shows increased lung volume, but this time there are *patchy* opacities throughout both medial lungs. Meconium in the tracheobronchial tree and lung parenchyma presents a striking picture (see Fig 4.13).

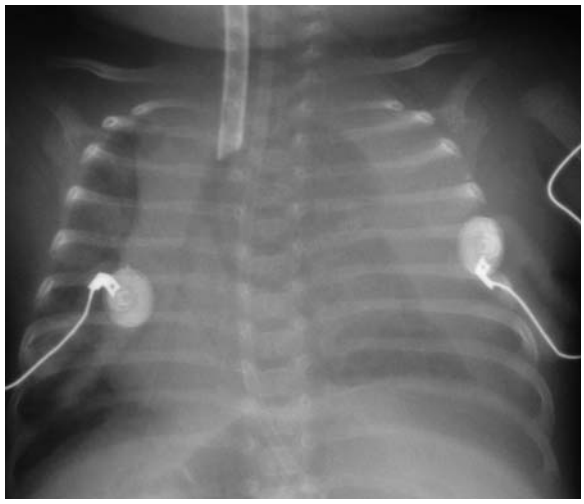

Fig. 4.14. Group B β-hemolytic streptococcal disease. The frontal view of a 2-day-old shows extensive opacity in the left side of the chest due to both an infiltrate and a large pleural effusion. The mediastinum is shifted to the right

Early hyperexpansion of the neonatal lung may herald a localized infiltrate, such as a pneumonic consolidation that does not become visible for a few days (Fig. 4.14). In a neonate with congenital heart disease, the first radiographic sign may well be increased volume only. As pulmonary resistance decreases, signs of a left-to-right shunt or cardiac enlargement become evident. It is important to note that a large heart does not necessarily mean primary congenital heart disease; anemia, asphyxia, and other high-output states may cause cardiomegaly as well.

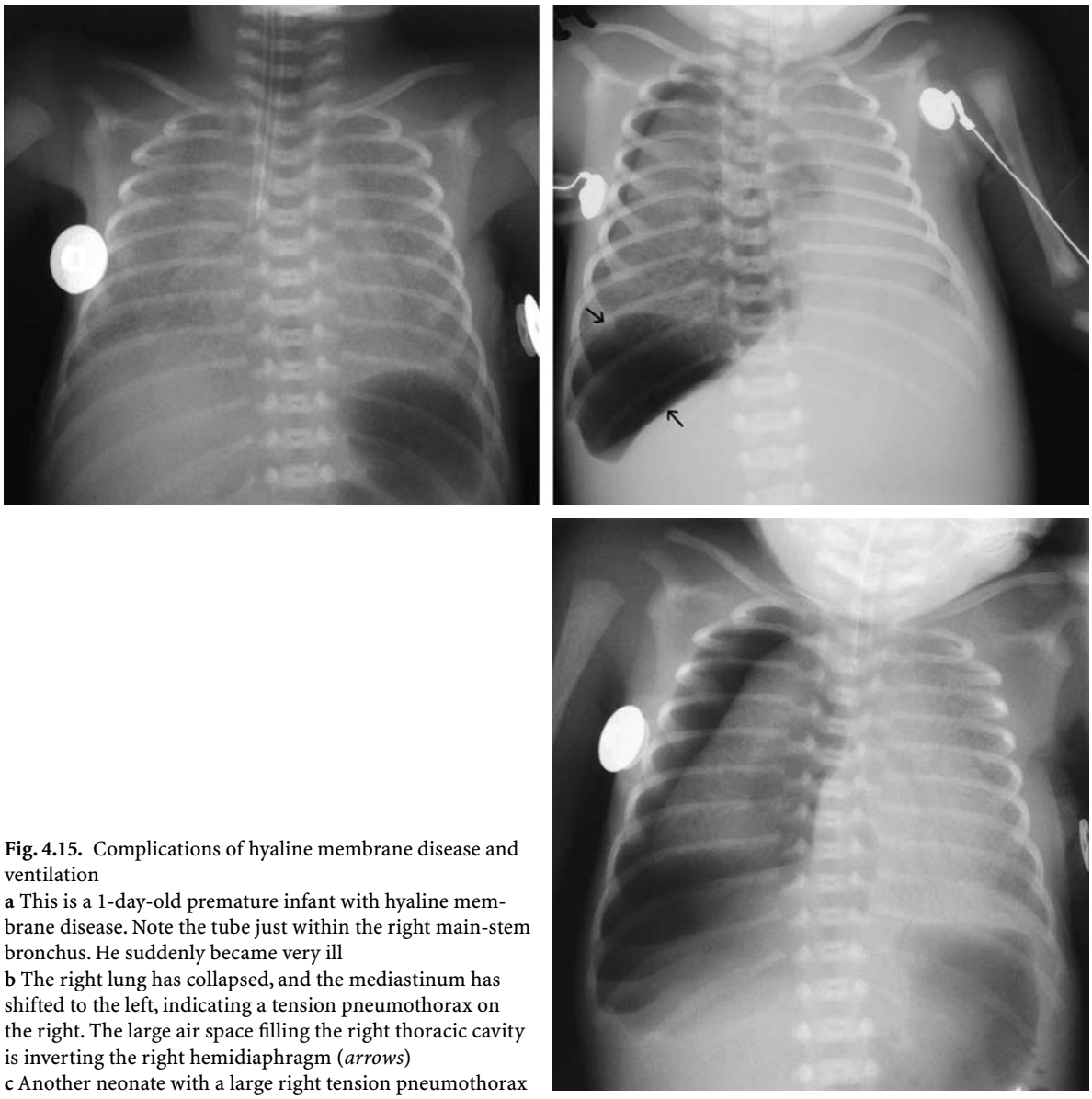

Fig. 4.15. Complications of hyaline membrane disease and ventilation
a This is a 1-day-old premature infant with hyaline membrane disease. Note the tube just within the right main-stem bronchus. He suddenly became very ill
b The right lung has collapsed, and the mediastinum has shifted to the left, indicating a tension pneumothorax on the right. The large air space filling the right thoracic cavity is inverting the right hemidiaphragm (*arrows*)
c Another neonate with a large right tension pneumothorax

Diseases with Normal or Decreased Lung Volume

The most common disease in this group is hyaline membrane disease. Unfortunately, group B β-hemolytic streptococcal pneumonia may appear indistinguishable from it. In both diseases homogeneous, fine opacities appear throughout the lungs with accompanying air bronchograms. This sign has been described as a "ground-glass appearance" (see Fig. 4.11). In hyaline membrane disease these changes are related to surfactant deficiency; therefore, the terminal air spaces tend to collapse, resulting in a low normal to decreased lung volume. The collapse of the terminal air spaces accounts for the fine, homogeneous granularity. Remember to look for air bronchograms. You must see the granularity or white dots all the way out the edge of the lungs to make a diagnosis of hyaline membrane disease. Prematurity and maternal diabetes are two of the more common underlying etiological factors predisposing to this disease. The classic picture of hyaline membrane disease has now been modified because surfactant is frequently given immediately after birth as soon as the child is intubated. This chest film is less severely af-

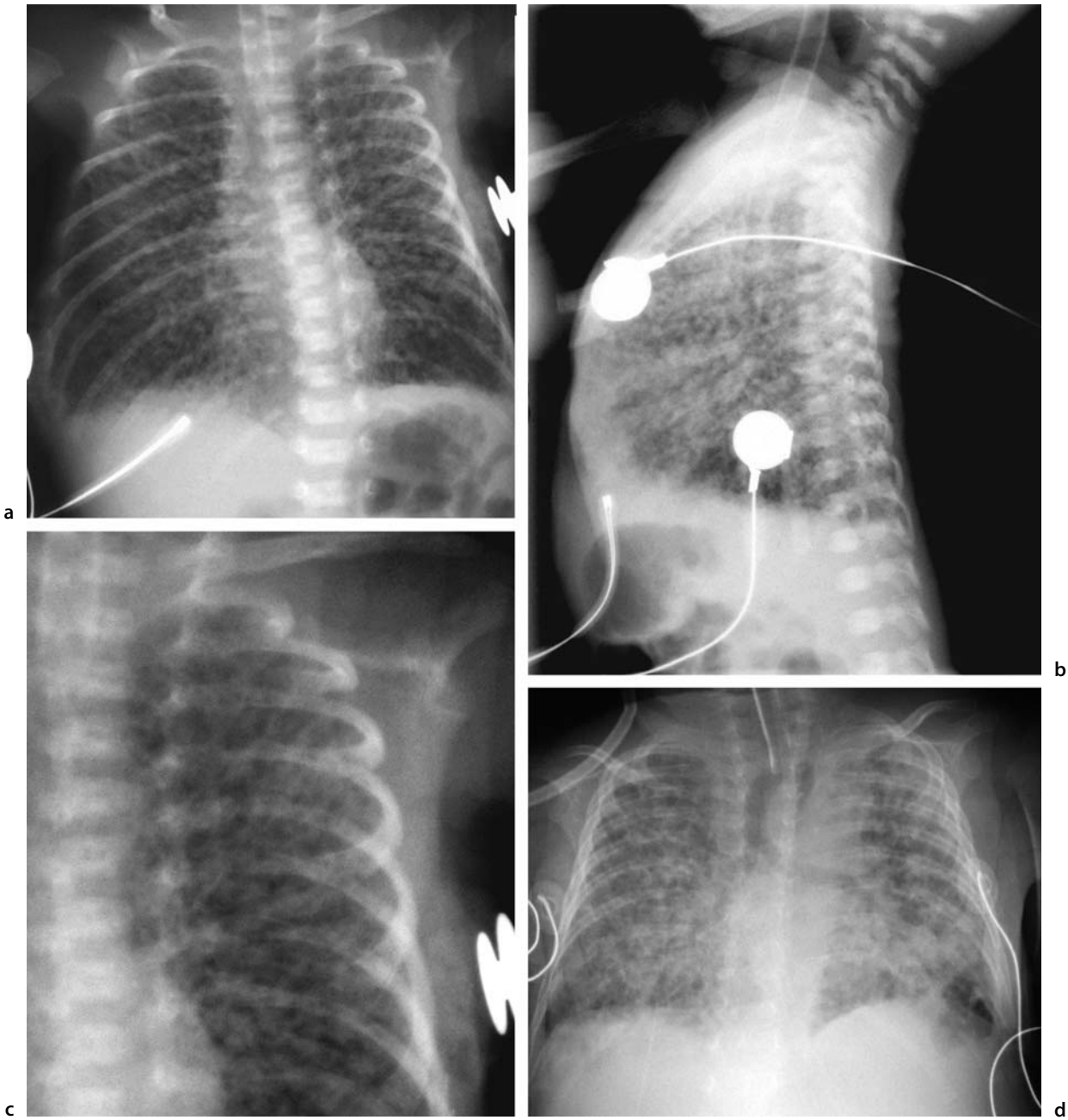

Fig. 4.16. Pulmonary interstitial emphysema
a On this film of a 6-day-old premature neonate, there is interstitial air manifest as black dots. The high pressures necessary to ventilate the child caused air to leak into the interstitium. This may compress the bronchus and, in fact, hinder aeration
b The lateral view showing interstitial air as small black dots. This complication of mechanical ventilation occurs when high pressures are used and ventilation is prolonged
c Magnified image of "black dots"
d An image of another patient with similar disease demonstrates the pulmonary interstitial emphysema

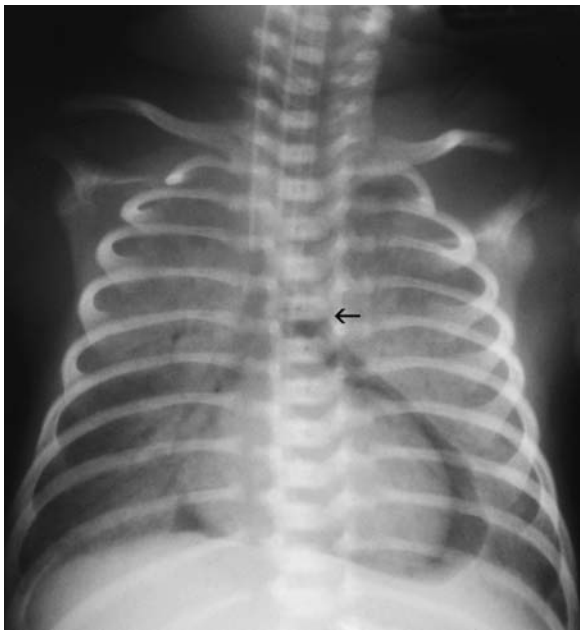

Fig. 4.17. A pneumopericardium
A frontal radiograph shows air around the heart. The air stops at the left aortic–pulmonary window where the pericardium attaches (*arrow*)

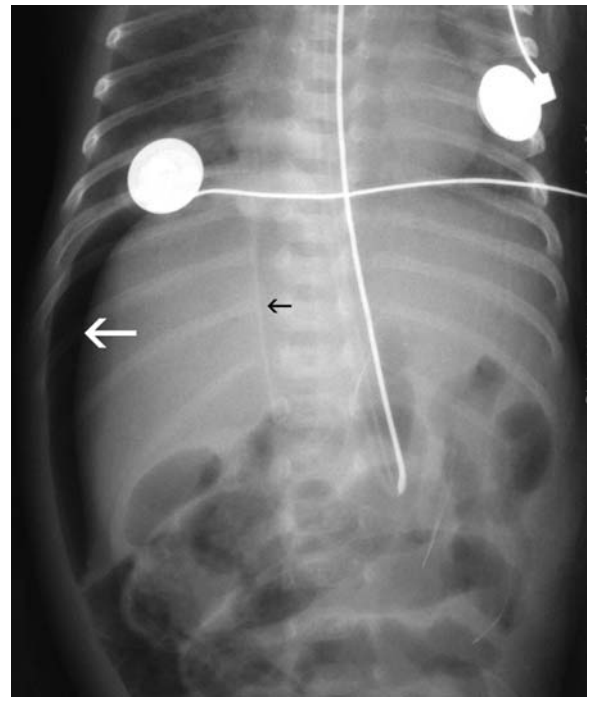

Fig. 4.18. Pneumopericardium or pneumomediastinum can pass through the various esophageal hiatus into the peritoneal cavity
On this decubitus roentgenograph with the baby's right side up, air is noted above the liver (*white arrow*). The falciform ligament is seen (*black arrow)*

fected and is asymmetrically involved because the surfactant (administered through the endotracheal tube) is randomly distributed throughout the lungs (Fig. 4.11).

Mechanical ventilation often causes air to leak into the interstitium of the lungs (pulmonary interstitial emphysema), into the mediastinum (pneumomediastinum), into the pleural space (pneumothorax), and occasionally into the pericardium (pneumopericardium; Figs. 4.15–4.17). Rarely, air dissects into the peritoneal cavity (Fig. 4.18). A summary of the complications of the premature infants' disease and therapy is found in Table 4.4.

One of the most difficult conditions for the novice to recognize is the pneumomediastinum. Radiographically, three different densities or shades of gray are visible on the frontal film (Fig. 4.19). The first is the white opacity of the heart. The second – the pneumomediastinum – is a radiolucent black area lateral to the heart and medial to the lungs that may elevate the thymus laterally and upward. The third is a gray opacity representing lung compressed laterally by trapped air.

Table 4.4. Complications of premature infant therapy

Air leak
Pulmonary interstitial emphysema
Pneumomediastinum
Pneumopericardium
Pneumothorax
Pneumoperitoneum
Air embolism
Misplaced and perforated tubes
Endotracheal
Oro- or nasogastric
Vascular catheters
Chest tube within the lung (bronchopleural fistula)
Nutritional deficiencies or complications of therapy
Rickets of premature
Gallstones – secondary to hyperalimentation
Renal stones – secondary to diuretic therapy (furosemide)
Other
Central nervous system hemorrhage
Line infection and vascular thrombosis
Sepsis
Oxygen toxicity – retinopathy of prematurity

With permission from [1].

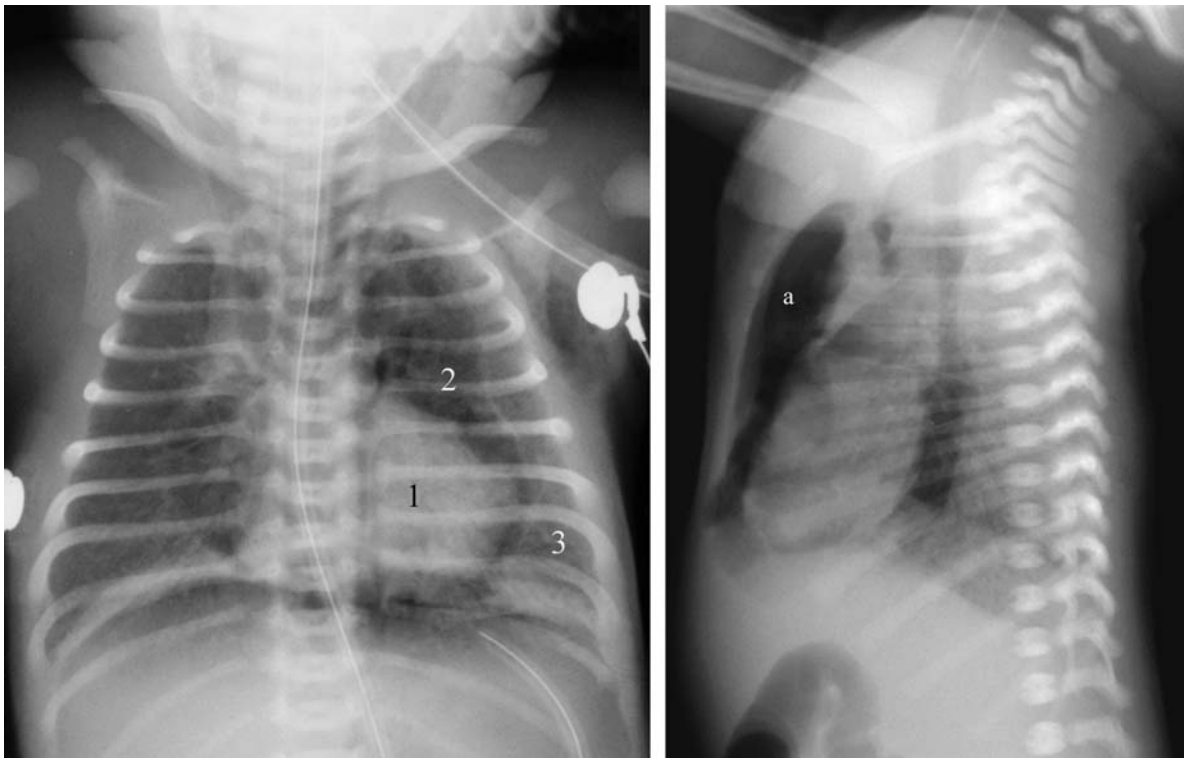

a b

Fig. 4.19. Pneumomediastinum
a This frontal view of the chest reveals three densities: *1,* heart; *2,* pneumomediastinum; and *3,* compressed lung. The abdomen is "lucent" because of air dissected down into the abdomen causing a pneumoperitoneum
b Lateral film showing air in the mediastinum (*a*)

A pneumomediastinum may be very small and difficult to differentiate from a pneumopericardium (see Fig. 4.17). When a pneumopericardium is present, separation of the aorta from the pulmonary artery is clearly seen on both frontal and lateral views, since the pericardium attaches at the base of the great vessels. In addition, the pericardial membrane may be visible when there is air on both sides of it.

Air can dissect upward into the subcutaneous tissues of the neck (unusual in a neonate) and downward through the same diaphragmatic hiatus as the aorta and esophagus pass, resulting in a pneumoperitoneum (see Fig 4.18).

The most important air leak, however, is that of a pneumothorax. Pneumothoraces are formed by rupture of air through the overlying pleura or by rupture of a subpleural bleb (see Fig. 4.15). Once there is a rupture of air by whatever mechanism into the pleural space, the lung begins to collapse. Since the infant is recumbent, an anterior and medial air space may appear first or may outline the inferior lung margins. Look for the pleural margins of the lobe of the lung. Beware of skin folds that may simulate pleura (Fig. 4.9). As the quantity of air increases and the lung collapses to its fullest, i.e., the elastic limit is reached, the pressure builds up and a *tension pneumothorax* develops. This results in: (a) shift of the mediastinum away from the midline and (b) flattening or even inversion of the diaphragm on the affected side. (If by chance the pneumothorax is bilateral, there may be no or less mediastinal shift, but then the heart is compressed and appears smaller.) At first, these changes may be so subtle that the pneumothorax becomes apparent only in comparison with previous films.

► ***Rule No. 8:*** Always review all old films to properly assess the new one. Subtle findings can easily be missed when a single previous examination is reviewed.

A common problem in infants with hyaline membrane disease is the patent ductus arteriosus, causing a left-to-right shunt. The classic roentgenographic

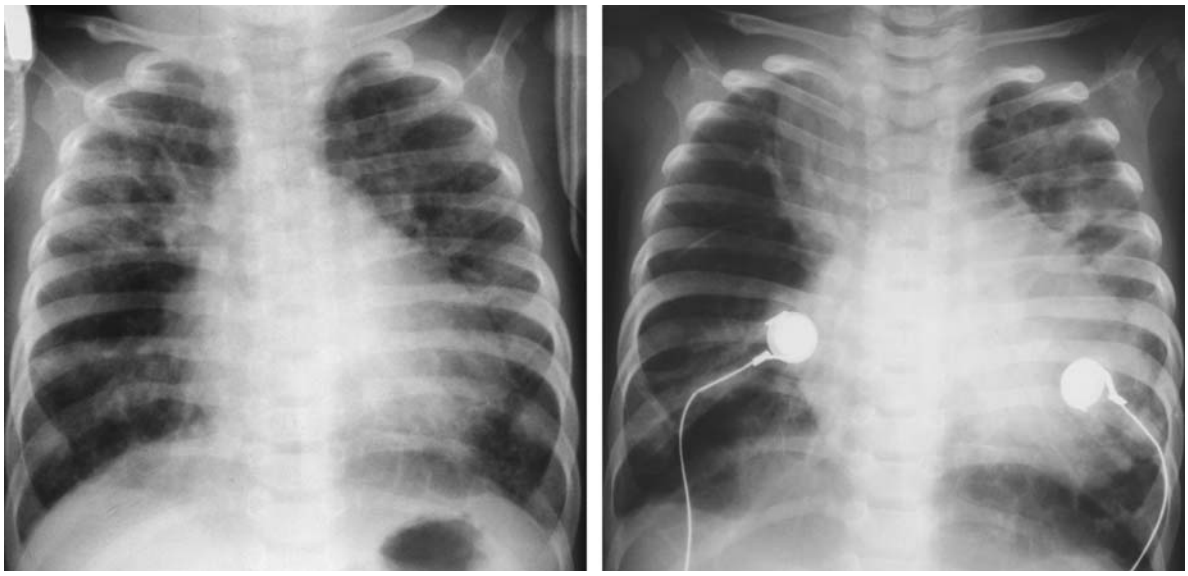

a b

Fig. 4.20. Sequelae of hyaline membrane disease and mechanical ventilation
a This 6-month-old had severe hyaline membrane disease requiring assisted ventilation for over 1 month; at the time this film was taken he was still on supplemental oxygen. The heart is enlarged, and there are fibrous changes throughout both lungs with uneven expansion. The lungs are very hyperexpanded
b At 1 year of age further enlargement of the heart has occurred, and there is increasing emphysema. The areas of fibrosis have now coalesced. There is some cyst formation in the left midlung and left base. This child died at 18 months of age of chronic respiratory insufficiency

signs of a patent ductus arteriosus are an enlarging heart, enlarging liver, and increasing pulmonary vascularity. These, however, are late signs and may be masked by the parenchymal changes of hyaline membrane disease. In infants with hyaline membrane disease, the only clues to a coexistent patent ductus arteriosus may be (a) lack of improvement after 3 days of adequate therapy for hyaline membrane disease and (b) increasing perihilar haze. These roentgenographic findings are frequently noted before the clinical signs of a bounding pulse or a murmur.

While most infants recover from hyaline membrane disease, 15 % go on to develop chronic lung disease of the newborn, formerly called bronchopulmonary dysplasia (Fig. 4.20). This disease is most likely the result of a combination of pulmonary insults due to severe hyaline membrane disease, high oxygen concentration, prematurity of lungs, and prolonged high-pressure mechanical ventilation (barotrauma). Cystic (air-trapped) areas appear in the lung parenchyma, intermixed with areas of fibrosis and atelectasis and generalized emphysema. The lungs become congested secondary to "leaking" capillaries.

Diseases with Variable Lung Volume

In utero, oxygenated blood flows from the placenta via the umbilical vein and then is divided, with half of the blood flowing to the liver and half going through the ductus venosus to the inferior vena cava and right heart. Since there is no need for blood flow in the lungs as no oxygenation is occurring in the lungs, the blood crosses the foramen ovale, fills the left atrium, left ventricle, and is ejected into ascending aorta to present the brain with oxygenated blood. Blood returning to the superior vena cava passes through the right heart and pulmonary artery to the ductus arteriosus into the descending aorta and back to the placenta. The shunting of blood away from the lungs occurs because of high pulmonary resistance. Persistence of this fetal circulation after birth is called persistent pulmonary hypertension. It is found in such diverse diseases as congenital diaphragmatic hernia, meconium aspiration, and, unfortunately, in cases in which there is no explanation. The radiographic finding is quite variable and no specific pattern is recognized as characteristic of persistent pulmonary hypertension. It is a clinical diagnosis made in the hypoxic neonate without structural heart disease.

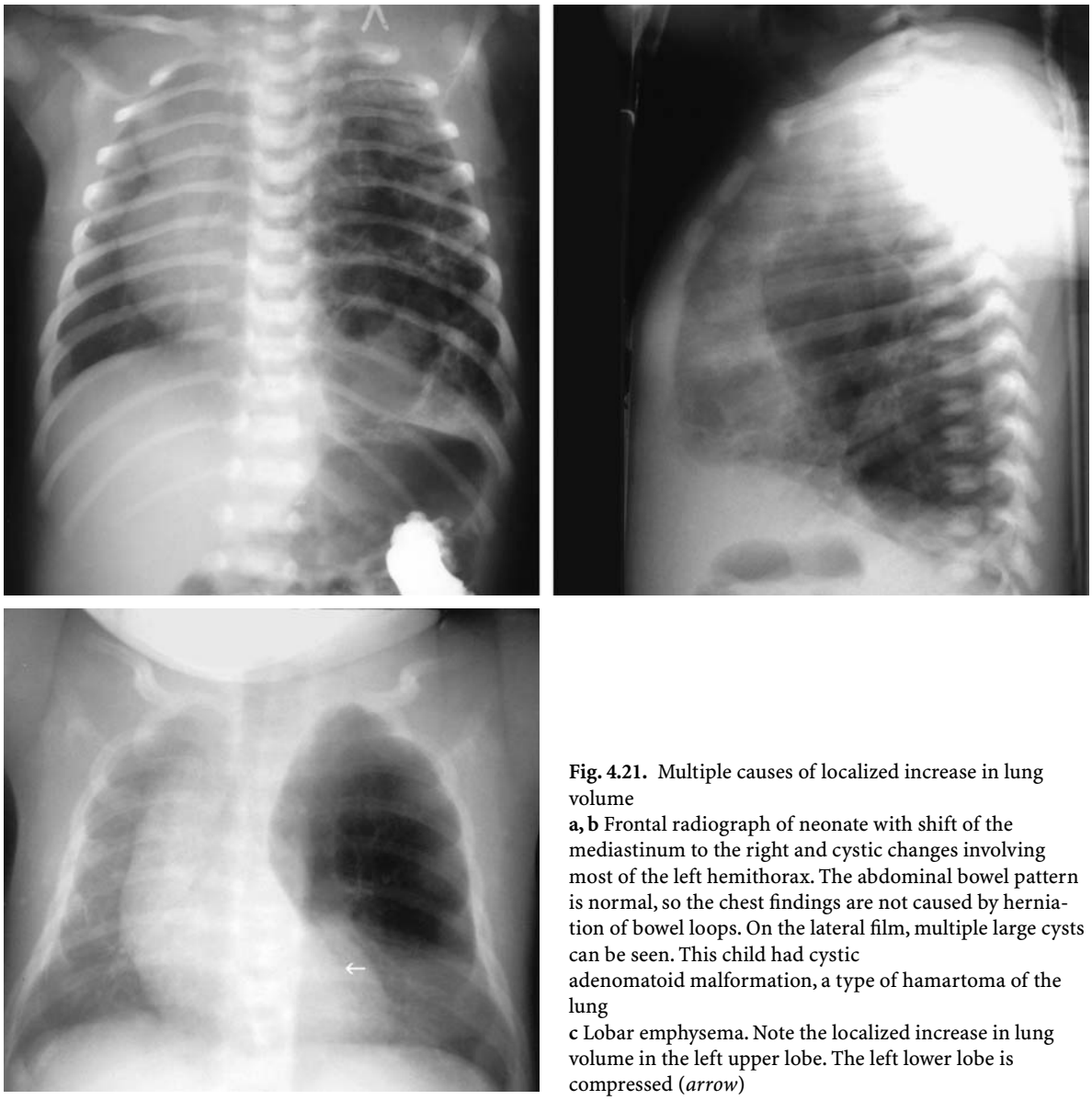

Fig. 4.21. Multiple causes of localized increase in lung volume
a, b Frontal radiograph of neonate with shift of the mediastinum to the right and cystic changes involving most of the left hemithorax. The abdominal bowel pattern is normal, so the chest findings are not caused by herniation of bowel loops. On the lateral film, multiple large cysts can be seen. This child had cystic adenomatoid malformation, a type of hamartoma of the lung
c Lobar emphysema. Note the localized increase in lung volume in the left upper lobe. The left lower lobe is compressed (*arrow*)

Localized Changes in Lung Volume

Localized increases in lung volume can be either air-filled or fluid-filled (Fig. 4.21). Since in utero the lung is filled with fluid, obstruction of a bronchus traps the fluid, delays resorption, and causes a localized increase in lung volume or a "mass" lesion. This compresses adjacent lobes and frequently shifts the mediastinum contralaterally. As the fluid is absorbed, it is replaced by air, but lung markings are not seen.

Classically this is associated with lobar emphysema or any condition obstructing a main-stem bronchus (e.g., intrinsic stenosis, bronchogenic cyst, pulmonary artery sling). Fine strands of tissue seen within the lucency indicate the presence of cysts. The commonest cystis lesion is congenital adenomatoid malformation. The lack of a defined *pleural* marking excludes pneumothorax.

- ***Rule No. 5:*** An esophagram must be performed in any child with unexplained respiratory disease. It is simple, inexpensive, and informative.

In the neonate as in the older child, unexplained airway disease should prompt an esophagram, which may be carried out initially with a tube in the esoph-

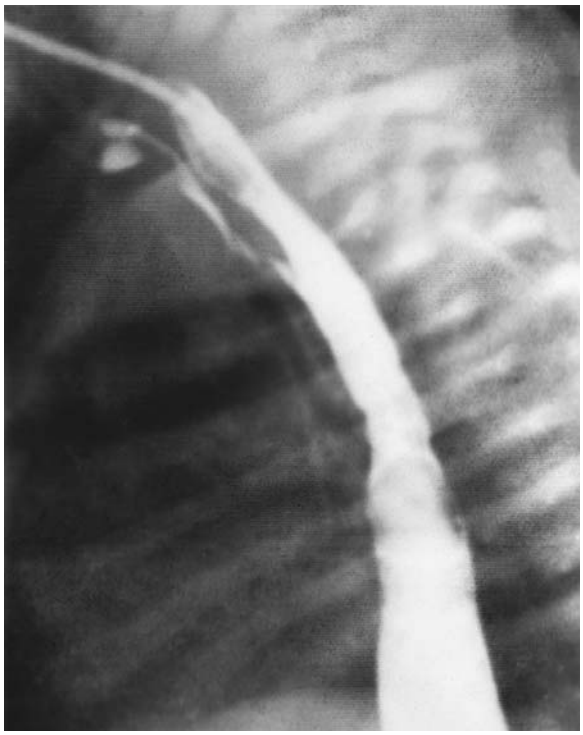

Fig. 4.22. "H-type" tracheoesophageal fistula in an infant with chronic pneumonia. This lateral view of an esophagram demonstrates an unusual finding. A small barium-filled tract can be seen from the esophagus running upward toward the trachea. Ingested formula could similarly be aspirated into the lungs

agus so that the "H-type" fistula between the trachea and the esophagus can be excluded (Fig. 4.22). If this fistula is not found, the infant is given a bottle, and the swallowing mechanism is evaluated. Look at the position, course, contour, and motility of the esophagus. A vascular ring, i. e., an anomaly of the great vessels, masses, or nodes, often makes an impression on the esophagus. Check for gastroesophageal reflux – chalasia – during this examination (see Chap. 5). In addition, under fluoroscopy, the diaphragm and mediastinum can be examined for diaphragmatic paralysis and unilateral air trapping.

If, after this study, further airway evaluation is necessary, or if the child continues to be a "noisy neonate," the airway can be studied fluoroscopically with the use of the magnification high-kilovoltage technique (see Chap. 3).

Remember: the most important question is: "Why am I ordering this set of films?" Once the diagnosis of hyaline membrane disease or severe chronic lung disease of the neonate is established, radiographs should be used to show correctable conditions, such as malpositioned tubes, airway obstruction, pneumonia, pneumothoraces, and vascular rings. Since the premature infant may be more acutely sensitive to the deleterious effects of radiation (Chap. 2), the timing and selection of radiographic examinations should be tempered with this consideration. Remember the ALARA concept (Chap. 2).

Structural Abnormalities

One lung may not develop (pulmonary atresia) and in these instances, there is only one main-stem bronchus and no carina. The lack of development of adequate amniotic fluid most often found in kidney dysfunction can lead to "Potter's sequence." The lack of amniotic fluid leads to compressive forces on the fetal thorax and inhibits growth of the lungs – pulmonary hypoplasia. A diaphragmatic hernia may cause hypoplasia of one lung, shift of the mediastinum away from the hernia, and is associated with persistent pulmonary hypertension. The spectrum of anomalies of the lung (pulmonary developmental abnormalies) includes pulmonary arteriovenous malformations, hypogenetic lung syndrome, bronchopulmonary sequestration (an isolated area of lung either in the thorax or abdomen), congenital cystic adenomatoid malformation (hamartoma), bronchogenic cyst (85% are mediastinal and may cause airway obstruction), and congenital lobar emphysema. All of these diseases can cause respiratory distress.

What abnormalities do you see in Fig. 4.23? The answer is in Appendix 2.

References and Further Reading

1. Kuhn JP, Slovis TL, Haller JO (eds) Caffey's pediatric diagnostic imaging, 10th edn. Mosby, Philadelphia, pp 48–103
2. Slovis TL (ed) (2003) Neonatal imaging. In: Kuhn JP, Slovis TL, Haller JO (eds) Caffey's pediatric diagnostic imaging, 10th edn. Mosby, Philadelphia, pp 48–103
3. Newman B (1999) Imaging of medical disease of the newborn lung. Radiol Clin North Am 37:1049–1065
4. Currarino G, Williams B (1985) Causes of congenital pulmonary hypoplasia: a study of 33 cases. Pediatr Radiol 115:15–24
5. Swischuk LE (2004) Imaging of the newborn, infant and young child, 5th edn. Lippincott Williams and Wilkins, Philadelphia

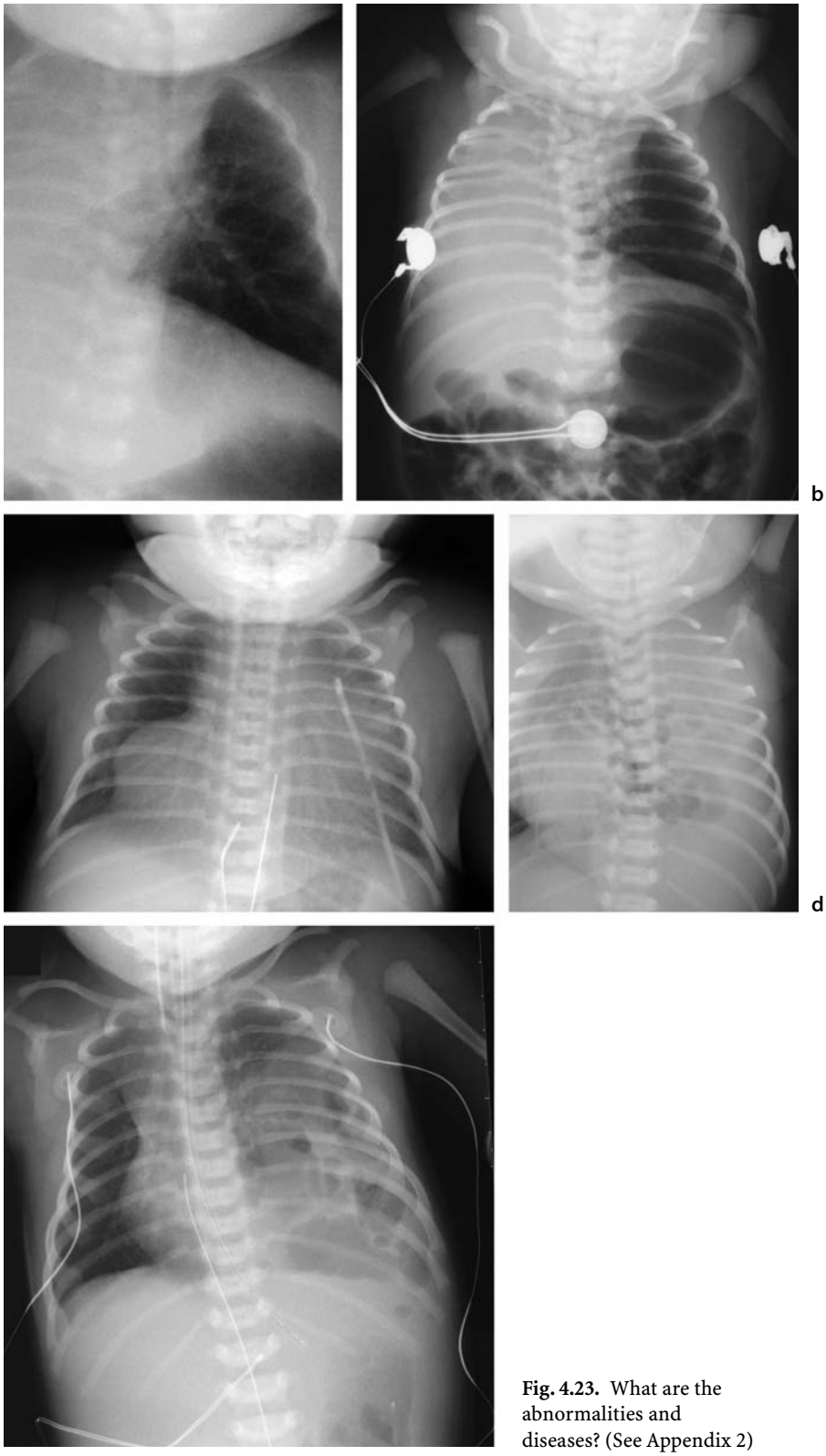

Fig. 4.23. What are the abnormalities and diseases? (See Appendix 2)

5 Abdominal Imaging

This chapter is a change from the earlier editions in that it includes imaging of the entire abdomen and pelvis. We have combined the gastrointestinal and urinary tract chapters because today's cross-sectional studies (ultrasound, CT, MR) image both systems at the same time. We will begin as always with the plain films and then discuss the normal ultrasound, CT, and MR examinations of the abdomen and pelvis. We will present imaging studies specifically tailored to study the bowel, the biliary system, the bladder, and the kidneys. We have chosen to do cross-sectional imaging ahead of specific studies since this is what is most often done in daily practice. The chapter will conclude with common pediatric abdominal problems and explain how to integrate the modalities and, when possible, chose the "best" single test.

Roentgenographic interpretation of a child's abdomen is a challenging experience, as there are many subtle clues to the nature of the disease process. Appropriate interpretation requires both knowledge of the technical aspects of how the film was made and a systematic approach.

Technical Factors

In the discussion of the chest we noted that observing gravitational effects is useful in assessing a film. This is also true in the abdomen, i.e., air always rises, fluid goes to the dependent area.

- ***Rule No. 9:*** The abdominal examination should include a minimum of three views: supine, prone, and erect.

One can think of the air in the abdomen as contrast medium; the purpose of obtaining three views is to move air into different loops of bowel so that the maximal quantity of bowel can be visualized. With the patient supine, what portions of the bowel are highest? The answer, of course, is the transverse colon and the body of the stomach. Therefore on the abdominal supine film air rises to these regions (Fig. 5.1). When the patient is prone, the highest portions of the bowel are ascending and descending colon, rectum, and fundus of the stomach. Therefore gas should rise to these areas (see Fig. 5.1). Remembering these facts can frequently help in distinguishing large from small bowel. Look carefully at the bones on the supine film. The iliac wings appear larger and more rounded than they do on the prone film (see Fig. 5.1).

The erect view is the last film in the series. A decubitus view is sufficient if the patient is too sick or unable to stand. How do you know if the film is an erect view? Once again, remember the effects of gravity. There may be an air–fluid level in the stomach. Similarly, if the bowel contains fluid, one sees air–fluid levels. Notice how most of the bowel falls into the lower abdomen and pelvis, while the gastric fundus remains fixed in the left upper quadrant. The colon is visible in the flanks, with the transverse segment extending from beneath the liver, across the abdomen below the stomach into the left upper quadrant.

The Radiologist's Circle and the ABCS

In a child with acute abdominal distress it is not uncommon to take sequential examinations of the abdomen. Therefore it is important to check the date and time of examination. Progressing in our imaginary circle, the ABCS should be reviewed, but this time in a different order: chest, bones and soft tissues, and (in this instance) abdomen.

- ***Rule No. 10:*** On every abdominal examination, evaluate the chest as if you were looking at a chest film.

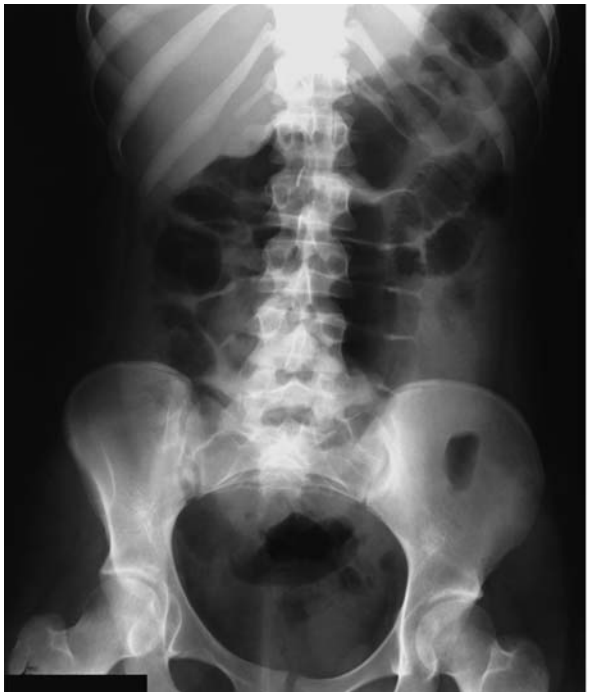

a

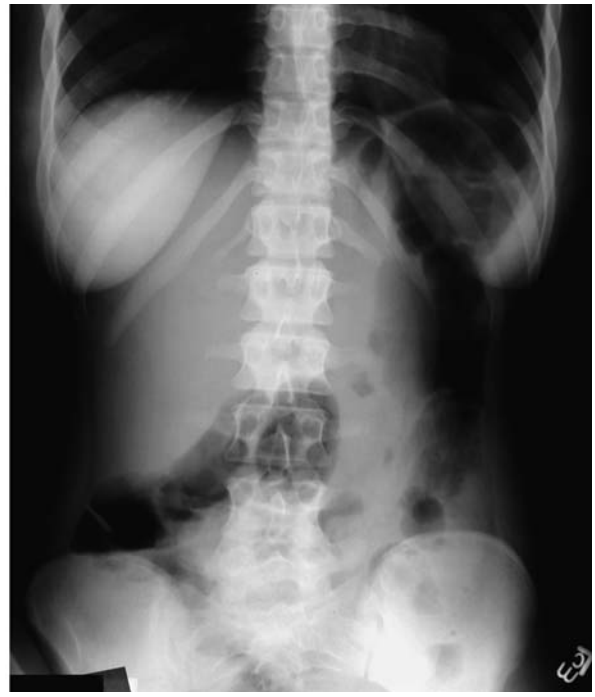

b

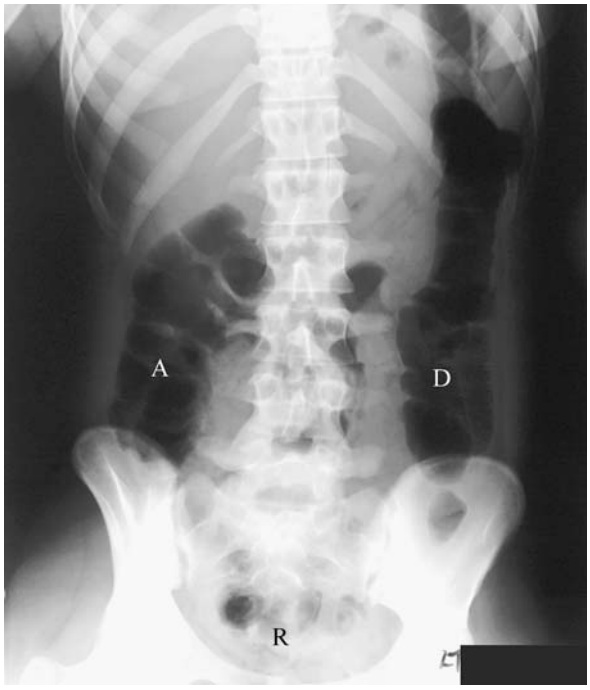

c

Fig. 5.1. The value of air as contrast medium by utilizing three views
a Supine roentgenograph in this 15-year-old girl with abdominal pain reveals multiple air-filled loops of bowel in the midabdomen but little gas within the rectum
b An erect film reveals that the base of the lungs is clear, and there is no free air under the diaphragm. There is gas in the hepatic flexure, transverse colon, and splenic flexure
c Prone examination reveals gas in the rectum (*R*), ascending (*A*), and descending (*D*) colon. The predominant pattern is that of colonic gas. The small bowel is not distended, and there is no evidence of obstruction

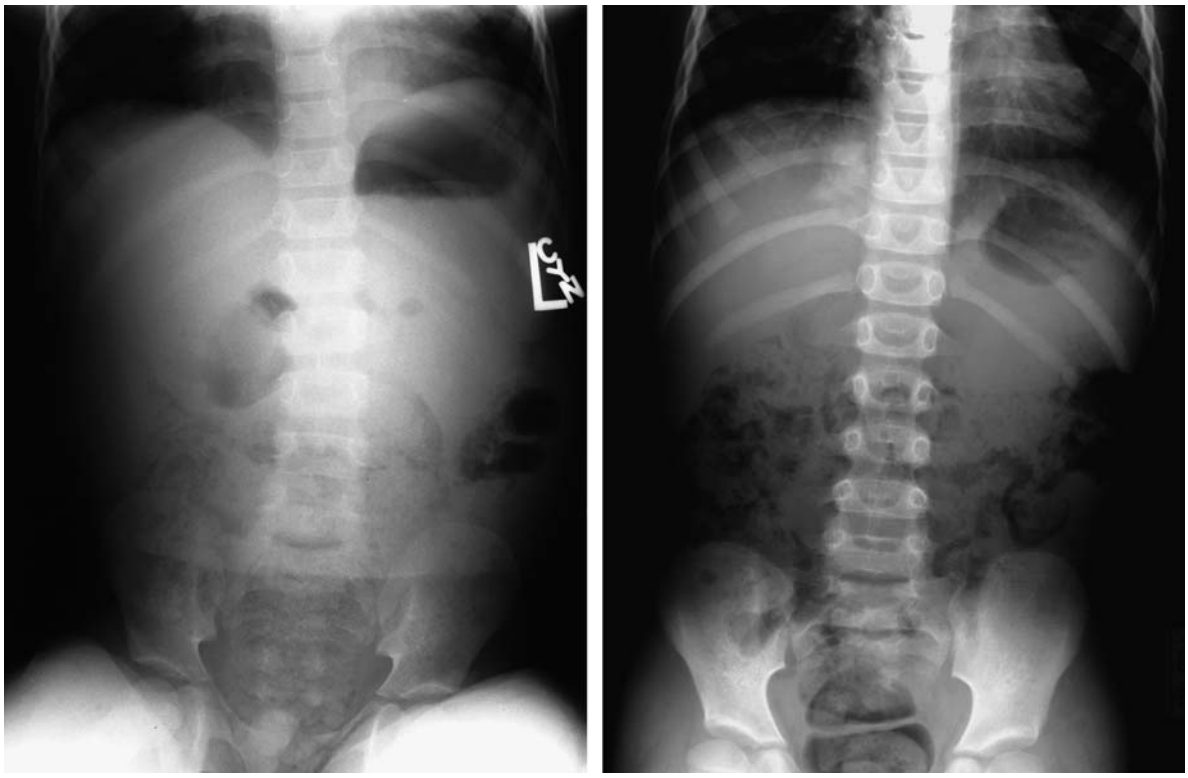

Fig. 5.2. On every abdominal film, examine the chest as if you were actually reading a chest film
a Upright abdominal film in a 4-year-old with abdominal pain. Is the left heart as transparent as the right? Did you see the opacity in the medial left chest at T9–10? It is a pneumonia
b A 6-year-old with right lower quadrant pain. You cannot see through the liver in the right medial region adjacent to T9–11. This opacity is also a pneumonia.

Chest

It is often easier to see basilar lung opacities, fractures of the lower ribs, and pleural reactions on an abdominal film than on a chest film (Fig. 5.2). In addition, the chest film may not adequately show a low thoracic paraspinal mass, which is readily observed on abdominal films. Remember, the posterior lung sulcus is located at the level of the 12th thoracic vertebra and the posterior diaphragms insert at L2. To find a thoracic paraspinal mass, you must look *through* the liver density on the right and the gastric air bubble on the left.

Bones and Soft Tissues

The bones and soft tissues can provide extremely valuable information. In making our imaginary radiologist's circle, note whether there is swelling or edema of the soft tissues. It is also important to identify the properitoneal fat line (Fig. 5.3). This black line is the lateral margin of the peritoneal cavity; the gas-filled ascending colon and frequently the descending colon are within 1–2 mm of this line on the prone film. A separation between the properitoneal fat line and the colon on the prone film indicates the presence of fluid or possibly an intra-abdominal mass. Remember, this sign is useful only if the colon has air in it! (See Fig. 5.3.)

The lower ribs, spine, pelvis, and hips are the major bones of concern on the abdominal film. Since specific abnormalities of these bones are discussed in Chap. 7, the major item of concern now is symmetry. Asymmetry must always be explained (Fig. 5.4). Once again, abnormalities of bone should lead to careful searching of neighboring intraabdominal contents; e.g., left lower rib fractures should suggest renal or splenic injury.

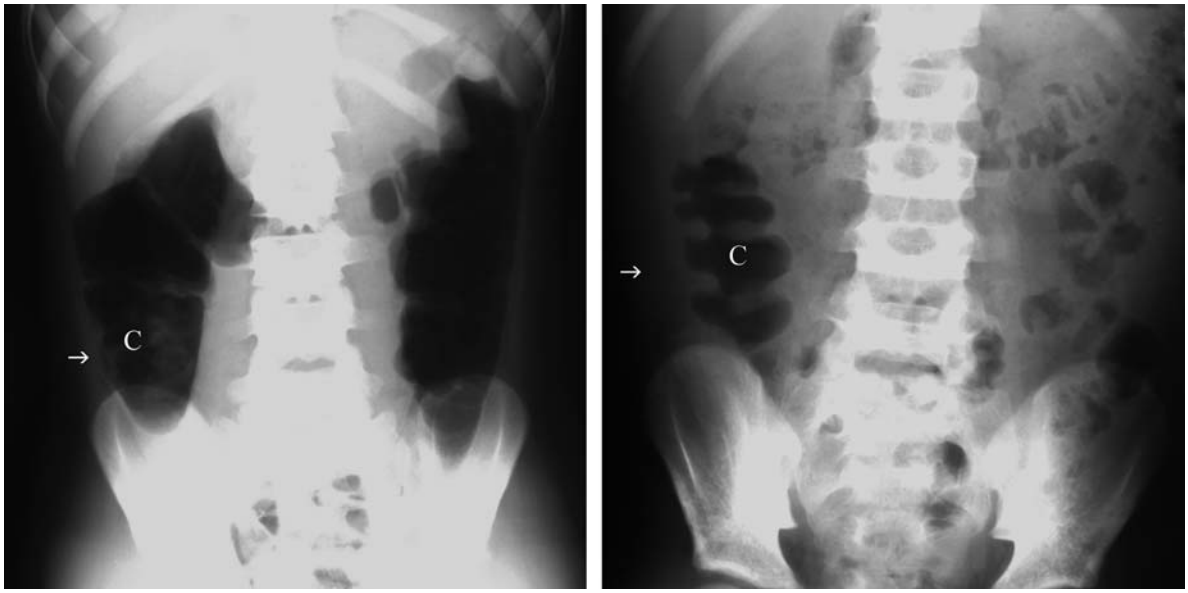

a b

Fig. 5.3. Properitoneal fat line
a Close-up prone view of the right lower quadrant in this normal 9-year-old. The black, linear properitoneal fat line (*arrow*) is seen, with the descending colon only a few millimeters away (*C*)
b In a 7-year-old child, the prone film reveals a separation of the colon (*C*) and the properitoneal fat line (*arrow*). This child had nephrotic syndrome and ascites

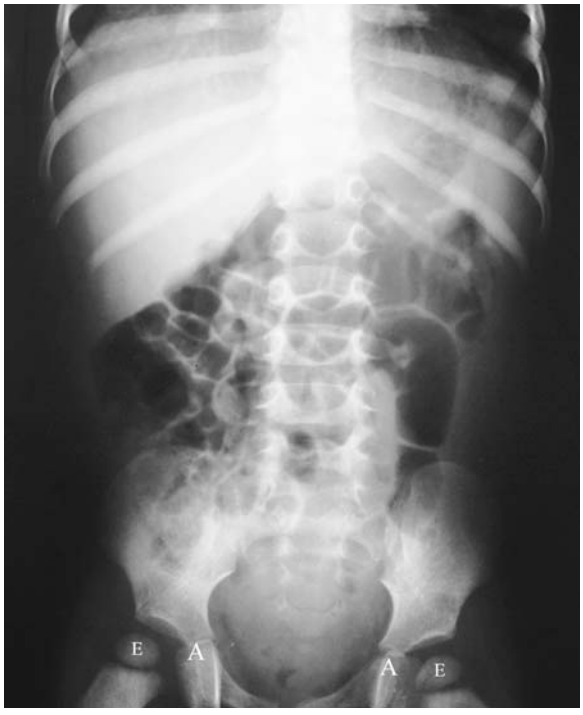

Fig. 5.4. Supine film of this 1-year-old with right-sided abdominal pain. Note the asymmetry of the hips. The right capital femoral epiphysis (*E*) is lateral to the medial acetabulum (*A*) when compared to the left. There was a joint effusion proven to be a septic arthritis

Abdomen

In the systematic approach, we look at the area for which the film was requested last. Therefore our approach to the intra-abdominal contents is to view the muscles, soft tissues, and viscera before examining the bowel gas pattern. Begin at the top of the film, most often with the erect film. The film must include the base of the lungs and diaphragm as well as the pubic bone (on at least one of the three films). If this film does not include the entire abdomen, valuable information may be lost (Fig. 5.5). Look for signs of free intraperitoneal air. As can be seen in Fig. 5.1, the diaphragm on the left is easily visible because of the stomach bubble. On the right the liver is directly beneath the diaphragm, and only the top margin – the thoracic margin – can be seen. Since air rises on the erect film, free air collects between the liver and diaphragm on the right and between the stomach bubble and the diaphragm on the left. On the supine film, however, air rises and fills the space above the viscera and beneath the umbilicus and the abdominal musculature. Free air is more difficult to see on this view but should nevertheless be recognized, as there is a subtle change in the soft tissue density of the gray abdomen (Fig. 5.6). When there is free air, the liver is blacker than the adjacent soft tissues. Therefore,

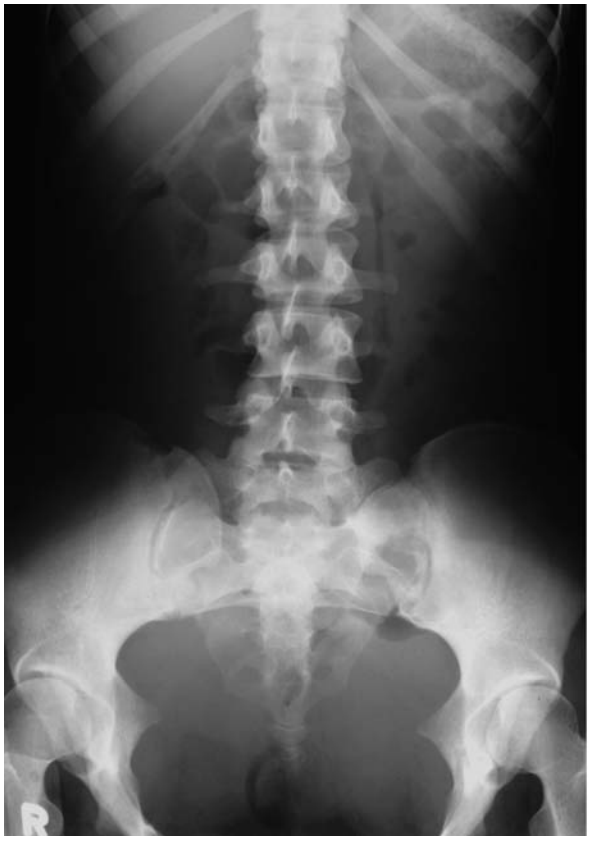

a

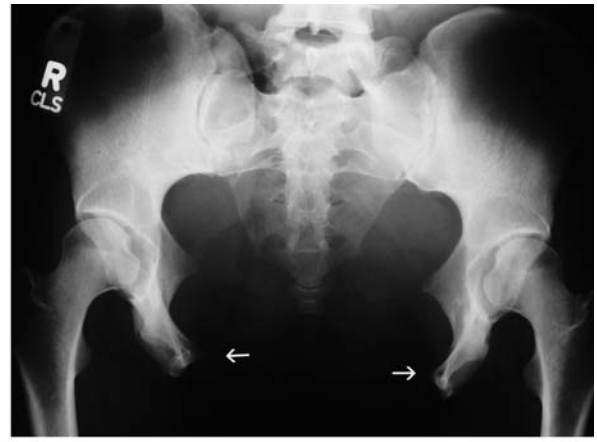

b

Fig. 5.5. Is this an adequate supine film?
a Teenager with abdominal pain
b Pelvis of the same young lady shows widespread pubic bones (*arrows*), a finding in patients who have had exstrophy of the bladder. Did you see the findings in **a**? The supine film includes neither the diaphragm nor the pubic bones

there are three densities, proceeding from the lateral aspect of the right side: (a) the soft tissue density – gray; (b) the liver with air over it, which is somewhat darker – dark gray to black; and (c) the stomach full of air, which is the darkest black. Normally there are only two densities – the gray soft tissues and liver (which are of equal density) and the air (black) in the stomach.

The falciform ligament is never normally visible; it can be seen only when surrounded by free intraperitoneal air. This ligament courses downward from its diaphragmatic attachment between the margin of the right and left lobes of the liver to the lowest aspect of the umbilical remnant. When there is free intraperitoneal air, the large bubble of free air assumes an oval configuration with the falciform ligament being central – the laces of a football – in the football sign (see Fig. 5.6).

Continuing with your appraisal of the film from the top down, look at the liver, spleen, and kidneys and assess their size, if possible (see Fig. 5.1). A radiologist measures liver size only infrequently; hepatic enlargement is usually an impression. The spleen is often obscured by bowel gas. Remember, a good inspiration pushes the liver down while a poor inspiration, in fact, lets it rise.

Determination of splenic size and position is usually possible by locating the inferior and medial margins. The stomach air bubble and gas in the splenic flexure of the colon lie immediately adjacent to the spleen, and both may be displaced, particularly if the spleen is enlarged (see Fig. 6.1) . Since one can feel beneath the costal margin to palpate a spleen, reference of the splenic density to this margin helps determine whether it is actually enlarged. Ask yourself, "Could I palpate it?" If so, "How big does it feel?"

Proceeding inferiorly on the film, note the iliopsoas muscles attached to the spine at the upper lumbar vertebra, and proceed diagonally and laterally to the lesser trochanters of the femora. The lateral margins of the psoas muscle can usually be seen. The key to identifying pathology of the psoas margins is asymmetry. If a portion of the muscle is not visible while the rest of the muscle and the opposite one are, abnormal soft-tissue densities in this region should be considered. The entire psoas margins sometimes cannot be seen on films of infants and children with abundant fecal material or bowel gas.

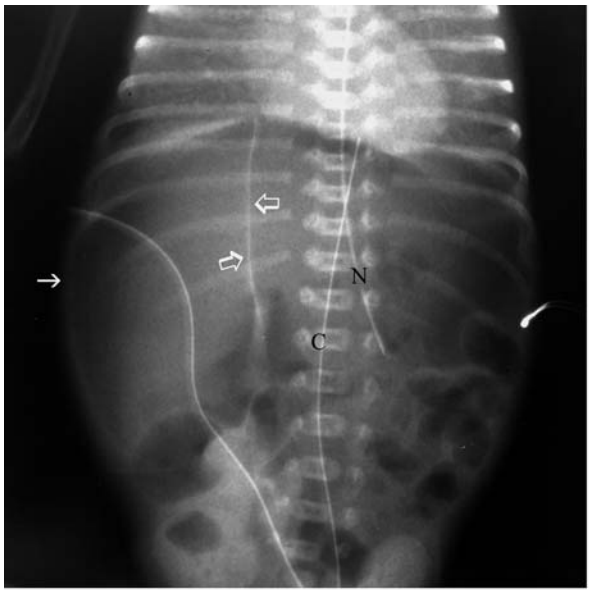

a

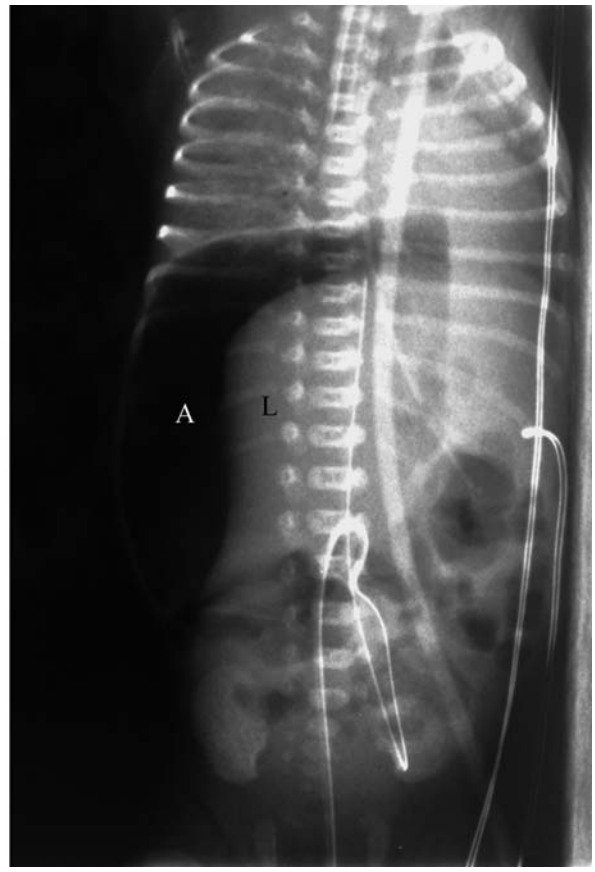

b

Fig. 5.6. Perforation of a viscus and free intraperitoneal air **a** Supine abdominal film reveals a change in density of the liver in relation to the lateral abdominal wall (*arrow*). The entire abdomen is more lucent or blacker. There is air on each side of the falciform ligament (*open arrows*). A nasogastric tube (*N*) and umbilical arterial catheter (*C*) are present
b Decubitus film (left side down) shows a massive amount of air (*A*) within the abdominal cavity. There is an air-fluid level on the left show me that there is both free air and fluid present. *L*, liver

The kidneys are adjacent to the lateral margin of the iliopsoas muscles. Renal size can often be estimated from the plain film. A rough guide to appropriate size is that the length from the top to the bottom of the kidney should be no greater than 4–4.5 vertebral bodies. The left kidney is usually slightly larger than the right (no greater than 1.5 cm difference). A kidney longer than five vertebral bodies is enlarged. The lower limits of normal are not as precise, but a kidney less than three vertebral bodies in length is abnormally small.

Look specifically for calcifications in all areas of the abdomen. Stones in the gallbladder, urinary tract, pancreas, or appendix may occur if there is stasis or an inflammation (Fig. 5.7). Benign and malignant neoplasms can calcify. Once a calcification has been identified and anatomically located, characterize it. Is it sharply marginated and of uniform density? Is it laminated (Fig. 5.7)? Lamination indicates that it has been there for a long time, and that the chemical processes have varied, and thus different layers have formed. Is it well formed and flocculent, as found in adrenal calcifications, or is it punctate with poorly defined margins, representing irregular deposition in a necrotic, rapidly growing neoplastic process? What is the calcification doing to the system in which it resides? Is it producing obstruction, or is it ulcerating? Does it look "physiological"? A phlebolith in an infant is definitely abnormal but it may be "normal" in an adult.

Continuing downward on the three views off the abdomen, evaluate the soft tissues of the pelvis for asymmetry. The bladder appears as a smooth and round soft tissue mass when distended. In infants it tends to extend up into the right lower quadrant.

Finally, look at the bowel gas pattern. Figure 5.1 shows a normal bowel gas pattern in an older child, while Fig. 5.8 shows a normal bowel gas pattern in a neonate. Even though there is a large amount of gas in the neonatal abdomen, the bowel loops have a recognizable, polygonal pattern. In neonates with bowel distention, the loops become "sausage-shaped." It is

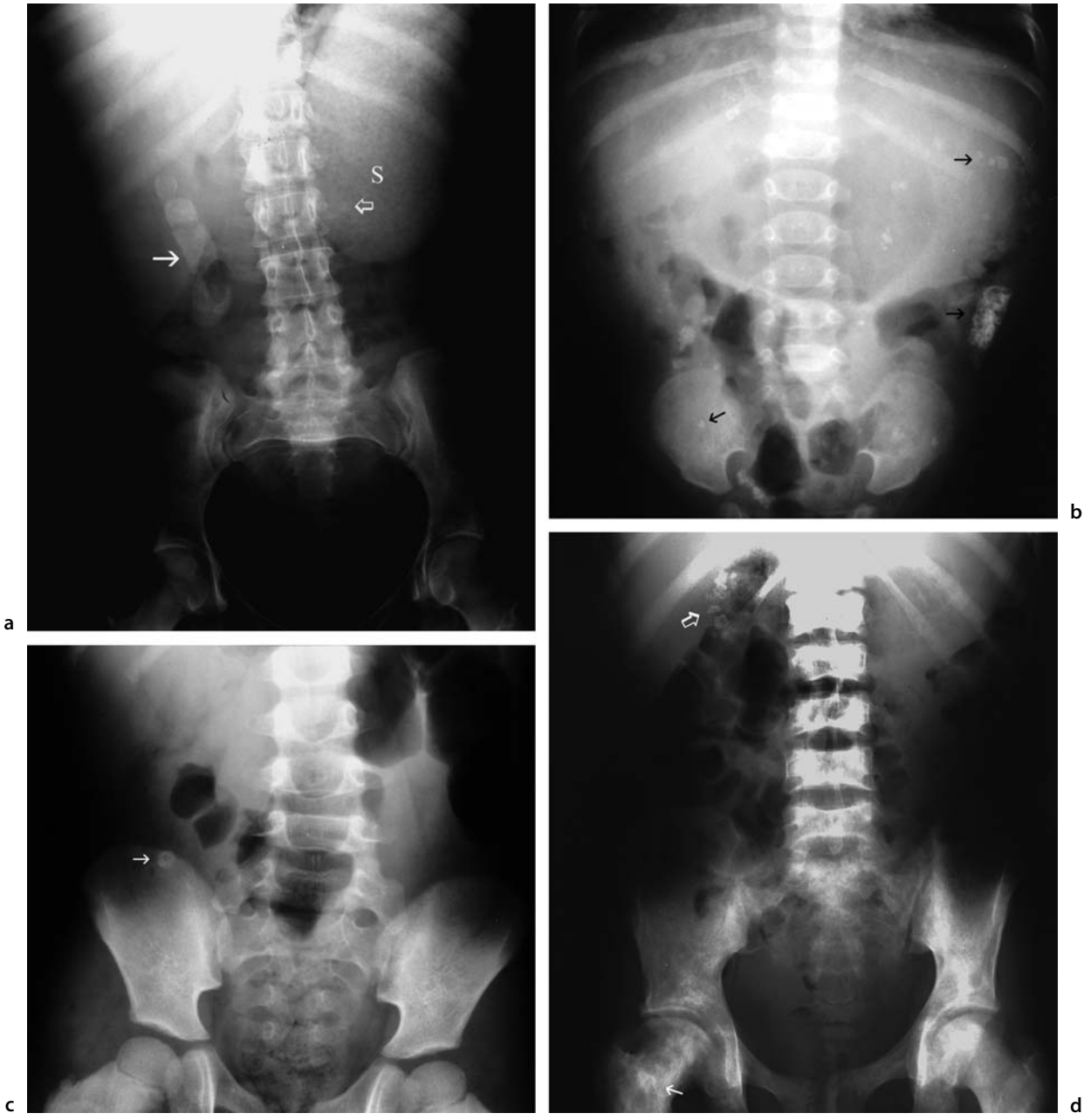

Fig. 5.7. Calcifications within the abdomen
a A 16-year-old with several areas of calcification. There is a tubular density in the right midabdomen. This is the gallbladder, which contains multiple radiopaque gallstones (*arrow*). There is a large viscus (*S*) in the left upper quadrant with punctate calcifications (*open arrow*) representing an enlarged spleen, which has undergone iron replacement secondary to multiple transfusions for hemolytic anemia (hemochromatosis)
b A 2-month-old with cystic fibrosis and large calcifications (*arrow*s) outlining the peritoneal cavity. This represents calcifications of meconium peritonitis from in utero perforation
c Appendicolith. Calcifications in the appendix (*arrow*) often have multiple concentric calcific rings (laminae) that aid in their identification
d A 15-year-old sickle cell patient with gallstones (*open arrow*) and multiple spine and femoral changes of bone infarction (*arrow*)

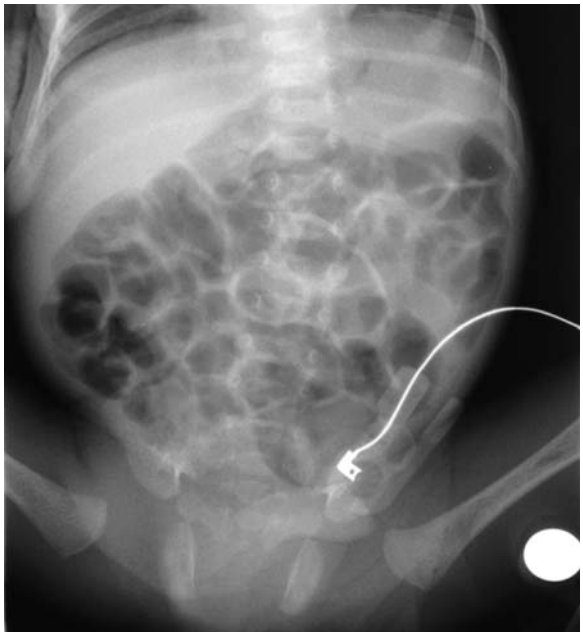

Fig. 5.8. Normal bowel pattern in a neonate. This supine abdominal film shows bowel loops that display a polygonal pattern. On this supine film gas is not seen in the rectum

frequently impossible to tell large from small bowel, but even here it helps to obtain the three views.

Observe the bowel gas pattern for position, contour, and size (distention). The bowel maybe displaced by a mass (Fig. 5.9 and also Chap. 6). Comparing Figs. 5.1 and 5.8 with Fig. 5.9, the presence of a soft tissue mass is striking. Free intraperitoneal fluid causes the bowel to move centrally and imparts a gray or hazy appearance to the abdomen (Fig. 5.9). The sharp liver angle (margin) is obscured by the fluid. Any fluid, be it lymph, blood, or pus, can give this appearance. Here again, however, we can use the effects of gravity to our advantage. Air in the bowel floats centrally, with the fluid in the dependent portions (see Fig. 5.9).

We use air as much as possible because it is a good contrast agent. The bowel margins should be smooth, not ragged or irregular. The contour should change as position changes, implying pliability; it should not be rigid. If a space-occupying lesion – a mass – pushes on adjacent segments of bowel and changes the contour, the wall appears stretched as a result of the extrinsic pressure.

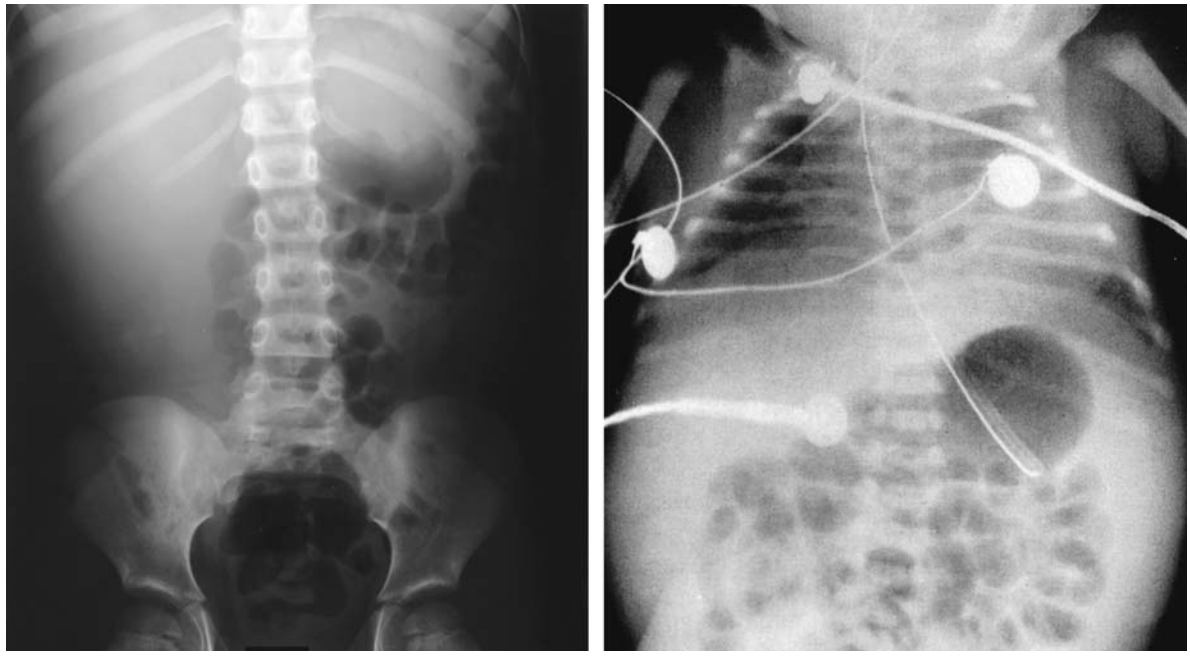

Fig. 5.9. Abnormal gas pattern
a A supine film of a 4-year-old with a protuberant abdomen reveals a large, homogeneous mass over the right and midabdomen. The bowel gas is pushed to the left. A sonographic examination confirmed the presence of a mesenteric cyst
b Ascites. On this supine radiograph of a 2-day-old male infant the bowel gas is pushed to the center, and there is a grayness to the flanks. The fluid moved appropriately on multiple views because it was free ascitic fluid secondary to urinary obstruction and posterior urethral valves. Note how the bowel loops float centrally instead of being displaced to one side by a mass, as in **a**

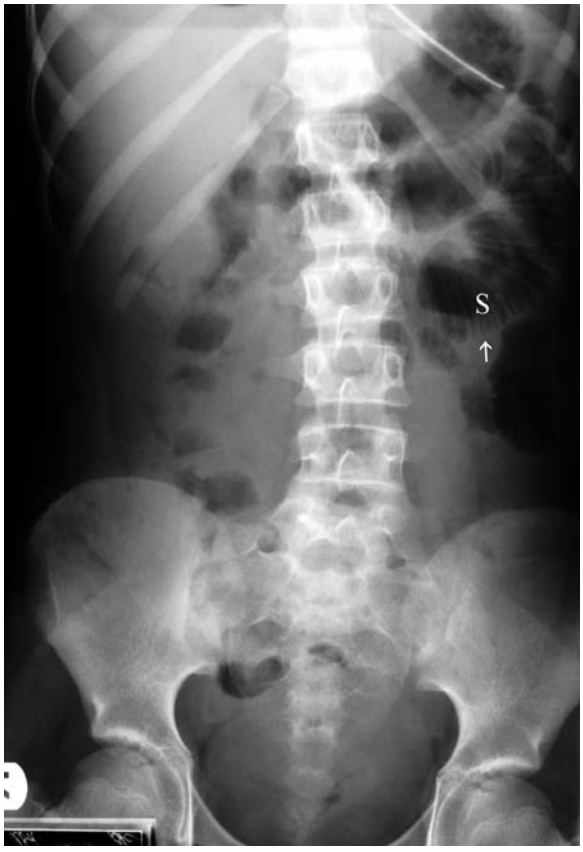

Fig. 5.10. Sentinel loop. On this supine film there is a localized distention of small bowel in the left upper quadrant (*S*). It is clearly identifiable as small bowel because of the valvulae conniventes (*arrow*). The sentinel loop remained in this region on multiple views. The child had blunt abdominal trauma, and the sentinel loop was anterior to an inflamed pancreas

An increase in the size and amount of bowel distention is crucial to the diagnosis of intra-abdominal disease. Children normally have some small bowel gas or (on the erect film) an air fluid level(s) in the colon. While multiple small bowel and colonic fluid levels are seen in mechanical bowel obstruction, they are also seen in infants as well as older children *without* obstructive bowel disease. Many of these children will have nothing more threatening than gastroenteritis. However, if you cannot see air in the colon or rectum on multiple views, or if there is a *localized* distention of bowel, you should be very suspicious of underlying pathological changes. In crying children the stomach may be quite large without any pathology. However, localized distention of small bowel provides a valuable clue to the site of disease – a "sentinel loop" (Fig. 5.10). Remember:

► ***Rule No. 2:*** Knowledge of anatomy is the key to correct radiographic diagnosis.

What viscera are these sentinel loops near? What vessels are found in this area? What type of pathology commonly occurs in this quadrant?

Increase in bowel size (distention) may occur in both small and large bowel without obstruction, but there is a *recognizable pattern to the distention.* The small bowel is less distended than the colon, and there is gas in the rectum. This condition has been called paralytic (without peristalsis) ileus (distention). Patients who have been given atropine derivatives or who have dysmotility syndrome may have the same radiographic picture. Since the patient with gastroenteritis has normal to increased peristalsis, and the patient given atropine derivatives has decreased peristalsis, the term "ileus" is somewhat confusing. It is best to describe the pattern and allow the clinician to fit it into the patient's status.

A more *uniform*, generalized increase of all or parts of the small or large bowel along with multiple air–fluid levels and no air in the rectum denotes mechanical bowel obstruction (Fig. 5.11). The site of obstruction is determined by how much bowel is distended. That is, many loops mean distal bowel obstruction, while a few distended loops mean proximal bowel obstruction (Fig. 5.12). In obstruction, the curvature or contour of the loops of distended bowel may be acute – hairpin turns – and the fluid levels may be uneven, i.e., a stepladder distribution (Fig. 5.11). Because of the hyperperistalsis, the bowel beyond the obstruction is devoid of gas (assuming the process has been present for some time).

A helpful mnemonic for assessing plain film is: stones, bones, gas, mass!

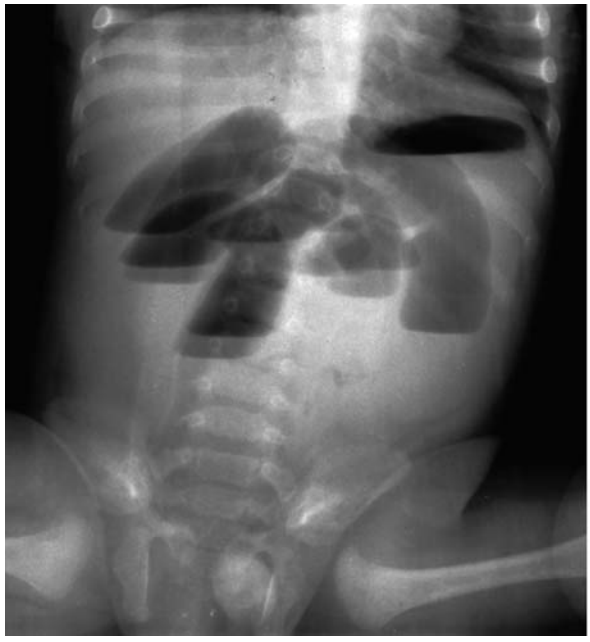

a

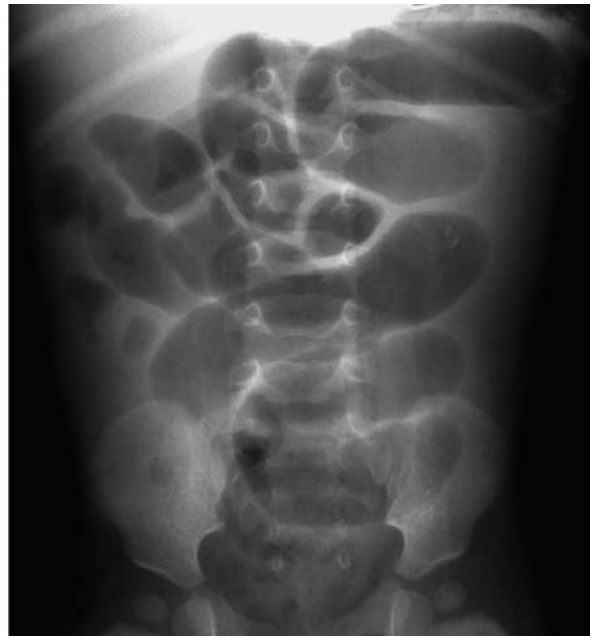

b

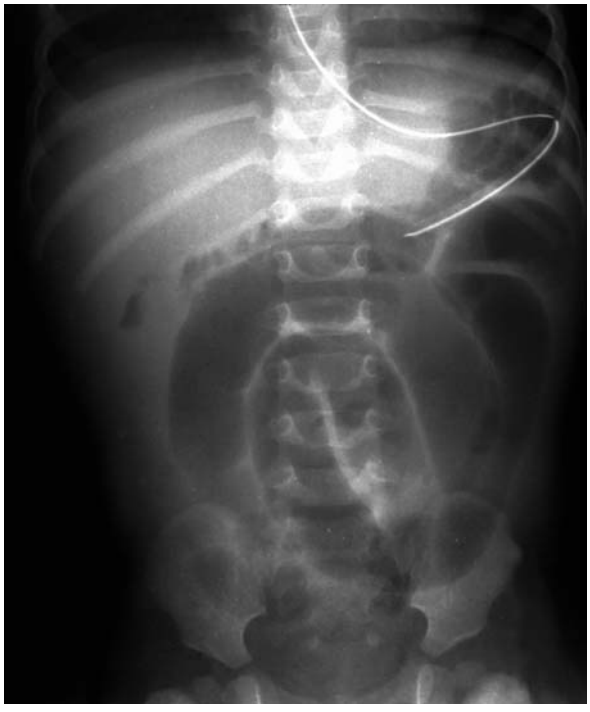

c

Fig. 5.11. Small bowel obstruction. This 1-year-old had an incarcerated inguinal hernia
a Erect film shows multiple air-fluid levels in a stepladder pattern (uneven levels in each loop). When this occurs, it suggests obstruction
b Supine radiograph shows large, distended loops in the midabdomen
c On the prone film, gas has not successfully shifted into the colon. The largest loops remain in the midabdomen. Small bowel obstruction is present

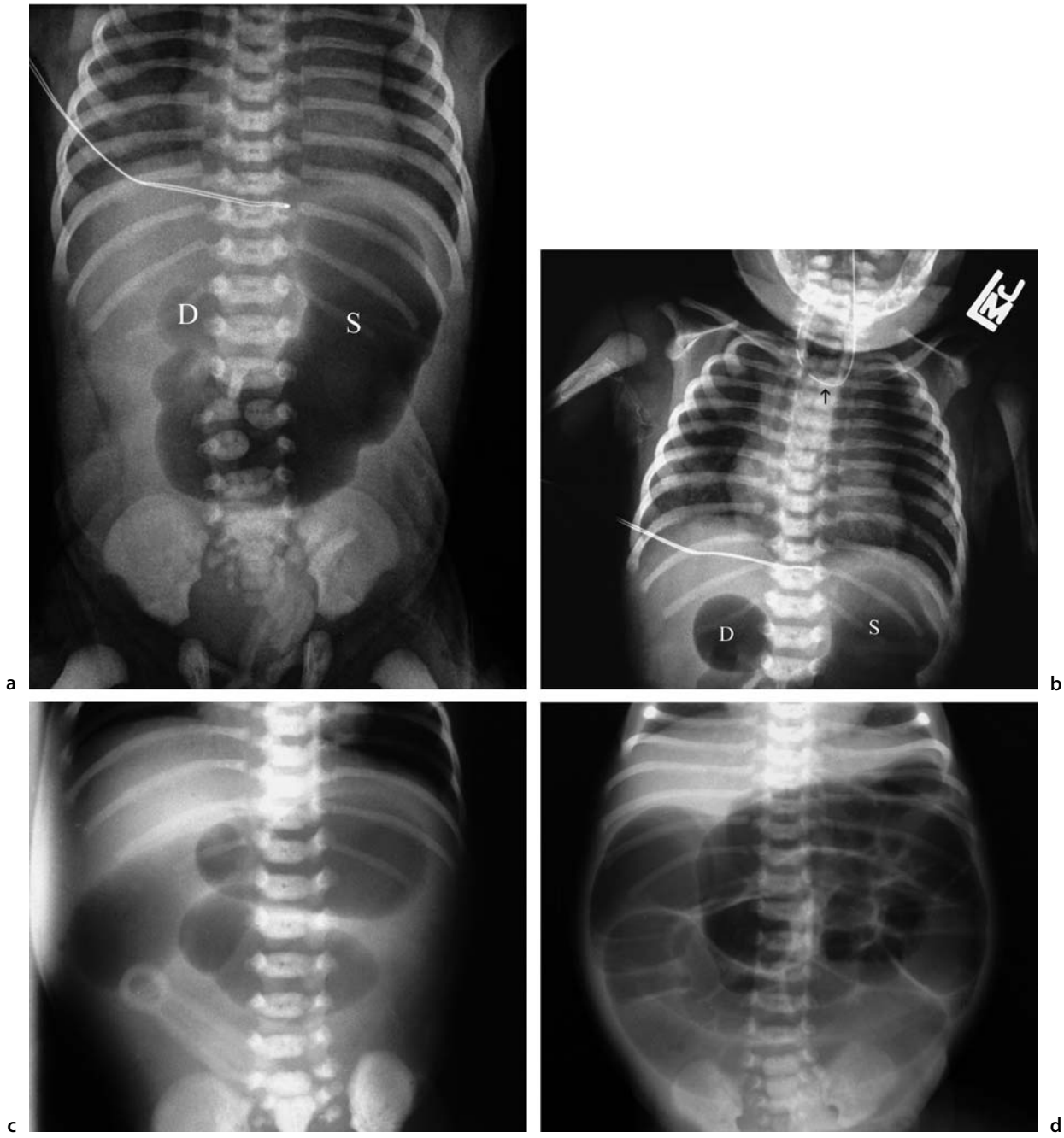

Fig. 5.12. Mechanical small bowel obstruction at various levels of the gastrointestinal tract. The more dilated loops are seen, the lower the obstruction

a This newborn presented with vomiting. The radiographs of the abdomen reveal two air–fluid levels (double bubble), one in the stomach (*S*) and one in the duodenum (*D*). This child had a high obstruction which was shown to be duodenal atresia. There are multiple lumbar vertebral anomalies

b Chest film on the same neonate. He has esophageal atresia with a coiled tube in the esophagus (*arrow*) and a tracheo-esophageal fistula as there is gas in the stomach and duodenum. He has Down's syndrome

c This 1-day-old presented abruptly with vomiting after feeding. Supine abdominal film reveals three air-containing structures: the stomach, duodenum, and jejunum. At surgery this child was found to have jejunal atresia

d This 2-day-old has multiple air-containing loops of bowel, signifying a more distal obstruction. The diagnosis at surgery was ileal atresia

Cross-Sectional Imaging Techniques

Ultrasound of the Abdomen and Pelvis

Ultrasound is a noncontrast tomographic study that in most instances requires no special patient preparation or sedation. There is no ionizing radiation and the examination can easily be performed portably. The study is tomographic in that thin slices of the viscera can be obtained, and the study can be performed in almost any plane. Since the examination is operator-dependent, it is important that all members of the ultrasound team perform the study in the same systematic fashion. The usual planes of study are transverse and longitudinal views with the transducer placed on the patient's abdomen. Views with the transducer on the flank (coronal view) may be obtained in longitudinal and transverse planes. Prone views are sometimes helpful, particularly for the kidneys. All examinations may be recorded on videotape or as multiple images on film or PACS.

We begin our ultrasound examinations with longitudinal "cuts" beginning on the patient's left and proceeding to the right (Fig. 5.13). It is on these views that one finds pleural and pericardial effusion. The transverse views begin high in the abdomen and progress from cephalad "cuts" to caudad (Fig. 5.14).

Transverse ultrasonic sections of the abdomen (as well as CT transverse sections) are oriented with the patient's right on the viewer's left; the superior aspect of the scan is the abdominal surface with the patient supine (Figs. 5.13, 5.14). In the longitudinal sections, the patient's head is oriented to the viewer's left.

Each organ has its own reproducible parenchymal architecture. Lack of echoes suggests a fluid-filled structure, such as a blood vessel or gallbladder. They appear black and are easily defined by color Doppler when there is any question as to whether a structure is a blood vessel (fills with color) or a cyst. It is not the purpose of this text to review the interpretation of ultrasonic scans, but rather to portray the anatomy. The liver, gallbladder, spleen, pancreas, kidneys, and great vessels are well seen except when there is overlying bowel gas or the patient is obese. It is fair to say, however, that ultrasonic evaluation of the gallbladder is the best method for demonstrating gallstones.

The three compartments (pararenal, perirenal, and renal) of the retroperitoneum are visualized (Fig. 5.15). The entire examination is carried out with high-frequency transducers and real-time technique so the examiner is able to see exquisite intrarenal detail, vascular pulsations, and dilated fluid-filled structures such as the ureters. With the use of color Doppler ultrasound, renal veins and arteries are easily seen (Fig. 5.16).

The internal architecture of the kidney changes with age. The reason for the different sonographic appearances is that the neonatal kidney is anatomically different. In the full-term neonate the maximum number of glomeruli are present in the cortex,

Fig. 5.13. Normal longitudinal ultrasound ▶
Our approach is always the same, beginning on the patient's left side with the patient's head directed to the viewer's left. The feet are to the viewer's right
a Left-most scan showing the kidney left (*K*) and the spleen (*S*). There are specular echoes (this means bright, sharp echoes) of the diaphragm (*D*)
b A section slightly more toward the center reveals the left lobe of the liver (*L*) and the heart (*H*)
c Just to the left of midline, one sees the aorta (*A*), the superior mesenteric artery (*arrow*) and the liver (*L*). Bowel is seen with fluid in the lumen (*LU*) and a relatively thick wall. Note how the aorta has branches and its cephalic portion is directed posteriorly. The esophageal–gastric junction (*EG*) seen directly over the aorta
d Slightly now to the right of midline one sees the heart and the most cephalic portion of the inferior vena cava (*IVC*)
e A full view of the inferior vena cava (*IVC*) with the liver above. Note the right renal artery behind the cava (*arrow*)
f Longitudinal right scan showing the hepatic veins (*arrow*) emptying into the superior cava and heart. *L*, liver
g Scan further to the right reveals the gallbladder (*GB*), the reverberations of air (*arrow*) in bowel, liver, and specular echoes of the diaphragm (*D*)
h More lateral scan shows the right kidney (*K*) with the liver above it

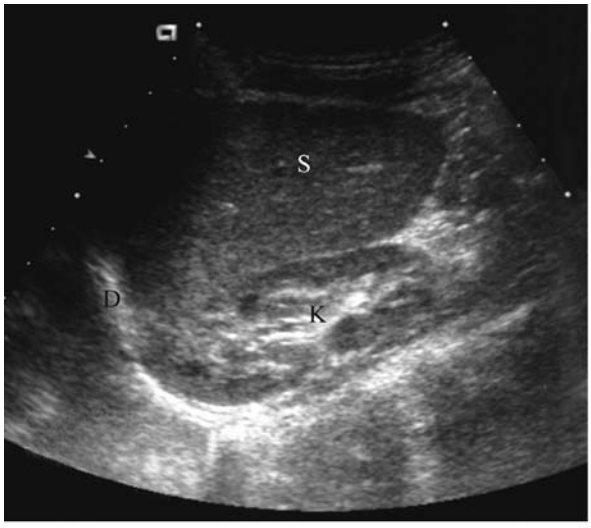

a

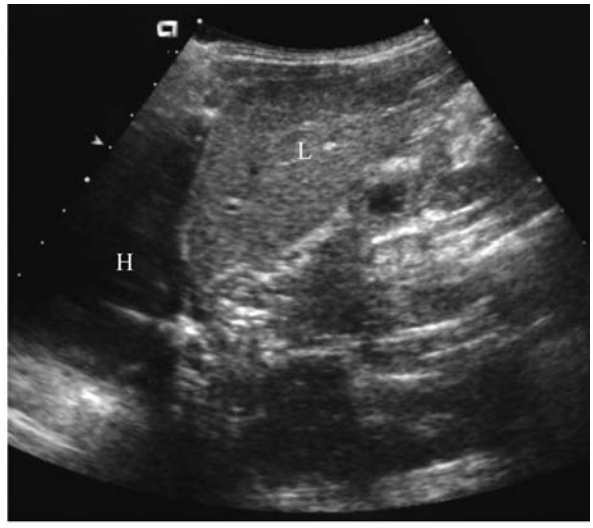

b

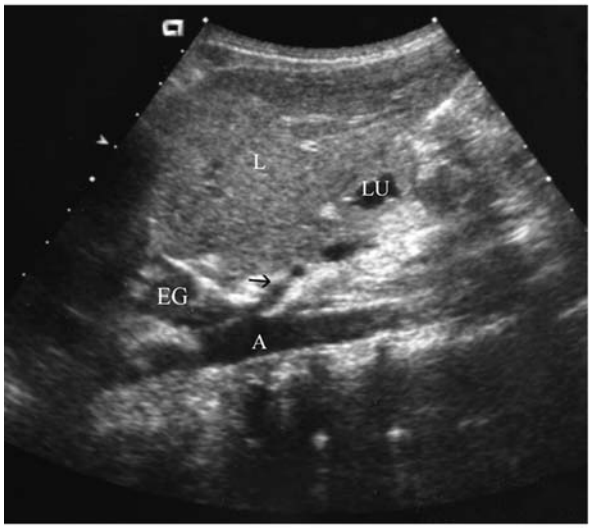

c

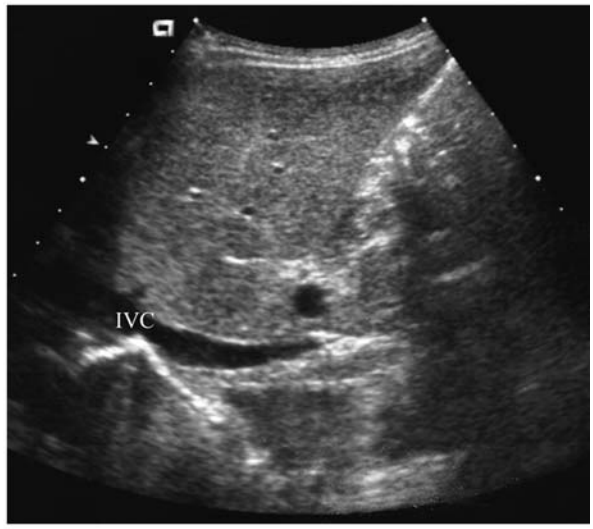

d

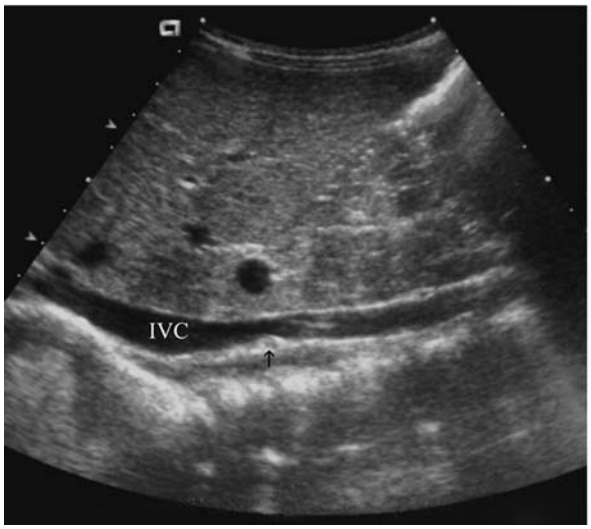

e

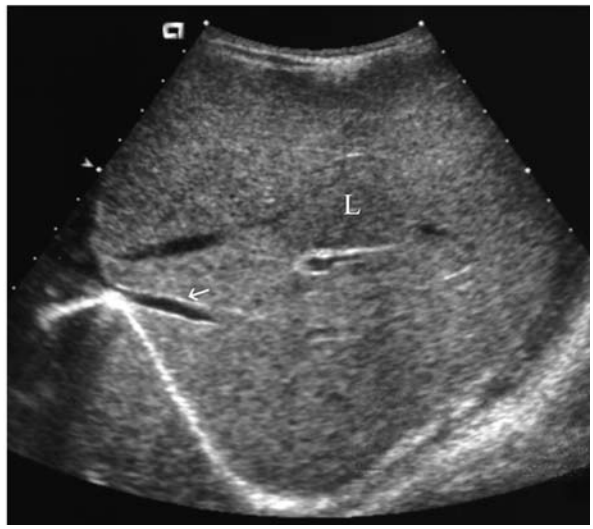

f

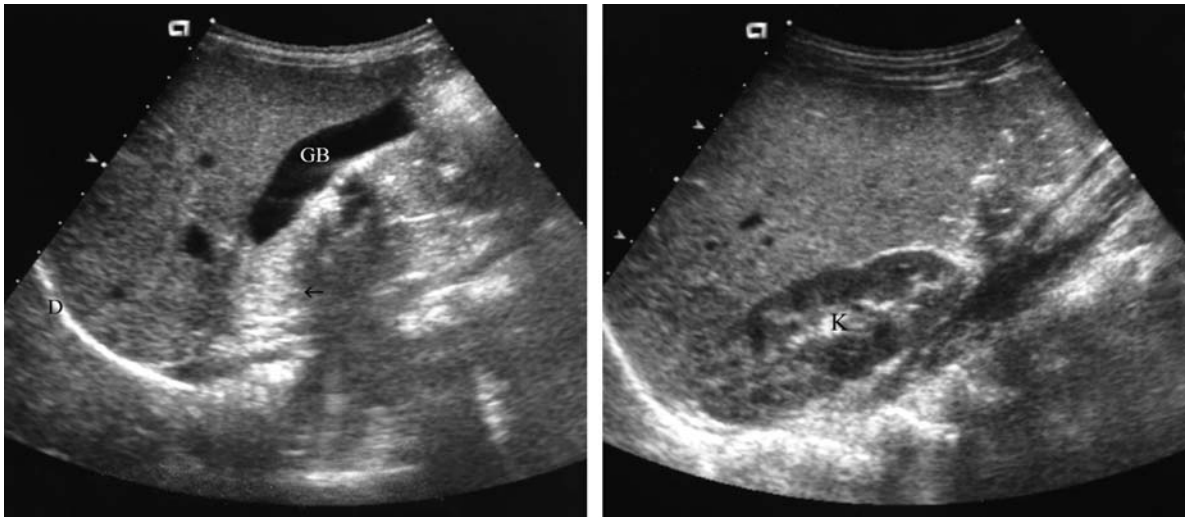

g h

Fig. 5.13. Legend see p. 96

but there are relatively few tubules (the cortex grows primarily by way of tubular growth). Thus in the neonate the glomeruli are crowded together in a volumetrically small cortex. Although quantitatively at a maximum, the neonatal glomeruli are qualitatively different from those seen later in life. The glomerular basement membrane is much more cellular in the neonate than the older child. Therefore it is not surprising that the neonatal renal cortex is echogenic and approximates or occasionally exceeds the echogenicity of the liver (Fig. 5.17). The renal medullae (the renal pyramids) are of greater relative volume now than they will ever be again, and the echo-free collecting ductules are visualized in striking relief against the echogenic cortex (Fig. 5.17). There is little fat in the neonate, and therefore the characteristic central sinus echogenic fat seen in the older child is not present. At all ages the renal pelvis and calyces can be seen if they are distended. It has been suggested that in well or overly hydrated patients the collecting system is seen more frequently. When the child has a full bladder the renal pelvis can be quite distended; however, with voiding the system returns to normal size.

Duplex Doppler imaging allows vascular evaluation of the kidney (Fig. 5.16). The image is obtained, a cursor is insonated in the appropriate vessel, and flow characteristics are evaluated. The major vessels (the main renal artery and vein) as well as smaller vessels can be insonated by the cursor and assessment of flow velocities and wave characteristics follows.

The viscera are in the upper three-quarters of the abdomen and the bladder, distal ureter, ovaries, uterus, and fallopian tubes are in the pelvis. Frequently bowel gas interferes with visualization of vessels between the bottom of the kidney and the viscera of the pelvis. Bladder wall thickness and volume is easily calculated when the patient has a full bladder. The degree of emptying can be ascertained by

Fig. 5.14. Normal transverse ultrasound ▶
a The most cephalic transverse section is through the liver (*L*) and the gallbladder (*GB*)
b Transverse section somewhat inferior to **a** showing the liver (*L*), kidney (*K*), and portal vein (*PV*)
c Transverse section through the head of pancreas (*P*) and splenic (*SV*) and portal vein (*PV*). The inferior vena cava (*I*) and aorta (*A*) are noted. *S*, spine
d Right transverse scan through the liver
e Left transverse scan through the spleen (*S*)
f Transverse scan showing the kidney (*K*), renal hilus, and gallbladder (*GB*). *S*, spine

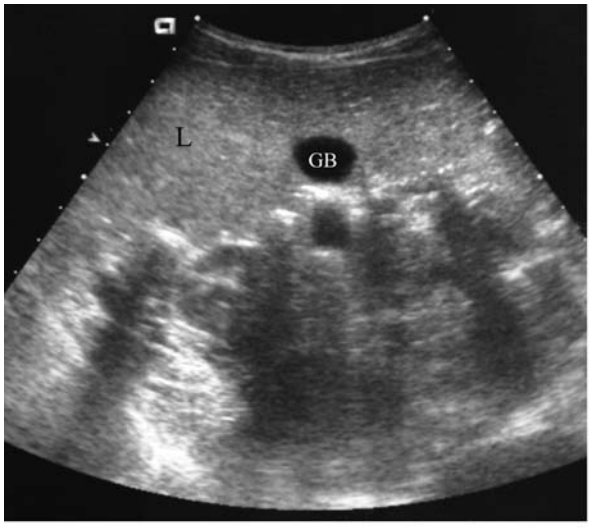

a

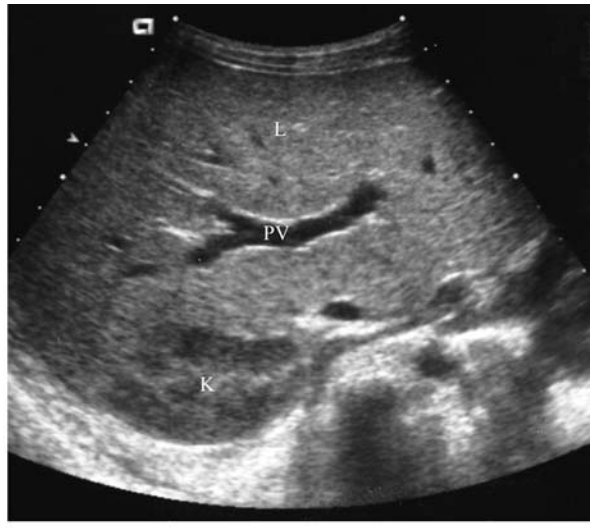

b

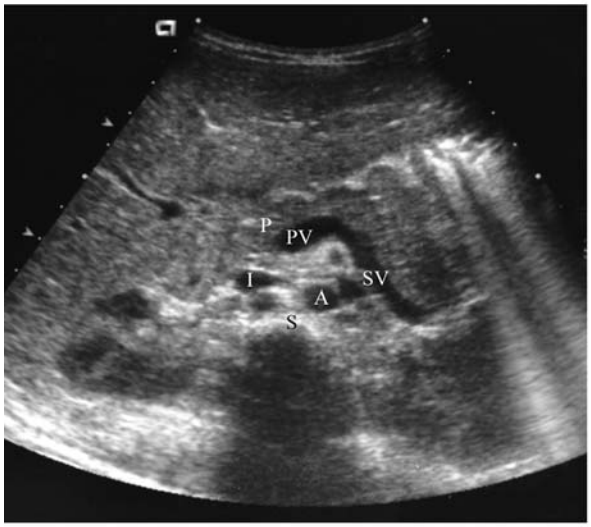

c

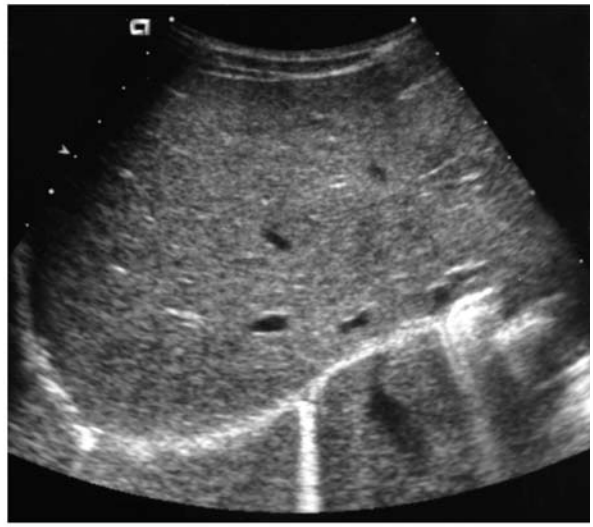

d

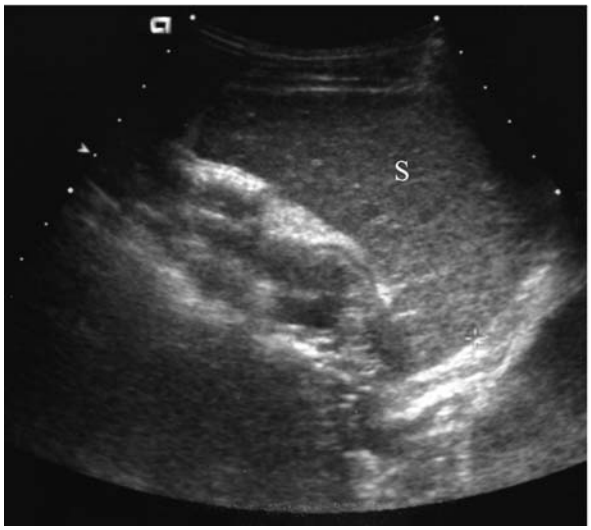

e

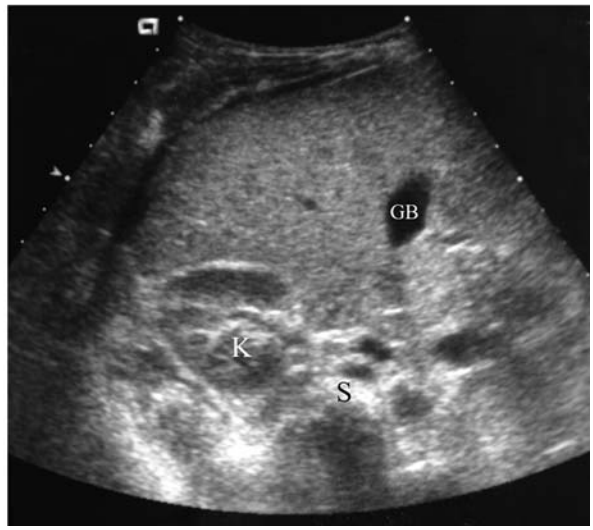

f

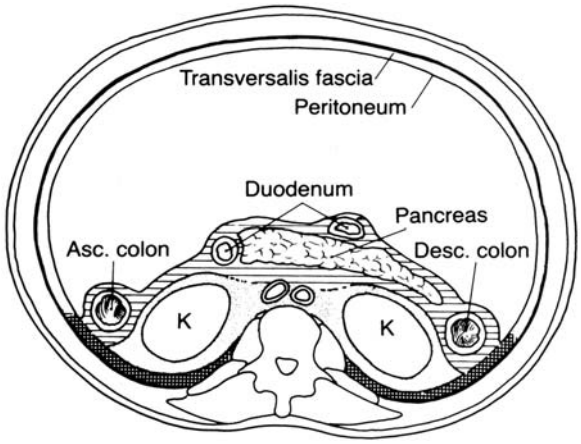

Fig. 5.15. The retroperitoneal spaces as described by Meyer et al [1]. *Striped area*, anterior pararenal space; *white areas* around kidneys, perirenal space; *cross-hatched areas*, posterior pararenal space. (From [1] with permission)

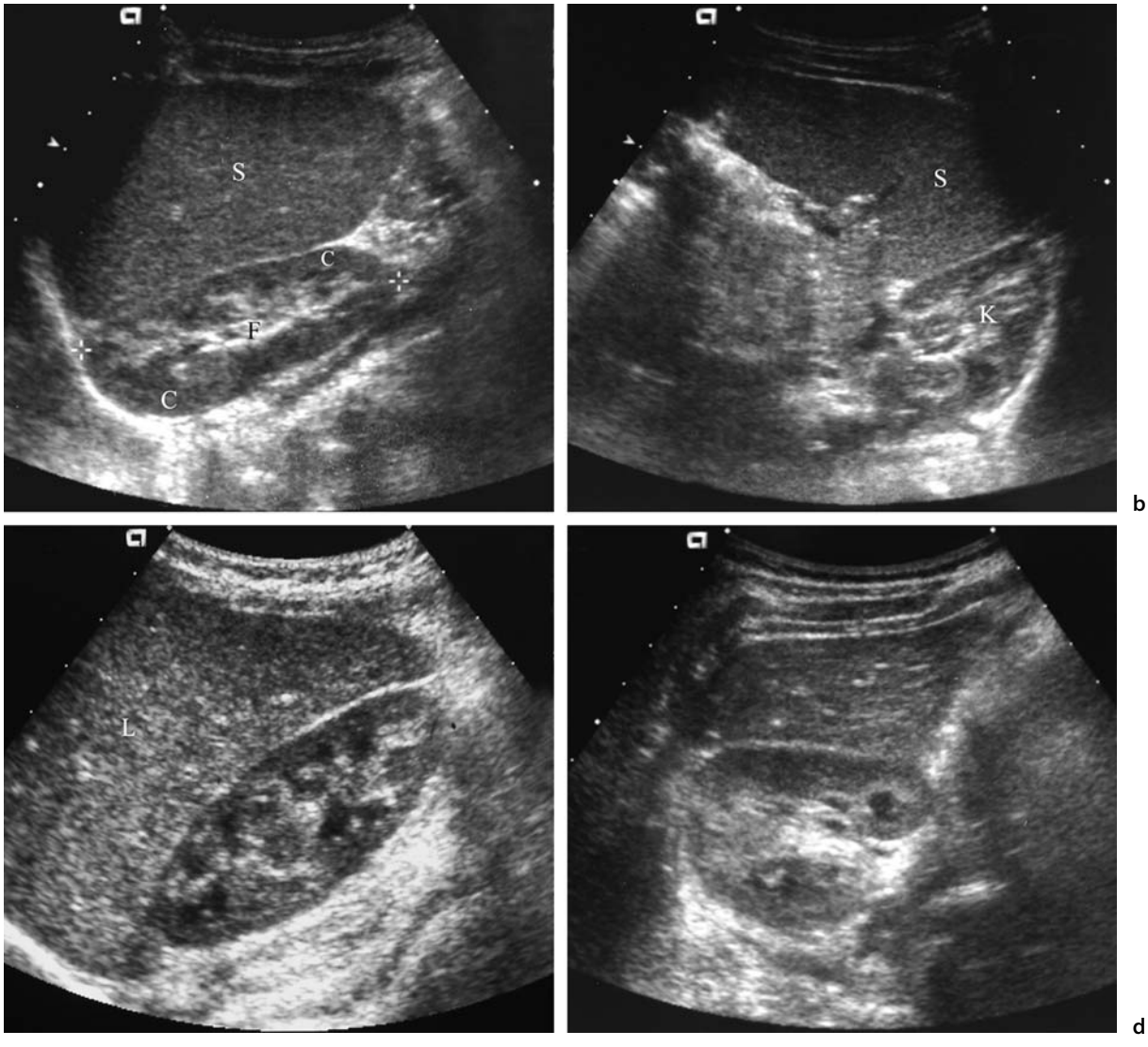

Fig. 5.16. Legend see p. 101

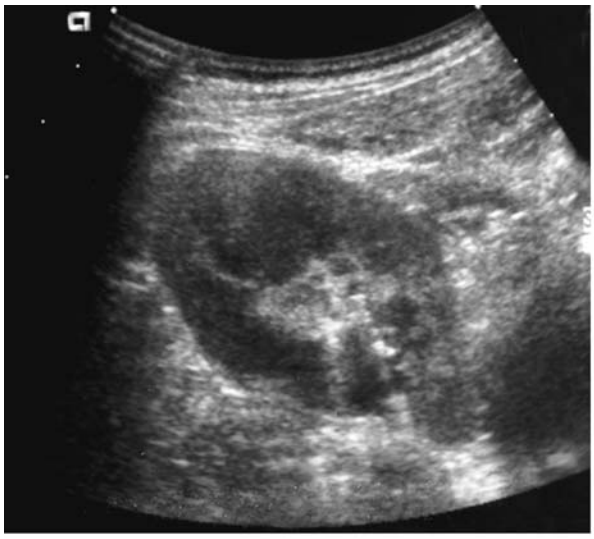

e

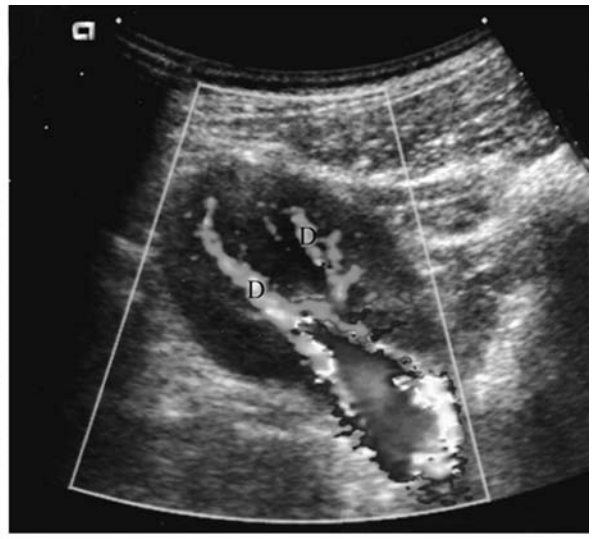

f

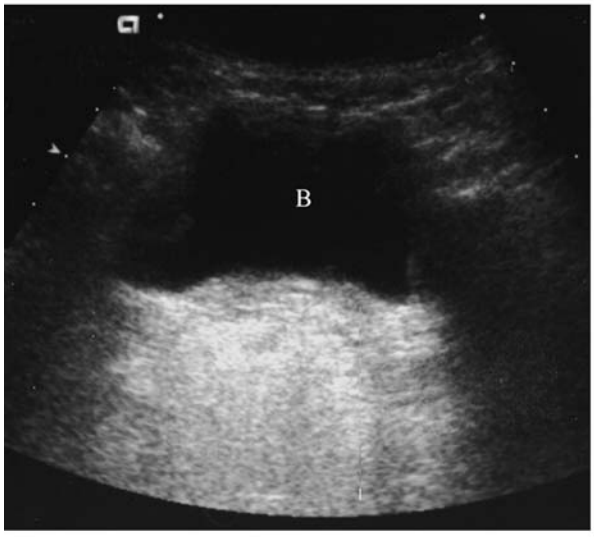

g

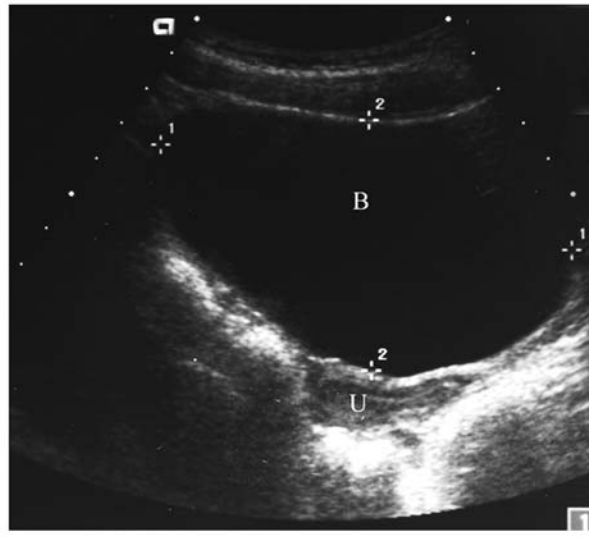

h

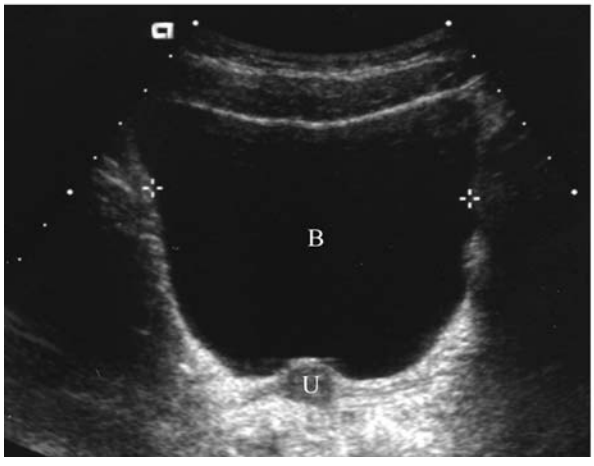

i

Fig. 5.16 (*continued*). Ultrasound of the kidney
a Longitudinal supine view of the normal left kidney in this normal 6-year-old. The spleen (*S*) is seen anteriorly. The renal cortex (*C*) is less echogenic (fewer white dots) than the spleen. There is fat (*F*) in the central sinus and around the kidney. Fat is echogenic (white)
b Transverse view of the left kidney (*K*) with the spleen (*S*) anterior
c Longitudinal right kidney with the liver (*L*) anterior to it. Both liver and spleen should not extend below the kidney on longitudinal views
d Transverse right kidney
e, f Transverse prone views of the right kidney. There is Doppler ultrasound (*D*) in renal vessels in **f**
g, h Transverse (**g**) and longitudinal (**h**) pelvic ultrasound shows the uterus (*U*) behind the bladder (*B*). This is a 2-year-old girl
i Transverse scan of the same patient as in **g** and **h** shows the uterus (*U*) below the bladder (*B*)

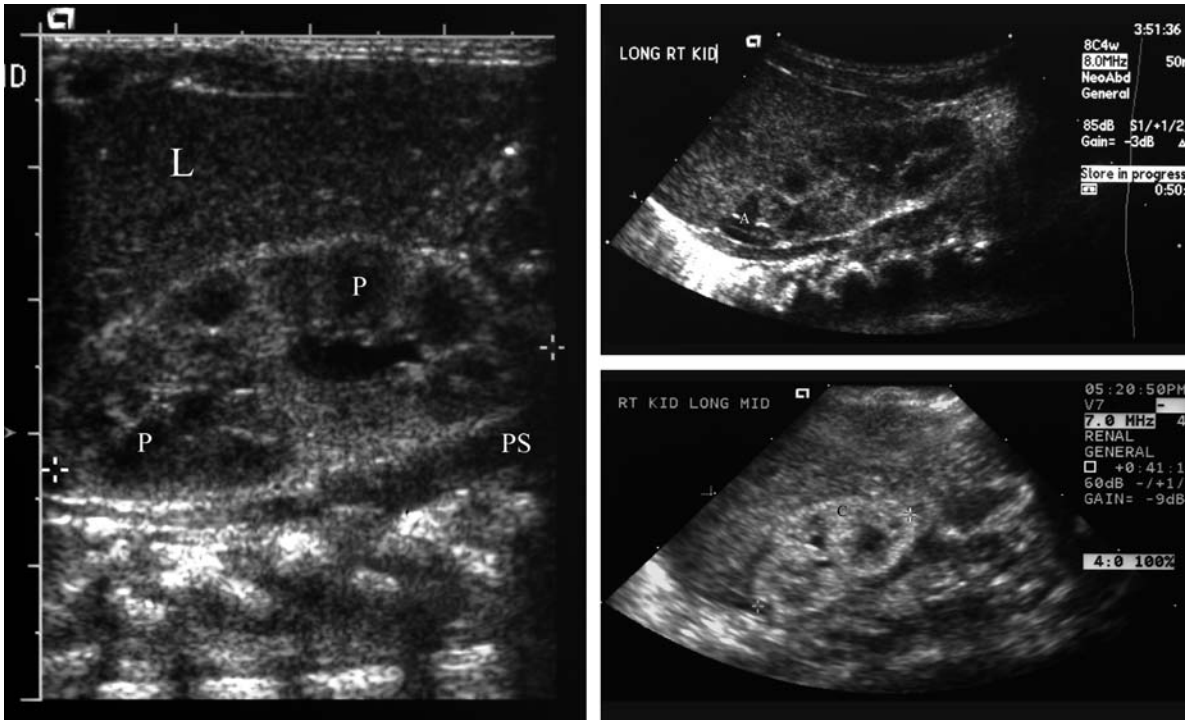

Fig. 5.17. Neonatal kidney
a Supine longitudinal view of the kidney reveals the anechoic medullary pyramids (*P*) arranged around the center of the kidney. There is no central sinus fat. The renal cortex is almost as echogenic as the liver. *L*, liver; *PS*, psoas muscle
b Supine longitudinal view in another neonate shows the adrenal (*A*)
c Another neonate with normal echogenic cortex (*C*). The echogenicity is greater than that of the liver

studying the bladder when it is full and after voiding (Fig. 5.18).

The vagina and uterus are easily identified (Fig 5.18). In the newborn, the cervix is equal to or larger than the body of the uterus. The prepubescent uterus is less than or equal to 2 cm. The ovaries may be more difficult to identify. The fallopian tubes are never normally seen.

It is important to study bowel with ultrasound. Though less sensitive to bowel abnormalities because of the interference by bowel gas, ultrasound can show the bowel signature of the wall, mucosa, and lumen. It reveals peristalsis and thickening as well as unyielding (noncompressible) abnormal bowel (see intussusception and appendicitis, Chap. 5, pp. 137–140). The use of color Doppler imaging aids in defining abnormal bowel.

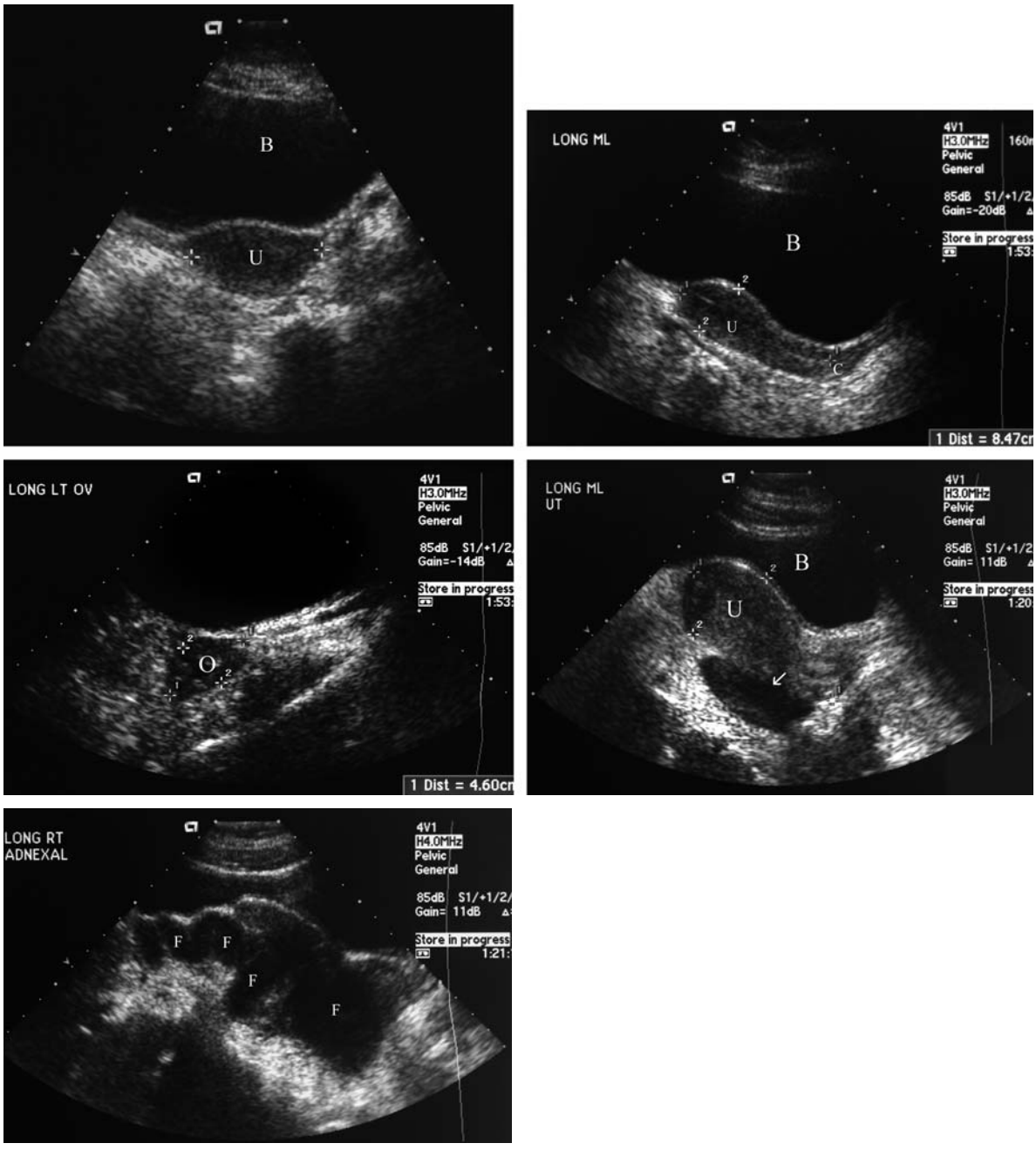

Fig. 5.18. Ultrasonography of the female pelvis
a Transverse scan through the full bladder reveals the bladder anteriorly (*B*) with the uterus behind (*U*)
b Longitudinal scan of the same adolescent patient shows the uterus (*U*) with the endometrial central line – the endometrial cavity. *B*, bladder; *C*, cervix
c The left ovary (*O*) in this same patient
d A 15-year-old female with abdominal pain. The bladder (*B*) seen anteriorly with the uterus (*U*) behind. Note a large "fluid collection" behind the bladder (*arrow*)
e This "fluid collection" was a convoluted fallopian tube (*F*) in a patient with pelvic inflammatory disease and tubal ovarian abscess

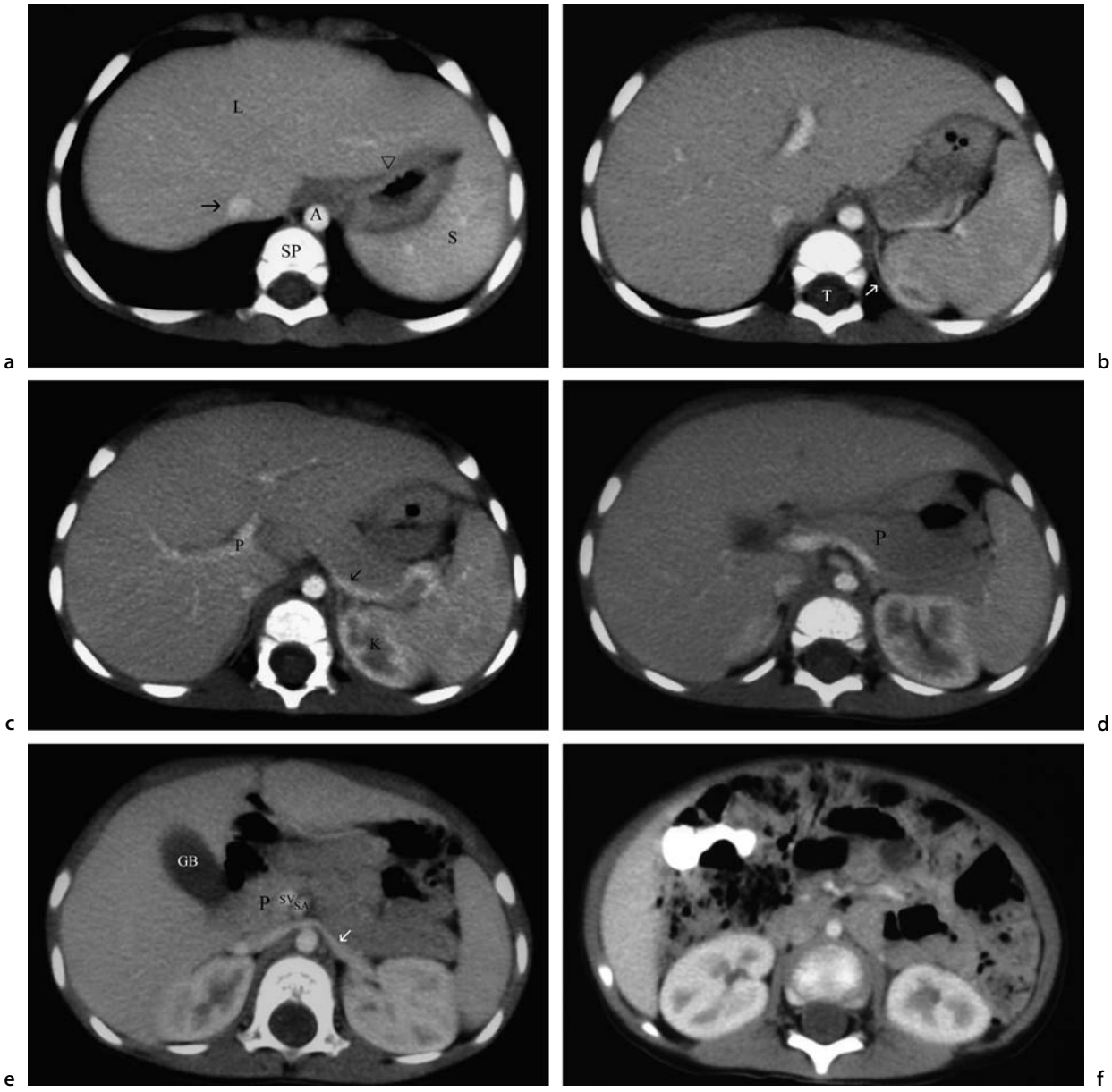

Fig. 5.19. Legend see p. 105

CT of the Abdomen and Pelvis

CT of the abdomen is quite exquisite in demonstrating all the viscera and bowel (Fig 5.19). With the new multidetector CT (MDCT), the examination is quick, complete, and in most instances will not require sedation. Most often oral contrast medium is given 2–5 h before the examination (depending on the indication) and intravenous contrast medium is given during the examination. Oral contrast medium is a dilute water-soluble agent with iodine to absorb the X-ray beam. The bowel lumen is white and this permits interpretation of nonbowel structures, such as lymph nodes or small masses. It allows better visualization of the pancreas. Clearly, any fluid collection which does not contain contrast medium in a well-prepared patient must be outside the gastrointestinal tract – an abscess or cystic mass. We try to do one exam (with contrast medium) to diminish radiation dose (examinations without and then with contrast medium give twice the radiation dose). The timing of intravenous injection and the beginning of the scan depend

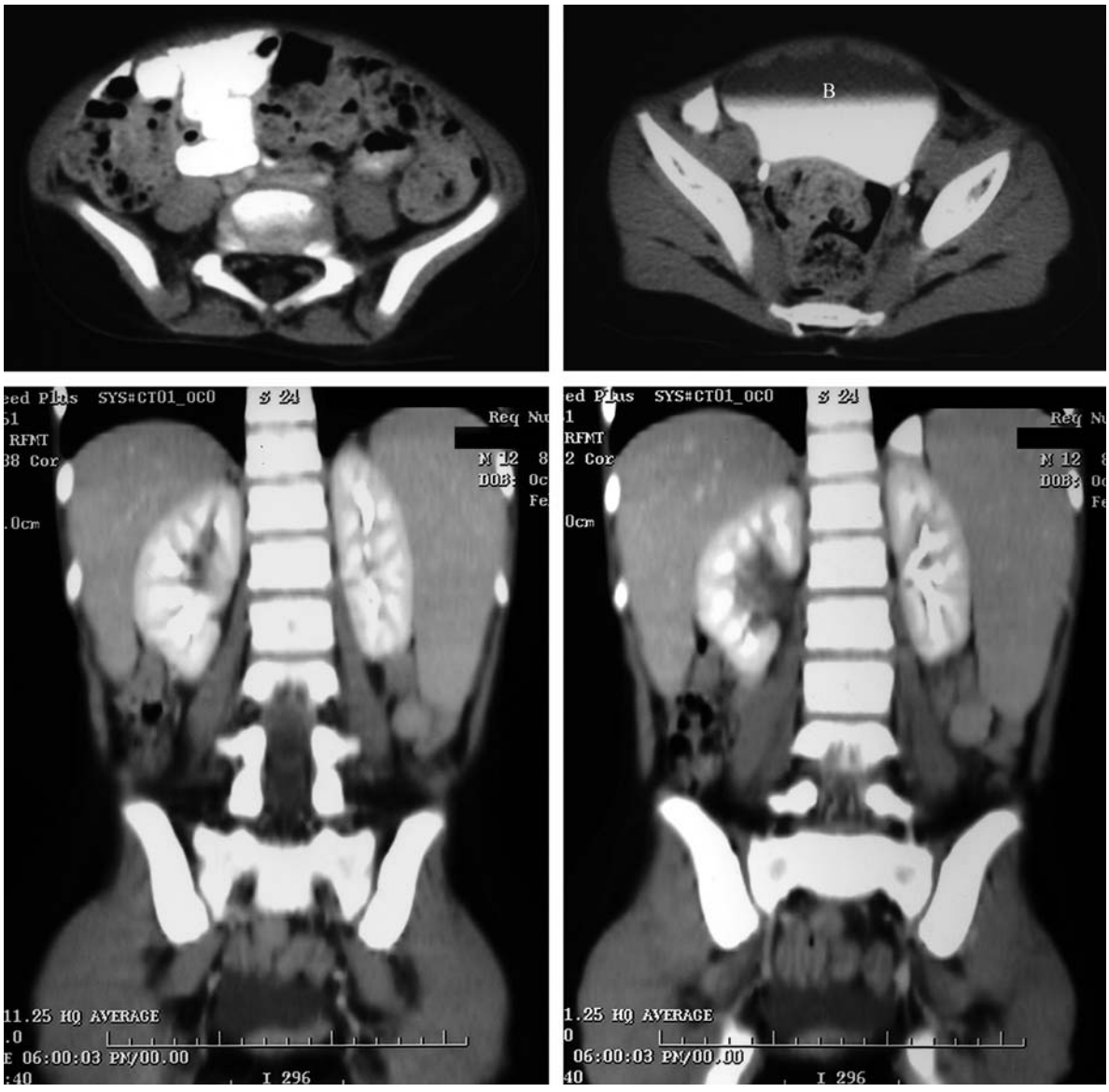

Fig. 5.19. CT of the abdomen and pelvis. Contrast-enhanced CT in a normal 2-year-old
a Section through the top of the liver reveals the inferior vena cava (*arrow*) and aorta (*A*). The liver (*L*), spleen (*S*), and stomach (*arrowhead*) are noted. The bony spine (*SP*) is seen posteriorly
b Scan somewhat more caudal through the liver, stomach, and spleen. The crux of the diaphragm (*arrow*) is seen, as is the thecal sac (*T*)
c Section slightly inferior to **b** shows the portal vessels (*P*) within the liver as well as the left kidney (*K*). Note the splenic vein (*arrow*) behind the tail of the pancreas
d Section through the pancreas. A better view of the tail and body of the pancreas (*P*) is obtained on this image
e Scan slightly more caudad reveals the head of the pancreas (*P*). The left renal vein (*arrow*) is noted passing above the aorta into the inferior vena cava. Note that the superior mesenteric vein (*SV*) is appropriately positioned to the right of the superior mesenteric artery (*SA*). The gallbladder is visualized (*GB*)
f View lower in the abdomen shows the patient has been given oral contrast medium. There is some in the bowel in the region of the hepatic flexure
g Section through the region of the top of the iliac crest continues to show bowel
h Section through the bladder (*B*) partially filled with contrast medium
i, j CT urogram done by coronal reconstruction. The right collecting system of the kidney is not filled with a contrast agent

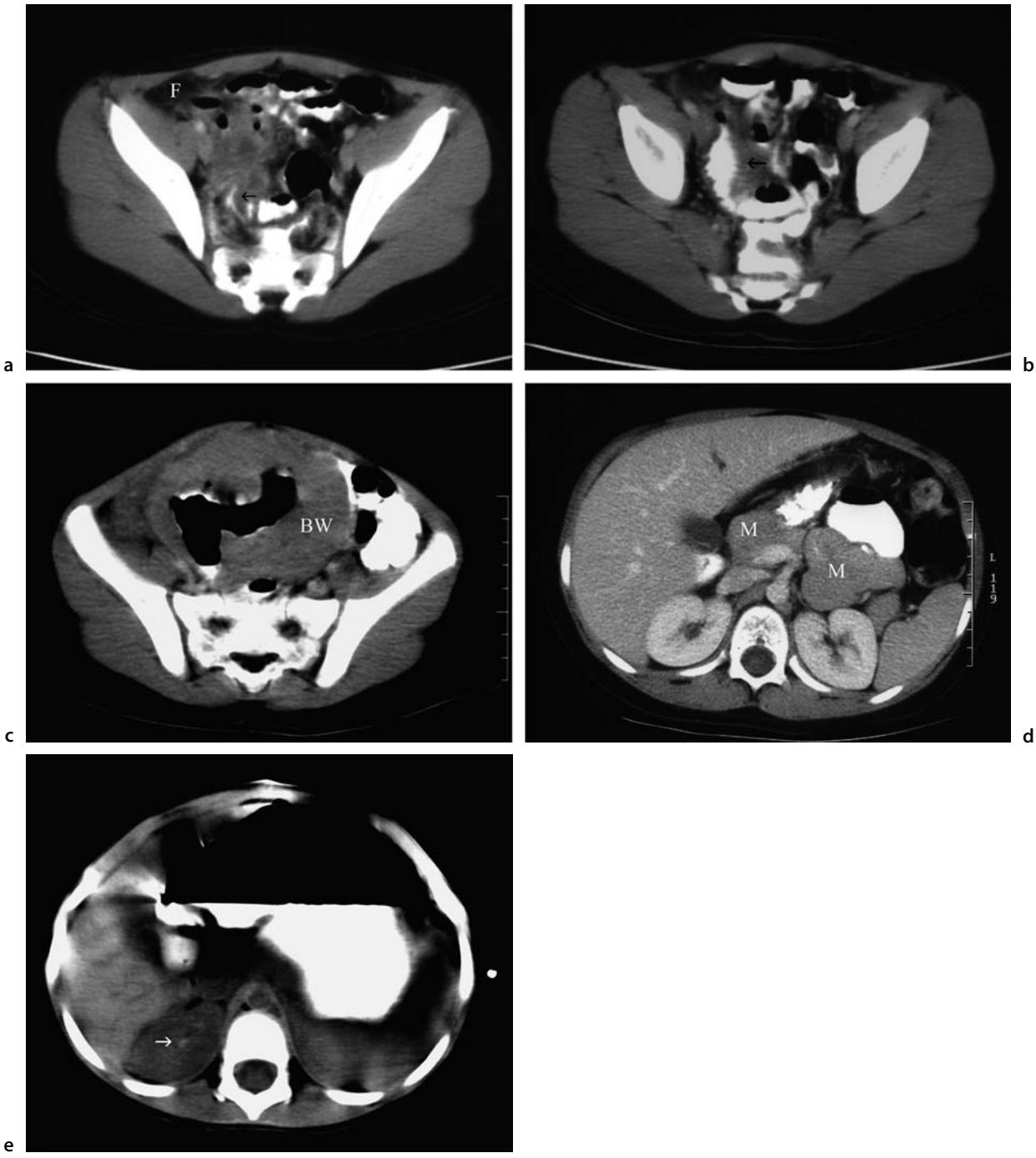

Fig. 5.20. Abnormal CT scans
a, b A 7-year-old with chronic abdominal pain. Two scans through the pelvis reveal the fat is inflamed and strand-like (*F*) and there is irregularity of the bowel wall (*arrow*) – all signs of inflammatory bowel disease
c, d A 3-year-old male with weight loss and failure to thrive. There is thickened bowel wall (*BW*) surrounding air within the lumen. This is the classic "aneurysmal dilatation" of bowel seen in lymphoma. Follow-up examination 2 years later shows now there are lymphomatous masses in the midabdomen (*M*)
e An 11-year-old with renal colic. Nonenhanced scan through the kidneys shows the right renal stone (*arrow*)

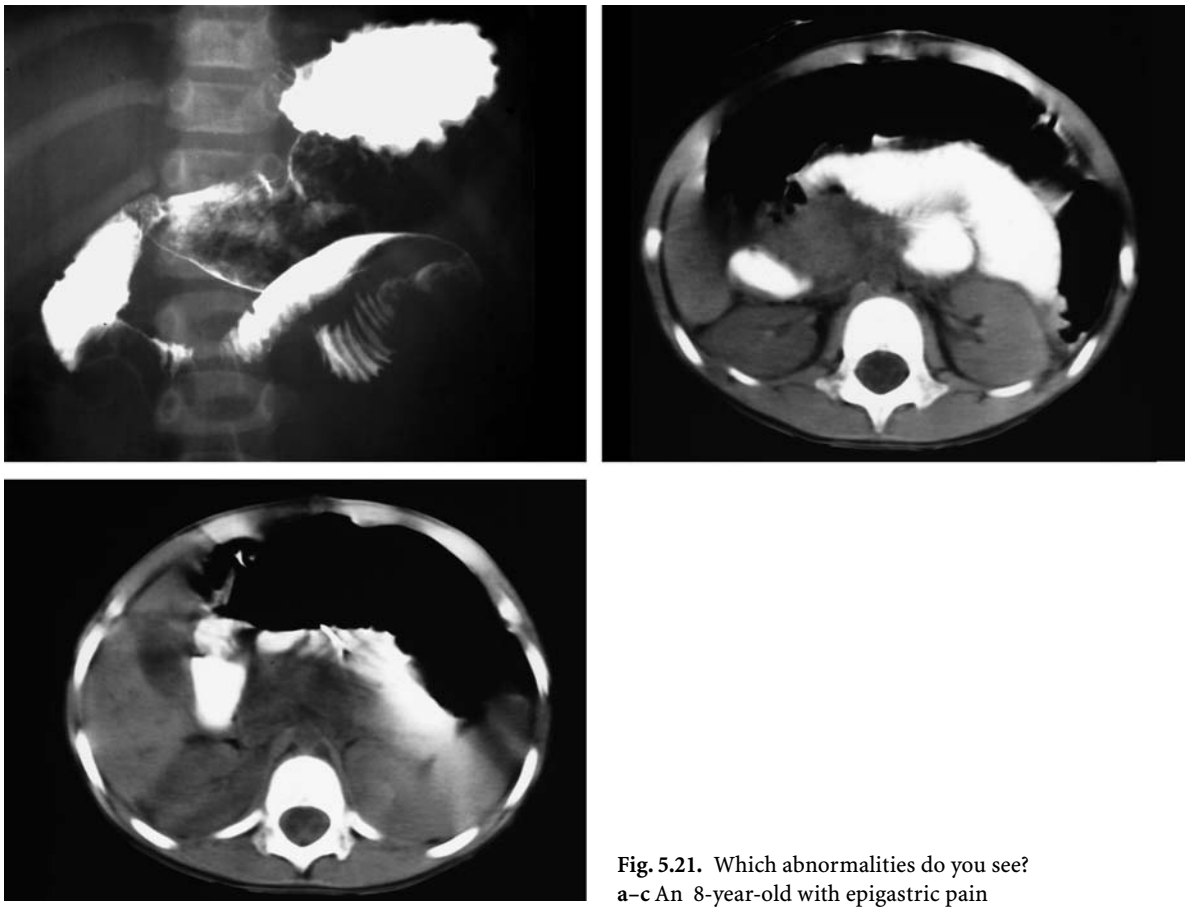

Fig. 5.21. Which abnormalities do you see?
a–c An 8-year-old with epigastric pain

on the reasons for the study and on which organ in particular one wants to evaluate.

MDCT allows acquisition of thicker slices (less radiation) and then reconstruction of thin slices for minute detail. It also lets us reconstruct images in multiple planes. CT angiography (Chap. 9) increases our ability to detect pathology.

The ability to define the entire retroperitoneum most precisely is a huge advantage of CT. The three components of the retroperitoneum are: (a) the anterior pararenal space, (b) the perirenal space, and (c) the posterior pararenal space (Fig. 5.15). The anterior pararenal space extends from the posterior peritoneum to the anterior renal fascia of Gerota. It contains the extraperitoneal portions of the gastrointestinal tract including the ascending and descending colon, the duodenal loop, and the pancreas. Because it contains the pancreas, it crosses the midline, and it is laterally confined by the lateroconal fascia. The perirenal space defined by the anterior and posterior layers of Gerota's fascia contains the adrenal gland and the kidney with its surrounding fat. These two fascial layers fuse laterally to form the paracolic gutters. The posterior pararenal compartment extends from the posterior renal fascia to the transversalis fascia and contains no viscera. This space continues laterally as the properitoneal fat of the abdominal wall.

CT of the kidneys without contrast medium allows the radiologist to detect calcifications. Contrast-enhanced CT is a very sensitive method for demonstrating renal infections and masses. With coronal reconstructions, MDCT has replaced the old excretory urogram (intravenous pyelogram). CT can show the uterus and ovaries but is less precise than ultrasound for identification of normal ovaries. The normal fallopian tubes are not visualized.

CT is superb for bowel and is not hindered by bowel gas. Bowel wall abnormalities such as thickening are easily seen. Inflammation and those diseases which infiltrate the fat causing stranding ("dirty fat") as well as bowel obstruction can be displayed (Fig. 5.20). What are the abnormalities in 5.21? See Appendix 2.

MR Imaging of the Abdomen

MR imaging of the abdomen is increasingly used in diagnosis and follow-up of tumors and renal evaluation. The principal problems with MR imaging are the difficulty of obtaining superb images because of motion artifacts (vascular, peristaltic, and body), the need for sedation or general anesthesia in patients less than 7 years of age, and timely access to the scanner.

The use of intravenous contrast medium (gadolinium) is mandatory. Some centers use gastrointestinal contrast medium. The appropriate coil and fast pulse sequences (Chap. 1) must be utilized to obtain the best images (Fig. 5.22). MR imaging is the best study

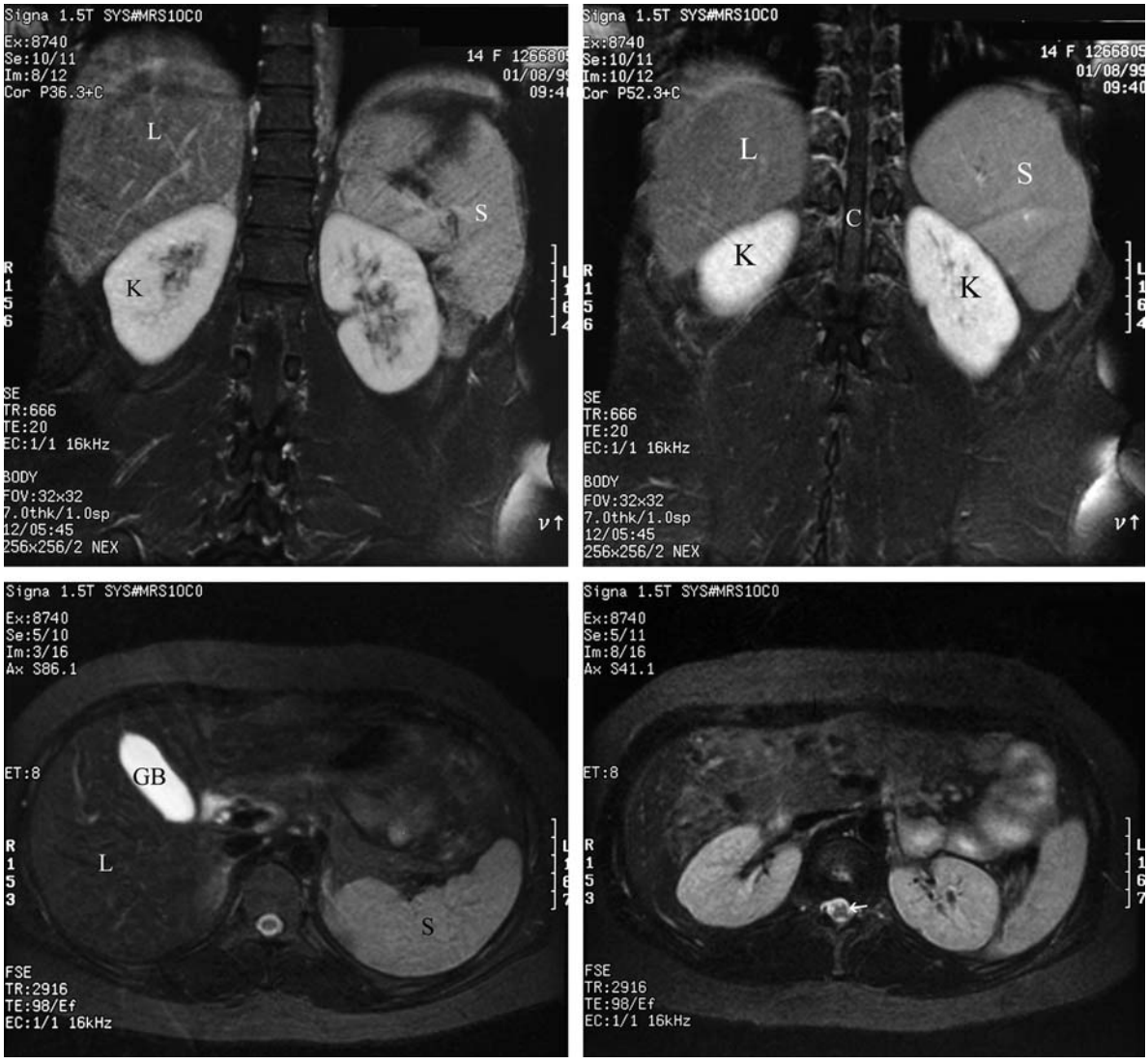

Fig. 5.22. Normal MR of the abdomen

a Coronal abdomen beginning at the level of vertebral bodies shows the liver (*L*), the kidneys (*K*), and the spleen (*S*). This is a fat-suppressed T1 image with intravenous contrast medium

b Similarly a more posterior coronal T1 contrast-enhanced image shows the right lobe of the liver (*L*) and the spleen (*S*), as well as the kidneys (*K*). Note the spinal cord (*C*)

c Transverse view of the abdomen through the gallbladder (*GB*) reveals the spleen (*S*) and liver (*L*). This is a T2 image as one can tell by the white spinal fluid and white bile

d T2 image somewhat lower shows the inferior margin of the liver and both kidneys. The renal hila are seen quite well. Note that the conus medullaris of the spinal cord (*arrow*) is at the level of the midportion of the kidneys

e see p.108

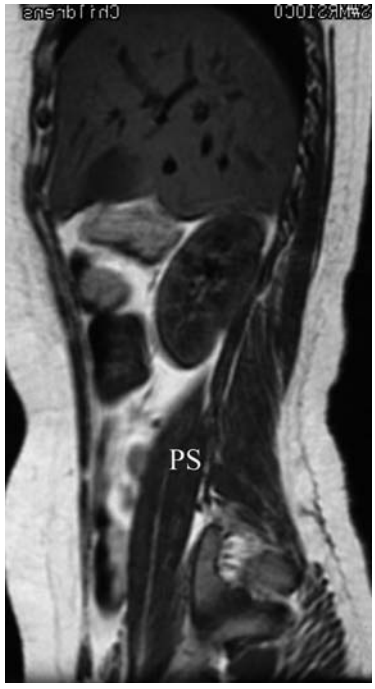

e

Fig. 5.22 (*continued*)
e Sagittal section on the right side through the liver and right kidney. Note the psoas muscle (*PS*)

to image the pelvic organs and the multiplanar aspects of the pelvis, provide important information by which to diagnose complex congenital anomalies (for example, in patients with ambiguous genitalia), and detect masses.

MR will probably become the primary modality following ultrasound for renal imaging. Dynamic contrast-enhanced MR urography reveals the kidney, ureter, and bladder in multiple planes with exquisite detail (Fig. 5.23). It can be used to diagnose congenital anomalies and obstruction and gives differential (each kidney) functional information. When diuretic MR urography is performed, the diuretic is given 15 min before the intravenous agent (gadolinium). Figure 5.23 shows the dynamic normal study with the cortical, parenchymal, and excretory stages.

MR angiography and cholangiography are important techniques just being popularized in pediatrics. MR angiography in cases of renal hypertension, vasculitis, venous anomalies, and thrombosis is promising. It will be used in renal transplantation evaluation.

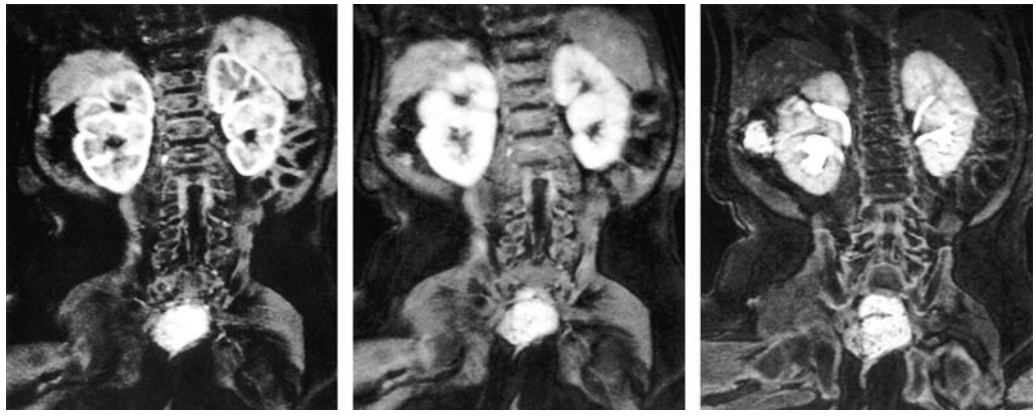

a–c

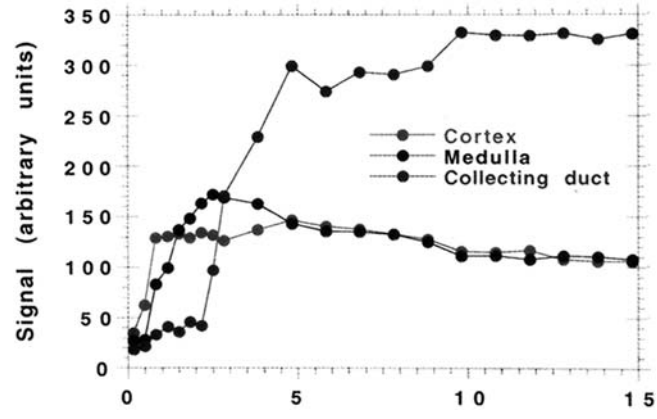

d

Fig. 5.23. Legend see p. 110

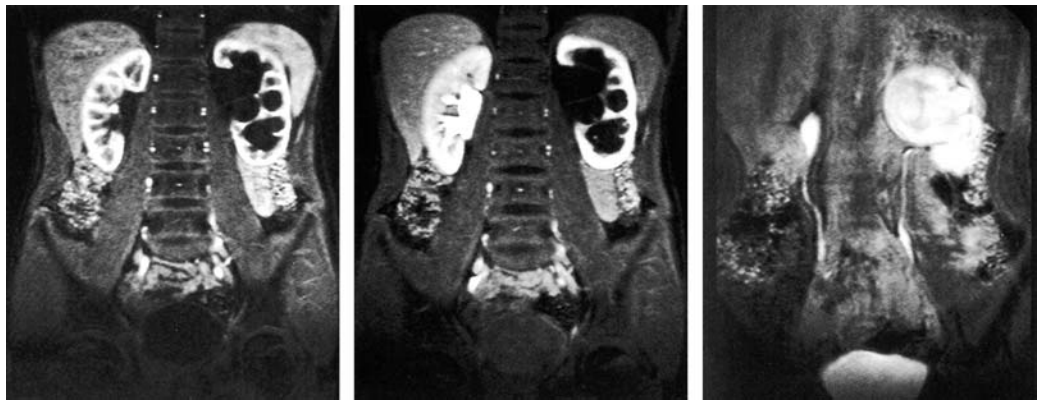

e–g

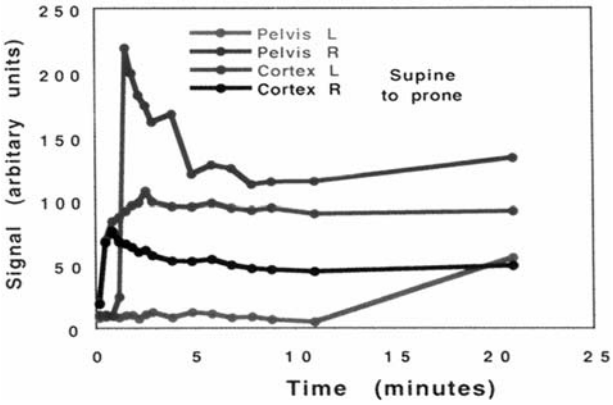

h

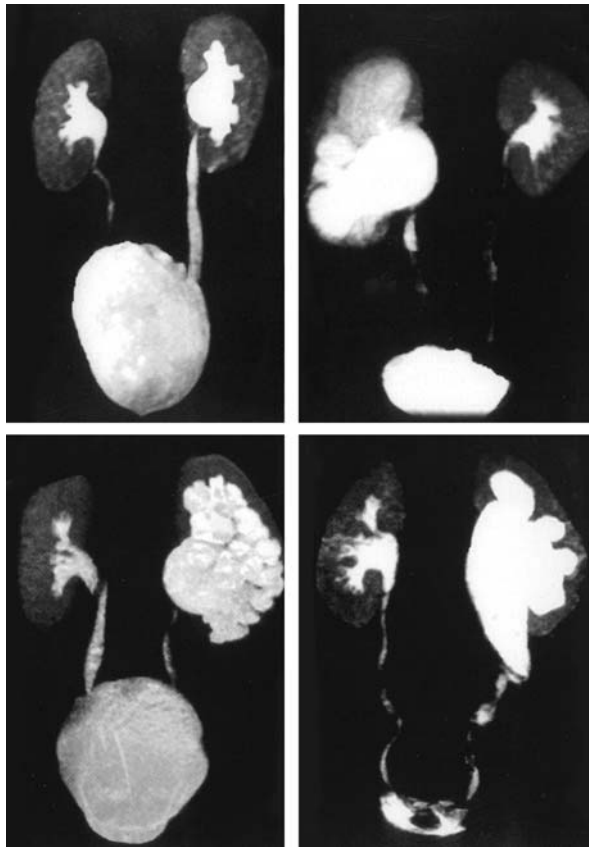

i, j

k, l

Fig. 5.23. Dynamic contrast-enhanced MR urography from [2] with permission.
a–d A 4-month-old girl with bilateral duplex kidneys showing normal excretion pattern. The immediate post-contrast image (**a**) demonstrates vivid and symmetric enhancement of the renal cortex. Image obtained just before contrast excretion (**b**) into the collecting system demonstrates enhancement of all the renal parenchyma including medulla. The renal parenchyma associated with upper and lower pole moieties is easily assessed. Approximately 2 min after contrast administration (**c**) there is symmetric excretion into the upper and lower pole moieties bilaterally. Signal intensity versus time curves (**d**) were generated to demonstrate signal changes in the cortex, the medulla, and the collecting systems. The pattern is reproducible in normal kidneys, and the renal transit time can be measured as the time from the initial enhancement in the renal cortex to appearance in the collecting system (From [2] with permission)
e–h A 12-year-old boy with left-sided ureteropelvic junction obstruction secondary to crossing vessel. Immediate images (**e**) show symmetric perfusion of the renal cortex with hydronephrosis on the left. Excretion was delayed on the obstructed left side (**f**). Contrast is seen in the right renal pelvis and ureter, but not on the left side. Also note the increased signal intensity associated with the nephrogram on the left. Delayed image at 20 min (**g**) shows contrast filling the dilated left renal pelvis with contrast, also noted in a normal-caliber ureter. The flow void at the level of the ureteropelvic junction represents the crossing vessel causing the obstruction. Signal intensity versus time curves (**h**) for the renal cortex and pelvis bilaterally. Note the symmetric enhancement of the kidneys with marked delay in excretion on the left. Also note the persistent higher signal intensity of the left renal cortex when compared to the right
i–l MIP images demonstrating morphology and anatomy of the urinary tracts. Upper left (**i**) a 2-year-old girl with mild narrowing of the UPJ considered nonobstructive. Upper right (**j**) a 6-week-old girl with typical rightsided UPJ. Lower left (**k**) a 6-month-old boy with over-left sided UPJ. Lower right (**l**) a 5-month-old boy with conical shape of the renal pelvis and tortuous proximal ureter. this child has persistent fetal folds

Imaging Studies for Specific Organs and Systems

Bowel

Barium sulfate is used to coat the *intraluminal surface* of the bowel in order to reveal mucosal, submucosal, and extrinsic masses impinging on or constricting the lumen. By viszalizing the bowel fill under fluoroscopic control the radiologist can observe distensibility, pliability, and intraluminal content. Peristaltic activity, particularly in the upper gastrointestinal tract, is also observed. These features are important when one suspects neoplasm or inflammation. The intricacies of these radiological examinations are beyond the scope of this text. In general, the patient is placed in multiple positions while barium is introduced either orally or rectally under direct vision, i.e., fluoroscopic control. Films are obtained with the patient in many positions so that air and barium coat different portions of the bowel.

Esophagus

Evaluation of the upper gastrointestinal tract begins with an esophagram (Fig. 5.24).

► ***Rule No. 5:*** An esophagram must be performed in any child with unexplained respiratory disease.

Many abnormalities of the esophagus (foreign body, duplication, etc.) and disorders of the swallowing mechanism may lead to respiratory distress secondary to aspiration and/or compression of the airway. On an esophagram the entire nasopharynx, oropharynx, and hypopharynx, as well as the esophagus from its origin at the inferior margin of the hypopharynx to the diaphragm, should be seen (see Fig. 5.24). It is important to see that the nasopharynx is not filled with contrast. As with all examinations, it is crucial to look at adjacent structures, for example, the airway, to make sure there is no compression, displacement, or contrast material within the trachea. It is important to study the esophagus for position, contour, and size. The fluoroscopist evaluates the motility of the esophagus, as this is difficult to ascertain on plain films alone.

In evaluating the *position* of the esophagus note that in the lateral projection there should be no separation between the anterior wall of the esophagus and the posterior wall of the trachea. On frontal examinations the esophagus overlies the right side of the spine, passing through the intrathoracic portion until it crosses the spine distally. The esophagogastric junction is to the left of the spine.

The *contours* of the esophagus are smooth, with specific, normal indentations (see Fig. 5.24). The first is the cricopharyngeal muscle, a smooth posterior indentation in the cervical region at the C5 level.

► ***Rule No. 11:*** In obstruction of a lumen there should be proximal distention.

It is unusual for the cricopharyngeal muscle to cause a problem, except in severe neurological impairment. The next two indentations on the barium column are seen on the frontal radiograph: the first at the level of the aortic arch and the next at the level of the left main-stem bronchus. Foreign bodies, when ingested, are usually found in these regions (see Fig. 5.25), as are vascular anomalies.

The *size* of the esophagus changes with peristalsis. The fluoroscopist sees a wave beginning above and proceeding uniformly through the esophagus until it empties its contents into the stomach. This is a stripping wave. Conditions with abnormal motility are usually detected at this time. On any single film one area of the esophagus may be may be more dilated or constricted than another, but this should be a transitory phenomenon. A specific area of normal intermittent widening is in the distal one-third of the esophagus, just above the gastroesophageal junction. This is a good place to detect esophageal varices or hiatal hernia. In our departments, we follow barium through the ligament of Treitz on every esophagram so we will not miss a malrotation.

Upper Gastrointestinal Series

The upper gastrointestinal series (Fig. 5.26) includes visualization of the esophagus, as well as the stomach, duodenum, and ligament of Treitz. This ligament is the fibrous band that fixes the duodenal–jejunal junction to the posterior peritoneal wall to the left of the spine at a cephalic height equal to that of the duodenal bulb. The upper gastrointestinal examination is useful for detecting ulcers or masses within the stomach, ulcers or obstruction of the duodenum, and malrotation, a condition in which the duodenal–jejunal junction is not properly fixed by the ligament of Treitz. Failure of this fixation often results in obstruction of the duodenum, either by peritoneal bands or

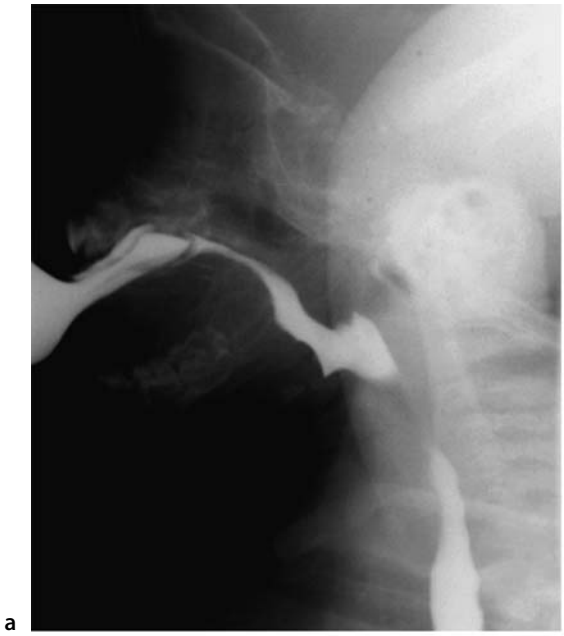

a

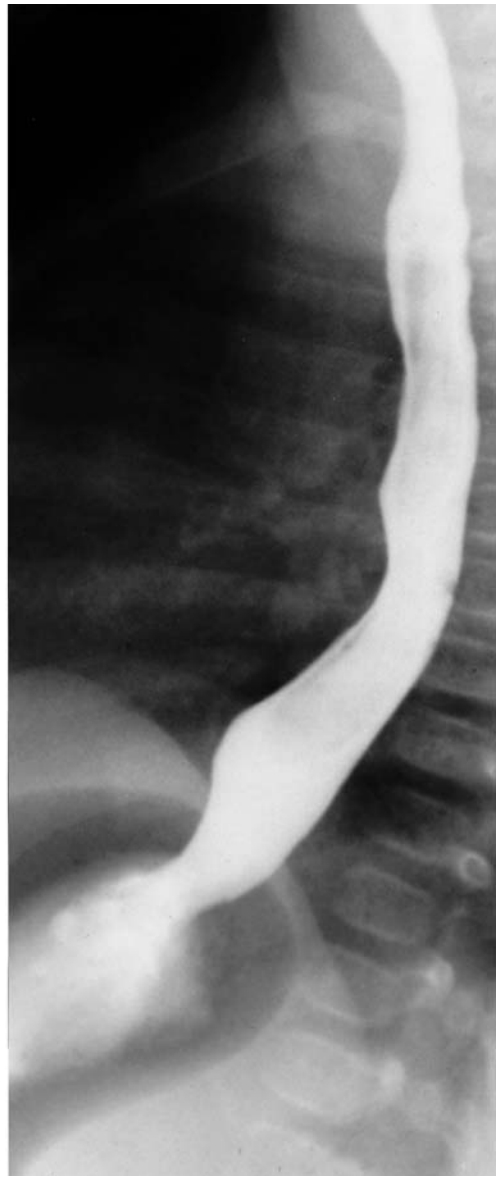

b

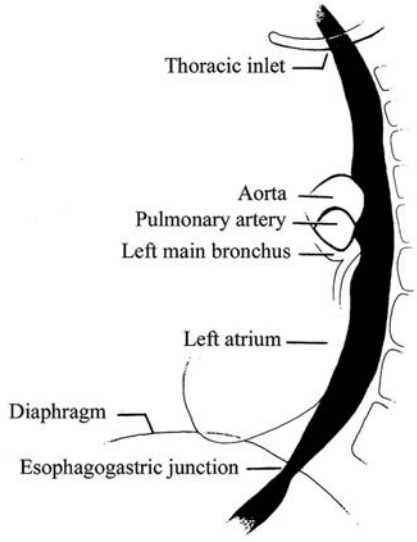

c

Fig. 5.24. The normal esophagram
a Films are taken routinely in the frontal and lateral projections. In this lateral view the swallowing mechanism is observed, and the contrast is noted at the oropharynx, hypopharynx, and proximal esophagus. There is no nasal reflux. Barium in the nasopharynx may indicate swallowing dysfunction
b The entire esophagus is visualized, including the esophagogastric junction. The walls are smooth and undulate gently. There are no mass impressions upon the esophagus
c Drawing of the lateral view of the barium-filled esophagus with the normal physiological areas of narrowing

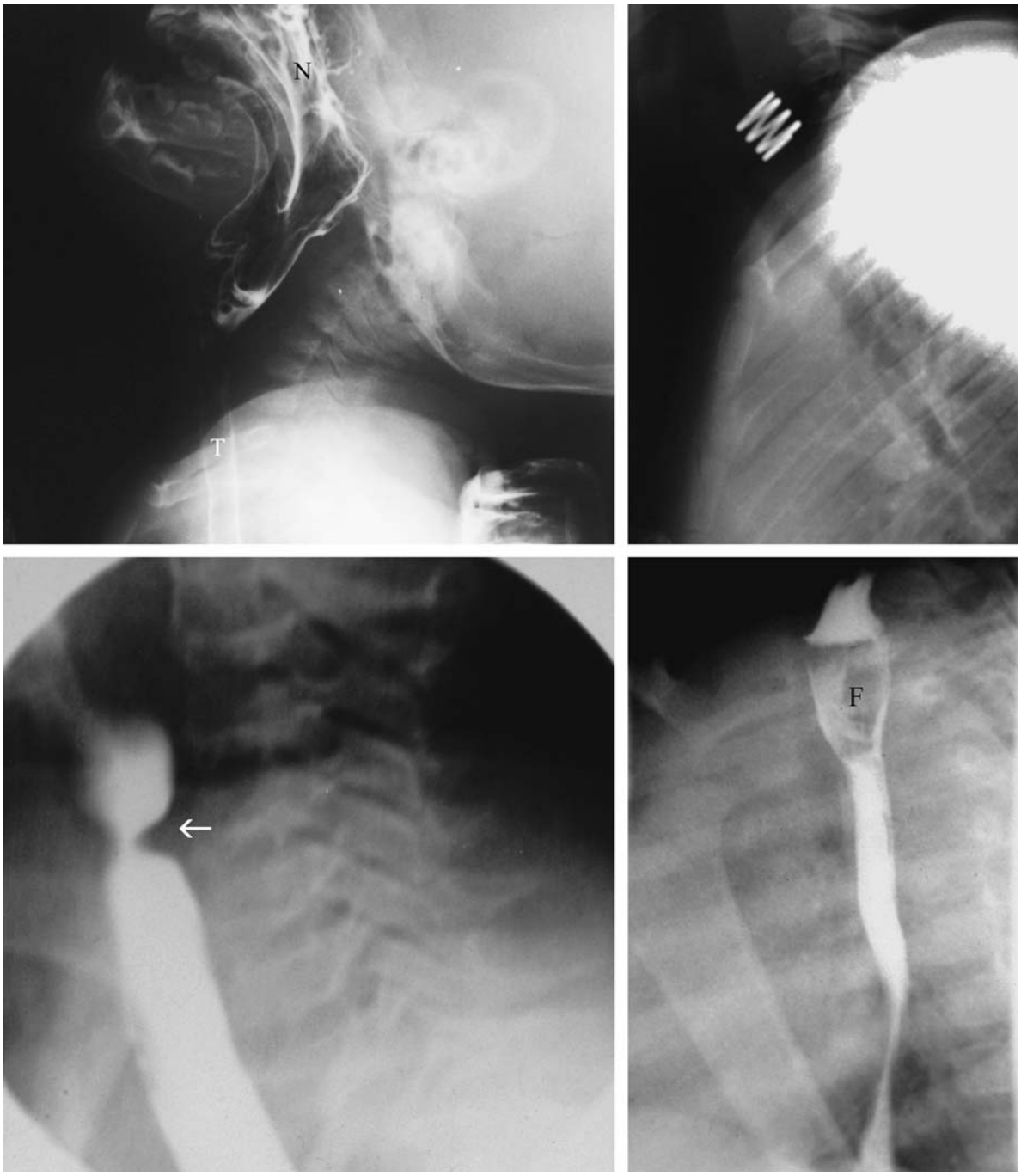

Fig. 5.25. Esophageal abnormalities
a This infant has swallowing difficulty and nasal reflux (*N*). The infant choked and aspirated the contrast medium into the trachea (*T*)
b This 16-month-old has a radiopaque spring in the cervical esophagus. The cricopharyngeal muscle at C5 is one of the areas of physiological narrowing. Children with esophageal foreign bodies frequently present with airway symptoms due to impingement on the trachea
c A 5-year-old with multiple episodes of choking. The posterior impression (*arrow*) in the esophagus is the cricopharyngeal muscle causing intermittent obstruction. This is cricopharyngeal achalasia
d The aortic arch is another site of physiological narrowing. When this food substance (*F*) was removed, no stricture was found. If a foreign body is stuck at an area other than a normal site of narrowing, a stricture should be suspected. Note the distention of the esophagus above the level of the aortic arch

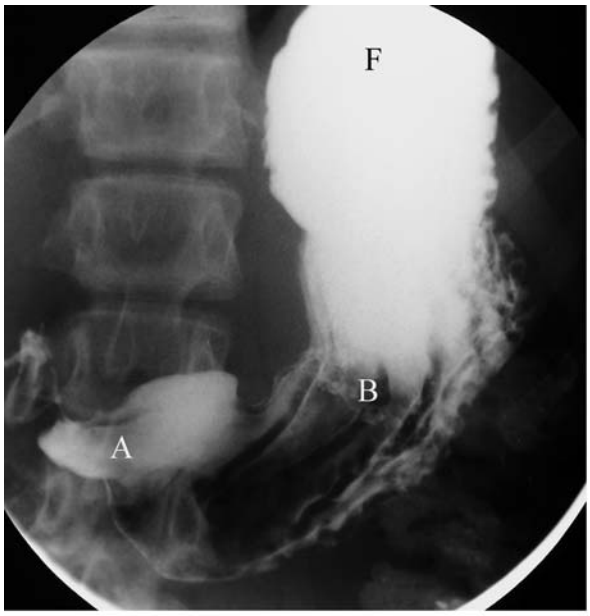

a

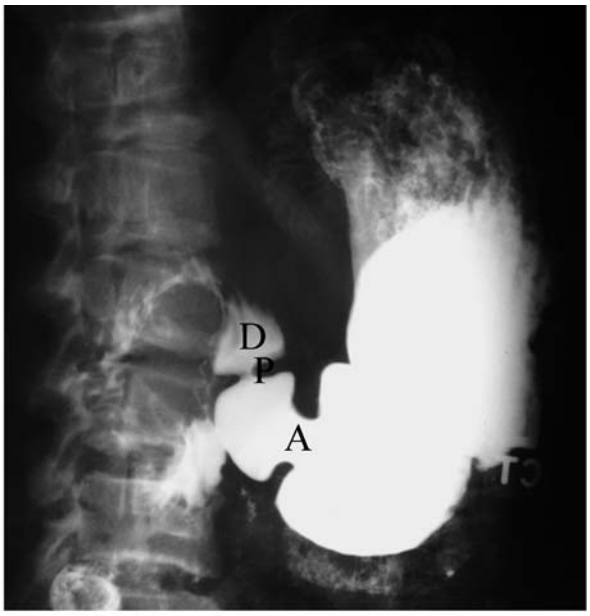

b

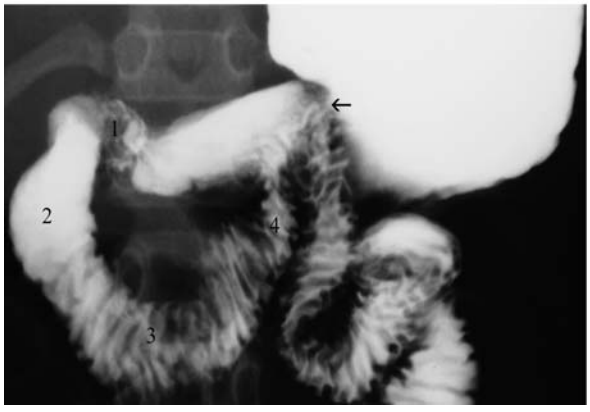

c

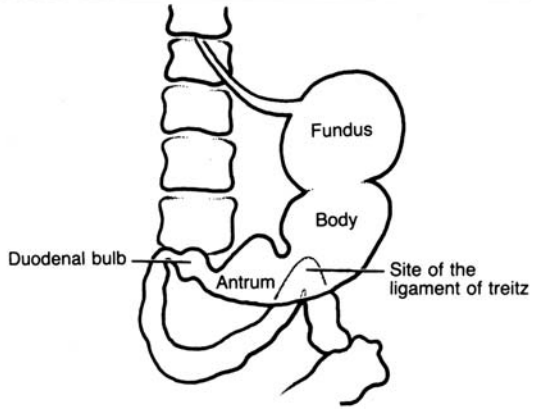

d

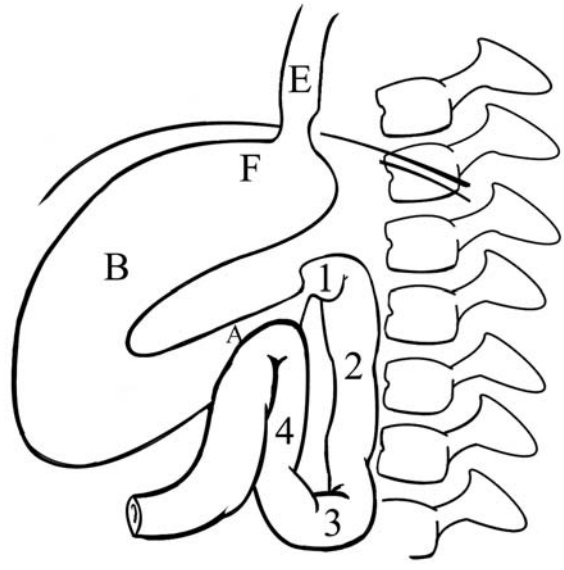

e

Fig. 5.26. The upper gastrointestinal series
a The stomach is visualized in multiple positions so that contrast agent moves through the fundus (*F*), body (*B*), and antrum (*A*). The mucosal pattern is smooth and regular without any disruption. Peristaltic waves can be deduced by the various shapes of the stomach, noted on multiple films as well as at fluoroscopy
b Oblique view shows to advantage the contraction at the antrum (*A*) and the pyloric channel (*P*). The duodenal bulb (*D*) is triangular and smooth. The duodenum is partially filled
c Further along in the study, the duodenum is entirely visualized, and the ligament of Treitz (*arrow*), behind the stomach, is at the level of the duodenal bulb. Note the four portions of the duodenum (*1*, *2*, *3*, *4*). The jejunal mucosal pattern appears feathery and unobstructed
d Drawing of the frontal view of the proximal stomach to the jejunum
e Drawing of the lateral projection. Duodenum parts *1–4*. *E*, esophagus; *F*, fundus; *B*, body; *A*, antrum

twisting of the duodenum and subsequent midgut volvulus. An upper gastrointestinal series can also detect masses within the epigastrium that may impinge on the duodenal sweep as well as inflammatory bowel disease of the duodenum. Congenital anomalies of the stomach and duodenum can be seen.

The stomach is then studied in its entirety by placing the patient in various positions and using the effects of gravity to move the liquid barium and air content from one area to another. The mucosal pattern is formed by the gastric rugae throughout the fundus, body, and antrum of the stomach. The *contours* of the stomach are smooth, and the stomach narrows in an expected manner at the pyloric channel, which readily opens into the duodenal bulb (see Fig. 5.26). It is important to recognize the normal pyloric channel, as this is the site of pyloric stenosis in young infants.

The duodenum is divided into four parts: the bulb, vertical portion, transverse portion, and ascending portion (see Fig. 5.26). The vertical and horizontal portions form the C-loop and are the retroperitoneal portions of the duodenum. The medial margin of the duodenum is adjacent to the head of the pancreas, while the lateral margin is adjacent to the liver and gallbladder. It is important to note the contours and position of the duodenum, as masses or abnormalities in adjacent structures affect the duodenum and cause distortion. It is also important to view the duodenum in frontal and lateral projections to detect anterior or posterior deviation. The horizontal portion of the duodenum crosses the spine from right to left, and the ascending portion ends at the ligament of Treitz to the left of the spine and assumes a position at the height of the duodenal bulb (see Fig. 5.26).

Small Bowel Follow-Through

This study (Fig. 5.27) includes visualization of the esophagus, upper gastrointestinal tract, and small bowel to the ileocecal valve. It is the examination used in children with suspected inflammatory bowel disease such as Crohn's disease. The study is also useful in defining partial distal small bowel obstruction. Immediately beyond the ligament of Treitz, the jejunum begins in the left upper quadrant and runs from left to right. The jejunal–ileal junction is *not* a clearly defined landmark. The mucosal pattern of the small bowel has been described as feathery. This is caused by the valvulae conniventes (Kerckring's folds). In contrast to the colon, these are transverse, circular muscles that convolute the mucosa (see Fig. 5.27).

The terminal ileum has a nodular appearance in children due to the lymphoid tissue of Peyer's patches. This is normal and not, as in the adult, associated with an immune-deficient state.

In a small bowel series it is important that all loops be filled at some point, and that adjacent loops not appear unduly separated when filled. The feathery mucosal pattern of the valvulae should have no irregularity or ulceration. Once the barium is swallowed, it takes between 30 min and 2 h to reach the ileocecal valve in most children, depending on the rate of gastric emptying and bowel motility.

Barium Enema

In this study (Fig. 5.28), contrast material is introduced through the rectum until the entire colon is filled. By coating the intraluminal surface of the colon, polyps, and diverticula, ulcerations and fistulous tracts as signs of inflammatory bowel disease can be diagnosed. Masses, both intraluminal and extraluminal, may be detected.

Let us begin with the barium enema and go through the usual film viewing pattern. The emphasis is on the normal anatomy and the method of looking at the examination. As with other films, use the parameters of position, contour, and size when evaluating the colon. The position of the rectum and sigmoid can be noted on the filled films. The rectum is in the midline on the frontal view, and the posterior wall lies immediately adjacent to the inner curve of the sacrum on the lateral view (see Fig. 5.28). The sigmoid colon extends into the right lower quadrant and then swings laterally to the left lower quadrant. The distal descending colon is seen at this level, with the proximal portions in the left flank and the left upper quadrant. Because of its contiguity with the spleen the highest curve is the splenic flexure. The transverse colon hangs from the mesentery in the midabdomen, suspended at the hepatic and splenic flexures. As mentioned above, this is an anterior structure. The hepatic flexure is in the right upper quadrant and more caudad (inferior) than the splenic flexure. It lies just below the liver. The ascending colon is in the right lateral gutter, and its most proximal portion is the cecum. It can be recognized by detecting either the appendix or the ileocecal valve or by the reflux into the terminal ileum. The cecum is normally in the right lower quadrant over-

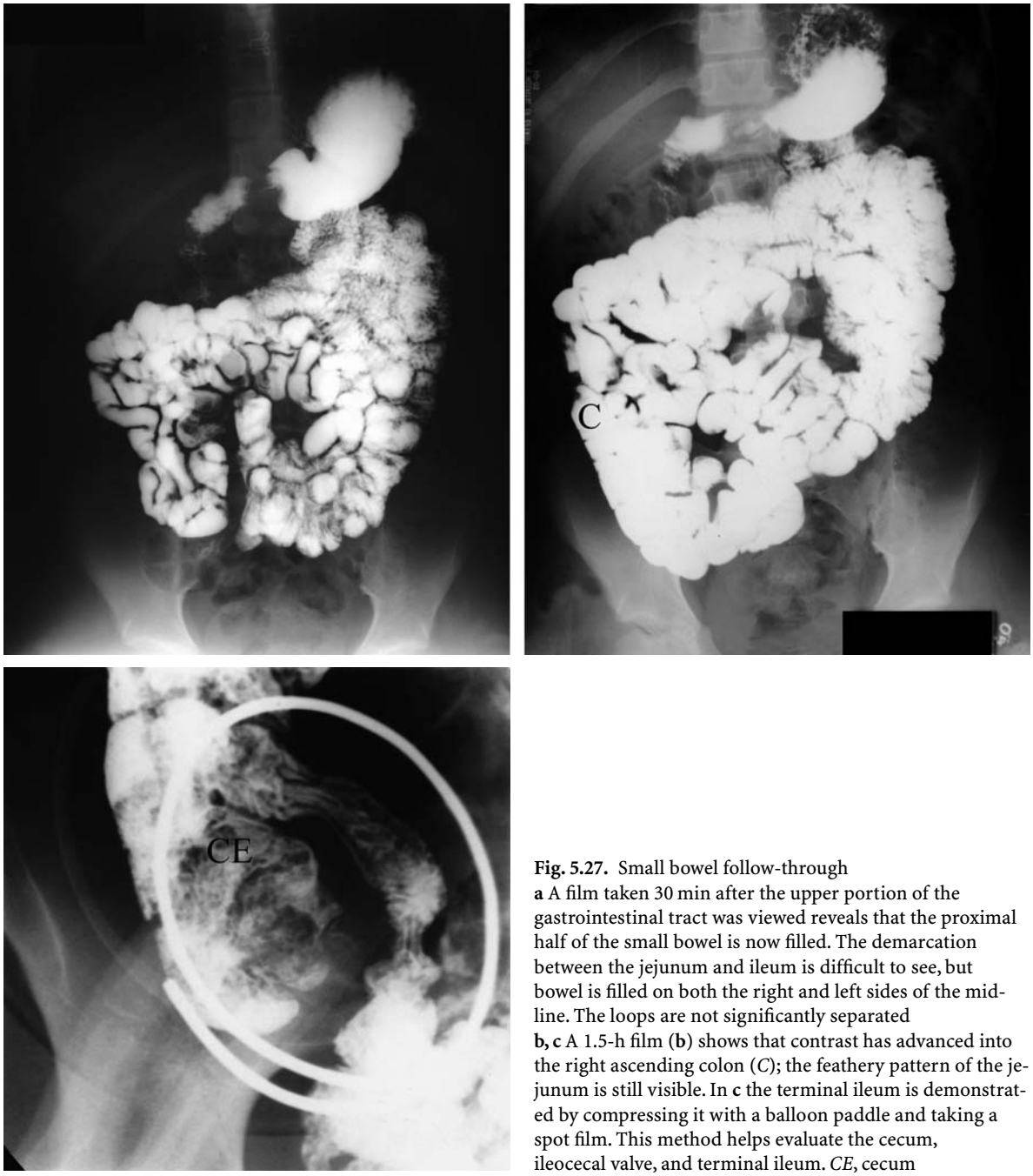

Fig. 5.27. Small bowel follow-through
a A film taken 30 min after the upper portion of the gastrointestinal tract was viewed reveals that the proximal half of the small bowel is now filled. The demarcation between the jejunum and ileum is difficult to see, but bowel is filled on both the right and left sides of the midline. The loops are not significantly separated
b, c A 1.5-h film (**b**) shows that contrast has advanced into the right ascending colon (*C*); the feathery pattern of the jejunum is still visible. In **c** the terminal ileum is demonstrated by compressing it with a balloon paddle and taking a spot film. This method helps evaluate the cecum, ileocecal valve, and terminal ileum. *CE*, cecum

lying the iliac crest; when it lies between the iliac crest and the hepatic flexure, it may be mobile due to a loose fixation of the mesentery. However, when the cecum is not in the right lower quadrant, suspect the congenital abnormality of malrotation or malfixation of the midgut (Fig. 5.29). By definition, the midgut extends from the ampulla of Vater in the duodenum to the midtransverse colon, with the foregut being all bowel proximal to this and the hindgut distal to the midgut.

The *contours* of the bowel lumen should be smooth and devoid of irregularities. When irregular-

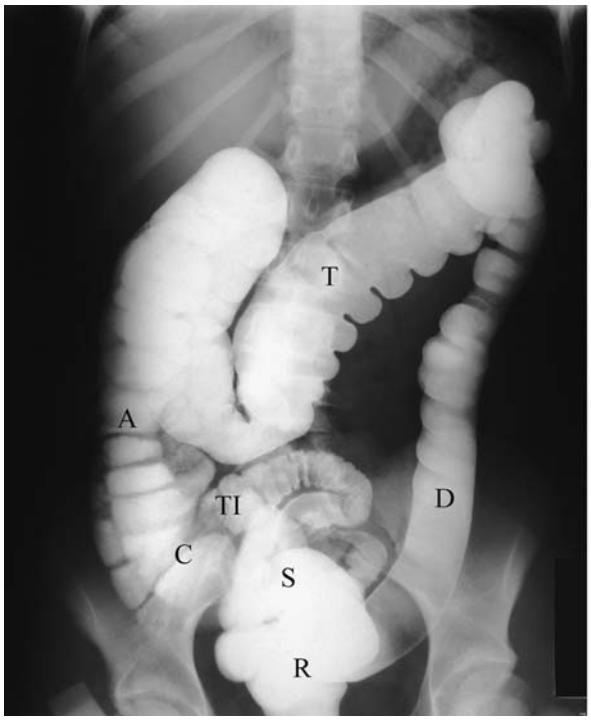

a

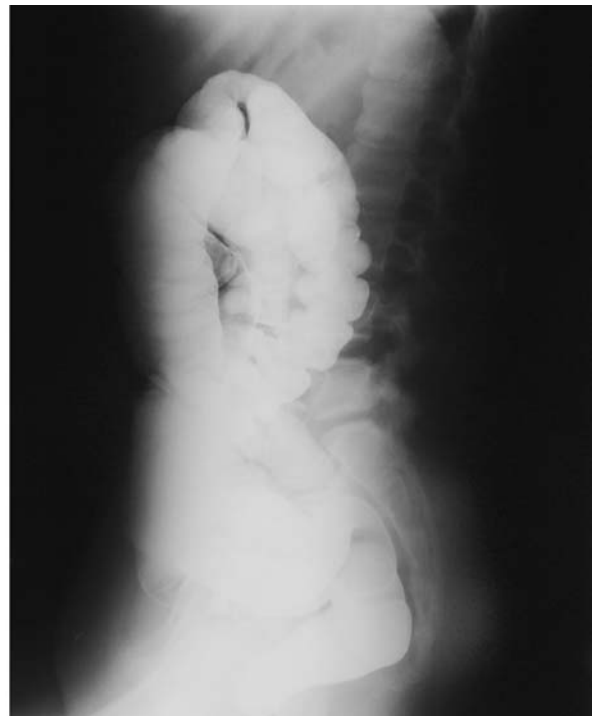

b

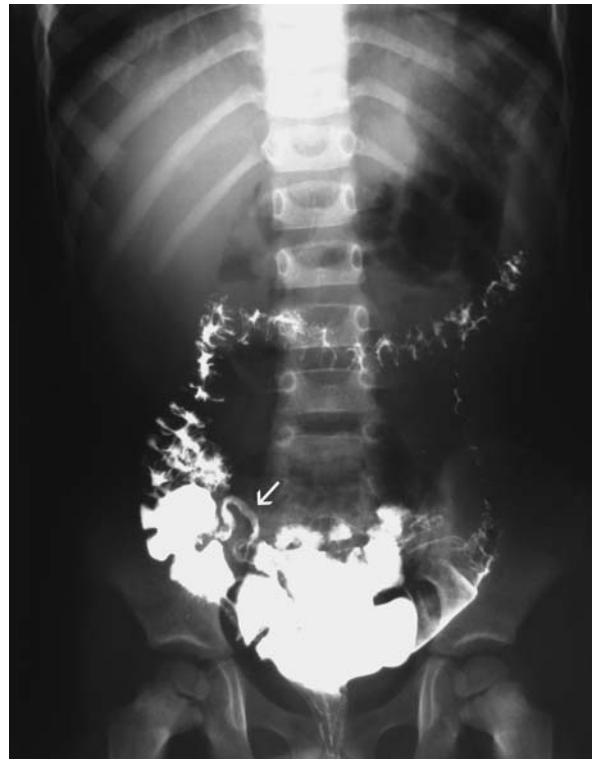

c

Fig. 5.28. Normal barium enema
a Frontal view of the barium-filled colon shows the midline rectum (*R*), tortuous sigmoid (*S*), and rather smooth-walled descending colon (*D*). The haustrated transverse colon (*T*), ascending colon (*A*), and the cecum (*C*) are also identified. Reflux into the terminal ileum (*TI*) is present
b Lateral projection affords a good view of the rectum and its proximity to the sacrum
c Postevacuation films show the bowel almost totally collapsed, with no filling defects. The thin, tubular, barium-filled appendix is seen in the right lower quadrant (*arrow*)

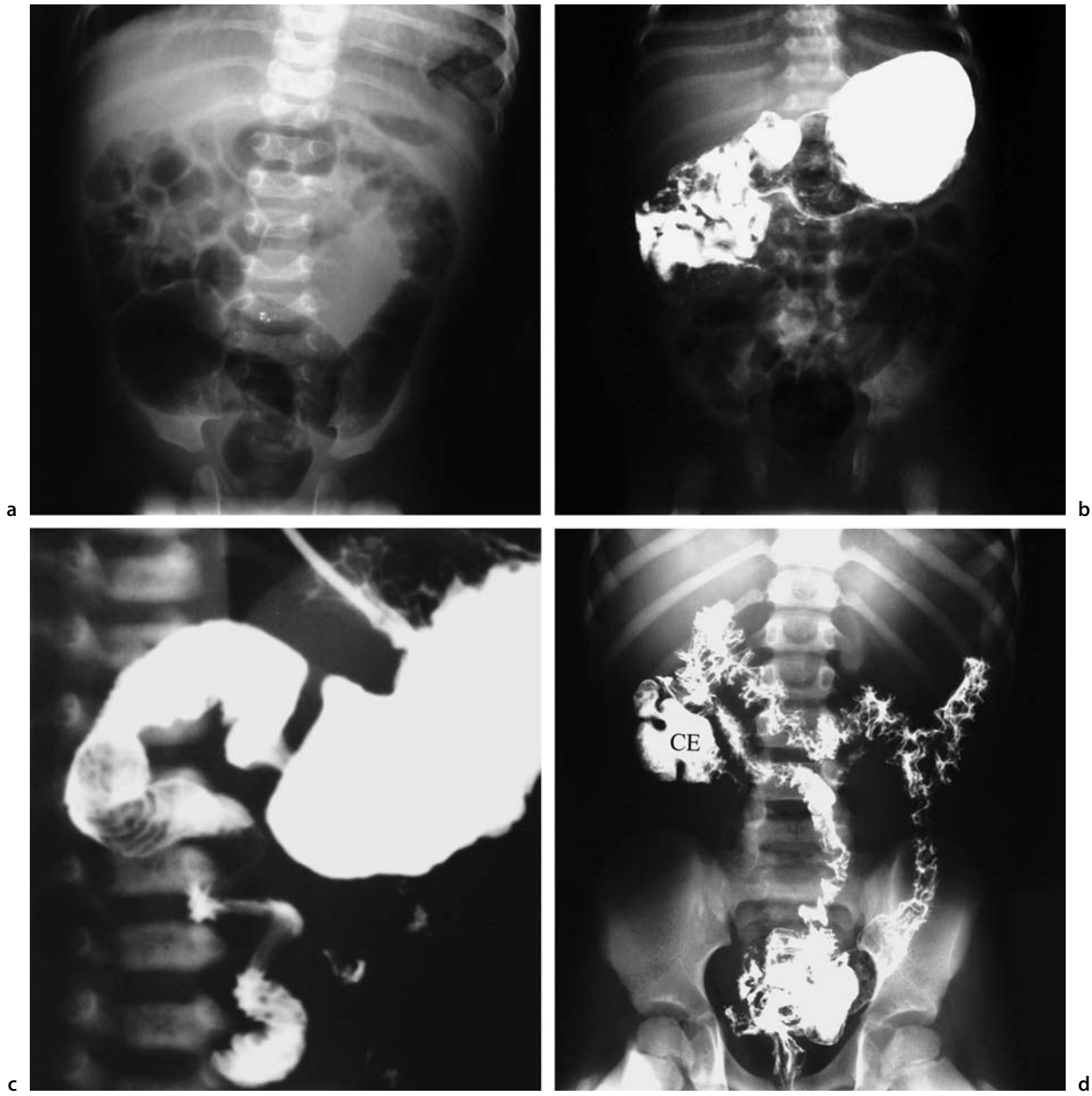

Fig. 5.29. Malrotation of midgut
a Plain film of the abdomen in this 5-year-old, who had been vomiting, reveals a cluster of small bowel loops to the right of the spine – a very "soft" finding of malrotation or mass. Frequently, the plain film is entirely normal
b A film after barium was given by mouth shows the jejunum entirely to the right of the abdomen. The ligament of Treitz is absent (see Fig. 5.26)
c Spot film of the duodenum in another child shows that the barium never goes to the normal location of the ligament of Treitz but forms a "corkscrew" pattern around the superior mesenteric artery (which is not visualized), typical of malrotation. If the superior mesenteric vessels get twisted, bowel ischemia results
d An evacuation film following a barium enema in another patient reveals the cecum (*CE*) high in the right upper quadrant. This is another sign of malrotation

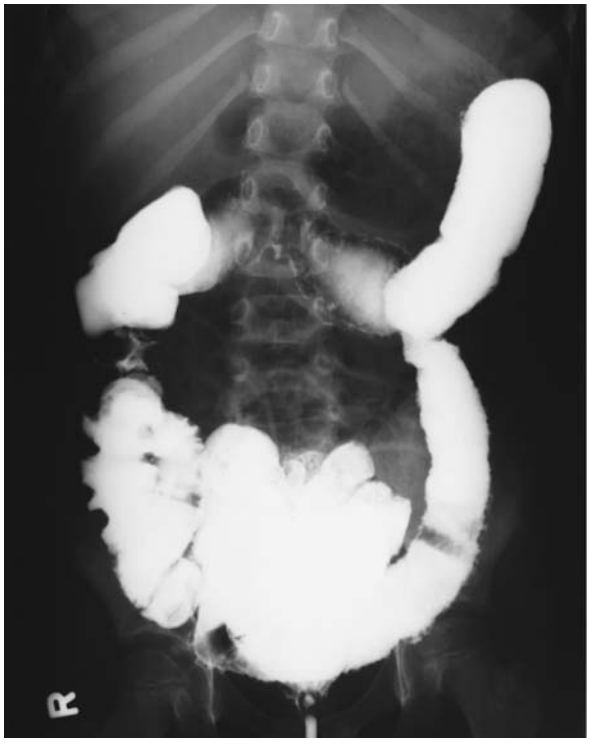

a

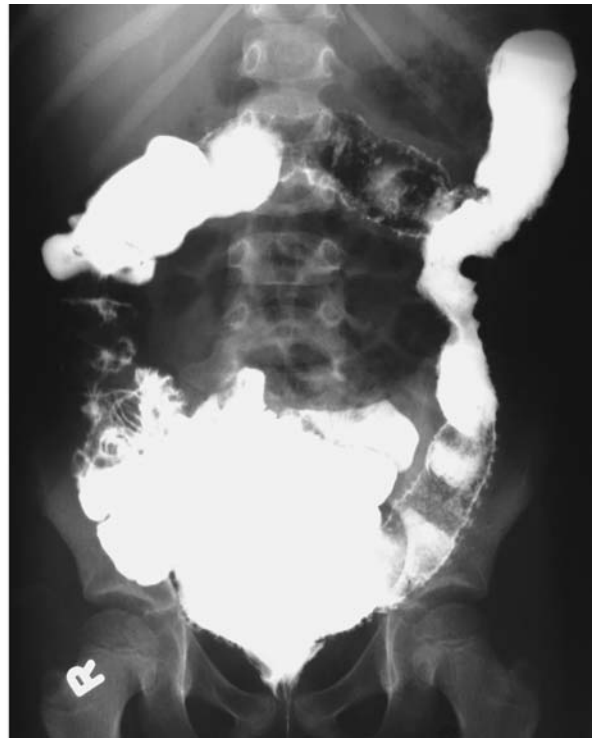

b

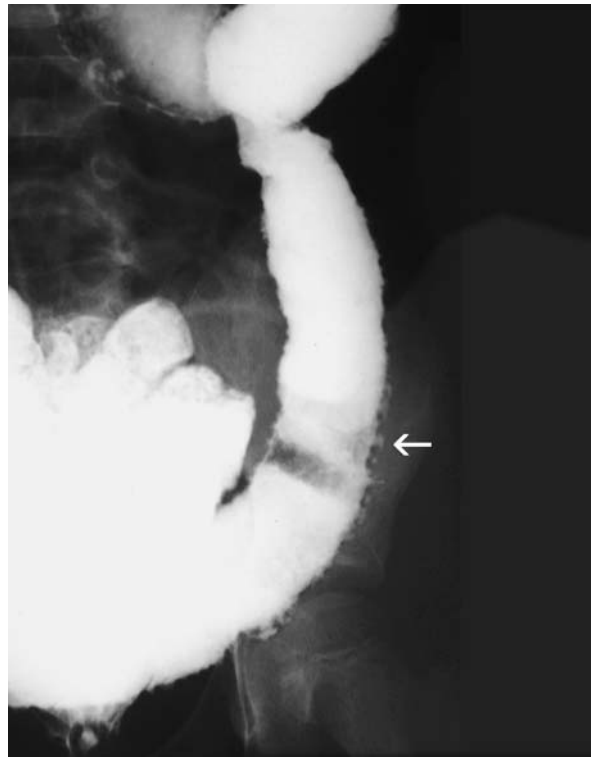

c

Fig. 5.30. Ulcerative colitis
a, b Frontal films from a barium enema reveals contrast material outside the lumen and in the wall, particularly evident in the descending colon. These are "collar-button" ulcerations
c Close-up shows the "collar button" (*arrow*) ulcerations. The key to diagnosis in this case is the abnormal contour of the bowel

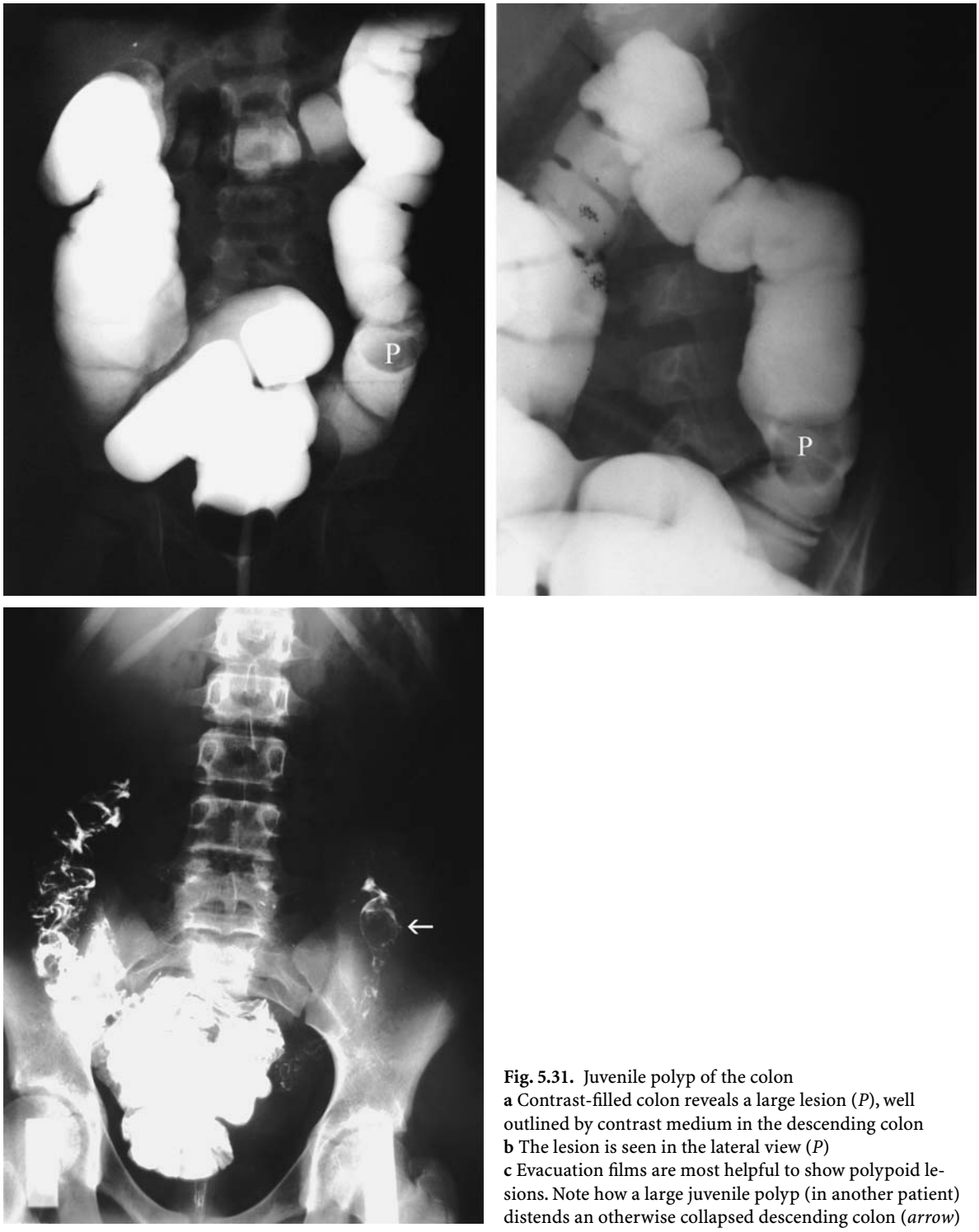

Fig. 5.31. Juvenile polyp of the colon
a Contrast-filled colon reveals a large lesion (*P*), well outlined by contrast medium in the descending colon
b The lesion is seen in the lateral view (*P*)
c Evacuation films are most helpful to show polypoid lesions. Note how a large juvenile polyp (in another patient) distends an otherwise collapsed descending colon (*arrow*)

ities are present, they may be due to either poor preparation (retained fecal material) or pathological conditions such as ulcerations of inflammatory bowel disease (Fig. 5.30; compare Fig. 5.28). The colon is normally indented at intervals by haustra or sacculations, which are smooth indentations caused by the longitudinal muscular band on the surface of the colon that compresses it like an accordion. The muscles of the longitudinal band are called taeniae coli. Normally, there are fewer haustral markings in the left colon than in the right.

After the colon has been filled and appropriate films taken, the patient is allowed to evacuate the contrast, and several postevacuation films (see Fig. 5.28) are obtained to evaluate the mucosal pattern. On these films, the mucosa is feathery and any mass within the colon, such as a polyp, disrupts this fine, regular, feathery pattern (Fig. 5.31).

The *size* of the colon is greatest at the rectum and cecum. The left colon may be slightly smaller than the rest of the colon.

The search for intraluminal filling defects is mandatory at fluoroscopy and also on filled and postevacuation films. Since these may represent polyps, look for a stalk. The most common intraluminal filling defect in children is fecal material, but the most common pathological intraluminal defect is a juvenile polyp (see Fig. 5.31).

Since it is easier and faster to evacuate the contrast from the colon, the barium enema precedes the upper gastrointestinal series when both are indicated for a gastrointestinal work-up. A delay of several days may be involved if the upper gastrointestinal series is performed before the enema study. If ultrasound, CT, or radionuclide examination is indicated, these examinations should also precede the barium study.

Liver and Biliary Tract

The liver and biliary tract are specifically studied with nuclear medicine techniques. The major indications relate to obstruction of the biliary system such as may be found in the jaundiced child.

An isotope scan of the liver is usually performed with technetium (a radioisotope) bound to compounds taken up by either the reticuloendothelial system (technetium sulfur colloid) or hepatocytes (technetium iminodiacetic compounds). Sequential scans over time are obtained so that function can be properly assessed (Fig. 5.32).

In the newborn, *prolonged* jaundice (over 2 weeks) is most commonly due to either neonatal hepatitis or biliary atresia. Ultrasound examination is the initial procedure of choice, as it reveals intrahepatic and bile duct dilatation, and any masses in the porta hepatis, such as a choledochal cyst (Fig. 5.33). The second imaging procedure is a radionuclide investigation with technetium-99m mebrofenin for the patency of the biliary system. The neonate with biliary atresia has good liver uptake of the radionuclide but no bowel excretion. The gallbladder is not seen. The neonate with hepatitis has poor liver uptake. When the findings are inconclusive, the neonate will need a liver biopsy. MR cholangiography is promising as an imaging test to show the biliary structures without any radiation.

In older children with jaundice, the most common diagnosis is viral hepatitis. These children do not need imaging evaluation except when their course is atypical or recurrent. In these instances ultrasound is an excellent, noninvasive starting method. Both gallstones and masses in the porta hepatis can be diagnosed. Intrahepatic biliary ductal obstruction with enlarged biliary radicals is easily seen. In the atypical case, procedures such as MR cholangiography, radionuclide study, CT evaluation, percutaneous transhepatic cholangiography, and endoscopic retrograde duct catheterization may be necessary. MR is becoming the procedure of choice (Fig. 5.33).

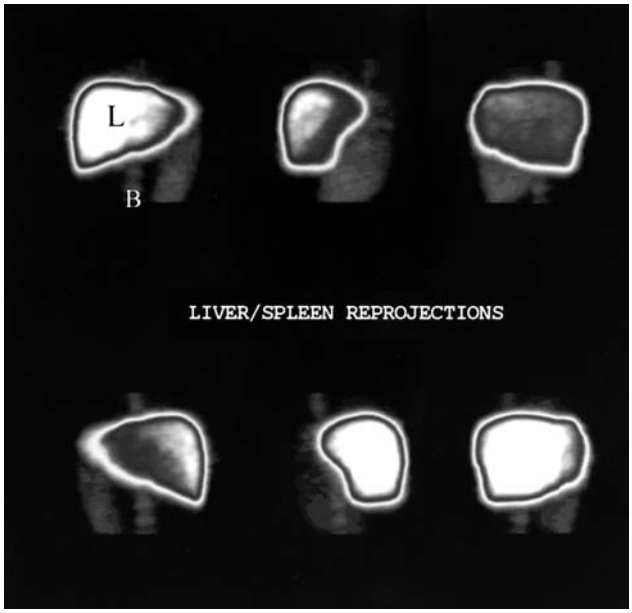

a

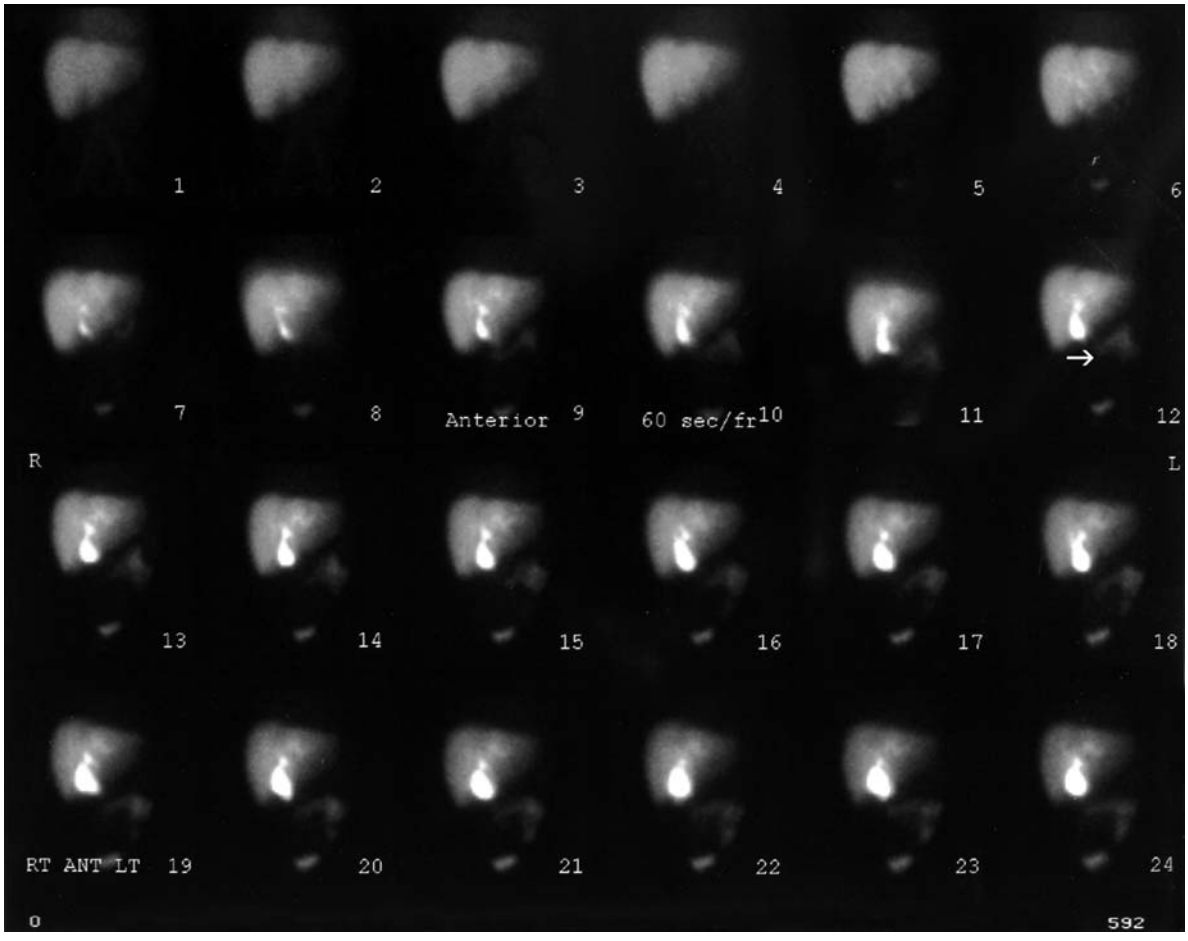

b

Fig. 5.32. Evaluation of the liver and biliary tract
a A technetium sulfacolloid scan for evaluation of the liver and spleen. Note that the spleen is not seen because the patient has sickle cell disease and the spleen is small and not functional, due to multiple infarctions. Another clue to the diagnosis of sickle cell disease is that there is marrow uptake in the spine. *L*, liver; *B*, bone marrow
b Hepatobiliary iminodiacetic acid (HIDA) scan in which the technetium isotope is taken up by the liver cells and excreted into the bile ducts and gallbladder. Note that the numbers on each picture relate to a 1-min time frame. The liver fills first, followed by the biliary ducts and the gallbladder. The gallbladder is the bright area. The liver should fill within 10 min, the gallbladder by 20 min, and the bowel in less than 30 min. Note that on the scans beginning at 12 min, the bowel (*arrow*) is filled. This is a normal system

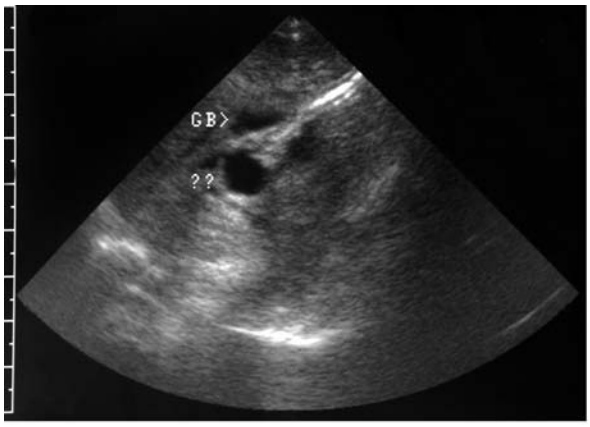

a

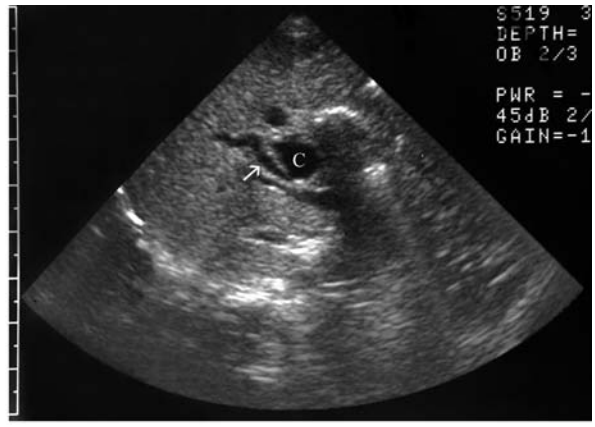

b

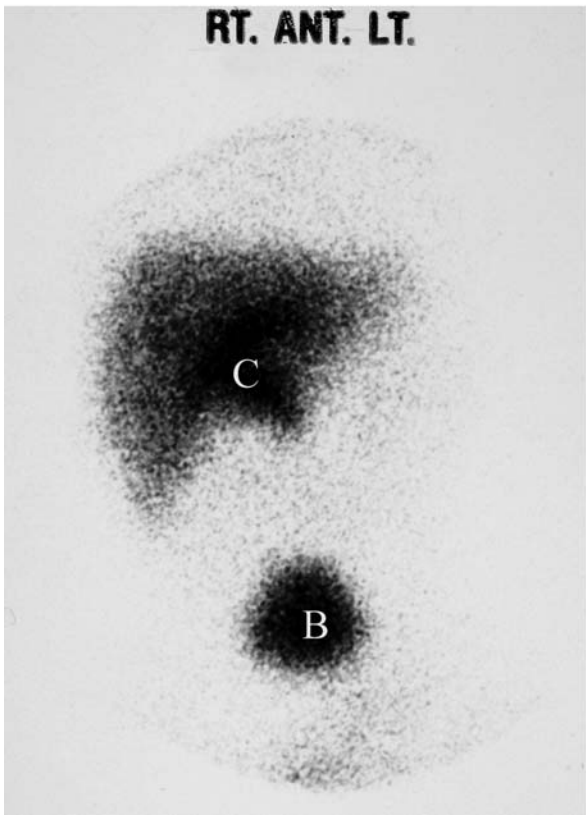

c

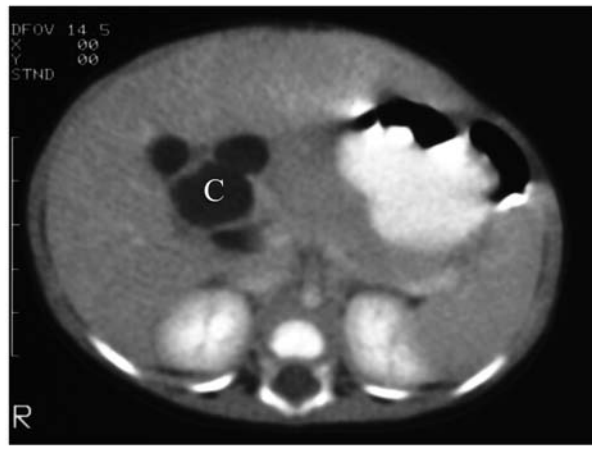

d

Fig. 5.33. Evaluation of the abnormal biliary tract.
a This is a 2-month-old who was born with duodenal atresia. Now, at 2 months, she has jaundice. Transverse ultrasound reveals the gallbladder (*GB*) and a cystic structure just inferior to it
b A scan somewhat more caudally reveals the bile duct (*arrow*) and a choledochal cyst (*C*)
c A HIDA scan reveals a radioisotope in the choledochal cyst (*C*) at 5 h after the examination. *B*, bladder
d The choledochal cyst (*C*) was confirmed on CT
e, f see p. 124

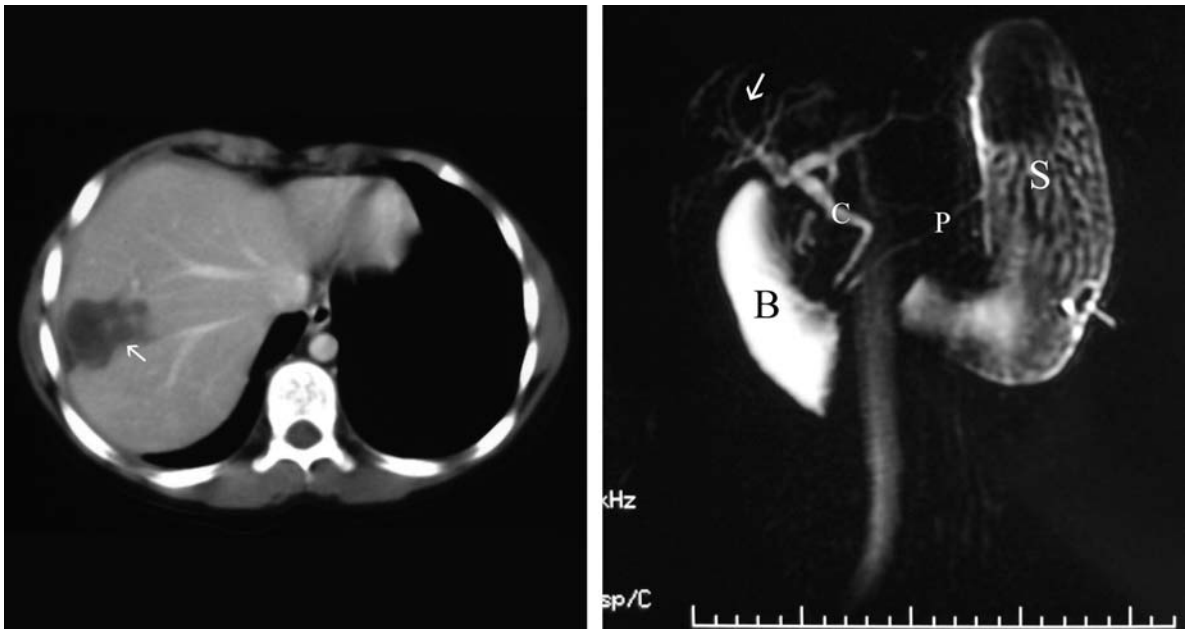

e f

Fig. 5.33 (*continued*)
e A 12-year-old male status post trauma. Enhanced CT of the abdomen shows a large low-attenuation collection (*arrow*) in the right lateral liver. This was a biloma secondary to trauma
f A teenage male with short gut from bowel infection secondary to malrotation. MR cholangiogram shows the pancreatic (*P*), common bile (*C*), and hepatic ducts (*arrow*). The hepatic and common bile ducts are dilated, while the pancreatic duct is normal. *S*, stomach, *B*, bowel

The Bladder

Radiographic Voiding Cystourethrogram

The purpose of the radiographic voiding cystourethrogram (VCU) is threefold: (a) to study the bladder and urethra for abnormalities of size, position, and contour, (b) to screen for vesicoureteral reflux (retrograde flow of contrast material into the ureters and/or kidneys), and (c) to evaluate pelvic abnormalities that impinge or invade the bladder.

If the VCU is to be performed alone, no preparation is necessary. The patient is asked to void, and then a small catheter (either a feeding tube or a straight catheter) is passed into the urethra and bladder. Residual urine is drained and the amount recorded. This is important because bladder dysfunction or distal obstruction can lead to retention after voiding. Contrast material is then instilled through the catheter into the bladder until it is filled to capacity. The contrast agent is a water-soluble dilute iodide-containing compound.

The bladder appears as a round, opaque density, symmetrically situated in the pelvis. The inferior margin of the filled bladder should be seen at the top of the pubic symphysis on a well-centered film. The bladder wall is smooth, and there should be no filling defects within the bladder. Irregularity of the wall may indicate mucosal edema or diverticulum formation. When the ureters are opacified with contrast there is incompetence of the ureterovesical junction and vesicoureteral reflux (Fig. 5.34). When the catheter is removed, the patient voids, allowing visualization of the urethra. This is much more crucial in a male, as significant pathology may exist in the posterior urethra – that portion of urethra between the bladder neck and the urogenital diaphragm (see Fig. 5.34). The male posterior urethra is divided into the prostatic and the membranous urethra. The prostatic and ejaculatory ducts terminate in the verumontanum, located on the posterior wall of the prostatic urethra. The membranous urethra is shorter, beginning at the inferior margin of the verumontanum and extending downward to the urogenital diaphragm. The anterior urethra of the male extends from the urogenital diaphragm distally to the urethral meatus and is divided into the bulbous and penile portions. When there are abnormalities such as posterior urethral valves, there is marked discrepancy between the anterior and posterior urethral calibers (Fig. 5.35).

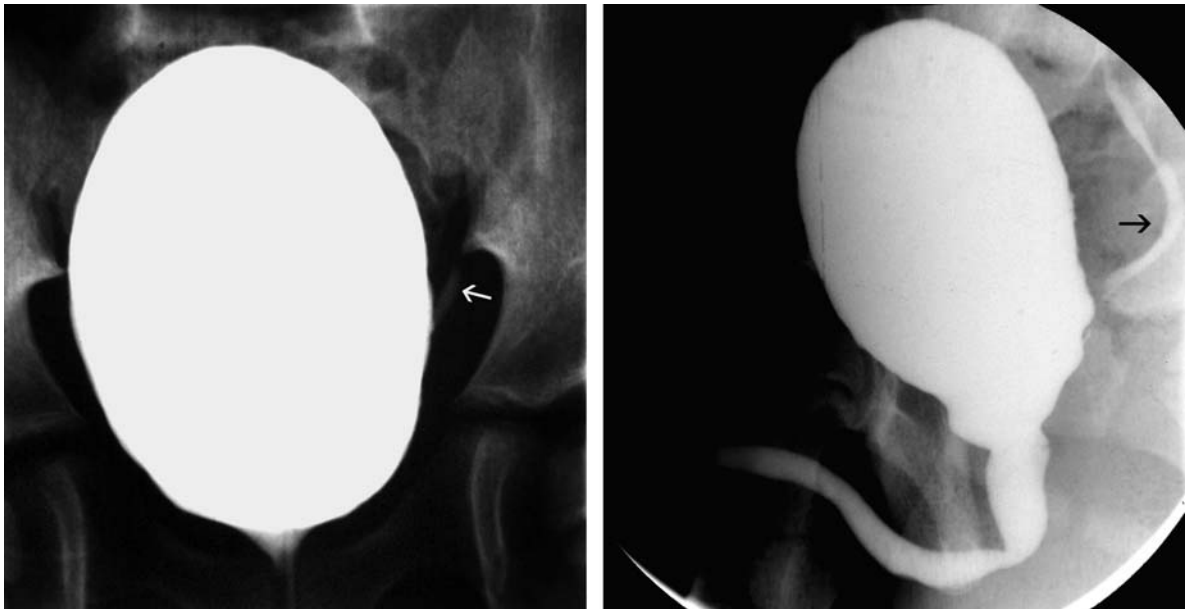

a b

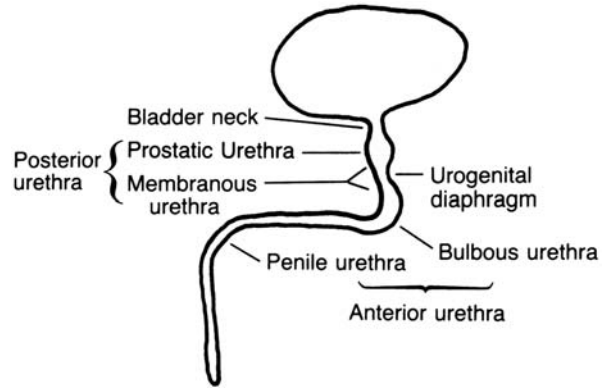

c

Fig. 5.34. Male voiding cystourethrogram (VCU)
a Filled bladder. The inferior margin is adjacent to the pubic bones, and the bladder is in the center of the pelvis. There is no mass impression on the bladder. The bladder contour is smooth. Incidentally noted is a small amount of refluxed contrast medium in the distal left ureter (*arrow*)
b Patient is placed in the oblique position, and the reflux into the left ureter is noted (*arrow*). As patient voids, the entire posterior urethra is easily seen as well. Slight irregularities at the base of the bladder posteriorly are expected during voiding
c The male urethra

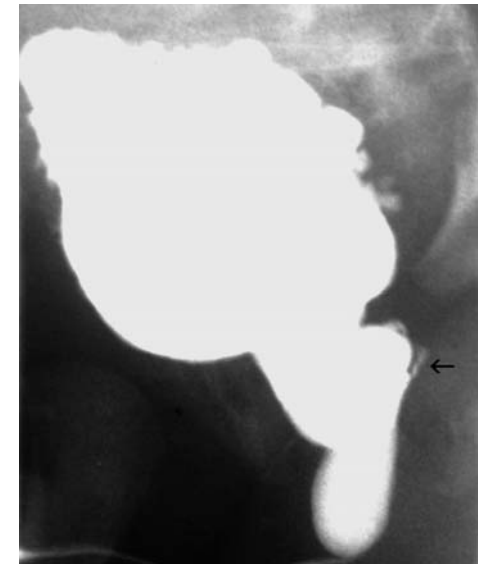

Fig. 5.35. Posterior urethral valves. This single oblique view during a VCU reveals the irregularity of the bladder wall. Large collections of contrast medium in saccules are due to bladder obstruction. The posterior urethra is quite dilated compared to the anterior urethra. The opening between the anterior and posterior urethra is located quite posteriorly and, of course, is narrowed (see normal urethra in Fig. 5.34). Reflux into the ejaculatory ducts is also present (*arrow*)

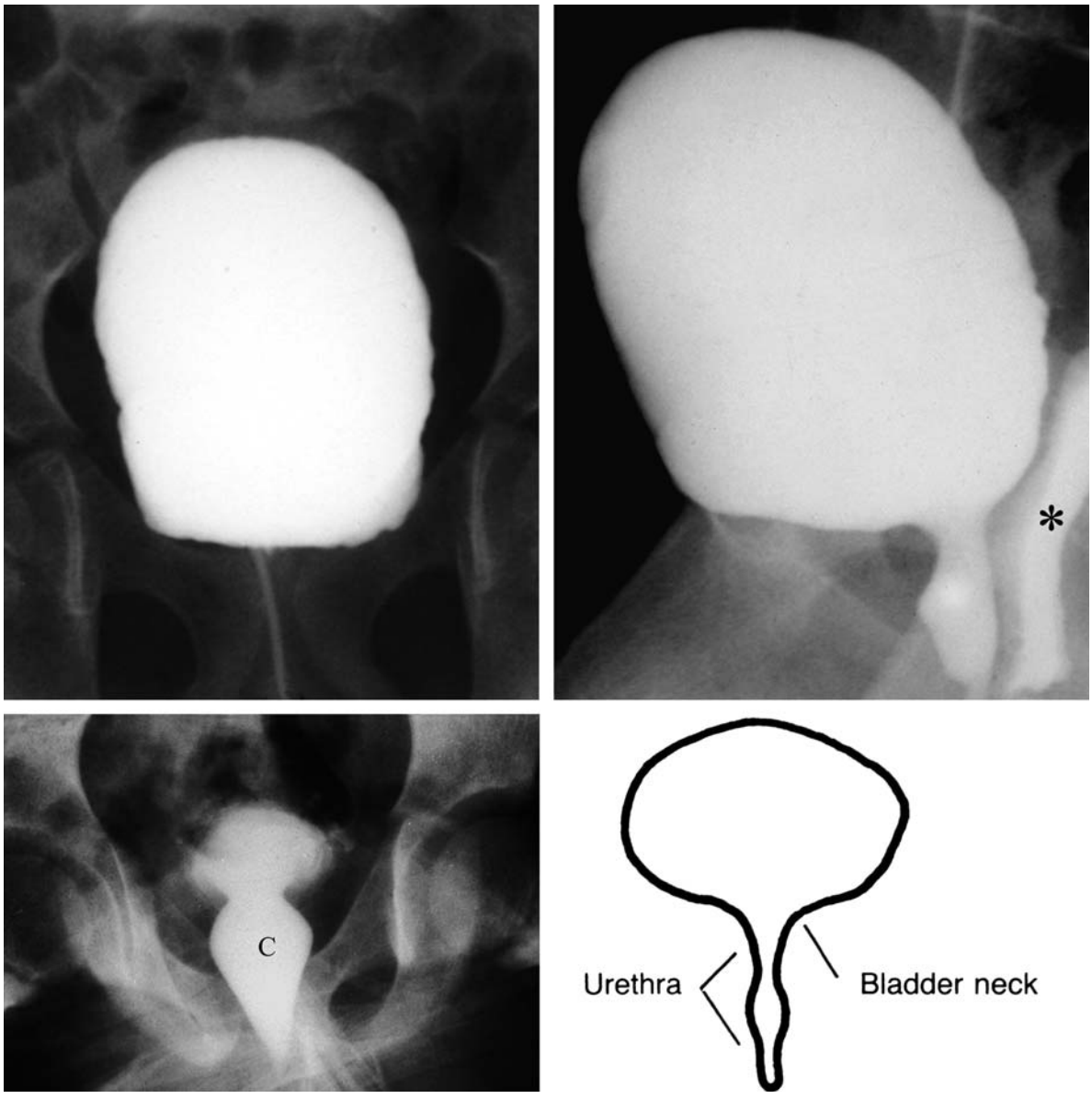

Fig. 5.36. The female urethra
a Filled bladder with catheter in place again reveals the central position of the bladder without any mass impinging on its wall
b, c On voiding, as seen on this oblique view, the posterior aspect of the bladder becomes slightly irregular. The urethra is much shorter in a female and often displays a "carrot-top" or "spinning-top" deformity (*C*). There is often reflux into the vagina when the patient voids in the recumbent position (*asterisk*)
d The female urethra

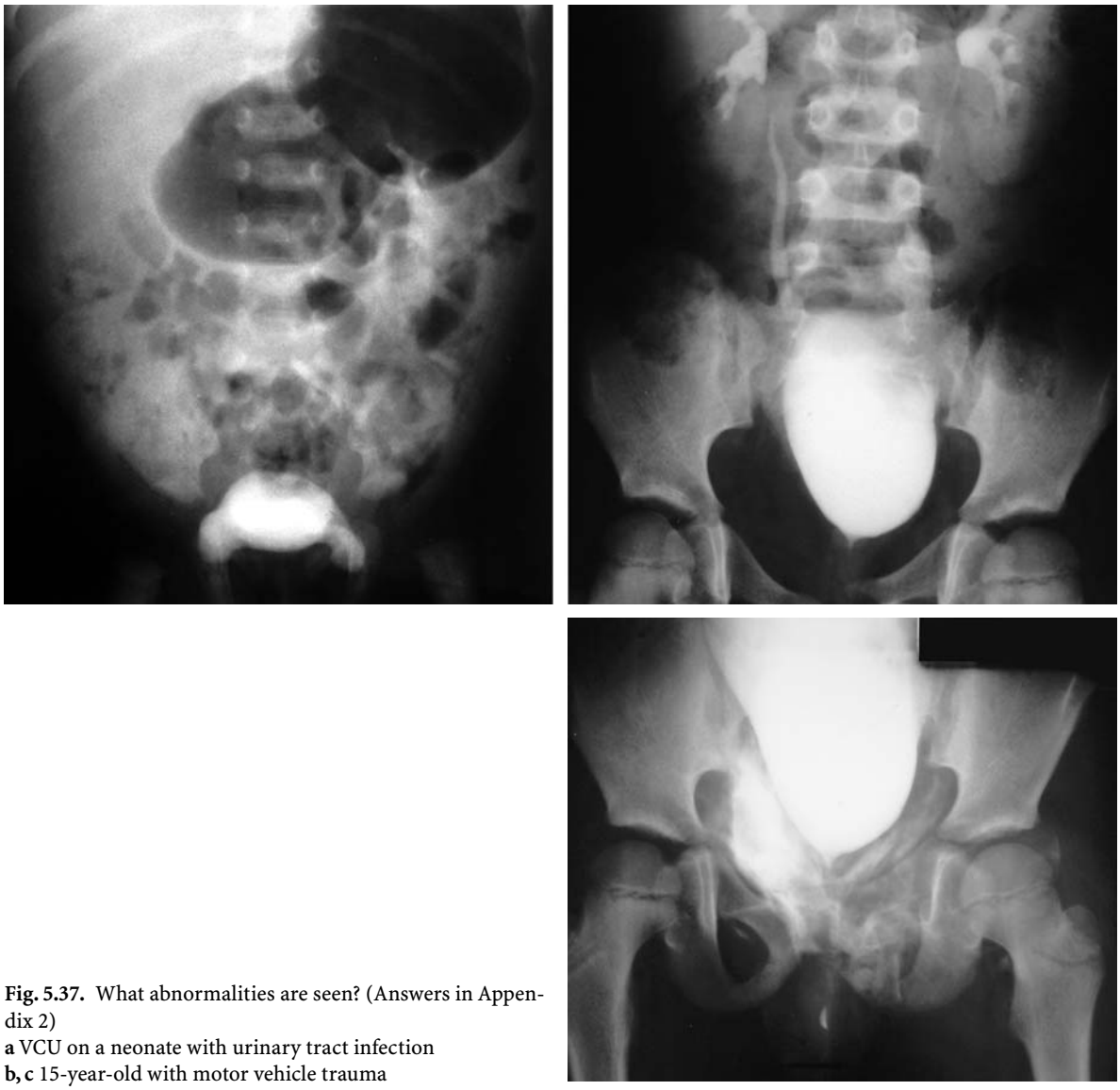

Fig. 5.37. What abnormalities are seen? (Answers in Appendix 2)
a VCU on a neonate with urinary tract infection
b, c 15-year-old with motor vehicle trauma

In the female, the urethra is shorter and is infrequently the site of significant pathology (Fig. 5.36). Voiding in the recumbent position often causes vaginal filling.

During fluoroscopy, the upper abdomen is viewed to make sure there is no evidence of reflux of contrast material from the bladder to the kidneys. This is important because reflux is one of the factors in the etiology of pyelonephritis and parenchymal scars. A postvoiding image is obtained to assess whether the bladder empties completely (see below, "Urinary Tract Infection").

In instances of trauma to the pelvis (particularly with fractures of the pelvic bones) the possibility of urethral disruption must be considered. The anterior portion of the urethra is best seen when a small catheter is placed within the urethral meatus and retrograde injection is made. If the urethra is intact, the catheter is passed into the bladder and a conventional VCU is performed to visualize the posterior urethra.

What abnormalities are visible in Fig. 5.37? See Appendix 2.

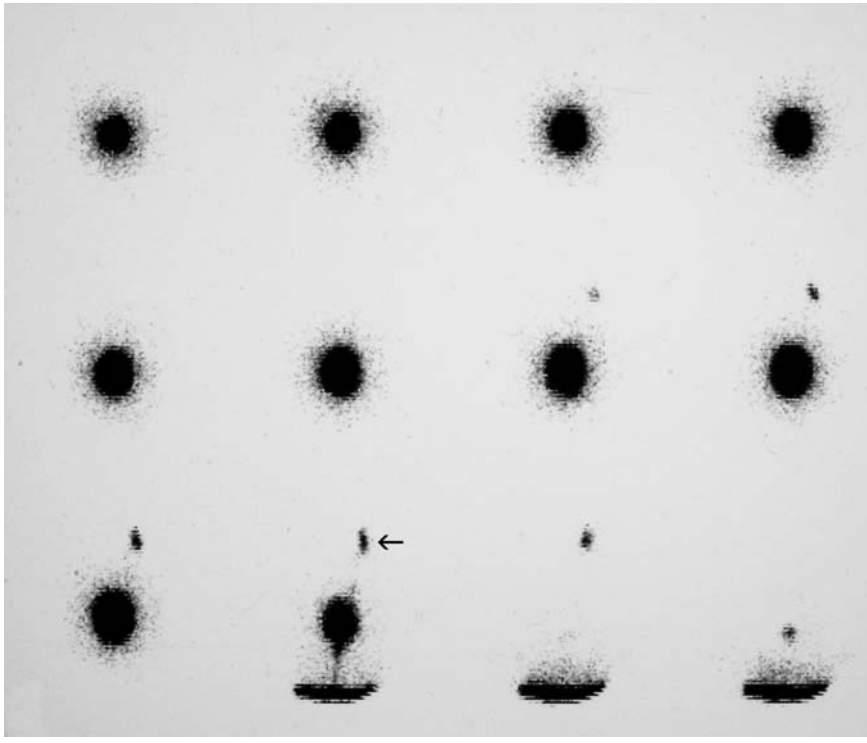

a

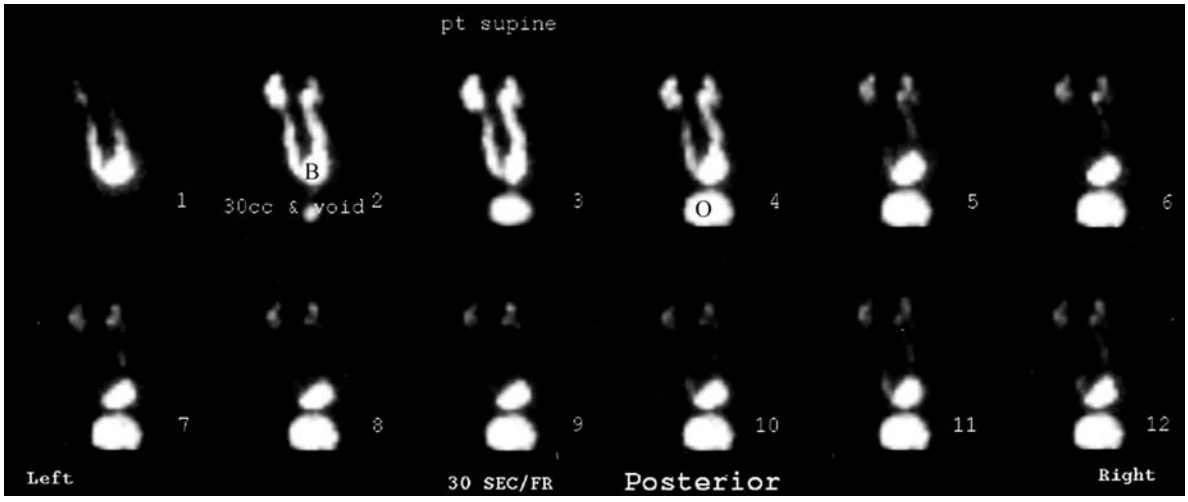

b

Fig. 5.38. Nuclear voiding cystogram
a The image at *top left* is the earliest film of the bladder. Progressing from *left* to *right*, the bladder is filling. The patient is being scanned from behind; therefore, the viewer's right is the patient's right. There is reflux into the right kidney with voiding (*arrow*)
b A child with bilateral reflux. *B*, bladder, *O*, tracer outside patient on a diaper

Nuclear Cystogram

In performing the nuclear cystogram, as with the VCU, a small catheter or feeding tube is placed into the urethra and into the bladder. The bladder is drained and normal saline with 1 microcurie (μCi) of technetium pertechnetate is infused into the bladder. The volume given varies with the child's age. The nuclear camera continually records during filling and voiding. Since there is continuous monitoring, this is a very sensitive test (Fig 5.38). There is considerably less radiation to the gonads, particularly in females, from a nuclear cystogram than from a radiographic cystogram. However, both grade I and intrarenal reflux will not be diagnosed (see below urinary tract infection).

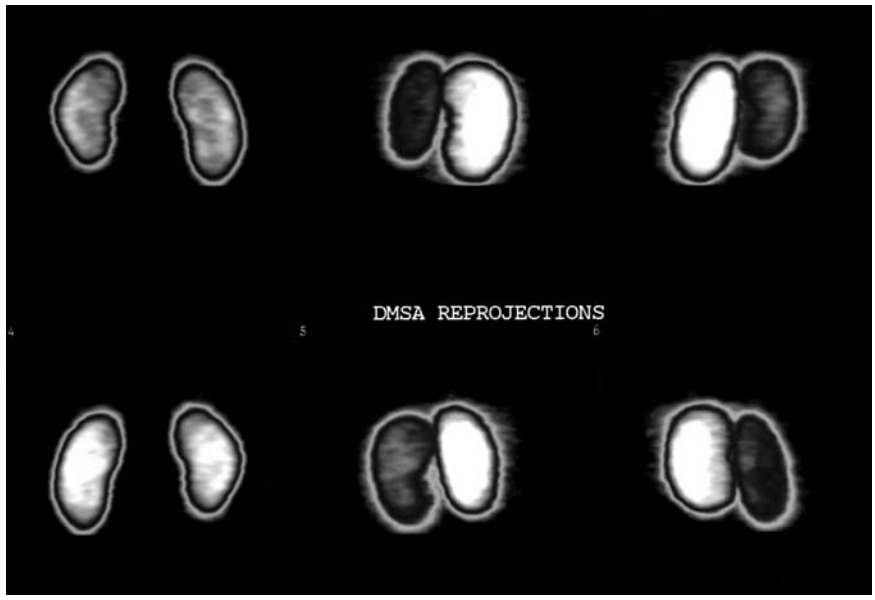

a

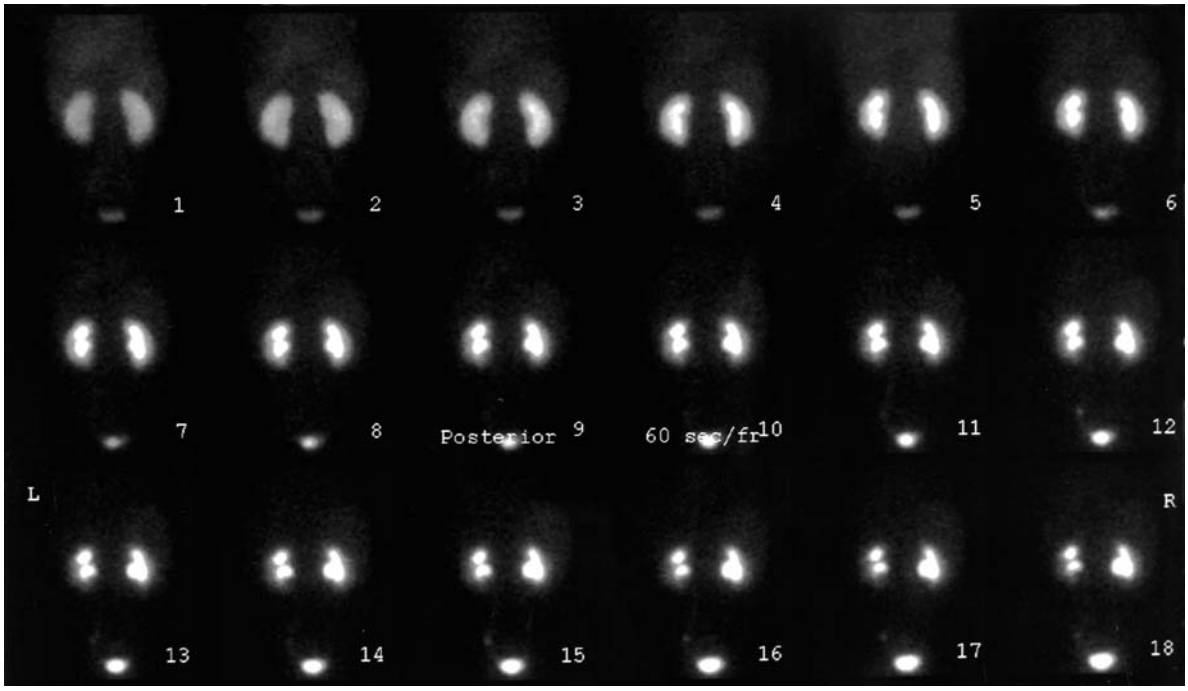

b

Fig. 5.39. Renal nuclear examination
a A cortical scan (DMSA) shows both kidneys well with no abnormal scars or changes of the cortex
b A MAG-3 study shows the renal parenchymal phase during the first several minutes and then the collecting system fill. By calculating washout, one can see the renogram and flow of both kidneys. The bladder begins to show significant activity by the 9- or 10-min frame. Diuretic can be given and washout flows established

Kidney

The anatomy of the kidney is seen on ultrasound, CT, and MR with more detail than on the intravenous pyelogram (excretory urogram, EU). The EU is infrequently used. Currently, nuclear medicine techniques remain the standard for evaluating renal function, although MR is promising in this regard.

The applications of nuclear medicine techniques to evaluate the pediatric urinary tract are probably more varied than those of any of the other modalities. Radionuclide imaging procedures have been developed to assess function of the kidneys by measuring effective renal plasma flow, glomerular filtration rate, and renal transit time. In addition, anatomic information such as cortical integrity can be shown in exquisite detail.

Little patient preparation is necessary for nuclear medicine examinations. It is crucial, however, that barium procedures do not precede the radioisotope or ultrasound examinations. In most instances the patient is catheterized, and in all cases intravenous injection of radiopharmaceutical is necessary.

Renal imaging depends predominantly on technetium-labeled compounds. These compounds differ in the manner by which they are eliminated by the kidney. ^{99m}Tc-labeled diethylenetriamine pentaacetic acid (^{99m}Tc-DTPA) is eliminated by glomerular filtration without any adherence to the renal tubules, whereas ^{99m}Tc-labeled glucoheptonate (^{99m}Tc-GH) and ^{99m}Tc-labeled dimercaptosuccinate (^{99m}Tc-DMSA) are to some extent bound to the tubular epithelial cells. Tubular transport agents are utilized in the neonate because of their higher removal from the circulation and the low glomerular filtration rate of the baby. The agent of choice is ^{99m}Tc-labeled mercaptoacetyl triglycine (MAG-3) (Fig. 5.39).

Tubular-bound chelates are used for evaluation of the renal cortex in such clinical conditions as renal infection, infarction, renal abscess (lobar nephronia), and acute tubular or cortical necrosis (Fig. 5.39).

Diuretic renography is utilized to evaluate hydronephrosis and to reveal the extent (if any) of obstruction of the collecting system (Fig. 5.39).

The indications for the EU to evaluate the kidney have virtually disappeared. A coronal reconstruction of contrast-enhanced MR or CT gives the same information (see Figs. 5.19 and 5.22). However, some centers use the intravenous pyelogram for evaluation of obstruction of the kidney and, therefore, it is briefly described. It is a plain film study with an abdominal film obtained prior to injection of the low-osmolarity contrast medium.

A 1-min coned-down prone radiograph of the kidneys – the total body opacification film – shows the parenchyma most advantageously (Fig. 5.40). The image on the nephrogram film is predicated on the principle that the peak plasma level of contrast agent is obtained immediately after a bolus injection. This vascular phase film shows the renal parenchyma very well because of the high renal blood flow (25% of cardiac output) and rapid removal of contrast agent by the glomeruli. Films in this phase also show avascular structures such as cysts or masses as negative defects. It is important to note that in the neonatal period renal blood flow is considerably reduced compared with that in the older child, and therefore that the parenchymal phase is delayed.

The imaging differential diagnoses on any of the various modalities or techniques for abnormal size or number of kidneys are found in Table 5.1.

What are the abnormalities seen in Figure 5.41?

Table 5.1. Differential diagnosis of abnormal size, number or visualization of the kidney(s)

A.	Single large kidney
	Tumor
	Renal vein thrombosis
	Pyelonephritis
	Abscess
	Hematoma
	Obstruction or reflux
B.	Two large kidneys
	Polycystic disease
	Hydronephrosis due to neurogenic bladder, posterior urethral valves, or other obstruction
	Leukemia, lymphoma
	Sickle cell disease
	Glycogen storage disease
	Amyloidosis
	Bilateral Wilms' tumor
	Acute glomerulonephritis
	Acquired immune deficiency syndrome (AIDS)
C.	Single small kidney
	Congenital hypoplastic kidney (renal artery stenosis)
	Postinfectious nephropathy
	Reflux
D.	Two small kidneys
	Reflux
	Postinfectious nephropathy
E.	Nonvisualized kidney
	Congenital absence of the kidney
	Surgically removed kidney
	Ectopic kidney with abnormal function
	Multicystic dysplastic kidney
	Renal artery thrombosis
	Renal vein thrombosis
	Tumor

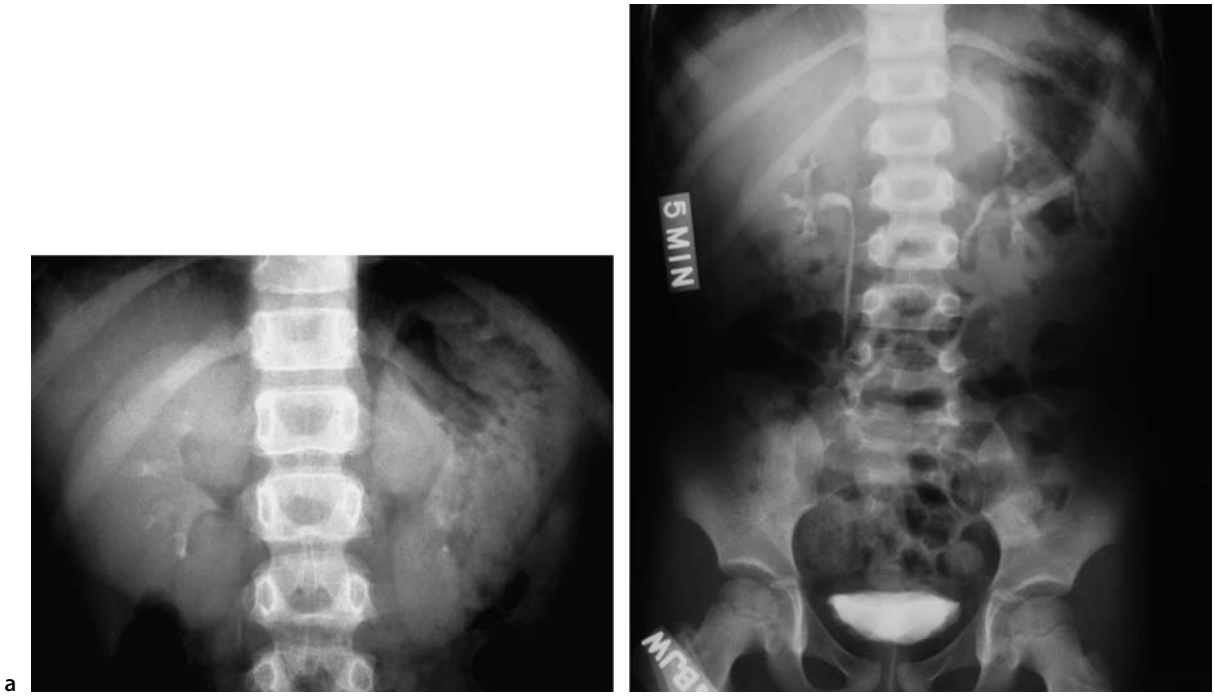

a b

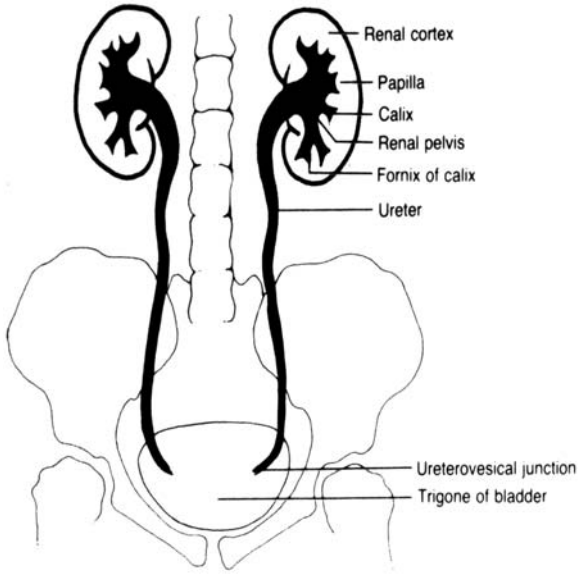

c

Fig. 5.40. The normal excretory urogram (EU)
a Prone coned-down view shows the nephrogram effect. The kidneys are homogeneous, and there is little contrast material in the collecting systems. Occasionally such a film is taken 1–2 min after injection; the collecting systems are then seen to better advantage. On this initial film the renal axis is noted with the upper pole being closer to the spine than the lower pole. The renal contours are evaluated and should be smooth without scarring or indentations
b This 5-min film reveals the renal collecting system – the calyces and infundibula leading to the renal pelvis and ureter. Any deviation or blunting of the collecting system is seen at this time. The renal pelvis then tapers into the ureter. The ureters pass inferiorly, crossing the margins of the transverse processes of the vertebrae. The bladder is separate from the pubic bones because it is partially filled. A 10-min frontal film is usually obtained to view the entire system to see if there has been any change secondary to osmotic load
c The normal intrarenal anatomy as see on the EU

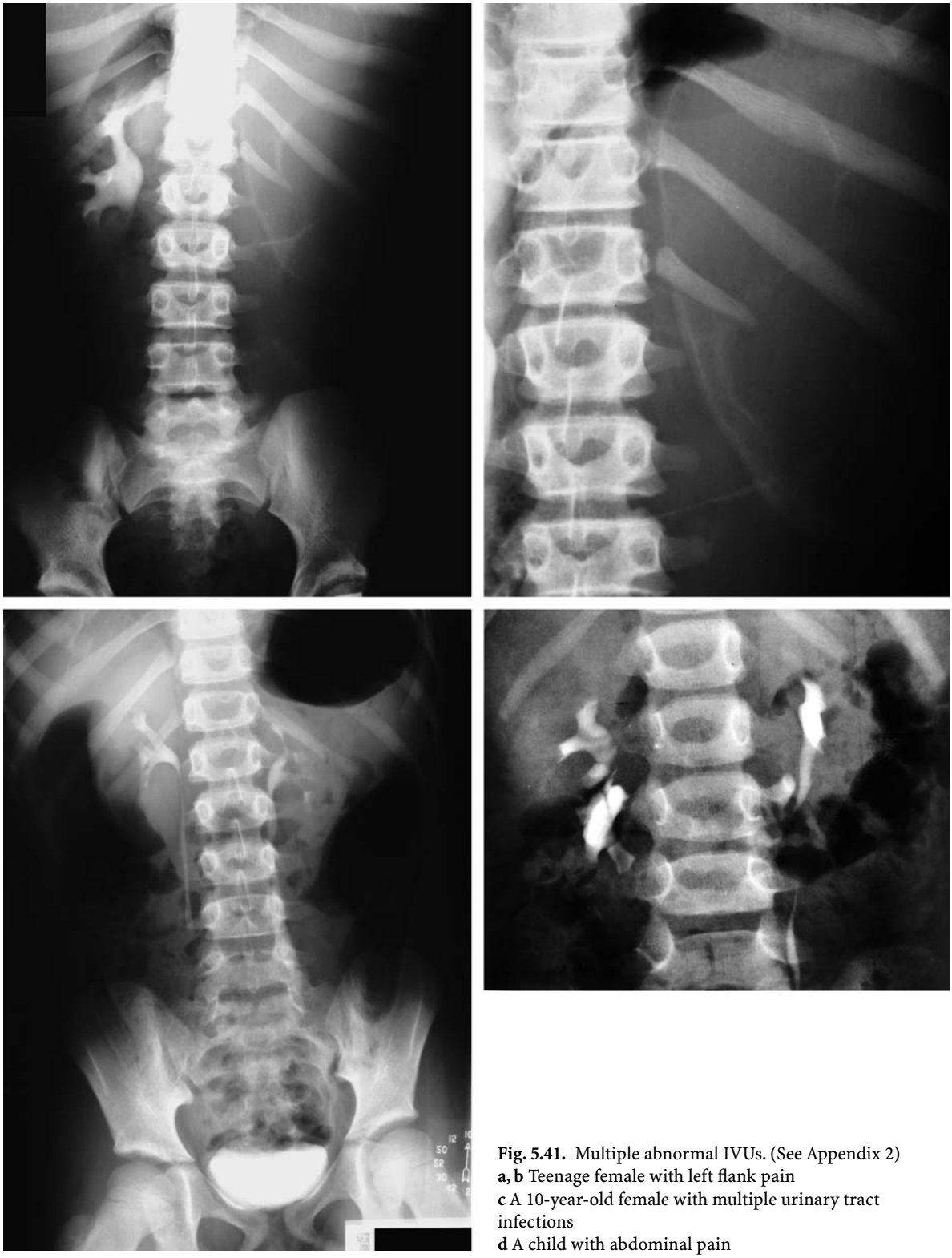

Fig. 5.41. Multiple abnormal IVUs. (See Appendix 2)
a, b Teenage female with left flank pain
c A 10-year-old female with multiple urinary tract infections
d A child with abdominal pain

Common Indications for Imaging the Abdomen in Pediatrics

The basic questions to ask before ordering an imaging modality of the abdomen are:

- Why am I doing the study?
- What do I hope to learn?
- Do I want an anatomical evaluation (e.g., tumor, anomaly, or obstruction) or a functional evaluation (e.g., renal function)?

Table 5.2. Signs or symptoms which may lead to imaging (listed alphabetically)

Abdominal mass (Chap. 6)
Abdominal–pelvic pain Acute (particularly right lower quadrant) Chronic (imaging only after clinical observation)
Bowel obstruction
Child abuse
Constipation (chronic and severe except in neonates)
Enuresis (imaging usually not necessary)
Failure to thrive
Gastrointestinal bleeding
Gastrointestinal perforation
Hematuria
Jaundice of uncertain etiology
Lymphadenopathy (systemic)
Malformations including meningomyelocele Anorectal abnormalities Genital abnormalities
Renal transplant
Screen for monitoring spread of known tumor
Screen for conditions/syndromes with abdominal components Aniridia (Wilms') Beckwith's syndrome (Wilms') Sickle cell disease (gallstones) Tuberous sclerosis (renal cysts and renal angiomyolipoma)
Scrotal pain
Systemic infection
Trauma (with appropriate history and/or significant physical or laboratory findings)
Urinary tract infection
Vomiting

An appropriate imaging modality can be selected only after the goals are clear in your mind. The decision as to which imaging modality one selects is really a tradeoff. In screening or looking for a low-yield abnormality, the appropriate procedure is the one that can provide the answer with the least radiation and least chance of a reaction or complication. It is for this reason that ultrasound is frequently selected as the first imaging modality. On the other hand, in evaluating a tumor, the most precise information is crucial; therefore, MR and CT studies are frequently utilized. The imaging modalities and techniques discussed in this chapter may be complementary. For example, an anechoic lesion on ultrasound may be a renal cyst, hydronephrosis, or a duplicated kidney. In the proper clinical setting, the work-up may end here (cyst), a functional study (hydronephrosis), or a confirmatory study (duplication) may be obtained.

The reasons one can obtain an imaging study of the abdomen and pelvis are almost unlimited. However, usually clinical observation and clinical follow-up settle most problems and no imaging is necessary. Table 5.2 is a partial list of complaints that might require an imaging study.

Common Clinical Problems

Vomiting

Vomiting is extremely common during childhood and is so nonspecific that history and physical examination are crucial to diagnosis. The character of the vomitus as well as the age of the child play an important role in the differential diagnosis (Table 5.3).

From age 1 day to 2 months the most common cause of nonbilious vomiting that may be imaged is chalasia – gastroesophageal reflux. Immaturity of the esophagogastric junction results in food substances (or contrast medium during an esophagram) flowing back from the stomach into the esophagus. This is imaged best with nuclear scintigraphy (best sensitivity) (Fig. 5.42). It also can be detected during the fluoroscopy phase of the esophagram or upper gastrointestinal examination. The diagnosis can also be made on the delayed film if there is contrast in the esophagus long after the patient has been given the barium. In most children this is not accompanied by a hiatal hernia and is a self-limiting disorder. The best nonimaging technique is the pH monitor – a probe placed at the end of a feed-

ing tube. It is positioned in the distal end of the esophagus and the patient is monitored for 24 h. When reflux is the primary consideration, a nuclear scan may suffice. When there are other anatomical considerations, a radiographic contrast study is indicated.

Another common cause of nonbilious vomiting in this age group is pyloric stenosis (Figs. 5.43, 5.44).

Table 5.3. Differential diagnosis of vomiting

A. Neonate to 2 months:
   1. Nonbilious
      a) Overfeeding
      b) Chalasia (gastroesophageal reflux)
      c) Pyloric stenosis
   2. Bilious
      a) Midgut volvulus
      b) Small bowel obstruction
      c) Bowel atresia in newborn
      d) Hirschsprung's disease

B. In infants aged 2 months to 2 years the possibilities include:
   1. Nonbilious (rarely an organic cause other than chalasia). May be diseases in other organ systems such as meningitis, urinary tract infection, etc.
   2. Bilious
      a) Midgut volvulus
      b) Small bowel obstruction
      c) Intussusception

C. In children over 2 years old:
   Most causes not related to gastrointestinal tract obstructions

These children usually have projectile, nonbilious vomiting. If it persists for some time, the baby loses weight, and electrolyte abnormalities (alkalosis with low chloride) become apparent. On careful physical examination the hypertrophied pyloric muscle can be palpated and feels somewhat like an olive. Some pediatric surgeons feel confident enough with this finding to operate and order an imaging examination only in those patients in whom the finding is absent. When one is quite certain of the diagnosis of pyloric stenosis but would like imaging confirmation, an ultrasound can be performed. Reliable criteria have been worked out for the hypertrophied pylorus (>4 mm muscle thickness and >15 mm pyloric channel length; Fig. 5.43).

When one is less certain of the diagnosis and is concerned about other anomalies, an upper gastrointestinal series is the correct procedure. The examination series defines the elongated, upturned, curved pyloric canal with the "railroad track" sign (Fig. 5.44).

In the neonate and infant up to 2 months of age, bilious vomiting strongly suggests obstruction distal to the entrance of the common bile duct into the duodenum. In the first days of life midgut volvulus and atresias of the small bowel are suspected. By using air as a contrast medium, the level of obstruction can be diagnosed by the number of air-filled, distended loops of bowel seen on the plain film (see Fig. 5.12). Midgut volvulus is the most important emergent condition to consider. In these situations there is developmental abnormality of rotation and fixation

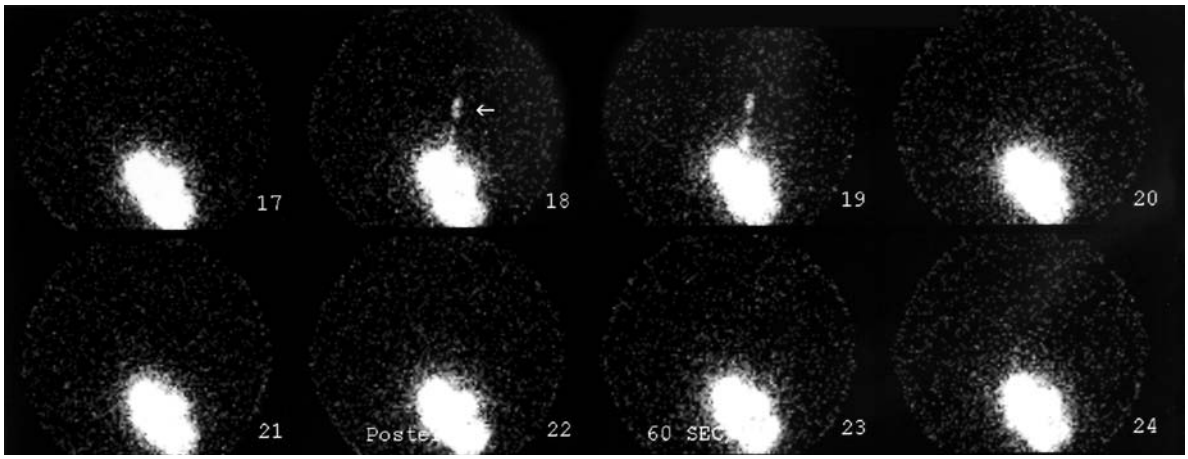

Fig. 5.42. Gastroesophageal reflux study. The patient was given technetium sulfacolloid in formula. Posterior imaging was done at 1-min intervals. The stomach is seen without reflux (*image 17*) and with gastroesophageal reflux (*image 18 and 19*)

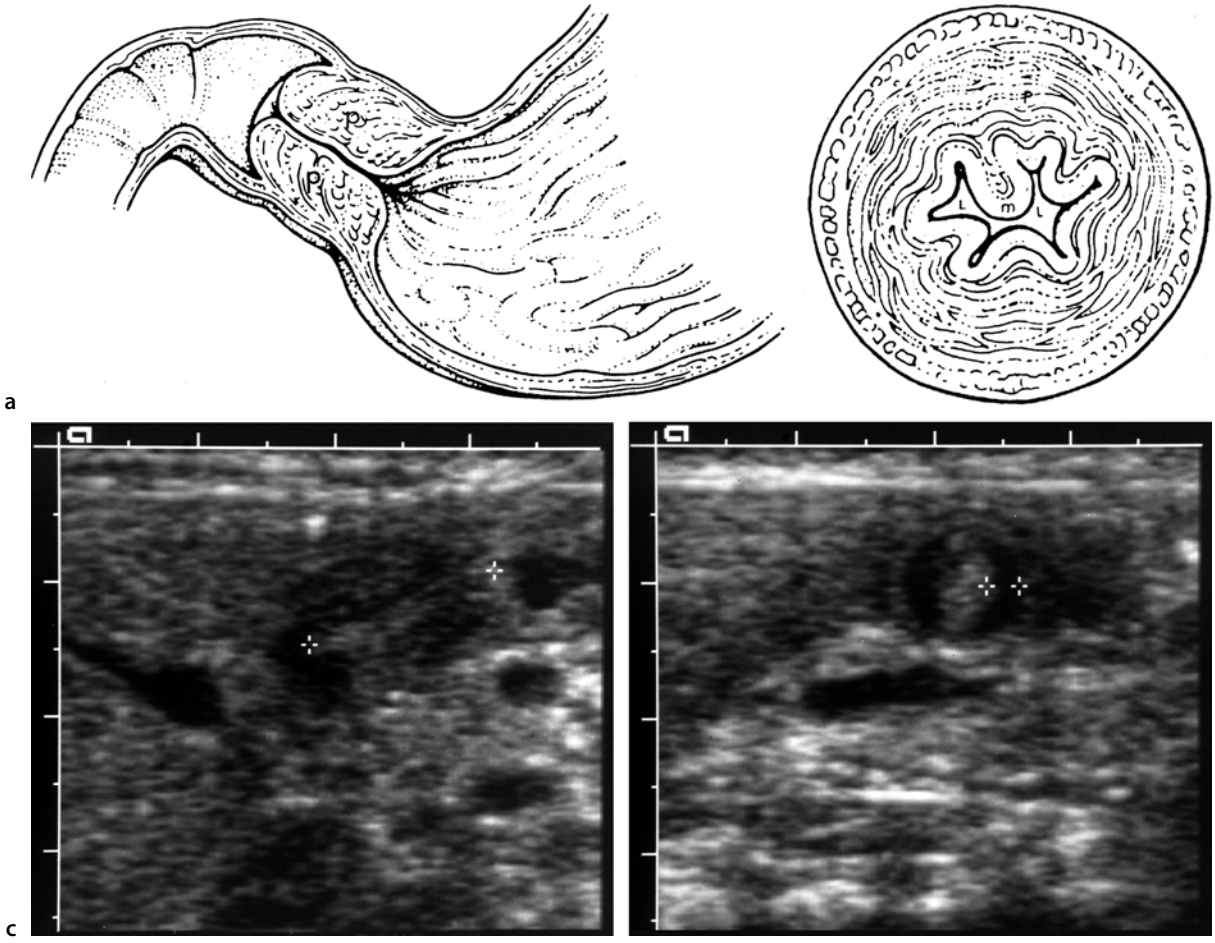

Fig. 5.43. Pyloric stenosis ultrasound diagnosis
a Drawing of longitudinal section through hypertrophied muscle (*P*)
b Drawing of transverse scan through thickened pylorus. *P*, pylorus; *M*, mucosa; *L*, lumen
c Longitudinal sonogram corresponding to **a**; cursors delineate length of pylorus
d Transverse ultrasound corresponding to **b**; cursors delineate muscle thickness. (From [3] with permission)

of the midbowel from the ligament of Treitz to the splenic flexure. The ligament of Treitz is absent. Lack of proper fixation provides the mechanical basis that permits the bowel to twist (volvulus), leading to vascular compromise (superior mesenteric vessels). Initially, venous return is occluded, followed by arterial obstruction involving the superior mesenteric artery (see Fig. 5.29).

Causes of more distal abdominal obstruction presenting in the newborn include ileal and colonic atresia and aganglionosis (Hirschsprung's disease). In the latter, there is extensive dilatation of bowel loops indicating low obstruction. When a barium enema is performed, a discrepancy between the dilated proximal ganglionic portion of bowel and the abnormal aganglionic distal portion of bowel is seen. This transition zone, together with the child's failure to satisfactorily evacuate the barium after 24 h, confirms the presence of mechanical bowel obstruction proximal to the malfunctioning colon segment.

Between 2 months and 2 years of age the major cause of nonbilious vomiting continues to be chalasia (gastroesophageal reflux). Bilious vomiting in this age group suggests malrotation, small bowel obstruction, or intussusception.

In children over 2 years of age most causes of vomiting are not related to gastrointestinal tract anomalies, although certainly small bowel obstruction, midgut volvulus, and intussusception do occur.

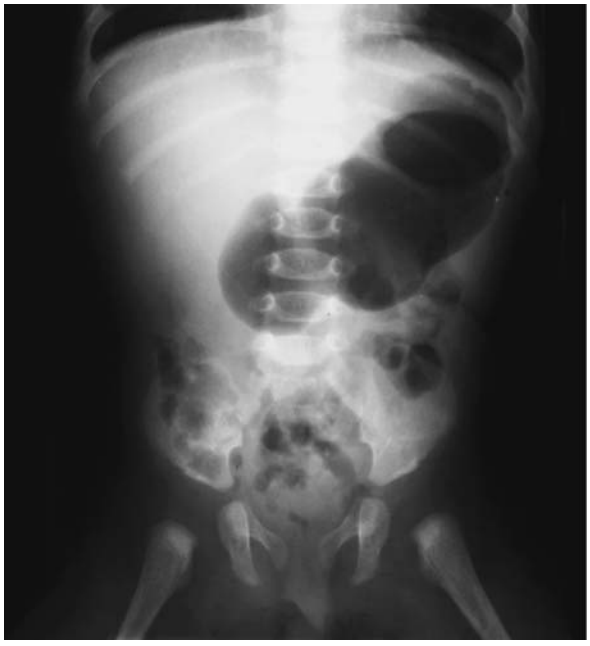

a

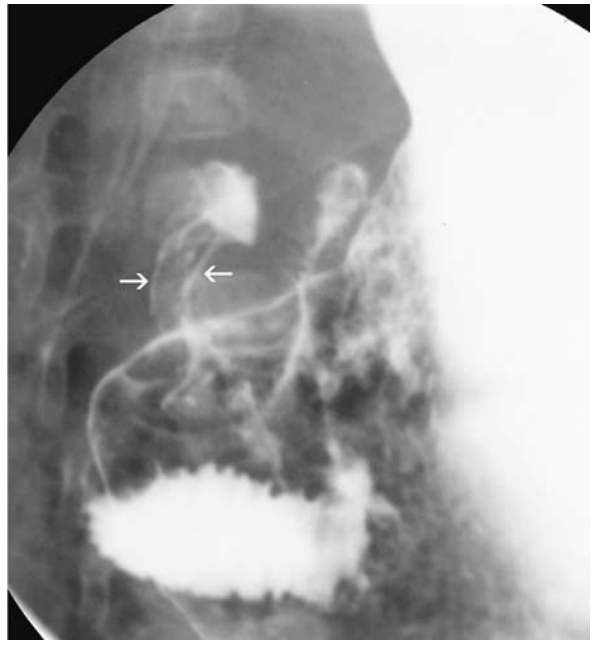

b

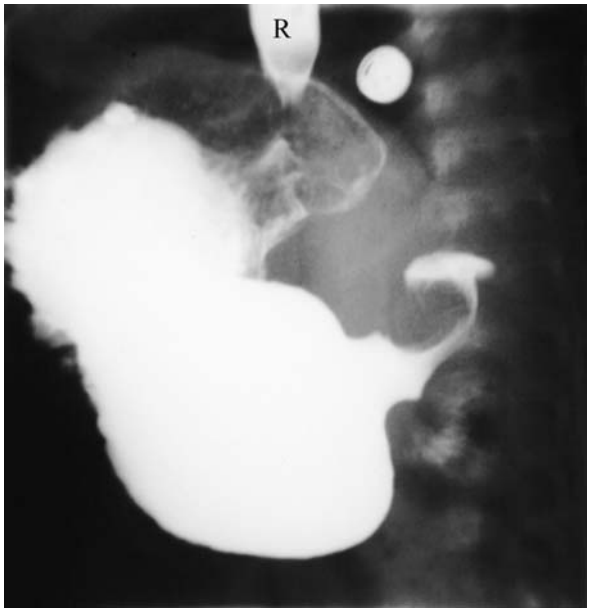

c

Fig. 5.44. Pyloric stenosis
a Supine film of the abdomen reveals distention of the stomach. Multiple peristaltic waves (contractions) are visible by the shape of the stomach. This is one of the plain film findings of gastric outlet obstruction
b Upper gastrointestinal series reveals the elongated, upturned pyloric channel (*arrow*). Note there are two contrast-filled tracts (railroad tracks) because of asymmetric hypertrophy of the muscle
c Oblique view in another child with pyloric stenosis shows the long pyloric channel. There is gastroesophageal reflux (*R*)

Abdominal Pain

This is an extremely common complaint in the pediatric age group. It can be divided into acute and chronic abdominal pain. In chronic abdominal pain most clinicians have found imaging studies to be futile when pain is the *only* complaint. However, when this symptom is coupled with weight loss, diarrhea, and/or blood in the stool, inflammatory bowel disease is frequently found. The term "inflammatory bowel disease" includes regional enteritis and ulcerative colitis and can be diagnosed by various imaging and endoscopic investigations of the upper and lower gastrointestinal tract (see Fig. 5.30).

Although acute abdominal pain in children is most often due to medical conditions such as gastroenteritis, the radiologist must be alert for surgical causes of abdominal pain, the most common of which are incarcerated hernia, intussusception, and appendicitis.

The diagnosis of *incarcerated hernia* is usually made clinically but can be noted on plain film examination by signs of small bowel obstruction and the abnormal position of bowel gas, frequently in the inguinal canal or scrotum (Fig. 5.45).

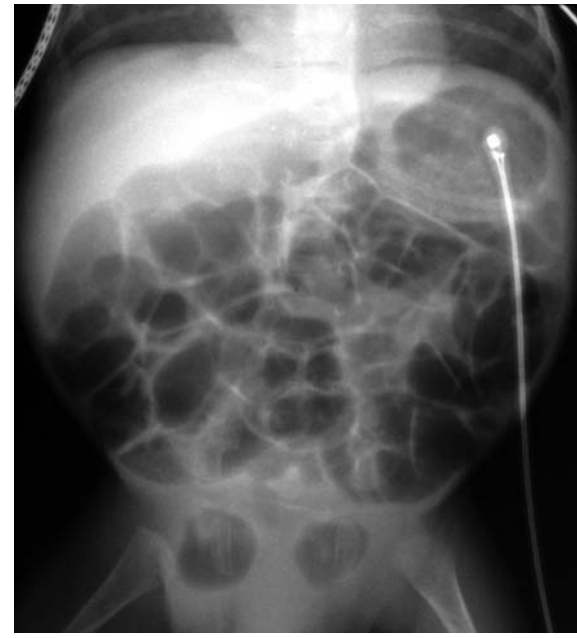

Fig. 5.45. Hernia on plain film
This young infant is quite distended and irritable. You can see gas in both inguinal canals. The child has bilateral inguinal hernias

Intussusception occurs when small bowel invaginates into small bowel and/or colon, causing obstruction and eventual ischemia of the telescoped portion of the bowel – the colon (Fig. 5.46). Most often, intussusception is manifest clinically by acute, colicky abdominal pain (see below) and in late stages by bloody diarrhea and signs of intestinal obstruction. The obstruction often results in bilious vomiting.

The plain film findings include demonstration of:

- A mass
- Signs of bowel obstruction

However, the plain film may be normal. For this reason, some centers have been screening patients suspected of having intussusception with ultrasound (Fig. 5.46). When the ultrasound is positive, a therapeutic enema (in most centers air is the contrast agent, while some still use barium) is performed. On barium examination, the mass as well as the "coiled spring" appearance of contrast around the mass is seen. The coiled spring is contrast in the colon surrounding the small bowel. The mass must be pushed back (reduced) through the ileal cecal valve and into the small bowel. The findings on air enema are identification of the small bowel (the mass) within the colon (Fig. 5.47).

Appendicitis is a common cause of abdominal pain and the most common cause of a surgical abdomen in children. It occurs less frequently in infants between 2 and 5 years and is often perforated by the time the diagnosis is made. At any age, the morbitity (and fatality) is entirely secondary to complications of perforation. It is therefore important to make a quick, correct diagnosis of acute appendicitis. The plain film findings of acute appendicitis include (Fig. 5.48):

- Appendicolith (10%)
- Free fluid in the right lower quadrant (best seen on a prone film by separation of the colon from the properitoneal fat line)
- Sentinel loop of bowel of localized air–fluid level in the right lower quadrant
- Scoliosis with concavity to the right (splinting)

However, plain film findings are present in the minority of cases imaged. For this reason, two imaging tests have been utilized to help make the diagnosis.

While ultrasonography has long been used to diagnose the complications of appendicitis, such as periappendiceal abscess, only in the last decade has it been reliably used to diagnose the nonperforated,

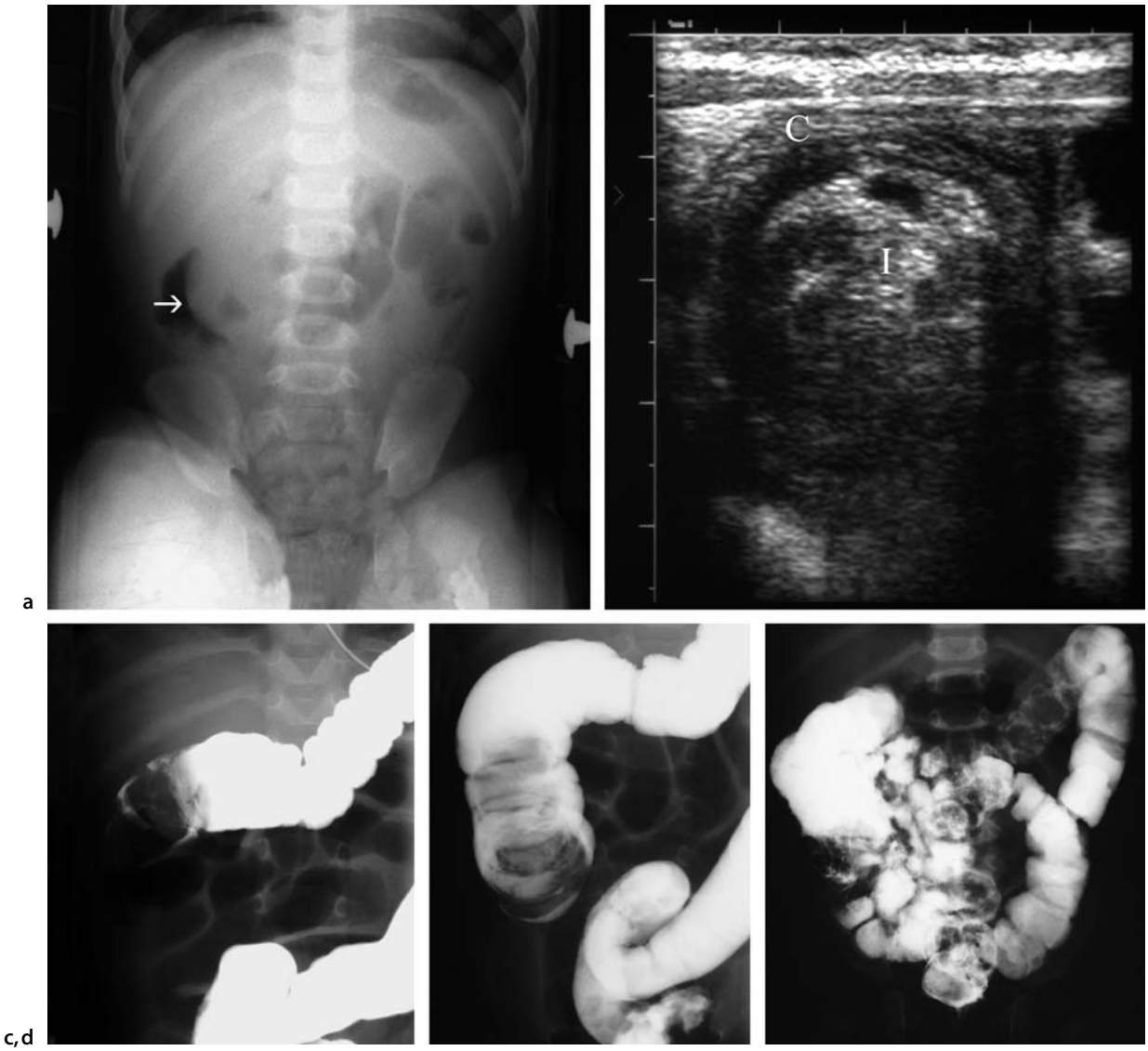

Fig. 5.46. Intussusception
a Upright abdominal film in this 8-month-old with acute, colicky abdominal pain reveals a mass (*arrow*) in the region of the hepatic flexure. This finding was consistent on all films
b Ultrasound of intussusception. Small bowel (ilium) (*I*) is within the colon (*C*)
c A barium enema was performed, and a large filling defect is seen in this region
d The mass was pushed back to the cecum by barium enema
e There was abundant small bowel reflux and the mass is no longer visible

uncomplicated, inflamed appendix. Using criteria of greater than 6 mm in width and noncompressibility of the appendix, and with the addition of color Doppler (flow may be increased in the inflamed appendix), appendicitis can be readily diagnosed by ultrasound (Fig. 5.48)

Ultrasound is examiner-dependent while CT is a more sensitive and accurate test but entails radiation exposure. CT can be focused to the region below the kidneys, although many favor scanning the entire abdomen for other causes of abdominal pain. The patient may or may not receive oral or intravenous contrast material. The CT findings of acute appendicitis are (Fig. 5.49):

- Distended appendix greater than 6 mm
- Fatty infiltration (stranding)
- An appendicolith (20–40 % – much more sensitive than the plain films)

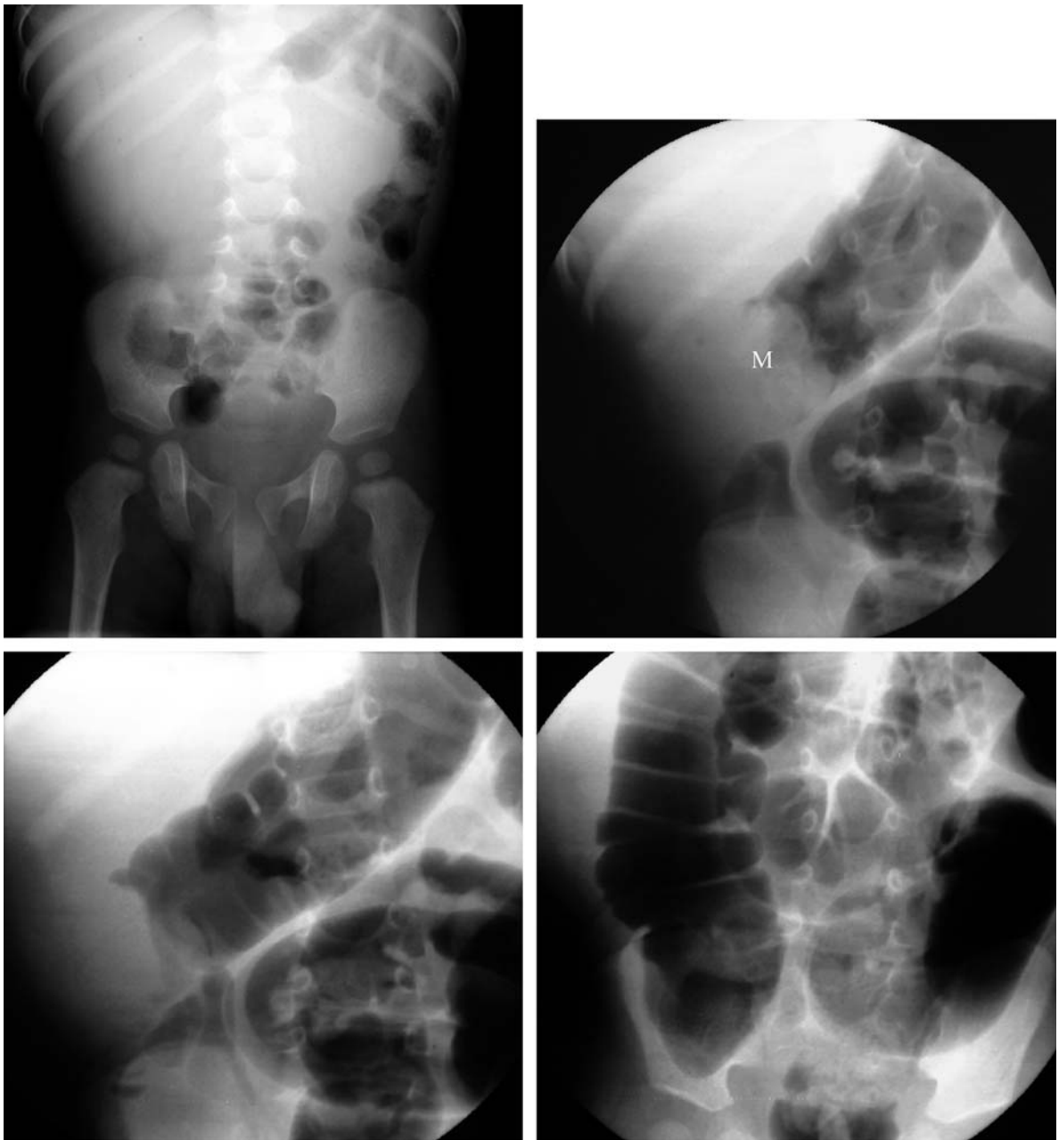

Fig. 5.47. Air reduction of intussusception
a On the plain film there is a suggestion of a mass in the midabdomen in this 13-month-old with colicky abdominal pain
b Air enema shows mass (*M*) within the transverse colon
c The intussusception was pushed to the descending colon
d The mass has disappeared with abundant air refluxing into small bowel

- Complications of perforated appendicitis – abscess and/or fluid (pus) in the abdomen

Another important cause of abdominal pain is urinary colic, either a kidney or ureteral stone. An acute renal stone may not cause a great deal of distention of the renal pelvis and therefore plain film and ultrasound are not as sensitive as CT in detecting calcium. The standard imaging is now a non-contrast-enhanced CT (Fig. 5.20).

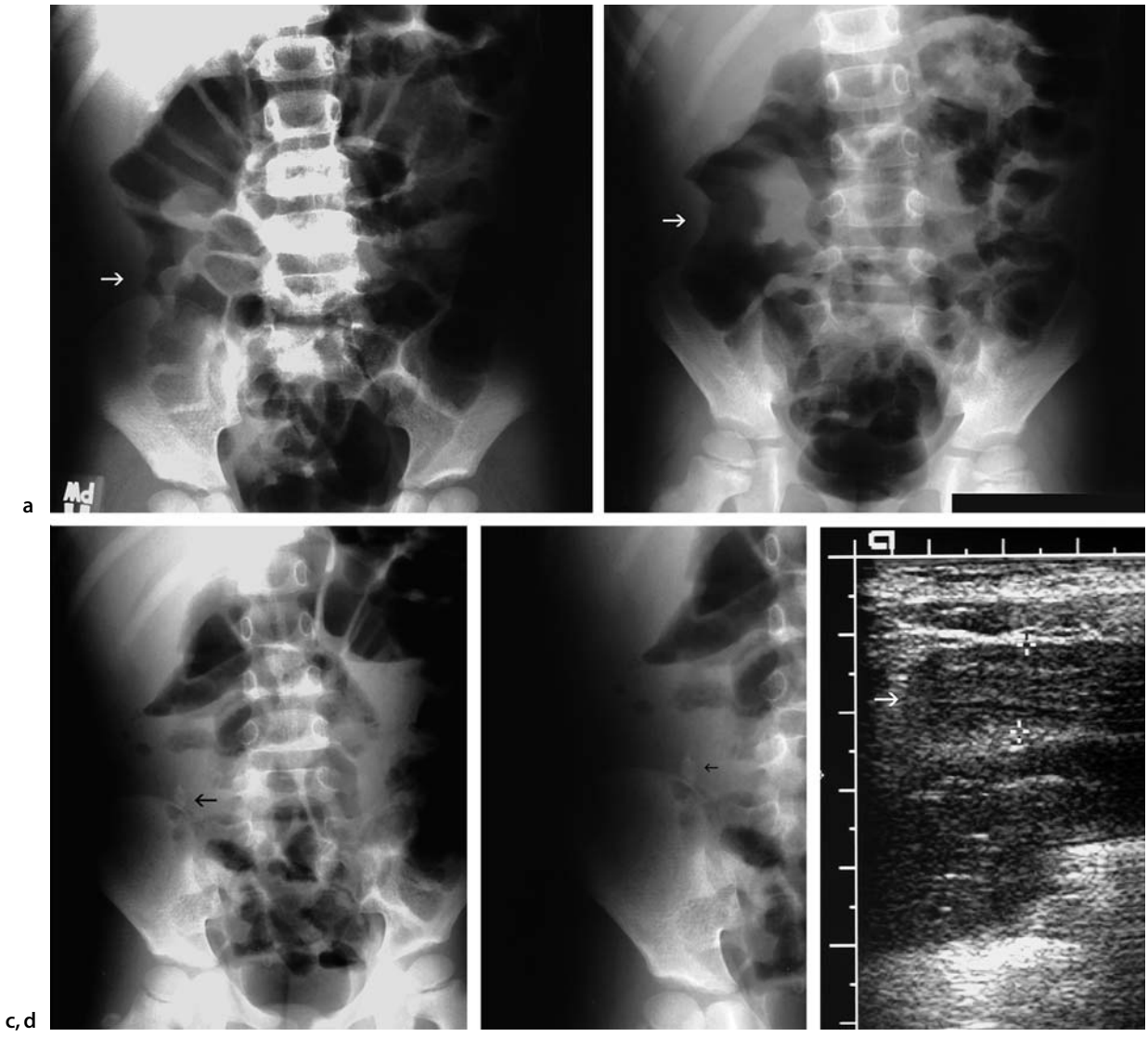

Fig. 5.48. Plain film and ultrasound of appendicitis

a, b A 5-year-old male presented with acute right abdominal pain. On both the supine (**a**) and the prone (**b**) film there is deviation of the colon from the properitoneal fat stripe. Note the irregularity of the colon (*arrow*)

c An erect film on another child.
A fecalith is seen (*arrow*). It is laminated. There is also a paucity of gas in the right lower quadrant

d Close-up of **c**

e Transverse ultrasound of the right lower quadrant reveals noncompressible bowel over 6 mm in diameter (*arrow*). This is the ultrasonic finding of acute inflamed appendix

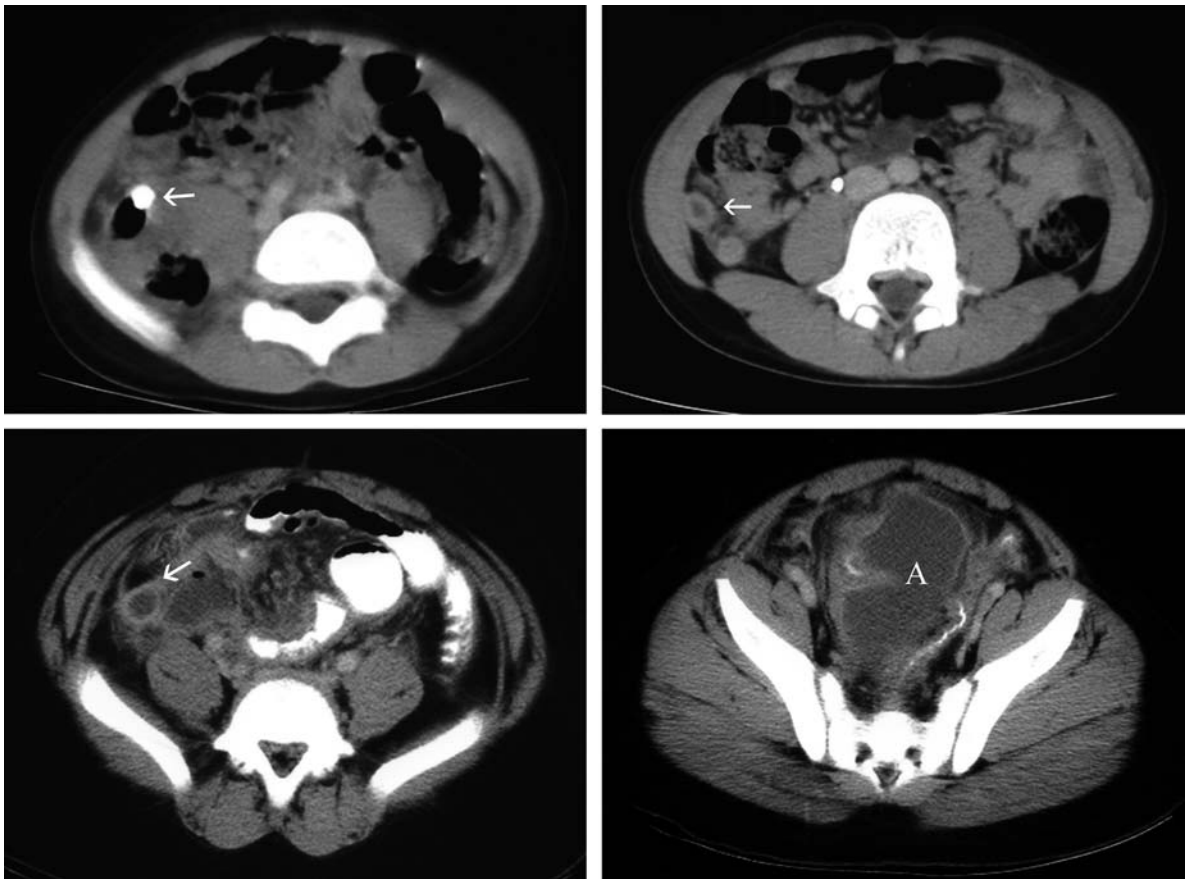

Fig. 5.49. CT of appendicitis
a A 4-year-old girl with right lower quadrant pain. Transverse scan through the region just above the iliac crest reveals a large appendicolith (*arrow*) in the right lower quadrant. This was only seen retrospectively on plain films
b An 8-year-old boy with lower abdominal pain reveals a thickened appendix (*arrow*) in the retrocecal region. This also was acute appendicitis. There is contrast in the right ureter
c, d A 10-year-old male with a several-day history of abdominal pain. Transverse scans at the region of the iliac crest (**c**) and in the pelvis (**d**) reveals a thickened inflamed appendix (*arrow*) and adjacent fluid (an abscess). There is a large abscess (*A*) displacing bowel and sitting on top of the bladder (bladder not shown)

Blunt Abdominal Trauma

Plain films of the abdomen may be extremely valuable in blunt abdominal trauma because free air, free fluid, and sentinel loops as well as fractured ribs and transverse processes of the spine can be found. Remember the radiologist's circle and the ABCS (Fig. 5.50).

CT is indicated in children with a history of high-velocity injury, abnormal abdominal examination, or laboratory evidence of elevation of liver enzymes or microscopic hematuria (which does not clear).

CT has become well established as routine in the diagnosis and management of children with blunt abdominal trauma (Fig. 5.51). Diagnostic peritoneal lavage is usually not necessary, especially in children who are hemodynamically stable. Visceral injuries are treated medically in most centers, and there has been a reduction in the need for exploratory laparotomy. The beauty of CT is that it allows the detection, localization, and characterization of hepatic, splenic, adrenal, and renal injuries. Mesenteric lesions and bowel injury are not as well visualized. With the trend toward nonoperative management of many of these visceral injuries, CT has been invaluable in the management of these children. When there is fracture of the bones of the pelvis, a retrograde urethrogram is necessary to rule out anterior urethral injury.

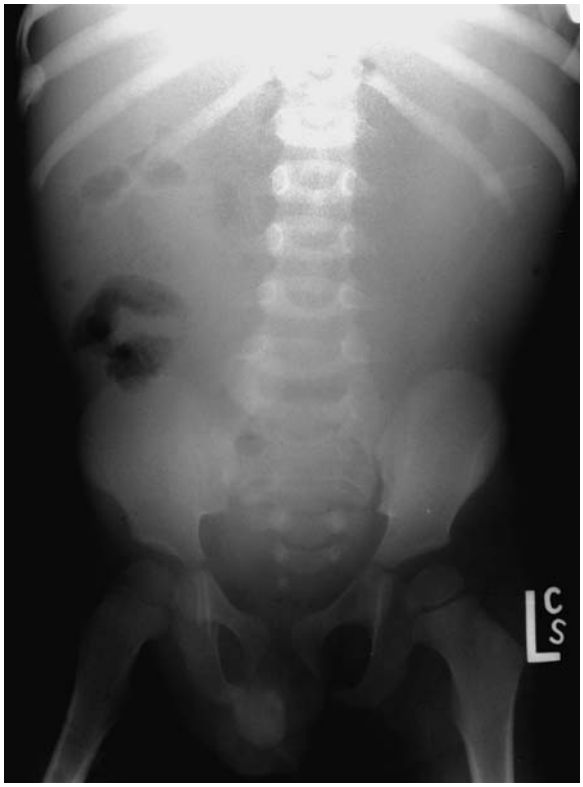

Fig. 5.50. This child presented to the emergency room with abdominal pain. A 2-year-old with paucity of bowel gas. The astute radiologist picked up something else. Do you see it? Look at the healing right lateral rib fracture at T10. This child was a victim of child abuse

Constipation

Late onset of symptoms, particularly after toilet training has begun, suggests a functional basis for this disorder. After appropriate follow-up and therapeutic maneuvers, imaging may be performed if the child has not improved. In most children with functional constipation, plain film studies reveal a dilated rectum and colon distended with stool. The barium enema confirms the presence of a large, capacious rectum, and postevacuation studies show no segment of narrowing, i.e., transition zone between dilated and nondilated bowel. However, if the patient has had a history of constipation from birth, one must consider a diagnosis of Hirschsprung's disease (Fig. 5.52). The barium enema differentiates the findings of functional constipation from those of a malfunctioning distal aganglionic segment. This may be seen most graphically on the postevacuation films, where the caliber disparity (the transition zone) is striking. Since the examination attempts to show not only anatomical abnormality but also pathophysiology, the usual preparation prior to the enema (colonic emptying with purgatives and enemas) should be omitted.

Gastrointestinal Bleeding

Rectal bleeding varies from guaiac-positive stools to frank bright red blood. There are many causes, and the proper approach is determined by the suspected etiology in each case. Table 5.4 outlines the various causes and possible diagnostic procedures.

Table 5.4. Gastrointestinal bleeding

Suspected causes	Kind of bleeding	Procedure of choice
Peptic ulcer	Melena	Endoscopy and/or upper gastrointestinal series
Anal fissure	Blood-streaked stool	None; physical examination
Polyps	Red blood mixed with stool	Endoscopy and/or barium enema
Intussusception	See abdominal pain and vomiting in text	Enema with air or opaque contrast reduction
Meckel's diverticulum	Voluminous, bright-red blood	Technetium radionuclide study
Inflammatory bowel disease	Bright red blood and/or streaking in stool	Endoscopy, upper gastrointestinal series with small bowel follow-through, barium enema
Necrotizing enterocolitis	Variable	Plain film. Radiographic signs in newborns include: (1) dilated bowel loops, (2) pneumatosis intestinalis (air in wall of the bowel), (3) portal venous gas, (4) free air

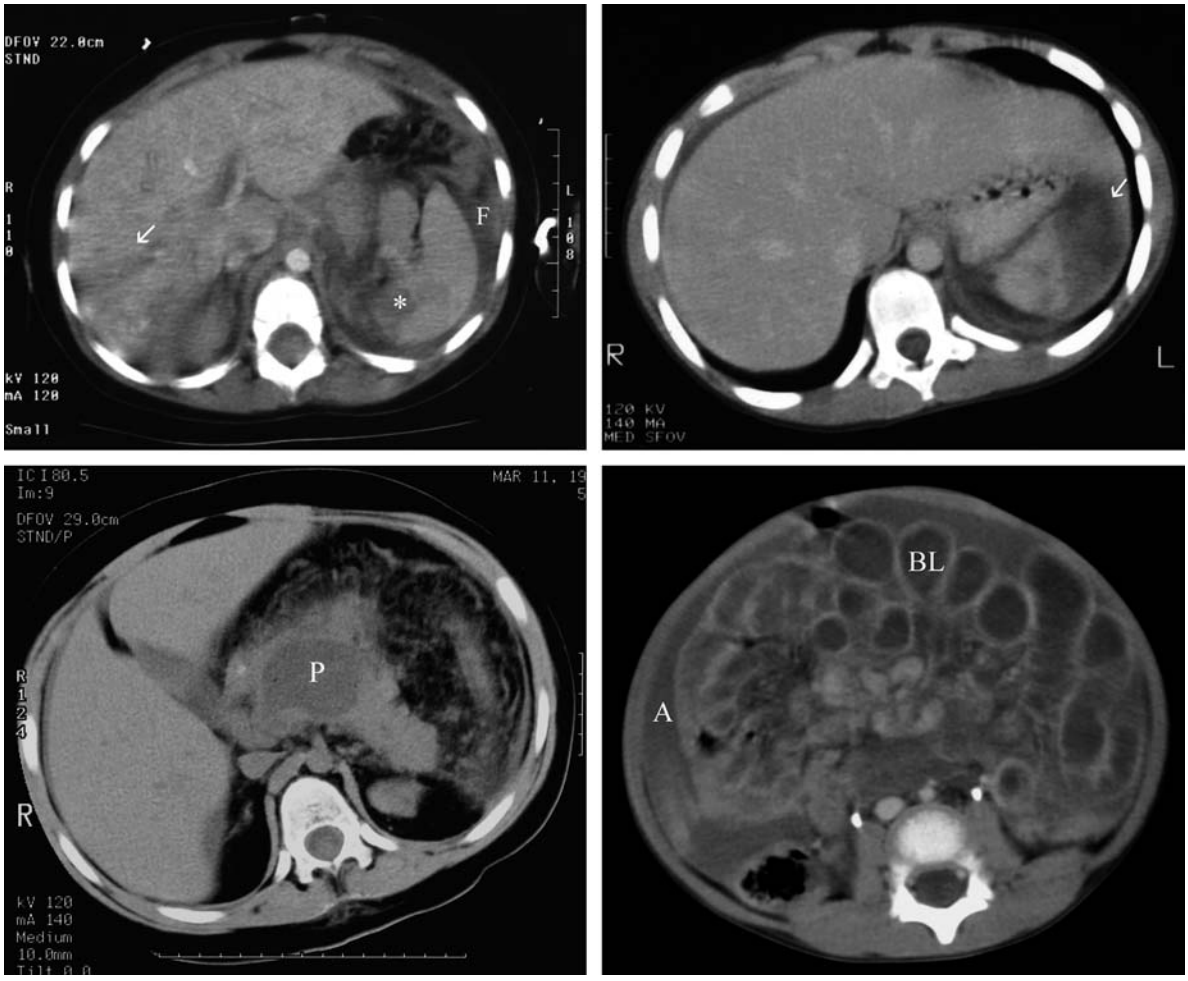

Fig. 5.51. CT trauma of the abdomen
a This patient was hit by a car. Laceration of the right lobe of the liver (*arrow*) and fractured spleen (*asterisk*) are present. There is free abdominal fluid (*F*)
b Another child with a fractured spleen (*arrow*) from a motor vehicle accident
c A 10-year-old who fell into the handle bars of his bicycle 1 week previously. He has a pancreatic pseudocyst (*P*)
d A 2-year-old passenger without proper car seat restraint in a motor vehicle accident. He is in shock with multiple fluid-filled bowel loops (*BL*). He has ascites (*A*) and the aorta and vena cava are small. There is contrast in both ureters

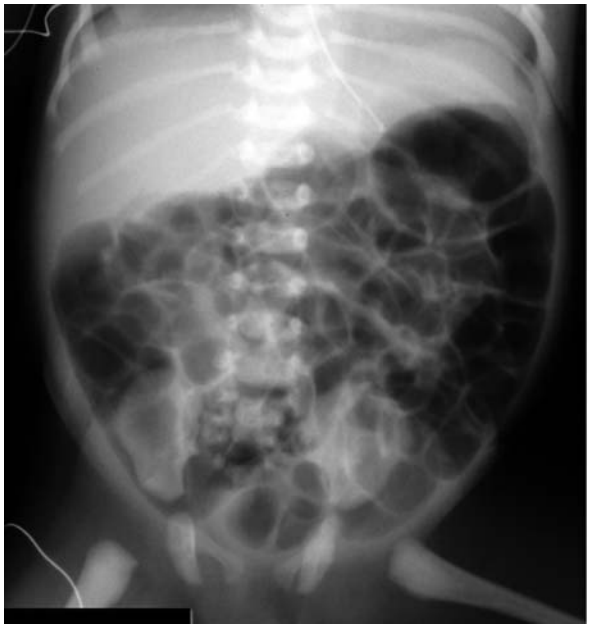

a

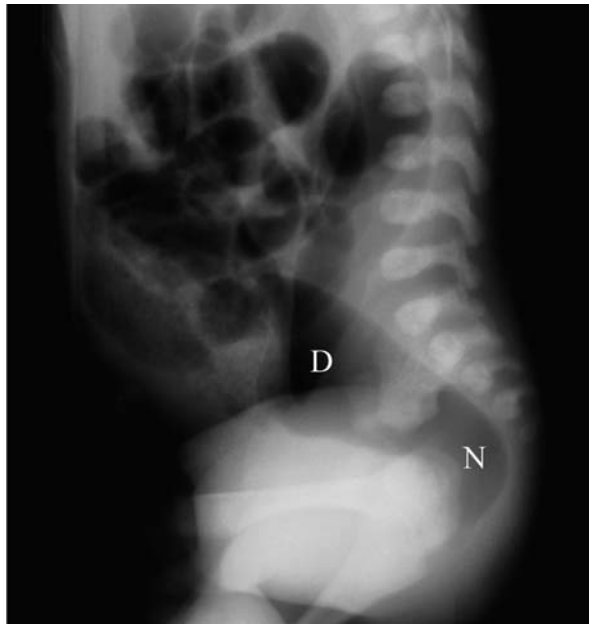

b

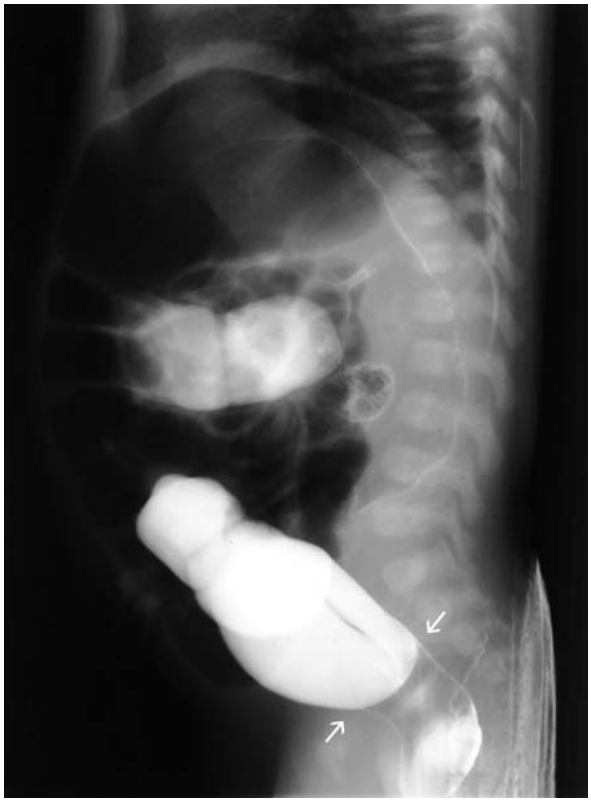

c

Fig. 5.52. Hirschsprung's disease
a Abdominal film in a 5-day-old reveals distention of the bowel with gas all the way down into the pelvis
b On lateral films the rectum is considerably smaller than any portion of the colon, and there is a transition zone between the nondilated (*N*) and dilated (*D*) portions of the bowel
c Lateral postevacuation film reveals that the rectum is not the most dilated portion of the colon. Transition zone (*arrows*) between the nondistensible, aganglionic distal colon and the dilated, ganglionic proximal colon. Note how much of the colon is dilated. The rectum is nondistensible

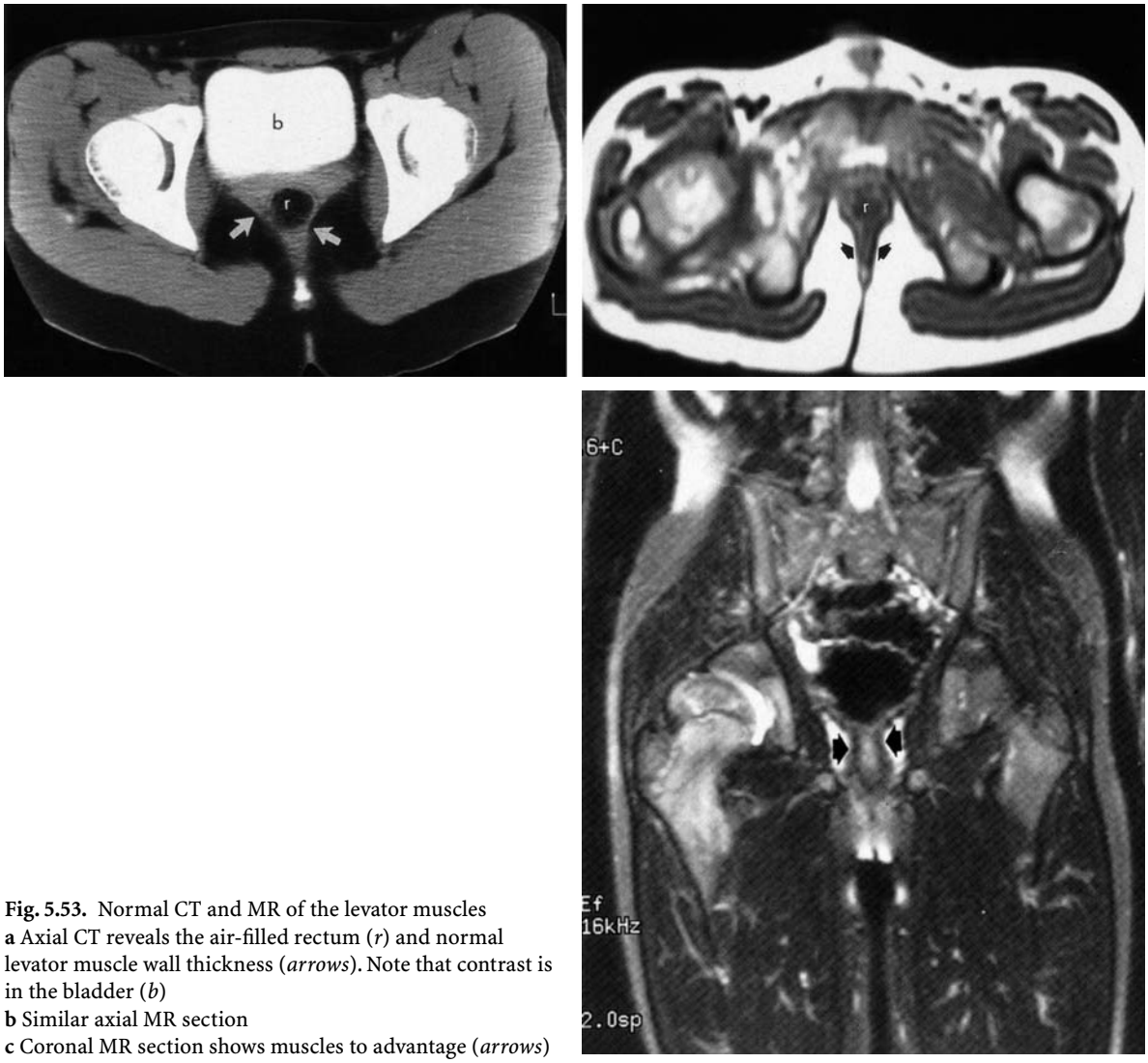

Fig. 5.53. Normal CT and MR of the levator muscles
a Axial CT reveals the air-filled rectum (*r*) and normal levator muscle wall thickness (*arrows*). Note that contrast is in the bladder (*b*)
b Similar axial MR section
c Coronal MR section shows muscles to advantage (*arrows*)

Anal–Rectal Malformations

In the past the invertogram (holding the baby upside down so that colonic gas rises and estimating how close the distal rectum comes to the anal dimple) was used to assess the level of imperforate anus. However, this technique was always unreliable, as meconium can block air from going distally. Prone cross-table lateral films are probably more reliable. Now, however, with the advent of MR we can depict the anal canal and distal rectum and with much greater accuracy. Visualizing the levator muscle is key to successful operative repair of this anomaly. MR also allows the visualization of associated renal and spinal anomalies (10% of imperforate anus cases) (Fig. 5.53). Postoperatively, the rectal pull-through procedure is nicely assessed with MR as well.

Urinary Tract Infection

Upper urinary tract infection must be documented before radiographic studies are requested. Although the presence of bacteria on Gram stains of a fresh, unspun, clean-catch specimen is very suggestive of a urinary tract infection, this must be confirmed with a quantitative urine culture. A colony count of 100,000

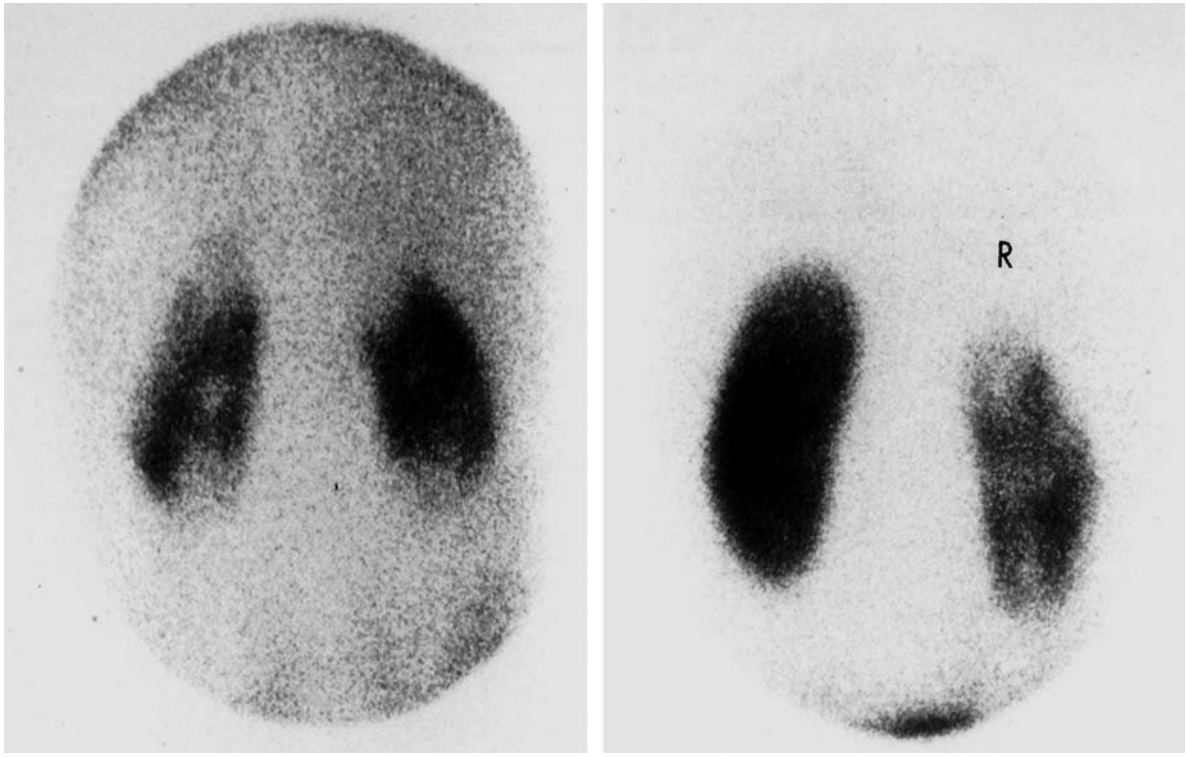

a b

Fig. 5.54. Nuclear studies of acute pyelonephritis
a Posterior scan with ^{99m}Tc-GH shows large photon-deficient areas in both kidneys corresponding to areas of infection in this 2-year-old girl
b Posterior scan of the right kidney in another child shows photon-deficient areas most prominent in the upper and lower poles. The left kidney is normal. This child complained of right flank pain and was febrile

per cubic millimeter of midstream voided specimen is considered a positive urine culture.

Recently, the need to image the first urinary tract infection in both boys and girls has been questioned. In infants less than 1 year of age and in older boys the first infection should be investigated. Historical information of a familial history of vesicoureteral reflux is a factor in early imaging. The history of the dysfunctional voiding (urgency with or without frequency) secondary to detrusor muscle irritability is an important but controversial indication for early imaging. The real question that provoked the debate on imaging is the lack of evidence that, when imaging detects an abnormality (i.e., reflux), treatment prevents or alters the progression to end-stage renal disease.

There is general agreement that the younger the child, the greater the risk of kidney damage from infection, and that pyelonephritis must be present to lead to scarred kidney and renal damage. In the past it was thought that ureterovesical reflux is the major risk factor for pyelonephritis. However, 40–50% of children with sequelae of pyelonephritis never have documented reflux. Therefore it appears that imaging the kidney for pyelonephritis is the most appropriate first step in the high-risk groups (neonate to 3 years). This should be conducted with ^{99m}Tc -DMSA or ^{99m}Tc-GH (Fig. 5.54). If positive, ultrasound and voiding studies are usually carried out (Fig. 5.55).

In low-risk groups (age >3 years), a DMSA scan might be all that is necessary. Reflux decreases with age.

Enuresis

Most nocturnal bedwetters do not require any imaging studies. Careful history, centering on the symptoms of urinary tract infection, neurogenic bladder, and persistent versus intermittent wetting, should clarify the problem. If an imaging work-up is pursued, an ultrasound to rule out anomalies and a VCU to detect a neurogenic bladder or abnormalities such as an ectopic ureteral insertion are performed.

Abdominal Mass

This is discussed fully in Chap. 6.

Hematuria

In nontraumatic hematuria, the need for an imaging study reflects the clinical diagnosis. Acute streptococcal glomerulonephritis and Henoch-Schönlein purpura are not indications for imaging. However, since tumors can present with hematuria, a precise anatomical evaluation is appropriate if the diagnosis is uncertain. Because of the lower radiation dose and, in many instances, the ease of obtaining the examination, an ultrasound scan is usually performed first.

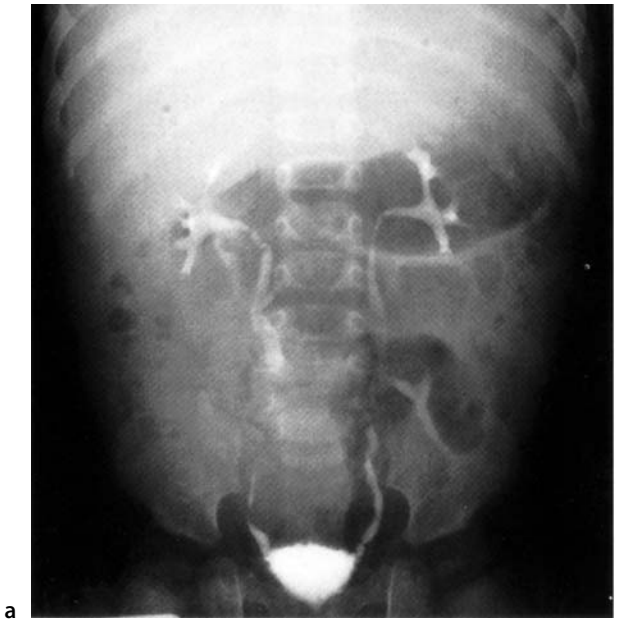

a

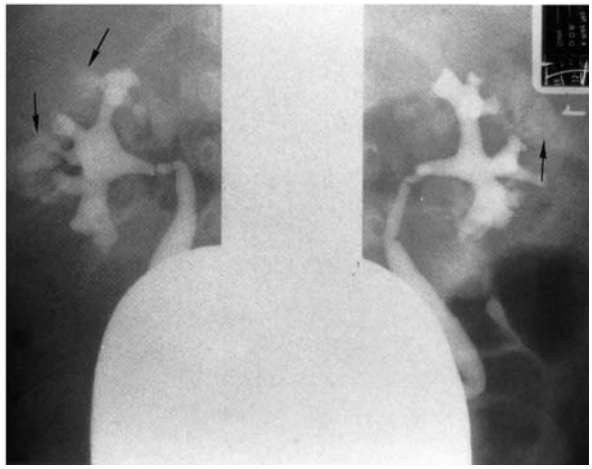

b

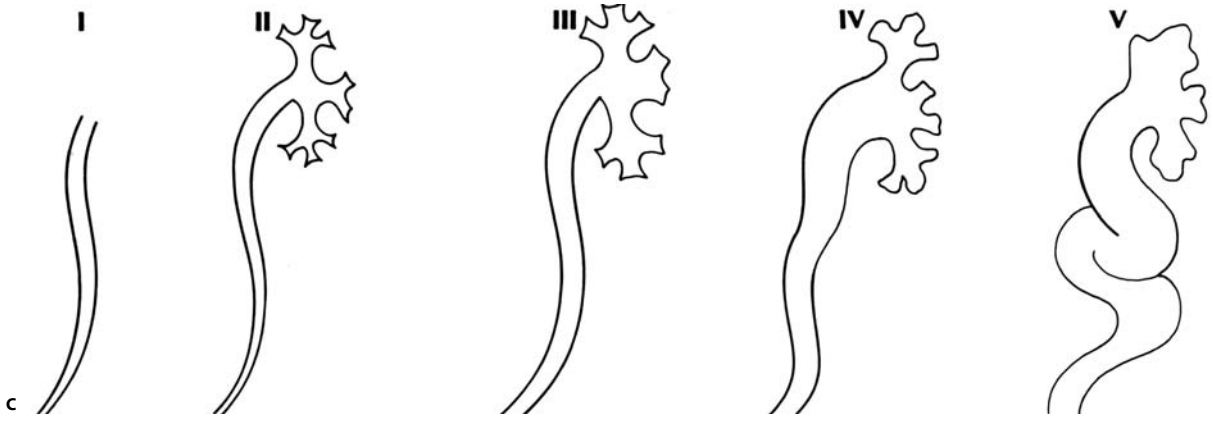

c

Fig. 5.55. Reflux
a This infant demonstrates bilateral grade II reflux (contrast material refluxes to calyces without distention)
b Bilateral grade IV reflux is seen (moderate distention of calyces). There is also bilateral intrarenal reflux (into the parenchyma) an ominous sign (*arrow*)
c Chart depicting grades of reflux. (From [4] with permission)

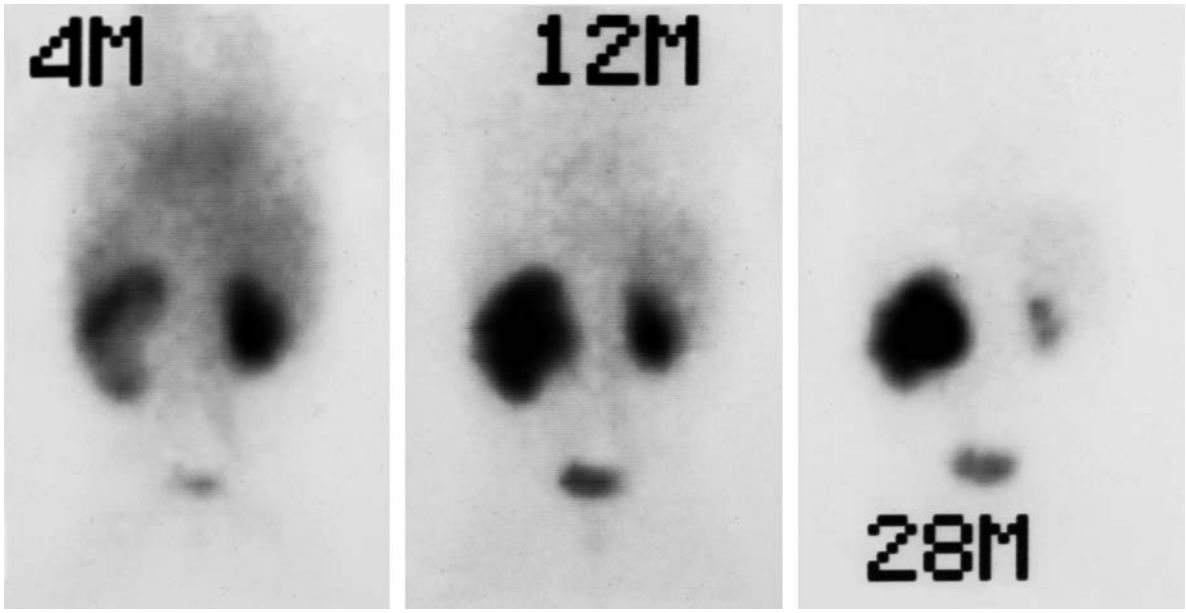

a, b c

Fig. 5.56. Neonatal hydronephrosis
This neonate had left hydronephrosis on prenatal ultrasound. Posterior ^{99m}Tc-DTPA scan was performed; remember, the patient's left is the viewer's left. Scans at 4 min (**a**), 12 min (**b**), and 28 min (**c**). At 4 min the left kidney is bigger, and there is lack of isotope in the renal pelvis. By 12 min the renal pelvis has filled. Lasix (furosemide) was given, and at 28 min the right kidney is almost empty, but the large dilated left renal pelvis remains. This was a ureteral pelvic junction obstruction on the left

Dilated Collecting System Seen on Antenatal Ultrasound Examination

Because of ever-increasing use of prenatal sonographic screening, pediatricians are confronted with a relatively new problem: the neonate who is found on prenatal ultrasound to have fullness or dilated collecting system. The postnatal follow-up, however, is relatively simple. The infant will need a follow-up ultrasound (preferably after the first few days of life). If this is normal, many centers would follow with repeated ultrasound over the first year. We assume that the baby had reflux which has resolved. When the urinary system is dilated, a cystogram is performed to detect reflux. When there is no reflux, but there is a dilated renal pelvis, a diuretic radionuclide scan (MAG-3) to rule out obstruction is necessary. This should be performed with Lasix (furosemide) to determine the exact degree of obstruction (Fig. 5.56). What are the abnormalities seen in Figure 5.57–5.60? After you look at them, see Appendix 2.

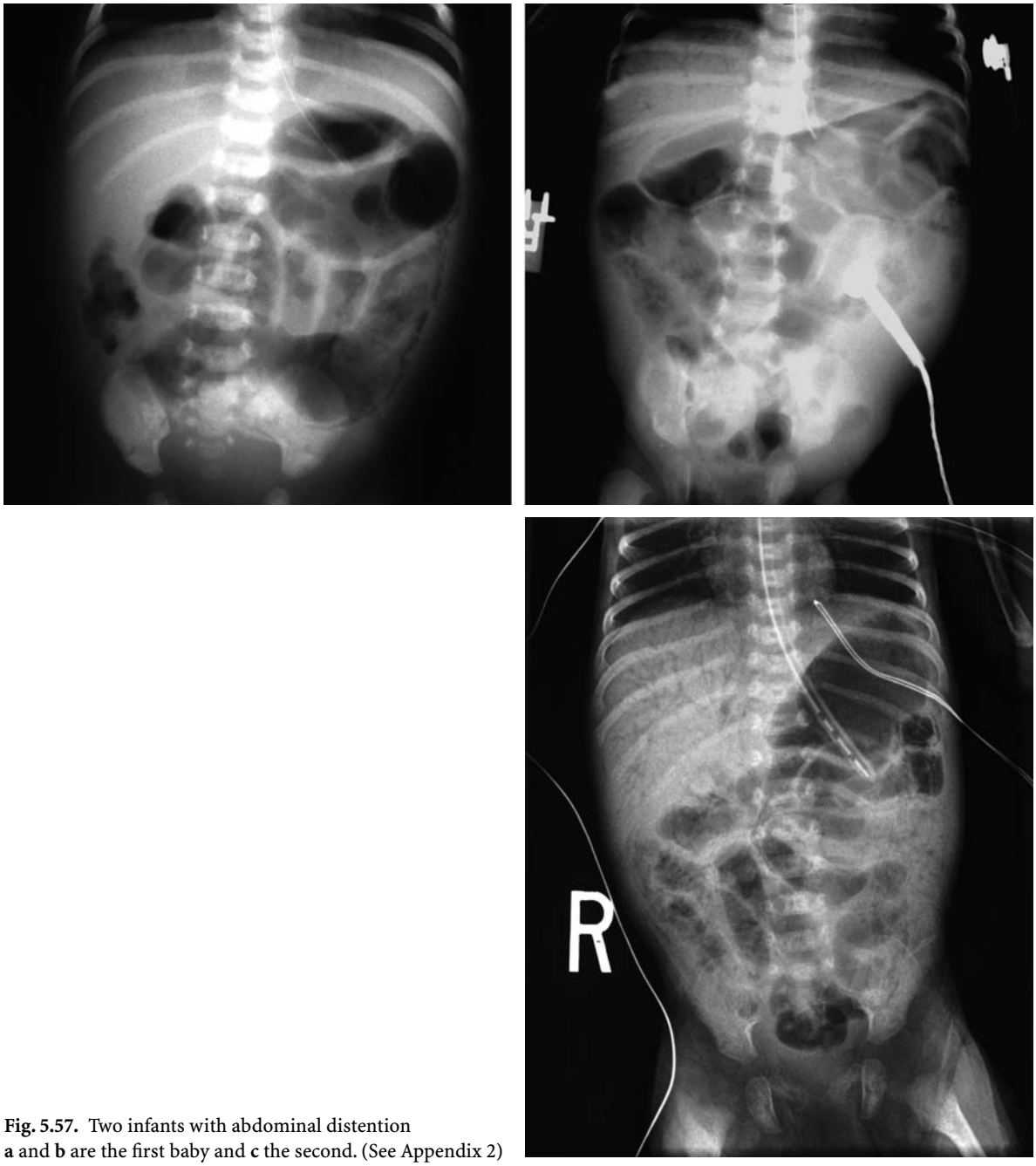

Fig. 5.57. Two infants with abdominal distention
a and **b** are the first baby and **c** the second. (See Appendix 2)

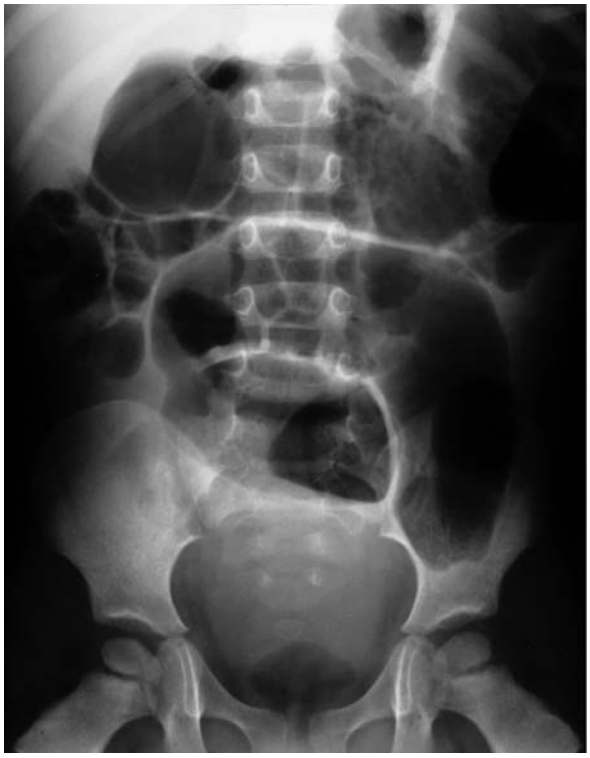

a

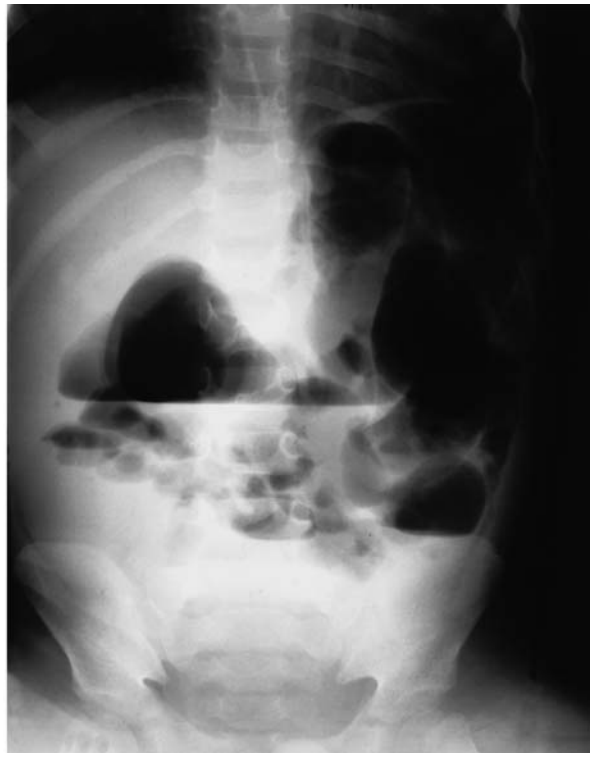

b

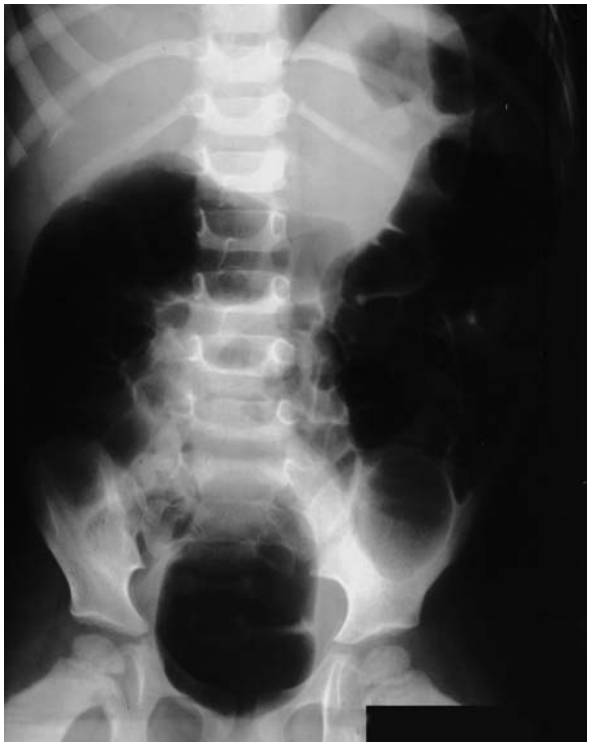

c

Fig. 5.58. A 1-year-old with abdominal pain and distension. (See Appendix 2)

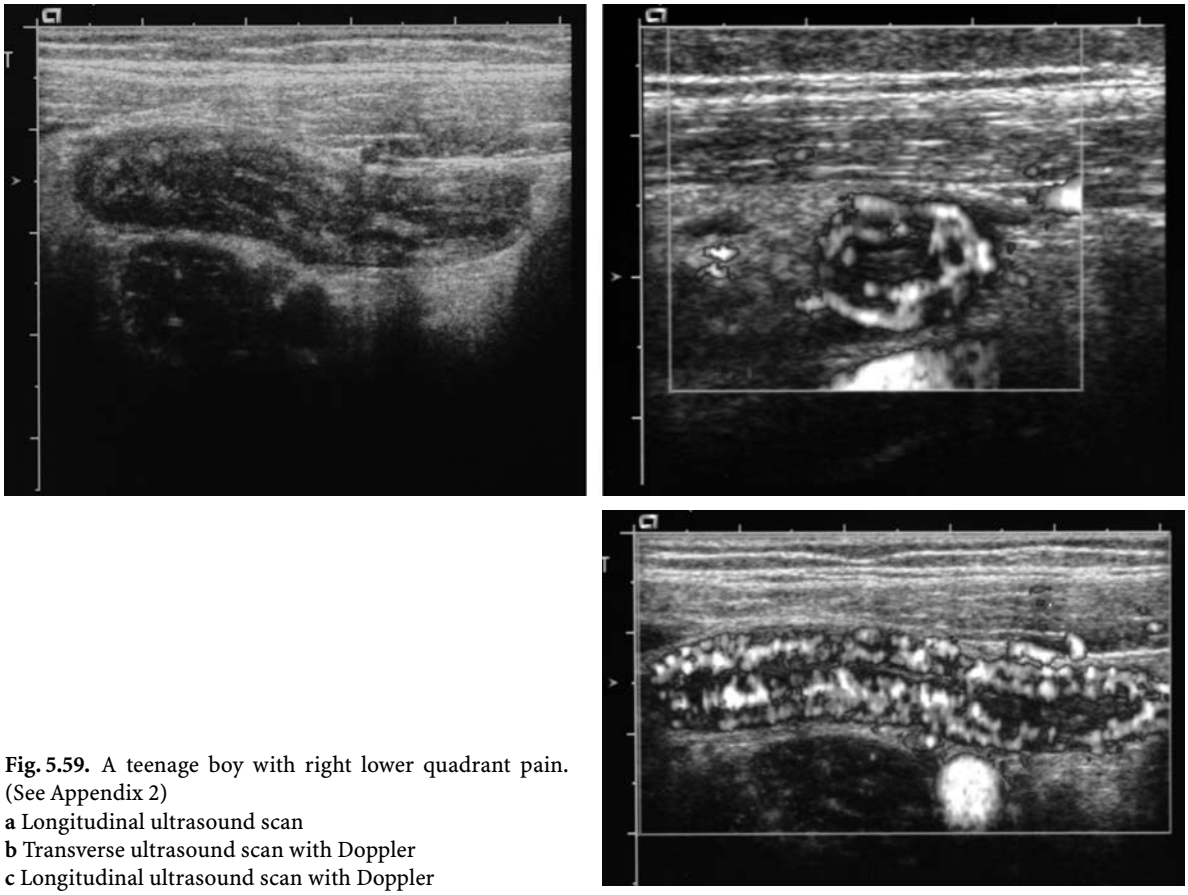

Fig. 5.59. A teenage boy with right lower quadrant pain. (See Appendix 2)
a Longitudinal ultrasound scan
b Transverse ultrasound scan with Doppler
c Longitudinal ultrasound scan with Doppler

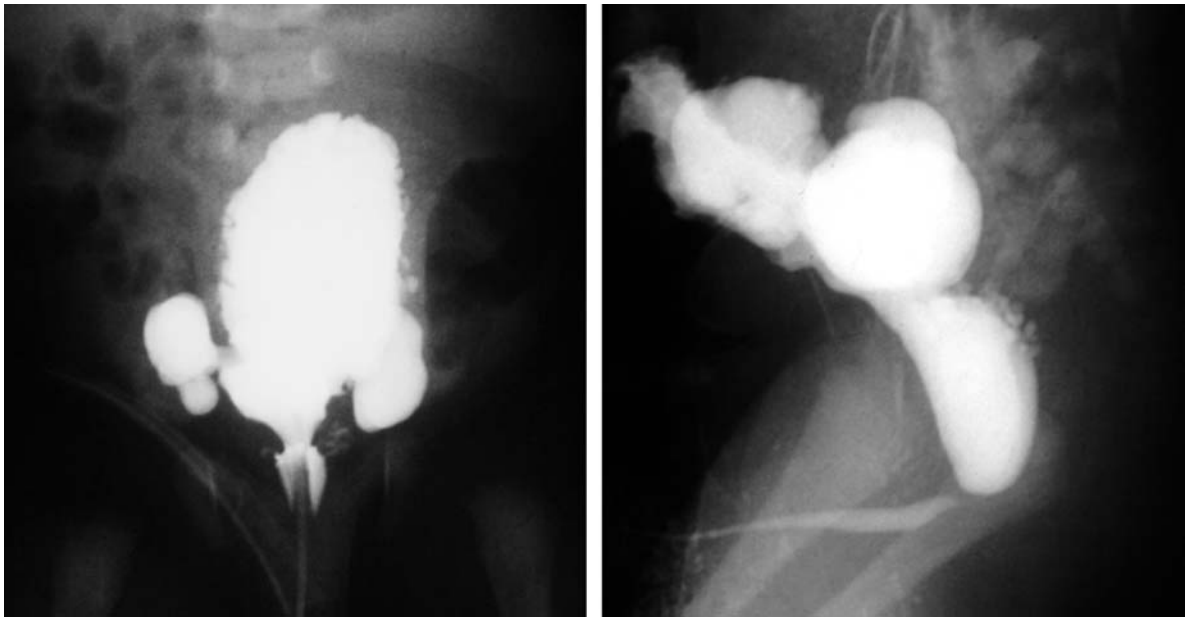

Fig. 5.60. Cystogram on a 3-year-old with poor urinary stream. (See Appendix 2)

References and Further Reading

1. Meyer JS, Harty MP, Khademian Z (2002) Imaging of neuroblastoma and Wilms' tumor. Magn Reson Imaging Clin N Am 10:275–302
2. Grattan-Smith JD, Perez-Bayfield MR, Jones RA, Little S, Broecker B, Smith EA, Scherz HC, Kirsch AJ (2003) MR imaging of kidneys: functional evaluation using F-15 perfusion imaging. Pediatr Radiol 33:293–304
3. Haller JO, Cohen HL (1986) Hypertrophic pyloric stenosis: sonographic evaluation. Radiology 161:335–339
4. Edelmann CM Jr (ed) (1992) Pediatric kidney disease. Little Brown, Boston.
5. Anupindi S, Jaramillo D (2002) Pediatric magnetic resonance imaging techniques. Magn Reson Imaging Clin N Am 10:189–207
6. Hoberman A, Charron M, Hickey RW, Basin M, Kearney DH, Wald ER (2003) Imaging studies after a first febrile urinary tract infection in young children. N Engl J Med 348:195–202
7. Kuhn JP, Slovis TL, Haller JO (eds) (2004) Part IV, Neonatal gastrointestinal tract. In: Caffey's pediatric diagnostic imaging, 10th edn. Mosby, Philadelphia
8. Kuhn JP, Slovis TL, Haller JO (eds) (2004) Part V, Neonatal genitourinary tract. In: Caffey's pediatric diagnostic imaging, 10th ed. Mosby, Philadelphia
9. Riccabona M, Fotter R (2004) Reorientation and future trends in paediatric uroradiology. Minutes of a symposium held in Graz, 5–6 September 2002. Pediatr Radiol 34:295–301

6 Abdominal and Pelvic Masses

The pediatrician frequently asks the pediatric radiologist to verify the existence of an abdominal or pelvic mass and to suggest possible diagnoses. The imaging approach to such problems varies, but these basic principles must be followed:

- The initial procedure should be a three-view abdominal series (Chap. 5).
- When there is only a *question* of a mass, the least invasive procedure should be done first.
- Once a mass has been established, the work-up is guided by the patient's age, the location of the mass, and the symptoms (Table 6.1).
- The following priorities should be kept in mind: (a) since bowel contrast may interfere with other examinations-ultrasound, CT, MR, and radionuclide imaging when necessary have priority; (b) if both a barium enema and an upper gastrointestinal series are necessary, the barium enema should be performed first because barium is more readily cleared from the colon.
- The pediatric radiologist is the best source of information as to how the imaging work-up should proceed.

Begin the Work-Up with an Abdominal Series

Almost every child who presents with an abdominal mass should have abdominal films as an initial screening procedure (except for girls over 9 years of age, who may be pregnant). Plain film findings and abdominal series are discussed in Chap. 5. Specifically, one should look for a mass, the effects of the mass, and calcifications.

Mass effect (Fig. 6.1) is the effect of the mass on contiguous structures, such as bowel or viscera. Divide the abdomen into quadrants and apply your knowledge of anatomical structures in each quadrant.

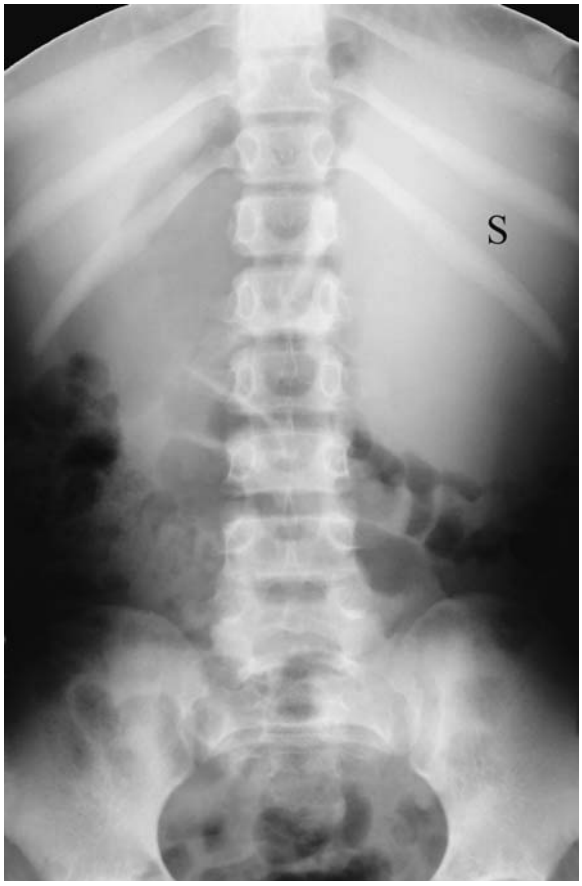

Fig. 6.1. Left upper quadrant mass
There is an enlarged spleen (*S*). The gas-filled bowel is displaced inferiorly and to the right – mass effect. The differential diagnosis of anatomical origin for the mass includes muscle, peritoneum, stomach, kidney, spleen, and adrenal gland. These are the structures that are found "skin to skin." This child had isolated splenomegaly due to portal hypertension

Table 6.1. Most frequent abdominal and pelvic masses by age. (Modified from [1] and [2])

Age and type of mass	Incidence %	
Neonate		
Renal	55	70
Hydronephrosis		
Ureteropelvic junction obstruction		
Ureterovesical junction obstruction		
Reflux (includes valves)		
Multicystic kidney		
Genital	15	
Hydrometrocolpos		
Ovarian lesions		
Gastrointestinal	15	
Duplications		
Volvulus		
Nonrenal retroperitoneal	10	
Adrenal hemorrhage		
Neuroblastoma		
Teratoma		
Hepatosplenobiliary	5	
1 month to 2 years		
Renal	55	78
Wilms tumor		
Hydronephrosis		
Nonrenal retroperitoneal	23	
Neuroblastoma		
Teratoma		
Gastrointestinal (including biliary masses and appendiceal abscess and intussusception)	18	
Genital, miscellaneous	4	
Older than 2 years[a]		
Visceromegaly secondary to infection, leukemia, lymphoma, splenomegaly secondary to portal hypertension	Frequent	
Wilms tumor and neuroblastoma	Frequent to age 5; decreases thereafter	
Appendiceal abscess	Frequent over 5	
Intussusception	Most frequent at age 2; decreases thereafter	
Pregnancy	A common pelvic mass in pubescent females	

[a] It is difficult to obtain precise numbers for this age group.

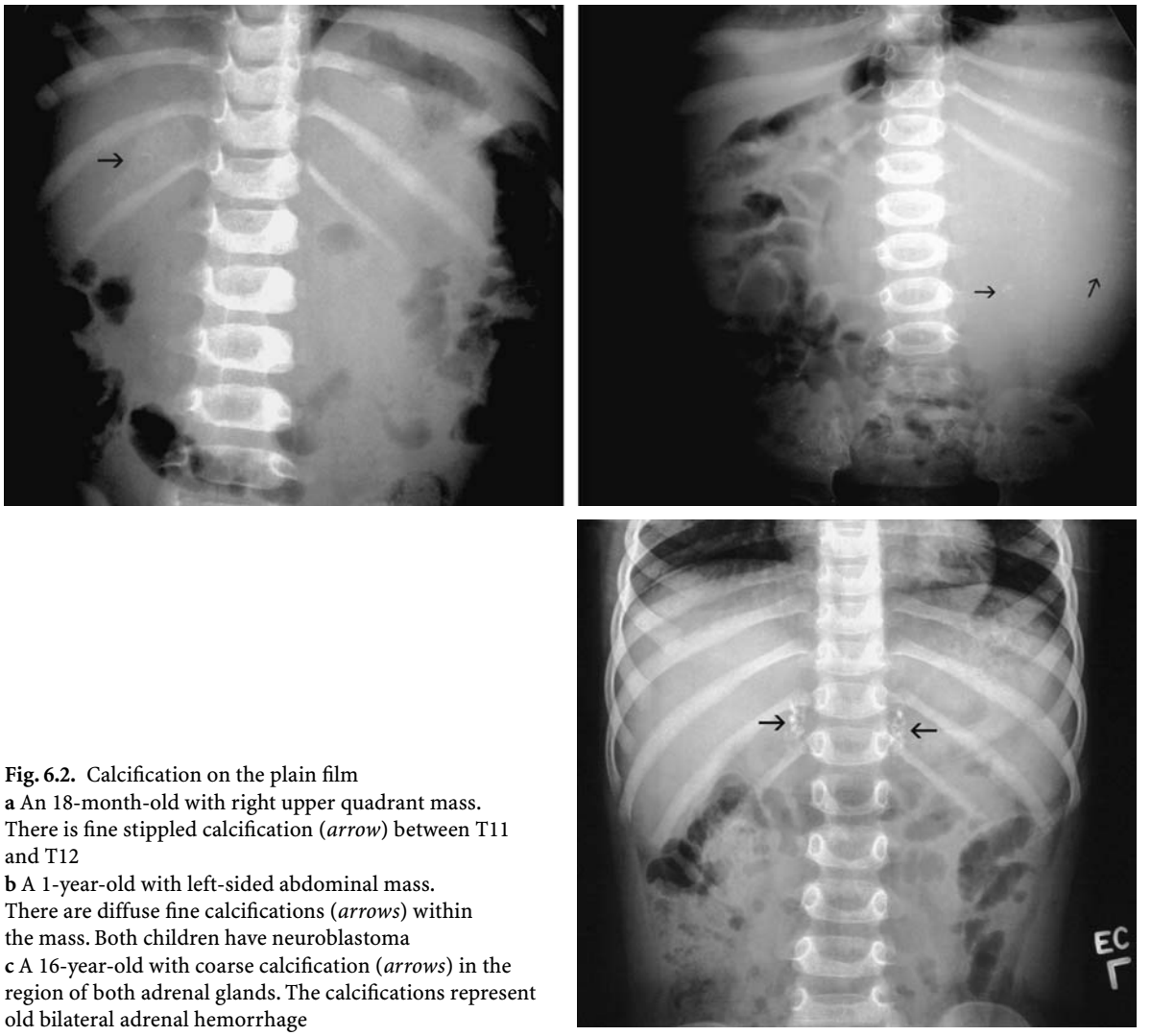

Fig. 6.2. Calcification on the plain film
a An 18-month-old with right upper quadrant mass. There is fine stippled calcification (*arrow*) between T11 and T12
b A 1-year-old with left-sided abdominal mass. There are diffuse fine calcifications (*arrows*) within the mass. Both children have neuroblastoma
c A 16-year-old with coarse calcification (*arrows*) in the region of both adrenal glands. The calcifications represent old bilateral adrenal hemorrhage

► ***Rule No. 12:*** Try to find the effects of the mass on adjacent organs on each abdominal film. Draw the mass, if necessary.

Calcifications (Fig. 6.2) are an important clue to the type of mass present. Fine, punctate calcifications next to the upper pole of the kidney might well represent an adrenal neuroblastoma, while large, coarse calcifications may merely mean the presence of calcified adrenal hemorrhage. It is common for the neuroblastoma to calcify, while it is distinctly less common for a Wilms tumor to calcify. An appendicolith is ordinarily round, solitary, and laminated, while a calcification in a dermoid or teratoma may have a structure similar to a tooth within it (Fig. 6.3). It must then be determined where the mass originated, and whether it is neoplastic, inflammatory, etc.

► ***Rule No. 13:*** After the mass has been defined, find the center of the lesion. Then consider all the structures, gross and microscopic, near the center of the lesion as possible sources of the mass. Think skin to skin.

Remember, an abdominal mass may be an enlarged organ such as the liver, spleen, or kidney, or it may be abnormal bowel. Frequently children with leukemia have visceromegaly. Isolated splenomegaly is found in portal hypertension (see Fig. 6.1). Obstructed or inflamed bowel loops may appear as a mass, as in the case of intussusception (Fig. 6.4).

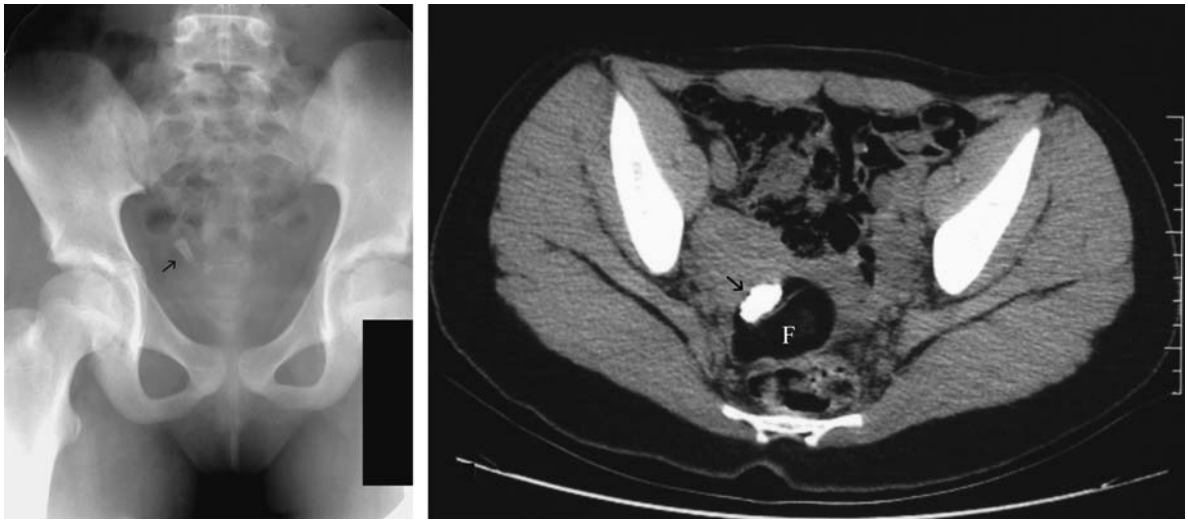

a b

Fig. 6.3. Dermoid tumors
a An 8-year-old girl with pelvic mass. The plain film revealed a calcified lesion resembling a tooth in the right hemipelvis (*arrow*)
b CT scan of a different patient. The CT shows calcified (*arrow*) and fatty (*F*) components of an ovarian dermoid

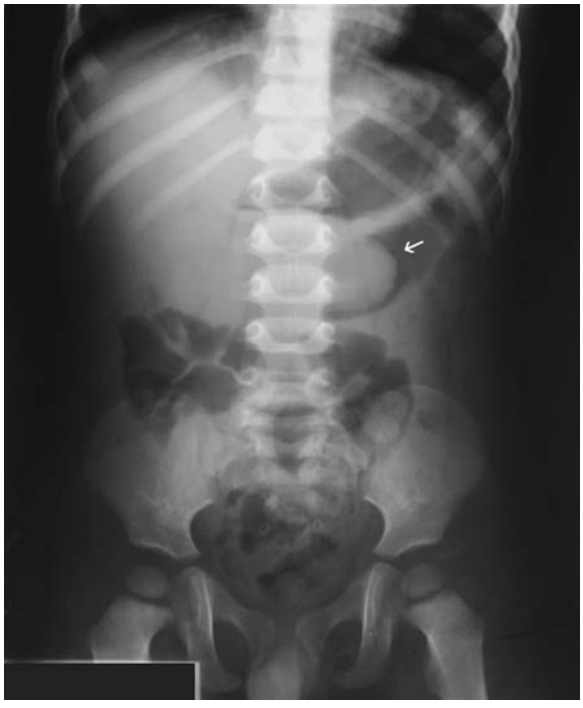

Fig. 6.4. Intussusception
The radiograph in this child with abdominal pain shows a left upper quadrant mass (*arrow*) which on subsequent contrast enema was proven to be an ileocolic intussusception

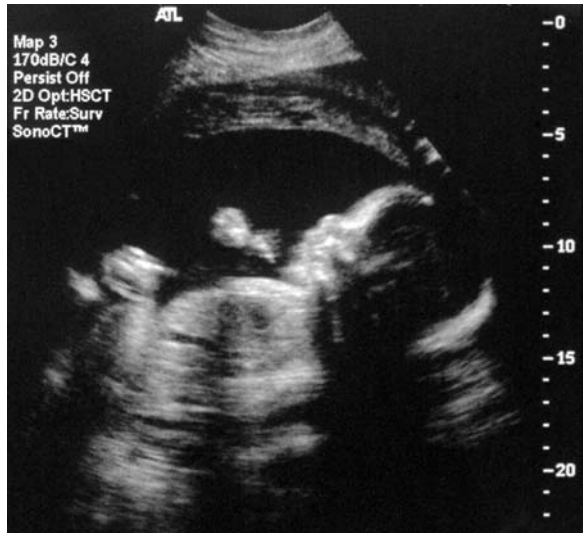

Fig. 6.5. Intrauterine pregnancy
Ultrasound should be the first imaging exam performed in older girls with a pelvic mass, as it may show an intrauterine fetus (seen in profile here)

Begin with the Least Invasive Study When There is a Questionable Mass

Frequently the clinician is not sure whether there is a mass. In the constipated child, fecal masses in the colon are easily palpated and may be mistaken for a lesion. Other putative masses include the distended urinary bladder and the abdominal aorta in a particularly thin child. Therefore, evacuation of both bowel and bladder contents should precede any work-up to obviate the majority of "pseudomasses."

In girls over the age of 9 years any pelvic mass should be considered an intrauterine pregnancy until proved otherwise. For this reason, ultrasound is initially utilized because it is the least invasive modality, with no ionizing radiation (Fig. 6.5).

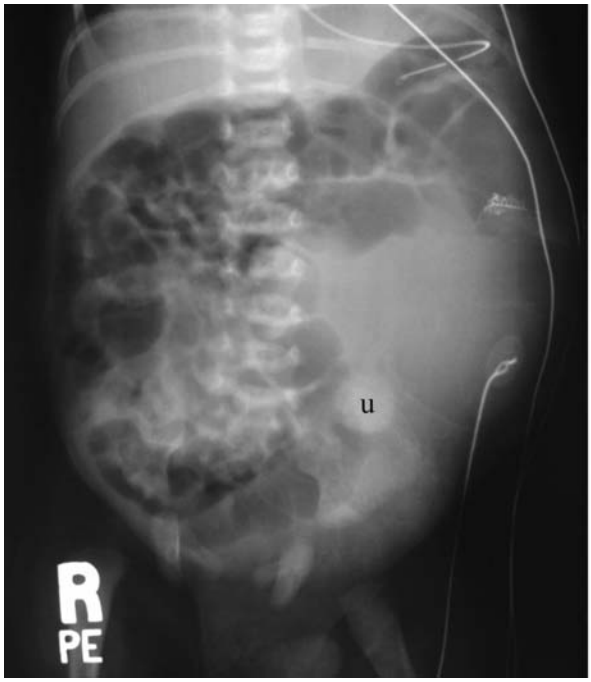

a

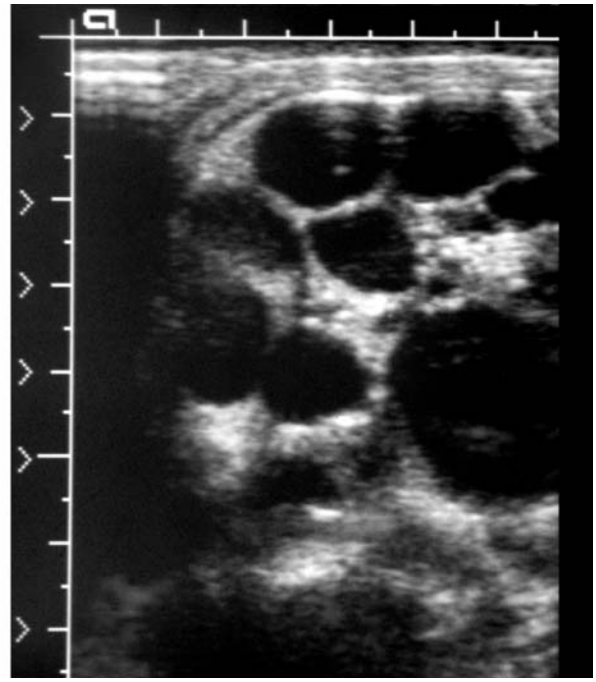

b

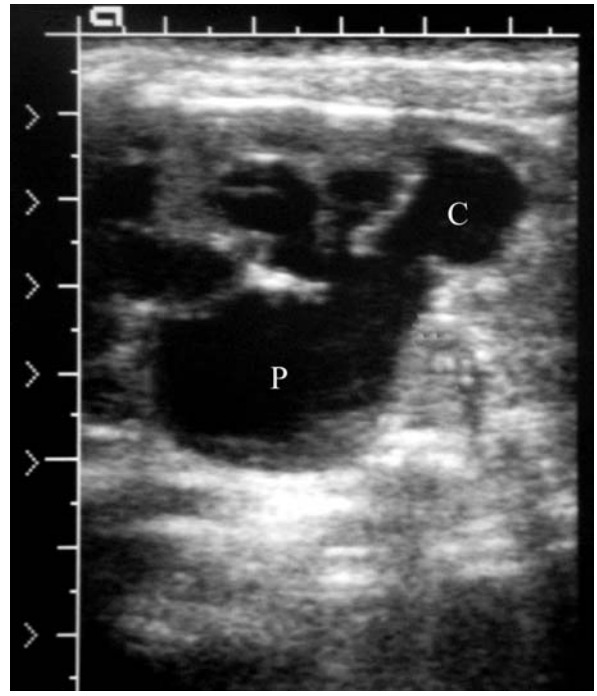

c

Fig. 6.6. Abdominal masses of renal origin
a Abdominal radiograph of newborn with left flank mass; gas-filled bowel is displaced to the right. This was subsequently shown to be a multicystic dysplastic kidney. Note rounded soft tissue density in the lower abdomen, representing the umbilicus (*u*)
b, c Ultrasound images from a different patient. Noncommunicating cysts of varying sizes in the left renal fossa (**b**) are consistent with a multicystic dysplastic kidney. Ultrasound image of the contralateral side (**c**) shows dilated renal pelvis (*P*) and calyces (*C*) secondary to ureteropelvic junction obstruction

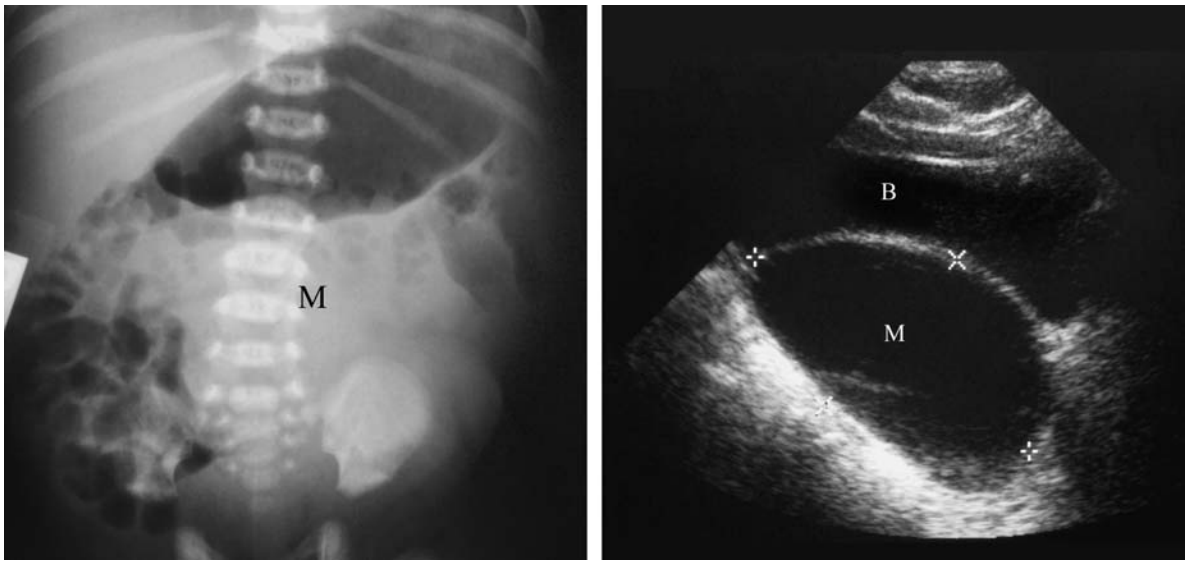

a b

Fig. 6.7. Ovarian cysts
a Abdominal radiograph of a newborn girl shows a large mass (*M*) in the left abdomen, displacing gas-filled bowel loops rightward and superiorly
b Ultrasound image from a 12-year-old girl shows a cystic mass (*M*, defined by calipers) posterior to the urinary bladder (*B*). There is a fluid – debris level suggesting the diagnosis of a haemorrhagic ovarian cyst

Let the Patient's Age and Symptoms and the Location of the Mass Direct the Work-Up

Newborn

Seventy percent of abdominal and pelvic masses in neonates originate in the genitourinary tract. Hydronephrosis (ureteropelvic junction obstruction, ureterovesical junction obstruction, and reflux) and multicystic kidneys account for the majority of urinary masses (Table 6.1, Fig. 6.6), while the most common genital masses are hydrometrocolpos and ovarian cysts (Fig. 6.7). Malignant abdominal masses are uncommon in this age group (although neuroblastoma occurs rarely), but pelvic masses with malignant potential (e.g., sacrococcygeal teratoma) do occur.

Since prenatal ultrasound is now so commonly performed, as many as 50% of masses which used to be initially detected in the neonatal period are now diagnosed antenatally.

One Month to 2 Years of Age

Once again, urinary masses predominate, with Wilms tumor occurring frequently. Nonrenal retroperitoneal masses such as neuroblastoma now become more common (Fig. 6.8). The gastrointestinal mass of most concern now becomes the intussusception (Chap. 5) (see Fig 6.4).

Older than 2 Years

Once a child reaches 2 years of age, the incidence of urinary masses declines, and the differential diagnoses broaden. Traumatic lesions, inflammatory processes (e.g., from a perforated appendix; see Chap. 5), and the more unusual hepatic lesions are now considered. However, Wilms tumor and neuroblastoma remain high in the differential diagnoses. The lymphomatous masses in the abdomen become a strong consideration in the older age group (Fig. 6.9).

Location of the Mass

After age, the location of the mass is the next most important consideration. If a neonate has a flank mass, the chances are great that it will be a hydronephrotic or multicystic kidney. A less likely right upper quadrant mass is a hepatoblastoma. In a 2-year-old, a right upper quadrant mass suggests a neuroblastoma or Wilms tumor. A good trick is to put your finger where you think the center of the mass is and consider all the normal viscera under your finger from skin to skin. Then think of a common pathology affecting those viscera. This helps form the differential diagnosis.

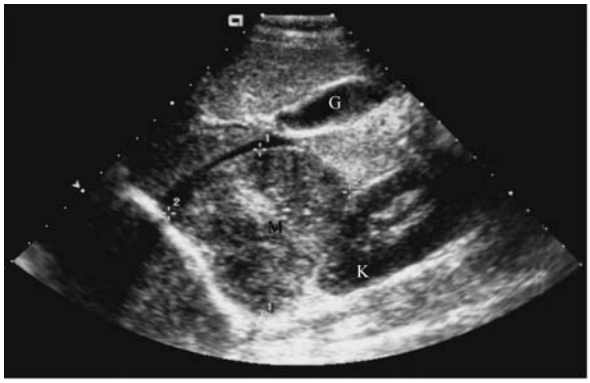

a

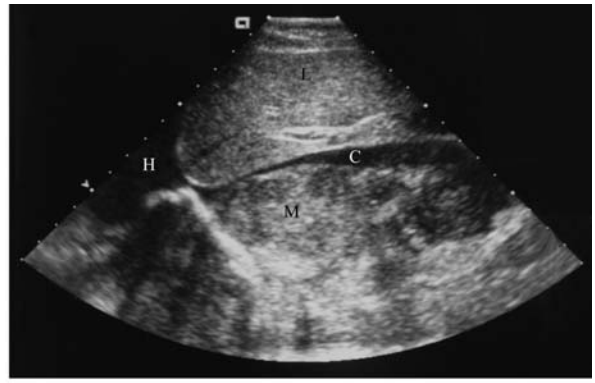

b

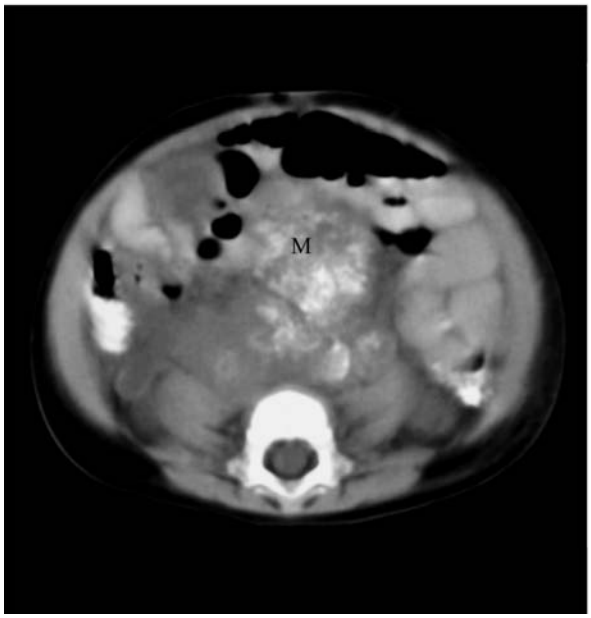

c

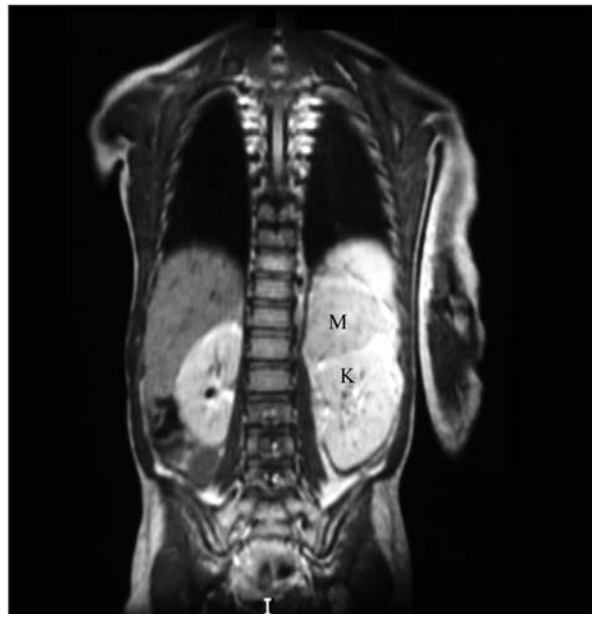

d

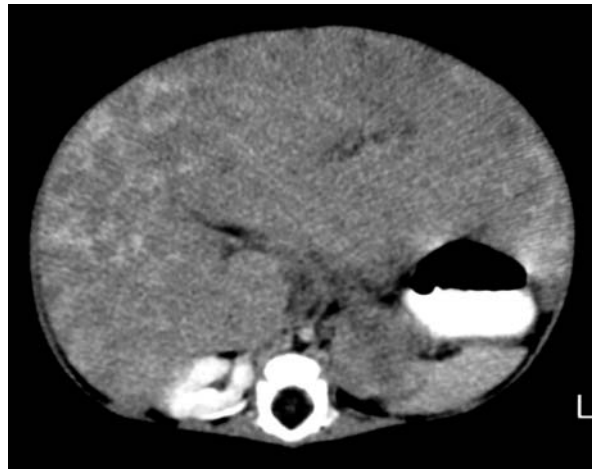

e

Fig. 6.8. Neuroblastoma
a, b Longitudinal ultrasound images demonstrate a large right adrenal mass (*M*), resulting in flattening of the right kidney (*K*). The mass compresses the inferior vena cava (*C*). Note heart (*H*), gallbladder (*G*), and liver (*L*)
c Contrast-enhanced axial CT image in a different patient shows a large, extensively calcified retroperitoneal mass (*M*)
d Coronal T1-weighted MR image of another patient with a left adrenal mass (*M*) that flattens the upper pole of the left kidney (*K*)
e Contrast-enhanced axial CT image of another patient with left adrenal neuroblastoma. The liver is enlarged and heterogeneous because of diffuse metastatic involvement

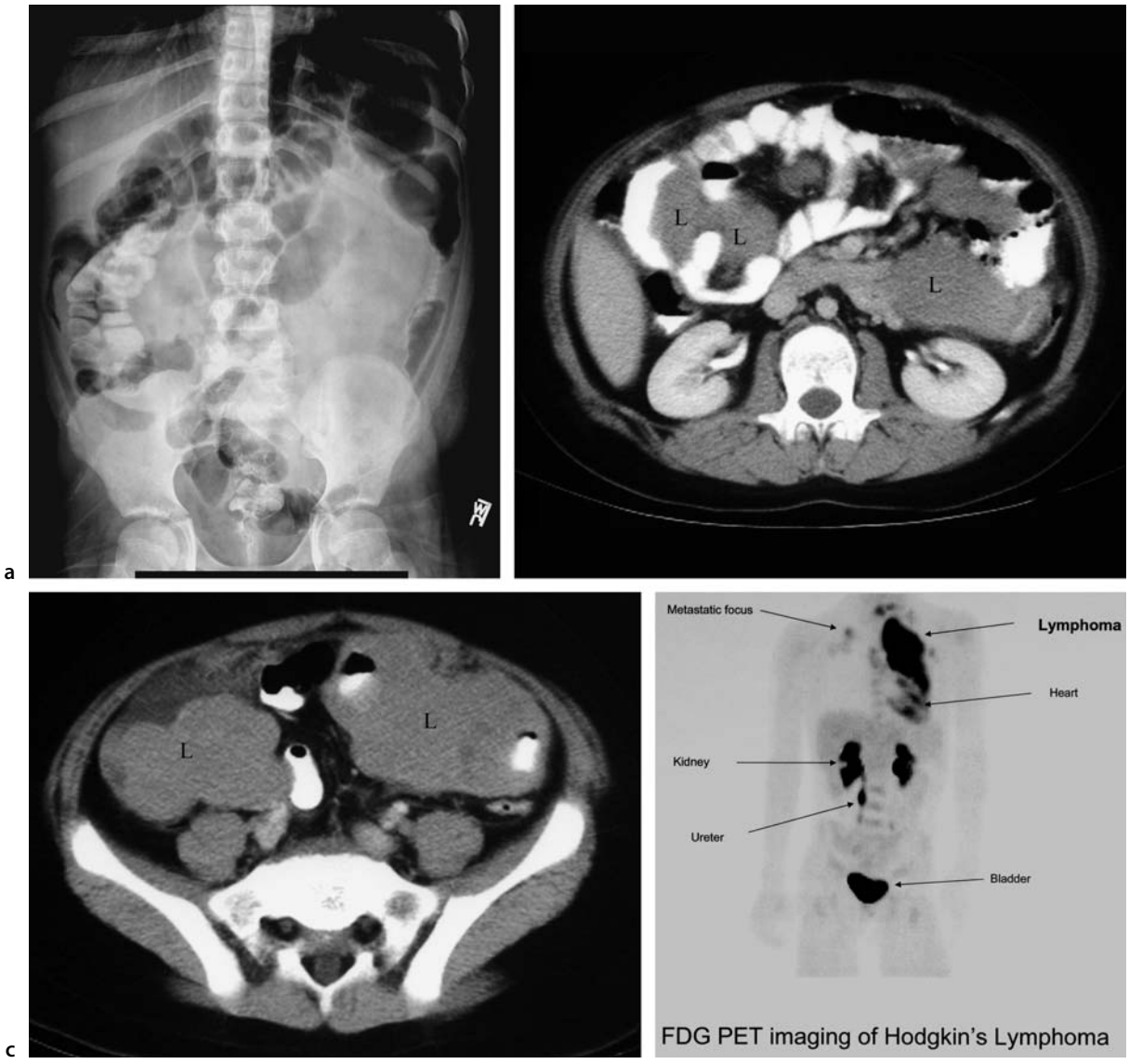

Fig. 6.9. Lymphoma
a–c A 13-year-old boy with Burkitt-type non-Hodgkin's lymphoma presented initially with vomiting and weight loss. Abdominal radiograph (**a**) shows a paucity of bowel gas in the left side of the abdomen. Contrast-enhanced CT images (**b, c**) show multiple soft tissue masses (*L*) around and between bowel loops on both sides of the abdomen
d PET imaging from a different patient with Hodgkin's lymphoma shows FDG accumulation in the hypermetabolic large mediastinal mass as well as in metastatic foci. Normal accumulation of FDG is seen in the heart, and normal excretion in the kidneys, ureters, and urinary bladder

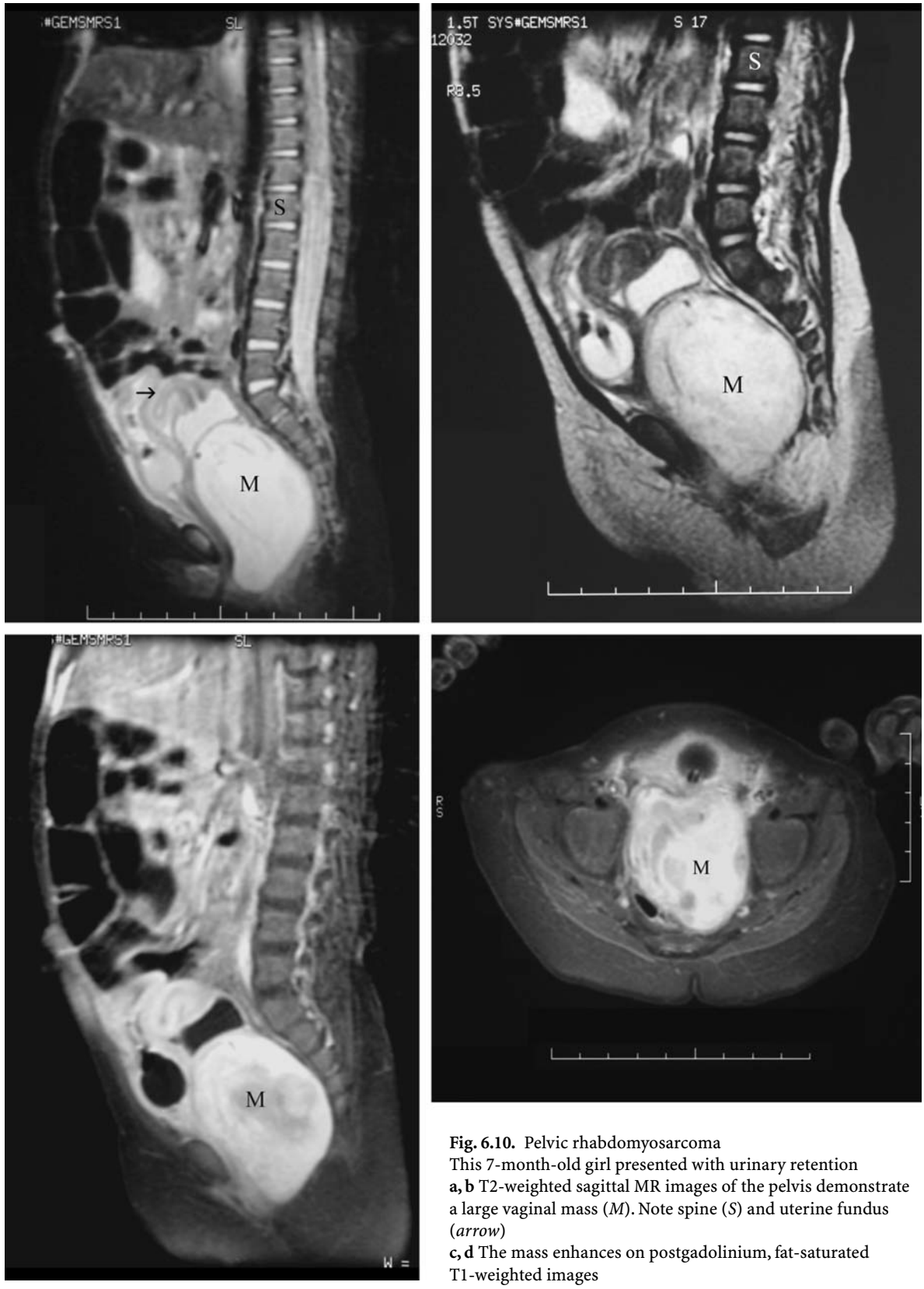

Fig. 6.10. Pelvic rhabdomyosarcoma
This 7-month-old girl presented with urinary retention
a, b T2-weighted sagittal MR images of the pelvis demonstrate a large vaginal mass (*M*). Note spine (*S*) and uterine fundus (*arrow*)
c, d The mass enhances on postgadolinium, fat-saturated T1-weighted images

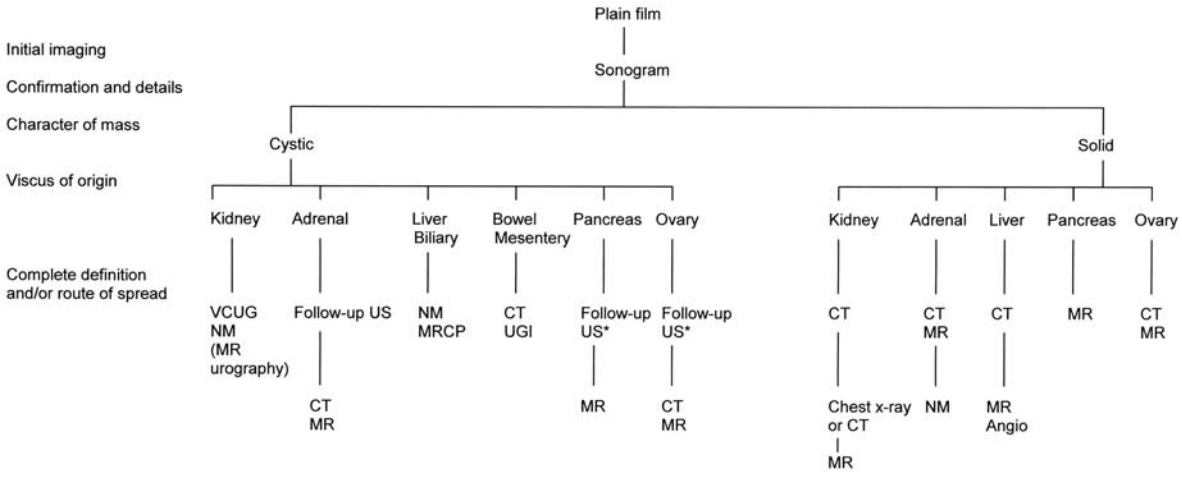

Fig. 6.11. Imaging work-up of a child with an abdominal mass
NM, nuclear medicine; *US*, ultrasound; *VCUG*, voiding cystourethrogram; *MR*, magnetic resonance; *CT*, computed tomography; *UGI*, upper gastrointestinal examination; * confirms changing size

Symptoms

In many instances when a mass is palpated, either by the parents or a physician, the child experiences no symptoms. However, symptoms or signs such as jaundice or profuse diarrhea provide clues. A jaundiced patient with a right upper quadrant mass may have a choledochal cyst, while one with a flank mass and profuse secretory diarrhea may have a catecholamine-secreting neuroblastoma. Specific attention should be paid to symptoms in children with pelvic masses. Because of the relationship of the pelvic mass to the bladder, bowel, and sacral nerve complex, these children may present with dysfunction of one or more of these systems (Fig. 6.10). Since masses (other than those associated with the ovaries and uterus) occur in the pelvis nearly as frequently as they do in the upper abdominal retroperitoneal areas, any child with bladder, bowel, or gait disturbance should be suspected of having a pelvic mass. The diagnostic work-up – appropriate history, physical examination and imaging procedures (algorithm in Fig. 6.11) – should proceed accordingly.

Imaging Principles

Many of these principles are discussed in previous chapters. For newborns, after initial plain abdominal films, ultrasound is generally the first test because most masses are of genitourinary origin (hydronephrosis, multicystic kidney), and most of them are cystic with characteristic ultrasonic appearance.

Once the presence of a mass is firmly established and its site determined, the extent of the lesion should be defined. CT and MR imaging are the most precise imaging methods to define the intra-abdominal and pelvic extent of a tumor. MR should be favored if the diagnostic sensitivity is equal as it involves no ionizing radiation.

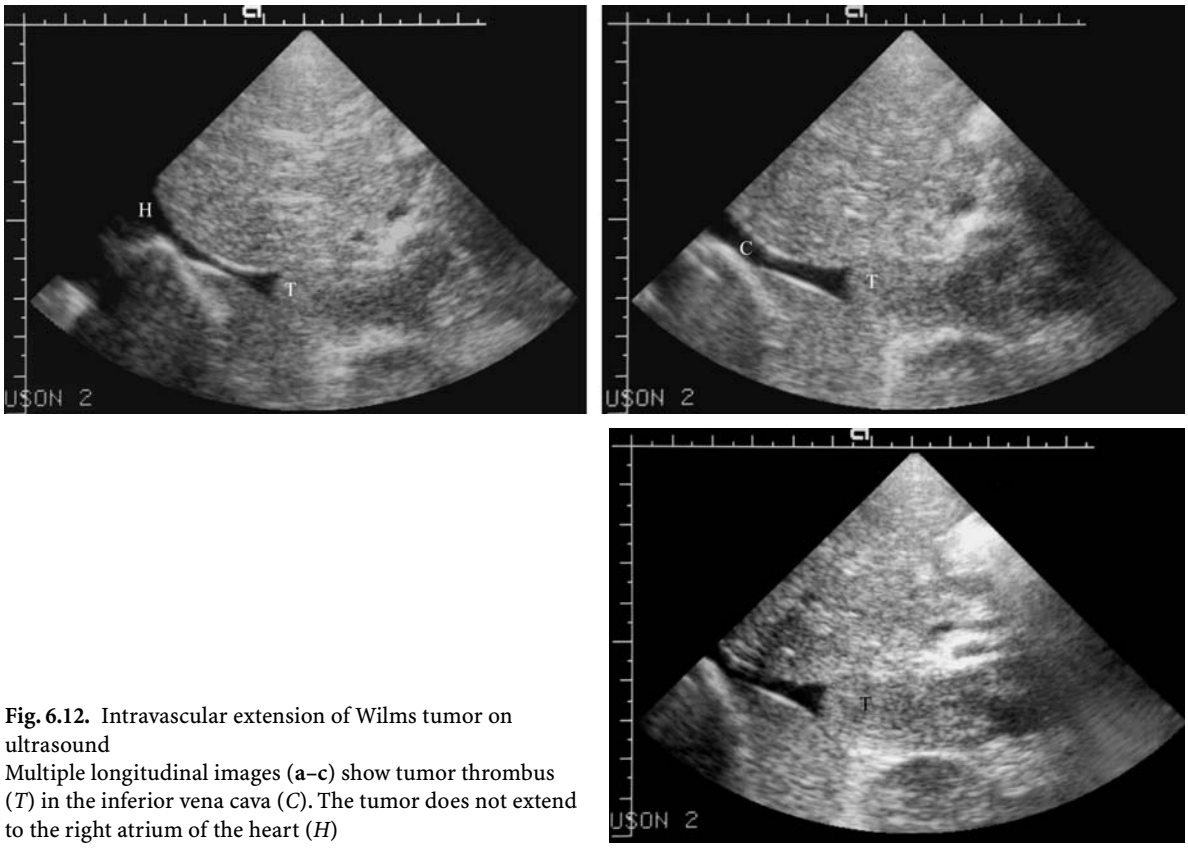

Fig. 6.12. Intravascular extension of Wilms tumor on ultrasound
Multiple longitudinal images (**a–c**) show tumor thrombus (*T*) in the inferior vena cava (*C*). The tumor does not extend to the right atrium of the heart (*H*)

Specific Lesions

The most common abdominal or pelvic tumors of childhood are Wilms tumor and neuroblastoma. The following are helpful clues for identifying the abdominal mass on ultrasound and CT:

- Tumor motion on ultrasound: this helps separate tumor from organs not invaded by the tumor (e.g., liver, kidney)
- Fat displacement: helps to distinguish visceral (renal) from extravisceral (nonrenal) tumors
- Compressed rim of liver tissue: when present, suggests extravisceral as opposed to intravisceral tumor; if tumor is growing out of an organ, the organ's tissue "surrounds" the tumor – the claw sign
- Caval thrombus: Wilms tumor, hepatoblastoma (Fig. 6.12)
- Calcium: more common in neuroblastoma
- Spinal involvement: most often neuroblastoma
- Nodal encasement: more common in neuroblastoma
- Portal vein displacement: suggests extrahepatic origin as opposed to hepatic invasion

Wilms Tumor

Wilms tumor is an intrarenal tumor (Fig. 6.13) with peak incidence between 2 and 5 years of age. Although the presenting symptom is frequently an abdominal flank mass, the tumor is associated with hematuria in 20% of patients. The patient is commonly asymptomatic, but occasionally fever and pain are seen. Hypertension may be present. The radiographic findings are those of distortion of the internal renal architecture. Infrequently, the tumor is large enough to completely obstruct the kidney. It is uncommon to see calcification. In general, the prognosis is good, but it depends almost entirely on the histological type (favorable versus unfavorable) and staging of the lesion. For the work-up of a child with an abdominal mass, see Fig. 6.11. However, once the primary diagnosis is made, the extent of the tumor should be evaluated on the basis of the biological behavior of tumor spread and sites of common metastases. Its routes of spread may be:

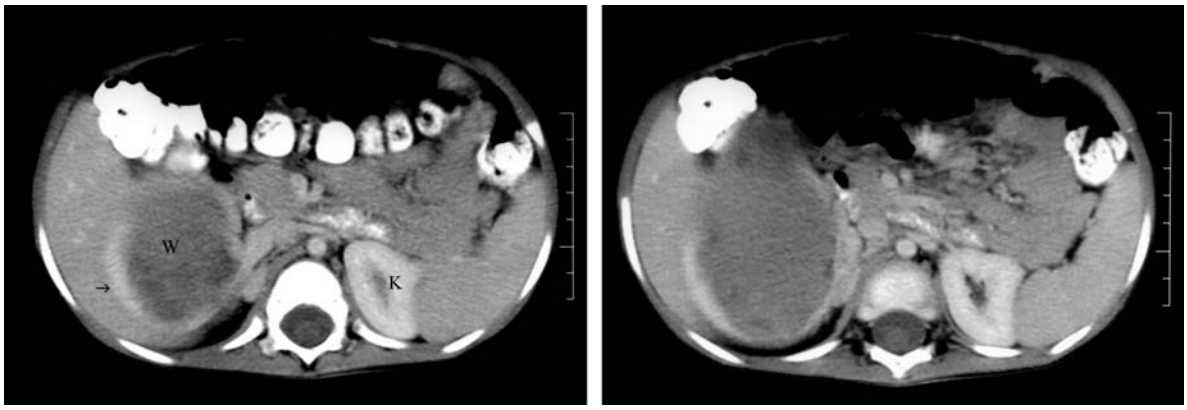

Fig. 6.13. Wilms tumor on CT
A 4-year-old with a right abdominal mass. Contrast-enhanced CT images (**a, b**) show a mass (*W*) in the right kidney. A rim of enhancing renal tissue (*arrow*) is seen around the lower attenuation mass. Compare this with the normal left kidney (*K*)

- Local
  - Renal vein
  - Inferior vena cava (Fig. 6.12)
  - Perirenal lymph nodes
  - Contiguous invasion of the liver
- Remote
  - Lungs: "cannonball" metastases
- Rare
  - Hematogenous to the liver
  - Bone

With Wilms tumor, it is crucial that the inferior vena cava be evaluated, as the tumor often grows directly into the renal veins, the inferior vena cava, and occasionally the heart. Detection of tumor in this region determines whether thoracoabdominal exploration is necessary. The vena cava is best and least invasively evaluated by real-time ultrasound or MR imaging. The other kidney must also be examined to rule out bilateral Wilms tumor and/or the presence of nephroblastomatosis (primitive rests of cells with tumor potential), a precursor of Wilms tumor. Evaluation of the chest, liver, and lymph nodes – common sites of tumor metastases – is best done by MR or CT.

Neuroblastoma

Neuroblastoma is a lesion of the sympathetic nerve chain and may arise anywhere along the axis of these sympathetic nerves (see Fig. 6.8). About 66% of these tumors arise in the abdomen and appear most frequently in the adrenal gland – the suprarenal region. The possible routes of spread are:

- Local
  - Lymph nodes and extensive nodal masses
  - Invasion of neural foramina, causing deviation of dural sac
  - Encasement of great vessels
- Remote (hematogenous)
  - Bone
  - Liver
  - Central nervous system: extradural space and orbit region

The majority of cases of neuroblastomas occur in children aged 6 months to 5 years. Unlike the asymptomatic presentation of a child with Wilms tumor, most children with neuroblastoma present with weight loss, irritability, fever, and/or anemia. A few show excessive catecholamine production and have such symptoms as skin flushing, perspiration, diarrhea, and/or headaches. On physical examination, there may well be hypertension and tachypnea.

The plain film findings frequently show stippled calcification, with lateral and downward displacement of the kidney (Fig. 6.2). Abdominal neuroblastoma has a rather poor prognosis if the child is over 1 year of age. By the time it is diagnosed, it has frequently metastasized to the skeleton as well as to the bone marrow and liver.

Cross-sectional imaging with CT and MR helps to define the extent of the primary tumor and to detect liver metastases (Fig. 6.8). Because of the high frequency of intraspinal involvement with neuroblastoma, MR imaging is essential to the work-up. MR may also show metastatic disease in bone marrow.

Most neuroblastomas show increased activity on iodine-labeled metaiodobenzylguanidine (MIBG) scans, and so this type of nuclear medicine study is frequently useful in demonstrating metastatic disease as well as in follow-up for recurrence. Nuclear medicine whole body bone scan is best for showing bone involvement.

Hepatic Tumors

These lesions are certainly less common either Wilms tumor or neuroblastoma. They are presented here because their imaging evaluation is complex and demands the use of multiple modalities. The two malignant liver tumors seen most frequently are hepatoblastoma and hepatocellular carcinoma. The more common benign hepatic lesions are vascular, such as the hemangioendothelioma. Children with malignant tumors come to the physician with complaints either of a mass in the upper abdomen or enlargement of the abdomen. Liver dysfunction with jaundice and ascites is seen less frequently.

Hepatoblastoma typically occurs in children under the age of 5 years. Cross-sectional imaging usually shows a well-circumscribed, solitary mass, though multifocal disease at presentation is not uncommon (Fig. 6.14).

The lesion extends into the portal and hepatic veins, and may enter the inferior vena cava. Its routes of spread include:

- Local
  - Lymph nodes
  - Diaphragm
  - Peritoneum
- Remote
  - Pulmonary metastases

An interesting recent observation regarding hepatoblastoma is its disproportionate occurrence in former premature infants; although only 7% of all births are premature, approximately 40% of hepatoblastomas occur in children with a history of prematurity. Since premature infants as a group are radiographed frequently for pulmonary and abdominal signs or symptoms, one may wonder whether the cumulative radiation dose to the developing liver from multiple radiographs plays a role in the occurrence of this tumor.

Hepatic hemangioendothelioma is the most common benign liver tumor in infants, and most hepatic hemangioendotheliomas are diagnosed within the first 6 months of life. Hepatomegaly and high-output congestive heart failure are the most frequent presenting signs. Less common presentations include platelet sequestration with resultant bleeding diathesis (Kasabach–Merritt syndrome), consumptive coagulopathy secondary to disseminated intravascular coagulation, tumor rupture leading to hemoperitoneum, and jaundice.

The initial imaging procedure, after the plain film, is ultrasonography of the right upper quadrant (Fig. 6.15). Doppler is used with ultrasound to diagnose arteriovenous malformations, hemangiomas, and portal vein patency. Because in most instances the surgeon would like to know about the resectability of the lesion, the studies that best demonstrate anatomical detail are performed next. These include CT and/or MRI/MRA. The latter is the preferred imaging modality in preoperative staging of liver tumors because it gives excellent soft tissue contrast while allowing visualization of hepatic vascular structures to rule out possible tumor invasion. Knowledge of the natural history of the disease, as well as the necessity for precise anatomical detail for surgical resection, demands an extensive multimodality preoperative work-up.

Lymphoma

Hodgkin's and non-Hodgkin's lymphomas are frequent malignancies of childhood. Approximately 40% of childhood lymphomas are of the Hodgkin's type and 60% are non-Hodgkin's. Although most children with lymphoma do not present with an abdominal mass, occasionally a palpable abdominal mass is the initial presenting sign. In most cases, this is due to lymphomatous infiltration of abdominal viscera (spleen, kidneys or liver). The Burkitt type of non-Hodgkin's lymphoma may arise from mesenteric lymph nodes or from the gastrointestinal tract, so these patients frequently present with an abdominal mass (Fig. 6.9).

In the past, CT and gallium 67 scintigraphy have been used for initial staging of lymphomas, to monitor response to treatment, and to evaluate for disease recurrence. FDG-PET is the current, more sensitive method for staging, to assess response to therapy, and for routine follow-up (Fig. 6.9).

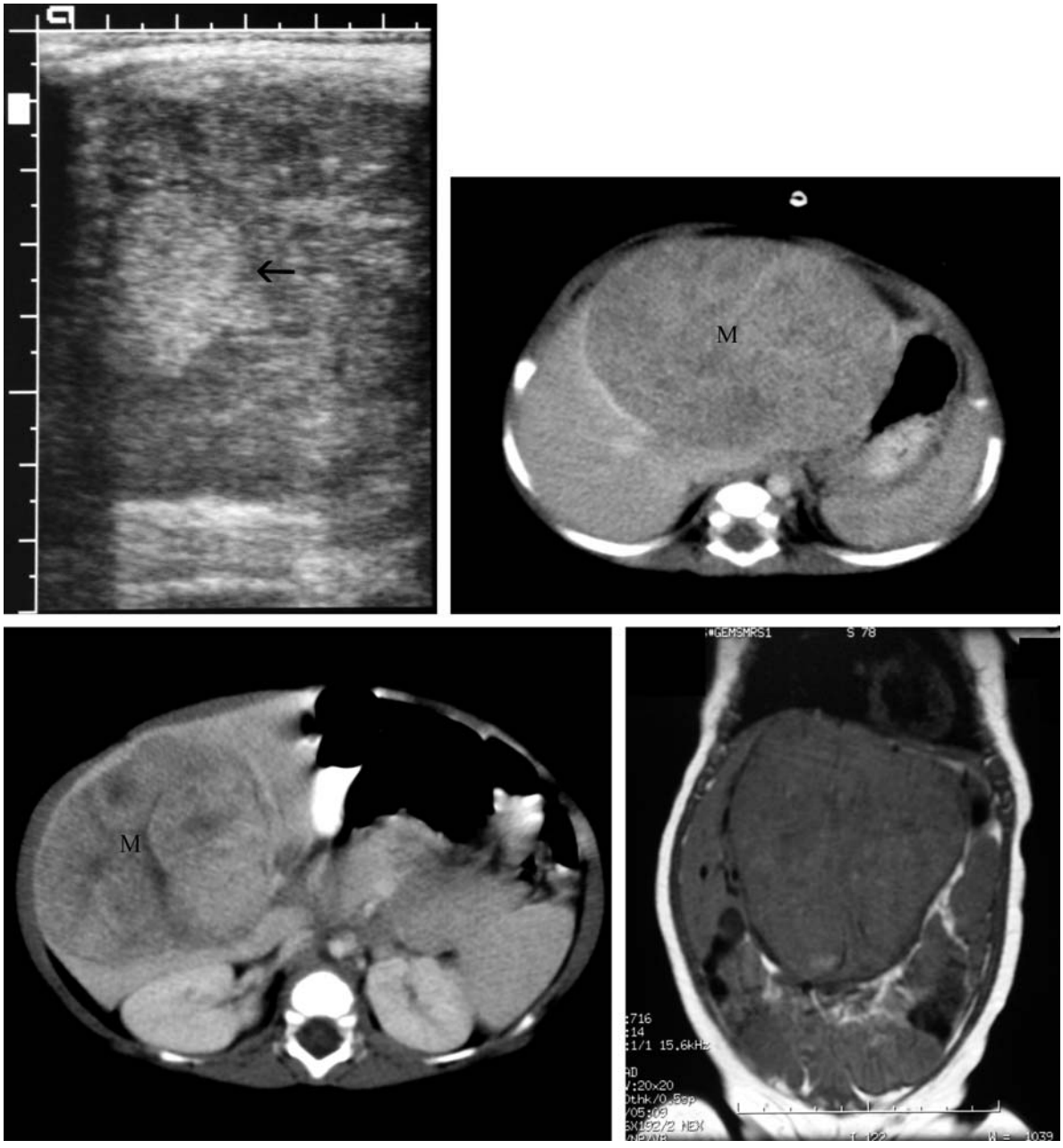

Fig. 6.14. Legend see p. 167

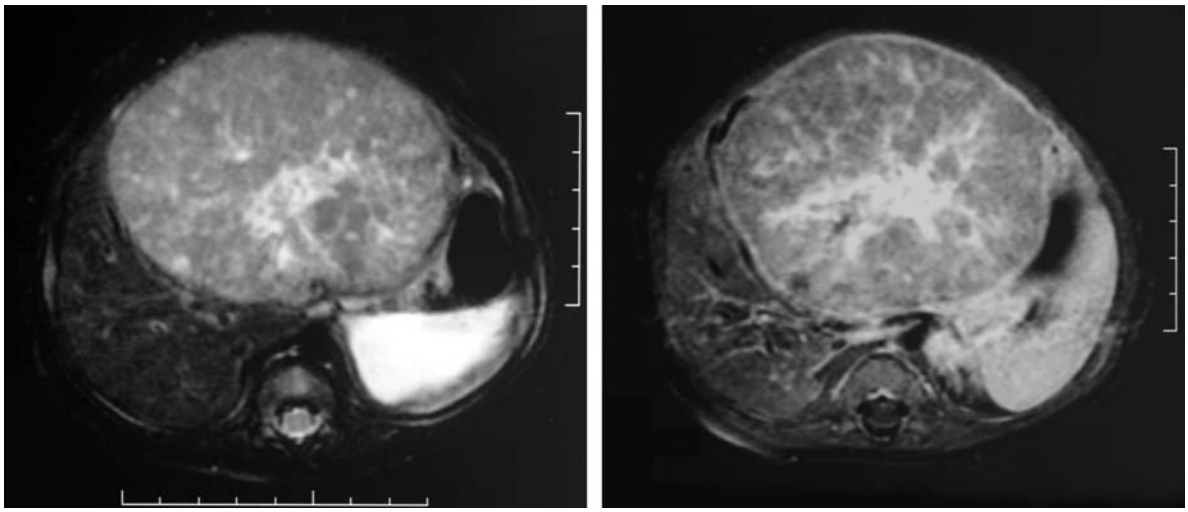

e f

Fig. 6.14. Hepatoblastoma
a Ultrasound of an infant's liver shows a hyperechoic mass (*arrow*) within the hepatic parenchyma
b–f Four-month-old boy, with abdominal mass (*M*). Axial contrast-enhanced CT (**b, c**), coronal T1-weighted (**d**), axial T2-weighted fat-saturated (**e**), and postgadolinium axial T1-weighted fat-saturated (**f**) images demonstrate a large, heterogeneously enhancing mass in the left lobe of the liver

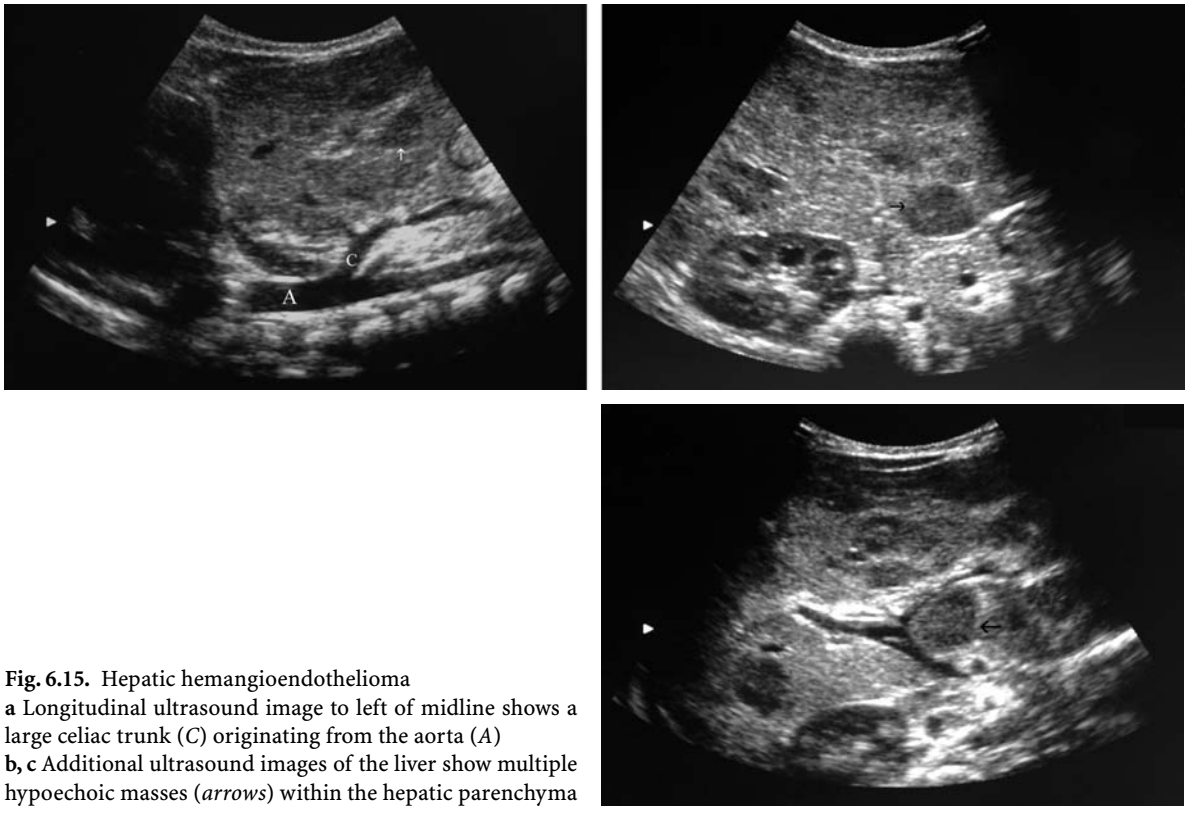

a b c

Fig. 6.15. Hepatic hemangioendothelioma
a Longitudinal ultrasound image to left of midline shows a large celiac trunk (*C*) originating from the aorta (*A*)
b, c Additional ultrasound images of the liver show multiple hypoechoic masses (*arrows*) within the hepatic parenchyma

Rhabdomyosarcoma

Rhabdomyosarcoma is the most common soft tissue tumor in children. It originates from the same embryonic mesenchyme that gives rise to skeletal muscle and is a major diagnostic consideration in the case of a solid pelvic mass. Sixteen percent of rhabdomyosarcomas originate in the genitourinary system. The vagina, bladder, testicular–paratesticular tissues, or prostate may be the primary site. Patients with bladder or prostatic rhabdomyosarcomas may present with urinary symptoms, including hematuria, urinary retention or urinary frequency, or with a palpable suprapubic mass. In addition to the above symptoms, girls with vaginal rhabdomyosarcoma may present with vaginal bleeding or prolapsing vaginal mass.

Rhabdomyosarcoma occurs in any age group, with 65% of the children being under 11 years of age. The tumor's routes of spread include:

- Local
  - Direct invasion of adjacent viscera
  - Retroperitoneal lymph nodes
- Remote (hematogenous)
  - Lungs
  - Bone
  - Liver

Since these patients typically present with either urinary symptoms or a palpable mass, their initial imaging exam is either ultrasound or cystography. After the presence of a genitourinary mass is established, CT or MRI of the pelvis is performed to better delineate tumor extent. MRI is better able than CT to evaluate the relationship between tumor and adjacent viscera. Metastatic work-up should include CT of the thorax for pulmonary metastasis, either CT or MRI of the upper abdomen for hepatic metastasis, and whole body bone scan for skeletal metastasis.

Pregnancy: The Most Common Pelvic Mass in Girls

Evaluation of pelvic masses begins, for girls over 9 years of age, with a pregnancy test or an ultrasound study (see Fig. 6.5). Careful longitudinal and transverse scans are done to rule out the easily diagnosable intrauterine pregnancy. The pelvic mass is defined, and the diagnostic possibilities may be limited to a select few. Ovarian lesions are also detected by ultrasound.

Risk Factors for Abdominal Masses

Children with certain conditions are at increased risk for developing the abdominal masses discussed in this chapter. Ten percent of patients with Beckwith–Wiedemann syndrome (a triad of macroglossia, omphalocele, and visceromegaly) develop an abdominal tumor, usually Wilms tumor, hepatoblastoma, or adrenal cortical carcinoma. Children with hemihypertrophy have a predilection for Wilms tumor and hepatoblastoma. Approximately one-third of children with sporadic aniridia develop Wilms tumor, and some of these have the WAGR syndrome (Wilms tumor, aniridia, genitourinary abnormalities, and mental retardation). There also appears to be an association of trisomy 18 with both Wilms tumor and hepatoblastoma. Other conditions associated with Wilms tumor include the Drash syndrome (male pseudohermaphroditism, glomerular disease and Wilms tumor) and tuberous sclerosis. Other risk factors for development of hepatoblastoma include fetal alcohol syndrome and familial adenomatous polyposis.

References and Further Readings

1. Griscom NT (1965) The roentgenology of neonatal abdominal masses. AJR Am J Roentgenol 93:447
2. Kasper TE et al (1967) Urological abdominal masses in infants and children. J Urol 116:629
3. Slovis TL, Sty JR, Haller JO (1989) Imaging of the pediatric urinary tract. Saunders, Philadelphia
4. Kuhn JP, Slovis TL, Haller JO (eds) (2004) Caffey's pediatric diagnostic imaging, 10th edn. Philadelphia, Mosby
5. Faerber EN (ed) (1997) Pediatric oncology imaging. Radiol Clin North Am 35:1251
6. Isaacs H Jr (ed) (1997) Tumors of the fetus and newborn. Saunders, Philadelphia

7 Skeleton

The second most frequent radiographic study, after the chest film, is that of the pediatric skeleton. The most common indication for such studies is of course trauma. In order to understand the disease processes that occur in the pediatric age group one must first know the skeletal anatomy. The skull and spine are covered in Chap. 8.

Anatomy

Long Bones

The two physiological mechanisms of bone production and development are endochondral (long bones) and intramembranous ossification (flat bones). The long bone of a child is divided into four areas (Fig. 7.1):

- Diaphysis: the shaft of the long bone
- Metaphysis: from the area where the bone widens to the physis
- Physis: the lucent line where growth takes place prior to calcification of the cartilage
- Epiphysis, or secondary ossification center: a portion of which interfaces with the joint as the articular cartilage and allows movement within the joint

The center of the long bone is the medullary cavity, while the outer bone is called the cortex. Some long bones (e.g., the femur) have a nonarticulating *apophysis* (see Fig. 7.1), which is similar to the epiphysis but does not contribute to the length of the bone (e.g., the greater trochanter of the femur). In the growing child's skeleton, blood supply is primarily to

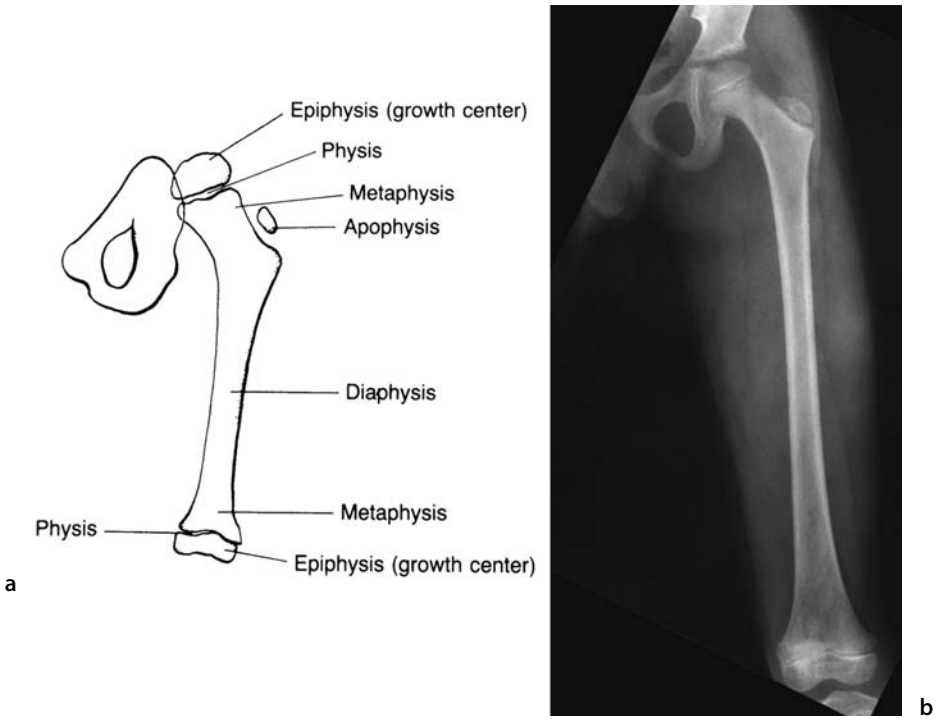

Fig. 7.1. The normal femur
a Schematic drawing of a normal femur
b Radiograph of a normal femur

the metaphysis, and many of the disease processes and roentgen findings are seen in this region. For example, hematogenous osteomyelitis is visible most often in the metaphysis; similarly, metastases travel hematogenously to the metaphysis.

Flat Bones

In contrast to long bones, flat or membranous bones do not have a single growth plate but rather a mesenchymal network or membrane that attracts osteoblasts, which form osteoid. There are equivalent diaphyseal, metaphyseal, and epiphyseal areas, however, which behave very similarly to their counterparts in the appendicular skeleton. Membranous bones include the mandible, pelvis, scapula, base of the skull, the clavicles, and the sternum.

Unique Features

The skeleton of children is quite different from that of adults. The child's bones are obviously still growing, developing, and modeling; therefore, many ossification centers are constantly appearing and fusing with the main skeleton (Fig. 7.2) (Table 7.1). Because these ossification centers may appear fragmented and may ossify in a multicentric fashion, they can easily simulate chip fractures. One should therefore obtain comparison views of the contralateral extremity if there is any question.

Insults from infection, tumor, or trauma to the metaphyseal region, physis, and epiphysis are much more damaging in children than in adults because the growth plate is disturbed. Fractures involving the growth plate are called Salter–Harris fractures and carry a prognostic rating according to the severity of the growth plate injury (I–V, with V being the worst; Fig. 7.3). Severe length discrepancies and other growth disturbances can occur from fractures in these regions.

Another unique difference between the child's and the adult's skeleton is the low incidence of dislocations (complete disruption of the joints with loss of contact between articulating surfaces) of otherwise normal joints. Because children's capsular and ligamentous structures are two to five times stronger than the weakest part of the growth plate, the growth plate fractures first, and dislocation occurs less frequently. The zone of calcifying cartilage (Fig. 7.4) is the weakest portion of the growth plate. The growing bones of children are also unique in that they are more "plastic" and more likely to bend before they fracture (Fig. 7.5). Because of this resiliency children are more likely to have "incomplete fractures," two of which have characteristic names – the *greenstick* fracture and the *torus* fracture. The greenstick fracture is characterized by a bowed long bone with a break on the convex surface but apparent cortical continuity on the concave surface. In the torus fracture there is buckling on one side of the cortex (see Fig. 7.5). In both of these fractures, however, microscopic examination shows nondisplaced fractures of osteoid across the bone.

Table 7.1. Approximate age of ossification of secondary centers in elbow

Center	Age (years)
Capitellum	1
Radial head	4
Inner (medial) epicondyle	7
Trochlea	10
Olecranon	10
External (lateral) epicondyle	11

In children the periosteum is constantly growing. Therefore it is less firmly attached to the diaphysis, or shaft, of the long bone and is more likely to tear and thus be elevated by trauma and hematoma formation. The periosteum reacts by laying down a thick layer of new bone. In contrast, the periosteum at the ends of the long bones is not loosely attached but rather firmly adherent to the metaphyseal regions. Twisting injuries here cause avulsion of a piece of bone from the metaphysis. This type of "bucket-handle" injury or avulsion "corner fracture" is commonly found in cases of child abuse (Fig. 7.6; discussed below).

Another difference between the adult and child is the ability to estimate bone maturation in those in the pediatric age range (discussed below, "Bone Age Determination").

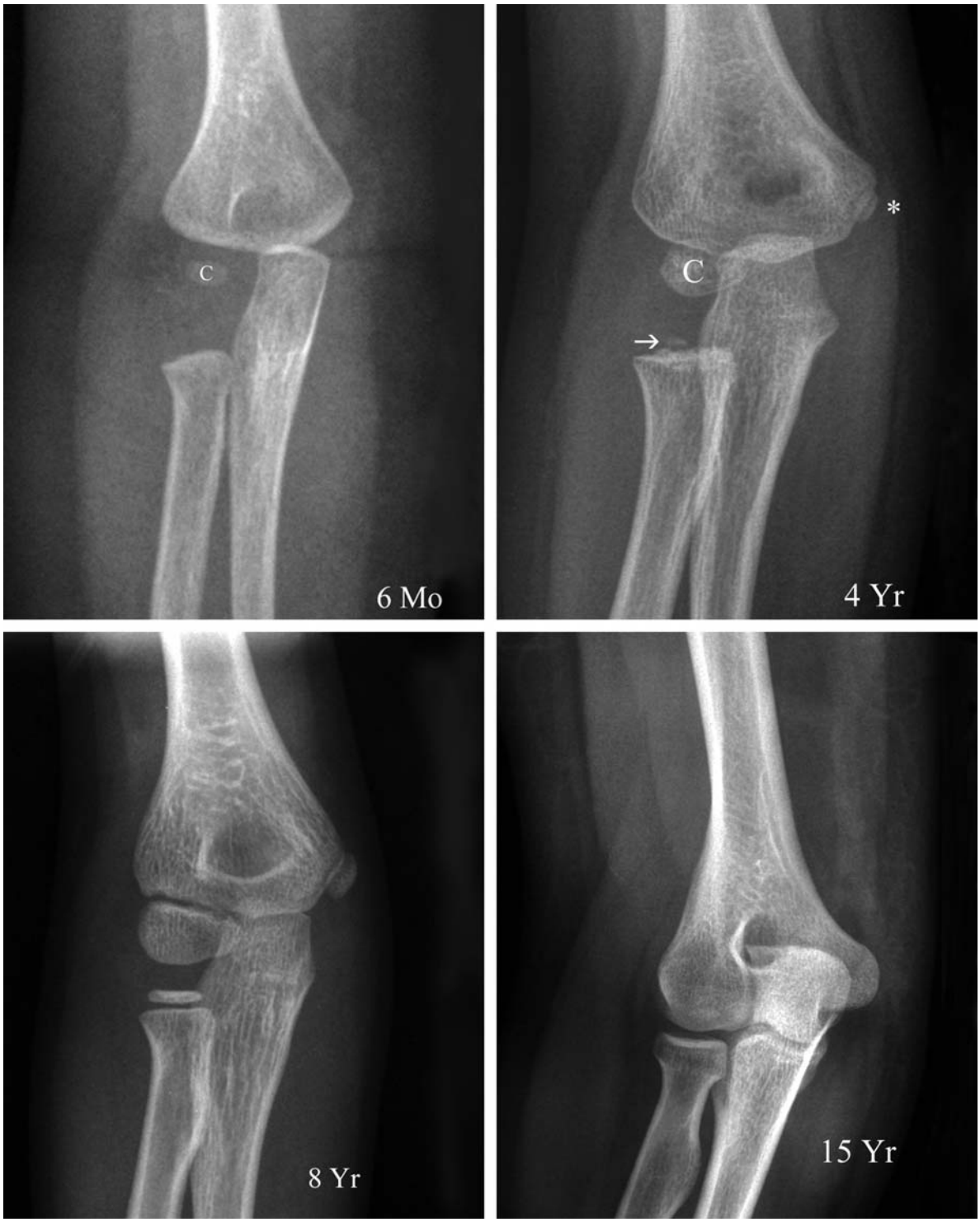

Fig. 7.2. The normal elbow at different stages of development
Note the appearance of the various ossification centers as the child matures (see Table 7.1)
a A 6-month-old. Capitellum (*C*) is ossified
b A 4-year-old. Radial head (*arrow*) and medial epicondyle (*asterisk*) have begun to ossify
c An 8-year-old. Secondary centers of ossification are larger
d A 15-year-old. Mature elbow with closure of the growth plates

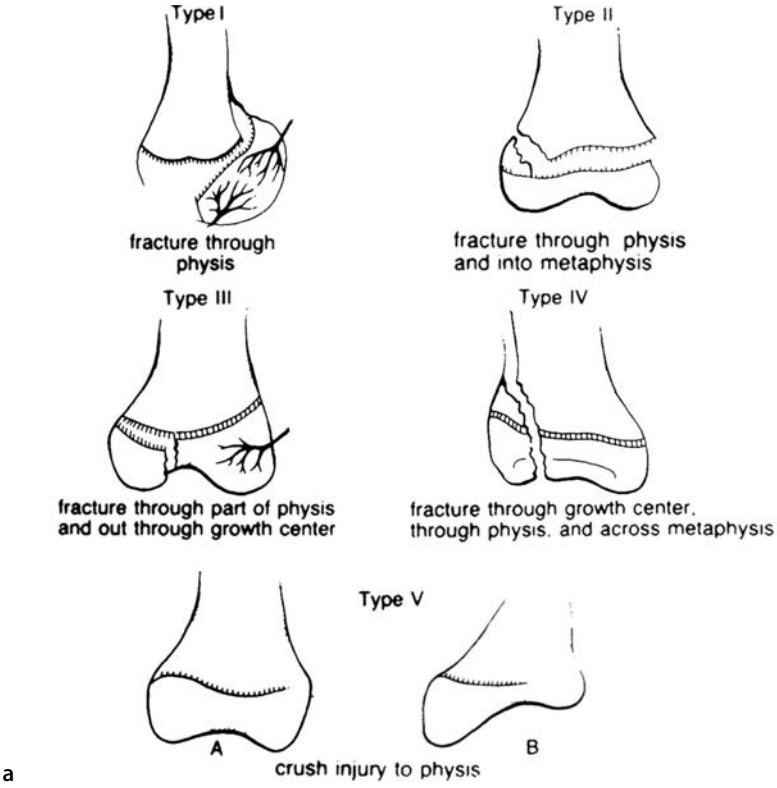

a

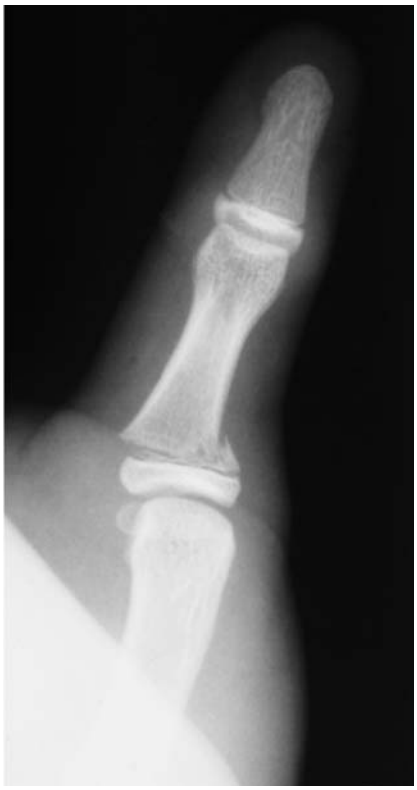

b

Fig. 7.3. Salter-Harris fractures
a Salter–Harris classification of fractures involving the growth plate. Prognosis depends on integrity of the blood supply and fracture type. Salter IV and V have a worse prognosis than I, II, and III
b Salter II fracture of the proximal phalanx of the thumb. The fracture involves the metaphysis and physis

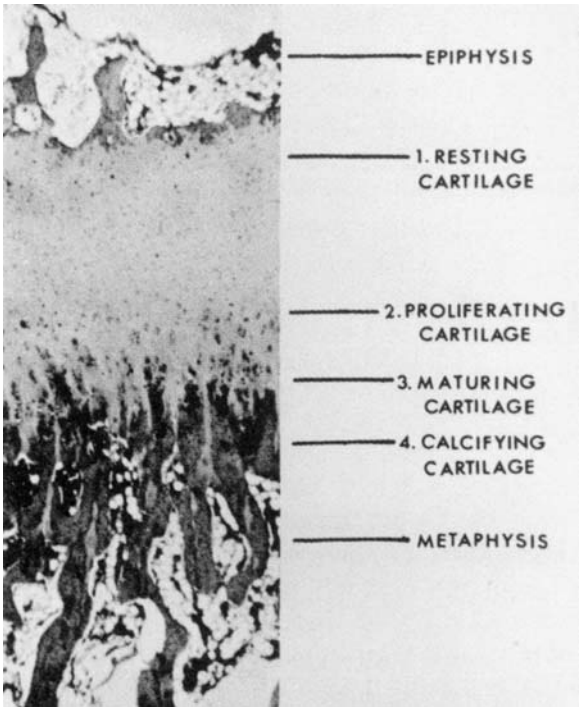

Fig. 7.4. Photomicrograph showing different zones of the growth plate
Shearing forces applied to the growth plate result in fracture through the zone of calcifying cartilage. (From [1] with permission)

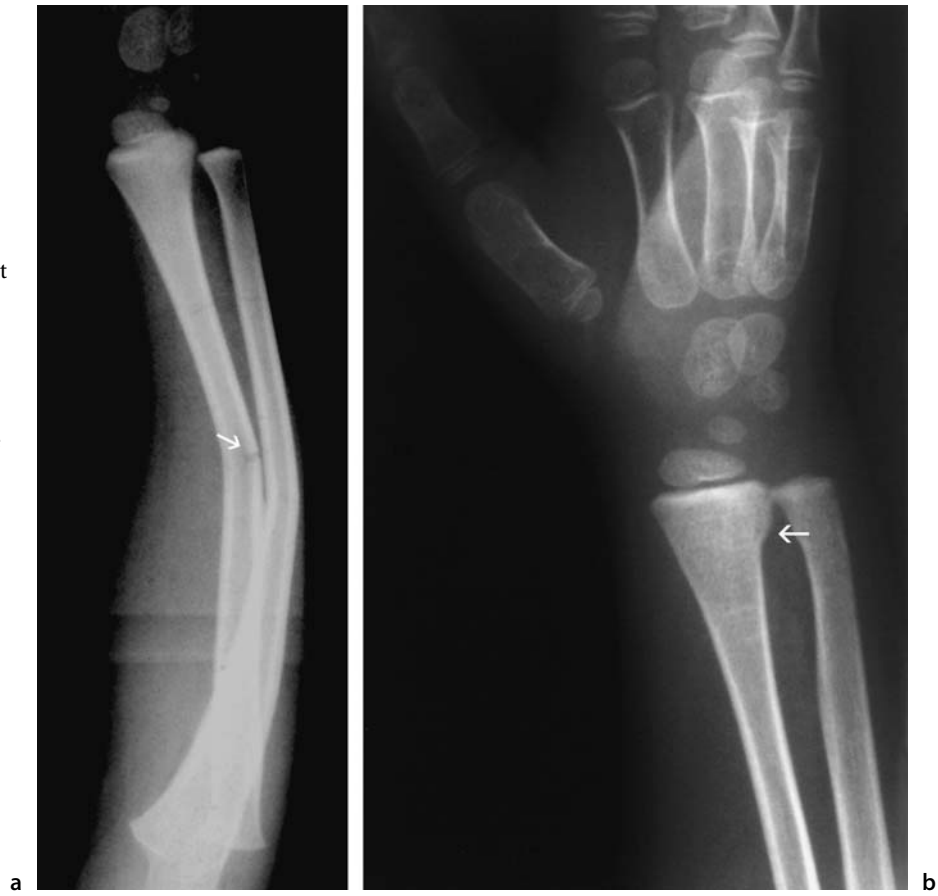

Fig. 7.5. Common pediatric fractures
a Greenstick fracture. The fracture appears to extend halfway through the diaphysis (*arrow*). Note the bowing of the radius and ulna
b Torus fracture. Note the buckling at the medial aspect of the distal radius (*arrow*). Microscopic examination of both greenstick and torus fractures show trabecular disruption across the entire horizontal width of the bone

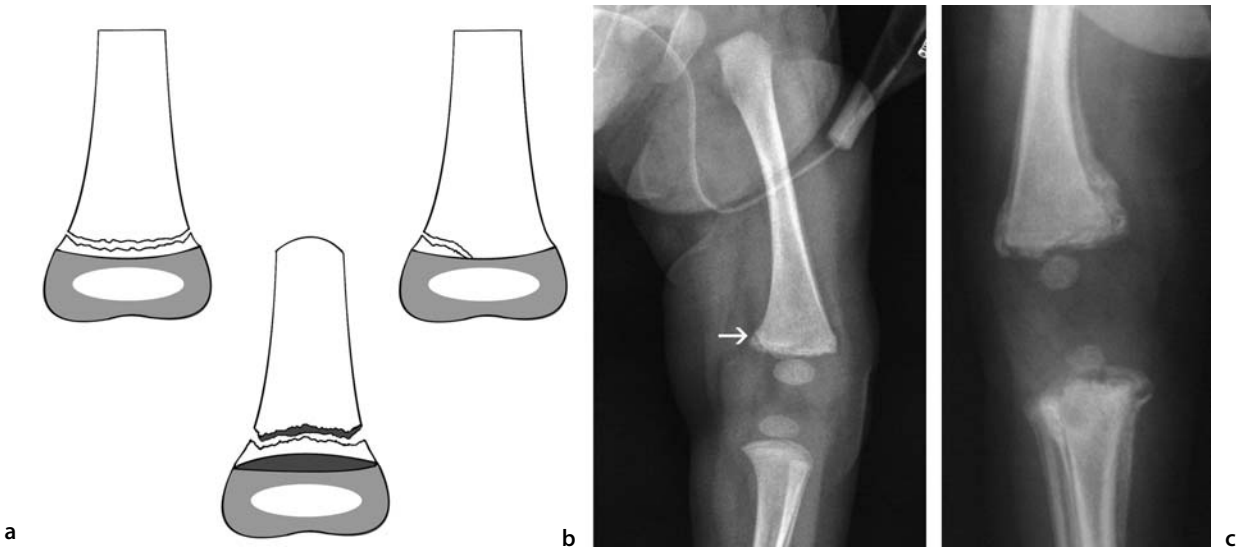

Fig. 7.6. Bucket-handle fractures
a Drawings of a metaphyseal fracture as it appears with various radiographic projections and distractions
b Bucket-handle fracture of distal femur. A thin avulsion of bone at the femoral metaphysis (*arrow*) resembles the resting handle of a bucket. This fracture is commonly seen in the battered child syndrome
c Another child with profuse periosteal reaction about the distal femur and proximal tibia. This defines the "bucket-handle" lesions

Imaging Modalities in Evaluating Musculoskeletal Disease

Plain Film Radiography

The plain film is the initial exam performed in the vast majority of cases of suspected musculoskeletal pathology. Although plain film radiography is not the most sensitive imaging exam for musculoskeletal pathology, it is readily available, inexpensive, and provides sufficient diagnostic information for most problems, including bone tumors.

Bone Age Determination

Plain radiographs are used to assess skeletal maturity. A child's bone age needs to be determined in several clinical situations (Table 7.2). For children over the age of 1 year, most endocrinologists and radiologists do this by comparing a PA view of the child's left hand with the standards in the Greulich–Pyle *Radiographic atlas of skeletal development of the hand and wrist* [2]. The atlas includes standards for males and females as well as the standard deviations in skeletal age at different chronologic ages.

One should keep several important points in mind when determining bone age:

1. The standards in the Greulich–Pyle atlas are based on the hand radiographs of "normal" white American children. How valid the atlas is for children of other races or ethnicities is not clear, and clinicians must take this into account. One should treat the bone age like growth and development curves.
2. Phalangeal age is more accurate than carpal age.
3. Phalangeal age is assessed by presence, relative width, shape, and fusion of various phalangeal epiphyseal ossification centers (see Fig. 7.7)
4. For the bone age to be considered normal, it should lie within two standard deviations from the patient's chronologic age.
5. In children under 1 year of age, bone age is usually determined by the Sontag method of totaling the number of visualized ossification centers (Table 7.3) in one side of the skeleton and comparing it with a standard table (Table 7.4).

Table 7.2. Indications for bone age determination

Short stature
Tall stature
Precocious puberty
Delayed puberty
Timing of orthopedic surgery (e.g., correction of limb length discrepancy, scoliosis)

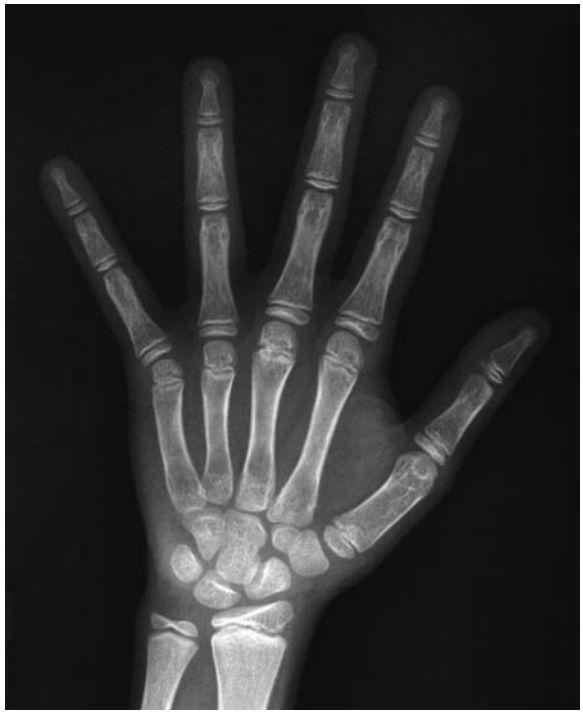

Fig. 7.7. Bone age
This male aged 13 years, 5 months has delayed puberty. His left hand radiograph most closely resembles the Greulich–Pyle standard for a male of 11 years, 6 months. The standard deviation for a 13-year-old male as given in the Greulich–Pyle atlas as 10 months. Therefore, his bone age is delayed (greater than two standard deviations below his chronologic age)

Table 7.3. List of ossification centers (total: 67). (From [3] with permission)

Shoulder	Femur
Coracoid	Proximal epiphysis
Humerus	Greater trochanter
Proximal medial epiphysis	Distal epiphysis
Proximal lateral epiphysis	Knee
Capitellum	Patella
Medial epicondyle	Tibia
Radius	Proximal epiphysis
Proximal epiphysis	Distal epiphysis
Distal epiphysis	Fibula
Hand	Proximal epiphysis
Capitatum	Distal epiphysis
Hamatum	Foot
Triquetrum	Cubiod
Lunate	First cuneiform
Navicular	Second cuneiform
Greater multangular bone	Third cuneiform
Lesser multangular bone	Navicular
5 distal phalangeal epiphyses	Epiphysis of calcaneus
4 middle phalangeal epiphyses	5 distal phalangeal epiphyses
5 proximal phalangeal epiphyses	4 middle phalangeal epiphyses
5 metacarpal epiphyses	5 proximal phalangeal epiphyses
	5 metatarsal epiphyses

Table 7.4. Mean total number of centers on the left side of the body ossified at the given ages. (From [3] with permission)

	Boys		Girls	
Age (months)	Mean no.	SD	Mean no.	SD
1	4.11	1.41	4.58	1.76
3	6.63	1.86	7.78	2.16
6	9.61	1.95	11.44	2.53
9	11.88	2.66	15.36	4.92
12	13.96	3.96	22.40	6.93
18	19.27	6.61	34.10	8.44
24	29.21	8.10	43.44	6.65
30	37.59	7.40	48.91	6.50
36	43.42	5.34	52.73	5.48
42	47.06	5.26	56.61	3.98
48	51.24	4.59	57.94	3.91
54	53.94	4.35	59.89	3.36
60	56.24	4.07	61.52	2.69

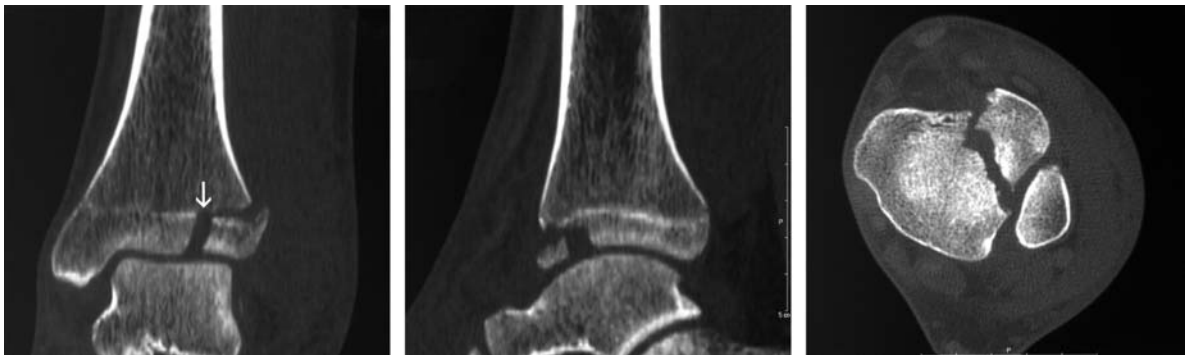

Fig. 7.8. CT of ankle reformatted in coronal (**a**) and sagittal (**b**) and the examined axial plane (**c**) show the juvenile Tillaux-type fracture and the anatomy of the distal tibial articular surface more clearly than the corresponding plain radiographs (see Fig. 7.13). There is a fracture through the epiphysis (*arrow*) and also through the physeal plate (fibrocartilage), making this a Salter–Harris type III fracture

Computed Tomography

CT can define osseous anatomy in more detail than the plain film, with greater definition of both the cortical bone and the medullary cavity. This is particularly valuable in confirming radiographically subtle fractures, diagnosing and localizing suspected osseous abnormalities (e.g., sequestrum, bone- or calcium-producing lesion, etc.), and evaluating difficult areas (e.g., sacrum, sternum, scapula, bones in cast). CT images can be reformatted in various planes and reconstructed to three-dimensional images. This helps orthopedic surgeons in preoperative planning (Fig. 7.8).

Magnetic Resonance Imaging

MR demonstrates the bone marrow, joints, cartilage and soft tissues in exquisite detail (Fig. 7.9), and is therefore very sensitive in detection of the extent of pathology involving these structures. Specifically, MR is frequently used in evaluation of ligamentous and cartilaginous injuries, joint pathology, soft tissue tumors, musculoskeletal infection, and avascular necrosis. It does not show detail of cortical bone or calcification as well as CT. Other disadvantages of MR include its expense, the frequent need for sedation in younger patients, and limited availability. It is always best to interpret MR scans in correlation with the plain films.

Nuclear Medicine

Most nuclear medicine imaging of bone is performed by injecting the patient with a phosphate compound labeled with the radioisotope technetium 99m. Over the next 2 h, the phosphate is incorporated into bone. The extent to which this incorporation occurs in different parts of the skeleton is determined by blood flow and by bone turnover. When the patient is imaged under a gamma camera, the distribution of radiopharmaceutical in the skeleton is shown (Fig. 7.10). Areas of abnormality usually show increased activity relative to the remainder of the skeleton.

Nuclear medicine bone scan is useful in evaluating diffuse processes (e.g., metastatic neoplasm), in detecting areas of abnormality that have not become radiographically visible (e.g., early osteomyelitis), and in localizing areas of pathology for more targeted imaging with CT or MR (e.g., back pain).

Bone scan imaging and interpretation can be difficult. Because the patients must remain sufficiently still for the gamma camera to measure the radioactivity from the skeleton, younger children need to be sedated for this exam. The technologists must pay particular detail to patient positioning and proper image acquisition. Nuclear medicine studies do not provide the anatomic detail that CT, MR, and plain radiography do, and so bone scans need to be interpreted in correlation with plain films.

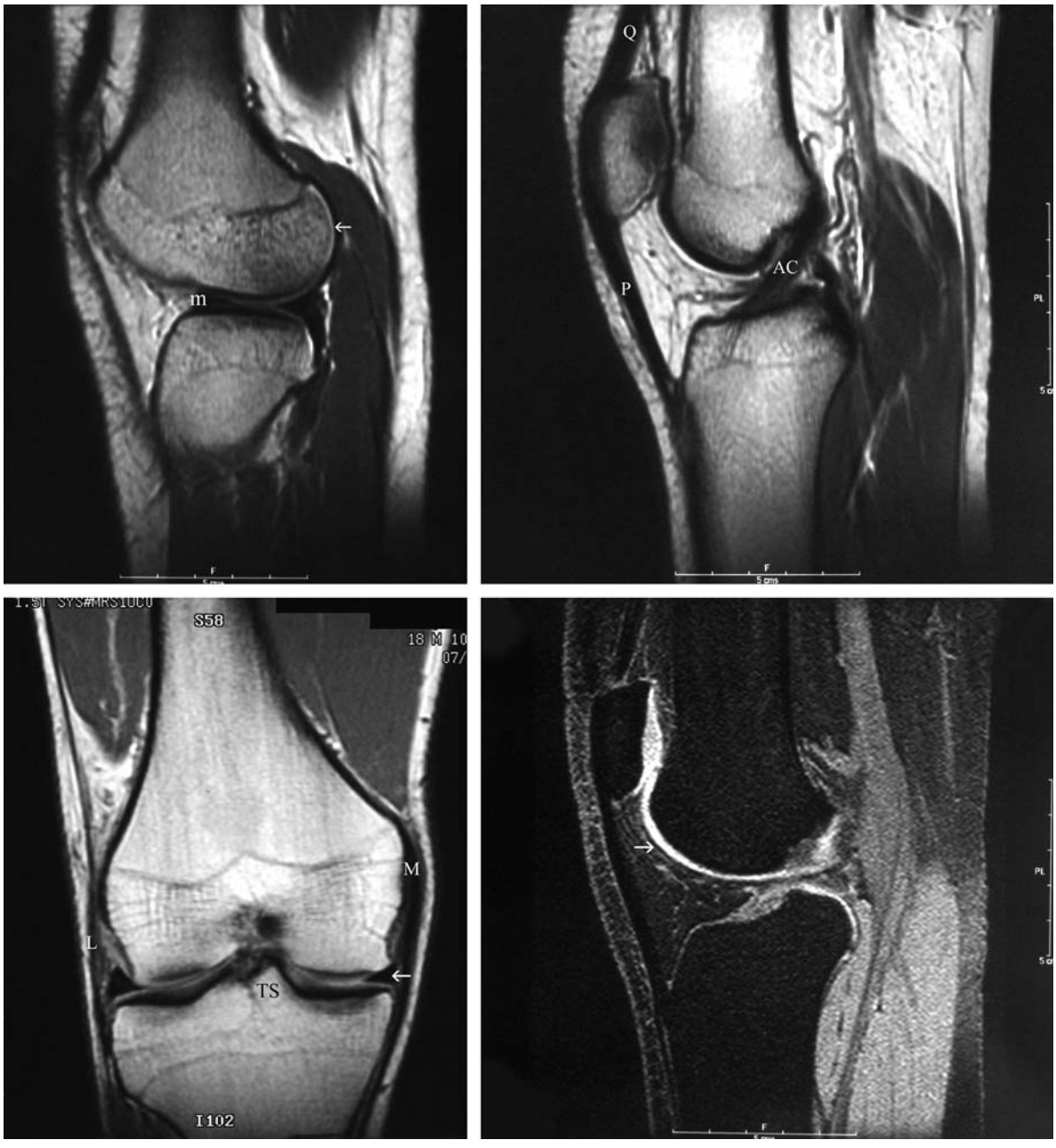

Fig. 7.9. MR of the normal knee
a Sagittal proton density view shows menisci of fibrocartilage (*m*) and articular (hyaline) cartilage (*arrow*)
b Sagittal proton density view reveals a normal anterior cruciate ligament (*AC*) and quadriceps (*Q*) and patellar (*P*) tendons
c Coronal T1-weighted view of the tibial spine (TS), meniscus (*arrow*) and collateral ligaments. *M*, medial; *L*, lateral
d Sagittal fat-saturated spoiled gradient image is best for evaluating the articular (hyaline) cartilage (*arrow*)

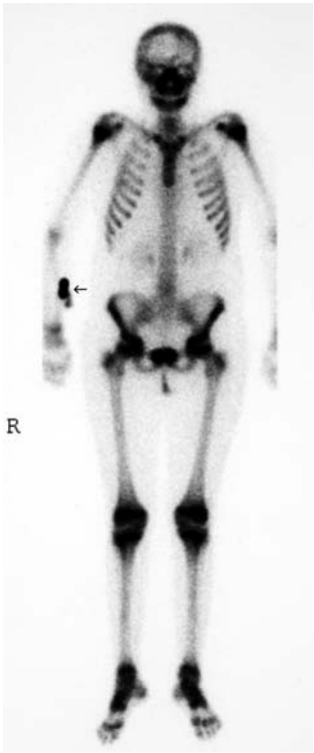

Fig. 7.10. Images from a normal whole body bone scan in a child
Note that there is relatively more activity in the metaphyses because of the greater blood supply to these zones of growth. The right arm (*arrow*) was the site of injection

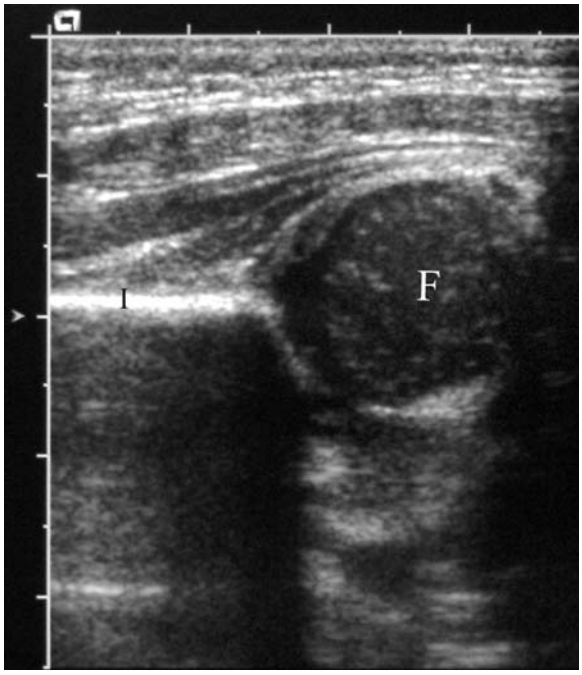

Fig. 7.11. Longitudinal sonographic view of a normal infant hip: the cartilaginous femoral head (*F*) is positioned in the acetabulum. *I*, ilium

Ultrasound

As a rule, ultrasound is not very helpful in evaluating intraosseous pathology, since bone is not a good conductor of sound. However, ultrasound can be useful in evaluating cartilaginous anatomy (e.g., the nonossified femoral head in an infant with developmental hip dysplasia; Fig. 7.11), diagnosing joint effusion, detecting nonopaque soft tissue foreign bodies, and evaluating soft tissue masses and synovial hypertrophy. In some centers, ultrasound is even used to evaluate tendons and ligaments, although this is more frequently done with MR.

General Approach to the Skeletal Plain Film

Before beginning to evaluate any images, the radiologist must know a few important clinical facts, such as the patient's age, sex, race, prior treatment, and whether this is a generalized or local bone disturbance. With this information, the radiologist can make intelligent decisions about the child's radiographs, as explained below.

Age. As discussed in the work-up of a child with an abdominal mass, the tendency of lesions to occur at different ages helps one to form the differential diagnosis. For example, a 6-year-old is more likely to have aseptic necrosis of the capital femoral epiphysis (Legg-Calvé-Perthes disease), while hip disease in a teenager is often a slipped capital femoral epiphysis.

Sex. Hemophilia affects only males; therefore it follows that arthropathy and bone changes are found only in males.

Race. Sickle cell anemia, Gaucher's disease, and thalassemia are important considerations in different racial and ethnic backgrounds–sickle cell disease in black children, Gaucher's disease in Jewish children, and thalassemia in children of Mediterranean ancestry.

Prior Treatment. It is important for the radiologist to know whether the lesion has already been partially treated, since it may display a very different roentgenographic appearance in the treated state. For example, a healing or treated bone cyst appears much different than the untreated variety.

Generalized or Local Disease. Finally, the radiologist must know whether this is the only bone involved, or whether the disease affects multiple bones. Langerhans cell histiocytosis, fibrous dysplasia, and metastases are systemic bone diseases, while simple bone cysts and Brodie's abscess are most commonly isolated focal disorders (Fig. 7.12). A skeletal survey or bone scan frequently is helpful in working up systemic disorders.

Before diagnosing specific bony abnormalities it is important to evaluate exposure. Is the film overexposed? This can be judged by looking at the soft tissues and seeing whether they are "burnt out" or clearly visible. If they are not clearly visible, the film is overexposed. If the bones are so light that the trabecular pattern is indistinct or invisible, the film is underexposed. Improperly exposed digital radiographs may be postprocessed to show adequate bone and soft tissue detail, but the radiation dose cannot be determined by the final product. It is important to look at the exposure factors on all films.

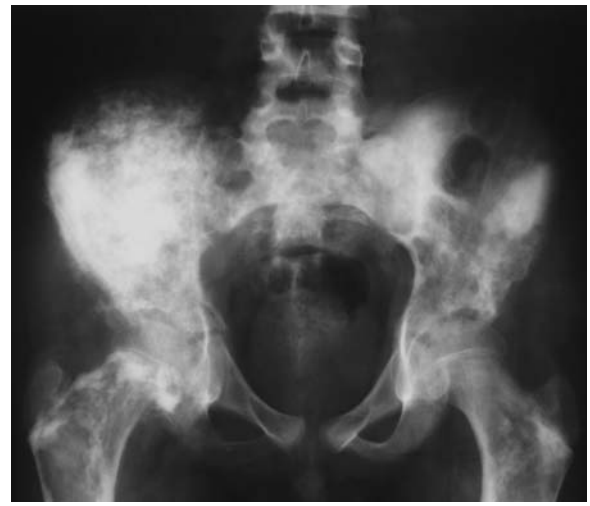

Fig. 7.12. Metastasis
Careful attention to the texture of the bone shows areas of lucency (black) and sclerosis (white). These correspond to lytic and blastic lesions caused by a medulloblastoma that metastasized to bone. While lytic metastases are commonly seen, blastic ones are quite infrequent

It is also important to look at any bony abnormality in two or more views. Fractures are easily missed if one relies on only a single view of the area. Comparison views are frequently necessary.

We use the same ABCS system to evaluate skeletal radiographs that we use to evaluate chest radiographs: *A*=abdomen (any part of the abdomen on the film is examined), *B*=bones (save for last; see below), *C*=chest (any part of the chest on the film is examined), *S*=soft tissues (give clues to the site and kind of injury, Table 7.5, Fig. 7.13).

Table 7.5. Abnormalities of soft tissue. (Modified from [4] with permission)

What to look for	Disease
Soft tissue swelling	Most likely site of bone abnormality. Can be hemorrhage, traumatic edema, inflammation or neoplastic abnormality
"Fat-pad" elevation	Fluid within a joint displacing the periarticular fat
Muscle wasting	Disuse, neuromuscular abnormality, chronic disease of any etiology requiring lots of immobilization
Calcifications	Old trauma; hemangiomas; metabolic, parasitic or connective tissue disorders (dermatomyositis, scleroderma)
Opaque foreign bodies	Glass (even nonleaded glass) is often visible on a radiograph
Gas in tissue planes	Penetrating trauma, infection by gas-forming bacteria
Adjacent surprises	Unsuspected renal or appendiceal calculi, especially on lumbar spine films

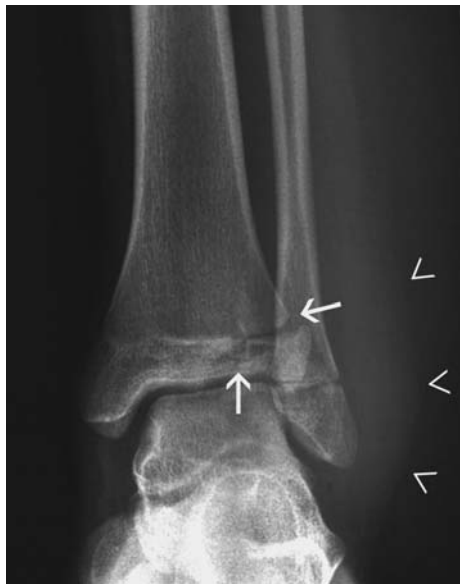

Fig. 7.13. Soft tissue swelling and fracture
There is extensive soft tissue swelling over the lateral malleolus (*arrowheads*) associated with the patient's distal tibial fracture of the physis and through epiphysis (*arrows*) (see Fig. 7.8)

In evaluation of the bones themselves, we use another ABC system [5]: *A*=alignment; *B*=bone size, shape, texture, mineralization, and maturation; *C*=cartilage and joint space.

Alignment of Bones. Disruption of bone cortex and articular surfaces is easy to spot when you look for it!

► ***Rule No. 14:*** When viewing an extremity, try to imagine the appearance of the patient. An excellent example is bowed legs or knock knees.

Bone Size, Shape, Texture, Mineralization, and Maturation. The configuration of the bone and its special relationship helps determine the presence of fractures, dislocations, or congenital anomalies. Many normal and abnormal findings can be detected by looking at the bone surface – the cortex. Periosteal reaction, with the exception of so-called physiological appositional new bone found symmetrically in infants 2–6 months of age (see below), should be regarded as abnormal. Remember, periosteum is *normally not visible*. It is seen only when it has been stimulated to lay down new bone, or the bone beneath it has been resorbed (Table 7.6). With an osteomyelitic process one can see cortical destruction along with reparative periosteal new bone (Fig. 7.14).

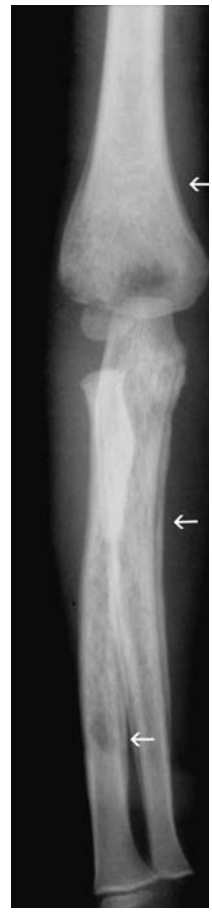

Fig. 7.14. Osteomyelitis
The ulna, radius, and humerus all exhibit a smooth periosteal reaction (*arrows*). The radius has a lytic defect at its distal position. This child has sickle cell disease with multifocal osteomyelitis

Table 7.6. Causes of periosteal reaction

Infection: osteomyelitis (includes congenital syphilis)
Trauma: nonaccidental injury, healing fracture
Metabolic: rickets, scurvy
Tumors/tumor-like diseases: osteosarcoma, Ewing's sarcoma, histiocytosis
Idiopathic: Caffey's disease
Iatrogenic/toxic: prostaglandin, hypervitaminosis A

► ***Rule No. 15:*** The periosteum is normally not seen.

Next we look at the texture of the bone with its normally uniform trabecular pattern and uniform mineralization. We diagnose metastatic disease and infection by the permeative destructive nature of bone involvement (see Fig. 7.12). These lesions do not have well-defined margins. At this time we can also detect metabolic disorders such as rickets and scurvy (Fig. 7.15). The medullary cavity is another impor-

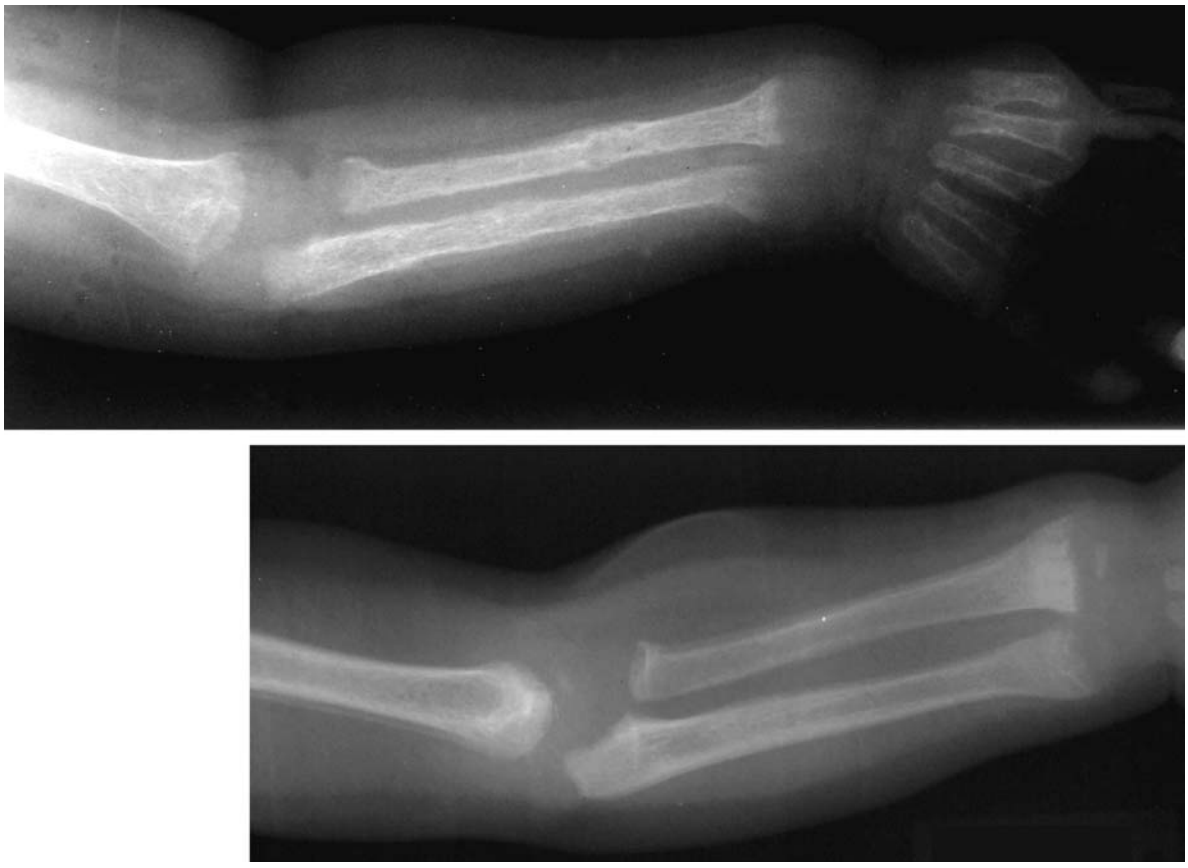

Fig. 7.15. Rickets
a In a young child the bones are demineralized and fractured. The distal radial and ulnar metaphysis are indistinct, frayed, and cupped
b In an older child, note how far the distal epiphysis is from the metaphysis

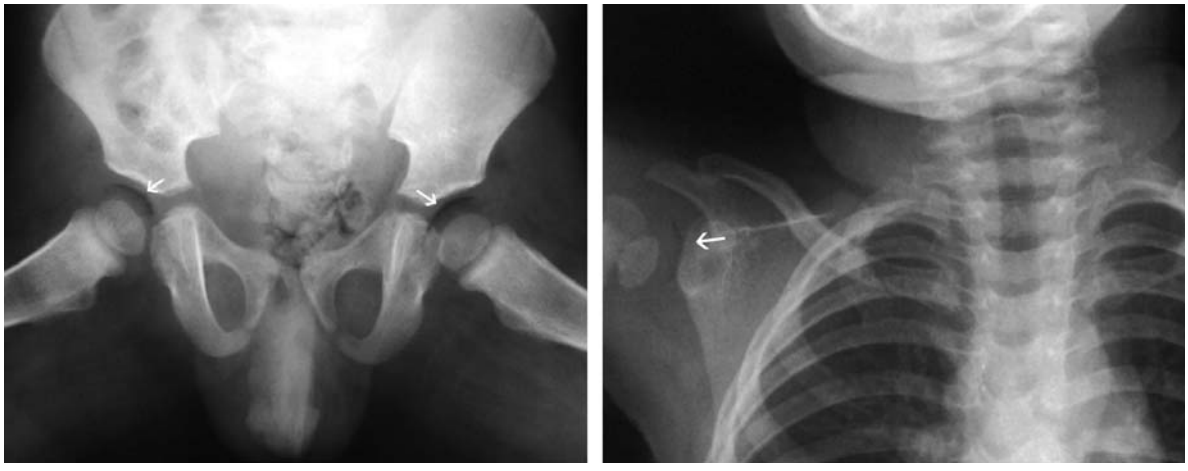

Fig. 7.16. Vacuum phenomenon
a Lucent (black) line outlines the cartilaginous head of the femur (*arrows*). This lucency, often seen in the large joints of children, is caused by pulling, resulting in a vacuum in the joint that allows nitrogen to enter and outline the articular cartilage of the bone
b Similar lucency outlines the humeral head (*arrow*)

tant component to evaluate. The major component of the medullary cavity – the bone marrow – is not seen on plain films but is seen extraordinarily well on MR (see below). Bone maturation (see above) becomes important when suspecting certain diseases such as hypothyroidism, where the bone age is markedly decreased.

Cartilage and Joint Space. Remember, one does not see the joint space alone on plain films – rather the noncalcified articular cartilage and joint space are viewed together (Fig. 7.16). Since only a small portion of this region is joint space, any narrowing may well be significant. The "joint space" should be symmetric and smooth without any calcifications or disruptions (see Fig. 7.16). The cartilage and joint space are superbly visualized by MR (see below).

Common Pediatric Problems

Trauma

Since trauma is the most frequent indication for skeletal examinations, it is important to know the normal variants that may appear. Two excellent sources of normal variants are found in the books of Keats [6] and Köhler [7]. It is important to compare both sides when one is in doubt about the presence of a fracture (Fig. 7.17).

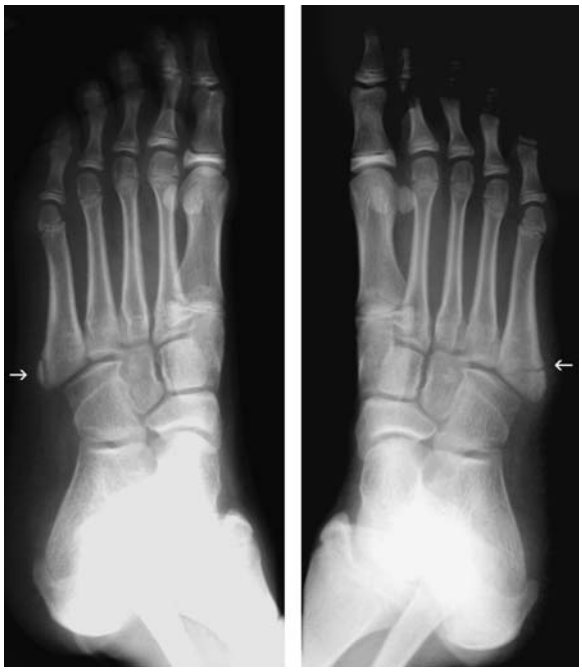

Fig. 7.17. Importance of familiarity with normal skeletal anatomy and symmetry
a The orientation of the normal apophysis (*arrow*) is parallel to the longitudinal axis of the fifth metatarsal bone
b Compare this to the fracture line at the base of the fifth metatarsal (*arrow*), which is oriented perpendicular to the bone

Let us start by looking at the fetus, which is rarely traumatized because it is in a protected environment – an amniotic fluid "water bath." Fractures, however, may occur in congenital diseases such as osteogenesis imperfecta. This disease is characterized by multiple partial and complete fractures in many bones (Fig. 7.18).

During difficult deliveries, such as breech presentations, fractures may be sustained; the most common ones involve the clavicles and skull. Since the infant is not very mobile during the first year of life, most injuries and fractures are secondary to various kinds of accidents. Particular findings, however, lead the radiologist to suspect child abuse (discussed below under "Nonaccidental Injury").

When it is necessary to determine the age of a fracture, remember: the younger the child, the faster the healing. In all children, however, the initial reparative process – periosteal reaction – begins 7–14 days after the original injury.

One must not, however, confuse the normal appositional new bone formation in infants from 2 to 6 months of age with pathological periosteal elevation. Rather, this is, as previously stated, normal periosteal bone deposition. It is bilaterally symmetric and found in the humeri, femora, and tibiae and extends to the metaphysis but no further. These are not fractures, nor do they denote any trauma (Fig. 7.19).

During the reading of children's radiographs we have found it useful to keep in mind the following "trauma tips" – factors unique to pediatrics:

- The clavicle is prone to greenstick fractures, which may be hard to visualize. One must take films in at least two views to make sure the child does not have a fracture.
- The elbow has so many secondary ossification centers that ossify at different ages that it is frequently necessary to view the opposite elbow for comparison (see Table 7.1).
- The *supermarket elbow* usually results from a sudden pull on a child's arm, as a parent is rushing through his/her shopping. If the radius is dislocated, the child will not move the arm (Fig. 7.20).

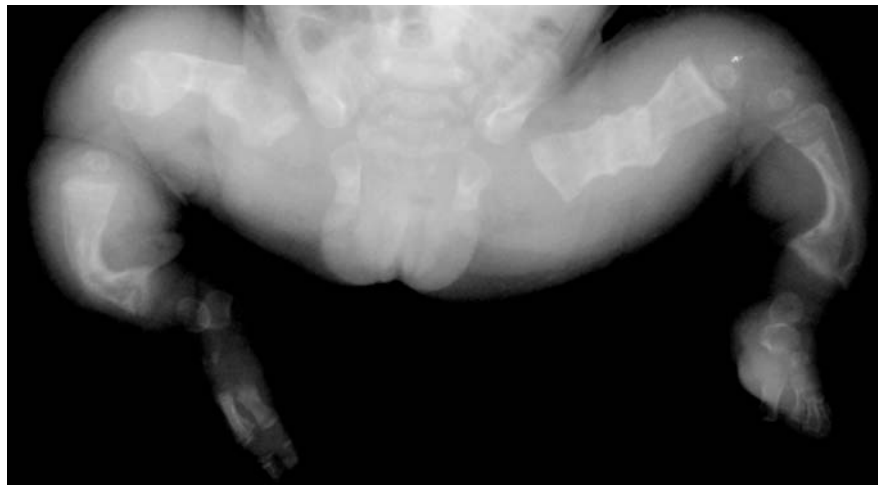

Fig. 7.18. Osteogenesis imperfecta
This newborn shows bowed and fractured lower extremities. Note the "crinkling" of the left femur. These fractures occurred in utero and resulted from unusually fragile bones due to a congenital defect in collagen architecture

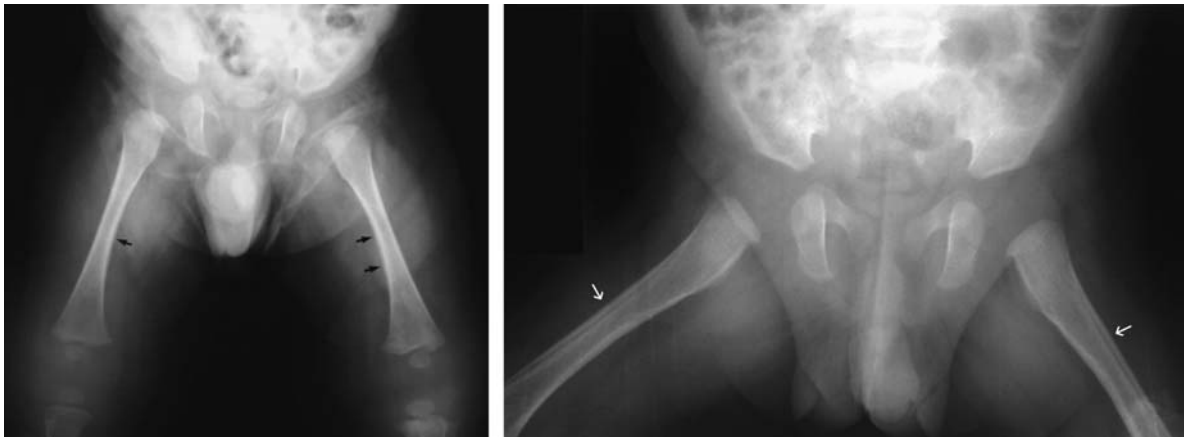

a **b**

Fig. 7.19. Appositional new bone formation
a This frontal view of a 2-month-old child shows what could be mistaken for pathological periosteal reaction on medial aspects of both the femora (*arrows*). This normal variant can be present up to 6 months of age and reflects rapid bone growth rather than a disease state
b Another example, more obvious, in a normal 5-month-old

The radius must be in direct relationship to the capitellum, regardless of the position of the elbow. The fat-pad sign is an especially valuable clue in trauma (Fig. 7.21).

- Stress fractures, although unusual, may occur in the proximal tibia, usually following extreme exercise (Fig. 7.22).
- A toddler's fracture, seen in children between the ages of 9 months and 3 years, is an oblique, nondisplaced fracture of the distal tibial shaft (Fig. 7.23).
- The slipped capital femoral epiphysis is a Salter I fracture of the femoral head (Fig. 7.24). This injury is found in adolescents, and there is a significant (25%) incidence of bilaterality.
- Metaphyseal corner fractures, multiple injuries, and, particularly, posterior rib fractures, are clues to child abuse (discussed below under "Nonaccidental Injury").

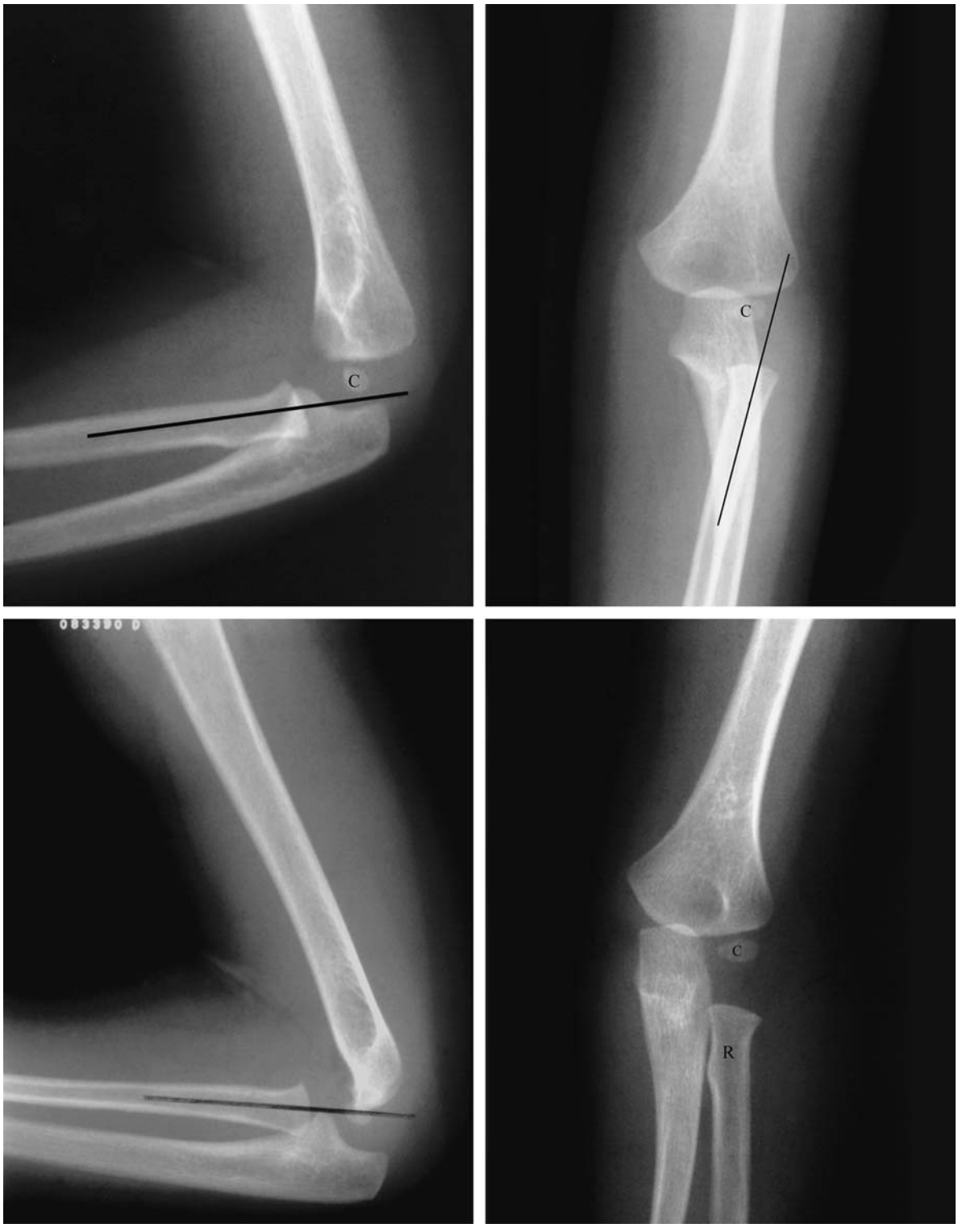

Fig. 7.20. "Nursemaid" or "supermarket" elbow
a, b Lateral and frontal elbow films with a line drawn through the shaft of the radius show that the radius does not articulate with the capitellum (*C*). This dislocation is caused by a sharp pulling motion, caused in the old days by a nursemaid and in more modern times by a parent or guardian pulling a child. It often occurs in the supermarket, hence the name
c, d Normal alignment. *R*, radius; *C*, capitellum

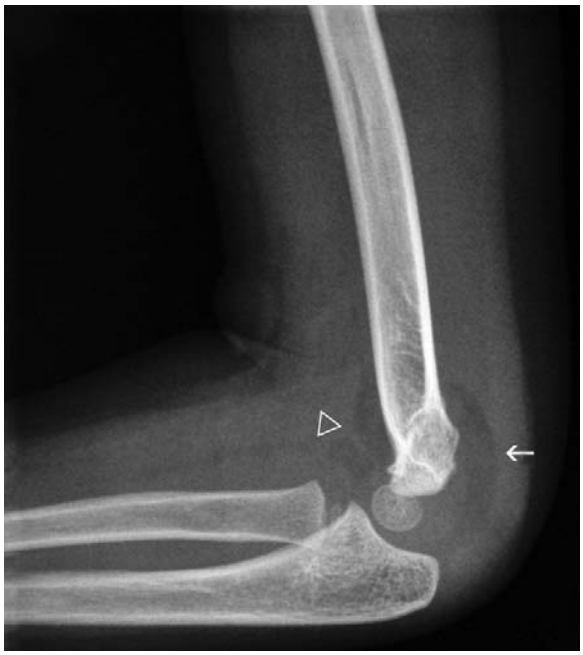

Fig. 7.21. Positive fat-pad sign
The posterior fat pad (black) is displaced so that it is now visible (*arrow*). This reflects joint effusion and, in the setting of trauma, is considered an indirect sign of fracture. There is also a large anterior fat-pad sign (*arrowhead*). This is less specific for a fracture

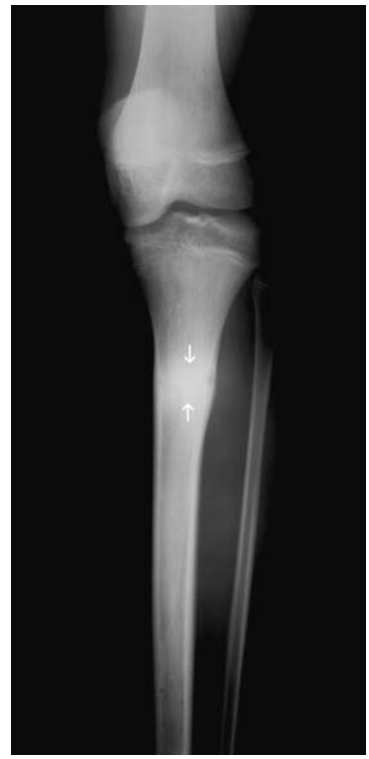

▲

Fig. 7.22. Stress fracture
Frontal radiograph of the tibia shows a zone of sclerosis (*arrows*) along the proximal shaft. There is also periosteal reaction

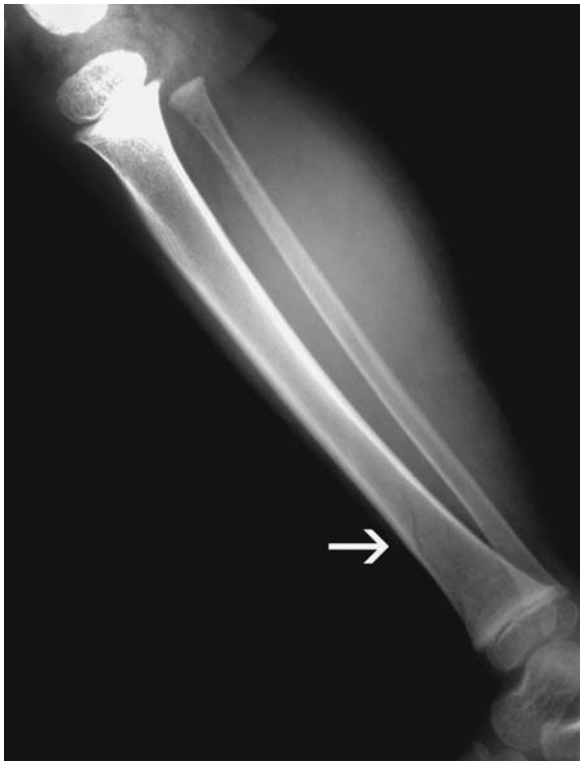

◀

Fig. 7.23. Toddler's fracture
An 18-month-old girl with a limp. This lateral view of the tibia shows a subtle oblique fracture (*arrow*). It was not seen in the frontal film (not shown)

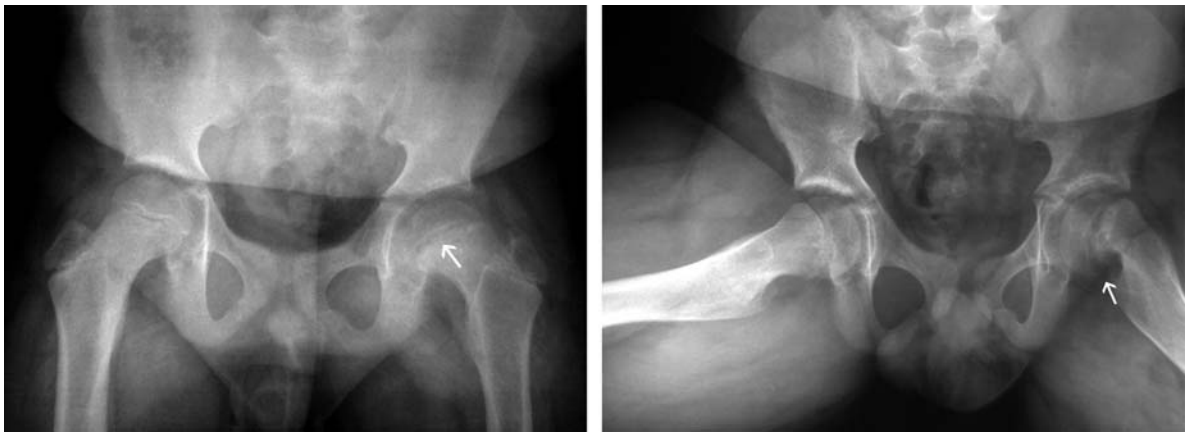

Fig. 7.24. Slipped capital femoral epiphysis
a This film of the hips in this teenager was taken in neutral position and shows asymmetry of the physis. The left physis appears wider (*arrow*), and the femoral head appears medially displaced. In all suspected cases of slipped capital femoral epiphyses, a frog-leg lateral film is taken
b Frog-leg lateral film shows complete separation of the left femoral head (*arrowhead*) and neck of the femur. This requires surgery – hip pinning

Cross-Sectional Imaging of Trauma

Suspicion of fracture on the plain film can be further investigated with CT. Some fracture dislocations are best evaluated with CT. It is also valuable in areas difficult to "see" with routine radiographs. These include the sacrum, pelvis, hips, and ankle (Fig. 7.25).

Where does MR fit in the work-up of skeletal trauma? MR is superb when one is interested in detecting injury to the growth plate or the formation of a cartilaginous bar crossing the growth plate (a bar may subsequently develop secondary to trauma and prevent further growth in that region; the entire bone can be deformed). MR is also indicated for osteochondritis dissecans, internal derangement of joints, and ligament and tendinous injury. This is especially true of knee injuries, where MR has revolutionized the work-up of trauma (Fig. 7.26). It is not unusual to find a lesion in the proximal tibia or distal femur which was not seen on plain film. This represents a bruise (or contusion) of bone and often can explain the patient's symptoms. It is of low signal on T1-weighted and high signal on T2-weighted sequences.

Even ultrasound has a place in the work-up of trauma. Radiopaque foreign bodies such as metal or glass are easily demonstrated by plain films. Sonography is excellent in finding and guiding the removal of nonopaque soft tissue foreign bodies. CT may also be good in this regard, although sonography is easier, quicker, involves no radiation, and is less costly.

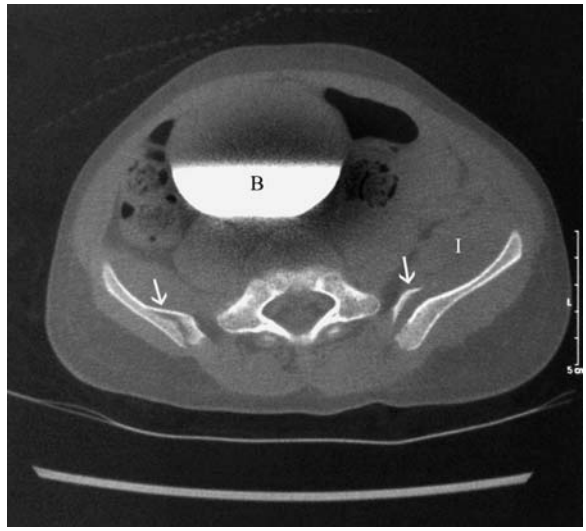

Fig. 7.25. Fractures on CT
CT of the pelvis in a motor vehicle accident victim shows subtle fractures of both iliac bones (*arrows*). Notice enlargement of the left iliacus (*I*) muscle from hematoma. The bladder (*B*) is half filled with contrast

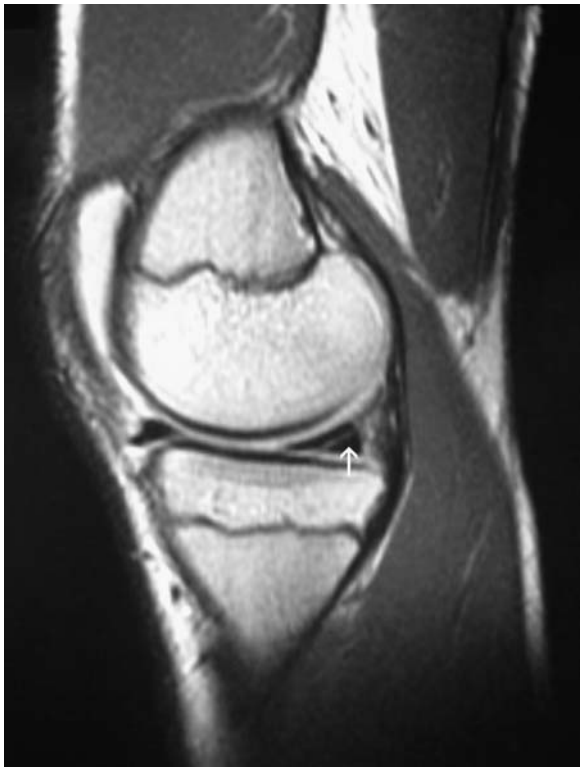

Fig. 7.26. Sagittal proton density image of the knee shows linear tear in the posterior horn of the medial meniscus extending to the inferior articular surface *(arrow)*

Table 7.7. Specificity of radiologic findings in non-accidental injury. (From [8] with permission)

High specificity
Classic metaphyseal lesions
Rib fractures, especially posterior
Scapular fractures
Spinous process fractures
Sternal fractures
Moderate specificity
Multiple fractures, especially bilateral
Fractures of different ages
Epiphyseal separations
Vertebral body fractures and subluxations
Digital fractures
Complex skull fractures
Common but low specificity
Subperiosteal new bone formation
Clavicular fractures
Long bone shaft fractures
Linear skull fractures

Table 7.8. Nonosseous manifestations of child abuse

Intracranial
Subdural hematoma (acute or chronic)
Brain contusion
Generalized hypoxic–ischemic injury
Axonal shearing injury
Thoracic
Pulmonary/cardiac contusion
Pneumothorax/hemothorax
Abdominal
Solid visceral laceration/contusion
Traumatic pancreatitis
Bowel injury
Duodenal hematoma
Bowel perforation

Nonaccidental Injury (Child Abuse, Battered Child)

The radiologist may be the first person to suggest the diagnosis of nonaccidental injury (child abuse, battered child syndrome, shaken baby syndrome). Since the infant is not very mobile during the first year of life, inflicted injury should always be considered in any infant who has a fracture without a plausible mechanism of injury. Although any fracture which is inconsistent with the given clinical history should be suspect, some particular types of fractures are considered highly specific for child abuse (Table 7.7). These include multiple fractures in different stages of healing (indicating multiple episodes of inflicted injury), metaphyseal corner ("bucket-handle") fractures, and posterior rib fractures (Fig. 7.27). In abused infants, one may also see periosteal new bone in the absence of fracture; this should not be confused with the normal appositional new bone formation in infants between 2 and 6 months of age.

In cases of suspected child abuse, the search for skeletal injury is performed with a full skeletal survey consisting of plain radiographs of the skull, spine, pelvis, thorax, and extremities. In cases of uncertainty or for follow-up, a nuclear medicine bone scan can be helpful.

Many nonosseous abnormalities may also be seen on radiological studies of children with nonaccidental injury (Table 7.8). Some of these are discussed elsewhere in this text.

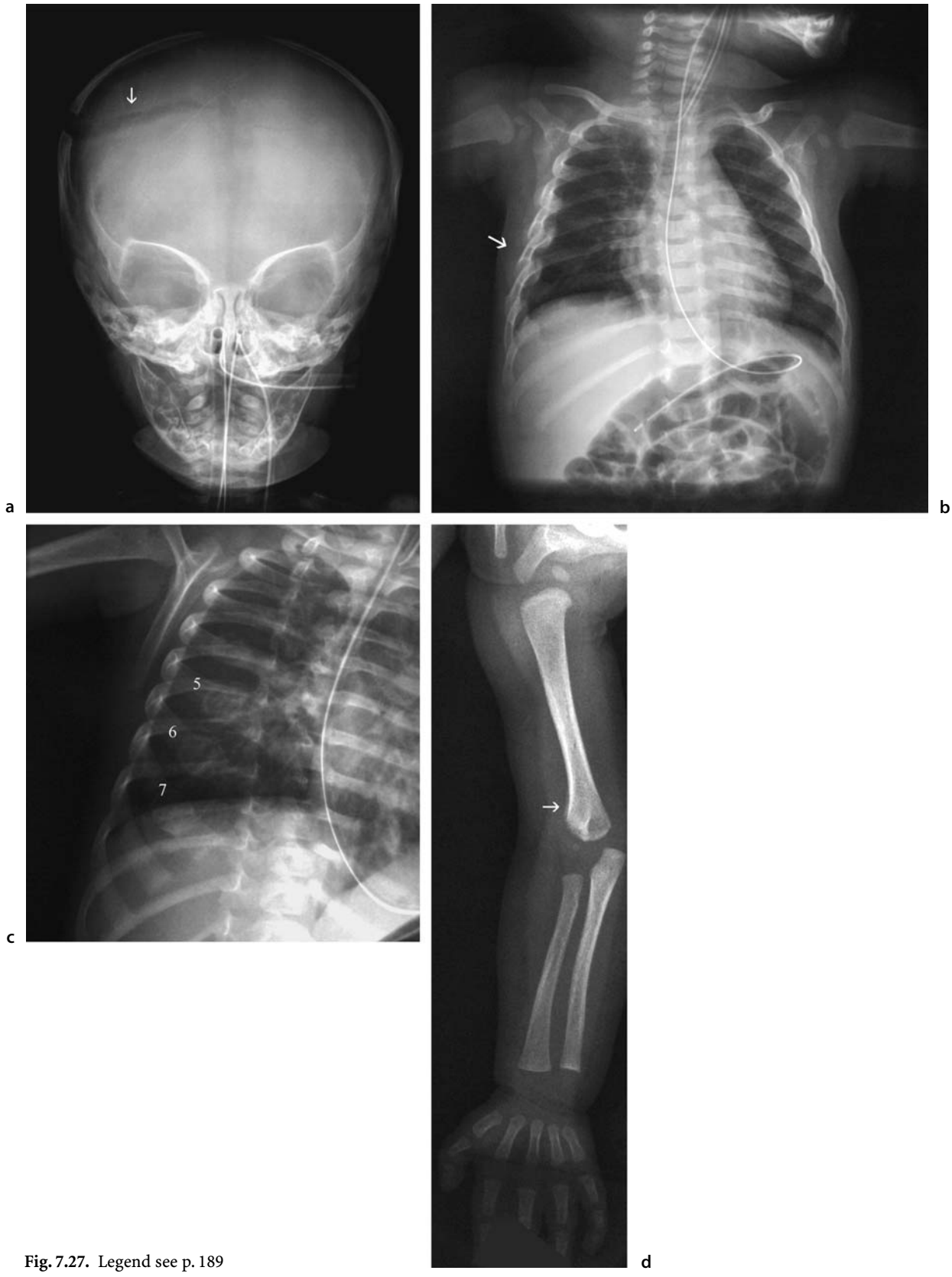

Fig. 7.27. Legend see p. 189

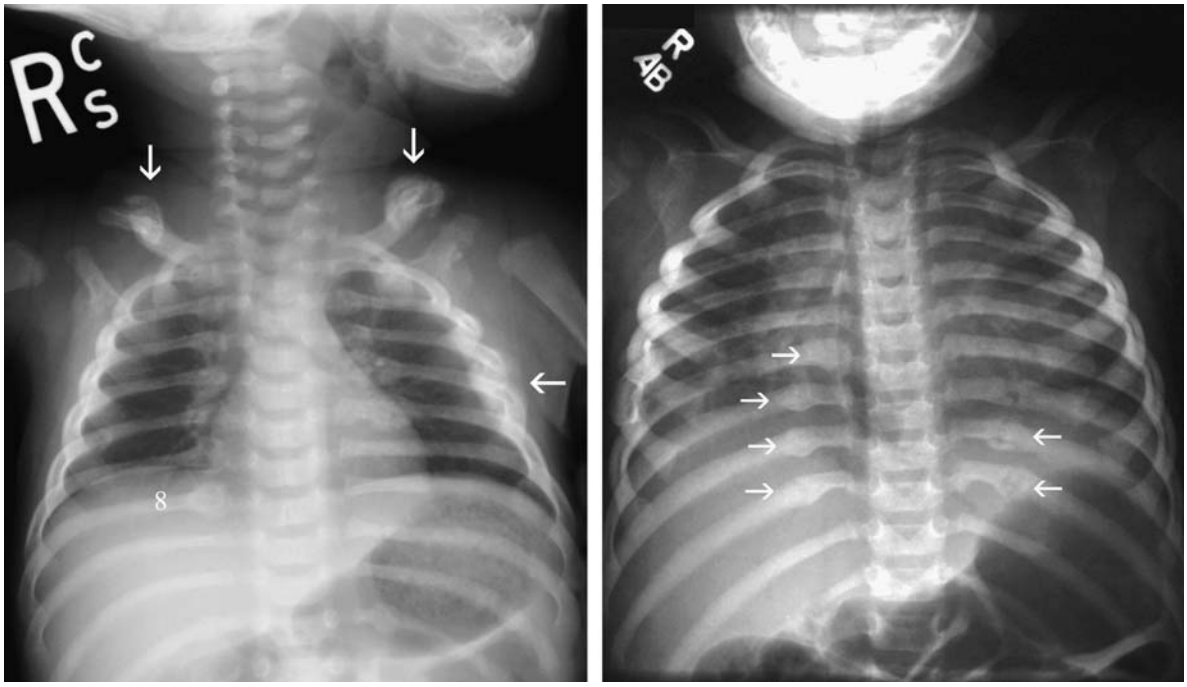

e f

Fig. 7.27. Child abuse
a Frontal view of an infant's skull shows a diastatic right parietal fracture (*arrow*)
b, c Frontal radiograph of the same patient's chest (**b**) and oblique view of the right ribs (**c**) demonstrate callus around multiple healing right rib fractures. Notice how the oblique view shows the healing fractures of ribs 5–7 particularly well
d The same patient's right upper extremity radiograph shows periosteal reaction at the distal humeral metaphysis secondary to a corner fracture
e Chest radiograph in another abused infant reveals multiple healing fractures (callus) in both clavicles (*downward arrows*), left lateral ribs (*horizontal arrow*), and posterior ribs including the right eighth rib (*8*)
f Chest radiograph of a different abused infant shows multiple bilateral posterior rib fractures with callus (*arrows*)

Developmental Dysplasia of the Hip

Developmental dysplasia of the hip occurs in about 1 in every 1000 neonates. Girls are more prone to this disorder than boys, with the left hip involved more frequently than the right. For years radiographic screening has been the best that we could do; instability is not diagnosed, but the persistently dislocated hip is readily seen. The hip is displaced laterally and posteriorly. On plain films lateral displacement of the femoral neck implies that the femoral head (not visible in young infants) is not covered by the acetabulum (Fig. 7.28). Currently, hip sonography is used to diagnose the unstable hip (Fig. 7.29). The hip may be scanned in neutral, flexed, adducted, and abducted positions with and without stress, and pre- and post-treatment evaluations can be made. CT and MRI may be used for evaluating the hip in plaster.

Osteomyelitis

Osteomyelitis is usually acquired via hematogenous spread of organisms to the bone. Since the greatest blood supply is in the metaphysis, this region has a predilection for osteomyelitis. A small focus of these purulent organisms causes abscess formation in the marrow with an increase in local pressure, followed by local deossification and destruction of the cortex (Fig. 7.30). The epiphysis is usually spared because of the tight adherence of the periosteum to the metaphysis. However, the shaft of the bone is readily permeable to infection as the periosteum is loosely adherent, and organisms may ascend the shaft of the bone or the medullary cavity.

Deep puncture wounds may also cause osteomyelitis in children. One of the more common organisms introduced via a puncture wound is *Pseudo-*

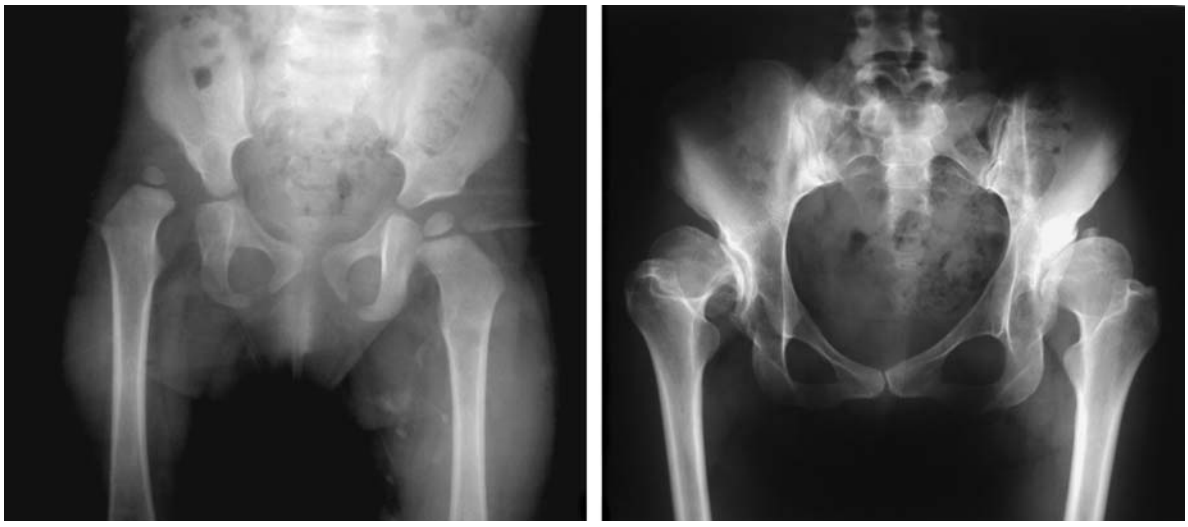

a b

Fig. 7.28. Dislocated hip on radiograph
a AP view of an infant's pelvis shows lateral displacement of the right femoral neck and femoral head. The involved femoral head ossification center is slightly smaller than on the normal left side
b A 31-year-old with congenital bilateral hip dislocation. There is pseudoacetabulum formation and coxa magna

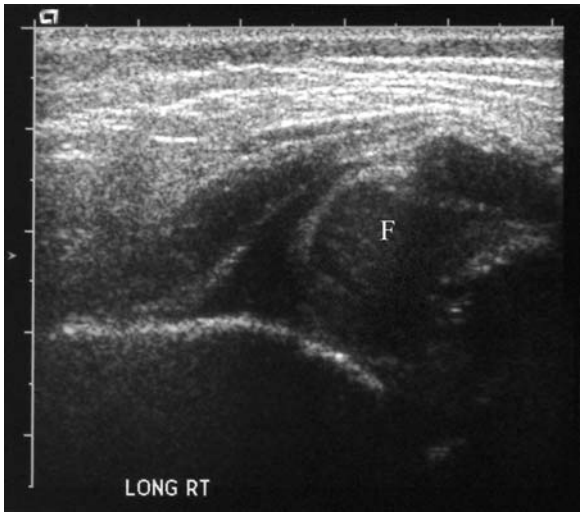

Fig. 7.29. Longitudinal sonographic view of a dislocated infant hip.
The femoral head (*F*) is not seated in the acetabulum, as it should be (compare with Fig. 7.11)

monas, while staphylococcal osteomyelitis is most common in hematogenously spread disease (see Fig. 7.14). Patients with sickle cell disease are susceptible to *Salmonella* osteomyelitis.

The clinical symptoms precede the radiographic findings by 7–14 days. For this reason a radioisotope study is frequently more helpful in the early diagnosis of acute osteomyelitis. The proper study is a "three-phase" bone scan with ^{99m}Tc-labeled diphosphonate. The initial phase is the blood pool and the second phase is soft tissue segment. These are obtained immediately after injection. Positive results mean increased blood flow and soft tissue infection (cellulitis). The delayed scan is the third phase, and is positive in osteomyelitis and septic arthritis (Fig. 7.31).

If the diagnosis is made promptly and treatment is successful, healing usually occurs without significant growth disturbance. However, prolonged infection prior to the diagnosis or severe involvement of a joint – septic arthritis – can have long-term sequelae.

The radiographic findings of acute, healing, and chronic osteomyelitis are summarized below:

- Acute osteomyelitis (0–2 weeks)
  - Soft tissue swelling initially
  - Loss of cortical margin
  - Focal demineralization of bone
  - Faint periosteal new bone formation (7–14 days after onset)
- Healing phase (>4 weeks)
  - Destroyed bone with irregular areas of sclerosis and lysis
  - Sequestrum: dense devascularized bone fragment within an area of pus amid granulation tissue

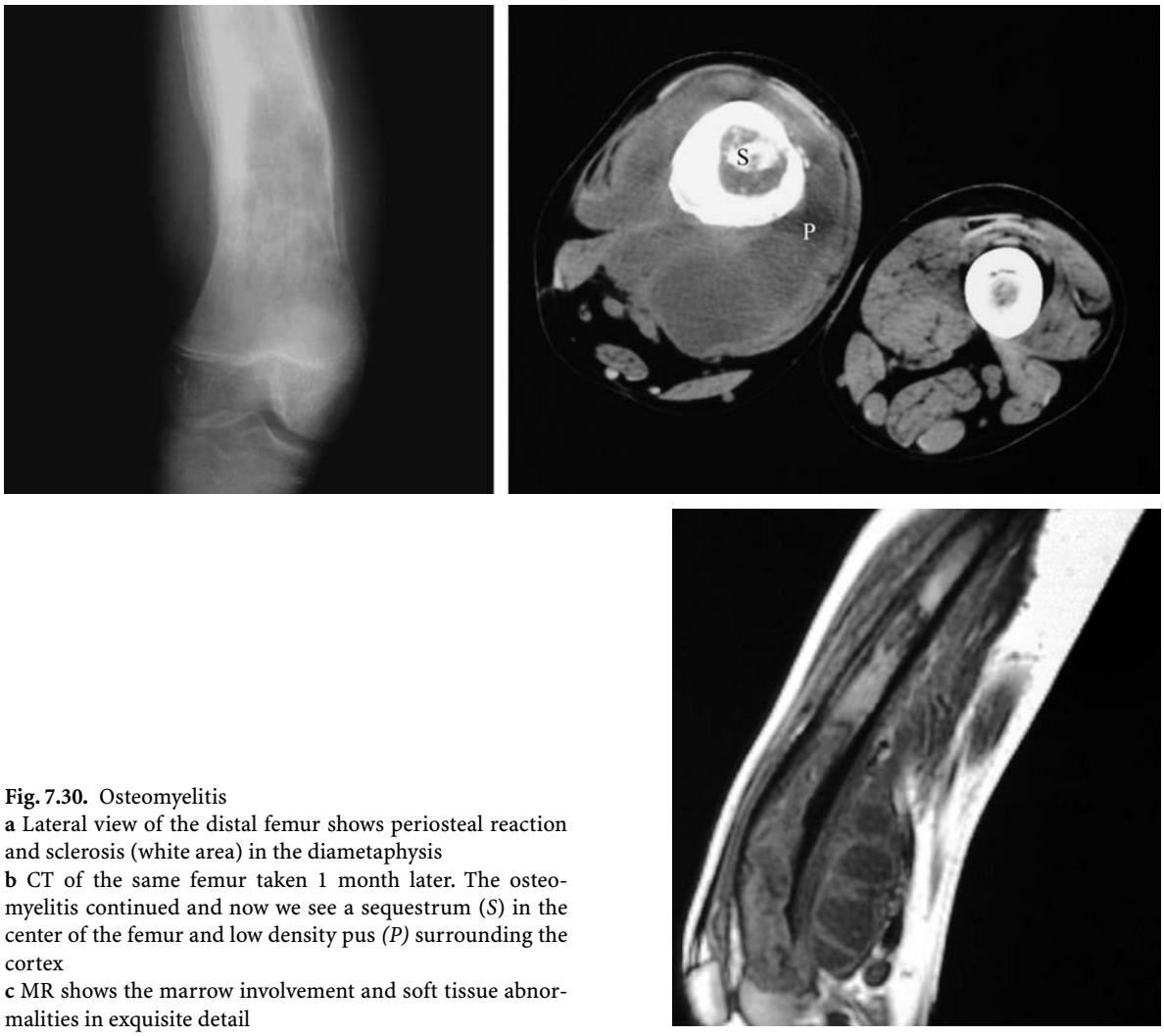

Fig. 7.30. Osteomyelitis
a Lateral view of the distal femur shows periosteal reaction and sclerosis (white area) in the diametaphysis
b CT of the same femur taken 1 month later. The osteomyelitis continued and now we see a sequestrum (*S*) in the center of the femur and low density pus *(P)* surrounding the cortex
c MR shows the marrow involvement and soft tissue abnormalities in exquisite detail

  - Involucrum: peripheral shell of supporting bone laid down by the periosteum around the old disease
- Chronic osteomyelitis (either unusual localized osteomyelitis or improperly treated)
  - Diffuse bone production with little or no destruction
  - Occasional draining sinus or lucent area in the midst of the sclerotic bone

MR has a definite role in the work-up of osteomyelitis, especially in the chronic and indolent form (Fig. 7.32). MR is especially useful in septic arthritis as it can demonstrate cartilage loss, joint effusion, synovial hypertrophy, and bone destruction. When the radiographic or scintigraphic findings are equivocal or hard to evaluate, MR is also useful. This is especially true when dealing with certain "flat" bones that are hard to visualize on plain radiographs such as the sternum, scapula, and pelvis (Fig. 7.33).

Certain children are at high risk for osteomyelitis and its complications. These include neonates who have a high incidence of both β-streptococcal osteomyelitis and septic arthritis. In neonates osteomyelitis is frequently multifocal. Patients with sickle cell disease have a high incidence of *Salmonella* osteomyelitis, which is also frequently multifocal, but the most common organism in bone infection of patients with sickle cell disease is *Staphylococcus.* Children with immune deficiencies such as chronic granulomatous disease and agammaglobulinemia are prone to multifocal osteomyelitis or osteomyelitis in unusual areas such as the iliac bones; this is frequently due to unusual organisms (Fig. 7.33).

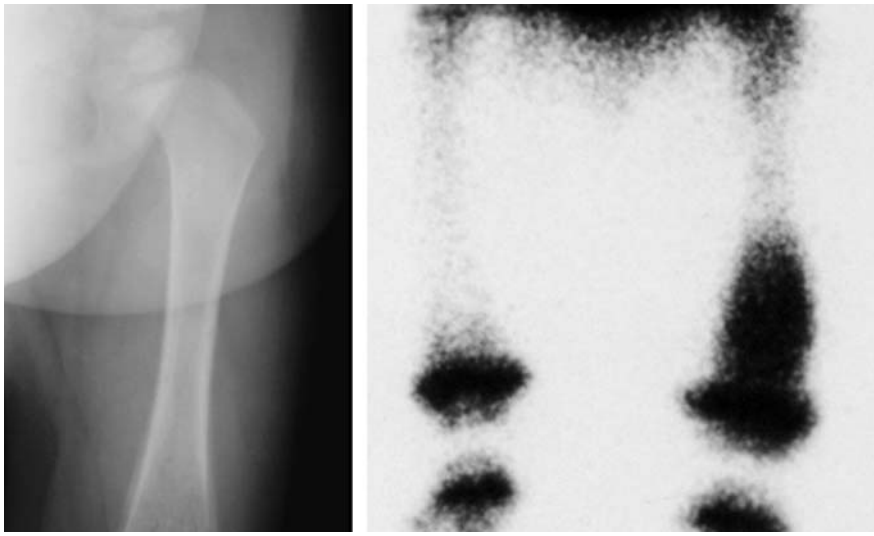

a b

Fig. 7.31. Osteomyelitis
a Left femur with distal periosteal reaction
b Anterior view of the femora on 2-h delayed images of ^{99m}Tc-labeled diphosphonate scan reveals increased uptake in the distal left femur

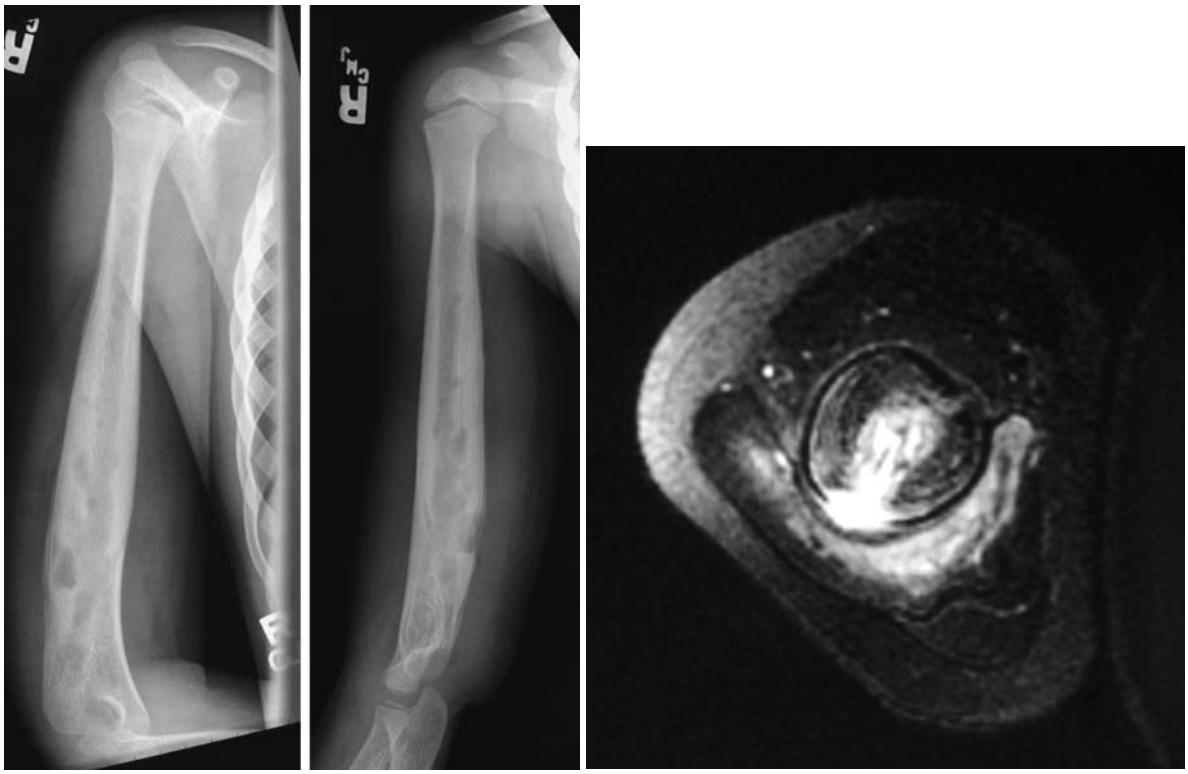

a,b c

Fig. 7.32. Chronic osteomyelitis
a, b Plain radiographs show dense cortical thickening and areas of lucency in the medullary cavity of the distal humerus
c Axial T2 fat-saturated MR demonstrates a sinus tract (white) through the posterior cortex of the bone and adjacent soft tissue inflammation

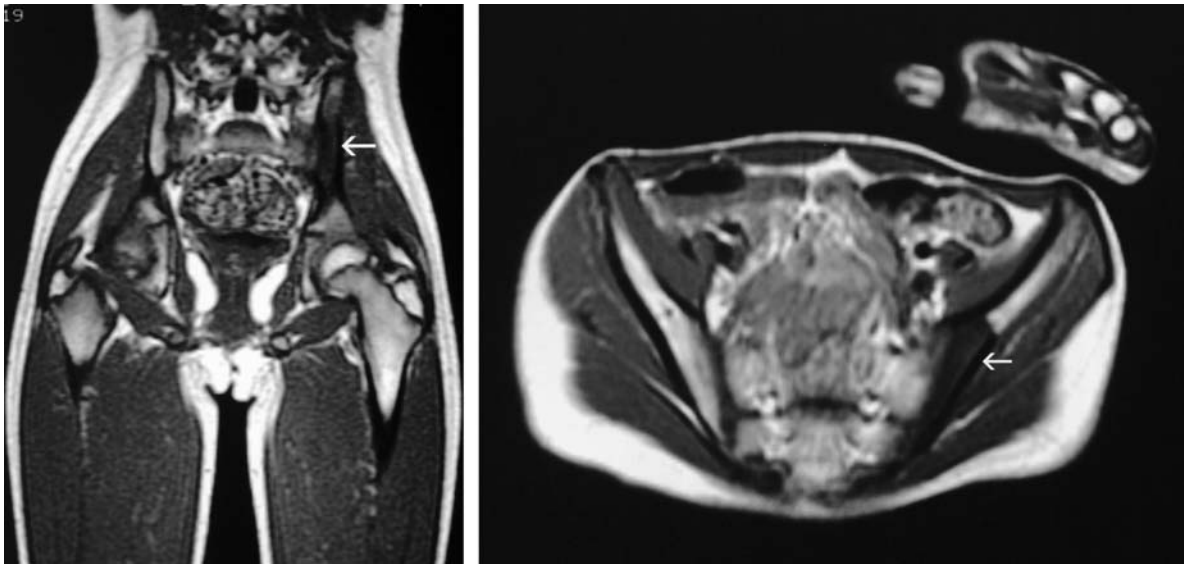

Fig. 7.33. MR of osteomyelitis
a Coronal T1 scan shows diminished signal in the left iliac bone marrow (*arrow*)
b This is confirmed in axial T1 images (*arrow*)

Bone Infarct

Bone infarcts are seen in a number of disorders, including sickle cell anemia, pancreatitis, Gaucher's disease, and steroid therapy. When it is idiopathic and affects the femoral head, it is called Legg-Calvé-Perthes disease (Fig. 7.34). Plain films are not able to differentiate infection from infarction in sickle cell disease, but in other disorders dense bone that eventually fragments is typical for infarction. MR is especially well suited for the diagnosis of infarction since it is a marrow disorder.

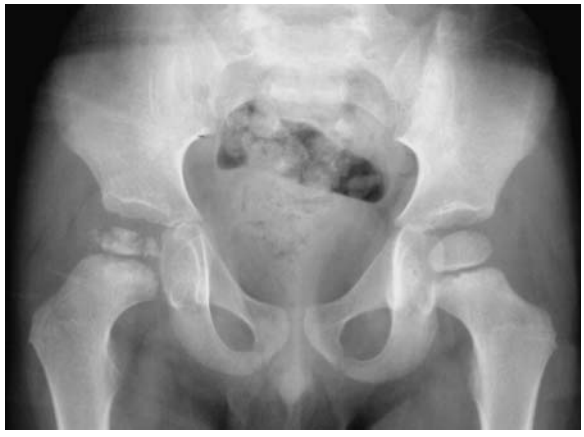

Fig. 7.34. Legg-Calvé-Perthes disease
Frontal view of the hips reveals fragmentation of the right capital femoral epiphysis

Metabolic Disorders

The growing skeleton is susceptible to many nutritional deficiencies and reflects the adequacy of the homeostatic mechanisms (gastrointestinal tract, liver, kidneys) for handling calcium. Two of the more common disturbances in this category are rickets and hyperparathyroidism. Both diseases are usually secondary to chronic renal disease.

Rickets. In rickets there is a deficiency of vitamin D and, therefore, poorly mineralized osteoid tissue. The trabeculae are fuzzy and irregular and certainly not as distinct as those in normal bone. The metaphyseal regions are irregular, with cupping and fraying of the bones (see Fig. 7.15). The apparent distance between the metaphysis and the ossification center is greater than normal, as there is an abundance of uncalcified cartilage. Despite all our advances, the most common cause of rickets in the world today is still nutritional vitamin D deficiency. However, in most medical centers the most common cause of rickets is chronic renal disease since the kidney cannot hydroxylate vita-

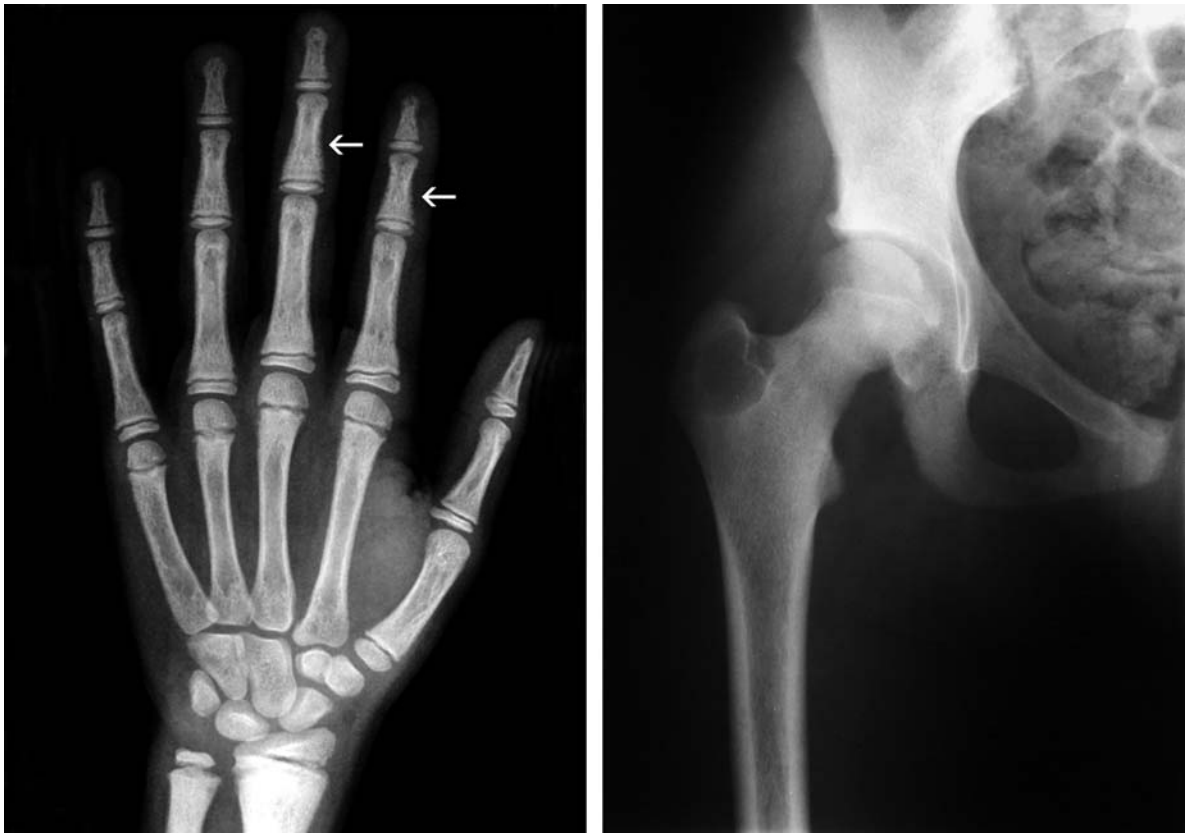

Fig. 7.35. Hyperparathyroidism
a Hand showing sclerosis at wrist and subperiosteal resorption of the radial aspects of the middle phalanges (*arrows*)
b The cortical margins of the neck (both medial and lateral) of the femur are not visible due to bone resorption (compare to neck of femur in Fig. 7.1). Also note the lytic lesion in the greater trochanter. This brown tumor is the result of accumulation of fibrous tissue and giant cells and has all the characteristics of a benign bone lesion. A sclerotic border and the clear zone of demarcation are evidence of its benignity

min D. Children with liver disease also may manifest rachitic changes because of the liver's role in vitamin D hydroxylation. In premature infants, the entire process of absorption and conversion of calcium into bone is impaired. Rickets of prematurity in this population is demonstrated by bright cortical bone and washed-out medullary cavity. The bones are not cupped or frayed because the infants are not growing.

Hyperparathyroidism. In this disorder bone resorption far exceeds bone proliferation (osteoclasis far exceeds osteoblastic activity), and as a result the bone is resorbed. Radiographically one sees subperiosteal bone resorption most often along the diaphyses of the phalanges (Fig. 7.35), at the distal clavicles, and along the lamina dura of the teeth. Diffuse demineralization and focal lucent lesions (brown tumors) are other signs of this disorder (Fig. 7.35). In chronic renal disease, calcium loss through the urinary system is usually so great that the parathyroids must draw calcium into the circulation from the existing stores in bones to maintain a normal calcium–phosphorus ratio.

Lead Intoxication. Heavy metals such as lead or bismuth stimulate increased calcification of cartilage, which causes increased density in the metaphyseal regions. The density is found in both large, weight-bearing bones as well as smaller ones (e.g., tibia and fibula) and in other areas where longitudinal bone growth is occurring most rapidly (Fig. 7.36). Remember: the ulna and fibula are the key bones for determining lead intoxication. The femur, humerus, and radius often have dense metaphyseal bands normally, but never the ulna and fibula. The finding of "lead lines" correlates with chronicity of exposure and not with blood lead levels or acute symptoms.

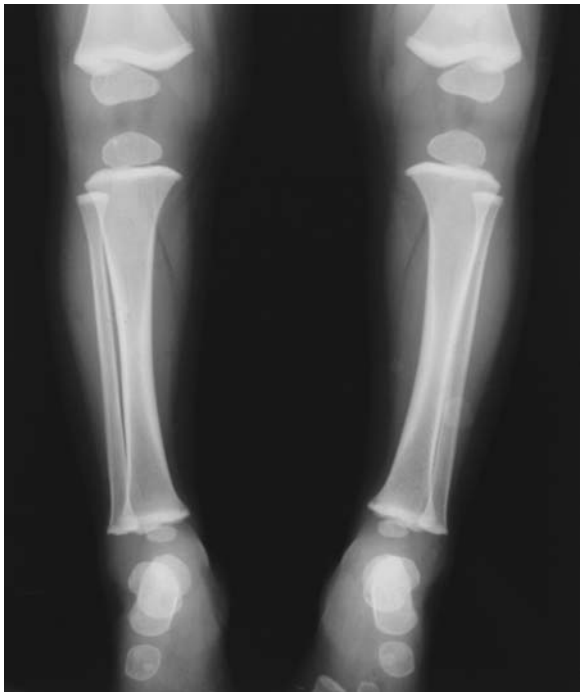

Fig. 7.36. Chronic lead intoxication
The metaphyses of all the bones, especially the fibula, are sclerotic. This is typical of heavy metal ingestion. While the femur, tibia, and humerus often have equivocal density in the metaphyses, the ulna and fibula should not be dense at all. Consequently, any metaphyseal density noted in the latter two bones should raise the suspicion of heavy-metal intoxication.

Bone Tumors

Malignant bone tumors are not common in children, but benign bone lesions are frequently seen. Some of the common benign and malignant lesions are described below.

Benign Lesions

Simple bone cyst is a lucent defect at the metaphysis of long bone near but not touching the physeal line. It is most often found in the humerus, femur, or tibia (Fig. 7.37). *Fibrous cortical defect* is a well-circumscribed, elliptical lucent lesion in the cortex at the end of a long bone, particularly the femur or tibia; the larger ones are called nonossifying fibromas. *Osteochondroma* (exostosis) is a protuberant growth of bone from the metaphysis that has contiguous cortical margins (Fig. 7.37). *Enchondroma* is a cartilaginous, cyst-like lesion often seen in the phalanges and rib (Fig. 7.37). *Osteoid osteoma* is a sclerotic lesion with a central lucent nidus. It occurs in many places, including the long bones and spine.

Malignant Lesions

Osteogenic sarcoma occurs mostly during adolescence, frequently in the long bones; this is the most common primary malignant tumor in the pediatric age group, and it is metaphyseal and bone-producing. *Ewing's sarcoma* is the second most common tumor in pediatric age group; it is more common than osteogenic sarcoma in those under 10 years of age (Fig. 7.38). This lesion may occur in any bone in the mid-diaphyseal region and is permeative. There is a large soft tissue component. It is frequently found in flat bones, such as those of the pelvis. Systemic malignancies of bone such as leukemia, neuroblastoma (metastatic), retinoblastoma (metastatic), and hepatoblastoma (metastatic), are important in the differential of permeative lesions. The appearances of these four diseases plus Ewing's sarcoma and osteomyelitis are all similar and frequently cannot be specifically diagnosed by X-ray.

The radiologist must decide whether the lesion is benign or malignant. Clear signs of a benign lesion include sharp demarcation between the lesion and the normal bone, a sclerotic margin around the lesion, and a nonaggressive pattern of growth. The characteristics most often associated with a malignancy include an accompanying soft tissue mass, periosteal reaction, an indistinct zone between the normal and abnormal bone – an indistinct zone of demarcation – and permeative, destructive changes in the bone (see Fig. 7.38). Plain film radiography is usually adequate to diagnose most benign tumors. Sometimes CT can add diagnostic information that can be helpful, such as in osteoid osteoma, where location of the nidus is critical for operative management. While plain film is still quite reliable for predicting the benign or malignant nature of lesions, MR is the modality of choice to define the extent of the abnormality once a malignant bone lesion has been suggested. The extent of the lesion means defining cortical and intramedullary invasion, epiphyseal, joint space, ligamentous, tendinous, and nerve bundle involvement. MR evaluation aids in the decision to perform a limb salvage procedure or an amputation and is helpful in following response to chemotherapy. Remember, however, that histological diagnoses can only be suggested; only a biopsy can result in a firm diagnosis.

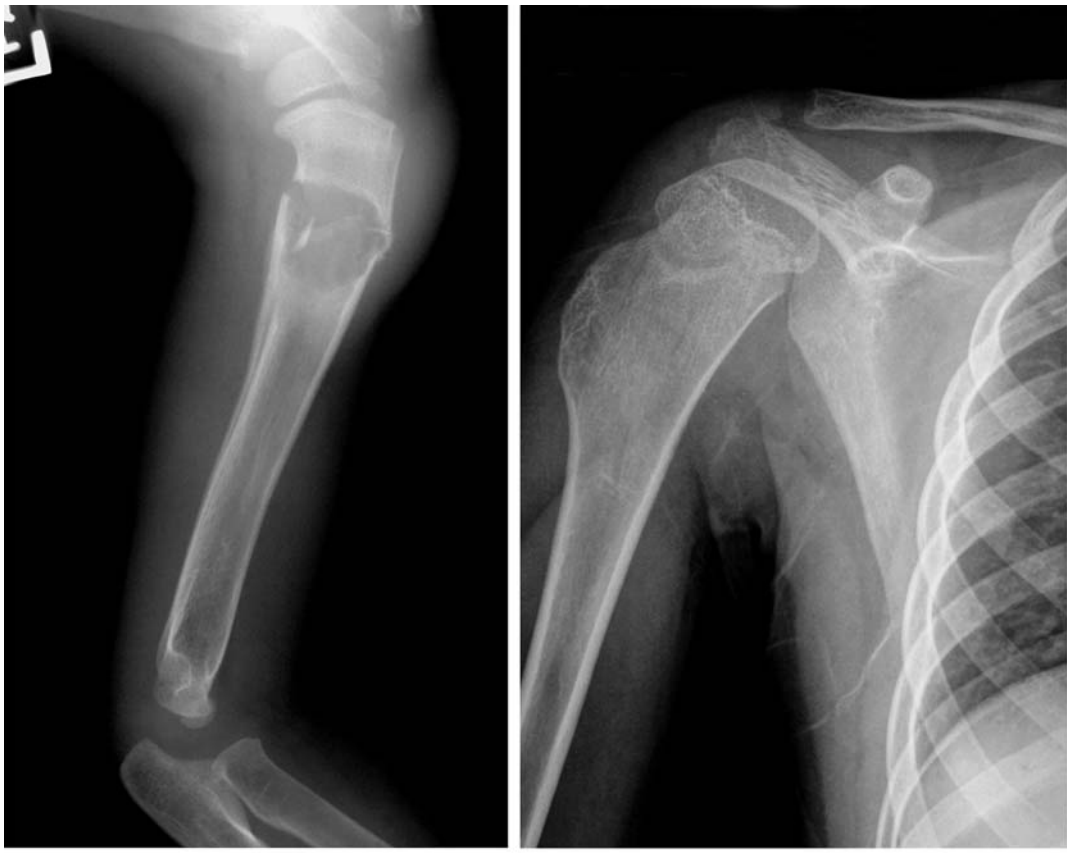

a b

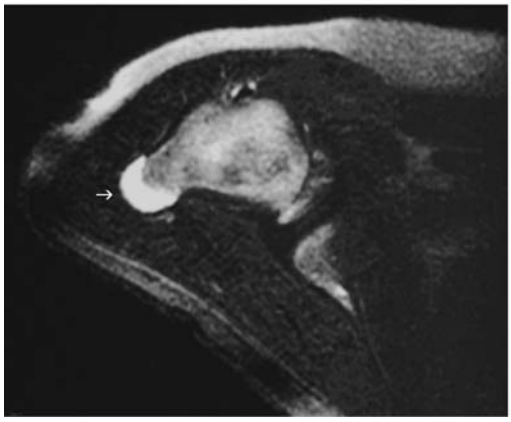

c

Fig. 7.37. Benign bone lesions
a Simple bone cyst. The proximal humeral lesion is well demarcated and is lucent. There is a pathologic fracture through the lesion. A "fallen fragment" of bone is seen within the cyst cavity
b, c Osteochondroma. The plain film (**b**) shows a broad-based lesion from the proximal humeral metaphysis. The medullary cavity of the lesion is contiguous with that of the bone. The axial T2-weighted MRI (**c**) shows the cap of cartilage (*arrow*) growing over the osteochondroma
d, e see p. 197

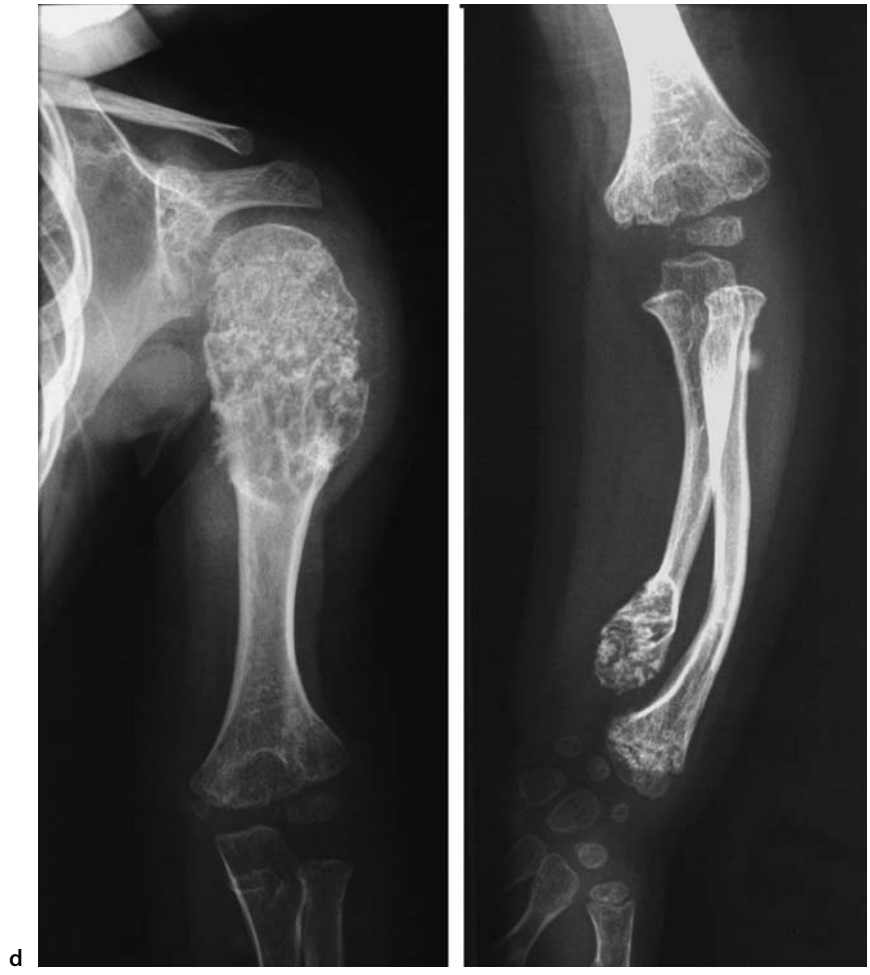

d e

Fig. 7.37 (*continued*).
d, e Enchondromas. This patient has multiple enchondromas on one side of her body, a condition known as Ollier's disease. These lesions contain multiple small, ring-like densities, a sign of cartilage. Notice the associated growth disturbance, foreshortening of the ulna, and bowing of the radius

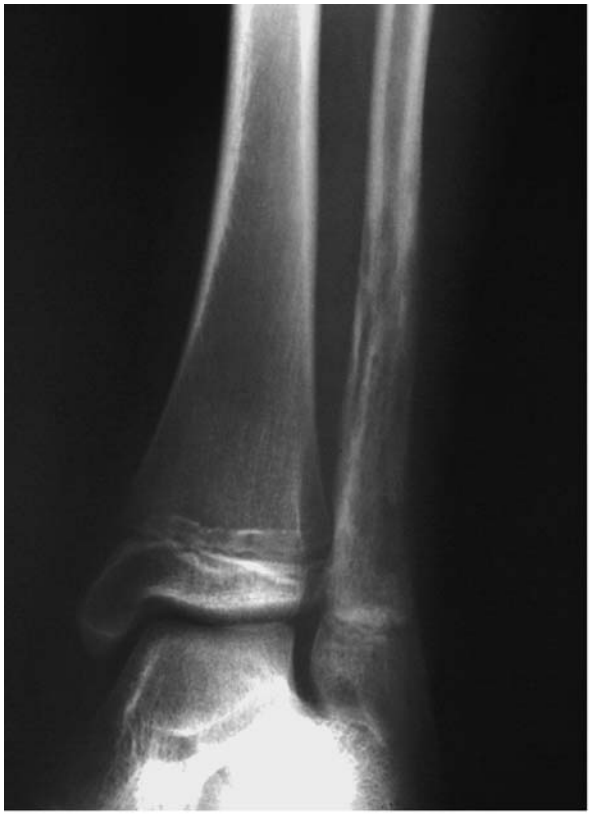

a

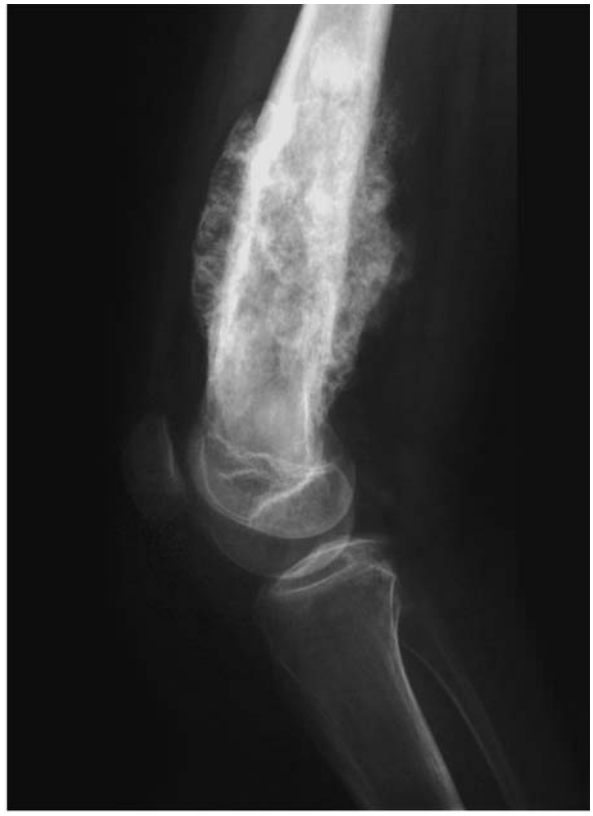

b

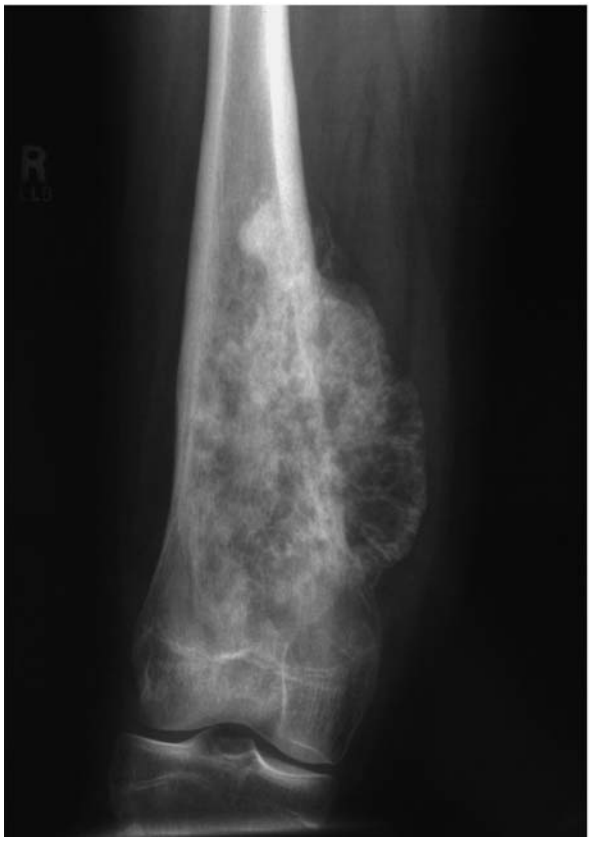

c

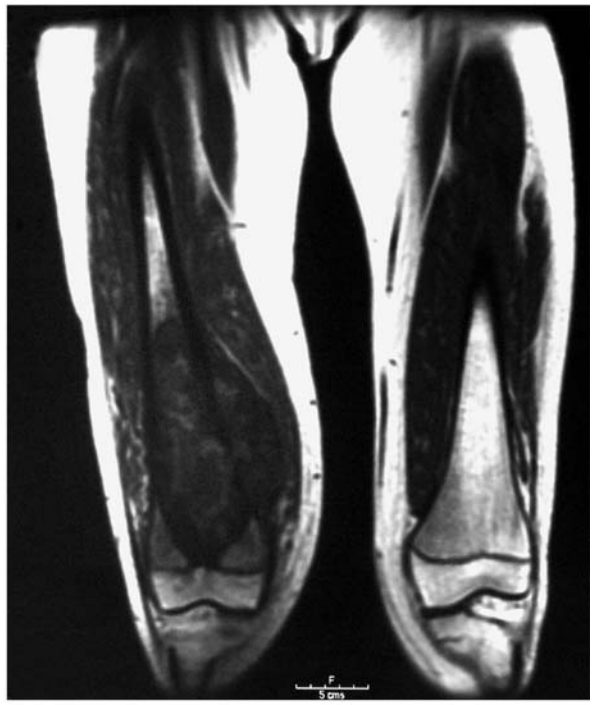

d

Fig. 7.38. Legend see p. 199

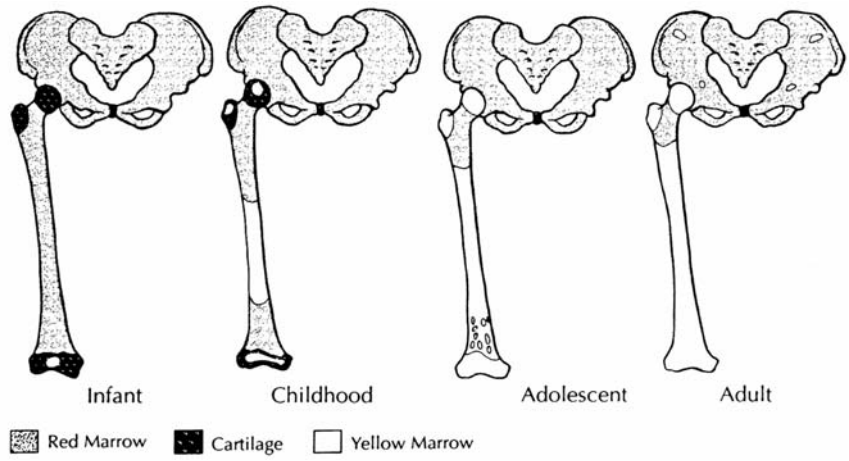

Fig. 7.39. Normal pattern of marrow conversion. (From [9] with permission)

Soft Tissue Tumors

The first examination in evaluating any soft tissue mass is still the plain film. When the patient has a palpable lesion, plain films can rule out underlying skeletal deformity, such as exostosis or callus formation overlying a fracture. Calcium, in the form of phlebolith in venous malformations or as periosteal reaction in myositis ossificans (calcifying hematoma and muscle damage after trauma), is an important clue. The plain film may also be helpful in detecting periosteal reaction, destruction, and remodeling of underlying bone.

MR is superb for the diagnosis of soft tissue tumors because it can rule out masses in virtually 100% of cases. Benign soft tissue masses tend to be sharply defined, encapsulated, and homogeneous with no peritumoral edema, while malignant masses tend to have indistinct margins, tend to be inhomogeneous, and have peritumoral edema in over 90% of cases. Specific diagnoses can be made for certain types of tumors if they contain fat or are vascular – lipoma, liposarcoma, hemangioma, arteriovenous malformation, pseudoaneurysm, ganglionic cyst, and hematomas. MR is also superb in detecting fluid levels inside certain lesions.

Marrow Disorders

It is important to be familiar with the normal pattern of conversion from hematopoietic to fatty marrow in the skeleton (Fig. 7.39). MR has become the modality of choice in evaluating diseases of the bone marrow. Because MR can separate fat from other tissues, it is excellent in appreciating the normal patterns of bone marrow distribution and the response of the marrow to the stress of disease. The disorders in which MR imaging is superb are:

- Myeloid hyperplasia (anemia, cyanotic heart disease)
- Marrow replacement disorders (leukemia, Gaucher's disease, neoplasms, lymphoma, metastases)
- Myeloid depletion (drugs, viral infections, radiation therapy toxins)
- Myelofibrosis (chemotherapy, radiation, infarction)

MR images the marrow by visualizing the fat content; fat-suppressing techniques aid in diagnosing infiltrative diseases. Marrow contains fat, and as the infant grows into adulthood, the amount of fat in the skele-

◀ **Fig. 7.38.** Malignant lesions
a Ewing's sarcoma. This radiograph of the distal fibula displays many of the findings of a malignant bone lesion. The fibula has disordered periosteal reaction both medially and laterally and the extensive bone destruction without a clear zone of demarcation between normal and abnormal suggests malignancy. The distal tibia is normal
b–d Osteogenic sarcoma. AP and lateral views of the distal femur (**b, c**) show dense, abundant periosteal reaction with a "sunburst" appearance and irregularity of the bony cortex. Coronal T1-weighted MR image (**d**) of the same patient demonstrates the extent of marrow involvement (compare to normal left side) as well as the soft tissue component of the tumor. The tumor extends distally to the growth plate but does not involve the epiphysis

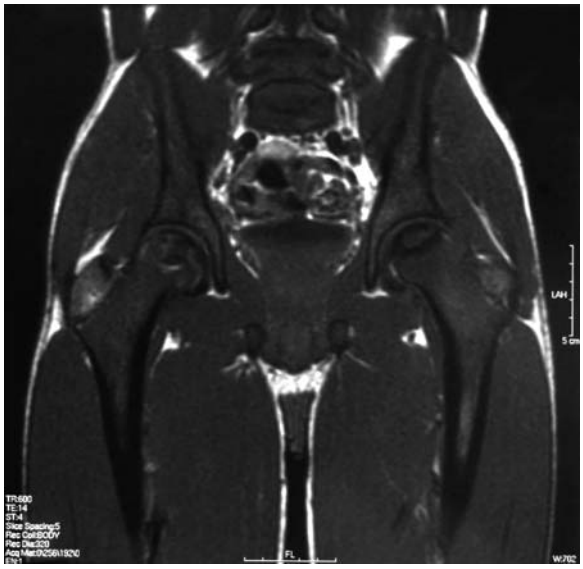

Fig. 7.40. Marrow evaluation with MR T1-weighted image of the pelvis in a 10-year-old with sickle cell anemia demonstrates diffuse myeloid hyperplasia. The marrow should be bright, but instead it is diffusely dark, including the epiphysis

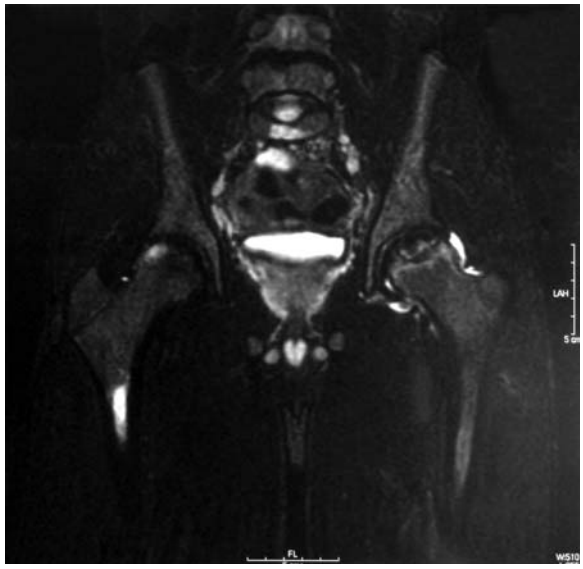

Fig. 7.41. Bone marrow infarction on MR
Fat-suppressed inversion recovery image of the pelvis in the same patient as Fig. 7.40 shows multiple bright areas of infarction, especially in the right capital femoral epiphysis and femoral diaphysis

ton increases and the amount of cellular (hematopoietic) marrow decreases. The marrow changes in the appendicular skeleton first and gradually moves centrally towards the axillary skeleton. Since the fatty marrow is bright and the cellular marrow is darker, abnormalities are easily recognized (Fig. 7.40). For example, the epiphysis almost always contains fatty marrow. Thus, an infarct in the epiphysis is readily detected (it is black on T1-weighted images and bright on fat-suppressed T2-weighted images; Fig. 7.41).

Arthritides

The most common cause of joint swelling in children is trauma. Usually the history is obtained, and the injury is short-lived. The second most common cause of "arthritis" is infectious – the septic joint. The common organisms in childhood are *Staphylococcus* and *Streptococcus,* but the ubiquitous gonococcus cannot be forgotten. Although radiographs may show evidence of joint effusion and swelling, ultrasound and MR are far more sensitive for effusion, synovial changes, and cartilaginous abnormalities. Appropriate clinical maneuvers such as tapping the joint are diagnostic. Less commonly, rheumatoid arthritis, hemophilic arthritis, and arthritides of collagen disease are found (Fig. 7.42).

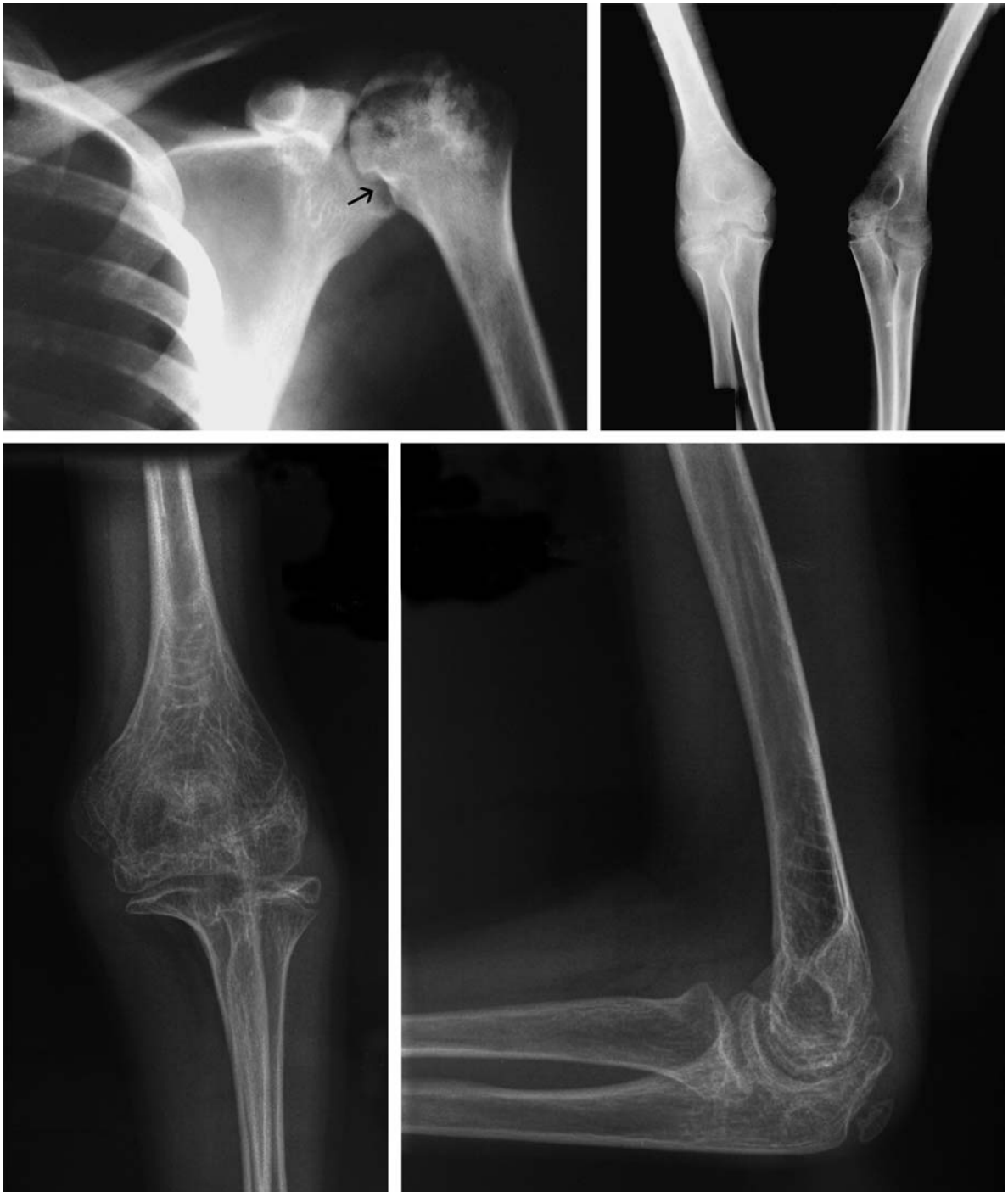

Fig. 7.42. Arthritides
a Hemophilia. Shoulder with bony erosions (*arrow*) and glenohumeral joint space narrowing. There is mixed sclerosis and lucency in the proximal humerus
b Hemophilia. There is overgrowth of the bones near the right elbow joint
c, d Late juvenile rheumatoid arthritis. AP and lateral views of this 8-year-old's elbow show periarticular osteopenia and loss of joint space. The articular surfaces are irregular

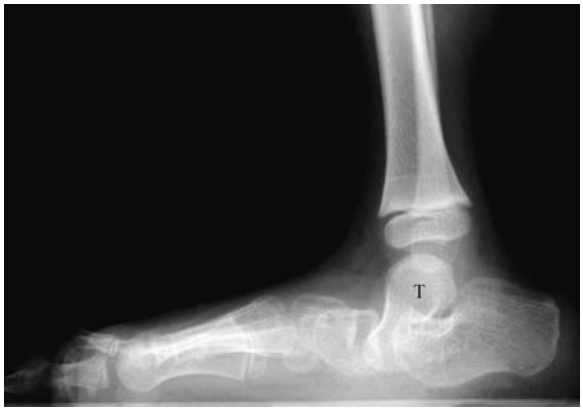

Fig. 7.43. Congenital vertical talus
The axis of the talus (*T*) should be more horizontally oriented and form a 120° angle with the calcaneus

Congenital Abnormalities

Congenital anomalies involve abnormalities of position (vertical talus; Fig. 7.43), number (polydactyly), size (achondroplasia; Fig. 7.44), and shape (proximal femoral focal deficiency – PFFD; Fig. 7.45) of bones. These may be accompanied by soft tissue anomalies, such as vascular malformation.

QUIZ CASE

What abnormalities do you see in Fig. 7.46?

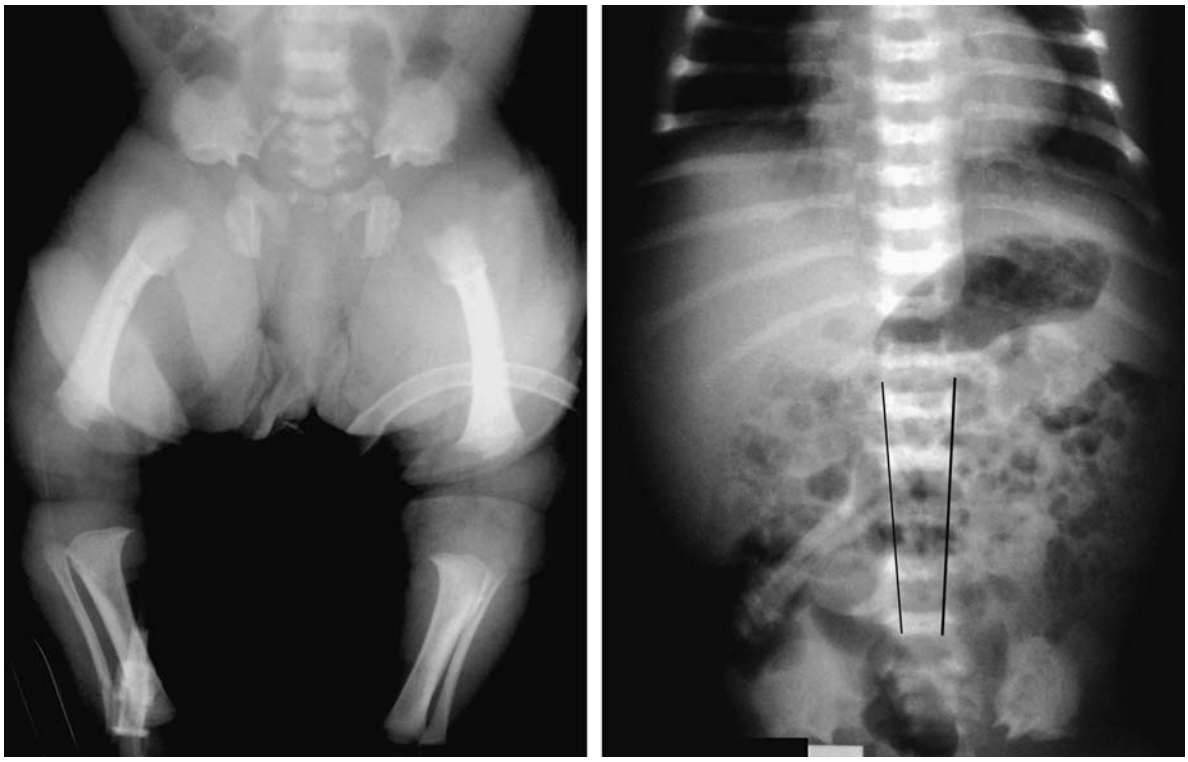

Fig. 7.44. Achondroplasia
a The proximal long bones of the extremities are short and the femora have an "ice cream scoop" appearance. The pelvis has a characteristic "champagne glass" configuration
b The interpediculate distances (*lines*) of the lumbar spine decrease rather than increasing as they should

Fig. 7.45. Proximal femoral focal deficiency
The right femur is shorter than the left and the proximal right femur is not ossified

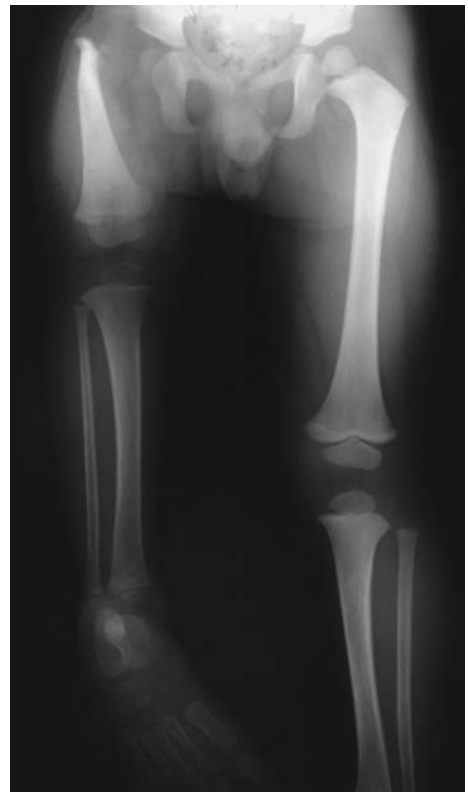

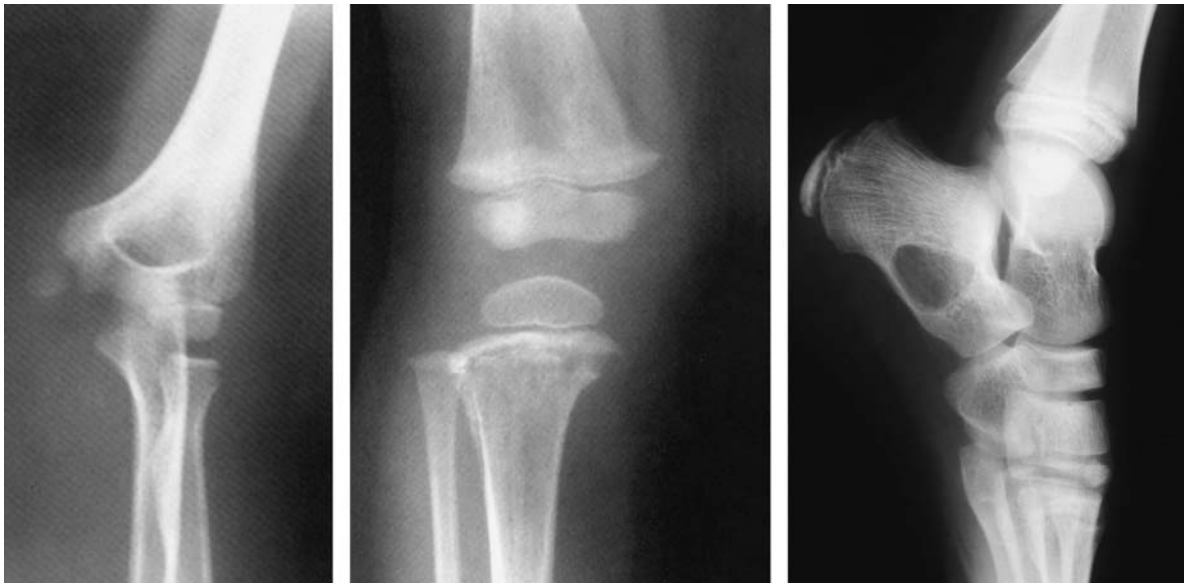

a, b **c**

Fig. 7.46. What are the abnormalities in these cases? (Answers in Appendix 2)
a A 10-year-old with elbow pain
b A 2-year-old with knee pain
c A teenager with heel pain
d–n see pp. 204, 205

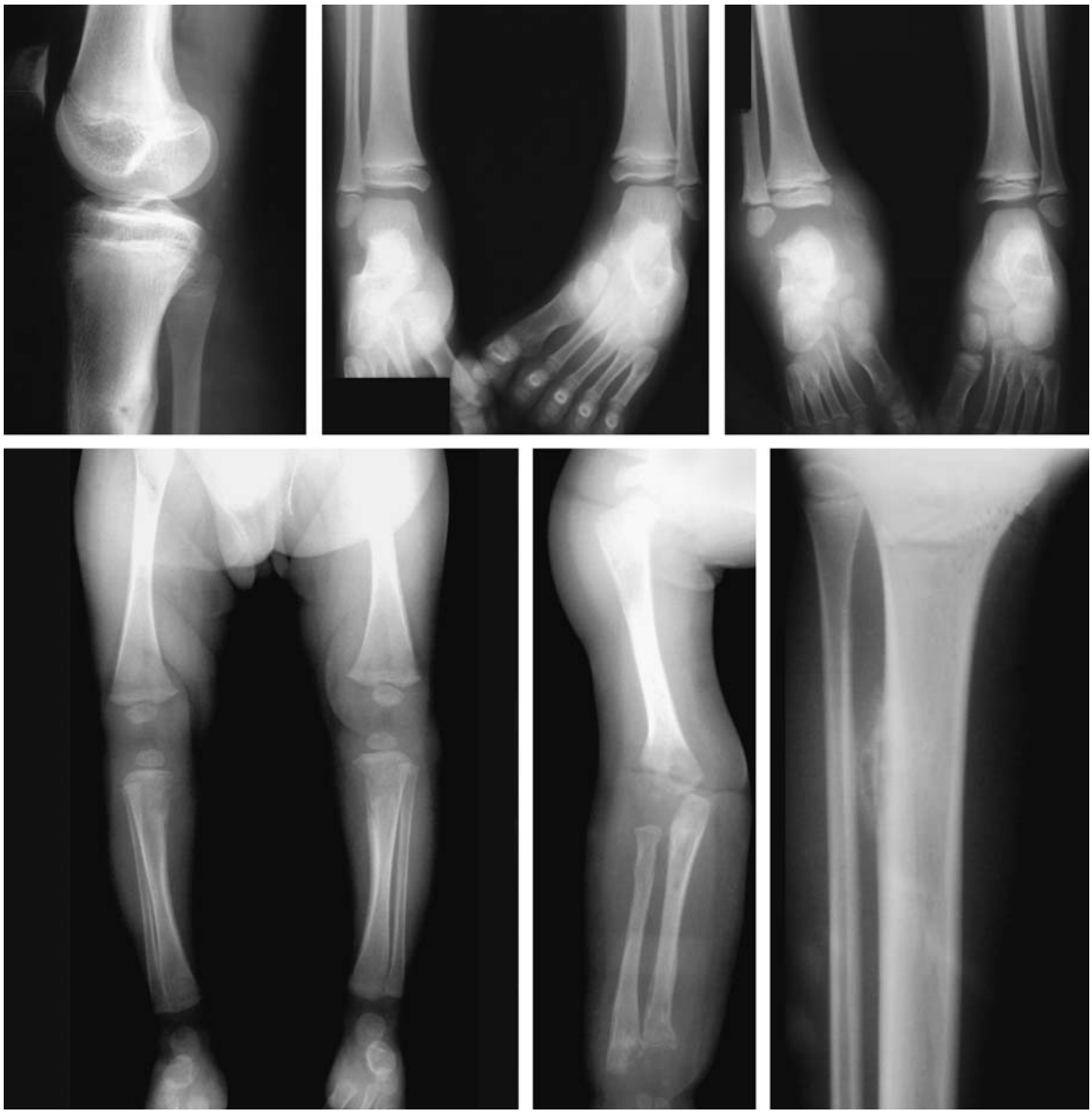

Fig. 7.46 (*continued*)
d A teenager with leg pain
e An 8-year-old with right ankle pain
f A 6-year-old with swollen right ankle
g, h A newborn with swollen extremities
i A 10-year-old with bump on leg

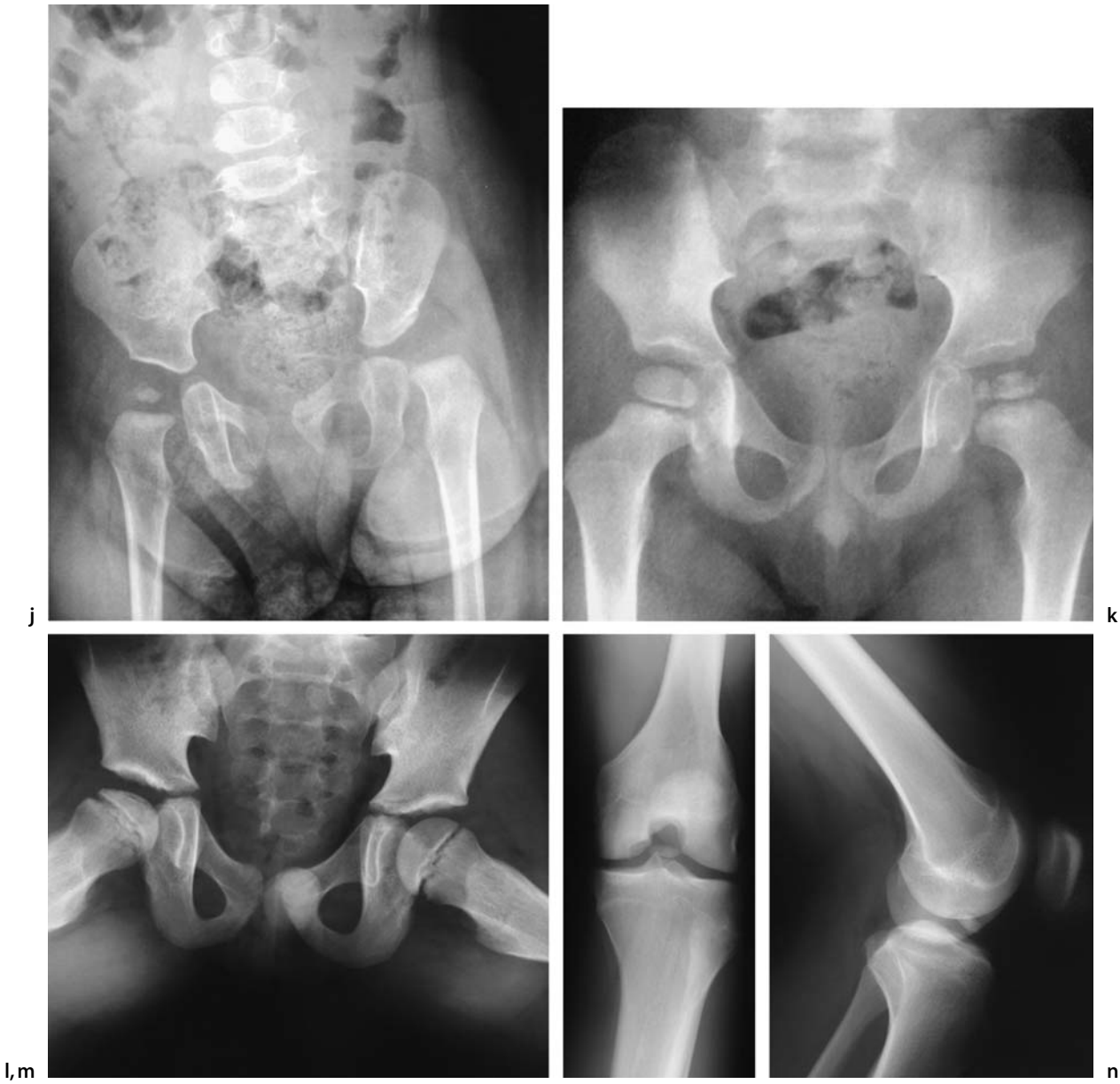

Fig. 7.46 (*continued*)
j An 8-month-old with asymmetric gluteal folds
k A 7-year-old with left hip pain
l A 5-year-old with right hip pain
m, n A teenager with right knee pain

References and Further Reading

1. RM Letts (ed) (1994) Management of pediatric fractures. Churchill Livingstone, Philadelphia
2. Greulich WW, Pyle SL (1970) Radiographic atlas of skeletal development of the hand and wrist, 2nd edn. Stanford University Press, Stanford
3. Keats TE, Sistrom C (eds) (2001) Atlas of radiologic measurement, 7th edn. Mosby, St Louis
4. Troupin RH (1978) Diagnostic radiology in clinical medicine, 2nd edn. Year Book Medical, Chicago
5. Forrester DM, Brown JC. Nesson JW (1987) Radiology of joint diseases, 3rd edn. Saunders, Philadelphia
6. Keats TE (ed) (2001) Atlas of normal roentgen variants that may simulate disease, 7th edn. Elsevier Science, Philadelphia
7. Schmidt H, Freyschmidt J, Holthusen W, Winter P (1993) Kohler/Zimmer borderlands of normal and early pathologic findings in skeletal radiography, 4th edn. Thieme Medical Publishers, New York
8. Kleinman PK (ed) (1998) Diagnostic imaging of child abuse, 2nd edn. Mosby, Philadelphia
9. Kaplan PA, Helms CA, Dussault R, Anderson MW, Major NM (eds) (2001) Musculoskeletal MRI. Saunders, Philadelphia
10. Kuhn JP, Slovis TL, Haller JO (eds) (2004) Caffey's pediatric diagnostic imaging, 10th edn. Mosby, Philadelphia
11. Ozonoff MB (1992) Pediatric orthopaedic radiology, 2nd edn. Saunders, Philadelphia
12. Schultz RJ (1990) The language of fractures, 2nd edn. Williams and Wilkins, Baltimore
13. Buchmann RF, Jaramillo D (2004) Imaging of articular disorders in children. Radiol Clin North Am 42:151–168
14. Laor T (2004) MR imaging of soft tissue tumors and tumor-like lesions. Pediatr Radiol 34:24–37

8 Central Nervous System

Cross-sectional imaging (ultrasound, CT, and MR) has completely revolutionized the way in which we look at the central nervous system. Once again, the ordering physician must ask, "What do I want to know?" If the concern is about the bony vault, a skull series may suffice, but if the real interest is diagnosing an intracranial lesion, one of the cross-sectional modalities should be used. We begin with the skull for anatomy of the cranial vault and then cover intracranial anatomy. Indications for imaging evaluation of the head, neck, and spine are then discussed.

Skull

The cranial sutures and fontanelles divide the skull into its major bones (Fig. 8.1). A suture is a nonossified portion of the membranous bone. (Remember: most of the skull is derived from membranous tissue, while the base of the skull and long bones are derived from enchondral ossification.) The metopic and coronal sutures begin at the large, diamond-shaped anterior fontanelle. The midline sagittal suture separates the parietal bones. It extends from the anterior fontanelle to the posterior fontanelle at the posterior aspect of the parietal bones. The lambdoid sutures extend from the posterior fontanelle.

The complex occipital bone is composed of six individual bones: two interparietal, one supraoccipital, two extraoccipital, and one basioccipital bone. The temporal bone, located inferior to the parietal bone and anterior to the occipital bone, includes the mastoid process and structures of the middle and internal ear. The temporal bone extends anteriorly to the sphenoid bone. The sphenoid bone is the dense structure at the base of the skull which includes the greater and lesser wings and the sella turcica. The largest bone of the face is the mandible. A routine skull examination should include the mandible, maxilla, orbital structures, and paranasal sinuses (sphenoidal maxillary, ethmoidal, and frontal).

The times of closure of various intracranial sutures and fontanelles and of the appearance of the paranasal sinuses are summarized in Table 8.1 (p. 211).

Figure 8.2 shows the multiple views necessary to evaluate the various portions of the skull. It is advisable to know these projections so that optimal visualization of particular sections of the calvarium can be obtained. The calvarium changes dramatically with age as the sutures and fontanelles close. Figure 8.3 shows the maturation process of the skull as seen in the lateral projection. The sutures become less obvious and the paranasal (maxillary, ethmoidal, sphenoidal, and frontal) and mastoid sinuses aerate.

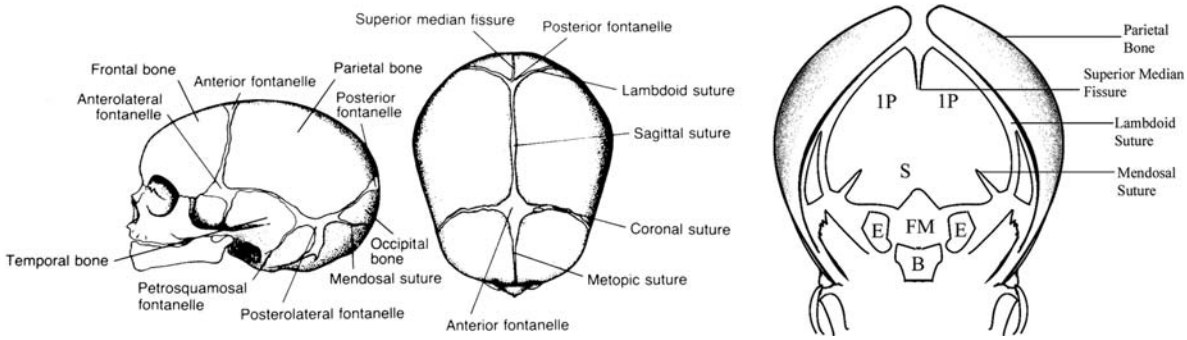

Fig. 8.1. The infant calvarium with major bones, sutures, and fontanelles in three different planes (lateral, from above, and from behind). *IP*, interparietal bone; *S*, superaoccipital bone; *E*, extraoccipital bone; *FM*, foramen magnum; *B*, basioccipital bone

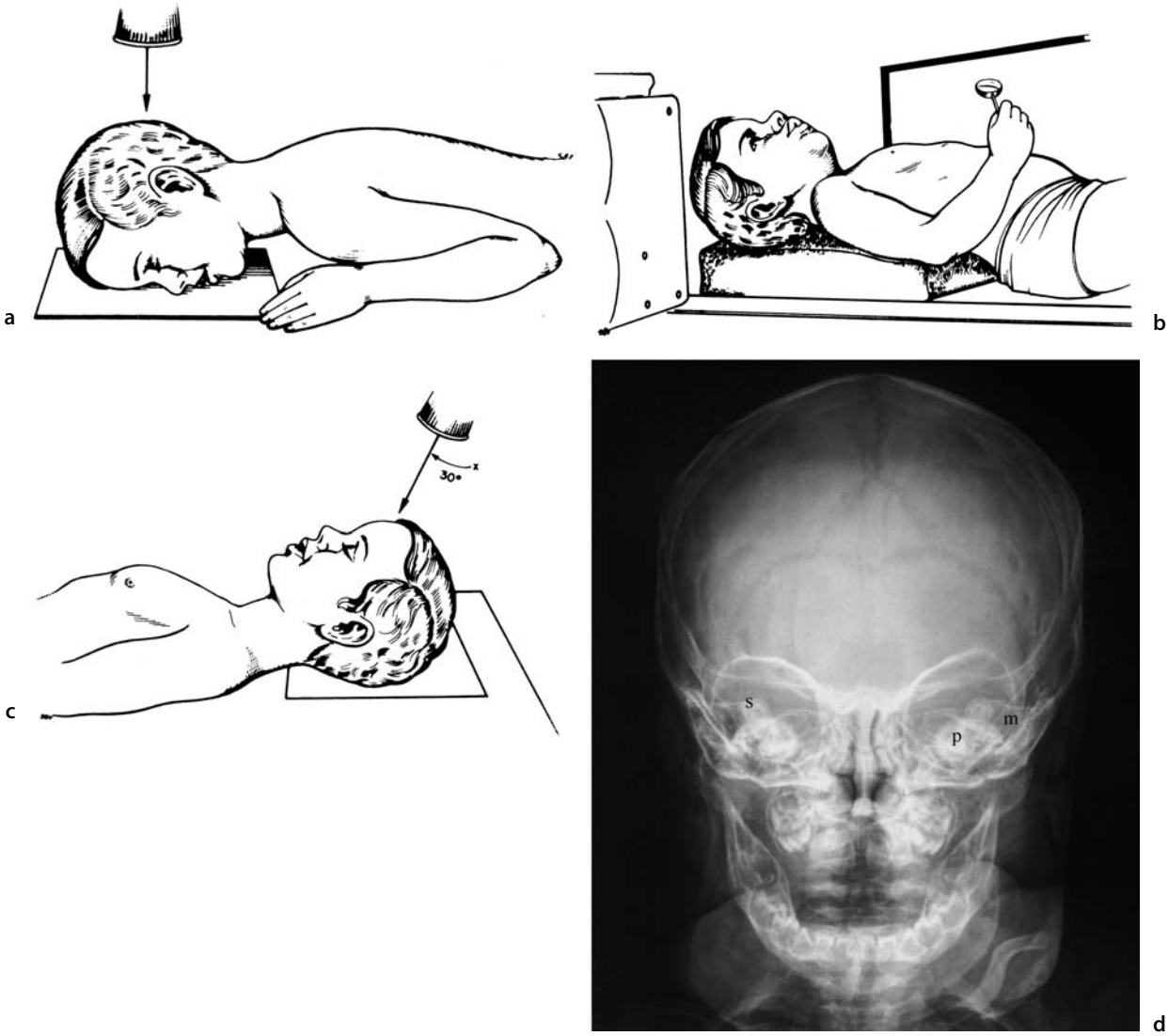

Fig. 8.2. Line drawings and radiographs of the various views of the skull
a In the PA view the beam enters the back of the child's head on a line perpendicular to the film, allowing visualization of the petrous pyramids, which are projected through the orbits
b In the cross-table lateral view the beam enters one side of the child's head while the film is on the other. In this way a horizontal lateral is achieved. This method allows the child to remain comfortable during the procedure, and the entire calvarium and the sella turcica and cervical spine are displayed
c In Towne's view the beam is directed front to back of the patient's head at a 30° angle to the perpendicular. This view is designed to demonstrate the occipital bone and the foramen magnum. Basal skull fractures are often seen best in this view
d A PA view of the calvarium with the petrous pyramids (*p*) visualized through the orbits. The round circular areas are the semi-circular canals of the middle ear (*s*). *M*, mastoid
e–h see p. 209

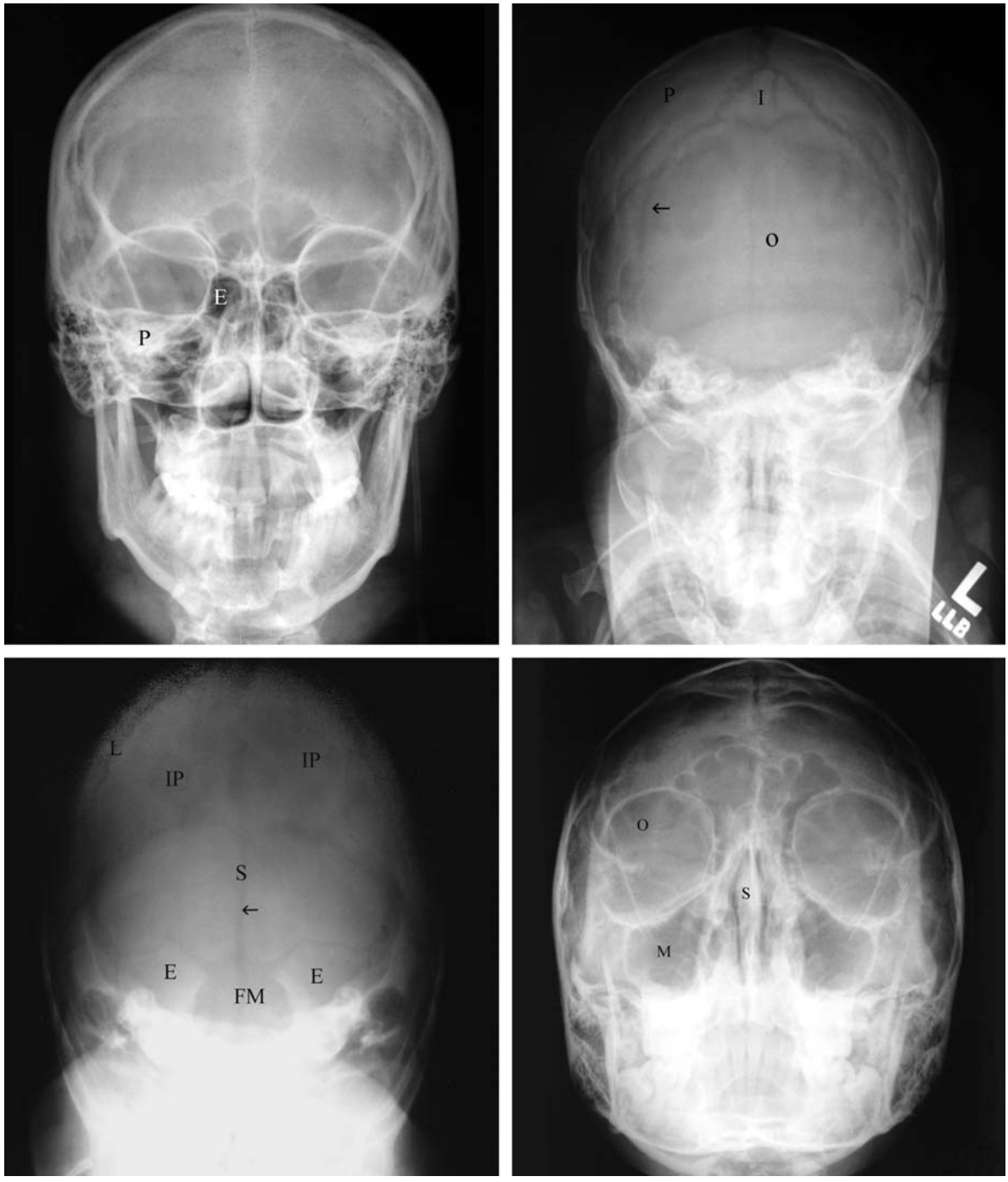

Fig. 8.2 (*continued*)
e A Caldwell view in which the beam is not so sharply angulated. The petrous pyramids (*P*) are at the lower rim of the orbit. *E*, ethmoid air cells
f Towne's view showing the lambdoid suture (*arrow*) and the occipital bone (*o*). *P*, parietal bone; *I*, a wormian bone called the inca bone. It is part of the occipital bone. In the Towne's view, we can see the most posterior aspects of the calvarium
g Coned-down Towne's view showing the various components: *L*, lambdoid suture; *IP*, interparietal bone; *S*, supraoccipital bone. Note that the *arrow* is on the metopic suture "shining through" from in front and there is no separation of the supra-occipital bone. *E*, extraoccipital bone; *FM*, foramen magnum
h A Waters' view is designed to show the maxillary sinuses. It is usually done with the patient in the erect position whenever possible to show air–fluid levels, maxillary (*M*) and ethmoidal and frontal sinuses. The ethmoid air cells seem to merge with the frontal air cells on this view. *O*, orbit; *S*, nasal system

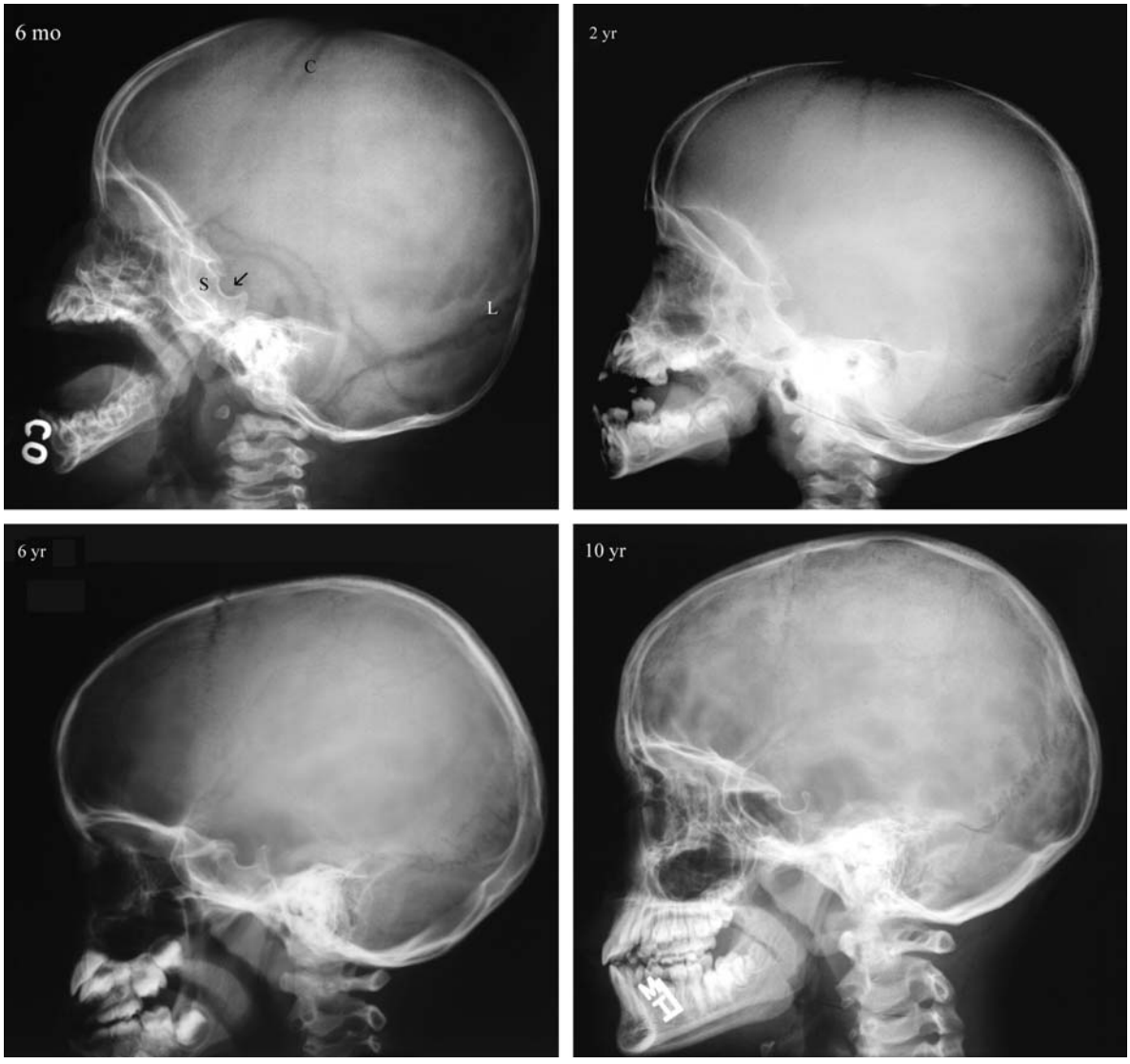

Fig. 8.3. Comparative views of the skull from early childhood through adolescence
a Six months
b Two years
c Six years
d Ten years
Note how the sutures become less obvious and the paranasal sinuses aerate. *S*, sphenoid; *C*, coronal suture; *L*, lambdoid suture; *arrow*, sella turcica. The face enlarges relative to the size of the skull

Table 8.1. Closure of sutures and fontanelles, appearance of the paranasal sinuses

Closure of fontanelles (average range/total range)
Anterior: 15–18 months/9–24 months
Posterior: 1–2 months/birth-3 months
Closure of sutures (from [5])
Mendosal: several weeks after birth (this suture separates the interparietal and supraoccipitaI portions of the occipital bone)
Metopic: variable (10% persist throughout life)
Coronal, sagittal, lambdoid: about age 30
Appearance of paranasal sinuses (great deal of variation)
Ethmoid sinuses: rudimentary air cells at birth but usually no air seen radiographically until 3–6 months
Maxillary sinuses: rudimentary air cells at birth but no air seen radiographically until 3–6 months
Sphenoidal sinuses: 1–3 years
Frontal sinuses: 4–12 years

Approach to the Plain Skull Film

A systematic approach for examining the skull is to begin from the external surface and work through the calvarium and down into the face and spine in all views.

Soft Tissues

Any bulge or enlargement of the soft tissues should be noted. This may be the site of trauma (we suggest looking harder in this region for a fracture) or protuberance of intracranial contents – an encephalocele – or, if at the fontanelle, evidence of increased intracranial pressure.

The Three Bony Tables

Outer Table. This is the most external bony margin of the skull. Irregularities or disruption of this cortex denote abnormality. Cephalohematoma, osteomyelitis, metastasis, and histiocytosis all affect this portion of the skull (Fig. 8.4).

Diploe. This is the middle table and contains the bone marrow. Severe hemolytic anemia can cause proliferation of bone marrow and enlargement of the diploe, giving a "hair-on-end" appearance (e.g., thalassemia, Fig. 8.4).

Inner Table. This portion of the bony calvarium is frequently affected by lesions within the cranial vault. The most common "erosion" is normal pacchionian granulation (Fig. 8.4).

Calvarium

Now we are looking through the bone as well as at the generalized bony covering. Pay close attention to the cranial suture. Search for possible fractures or intracranial calcifications. While common in adults, "normal calcifications" of the pineal, habenular commissure, choroid plexus, or dura are not usually seen in childhood (under the age of 15 years) on plain films; these calcifications can be frequently seen on CT in the younger age groups.

Sella Turcica

The sella houses the pituitary gland. It is a site commonly affected by increased intracranial pressure (see below).

The Frontal Film

When viewing the skull from the front (see Fig. 8.5), the easiest way to detect an abnormality is to look for asymmetry. This body is, for the most part, symmetric, and a line drawn down the middle of the frontal skull film should show each side of the skull as the mirror image of the other.

The Lateral Film

The soft tissues of the neck and nasopharynx, as well as the cervical spine, are clearly visible. Look for displacement of the air column by a mass (mass effect) or any bony destruction (see Chap. 3).

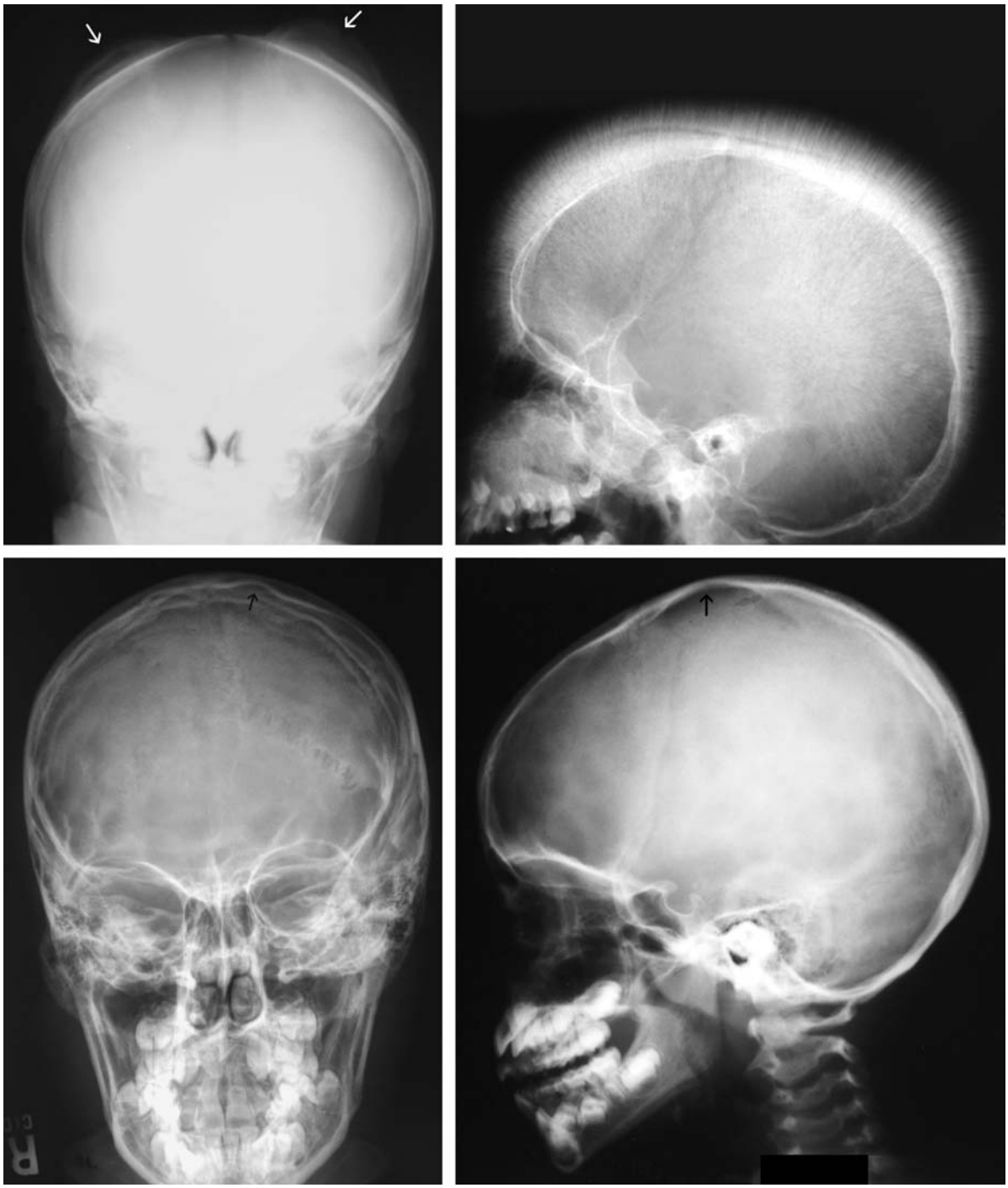

Fig. 8.4. Abnormalities of the tables of the calvarium
a Outer table – bilateral cephalohematomas. This picture was underexposed specifically to show the lesion. The outer table of the calvarium (*arrows*) is elevated by subperiosteal bleeding. The lesion does not cross the midline as it is limited by the periosteal attachment. This is an abnormality initially seen during the first days/weeks after birth. The subperiosteal blood calcifies, as in this child, and ultimately heals uneventfully
b Expansion of the diploe or middle table in a patient with thalassemia. The exuberant hematopoiesis that frequently occurs in patients with this disorder expands the diploic region of the calvarium – the middle table. The result is a "hair-on-end" appearance, which can be seen in any disorder causing rapid and extensive hematopoiesis
c, d Pacchionian granulation in two patients. The inner table (*arrow*) is elevated toward the diploe by rather abundant pacchionian granulation. These are arachnoid extensions that aid in spinal fluid resorption

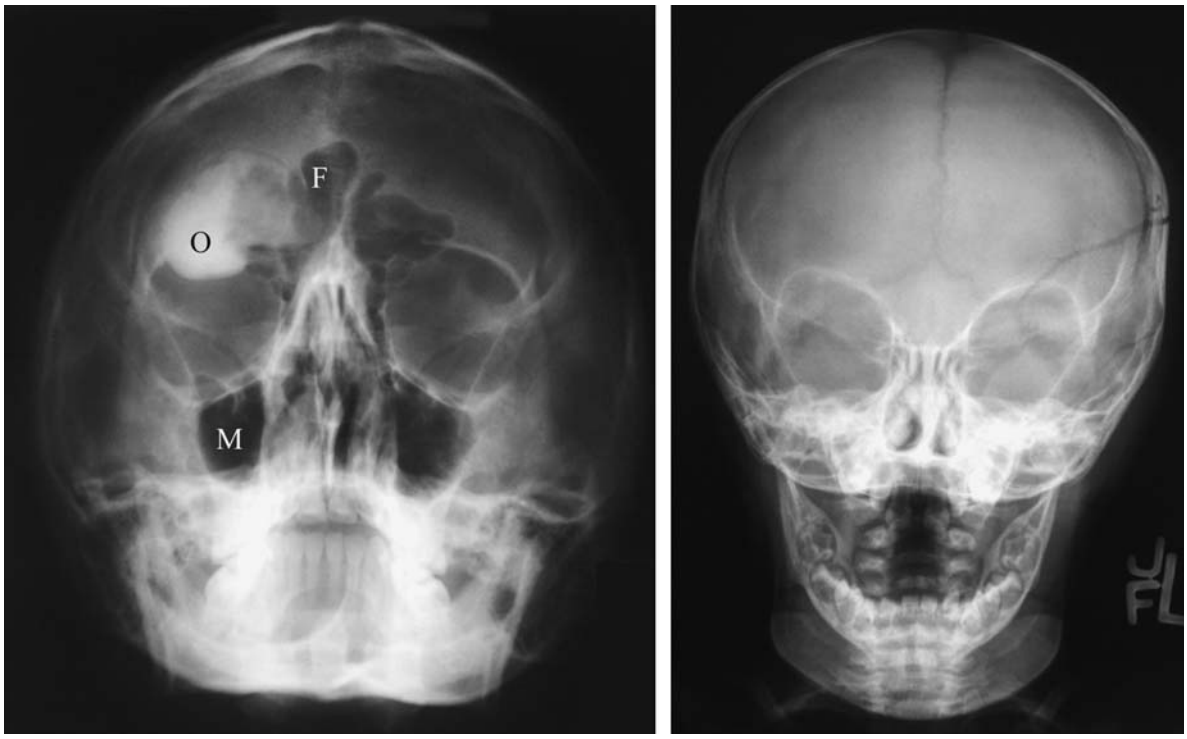

Fig. 8.5. Look for asymmetry
a Waters' view of the calvarium in this 15-year-old male. Careful attention to symmetry of the face allows one to detect the large, bony benign tumor (*O*) of the frontal sinus. It is an osteoma. Note the well-aerated maxillary (*M*), ethmoid, and frontal sinuses (*F*)
b The Caldwell view in another child shows a large black line on the left above the orbit – a diastatic fracture. Diastatic means that there are widely spread edges of bone. In both of these cases, you can find the abnormality by looking for asymmetry

Intracranial Contents

In the neonate and young infant, the brain and its meninges are easily identified by transfontanellar ultrasound. The two standard projections are the coronal and the sagittal (Fig. 8.6). These views are limited by the fontanelle size so they are always angled, i.e., paracoronal and parasagittal. These views are supplemented with a mastoid view (Fig. 8.6). The ventricles are used as landmarks, but the real key is seeing the parenchyma. Extra-axial fluid is easily seen (extra-axial means between the brain and bone, outside of the brain). The more premature the neonate, the less sulci and the larger the extra-axial space. At term, there is little extra-axial fluid, but from 2 months to 2–3 years a small amount of extra-axial fluid may be seen (Fig. 8.7).

The whole concept of extra-axial fluid is a good example of clinical concordance with the ultrasound finding. Benign extra-axial fluid is a diagnosis of exclusion. Fluid in the subdural space is found after trauma (both accidental and in child abuse) and with meningitis. Only when one knows that the child is not ill and is developmentally normal can the extra-axial fluid be ascribed to the "benign" category.

A more precise view of the parenchyma and meninges can be obtained with CT. These images are usually in the axial plane (a horizontal plane, approximately 20° above the orbital–meatal line, sparing the lens; Fig. 8.8). These anatomical sections can be as thin as 1 mm. For most intracranial imaging, 5- to 10-mm sections are performed. CT is superb for showing the bony structures, calcium, hemorrhage, and the supratentorial brain. It is less optimal for showing the posterior fossa, brain stem, distinguishing gray–white matter differentiation, and defining white matter abnormalities. Computerized reconstruction in multiple planes can be performed, but these images are not as good as those that can be obtained by MR.

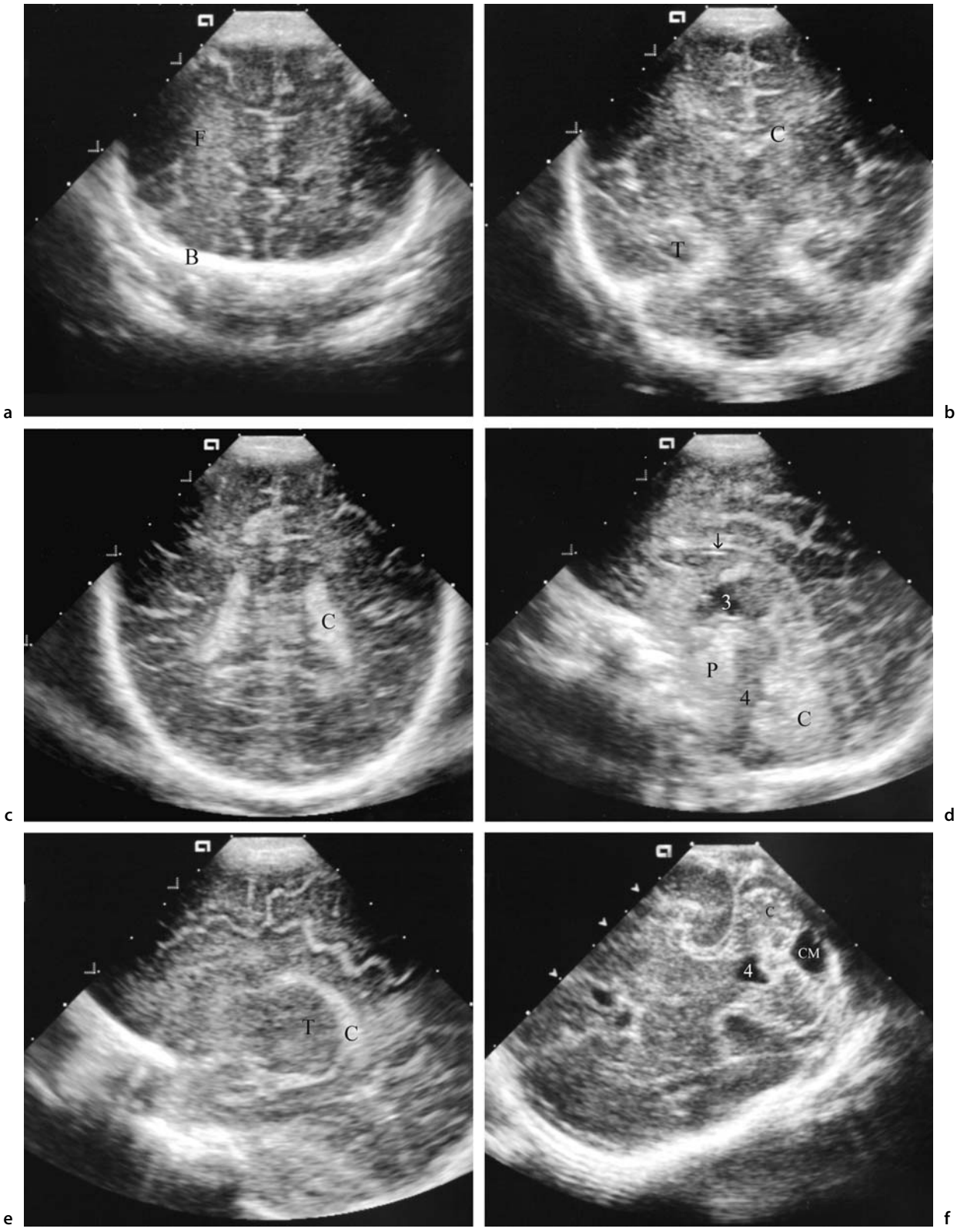

Fig. 8.6. Legend see p. 215

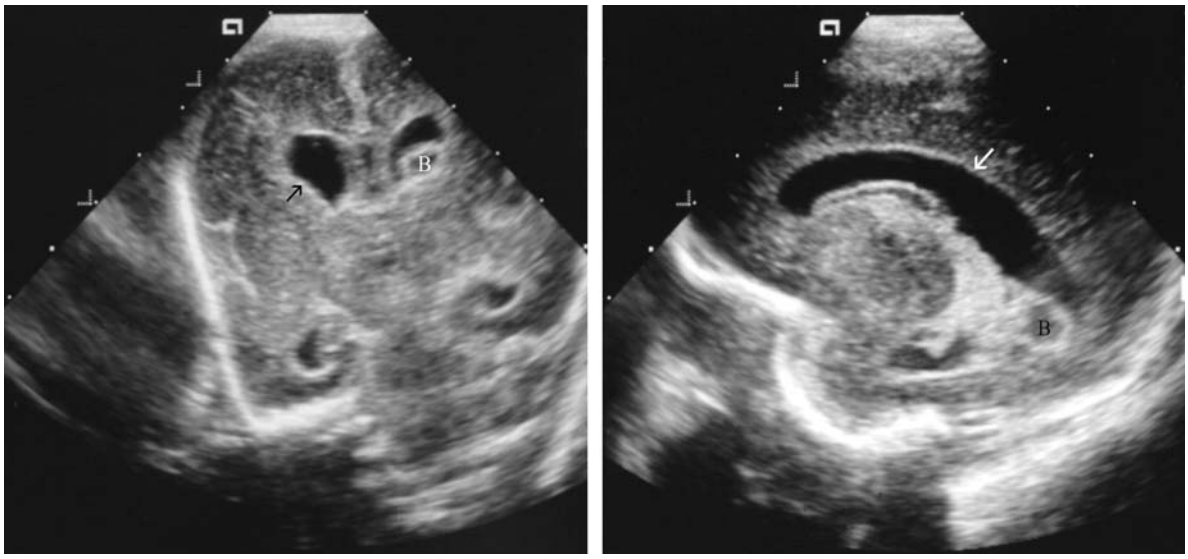

g h

Fig. 8.6. Ultrasonography of the neonatal brain
a Coronal section through the fontanelle with the patient's right side always on the viewer's left. In this extreme view angled toward the eyes, the frontal lobes (*F*) and the bony roofs of the orbits (*B*) are noted
b A coronal ultrasonic section at the level of the frontal horn. The ventricles are small, but one can see the choroid (*C*) in the floor of the lateral ventricle and entering into the foramen of Monro. *T*, temporal lobe
c Coronal ultrasonic section through the atria of the lateral ventricle. The echogenic symmetric structures (*C*) are the choroid plexus at the atria
d Sagittal midline cut with the patient's face always to the viewer's left (AN=anterior). The cerebellum (*C*), pons (*P*), third and fourth ventricles are labeled. The *arrow* is pointing to the hypoechoic corpus callosum
e Sagittal section through the thalamus (*T*). Note the choroid along the floor of the lateral ventricle (*C*). The lateral ventricle is noted to be small
f Mastoid view obtained in the axial plane through the temporal bone reveals a normal fourth (*4*) ventricle and cisterna magna (*CM*). The lateral lobe of the cerebellum (*P*) is noted
g A premature baby with ventricular dilatation and intracranial hemorrhage. This section through the frontal horns reveals the enlarged ventricles (*arrow*) and blood within the ventricles (*B*)
h Sagittal ultrasound study on the same baby shows the enlarged ventricle (*arrow*) as well as blood within the lateral ventricle above the thalamus. Note that the choroid adheres to the thalamus and is echogenic and homogeneous

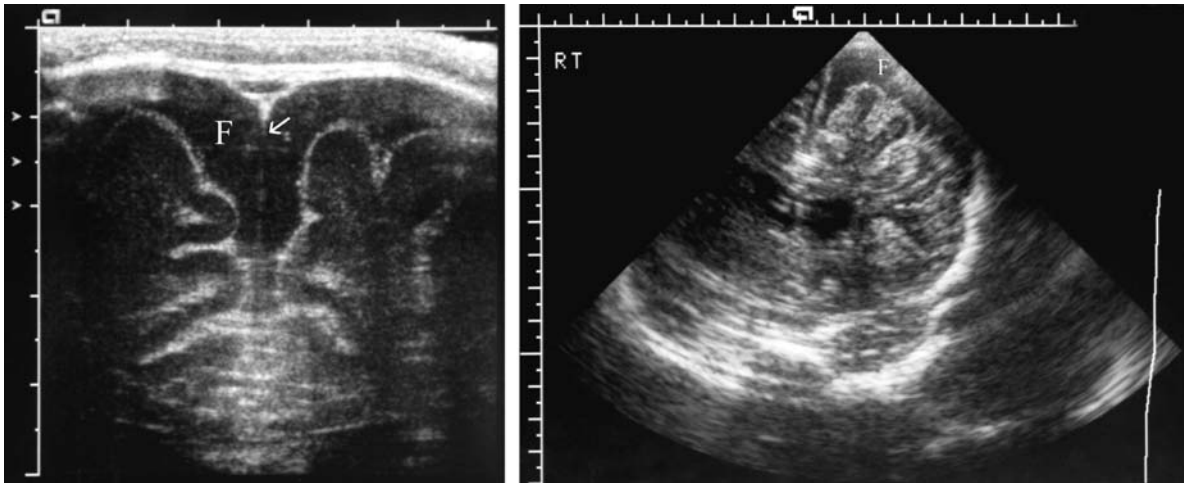

a b

Fig. 8.7. Extra-axial fluid
a Coronal section shows fluid (*F*) in the intrahemispheric fissure. The falx (*arrow*) is seen
b Angled coronal scan shows fluid (*F*) above the left frontoparietal region

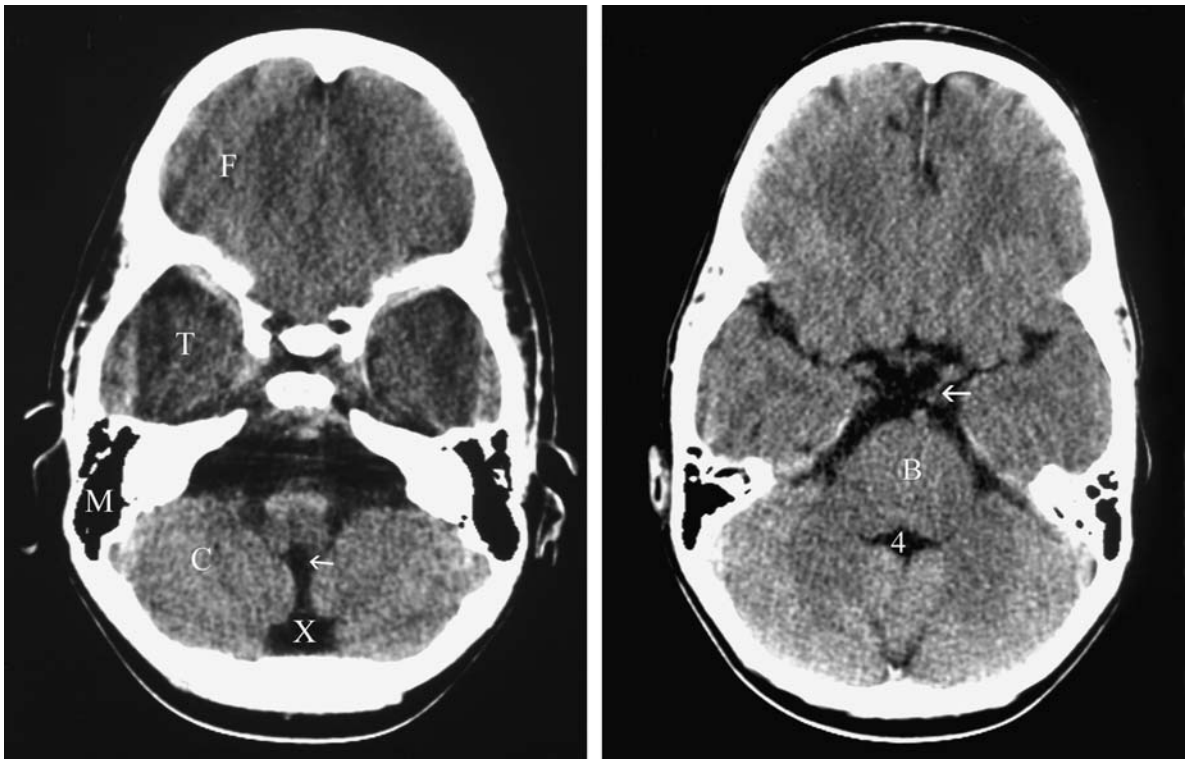

a b

Fig. 8.8. Normal CT scan of the brain.
a–e Unenhanced scans, that is, no intravenous contrast
f–j Comparable images with intravenous enhancement
a, f The most inferior (lowest caudad) section (**a** without enhancement, **f** with enhancement) reveals the mastoid air cells (*M*), the temporal lobes (*T*), and frontal lobes (*F*). The posterior fossa is seen with a normal fourth ventricle (*arrow*, **a**), vallecula, and cisterna magna (*X*). The cerebellar hemispheres are noted (*C*). With intravenous enhancement (**f**), note visualization of the basilar artery (*arrow*, **b**)
b, g The next superior cuts. The suprasellar cistern (*arrow*) is seen as well as the fourth ventricle (*4*) and brainstem (*B*). With enhancement the entire circle of Willis is noted. *M*, middle cerebral artery; *A*, anterior cerebral arteries.
c, h The next higher sections. The frontal horns of the lateral ventricle (*V*) and the third ventricle (*3*) are noted. The thalamus is next to the third ventricle (*T*) and the quadrigeminal plate cistern is seen (*arrow*)
d, i The next higher sections, showing the lateral ventricles. With enhancement, the straight sinus (*S*) is noted draining into the torcula
e, j The highest sections. Gray and white matter (*W*) differentiation can be seen and there is enhancement of the falx (midline white)
c–j see pp. 217, 218

CT is ideal for evaluating the temporal bone for trauma, inflammation, or congenital abnormalities. Thin sections (1.25 mm) are performed in two planes – the axial and coronal (Fig. 8.9). CT is also is the standard for paranasal sinus evaluation (Fig. 8.9).

MR is the most exquisite method of viewing brain parenchyma. It can be portrayed in any plane, has excellent tissue differentiation, and superbly defines the spine (Fig. 8.10). MR, however, is less advantageous than CT in showing bony abnormalities. An excellent text for learning the anatomy demonstrated by these modalities is that by Hayman and Hinck [1]. A comparison of modalities is found in Chap. 1, Table 1.1.

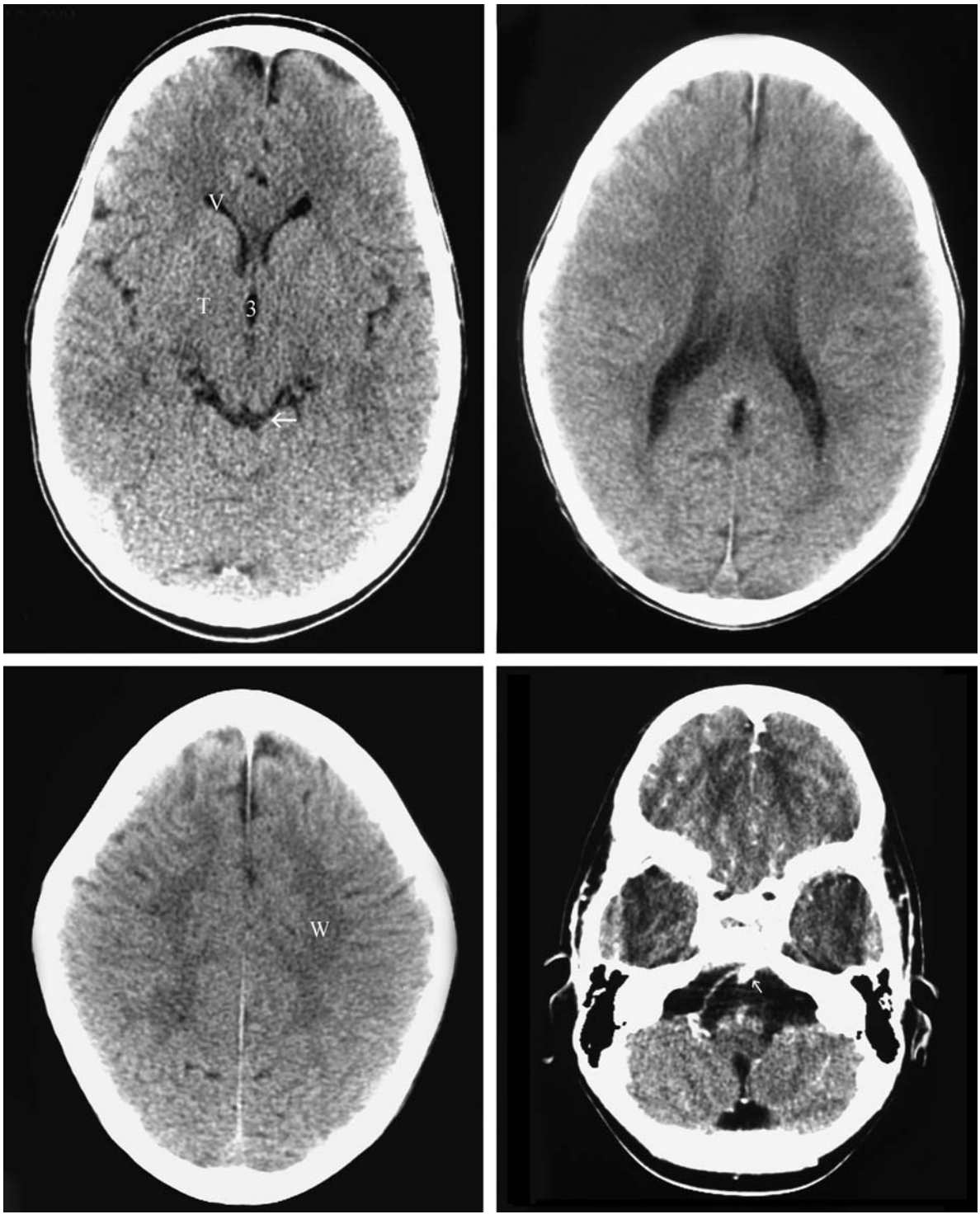

c d e f

Fig. 8.8. *(continued)*. Legend see p. 216

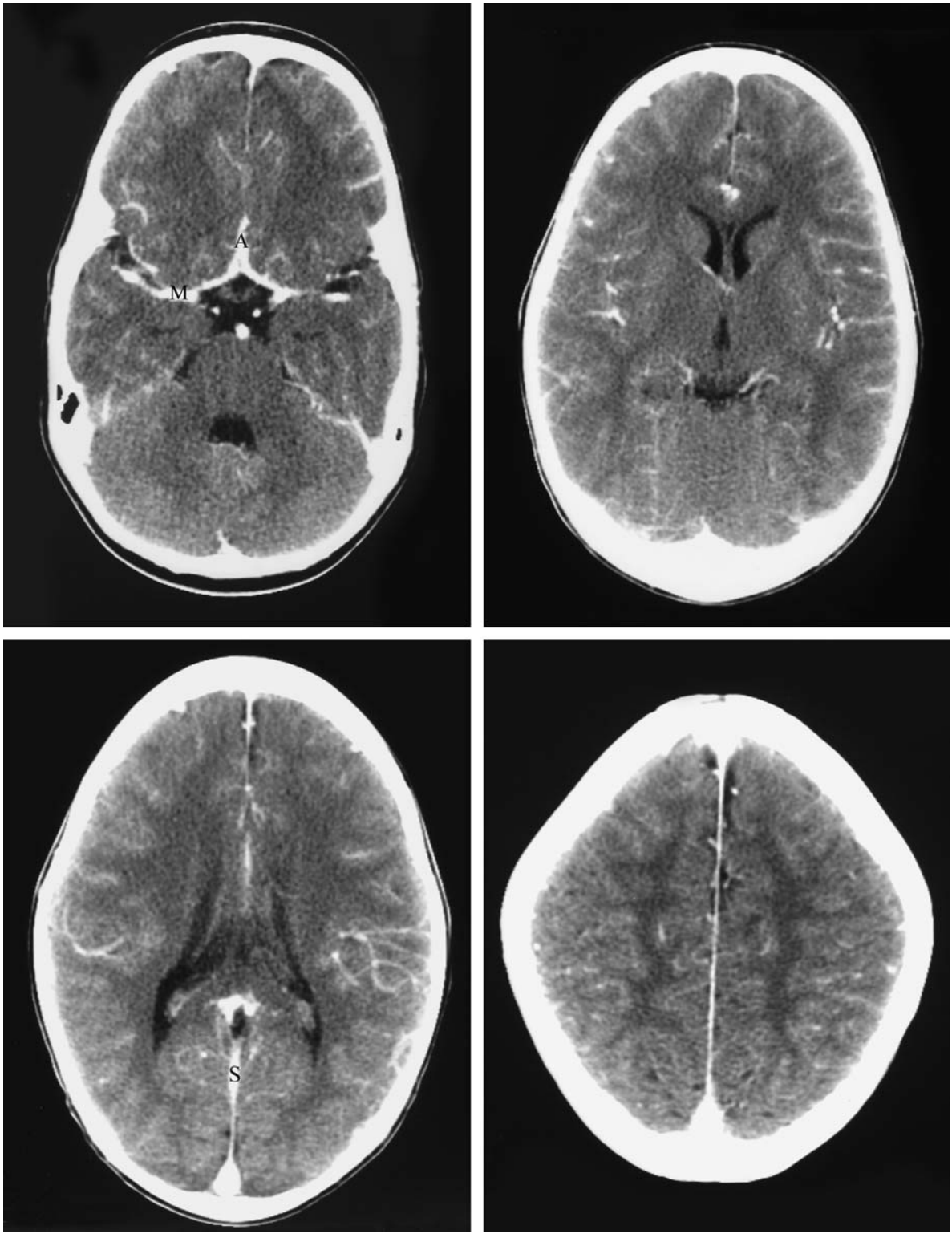

g h i j

Fig. 8.8. *(continued)*. Legend see p. 216

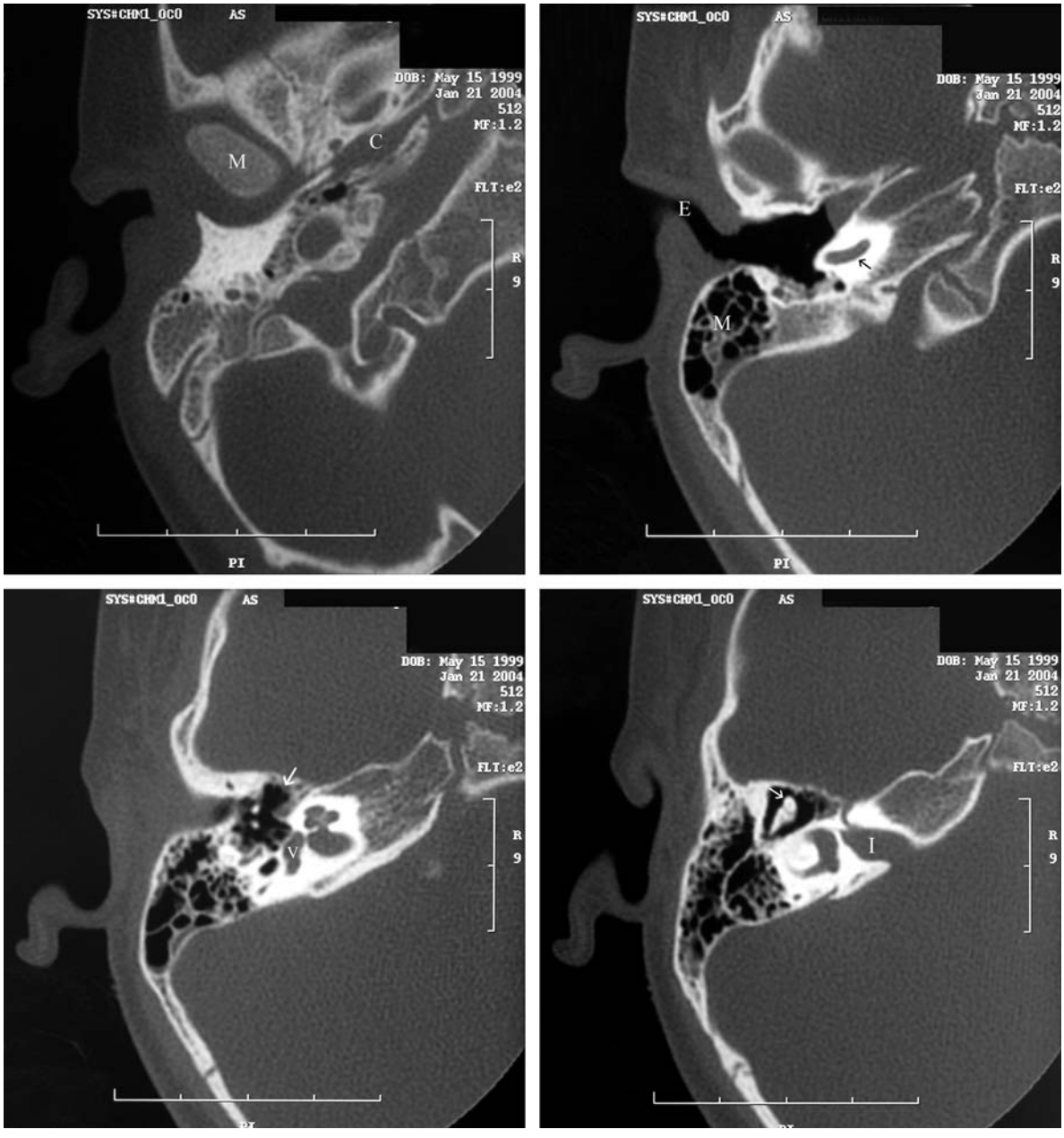

Fig. 8.9. CT of the temporal bones of a normal right ear and normal paranasal sinuses
a Axial section at the temporomandibular joint. The mandible (*M*) and the carotid canal (*C*) are visible. The mastoid air cells in this low cut are not yet aerated
b Axial section somewhat higher, at the level of the basal turn of the cochlea (*arrow*). The external canal (*E*) and the mastoid air cells (*M*) are noted. There is now aeration of the some of the mastoid air cells. The cochlea is one of the densest bones in the body
c Axial section at the vestibule (*V*) and inferior middle ear (*arrow*). The ossicles are just coming into view
d Axial cut at the level of the middle ear and internal auditory canal (*I*). The *arrow* is on the malleolus. The lucency inferior to the *arrow* is the mallear–incudal joint and the lower bone is the incus
e–h see pp. 220–222

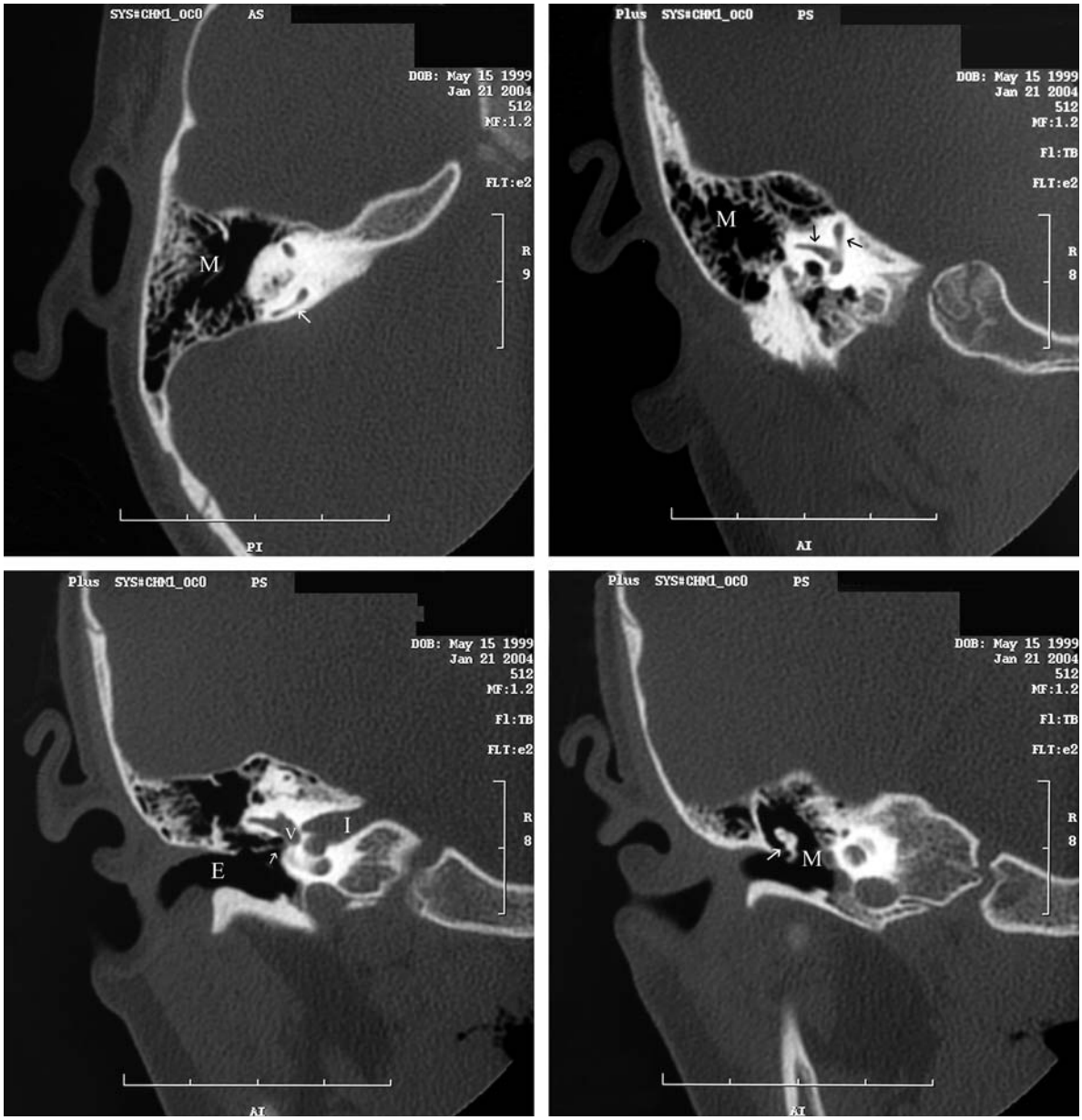

Fig. 8.9 (*continued*)
e Axial plane at the level of the semicircular canal (*arrow*). Note the aerated mastoid (*M*)
f Coronal cut in the most posterior aspect of the temporal bone. The *arrows* are pointing at the semicircular canals. *M*, mastoid air cells
g Coronal scan at the level of the external canal (*E*) shows the oval window (*arrow*), the vestibule (*V*), and the internal auditory canal (*I*)
h Axial cut at the level of the middle ear (*M*). The *arrow* is now pointing to the incus

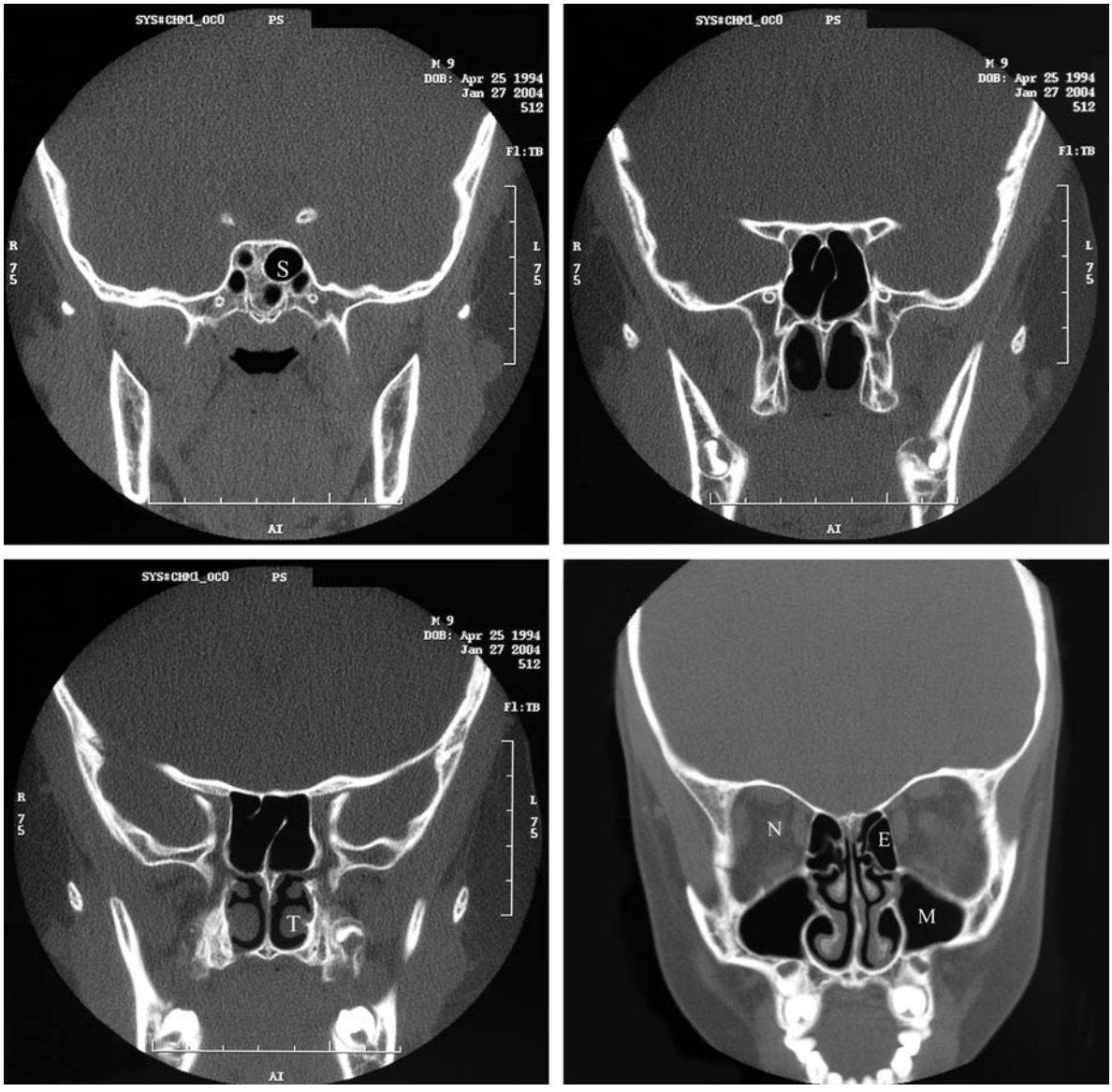

Fig. 8.9 (*continued*)

i Coronal CT examination of the paranasal sinuses. This first section is the most posterior through the sphenoid (*S*) which is only partially aerated

j Section somewhat anterior through the sphenoid and ethmoid junction

k A section more anterior through the turbinates (*T*). We are just at the most anterior aspect of the temporal lobes intracranially

l Coronal section through the orbits, as well as the ethmoidal and maxillary sinuses. The optic nerve is well seen (*N*). *M*, maxillary sinus; *E*, ethmoid sinus. Remember these are bone windows and not soft tissue windows. The orbital muscles and nerves can be seen much better on soft tissue windows

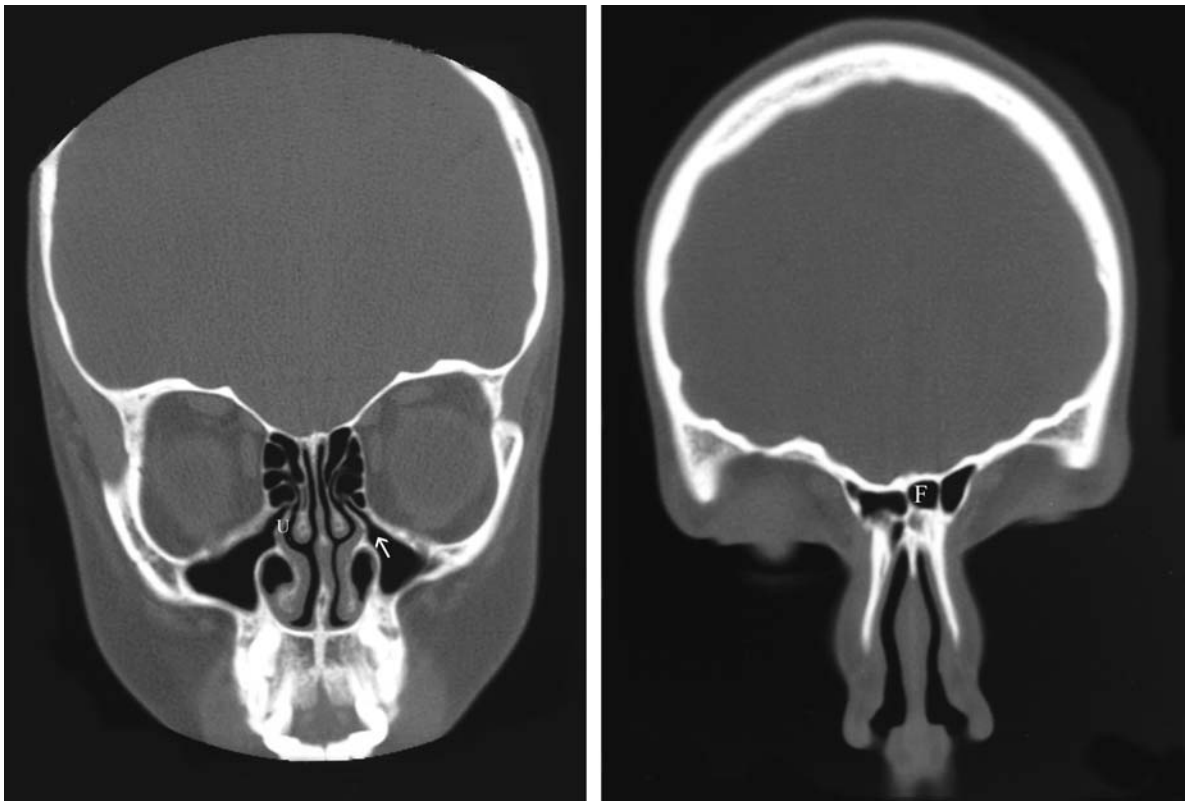

m n

Fig. 8.9 (*continued*)
m This section is through the osteomeatal complex (*arrow*). The opening is the ostia. The passage into the nose is the infundibulum or air space superior to the ostia and lateral to the uncinate process (*U*) of the inferior turbinate. The circular air space above the uncinate process is called the hiatus semilunaris
n The most anterior section shows the nasal bone and frontal sinus (*F*)

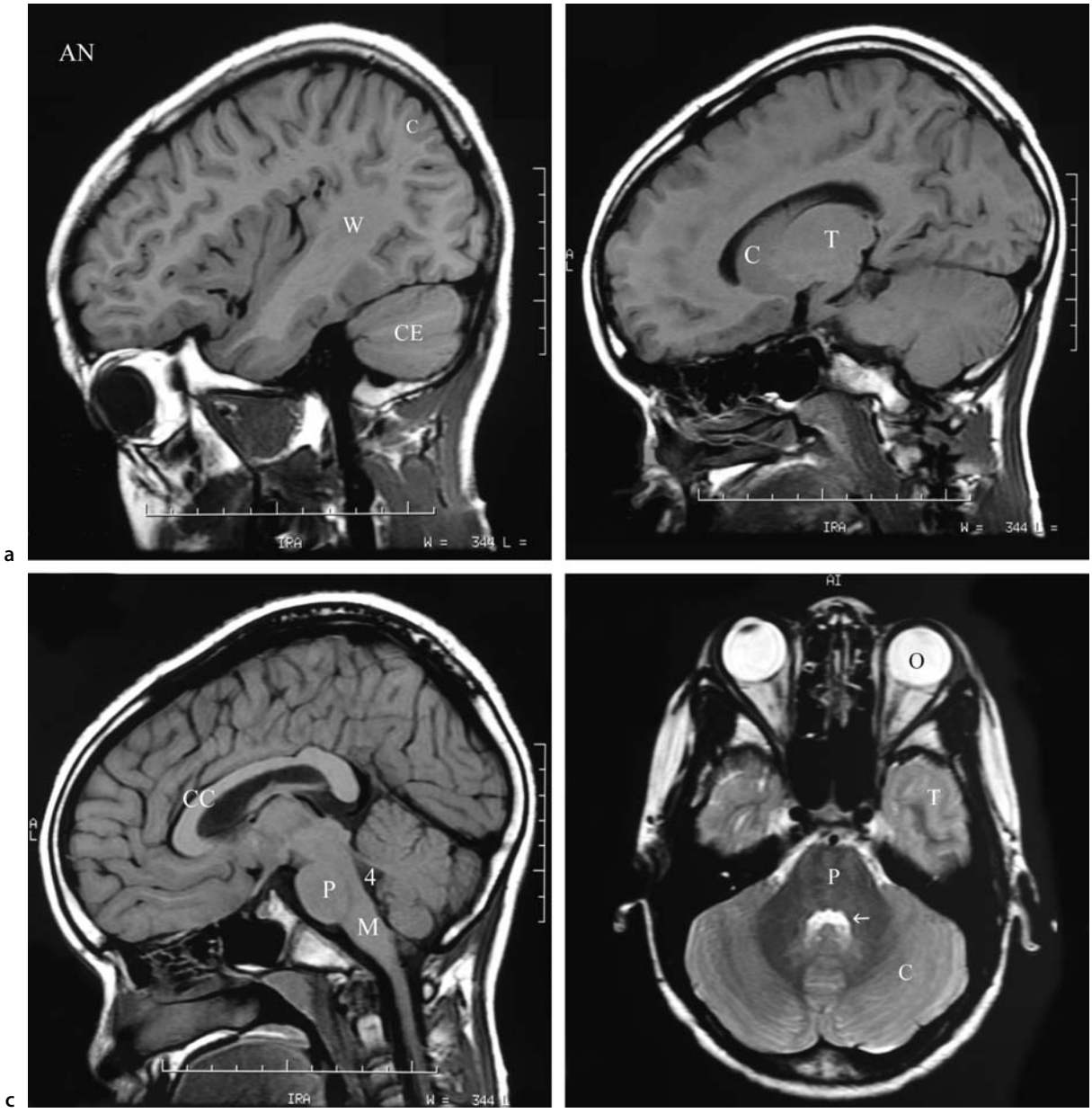

Fig. 8.10. Normal MRI
a Sagittal T1-weighted study shows the cerebellum (*CE*), white matter (*W*), and cortex (*C*). The patient is always looking to the reader's left, which is anterior (AN)
b Somewhat more medial sagittal T1-weighted cut shows the thalamus (*T*) and the caudate nucleus (*C*)
c Midline T1 sagittal cut reveals the corpus callosum (*CC*), the pons (*P*), the medulla (*M*), and the fourth ventricle (*4*). Note that there is no cerebellar tissue herniating downward below the craniocervical junction
d Axial T2-weighted images at the base of the skull. *O*, orbit; *T*, temporal lobe; *P*, pons; *C*, cerebellum. The *arrow* is pointing to the fourth ventricle. Remember on T2 weighted images, the cerebral spinal fluid appears white
e–r see pp. 224–227

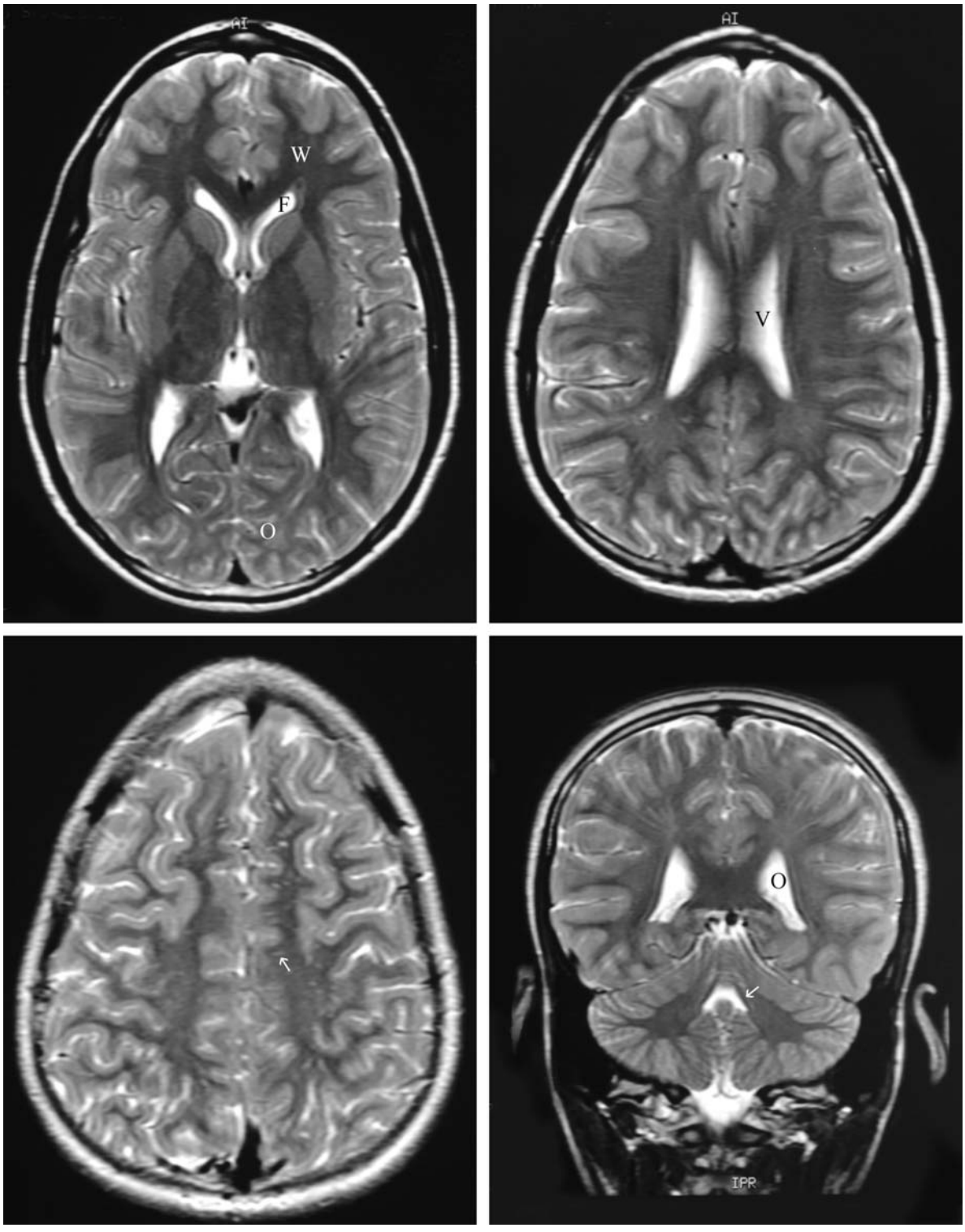

Fig. 8.10 (*continued*)
e T2 axial image at the level of the frontal horn (*F*) of the lateral ventricle. *W*, white matter; *O*, occipital lobe
f Higher axial T2 image showing the ventricles (*V*)
g Axial T2 image at the centrum semiovale. The *arrow* is pointing to a Virchow-Robin space. These are normal perivascular spaces
h Coronal T2 section posteriorly at the level of the occipital horns (*O*) of the lateral ventricles. The *arrow* is pointing to the fourth ventricle. Note the nice gray–white differentiation

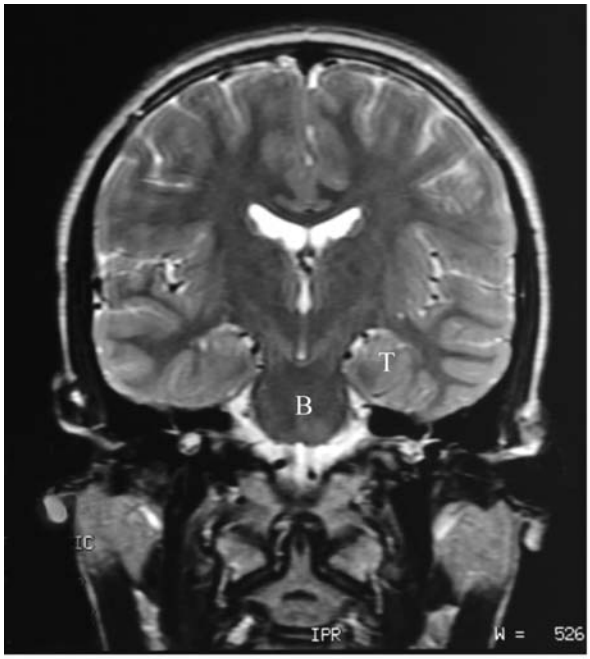

i

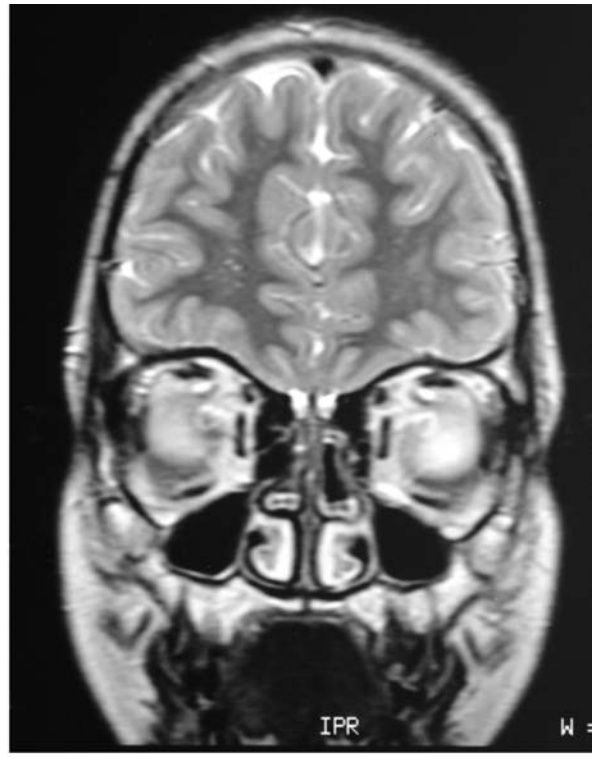

j

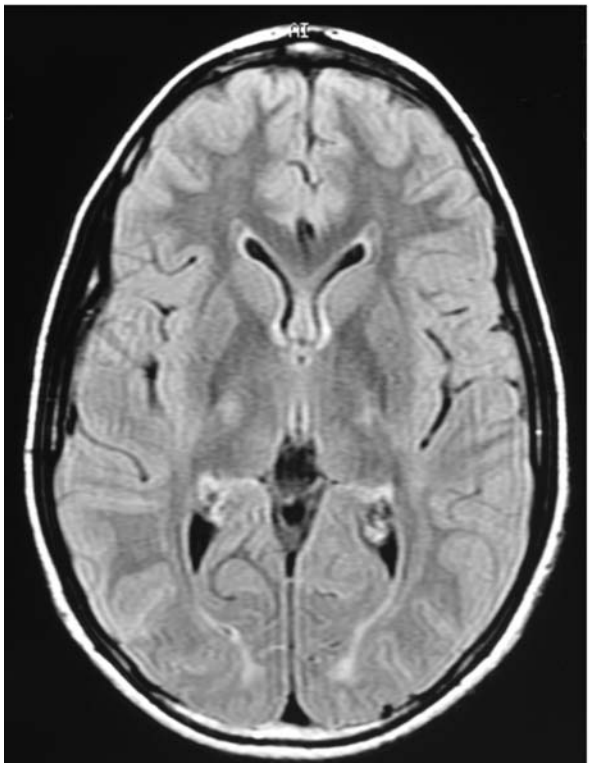

k

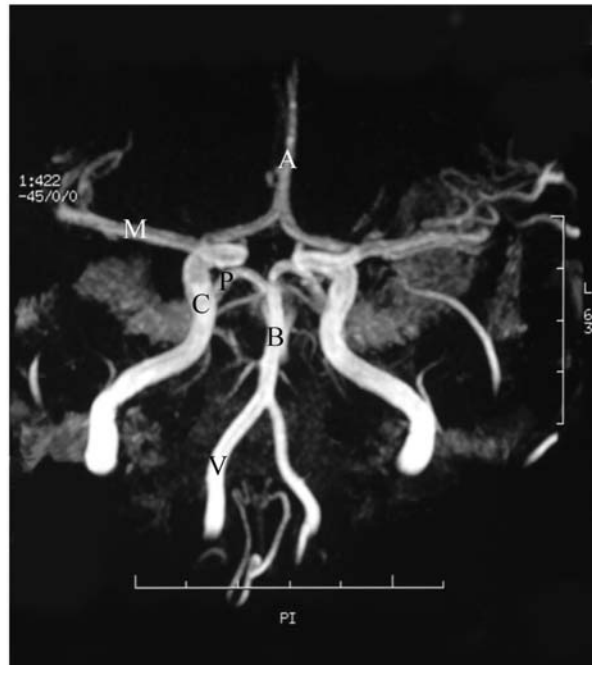

l

Fig. 8.10 (*continued*)
i More anterior coronal T2-weighted image showing the brain stem (*B*) and the temporal lobe (*T*)
j Coronal T2-weighted section through the paranasal sinuses and orbits
k Axial FLAIR image. FLAIR is a T2 image with black CSF. As on T2 images, any pathology would have high signal – white. Pathology in the periventricular region is much easier to see than on a T2 sequence
l Frontal MRA of the circle of Willis. *A*, anterior cerebral artery, *M*, middle cerebral artery; *P*, posterior cerebral artery; *B*, basilar artery; *V*, vertebral artery; *C*, carotid artery

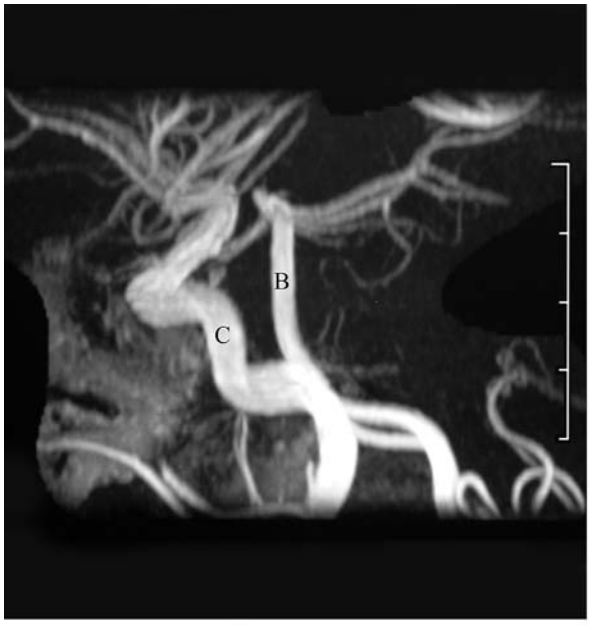

m

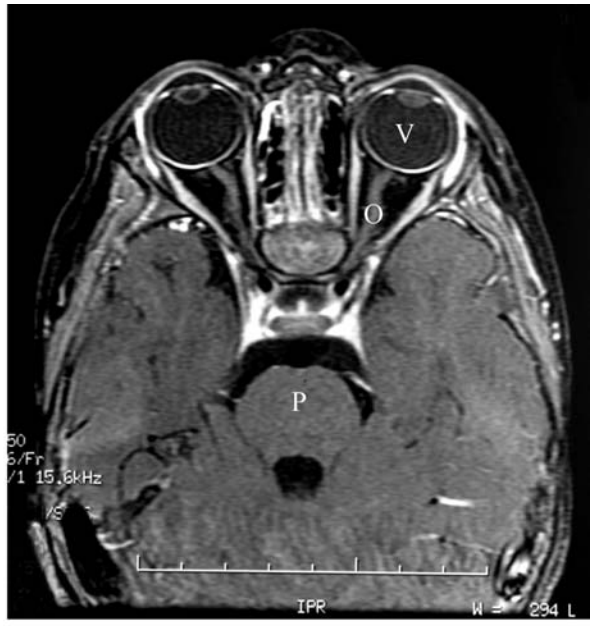

n

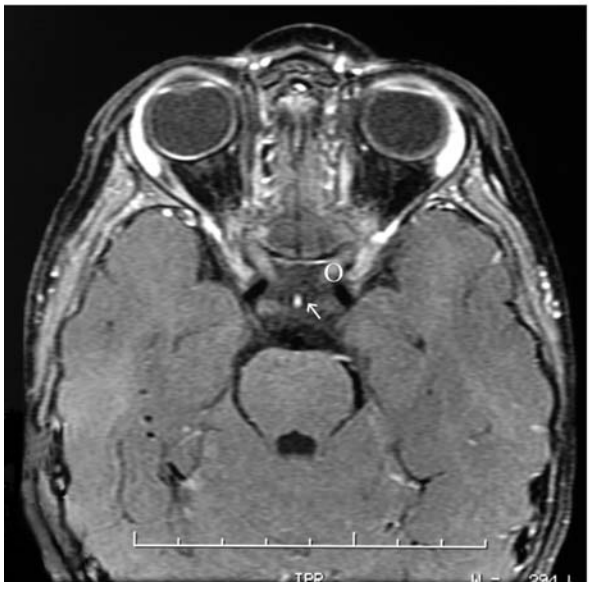

o

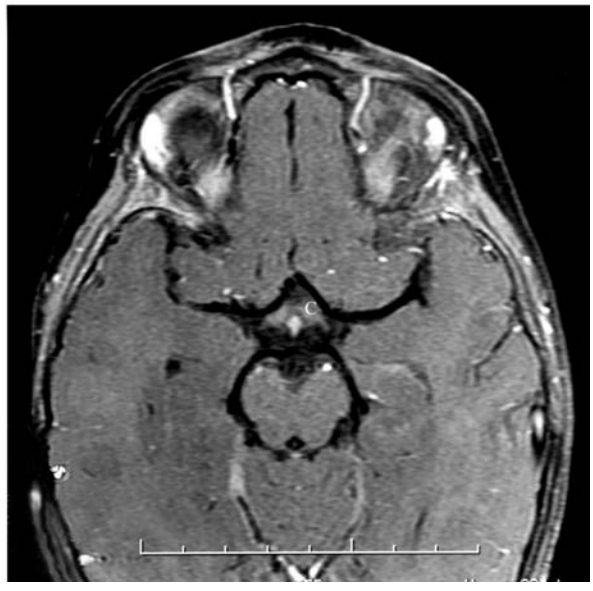

p

Fig. 8.10 (*continued*)
m Sagittal MRA at the circle of Willis showing the basilar (*B*) and carotid arteries (*C*)
n Fat-suppressed T1 image post-contrast of the orbits. *V*, vitreous chamber; *O*, optic nerve; *P*, pons
o Another contrast-enhanced axial T1 fat-suppressed image of the orbits shows the optic nerve (*O*) exiting from the optic canal and the enhancing pituitary stalk (*arrow*)
p A higher cut in the same sequence shows the optic chiasm (*C*)

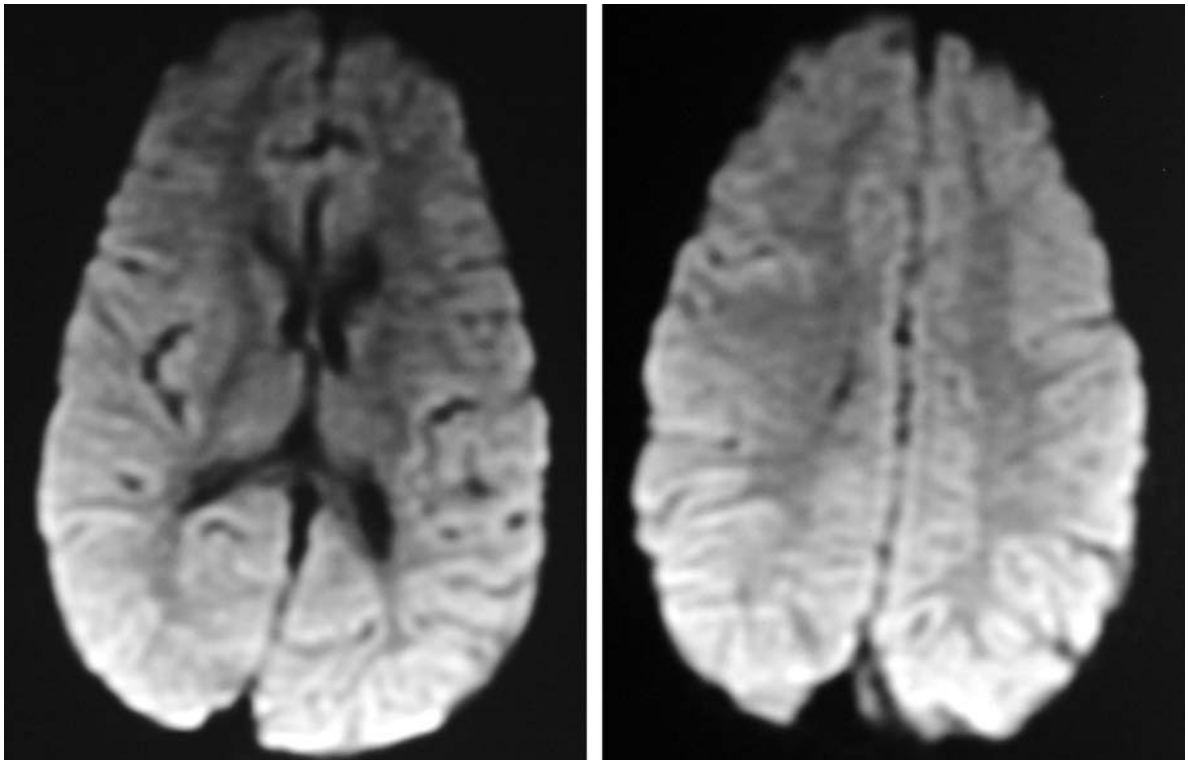

q r

Fig. 8.10 (*continued*)
q, r Two images from a diffusion-weighted study. Note the homogeneous gray appearance of the brain. If there were abnormalities, it would be a bright white high signal

Indications for Imaging Evaluation

Trauma

Over 50% of young children with epidural and subdural hematomas do not have changes in the bony skull, i.e., do not have skull fractures [2]. Thus, absence of fracture does not rule out damage to the brain. It is apparent, then, how useful seeing the intracranial contents really is. Similarly, not all children who have had trauma need imaging evaluation. The mechanism of injury must be considered. For example, patients with high-velocity injuries should be imaged. Children with altered sensorium, the unconscious child, the child with neurological findings, and the patient with a history of potential severe central nervous system trauma needs CT imaging to detect and define the extent of damage to the intracranial contents. MR is becoming faster and more accessible. It is more sensitive than CT for microhemorrhages, diffuse axonal shearing injuries, and infection. Since all of these occur in trauma, MR will play a greater role in the imaging of severely traumatized patients. The diffusion-weighted and fluid attenuated inversion recovery (FLAIR) techniques are most helpful (see Chap. 1).

As in all imaging evaluations, the patient should have stable vital signs before beginning this procedure. The goal of this evaluation is to detect parenchymal abnormalities or shifts of intracranial contents by either parenchymal or extra-axial lesions and changes in ventricular size or contour.

If a child is brought to the emergency room after trauma and is alert and apparently well *without* a history of unconsciousness, retrograde amnesia, or physical findings suggestive of central nervous system alteration (palpable bony malalignment, CSF discharge from either the ear or nose, tympanic membrane discoloration, absence of neurological findings), the chances of a significant fracture or the need for intracranial imaging are extremely small. However, there is still a role for limited and selective use of skull films, especially in cases of possible child abuse or unusual skull fractures. The latter include: (a) depressed fracture, where a fragment of bone is pushed in on intracranial contents; (b) diastatic fracture or growing skull fracture, in which the meninges

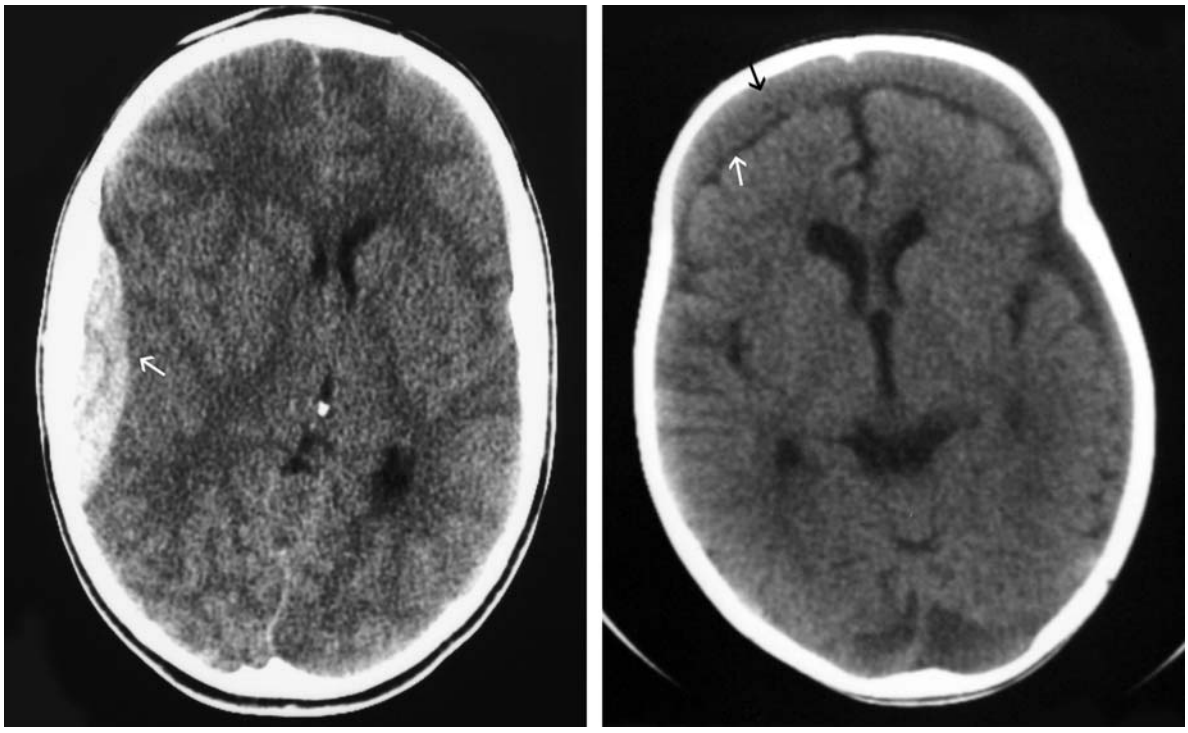

a b

Fig. 8.11. Extra-axial fluid collections
a This was an 11-year-old boy who was kicked while playing football and was unconscious for several minutes. He went home but then had acute intracranial symptoms and was brought to the emergency room. The CT scan shows a bright, white elliptical mass convex toward the brain (*arrow*). This is a classic epidural bleed and it is inhomogeneous, suggesting that bleeding may still be occurring
b A 1-year-old battered child shows complex extra-axial fluid collections (*black arrow*) which are neither black nor as gray as brain, but intermediate in attenuation. The subarachnoid fluid below is black (*white arrow*). This is a subacute subdural and is not an acute bleed. Its shape is concave toward the brain

may become entrapped and cause, by the vascular pulsations of CSF, bone erosion and enlargement of the fracture; (c) fracture through the sinuses; and (d) fractures crossing the path of the middle meningeal artery. If these lesions are seen, CT may be ordered to rule out the complications of these fractures. Remember, we are looking at the brain primarily for evidence of bleeding. Fresh blood appears white on a CT scan, and we therefore do not want to inject contrast because it too appears white and may obscure the findings. On CT of the head we routinely obtain three types of images: one that concentrates on the bony calvarium (bone windows), one that concentrates on the brain (brain windows), and one that emphasizes the extra-axial spaces so we may see less dense subdural and extradural collections (Fig. 8.11). These are obtained by postprocessing algorithms of a *single* examination of the brain.

The major indication for skull films is child abuse. The skull examination is merely the first of a series of skeletal examinations for detecting radiographic evidence of child abuse (see Chap. 7).

When looking for fractures on plain films, remember these rules:

- Soft tissue swelling often accompanies acute fractures.
- An acute fracture line is sharp, does not branch, and does not have sclerotic margins.
- With rare exceptions, there are no sutures within the parietal bone; therefore, any sharp, linear lucency in this region is a fracture until proven otherwise.
- There are so many vascular grooves and normal variants that it is important to have available one of the standard references for normal skull roentgen variants (see "References and Further Reading").

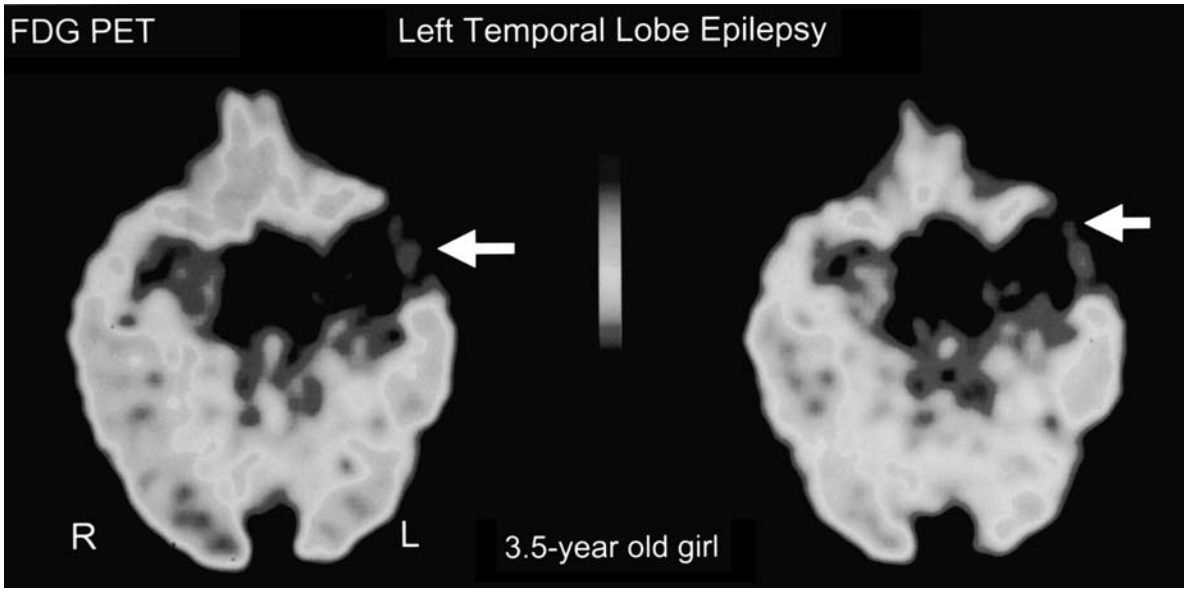

Fig. 8.12. PET for intractable seizures
This 3.5-year-old girl has an area of hypometabolism (*arrow*) in the left temporal lobe. With resection of the seizure foci, the seizure may be controlled or disappear completely

Seizures

An imaging procedure is usually not necessary for a child with febrile seizure. In most instances the major consideration is meningitis, for which a spinal tap is diagnostic. However, the work-up of a child with a nonfebrile seizure is a different matter. When there are no other neurological signs or symptoms and no personality or behavior changes, the probability of finding abnormalities on imaging is quite low. The major concern is that an intracranial mass lesion (tumor, subdural hematoma, etc.) is causing the seizure. One of the best (although nonspecific) tests is the EEG. This detects superficial masses as well as generalized electrical abnormalities. The most sensitive imaging test for detecting a mass lesion is MR. The yield of an MR study in demonstrating a treatable condition in nonfebrile seizure patients without other neurological findings is very low. However, the clinical standard for a child with nonfebrile seizures is to have one imaging procedure during the work-up (not acutely if seizure is the only symptom or sign), and MR appears to be the best modality. Remember: tumors and infections (both of which cause seizures) disrupt the blood–brain barrier. These abnormalities allow contrast to penetrate and enhance the areas of inflammation or tumor.

The role of nuclear medicine single-photon emission computed tomography (SPECT) and PET is for intractable seizures. These procedures are reserved for patients with the most severe and difficult conditions and are a prelude to therapy (seizure surgery) (Fig. 8.12).

Increased Intracranial Pressure or Enlarging Head Circumference

It is easy to evaluate a child with an open fontanelle for increasing intracranial pressure. The fontanelle bulges when the child is in a sitting position, and the child may also exhibit a high-pitched cry and irritability. Prior to fontanelle closure, ultrasound evaluation detects ventricular enlargement (Fig. 8.13). Once the fontanelle closes, the sutures may spread before the patient exhibits some of the clinical signs of increased pressure, such as papilledema. Because radiographic signs often precede the clinical clues, you should be familiar with the major plain film radiographic signs of increased intracranial pressure. Remember, however, that a skull film is not the kind of imaging most appropriate to solve this clinical problem.

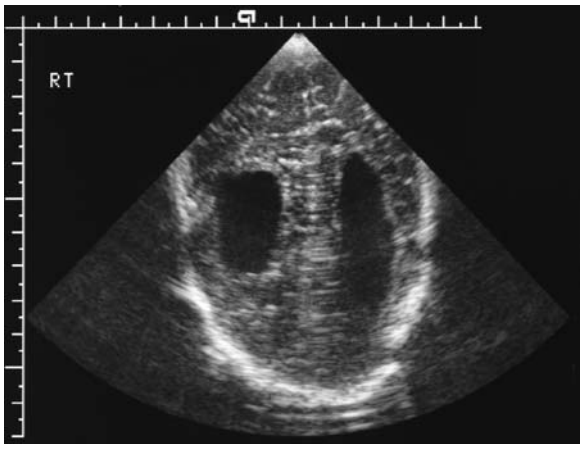

Fig. 8.13. Ventriculomegaly
This is a coronal ultrasound study through the anterior fontanelle at a level just behind the atria of the lateral ventricles. Note the large ventricles. Ultrasound is an anatomic study and cannot show whether increased pressure is causing the ventriculomegaly or whether there is merely ventricular enlargement in response to a damaged brain. Ultrasound cannot determine pressure

Spreading of the Cranial Sutures

The coronal suture widens first (due to increased intracranial pressure), but this is often difficult to interpret if it is the only finding. It is important to see all of the sutures widened to accurately diagnose increased intracranial pressure. The lateral view is *not* the best view to determine suture spread, as there may be superimposition of right and left sides; rather, the frontal projections – Towne's or PA – are best (Fig. 8.14). Children with increased intracranial pressure may have spread sutures before papilledema – up to the age of 10–12 years (see [3, 4]). Remember that in neglected or nutritionally starved children there may be a rebound growth with suture spread as the child recovers. In this instance the sutures are spread, but there is no increased intracranial pressure.

Alterations of the Sella Turcica

Ventricular enlargement produces pressure on the dorsum sellae and it may become thinned. This leads to eventual erosion of the dorsum. It becomes truncated and sharpened. The sella may enlarge (Fig. 8.14). Such changes reflect increased intracranial pressure and are not specific for the etiology.

Why is there increased intracranial pressure? The differential diagnoses in children include diverse etiologies not considered in adults, such as lead encephalopathy, congenitally obstructive hydrocephalus, and congenital arteriovenous malformations such as a vein of Galen malformation. Increased intracranial pressure is of course a major presenting sign in a child with a brain tumor.

The skull film, however, is not the most efficacious imaging test in a child suspected of having increased intracranial pressure; CT or MR (whichever can be obtained more quickly) should be performed to detect the etiology of the increased pressure. Unfortunately, one of the more common causes of increased intracranial pressure is subdural hematoma secondary to child abuse. Not all subdural hematomas are bright on CT (see Fig. 8.11); for this reason, if abuse is suspected, an MR can be obtained to date the hemorrhage (blood and hemosiderin appear differently).

Abnormal Head Shape or Size

The neonate or young infant with an abnormal configuration of the head should be examined radiographically for premature closure of a suture (craniosynostosis). We are more concerned about the cranial vault than the intracranial contents. The most common suture to close prematurely is the sagittal suture. These patients have an elongated head from front to back with a palpable bony ridge over the top. Radiographically only a portion of a suture needs to be closed to result in an abnormal cranial configuration (functionally the entire suture is closed) (Fig. 8.15).

The screening test for suture closure is the plain film, although there are some advocates of ultrasound. When necessary, 3D CT can be done at low mAs to define the problem (Fig. 8.15).

In the child with an enlarging head, skull films are not specific. In the young infant ultrasonography of the intracranial contents detects congenital anomalies and hydrocephalus (Fig. 8.13), while CT studies provide the answer in older children. The commonest reason for large ventricles necessitating therapy in our institution are: (1) post-hemorrhagic hydrocephalus of the premature, (2) the myelomeningocele patient, (3) other congenital central nervous system anomalies, (4) brain tumors, (5) trauma, and (6) post-meningitis.

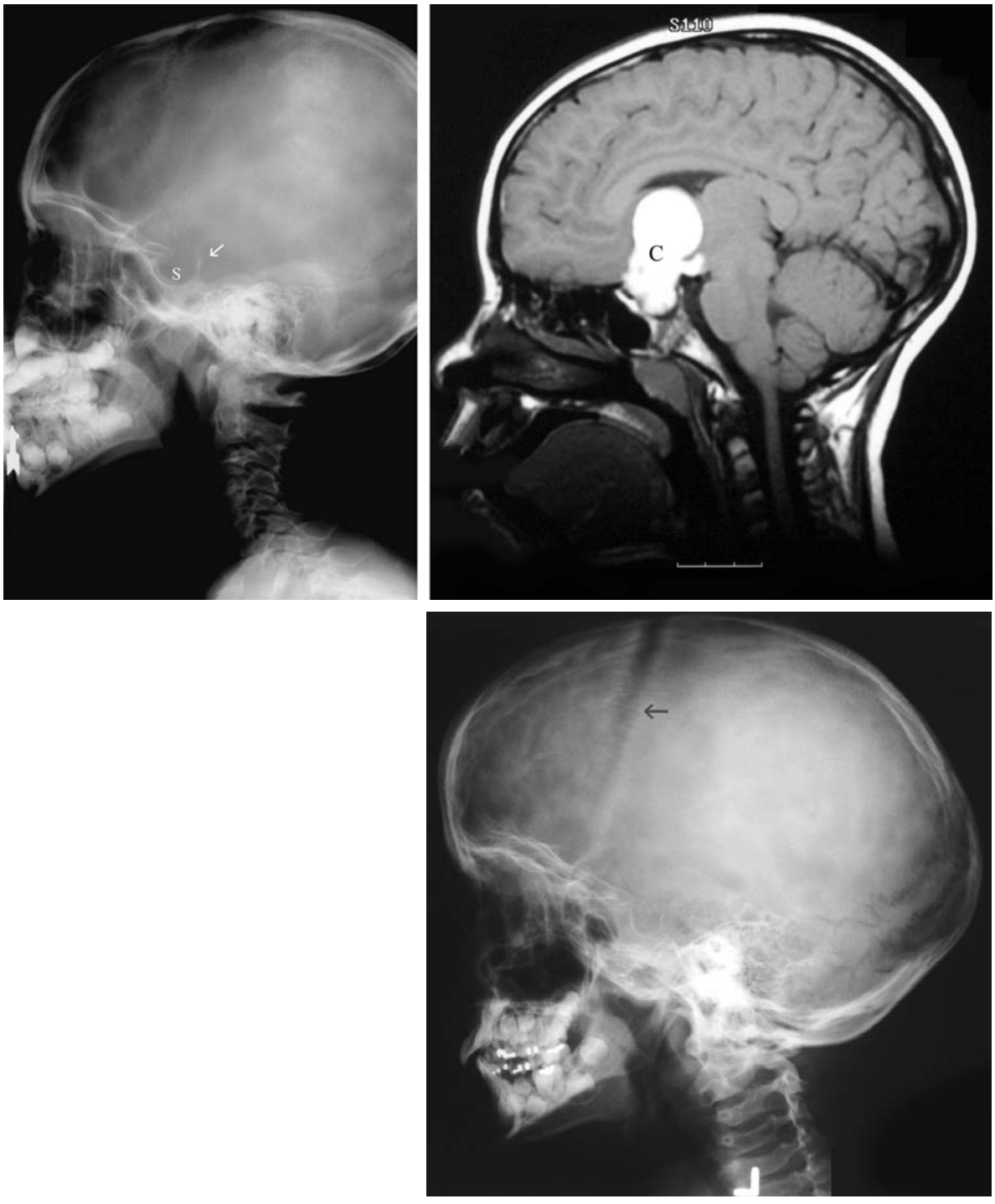

Fig. 8.14. Signs of intracranial pressure
a This is a 7-year-old with symptoms of visual disturbance and headaches. The lateral film shows an enlarged sella (*S*) and truncated dorsum sellae (*arrow*). There is some fine calcification present above the dorsum
b T1-weighted sagittal MR image shows a large craniopharyngioma (*C*) involving the sella
c Lateral film in another child with increased pressure. Although the lateral film is not the best to show spread sutures because the two sides may be superimposed, it is clear in this child that the coronal suture is widened (*arrow*)

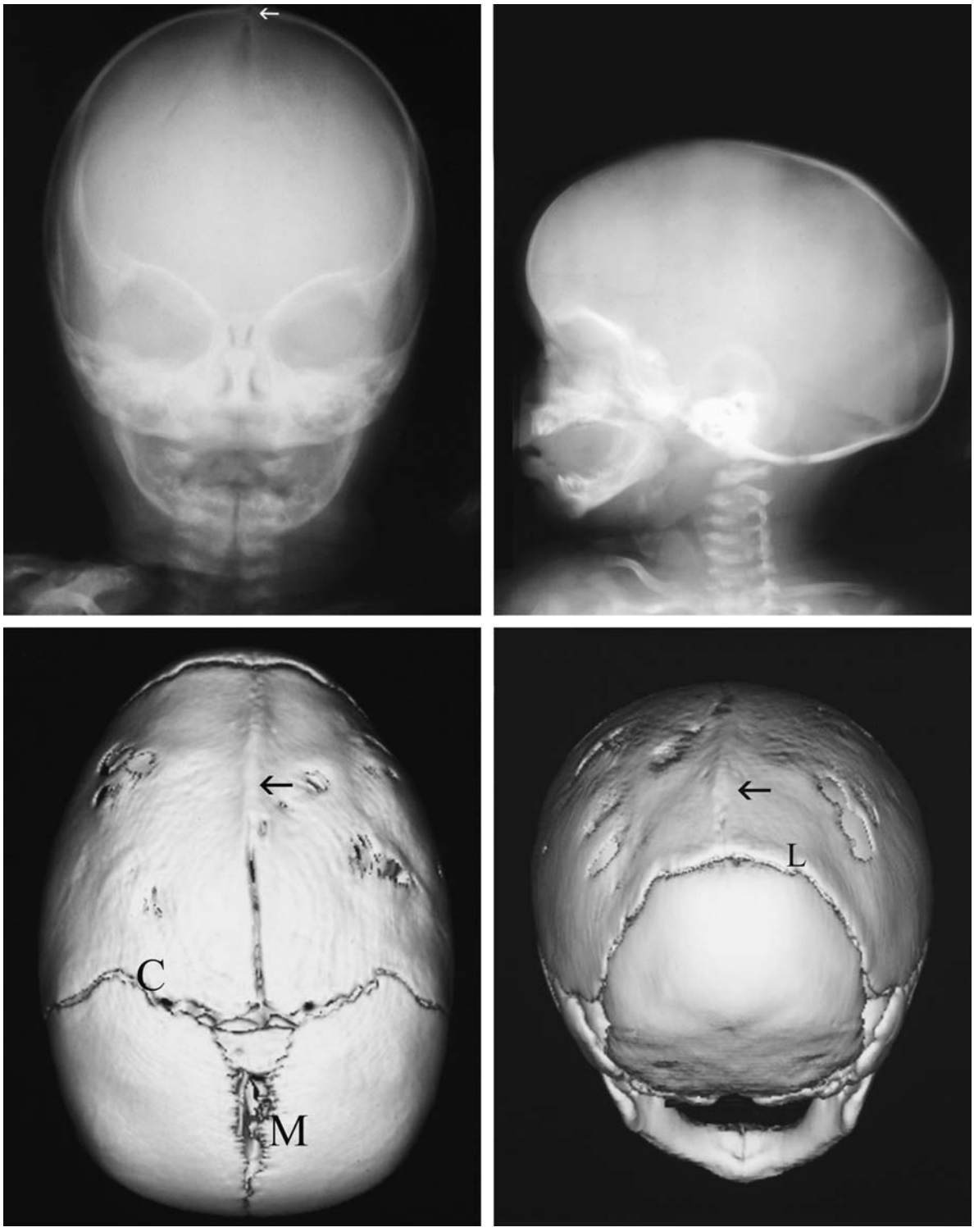

Fig. 8.15. Craniosynostosis
a Caldwell view showing the sagittal suture is closed (*arrow*)
b Lateral skull film of the same patient reveals increased head circumference from posterior to anterior – scaphocephaly. The child has sagittal suture craniosynostosis
c, d Three-dimensional "bird eye" (from the top) (**c**) and posterior (**d**) images of a child with a partially closed (*arrow*) sagittal suture – sagittal craniosynostosis. *C*, coronal suture; *M*, metopic suture; *L*, lambdoid suture
e–i see pp. 233, 234

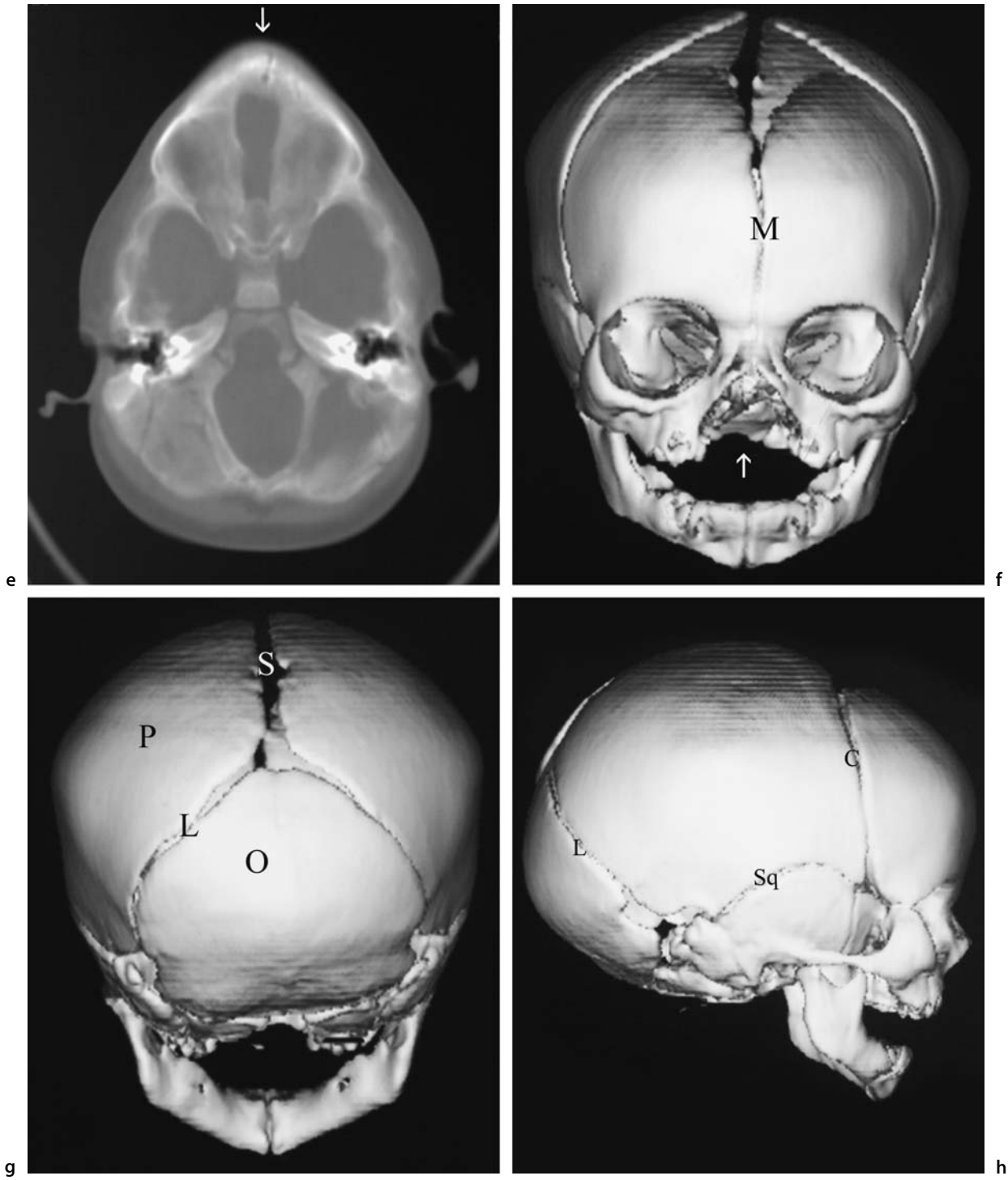

Fig. 8.15 (*continued*)
e Axial CT scan with bone windows shows the pointed forehead – trigonocephaly (*arrow*). This configuration resembles the keel of a boat and indicates metopic craniosynostosis
f–i 3D image reconstruction of a child with a recessed jaw and a cleft lip and plate (*arrow*). Compare the sutures in this patient with Figs. 8.1 and 8.2. *O*, occipital bone; *P*, parietal bone; *L*, lambdoid suture; *S*, sagittal suture; *M*, metopic suture; *C*, coronal suture; *Sq*, temporal squamosal suture; *AF*, anterior fontanelle

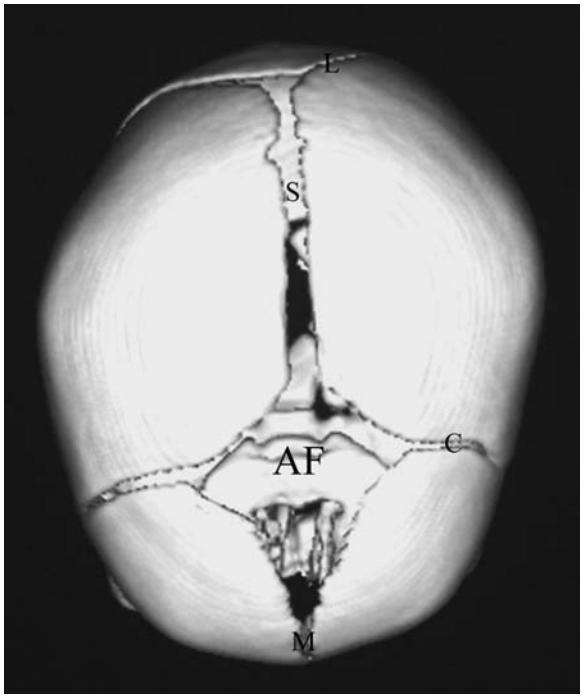

i

Fig. 8.15 (*continued*). Legend see p. 233

The child with a small head may well have one of the congenital infections– the TORCHS diseases (*to*xoplasmosis, *r*ubella, *c*ytomegalovirus, *h*erpes, *s*yphilis). While gross calcifications are easy to detect on plain films, more subtle calcific deposits are best detected by ultrasound and CT (Fig. 8.16). Contrast is not used when looking for intracranial calcium because calcium is white on CT, and contrast would therefore obscure the findings.

Other Indications for Imaging Evaluation of CNS

These include new or progressive neurological findings and metastatic disease – the latter with both skull films (if this is a primary tumor that commonly goes to bone) and MR (if intracranial metastasis is sought).

Tumors, stroke, metabolic diseases, and neurodegenerative diseases cause new and/or progressive neurological symptoms. The acuity of the presentation determines the imaging procedure of choice. CT will show masses and hemorrhage and is the most accessible test. However, it is not as good as MR in the posterior fossa nor in early (hours to days) stroke. It frequently is not helpful in metabolic/neurodegenerative diseases at their onset. Magnetic resonance spectroscopy (MRS) is a superb test for detecting metabolic (biochemical) abnormalities, frequently showing a high lactate peak (Fig. 8.17).

Tumors of the posterior fossa are more common than supratentorial lesions in children over 1 year of age. From birth to 1 year, supratentorial and infratentorial lesions are present in equal numbers (Table 8.2).

Table 8.2. Common brain tumors in childhood

Posterior fossa
Medulloblastoma
(includes primitive neuroectodermal tumors, PNET)
Astrocytoma (glioma)
Ependymoma
Supratentorial
Astrocytoma (glioma)
Craniopharyngioma
Pineal germ cell tumors
Metastatic
Neuroblastoma

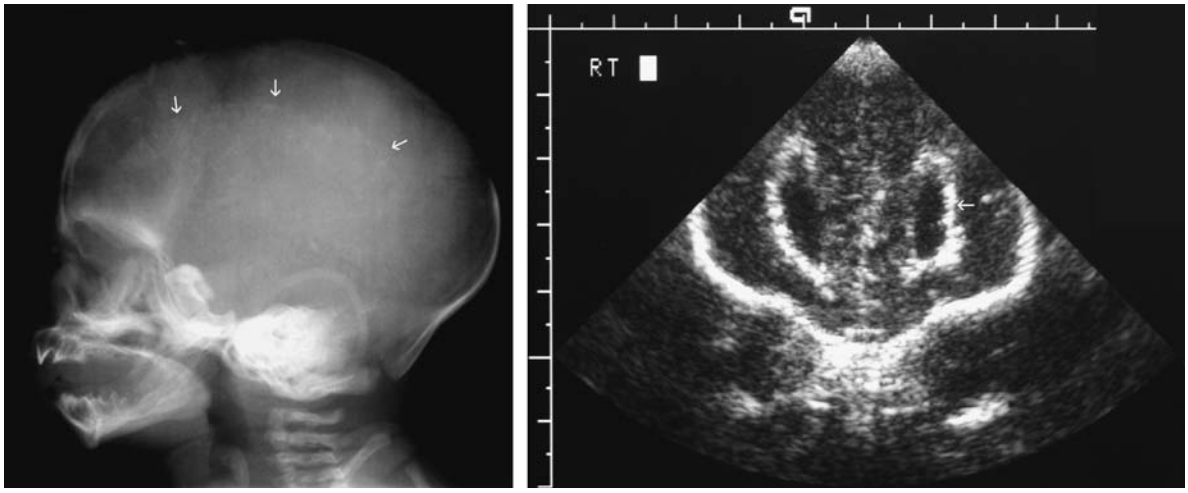

a b

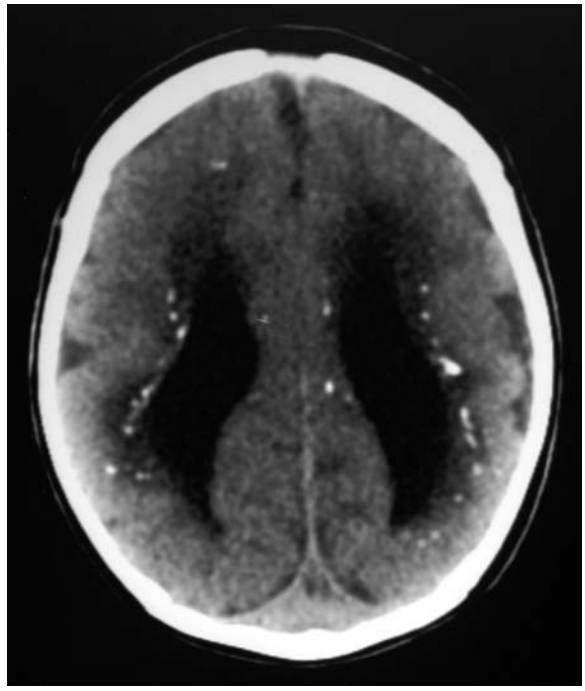

c

Fig. 8.16. TORCHS
a Lateral skull film in an infant with cytomegalovirus (CMV) reveals calcifications (*arrows*) in a periventricular location
b Ultrasound study of the same child shows the echogenic (*arrow*) periventricular calcification surrounding large ventricles
c CT scan in another patient reveals ventriculomegaly and periventricular calcifications

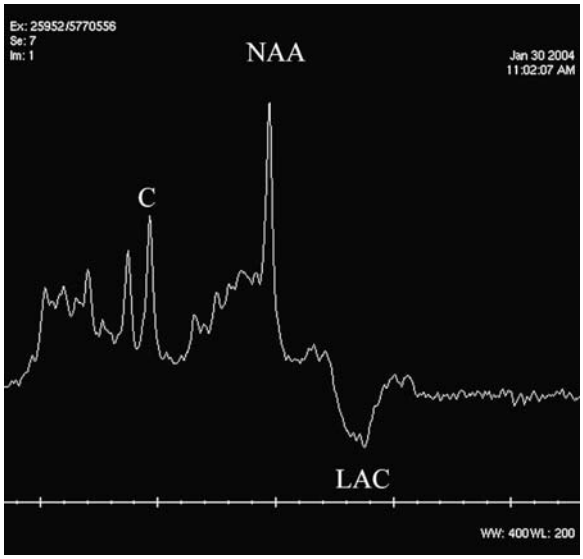

Fig. 8.17. Normal magnetic resonance spectroscopy (MRS). The horizontal axis indicates parts per million of the compound demonstrated. *N*-acetyl aspartate (*NAA*) is located at 2 parts per million, creatine (*C*) at 3 parts per million, lactate (*LAC*) is located 1 part per million. Lactate appears when there is a breakdown of aerobic metabolism within cells and a switch to anaerobic metabolism. Lactate elevation is seen in various metabolic disorders, following hypoxia, at times in tumors and abscesses, and in demyelination or inflammatory processes. It is never seen as a substantial normal peak

Supplementary Procedures in Evaluating the Central Nervous System

Arteriography. One performs arteriography by passing a catheter via the femoral artery to the carotid and/or vertebral arteries (see Chap. 9). The procedure helps map precise arterial anatomy before surgery and is frequently used in tumors to clarify and supplement CT/MR studies and for delineating vascular malformations.

MR Angiography. As discussed in Chap. 1, the computer (provided with the correct software) can provide images by MR of the cranial blood vessels (see Fig. 8.10).

Imaging the Paranasal Sinuses and Neck

The most common head and neck lesions in childhood are those related to infection – paranasal sinusitis, orbital cellulitis, and cervical adenitis. Plain films of the paranasal sinus are notoriously unreliable for diagnosing sinus involvement, except when there is an air–fluid level present – a clear sign of sinusitis (Figs. 8.18 and 8.19).

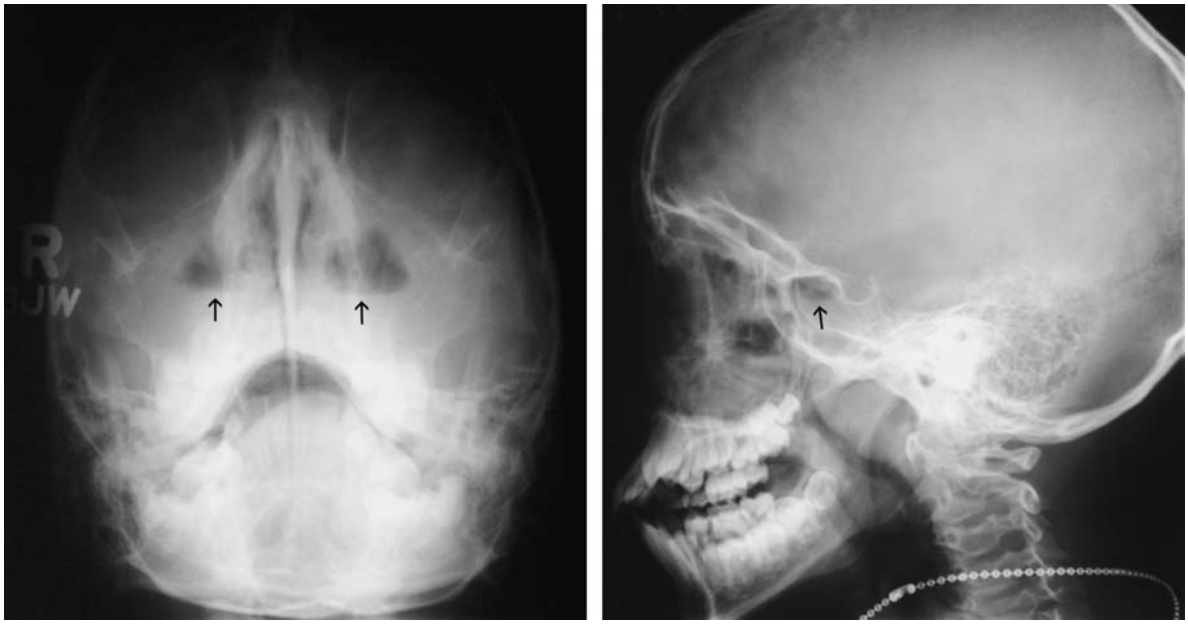

a b

Fig. 8.18. Acute sinusitis on plain films
a Waters' view in the erect position shows bilateral air–fluid levels in the maxillary sinus (*arrows*). Note the walls of the maxillary sinus and how much of the sinus is filled with fluid. The black areas are the residual air (compare to Fig. 8.5)
b Sphenoid sinus air–fluid level (*arrow*) in this erect lateral film. What other abnormalities do you see? There is a large amount of adenoid tissue present obscuring the nasopharyngeal air passage

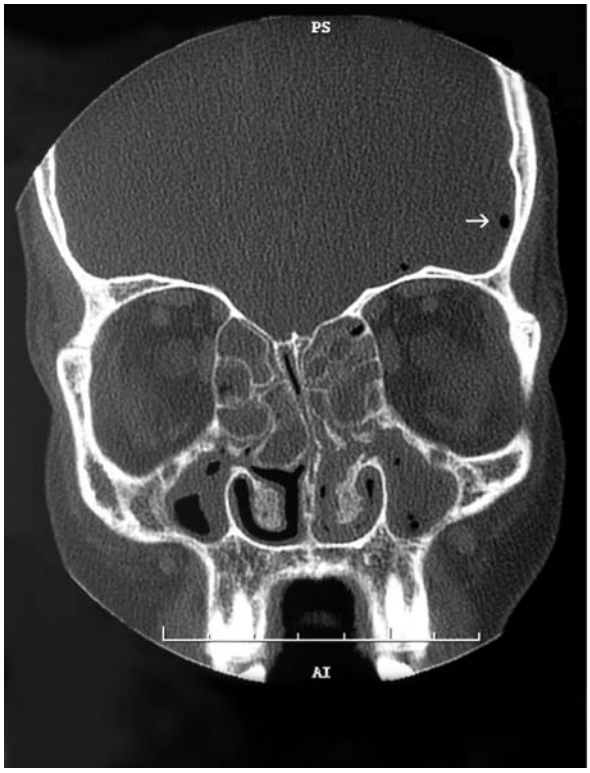

a

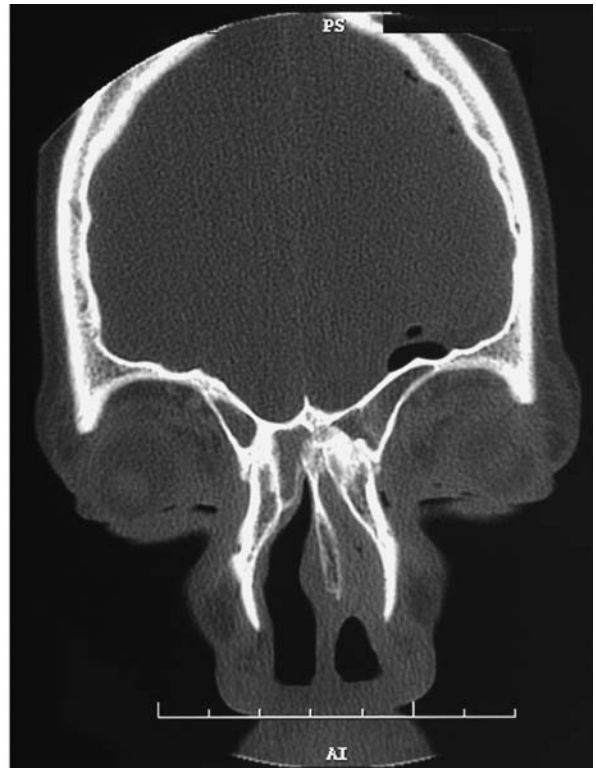

b

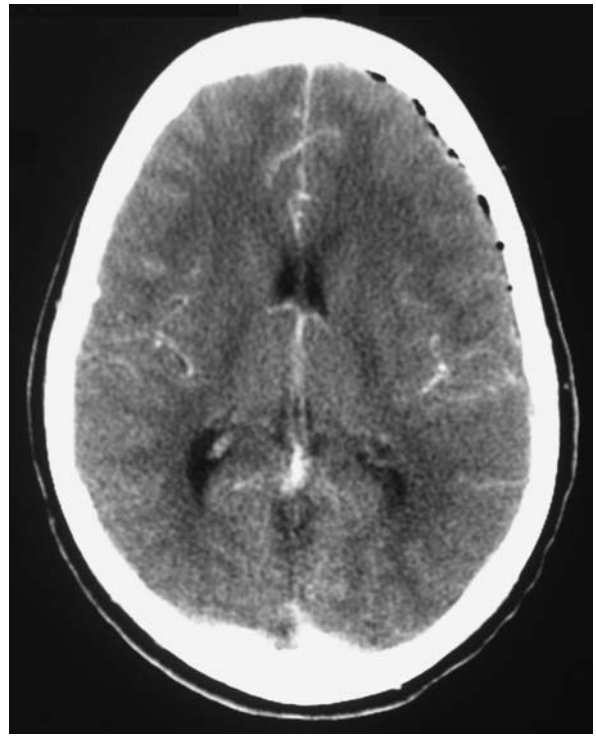

c

Fig. 8.19. Complication of sinusitis in a 15-year-old
a Coronal CT scan of the paranasal sinuses shows opacification of the maxillary and ethmoid sinuses. There is air (pneumocephalus) within the calvarium (*arrow*)
b Coronal scan at the level of the opaque left frontal sinuses. Once again the pneumocephalus is seen
c Enhanced axial CT of the brain shows the air to be extra-axial. These patient developed an epidural infection and a brain abscess

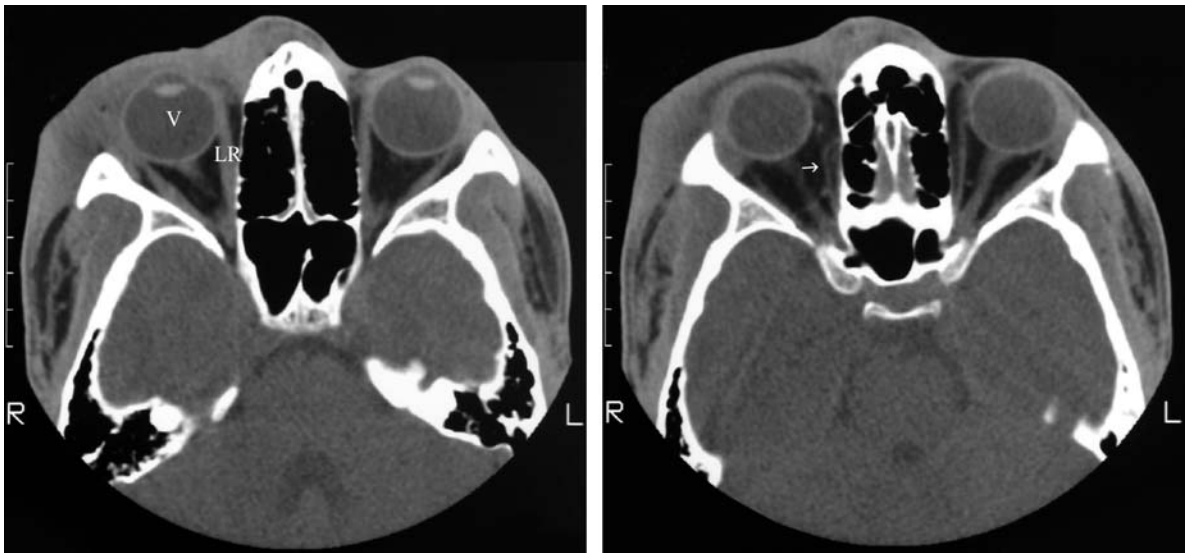

a b

Fig. 8.20. Orbital cellulitis in a 14-year-old with a swollen right eye
a The soft tissues anterior to the right eye are quite swollen. The swelling extends over the nose. This is the preseptal component. *LR*, lateral rectus; *V*, vitreous chamber
b There is a postseptal component with abscess formation (*arrow*). Compare to the opposite side. Remember, always look for asymmetry

Coronal CT is the best test for evaluating the paranasal sinuses and specifically the osteomeatal complex – the opening of the maxillary sinuses into the nose (see Fig. 8.9). Here again low mAs should be used to reduce radiation dose (Chap. 2). Orbital inflammation may be in front of the attachment of the tarsal plate of the eyelid (preseptal) or behind this attachment (postseptal) (Fig. 8.20). Postseptal orbital cellulitis originates in adjacent paranasal sinus infection.

The tarsal plates are a fibrous layer of tissue in each eyelid. They are semilunar in shape and attach medially (near the lacrimal sac) and laterally (at the lacrimal gland) to protect the eye. When the inflammation is in front of the tarsal plate – preseptal cellulitis – and there is full range of eye motion, no imaging is necessary.

Both CT and MR are excellent for evaluating masses of the neck. When it is important to detect bone involvement, CT is preferable. The most common mass is lymphadenopathy, while the most common malignant soft tissue tumor of the neck in childhood is rhabdomyosarcoma. With children, one must always think of congenital abnormalities such as infected thyroglossal duct or branchial cleft cyst.

Spine

Anatomy

The complexities of and differences among the cervical, thoracic, lumbar, and sacral segments are beyond the scope of this text; but knowledge of the general configuration of the bony anatomy is crucial (Fig. 8.21). The two major plain film views of the spine are the frontal and lateral. It is important to identify (a) the vertebral bodies, (b) the disc spaces between vertebral bodies, (c) the posterior elements, and (d) the spinous processes. The vertebral bodies become larger in a cephalic-to-caudal direction. The ring apophyses are best seen at the corner of the vertebral bodies on the lateral view.

The alignment of the bony spine is crucial in the radiographic diagnosis of trauma or scoliosis. This is especially true with the cervical spine; lines drawn from C1 through C7 along the anterior aspects of the vertebral bodies, posterior aspects of the vertebral bodies, and anterior aspects of the spinous processes should slope gently without sharp disruption (Fig. 8.22). Any abnormality in these lines suggests displacement. The exception is the pseudosubluxa-

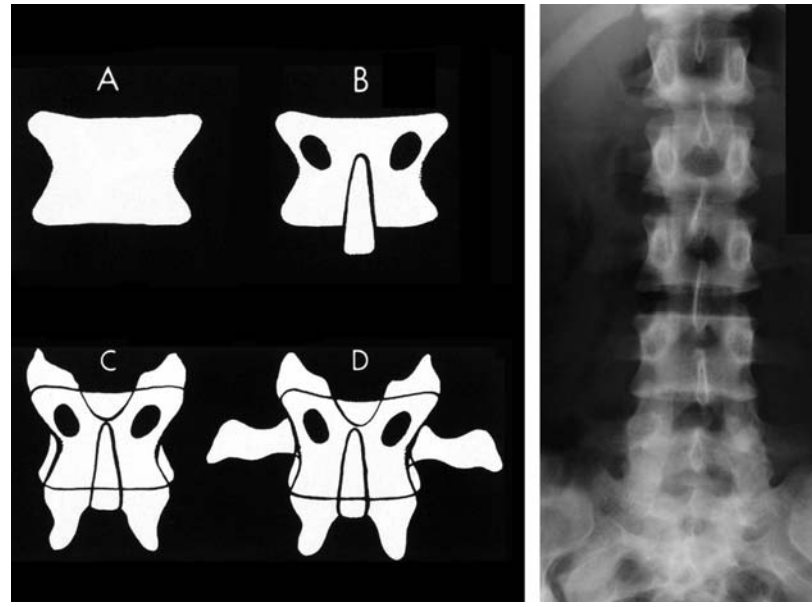

a b

Fig. 8.21. Spine
a Schematic diagram explaining the various structures and how they contribute to the final product. *A,* vertebral body; *B,* vertebral body plus pedicles in *black* and spinous process; *C,* superior/inferior articulating facets have been added; *D,* transverse processes added
b Frontal view of the lumbar spine. What is wrong with L5? (See Appendix 2)

tion of C2 and C3 due to the generalized laxity of ligaments in the infant. On the frontal projection, look for disruption of the cortex of the vertebral bodies, transverse processes, or pedicles, as well as paraspinal masses. The vertebral bodies are most frequently disrupted by infection or tumor, while the pedicles are disrupted by intraspinal processes. The pedicle is that portion of bone that borders the lateral aspect of the spinal cord and subarachnoid space. The medial aspects of the pedicles are convex; straightening of the concavity of these pedicles denotes a lesion within the subarachnoid space or spinal cord. The transverse processes are frequently affected by traumatic lesions.

We frequently ask questions about the spinal cord itself and not about its bony covering. Here MR is clearly the best test (Fig. 8.23). The entire spine can be visualized and the level of the conus medullaris demonstrated (normal T12–L2). The conus medullaris is the most inferior level of the spinal cord, with the nerve roots extending distally. Any intraspinal fluid collections (syrinx) or tumors will be seen. Swelling of the cord, traumatic lesions, and bleeding are all best detected by MR.

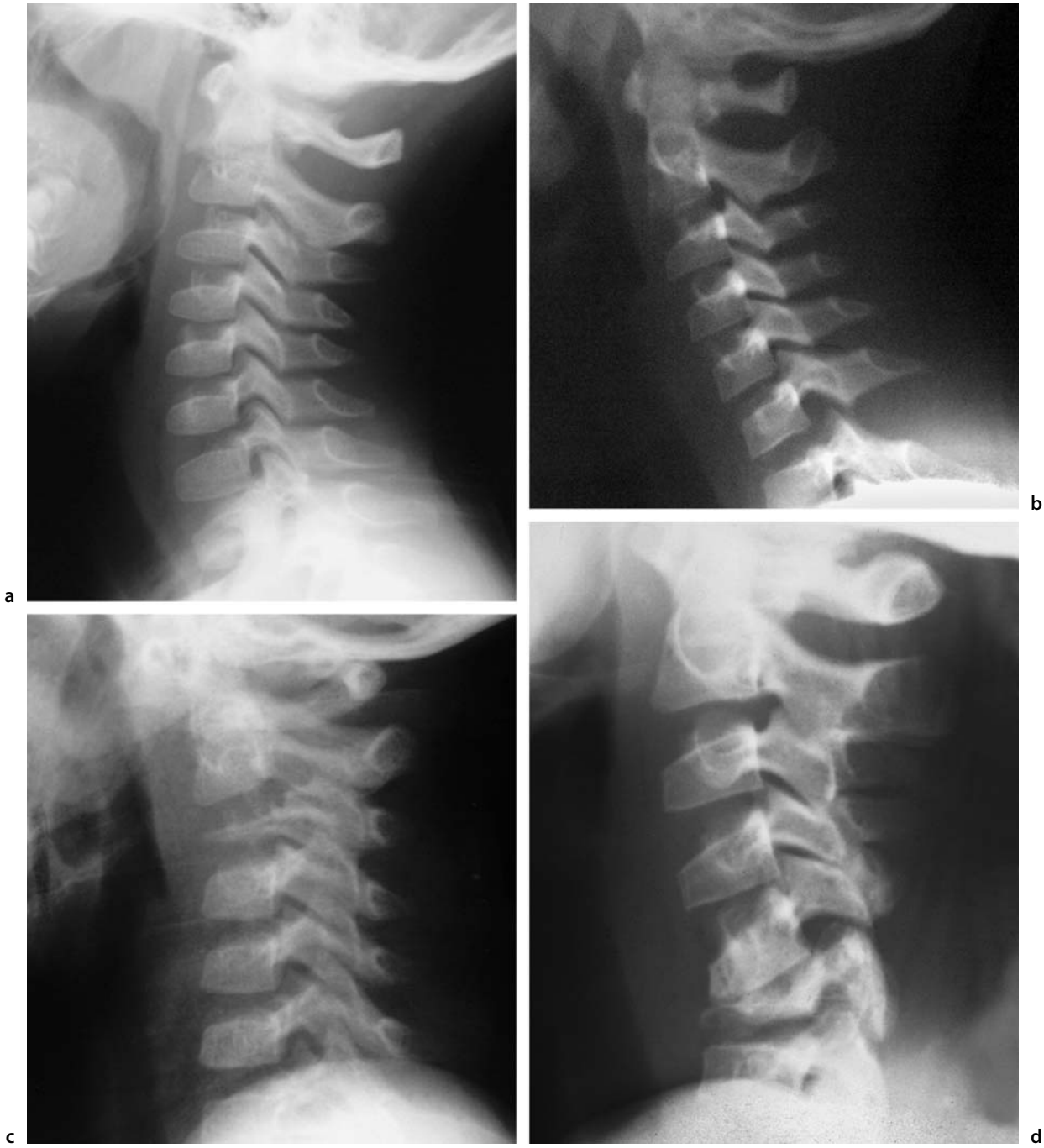

Fig. 8.22. Lateral cervical spine
a Normal lateral cervical view
b–d Can you identify the abnormalities? (See Appendix 2)

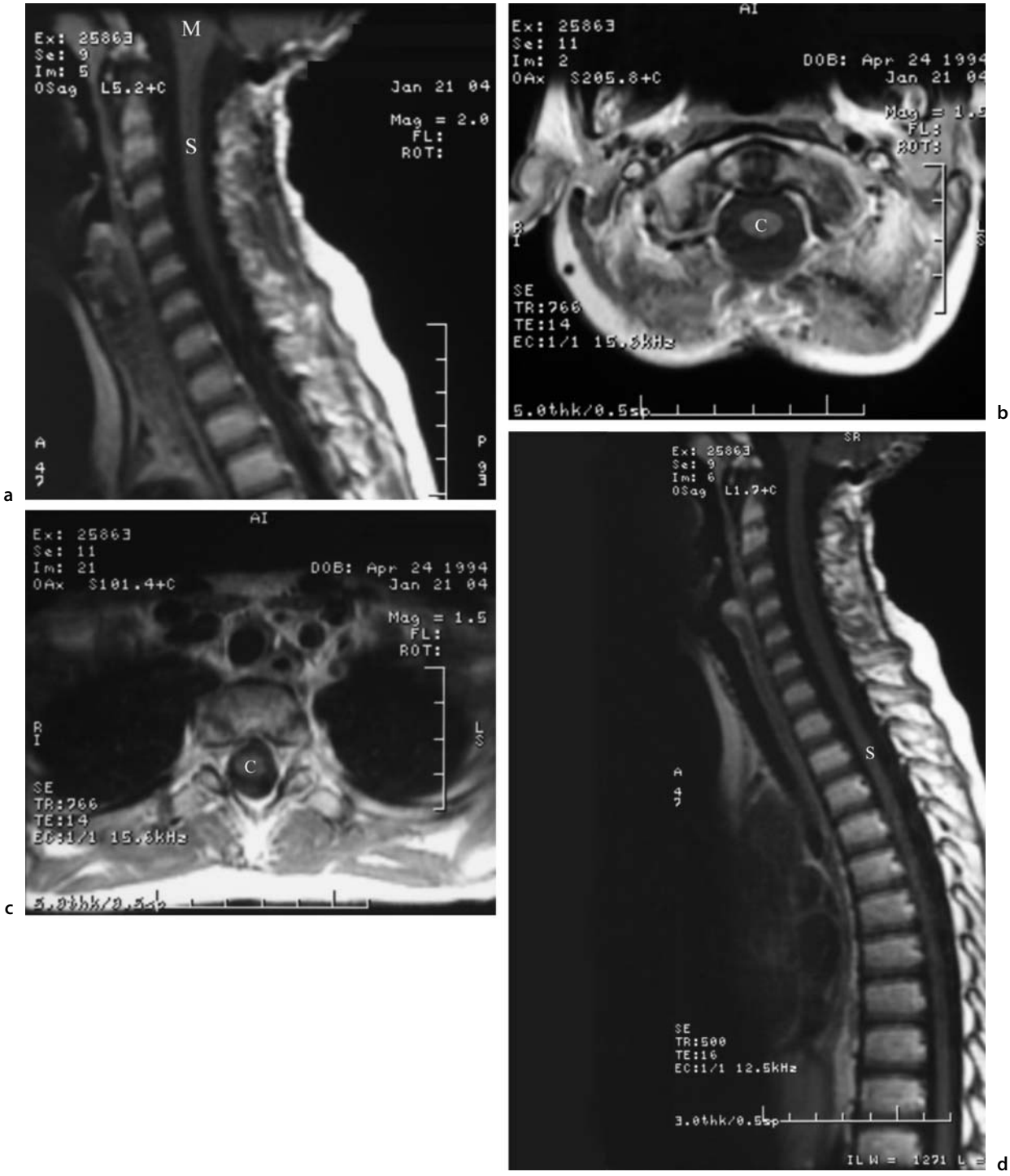

Fig. 8.23. MR of the spine

a T1 lateral midline section of the cervical spine shows the medulla (*M*) and the spinal cord (*S*). The bony vertebral bodies in this sequence are less distinct. Note that the cervical spinal cord fills less than 80% of the canal

b Axial T1 section of the same child shows the cervical spinal cord (*C*) normally positioned

c Axial T1 section of the thoracic spinal cord at the apex of the lung shows that the cord (*C*) is slightly smaller than that in **b** and is well positioned without mass

d–g Sagittal T1 (**d, f**) and T2 (**e, g**) of the thoracic and lumbar cord show the conus (*CO*) T12-L1. The cord spinal (*S*) is normal in position and shape. Note on **e** the flow artifacts (*arrow*) (dark spots) behind the spinal cord

e–j see pp. 242, 243

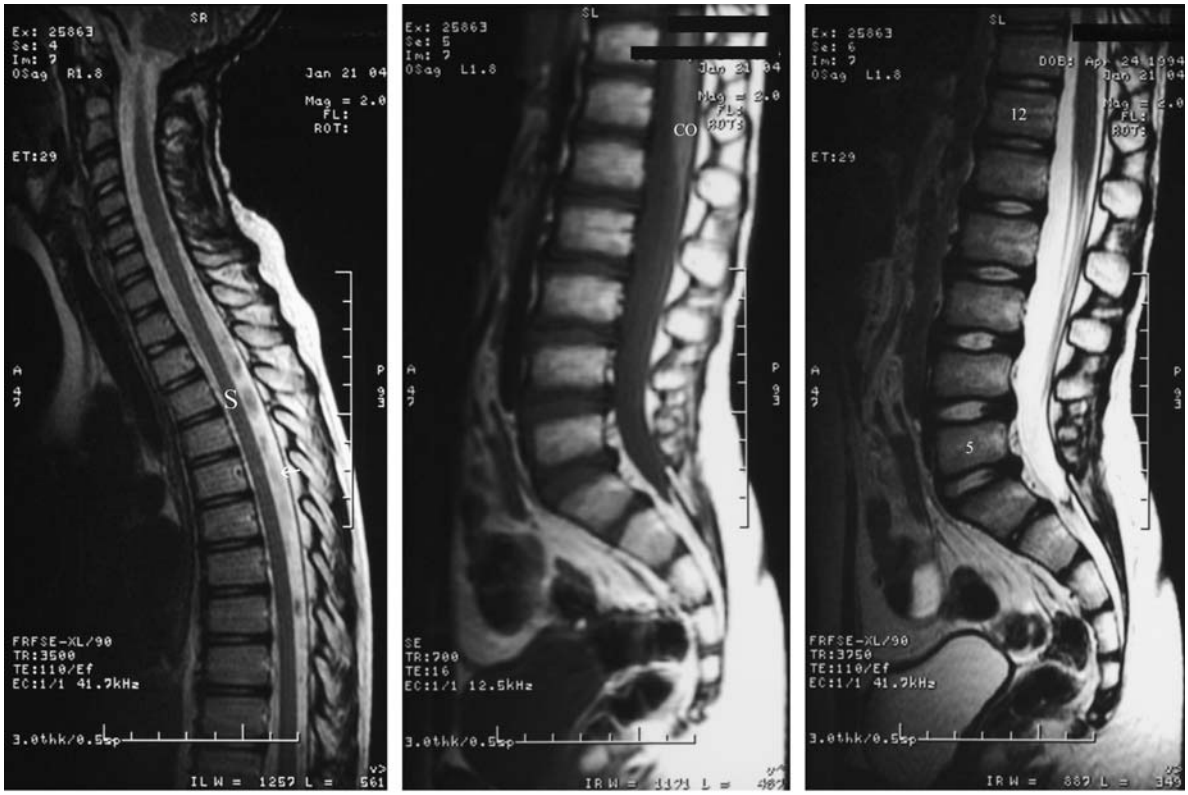

e, f g

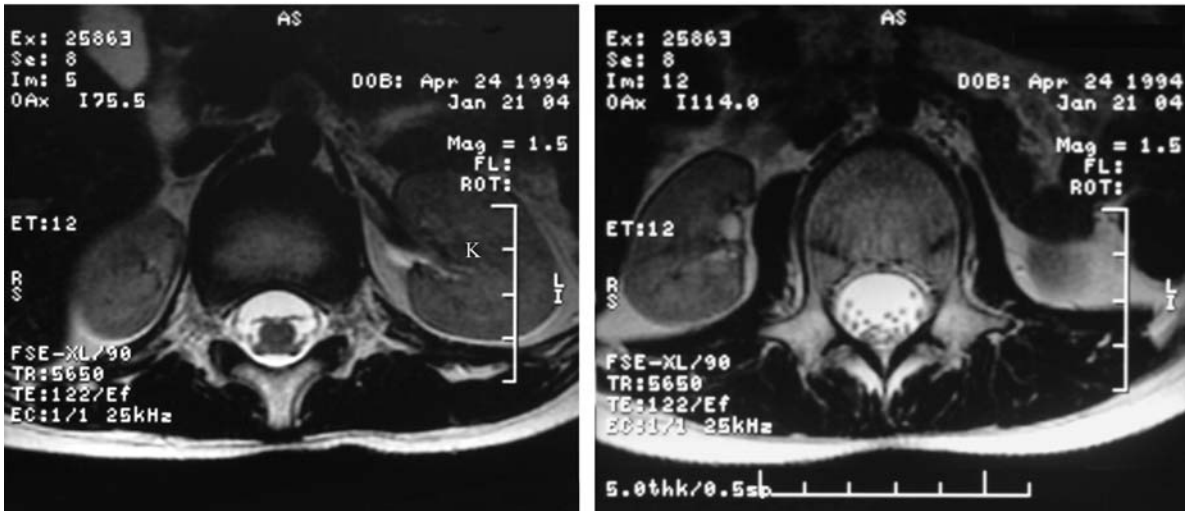

h i

Fig. 8.23. (*continued*). Legend see p. 241
h Axial T2 section at the level of the kidneys show the conus. *K*, kidney
i Axial T2 scan of the nerve roots

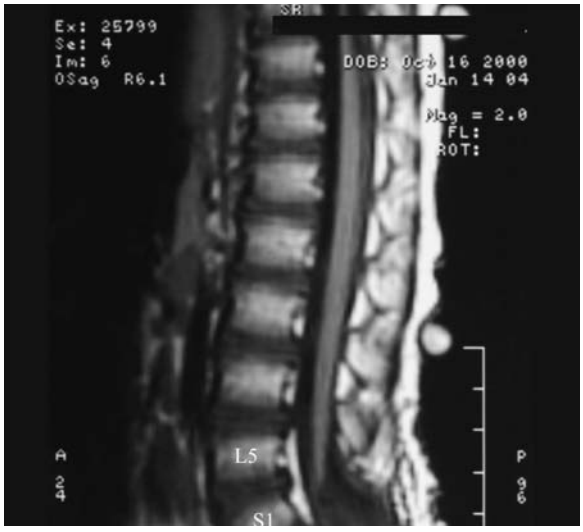

j

Fig. 8.23 (*continued*)
j Sagittal T1 scan of a meningomyelocele patient with tethered cord. The conus is at the level of L5. There is bone defect posteriorly

Indications for Imaging Evaluation of the Spine

The initial evaluation remains the frontal and lateral plain film, most often supplemented by oblique views and specific odontoid films if the cervical spine is to be evaluated. The major indication for this procedure is trauma.

Multidetector CT is excellent for fast evaluations of the bone for fracture. Reconstructions in multiple planes have enhanced our ability to diagnose fractures. When one suspects spinal cord injury on the basis of physical findings, MR is the best test. Sagittal and coronal views with multiple sequences will detect contusions, extra-axial hemorrhage, and ligamentous damage.

Other reasons for spinal imaging include back pain (an unusual complaint in childhood), weakness of lower extremities or gait problems, unusual bladder or bowel complaints (specifically of a regressive nature), or diseases that involve metastasis to the spine. Unusual curvatures of the spine (scoliosis) and congenital anomalies of the spine (spinal dysraphism, meningomyelocele) are diseases in which it is important to evaluate the nature of the spinal cord itself. In these instances, MR is necessary.

A specific abnormality seen in teenagers is herniation of the nucleus pulposus – Schmorl's node – from its normal position in the center of the disk.

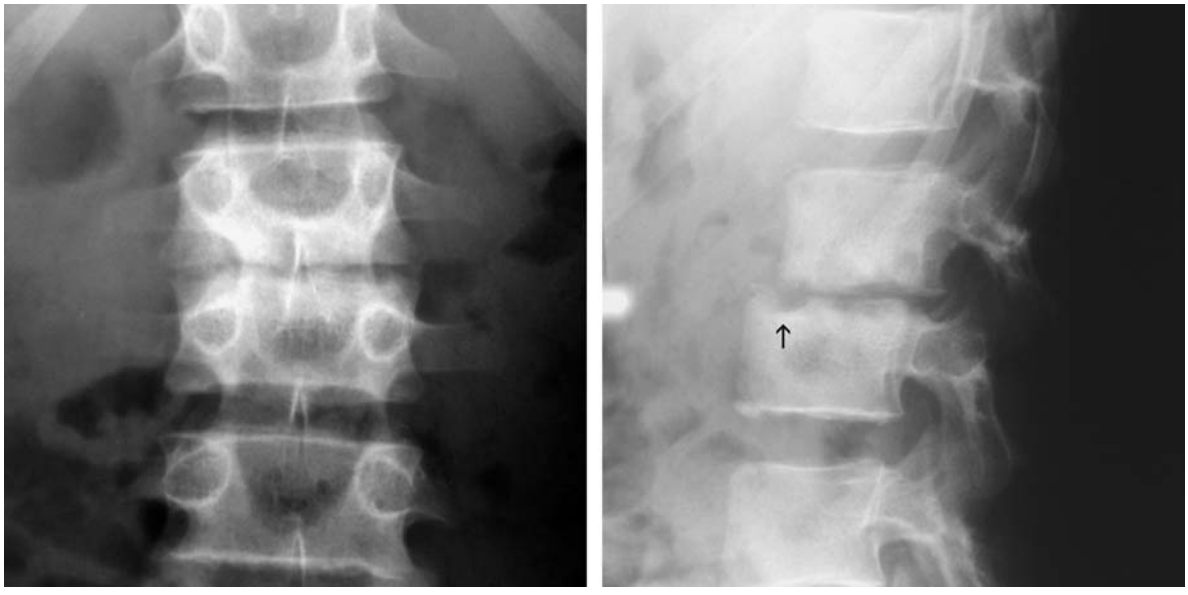

a b

Fig. 8.24. Herniation of the nucleus pulposus: Schmorl's node
a Frontal view of the lumbar spire reveals narrowed disk space between L2 and L3 with irregular margins
b Lateral view shows the narrow disk space and the large AP diameter of L3. The anterior defect (*arrow*) is the site where the nucleus pulposus has herniated and disrupted the ring apophysis of the vertebral body

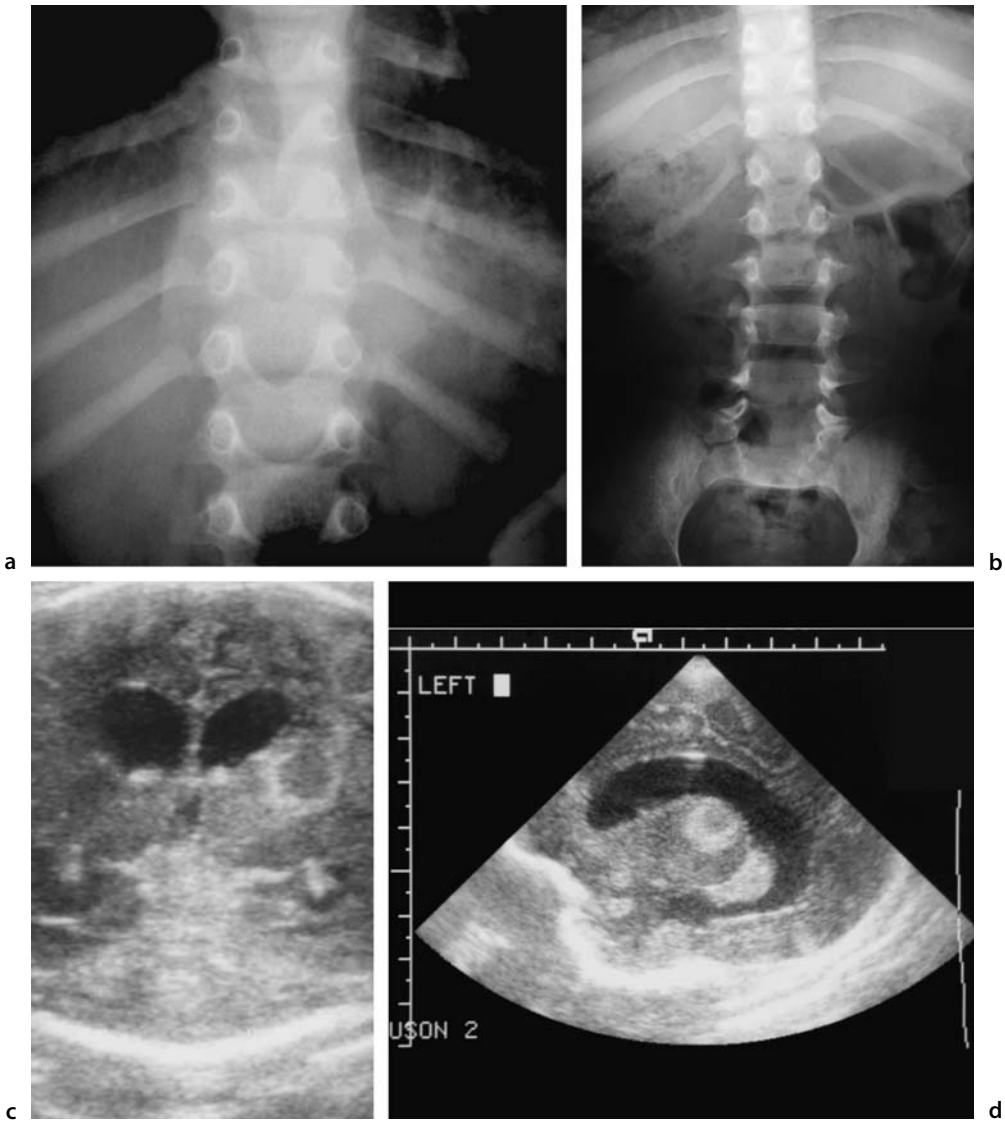

Fig. 8.25. What are these abnormalities? (See Appendix 2)
a A 2-year-old male with back pain
b A 9.5-year-old with congenital anomaly
c, d A 1-month-old female with history of abdominal wall defect and now thrombocytopenia

This herniation may occur in any direction. When anterior, it may displace the ring apophysis of the vertebral body, leaving the corners apparently "compressed" and the disc space narrowed (Fig. 8.24). The occurrence of this at multiple levels is called Scheuermann's disease, although many children with this roentgenographic finding are asymptomatic.

QUIZ CASE

What are the abnormalities in Figs. 8.25–8.30? (See Appendix 2 for the answers.)

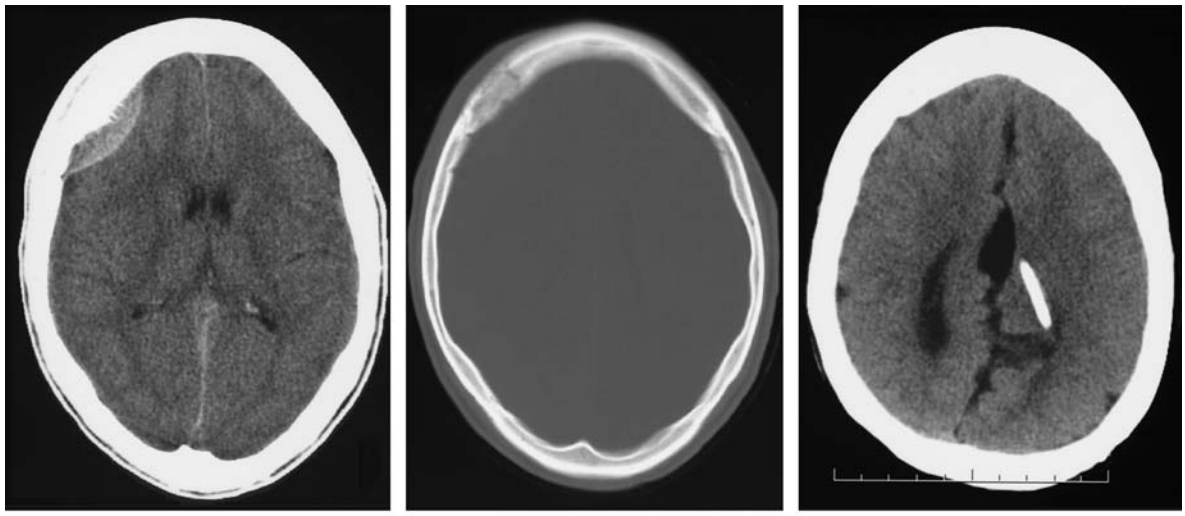

a, b

c

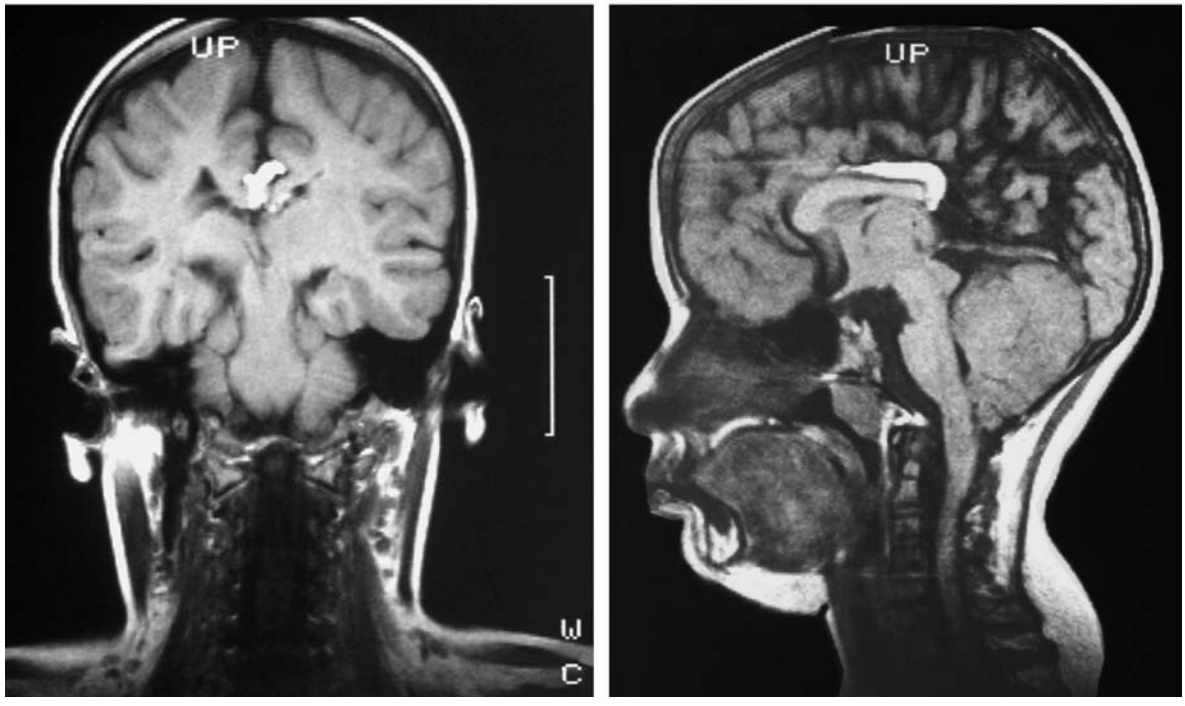

d

e

Fig. 8.26. What are the abnormalities? (See appendix 2)
a, b Follow-up head scan in a patient with known neuroblastoma
c–e Teenage myelomeningocele patient – CT and MR

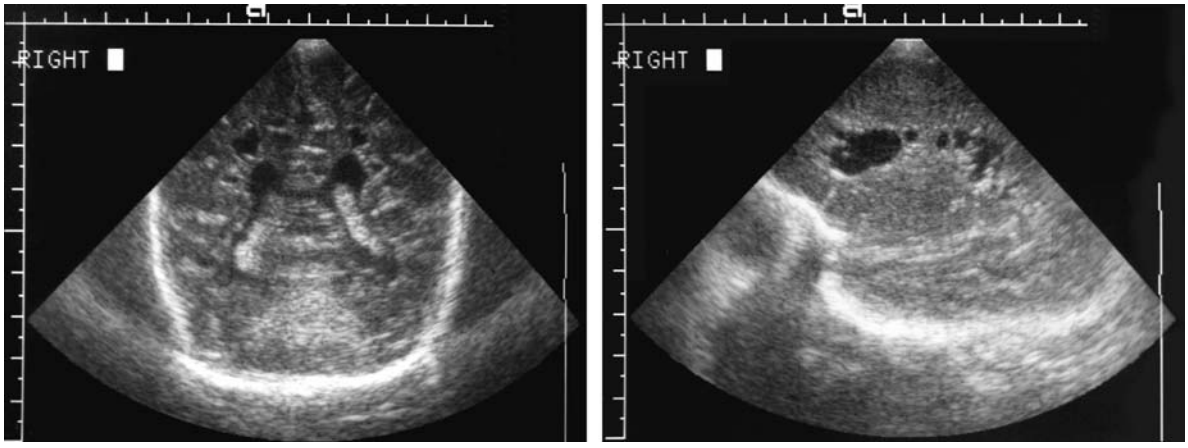

a b

Fig. 8.27. Ultrasound study of the head in a premature (26-week gestation) infant at 4 weeks of age (**a, b**)

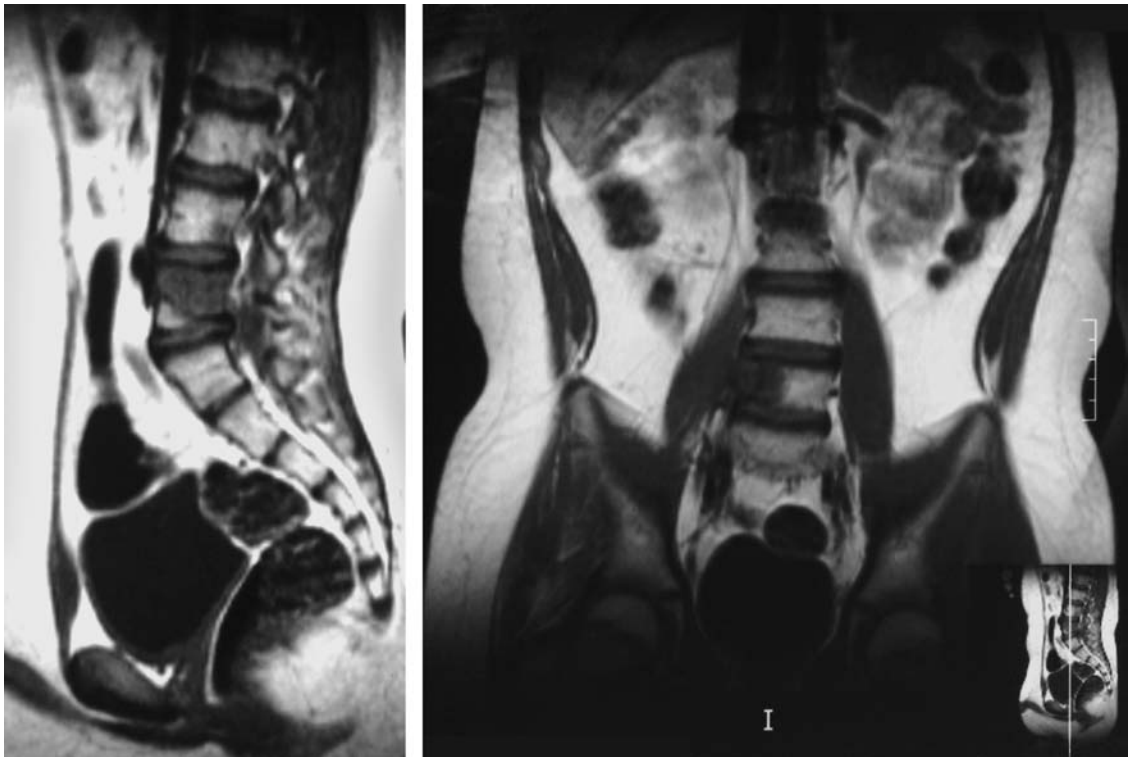

a b

Fig. 8.28. A 14-year-old with back pain (**a, b**)

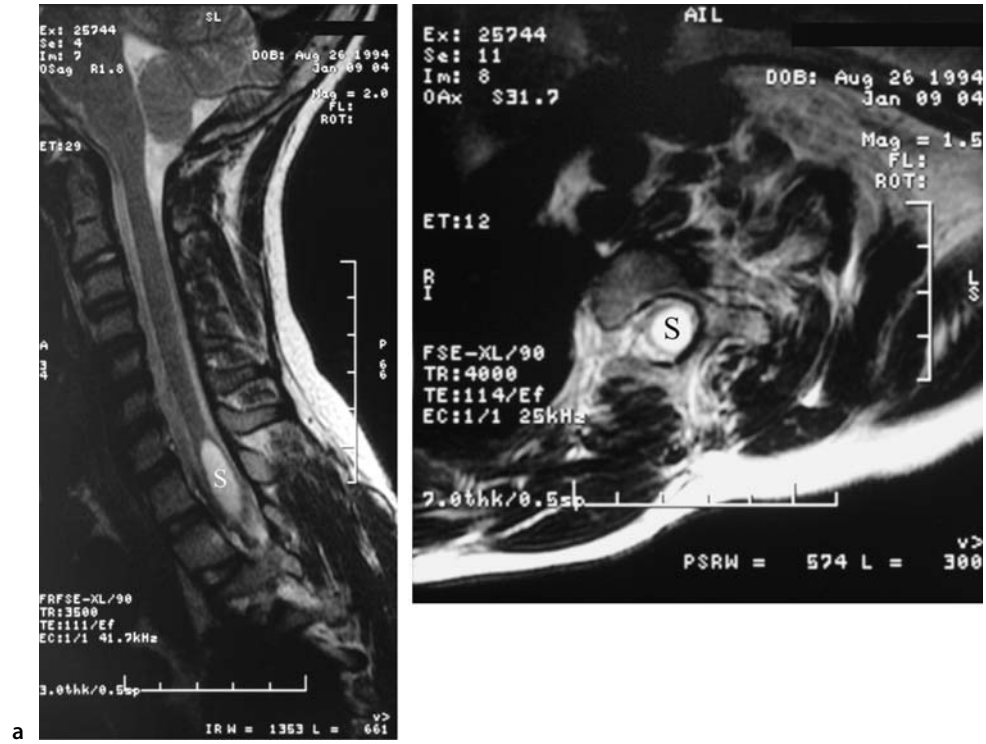

Fig. 8.29. A 10-year-old with weakness (**a, b**)

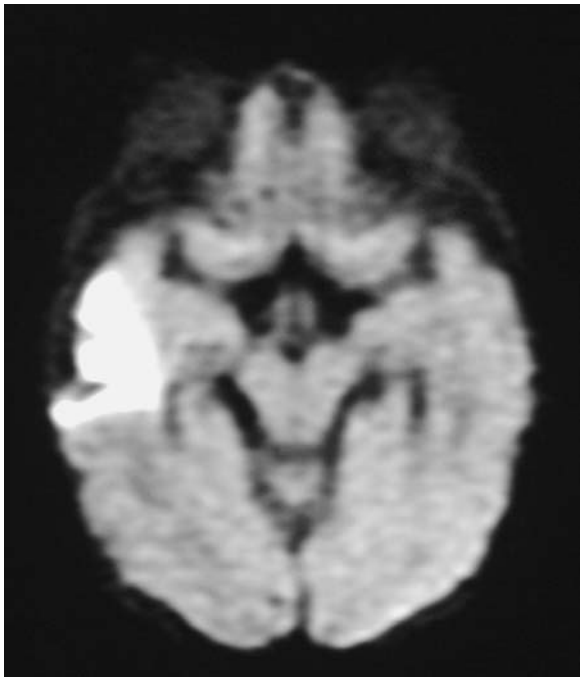

Fig. 8.30. A 1-month-old baby with encephalopathy

References and Further Reading

1. Hayman LA, Hinck CC (1992) Clinical brain imaging: normal structure and functional anatomy. Mosby, Chicago
2. Harwood-Nash DC, Hendrick EB, Hudson AR (1971) The significance of skull fractures in children-a study of 1,187 patients. Radiology 101:151
3. Bell WE, McCormick WF (1978) Increased intracranial pressure in children, 2nd edn. Saunders, Philadelphia
4. du Boulay GH (1980) Principles of X-ray diagnosis of the skull, 2nd edn. Butterworth, London
5. Gooding CA (1971) Cranial sutures and fontanelles. In: Newton TM, Potts DC (eds) Radiology of the skull and brain. Mosby, St Louis
6. Christenson PC (1977) The radiologic study of the normal spine: cervical, thoracic, lumbar, and sacral. Radiol Clin North Am 15:133–154
7. Keats TE (2001) An atlas of normal roentgen variants that may simulate disease, 7th edn. Mosby, Chicago
8. Swischuk EL (2004) Imaging of the newborn, infant and young child. 5th edn. Lippincott Williams and Wilkins, Philadelphia
9. Kuhn JP, Slovis TL, Haller JO (eds) (2004) Caffey's pediatric diagnostic imaging, 10th edn. Mosby, Philadelphia
10. Weinstein SL (2001) The pediatric spine: principles and practice, 2nd edn. Lippincott Williams and Wilkins, Philadelphia
11. Cohen MM, MacLean RE (2000) Craniosynostosis: diagnosis, evaluation and management. Oxford University Press, New York

9 Special Procedures

The first eight chapters of this volume discuss common pediatric imaging procedures. This chapter deals with the less common invasive procedures. The more invasive the procedure, the greater the skill and expertise required of the team. Some of the less invasive procedures (Table 9.1) are done by the general pediatric radiologist and other procedures involve more specialized skills and are done by the pediatric interventionalist. All of these physicians need to be current in sedation and monitoring practices.

Table 9.1. Pediatric interventional procedures

Less invasive procedures
Hip taps
Gastrointestinal tube changes or replacements
Sialograms
Esophageal foreign body extraction
Arthrography
More invasive procedures
Vascular access
Biopsies
Drainages of abscess and other collections
Angiography
Specific gastrointestinal procedures
Percutaneous gastrostomy and gastrojejunal tubes
Biliary stents
Balloon dilatation
Specific urinary system intervention
Percutaneous nephrostomy
Ureterostenting
Airway stenting
Vascular intervention
Neurological
Renal
Gastrointestinal
Vascular
Endovascular delivery of therapeutic agents such as chemotherapy

Sedation

A sedation protocol is essential in any pediatric interventional section. The choice of the sedating agent or whether to use general anesthesia is influenced by many factors, not the least of which is the experience of the pediatric interventionalist. Each center seems to have a different sedation protocol; this suggests that many approaches are acceptable if proper monitoring and expertise are available.

Less Invasive Procedures

Hip taps are done to diagnose or exclude the diagnosis of septic arthritis. This procedure is now usually done under ultrasound guidance for the removal of fluid; ultrasound cannot differentiate infected from sterile fluid or blood. The approach is from the anterior thigh (Fig. 9.1). Fluid is found in the two most common diseases that produce gait disturbances in children – toxic synovitis and septic arthritis/osteomyelitis – but pus only in septic arthritis. Contrast medium is injected into the joint space if a "dry tap" is obtained to make sure the needle was within the joint capsule (Fig. 9.2). Arthrography has been generally replaced by MRI to ascertain the appearance and amount of cartilage.

Opacification of the salivary ducts and glands by injecting contrast medium into the ostium (opening) of the duct is usually performed to investigate a mass (Fig. 9.3). The parotid gland is the one most often studied by this method. Injection of the duct is performed with digital subtraction images followed in certain cases by CT, as CT gives a more complete evaluation of the gland.

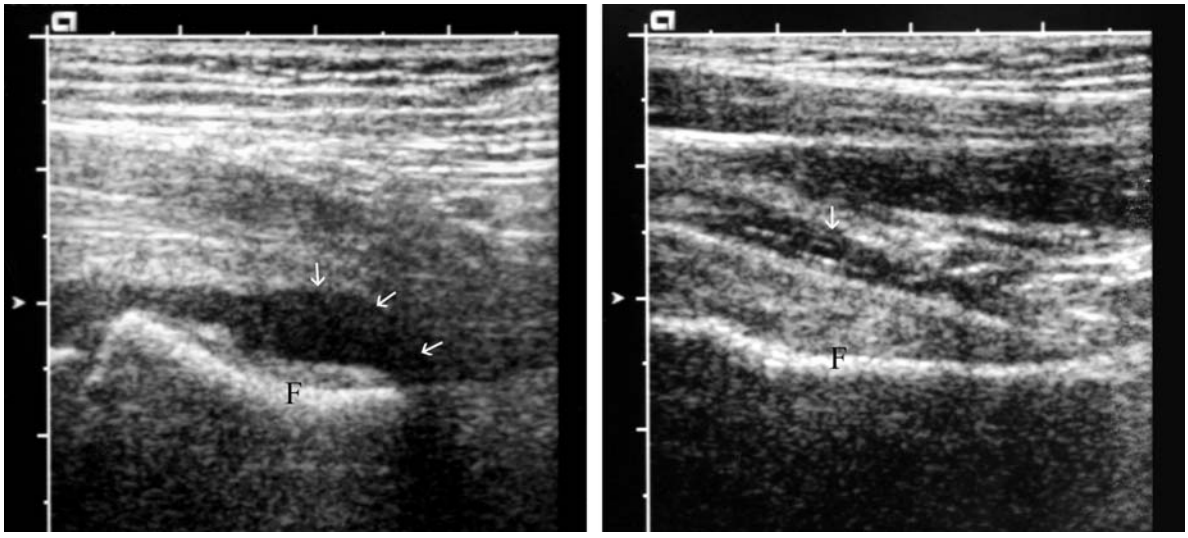

a b

Fig. 9.1. Hip tap
a Longitudinal ultrasound of the right hip with the transducer anteriorly on the thigh. There is large joint effusion (*arrows*) present. *F*, femur
b Longitudinal ultrasound of the normal left side shows no fluid but rather the hypoechoic muscle (*arrow*). *F*, femur

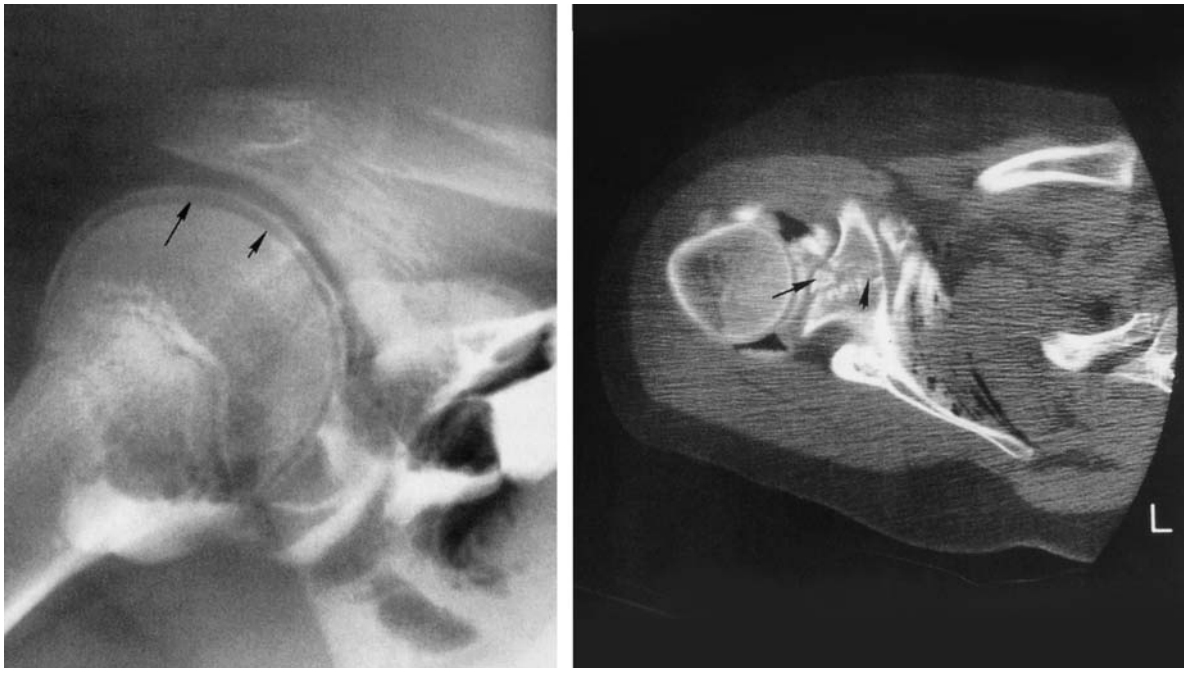

a b

Fig. 9.2. Arthrography in a patient who sustained a traumatic shoulder injury
a Upright double contrast (both air and contrast were inserted) arthrogram of the right shoulder reveals normal cartilaginous covering of the humeral head (*arrows*; gray is cartilage). However, it is difficult to evaluate the glenoid fossa on this view. Therefore, CT is carried out after the arthrogram
b CT of the same shoulder reveals a triangular fragment of bone (*arrow*) and linear fracture of the glenoid (*arrowhead*). The contrast (white) outlines the separation of the cartilaginous portion of the glenoid from the humeral head. Note that this glenoid fracture has not destroyed the overlying articular cartilage

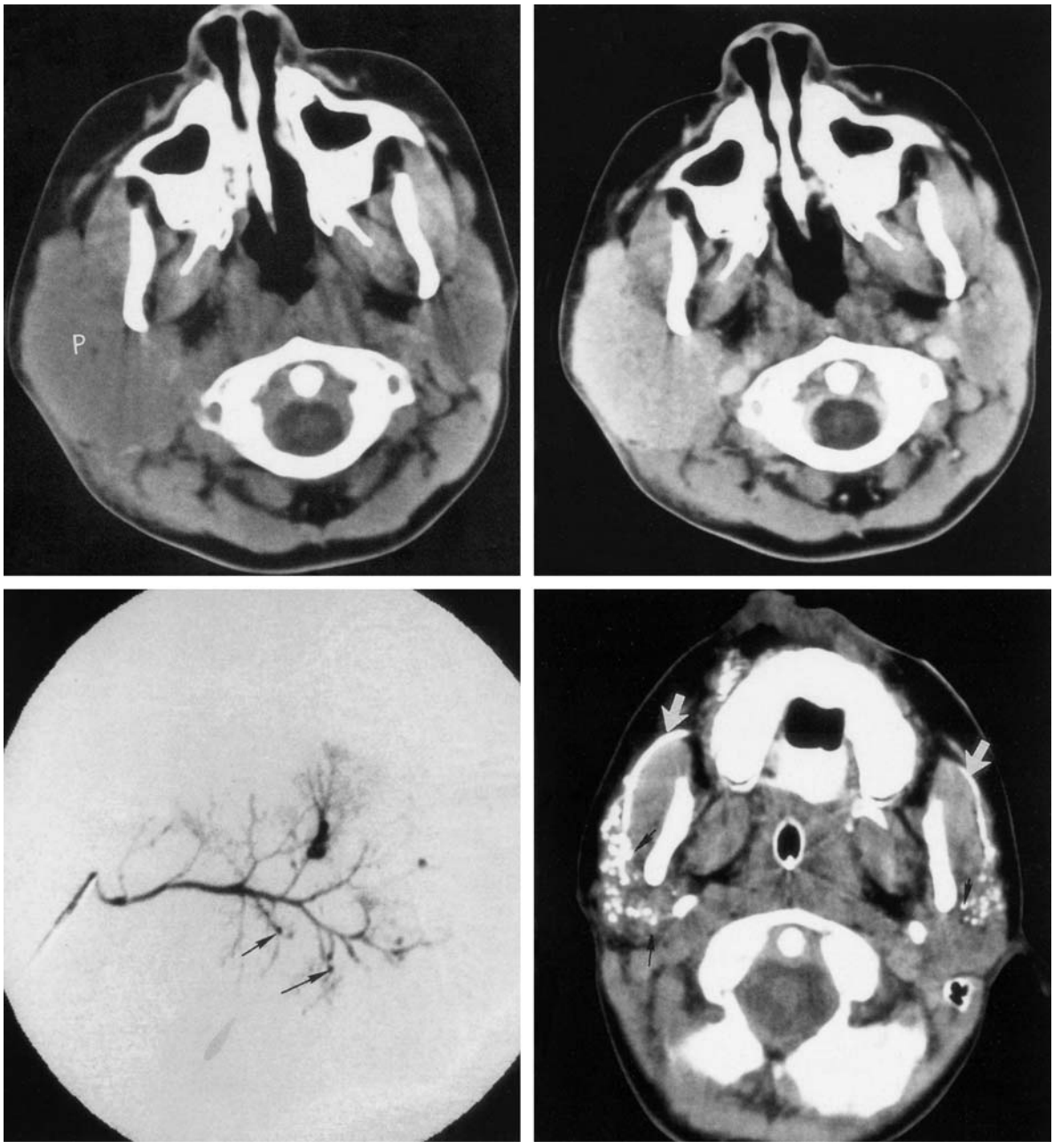

Fig. 9.3. Sialography
a Noncontrast CT of the parotid region shows uniformly enlarged right parotid gland (*P*) without calcification
b Enhanced CT (intravenous contrast) of the same region shows uniform enhancement of the gland similar in density to the opposite side. There is no focal region of abnormality
c Injection of the parotid duct on the affected side reveals no obstruction but small beaded areas of sialectasis (*arrows*). This represents chronic inflammation
d CT of another child after bilateral injection of Stensen's duct (the duct to the parotid gland, *white arrows*). There are multiple, small, white collections which represent sialectasis (*arrows*)

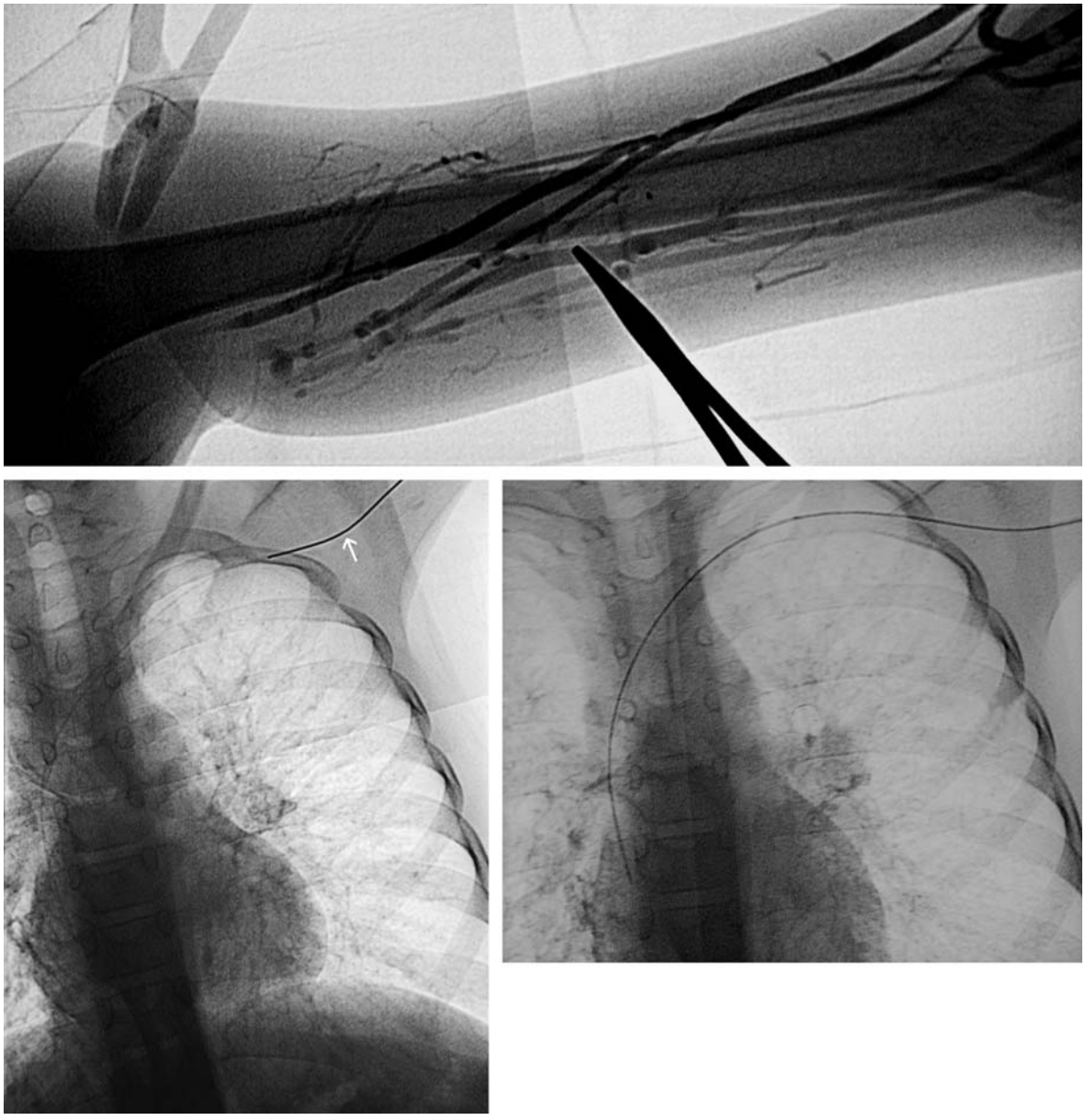

Fig. 9.4. Venous access
a An intravenous injection reveals the venogram and the towel clamp is on the basilic vein. The new needle and catheter were placed into the basilic vein
b After placement of the PICC line before removal of the guide wire, the PICC is in the right atrium and the guide wire is still at the level of the subclavian vein (*arrow*)
c After removal of the guide wire, contrast injection shows the PICC line is centrally placed in the right atrium

More Invasive Procedures

Venous Access

Venous access is crucial in many aspects of pediatric therapy including fluid administration, antibiotic therapy, parenteral nutrition, and blood sampling. Peripheral intravenous lines may be difficult to place and retain because of the problems of immobilization of the pediatric patient as well as the small size of the vessels. Dislodgment is common as the infant and young child constantly pull at the intravenous tubing. For these reasons, peripherally inserted central catheters (PICCs) have become important in pediatric care as they remain in place much longer than peripheral intravenous lines. These lines can be placed with either ultrasound or fluoroscopic guidance (Fig. 9.4) and are usually inserted in the basilic vein and placed centrally. Ultrasound guidance reduces the radiologic exposure. Sedation will be required in most children under 10 years of age and the overall success rate in experienced hands is well in excess of 90%. PICC lines are considered intermediate-term vascular access, lasting from 7 days to 3 months.

When a line is required for greater than 3 months, a subcutaneous venous access port or tunneled catheter can be placed percutaneously. Another percutaneously inserted line is the hemodialysis catheter.

Biopsies and Drainage

Imaging guidance for both biopsy and drainage is frequently performed in the pediatric radiology department. The interventionalist is guided by pulsed fluoroscopy, CT, or ultrasound. Perhaps the most frequent drainage procedure is that of a perforated appendiceal abscess (Fig. 9.5). Pelvic, subphrenic, liver, and splenic abscesses, as well as pancreatic pseudocysts are approached percutaneously. Drainage/sampling of pleural fluid is also performed. It is important to remember the principles of sedation and to keep the radiation dose to a minimum. Drainages can be accomplished by either the direct trocar method or by the Seldinger over-the-wire technique. In the latter, a needle is placed into the collection and a wire is placed through the needle to secure access. The needle is removed and a catheter is then placed over the wire.

The type of needle used for biopsy is determined by the amount of tissue necessary and the ability of the pathologists to reach diagnosis on either a core or a fine-needle specimen.

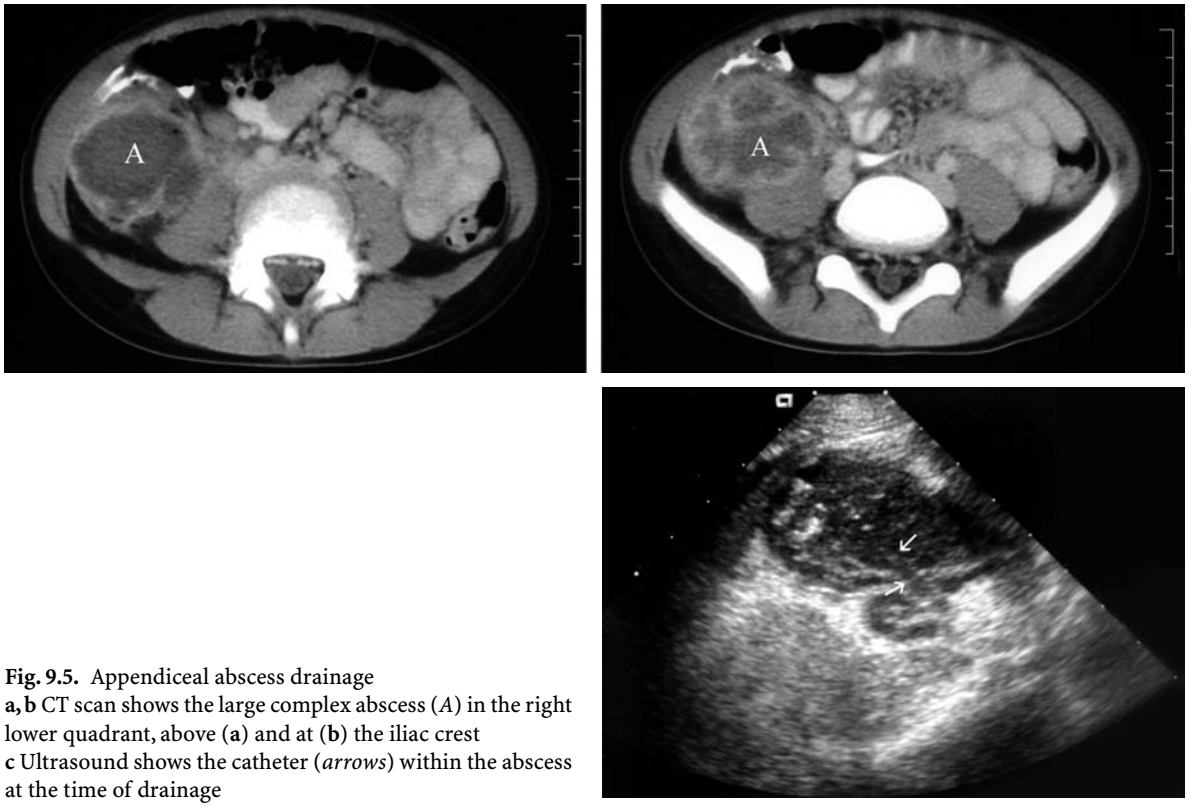

Fig. 9.5. Appendiceal abscess drainage
a, b CT scan shows the large complex abscess (*A*) in the right lower quadrant, above (**a**) and at (**b**) the iliac crest
c Ultrasound shows the catheter (*arrows*) within the abscess at the time of drainage

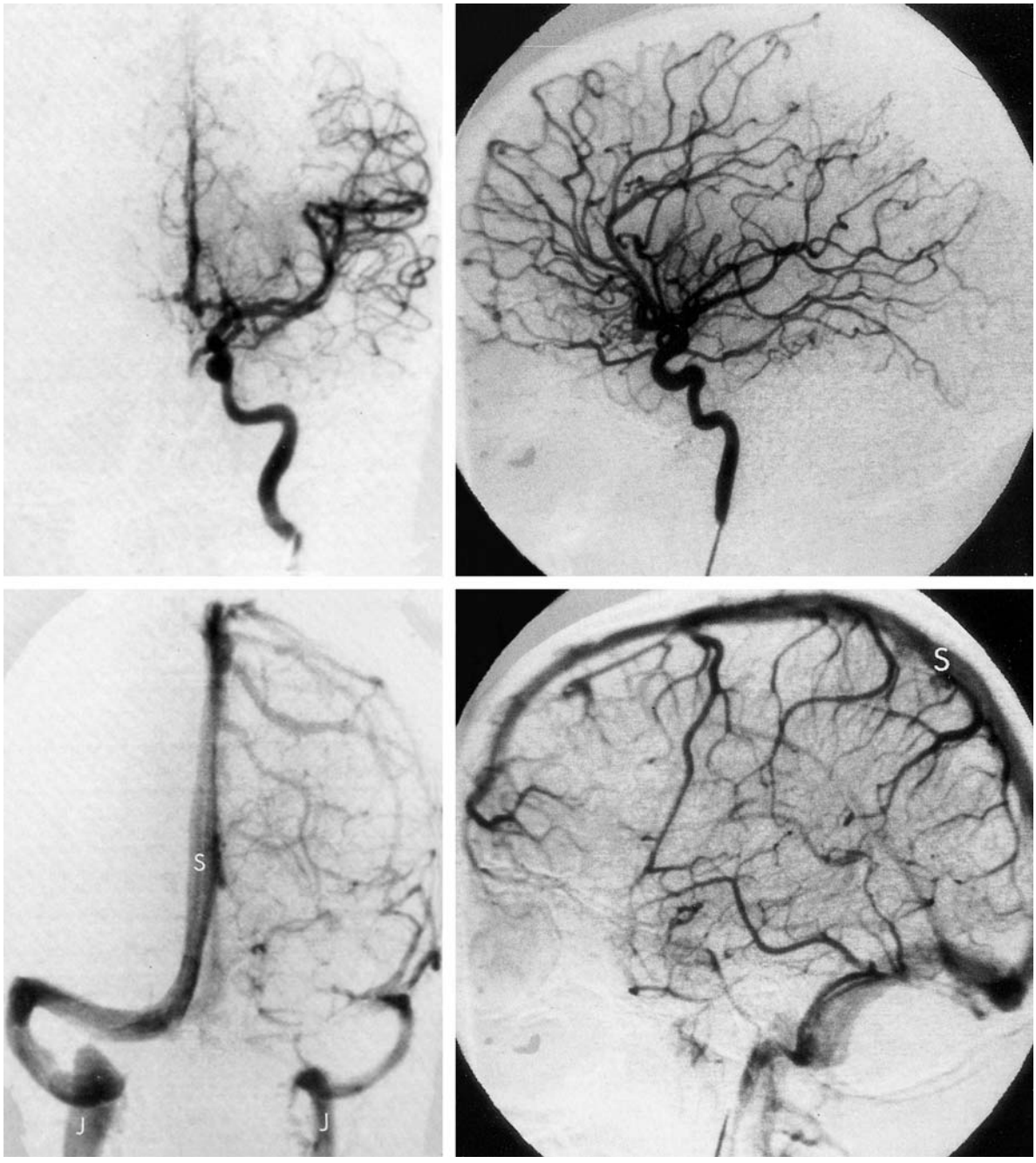

Fig. 9.6. Angiography
a Left internal carotid artery injection visualized in the AP projection reveals the middle and anterior cerebral arteries and their branches
b Same patient lateral view shows the normal vascular structures
c Venous phase of this same injection. This AP view shows contrast returning to the heart via the superior sagittal sinus (*S*) and eventually into the jugular vein (*J*). This patient demonstrates a normal variant – although we performed a left-sided injection – the predominant venous drainage is to the right
d Lateral view of the venous phase shows both deep and superficial venous drainage
e see p. 255

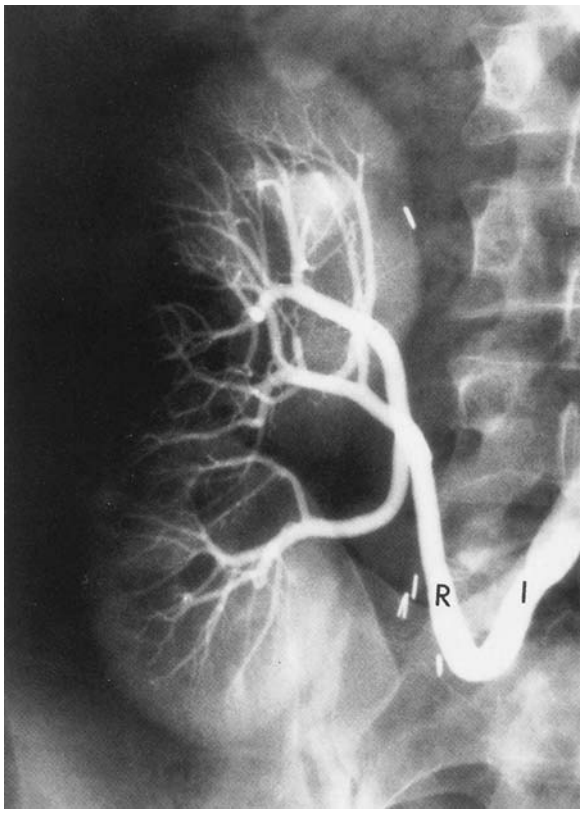

e

Fig. 9.6 (*continued*)
e Visceral angiogram. Arterial injection of a transplanted kidney showing the anastomosis of the renal artery (*R*) to the right iliac (*I*) artery. There is no stenosis of the major renal branches. This child was being evaluated for post-transplant hypertension

Angiography

Angiography, a contrast study of vessels, remains the gold standard against which to measure less invasive techniques such CT and MR angiography. Today no more than 50–100 angiographic procedures are performed in the course of a year in a busy children's hospital. Approximately 50% are investigating the central nervous system and 50% are peripheral angiographic procedures (Fig. 9.6).

The Seldinger method is utilized in arteriography. Most often this occurs via the femoral artery and the catheter is then placed in the appropriate vessel to be studied. In children arteriography is used to clarify central nervous system problems and as a map for interventional or surgical treatment for peripheral or visceral lesions.

Gastrointestinal Interventional Procedures

Aside from venous access, interventional gastrointestinal tract procedures comprise the largest part of most pediatric interventional practice. Since adequate nutrition is essential for normal growth and development, children who are unable to take in sufficient calories may need a route for feeding. Those who require short-term nutritional support of less than 6 weeks may have a nasogastric or, if gastroesophageal reflux is present, nasojejunal tube placed. However, when longer periods of nutritional support are necessary, percutaneous gastrostomy or gastrojejunostomy tube placement is recommended (Fig. 9.7). The majority of patients who undergo these procedures have neurological impairment. Other patients with congenital diseases such as cystic fibrosis or liver disease are also candidates for this procedure.

These tubes may be placed at a significantly lower cost in the interventional suite than in the operating room and may obviate the need for an antireflux procedure. We routinely check for malrotation (Chap. 5) prior to jejunal tube placement.

Recently, percutaneous cecostomy has been utilized to prevent overflow fecal incontinence. A tube in the cecum is access for regular antegrade enema, allowing colonic emptying at a prescribed time.

Urinary System Interventional Procedures

Relief of an obstructed kidney by placement of a nephrostomy tube is the most commonly performed urinary interventional procedure in children (Fig. 9.8). The most common indications are ureteropelvic junction obstruction or failed pyeloplasty (operative decompression of ureteropelvic junction obstruction). This percutaneous nephrostomy is a temporary urinary diversion.

Stent placement in ureters is another procedure performed by the pediatric interventionalist. A less frequently performed procedure is percutaneous stone removal or placement of a catheter into the renal pelvis and ureter so that the urologist easily defines the ureter at surgery.

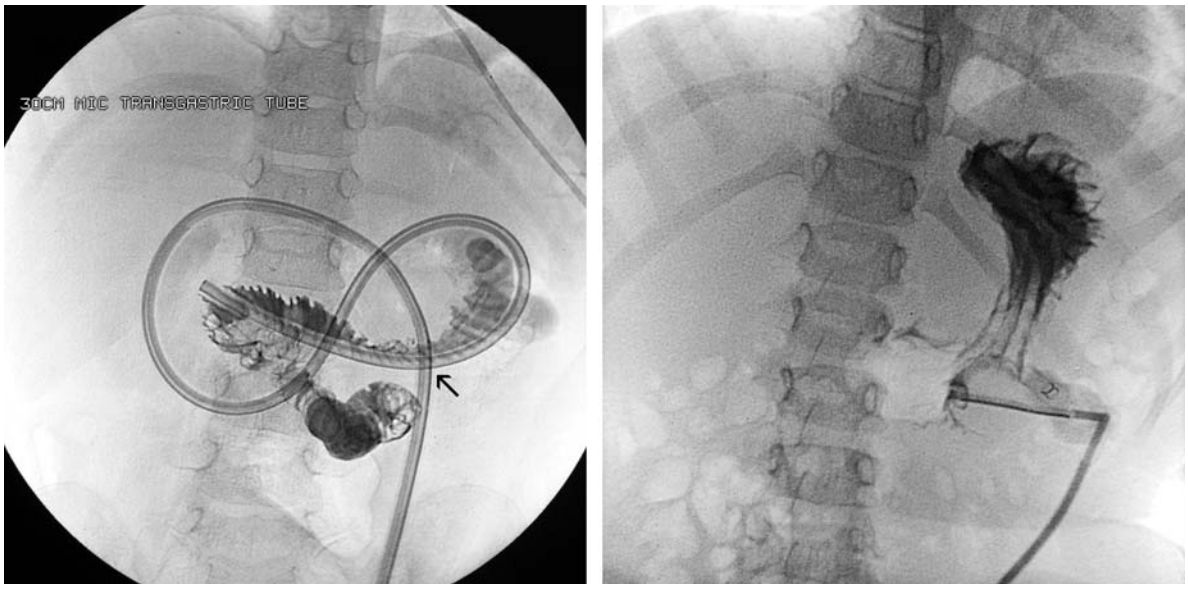

a b

Fig. 9.7. Gastrointestinal intervention
a Film showing a tube percutaneously inserted through the stomach (*arrow*) passing through the stomach into the duodenum. The injection of contrast is made within the jejunum. This is a gastrojejunostomy tube
b This patient has a tube within the stomach. It is a gastric button which allows the patient to be disconnected from the external tube during times of nonfeeding

Airway Interventional Procedures

There is a small group of patients with congenitally narrow airways who require stenting of the airway. Few procedures have been done in children up to this time.

Vascular Intervention

Neurovascular

Using the Seldinger technique, endovascular therapy is safely performed in neonates, infants, and children (Fig. 9.9). It is a standard of care in patients presenting with a vein of Galen malformation and dural arteriovenous shunts. It has become an important tool in managing arteriovenous malformations of the brain and spinal cord, as well as intervening in the rare pediatric aneurysm.

Renovascular

Endovascular therapy may be important in cases of renal trauma in an attempt to save the kidney. Subselective arterial embolization of bleeding sites may prevent nephrectomy. Renal vascular hypertension in children is more unusual than in adults. Renal artery stenosis may be treated by dilatation (angioplasty) or vascular stent placement.

Gastrointestinal

Localization of the exact source of bleeding and treatment by selective transcatheter embolization or vasopressin infusion is quite successful.

Vascular Embolization

Bleeding sites such as the bronchial arteries in a child with hemoptysis, or in preoperative vascular tumors of the head and neck, or in bleeding from traumatized viscera, have been treated with embolization therapy with great success.

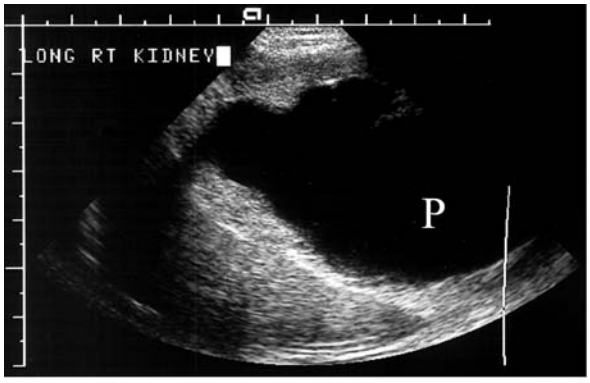

a

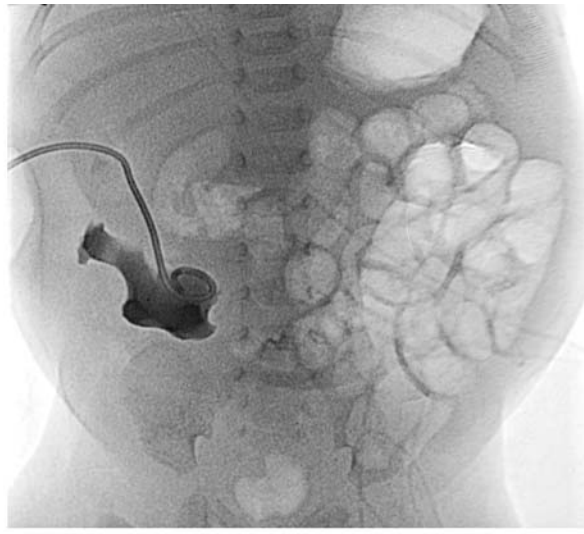

b

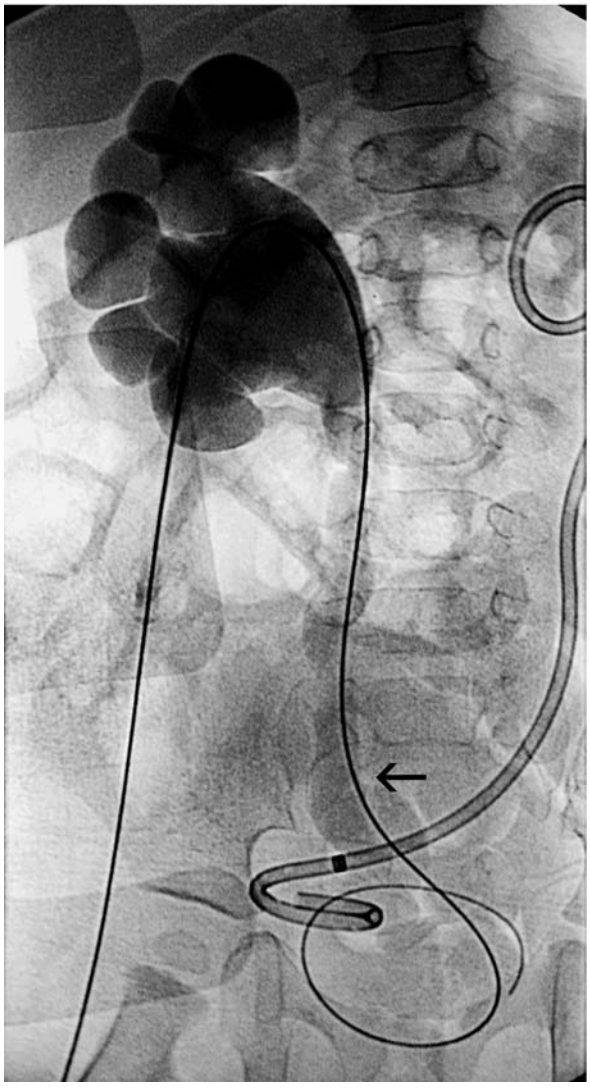

c

Fig. 9.8. Drainage of an obstructed kidney
a Longitudinal ultrasound shows a markedly enlarged renal pelvis (*P*) and collecting system on the right side
b Percutaneous nephrostogram was done and a pigtail catheter placed into the abnormal right kidney
c Another patient with obstruction of the distal ureters. There is contrast in the dilated renal collecting system and dilute contrast (*arrow*) in the right ureter. The guide wire remains in place from the kidney to the bladder. It is coiled distally in the bladder. There is a stent tube in the left kidney and ureter

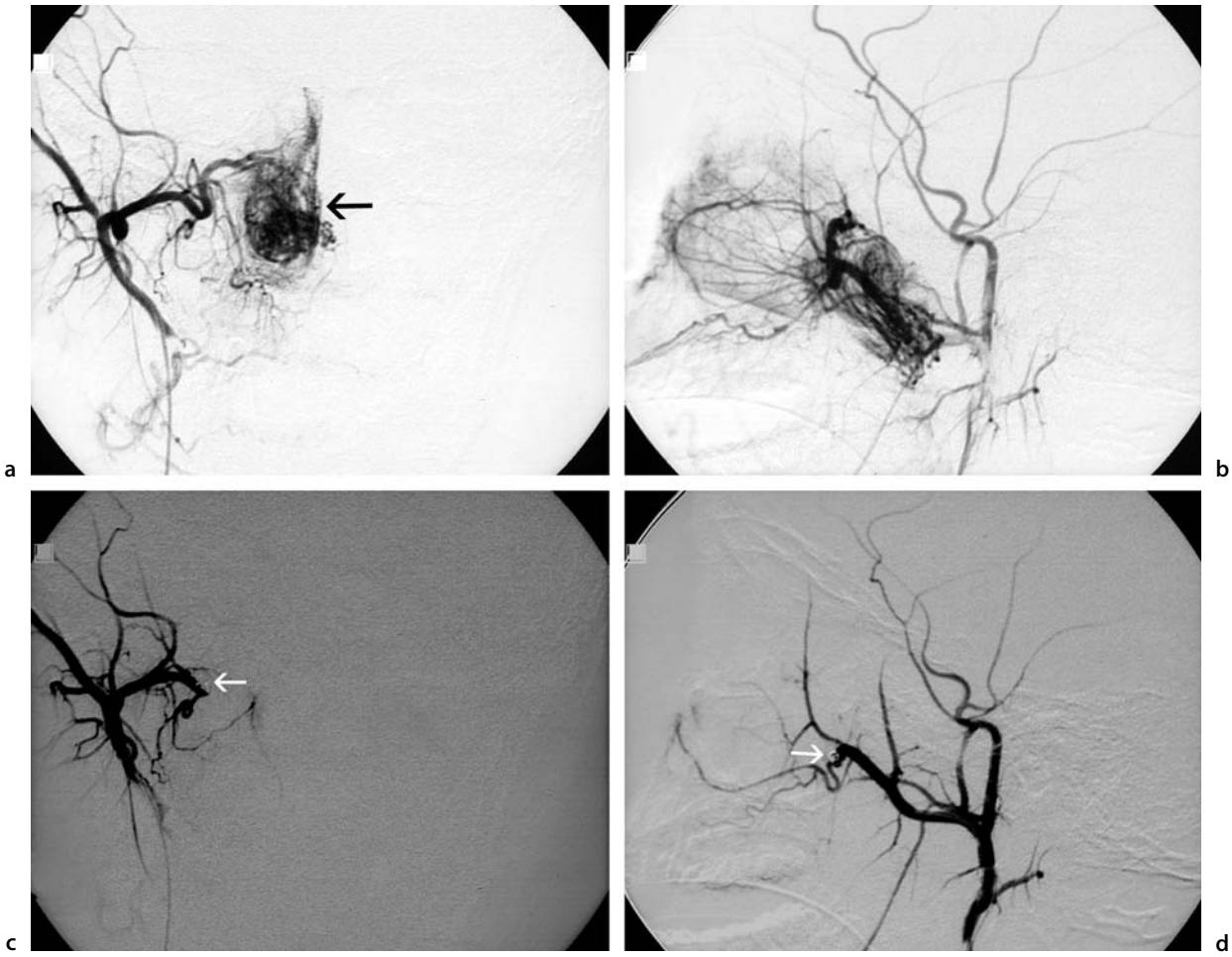

Fig. 9.9. Neurointervention. This is a 14-year-old with epistaxis. He was found to have a juvenile angiofibroma and the interventional service was asked to reduce the bleeding prior to surgery
a, b AP and lateral views of the external maxillary artery shows a great deal of contrast filling (*arrow*) of the vascular tumor
c, d Subselective injection in the internal maxillary artery allowed the placement of coils (*arrow*). The postoperative films show no tumor blush

Endovascular Delivery of Therapeutic Agents

The use of intrahepatic chemotherapy to deliver precise doses of therapeutic agent to tumor has been investigated. It is used with embolization so that the therapeutic agent is trapped within the tumor and can have maximum effect. Hepatoblastomas have been treated in this manner. Delivery of other agents besides chemotherapy is in the experimental stages.

Further Reading

1. Donaldson JS (ed) (2002) Pediatric interventional radiology. In: Mueller PR (ed) Semin Interv Radiol 19:1–99
2. Kaye RD, Sane SS, Towbin RB (2002) Pediatric intervention: an update. Part I. J Vasc Interv Radiol 11:683–697
3. Kaye RD, Sane SS, Towbin, RB (2002) Pediatric intervention: an update. Part II. J Vasc Interv Radiol 11:807–822
4. Crowley J (2003) Vascular access. In: Donaldson J (ed) Pediatric interventions. Tech Vasc Interv Radiol 6:176–181
5. Norman J (2001) Practical pediatric interventional radiology. Curr Probl Diagn Radiol 30:61–86

Appendix 1: Rules for Reading Pediatric X-Rays*

Read the ABCS:
A = abdomen, B = bone, C = chest, S = soft tissue

1. On every chest film, read the abdominal portion as you would read an abdominal film.
2. Knowledge of anatomy is the key to correct radiographic diagnosis.
3. The airway should be visible on all normal chest films.
4. A mass must be seen in two planes.
5. An esophagram must be performed in any child with unexplained respiratory disease.
6. In unilateral hyperexpansion of the lungs, you must see how the air moves. Air must move in and out of each lung. Mediastinal position is critical to this determination.
7. The heart and liver are transparent organs.
8. Always review all old films to properly assess the new one. Subtle findings can easily be missed when a single previous examination is reviewed.
9. The abdominal examination should include a minimum of three views: supine, prone, and erect.
10. On every abdominal examination, evaluate the chest as if you were looking at a chest film.
11. In obstruction of the lumen, there should be proximal distention.
12. Try to find the effects of the mass on adjacent organs on each abdominal film. Draw the mass, if necessary.
13. After the mass has been defined, find the center of the lesion. Then consider all structures, gross and microscopic, near the center of the lesion as possible sources of the mass. Think skin to skin.
14. When viewing an extremity, try to imagine the appearance of the patient. An excellent example is bowed legs or knock knees.
15. The periosteum is normally not seen.

* These rules were adopted from Joseph O. Reed, MD, chief of pediatric imaging at Children's Hospital of Michigan from 1957 through 1987. Throughout this text we include these fundamental concepts, which were used daily in his teaching sessions.

Appendix 2: Answers to Questions

Chapter 3

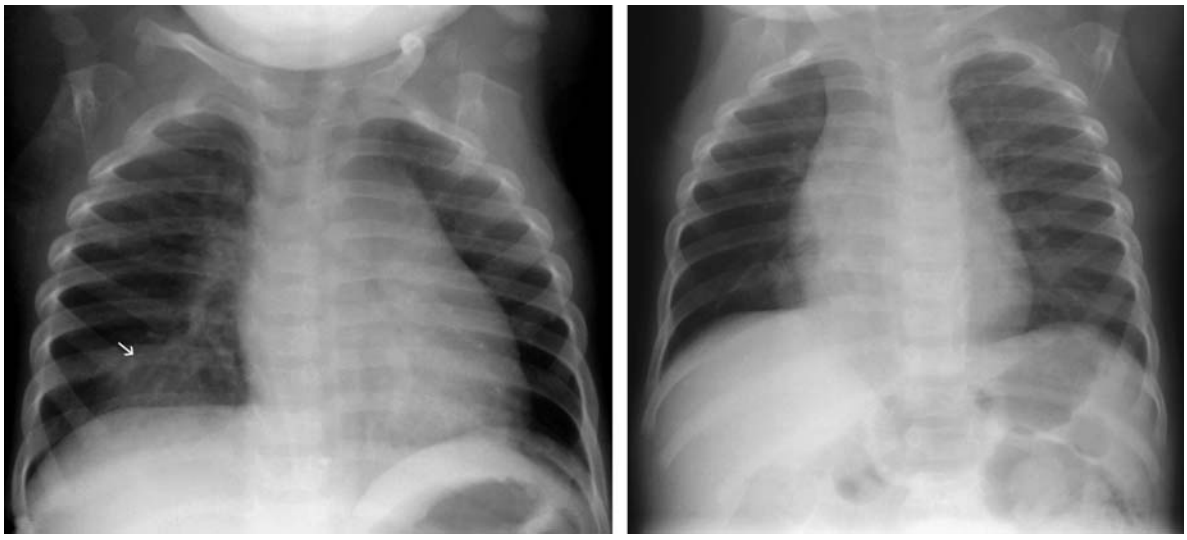

b e

Fig. 3.4. The patient in **b** is rotated to the left. The heart is appreciably in the left hemithorax, and the left side of the chest is relatively elongated, as compared to the right. Note the opacity in the right lower chest field (*arrow*). The reverse is true in **e**

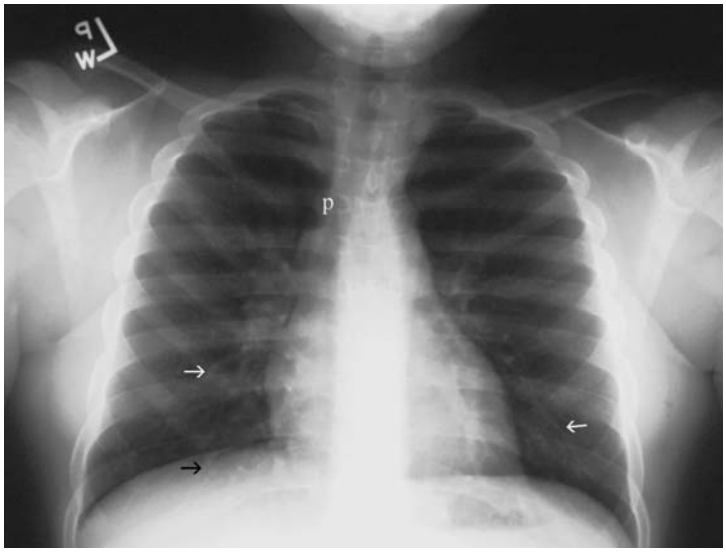

Fig. 3.8. The film is reversed (right to left) according to markers! *p*, pedicle; *white arrows* on anterior ribs; *black arrows* on vessels in base of lung. Remember, the heart and liver are transparent

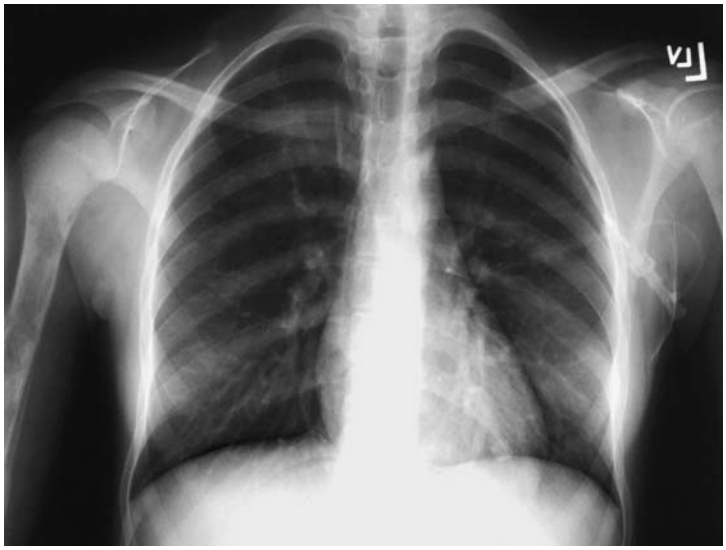

Fig. 3.13. Can you detect the abnormality on this chest film? Did you look at the bones? There is destructive process of the right humerus (dark spots with periosteal reaction) consistent with osteomyelitis in this sickle cell patient. There is a catheter entering from the left side extending into the right atrium for intravenous therapy

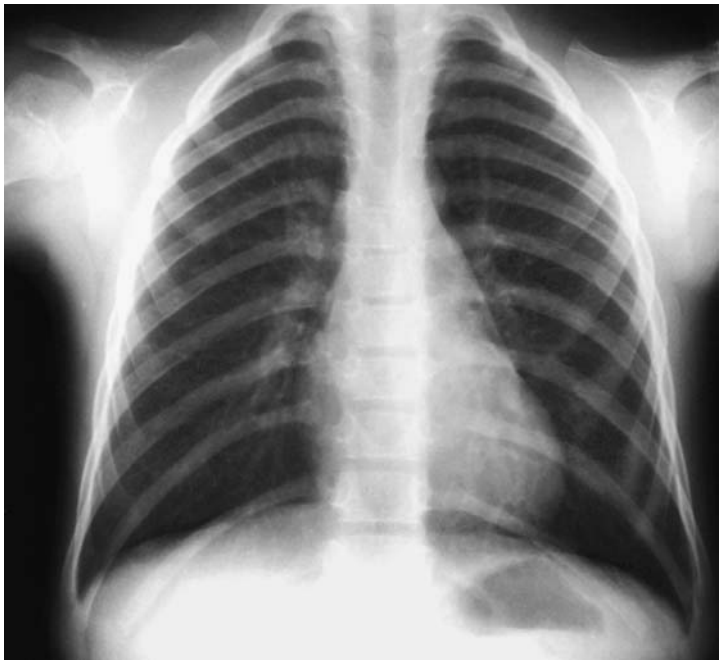

Fig. 3.14. A 9-year-old with a cough. Frontal chest film reveals the heart and lungs to be normal, but there is something missing – the clavicles. This patient has cleidocranial pubic dysostosis

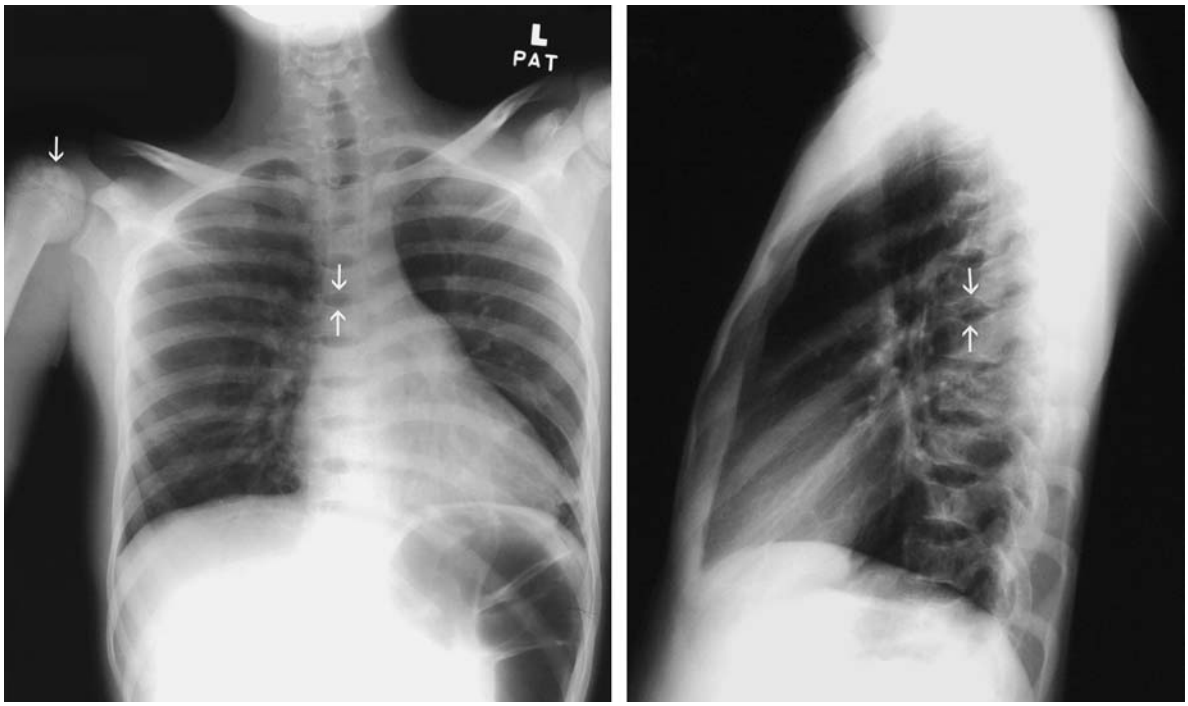

a b

Fig. 3.15. A 17-year-old boy with a cough. On the frontal film (**a**) the heart is large. See the sclerosis (white spots) in the right humerus (*arrow*) and the abnormal vertebrae (T8, T9) (*arrows*), which have decreased height in their midportion. On the lateral view (**b**), the cortical end plates of most of the thoracic vertebrae are depressed. This patient has sickle cell anemia, and the depressed end plates (*arrows)* are due to infarctions. These are called "H" vertebrae (look like old Lincoln cabin log toy pieces) and are typical of sickle cell disease

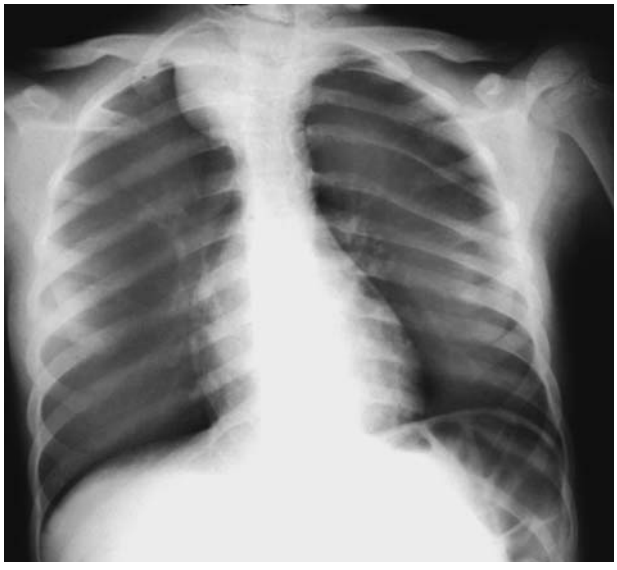

Fig. 3.16. This 12-year-old presented with café au lait spots and scoliosis. Aside from the obvious right large mediastinal mass superiorly there are ribbon-like irregularities of the left fourth through sixth ribs. The combination of the mediastinal mass, rib changes, and café au lait spots suggests a diagnosis of neurofibromatosis. The chest mass is either an anterior meningocele or a neurofibroma. The ribs are wavy secondary to dystrophic bone and hypertrophied intercostal tissue in the subcostal groove. The film is photographed for bone detail and lung markings are lost in this exposure

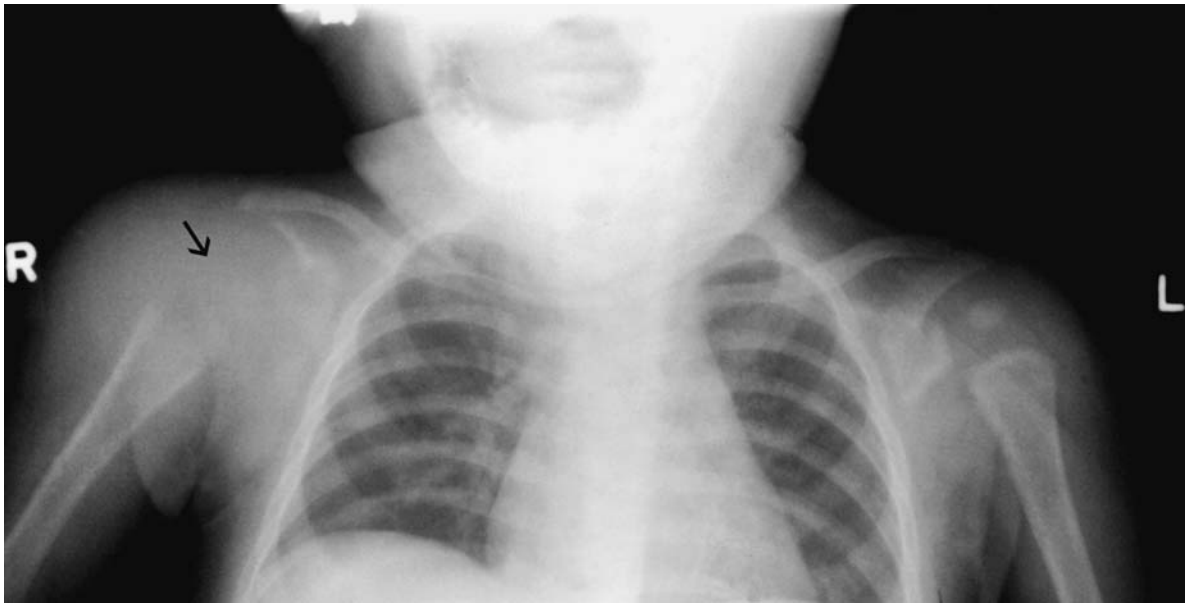

Fig. 3.17. A 6-month-old infant with fever. The frontal chest film shows a soft-tissue swelling of the right shoulder. This patient has osteomyelitis of the right humerus (*arrow*). Compare this to the normal left humerus

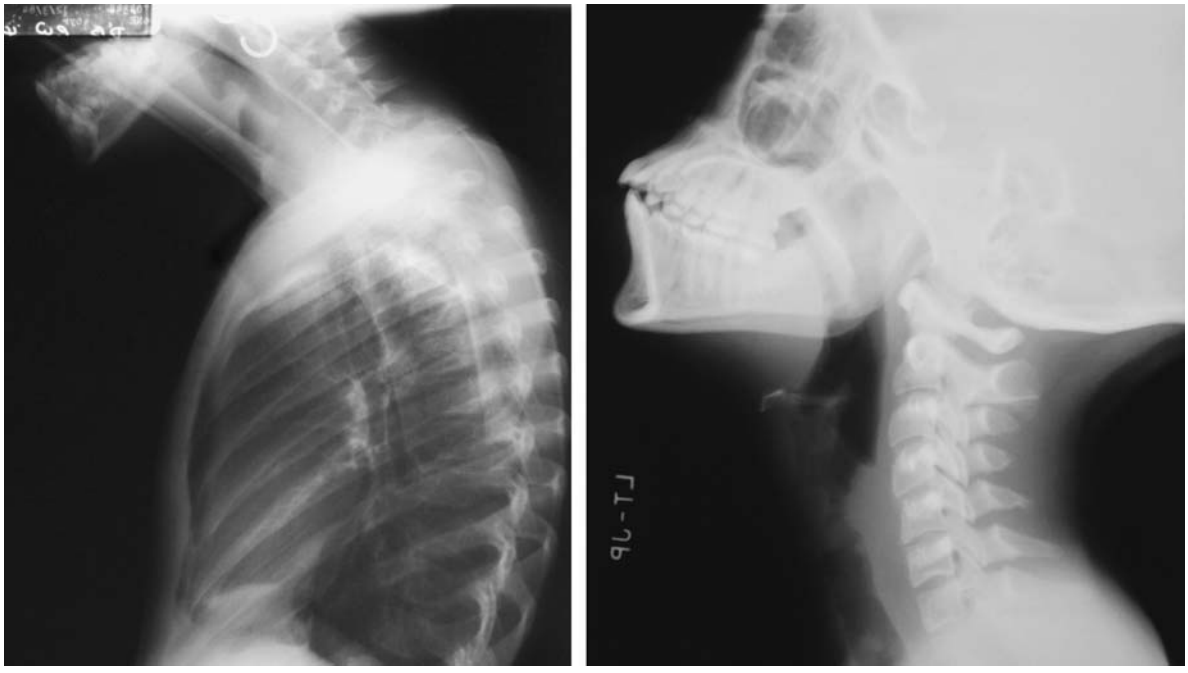

a b

Fig. 3.24. Airway abnormalities
a Acute epiglottis. This is a 3-year-old with respiratory distress. The lateral chest is normal, but the lateral neck shows an enlarged epiglottis and aryepiglottic folds
b Laryngeal papillomatosis. This 12-year-old has multiple growths in the airway. It is not black like the hypopharynx but rather mottled gray

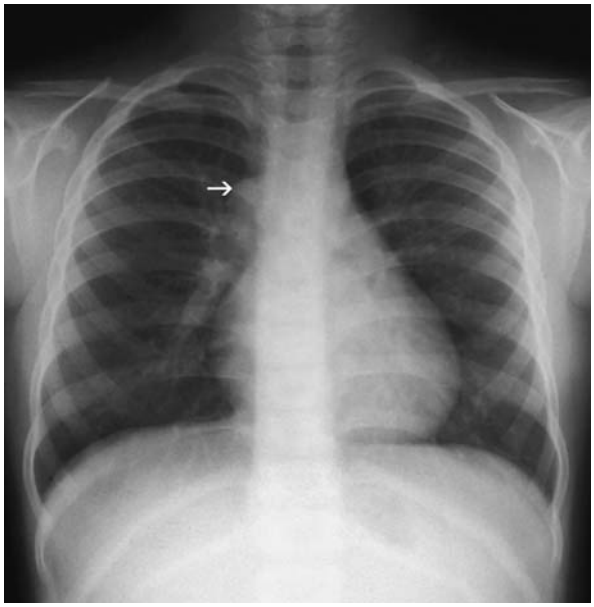

Fig. 3.33. In this 4-year-old asymptomatic girl, a bulge was noted at the junction of the right main-stem bronchus and trachea (*arrow*). It did not pulsate, nor did it affect the esophagus. It was not seen on the lateral film. At ultrasonic examination, the intrahepatic vena cava was found to be atretic, leaving just an infrarenal vena cava. The mass is the azygos vein, which returns blood from the abdomen to the heart. This condition is called azygous continuation of the inferior vena cava

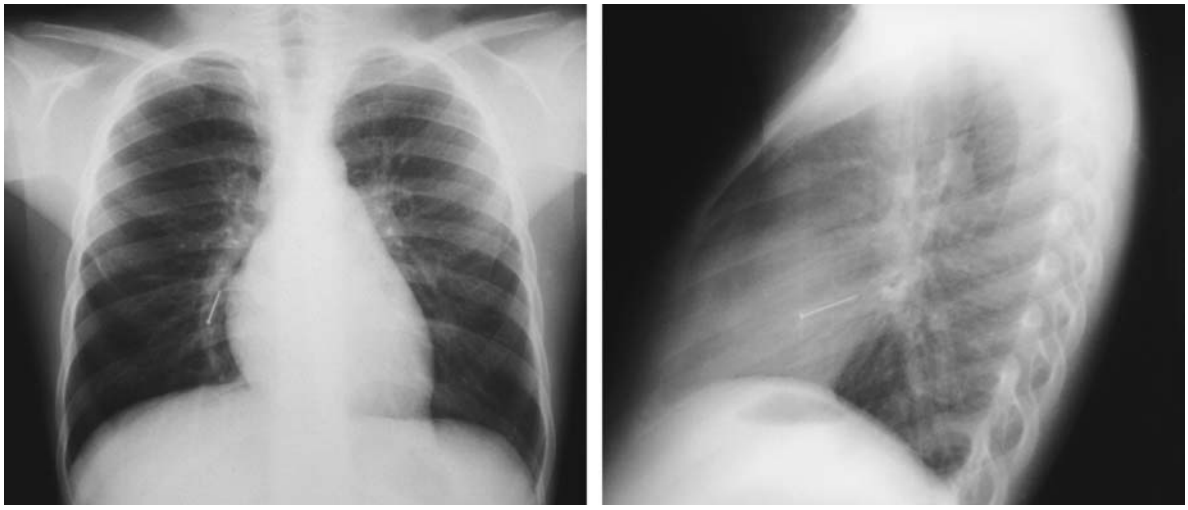

a b

Fig. 3.50. A child with onset of acute respiratory distress. Frontal (**a**) and lateral (**b**) films. Did you notice the white, linear density along the right heart border? The child aspirated a pin and it was removed endoscopically from the right main-stem bronchus

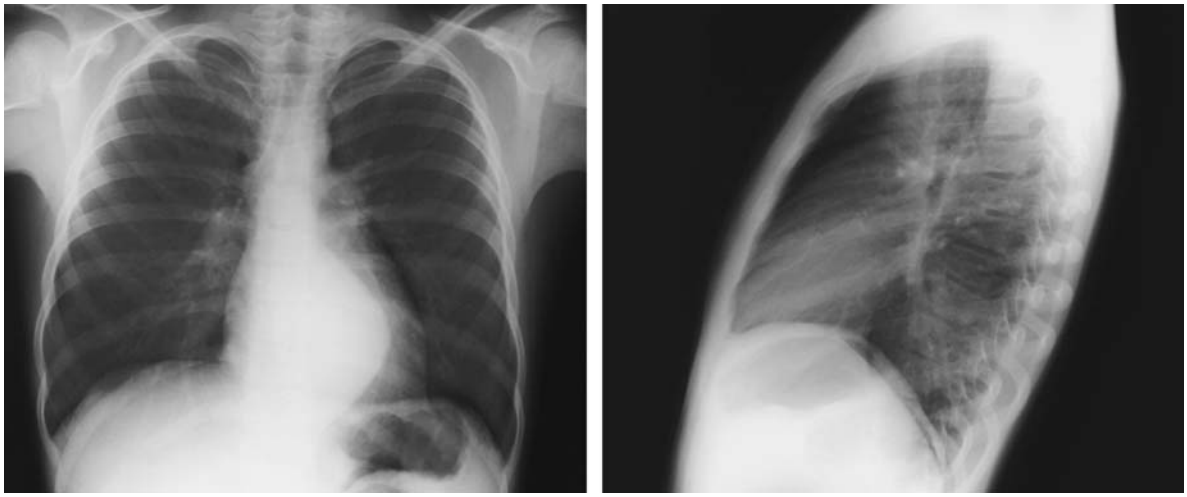

a b

Fig. 3.51. A 6-year-old with a cough. Frontal examination (**a**) reveals a large density extending to the left paraspinal line behind the heart. The heart is no longer transparent. The borders of the density are convex laterally, suggesting an extrapleural mass. On the lateral view (**b**) the mass is difficult to see. The vertebral bodies are whiter inferiorly than they are superiorly, indicating the mass is in the posterior aspect of the hemithorax. This was a ganglioneuroblastoma

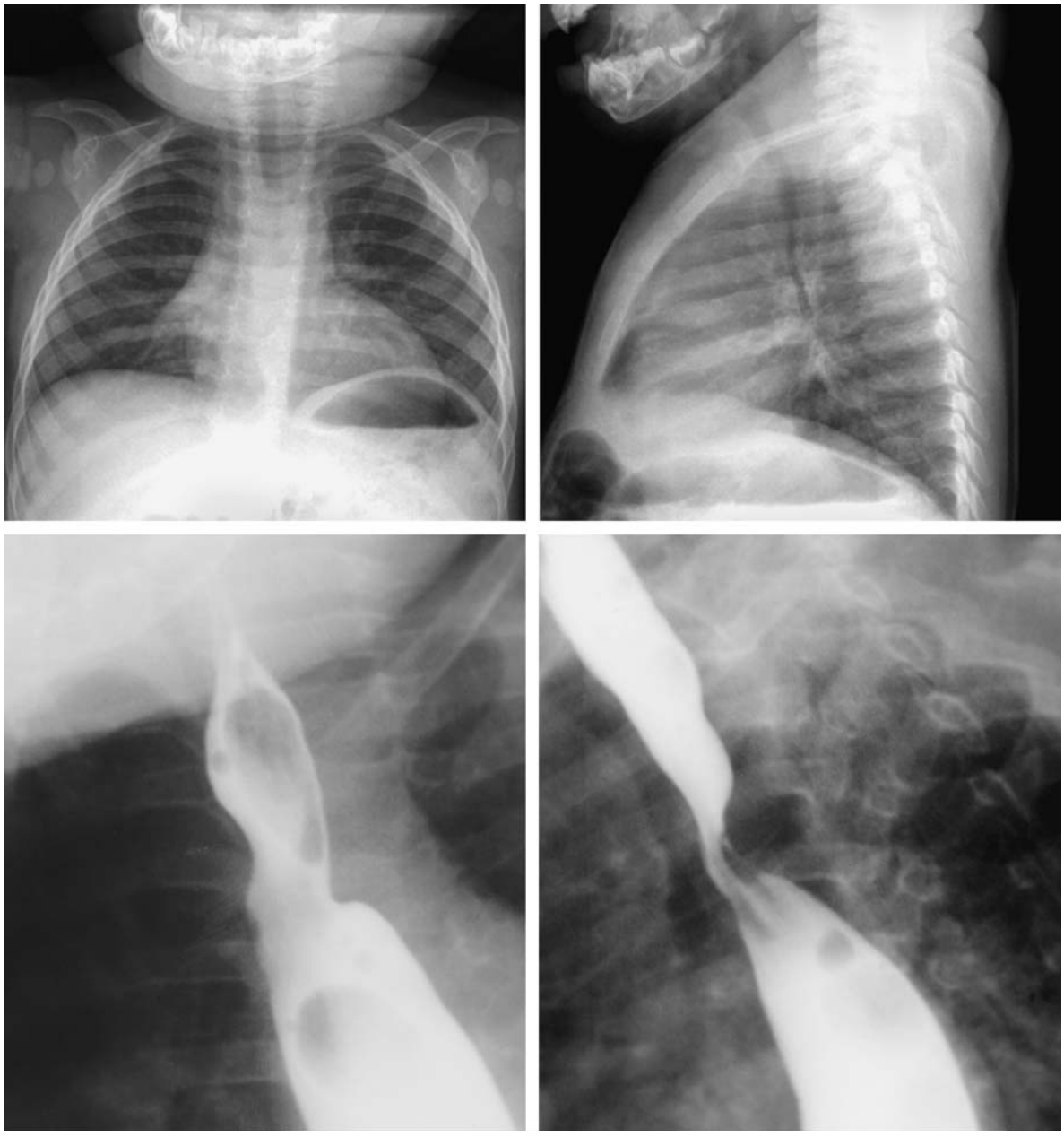

Fig. 3.52. A child with wheezing. The frontal radiograph (**a**) shows the distal trachea pushed to the left and effaced; the carina is not adjacent to the right pedicles. The lateral film (**b**) reveals the airway bowed forward and slightly narrowed. The frontal view of a barium swallow (**c**) shows the right and left indentations on the esophagus. The lateral view (**d**) reveals a bulge behind the esophagus and some narrowing and bowing of the airway. The patient has a vascular ring, specifically a double aortic arch

Chapter 4

Questions p. 63: Magnification of the chest occurs because of the portable technique. There is an apparent "large cardiomediastinal silhouette" because the tube-to-film distance is only 36–40 in. (91–102 cm). Since the child is supine, the vascularity of the upper and lower lungs is equal

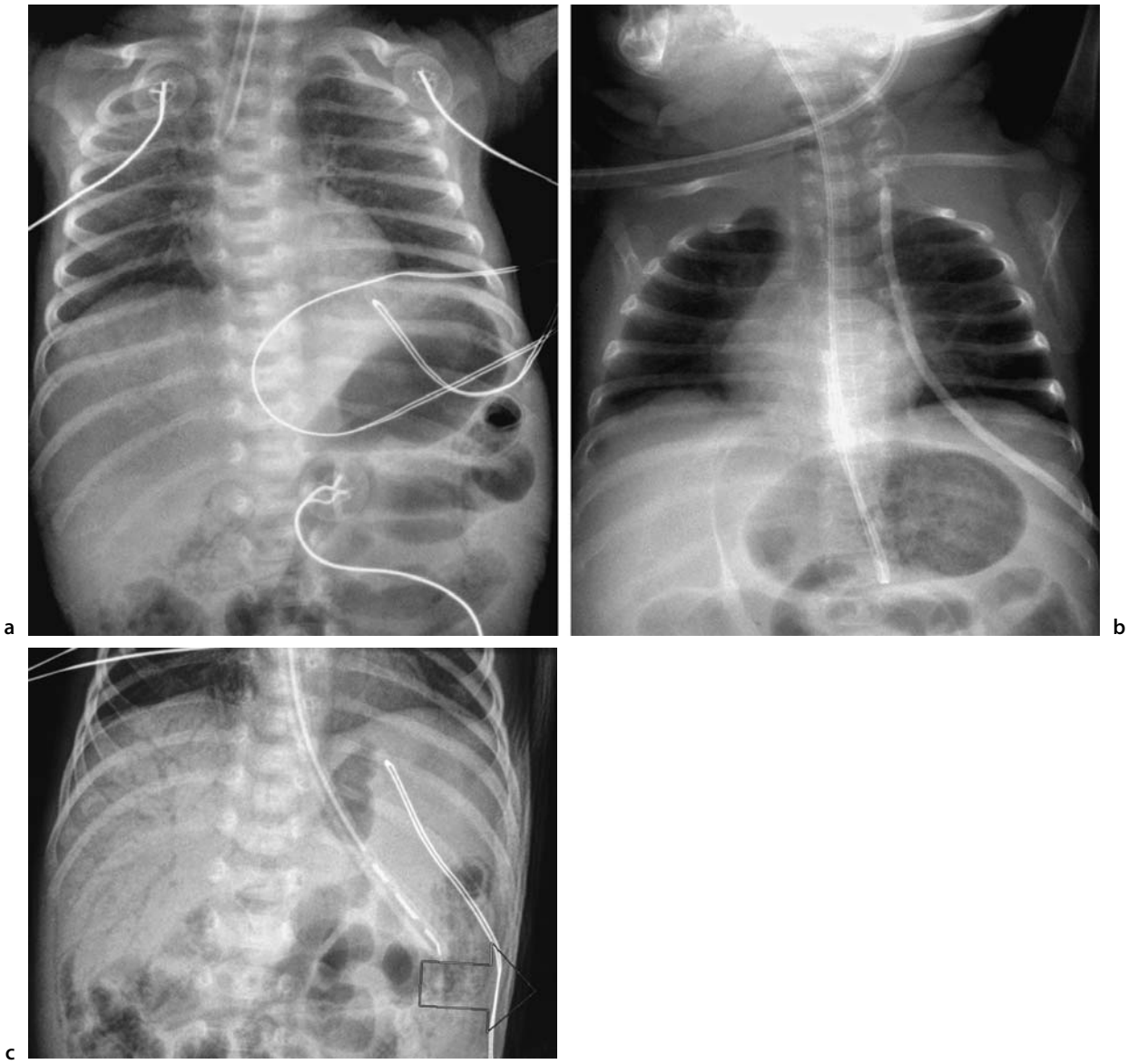

Fig. 4.6. Neonate with abdominal distension
a This intubated premature infant has gas within the liver (portal venous gas) and air in the bowel wall (pneumatosis), giving a bubbly appearance. See **c** for better appreciation of these findings. The baby has necrotizing enterocolitis. Always follow the ABCS
b In another neonate, there is free air in the peritoneum. The oblique white curved opacity extending from the diaphragm to the bottom of the film is the falciform ligament. It can only be seen when there is air on both sides of this thin ligament (attaches to the peritoneum posteriorly between lobes of the liver and inferiorly to the umbilicus). Multiple lines including a nasogastric tube are present
c Portal venous gas and pneumatosis in a baby with necrotizing enterocolitis. This is the same baby as in **a**

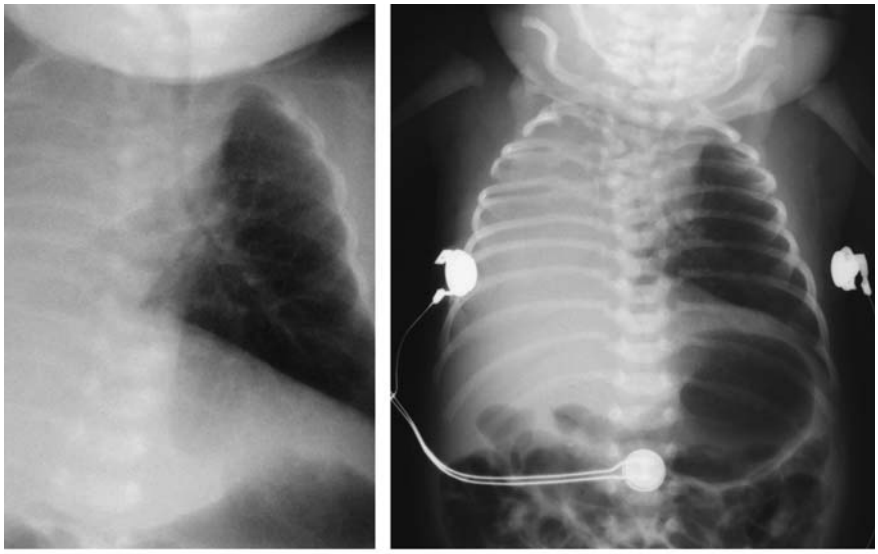

a, b

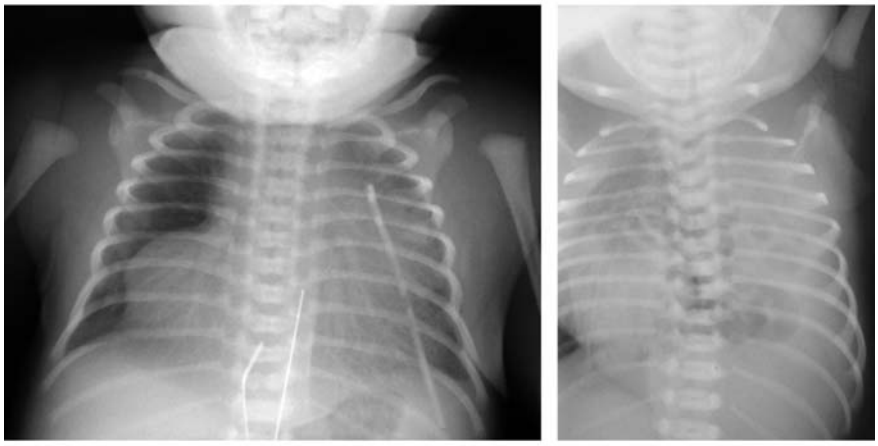

c, d

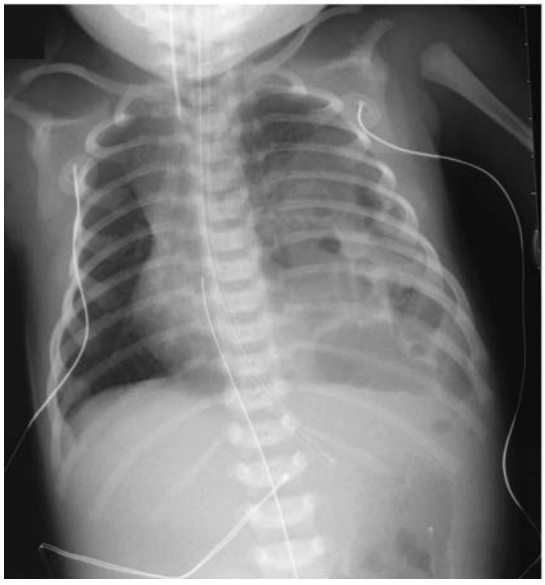

e

Fig. 4.23. Congenital neonatal anomalies
a Agenesis of the right lung. There is no carina, only a left main-stem bronchus. The mediastinum has shifted to the right
b Another child with agenesis of the right lung. It is common that vertebral and rib anomalies occur with this disorder
c Eventration of the right hemidiaphragm. Note how this acts as a mass and shifts the mediastinum to the left. When an eventration creates mass effect, it is treated as diaphragmatic hernia
d, e Two neonates with congenital left diaphragmatic hernias. Note the shift of the mediastinum to the right

Chapter 5

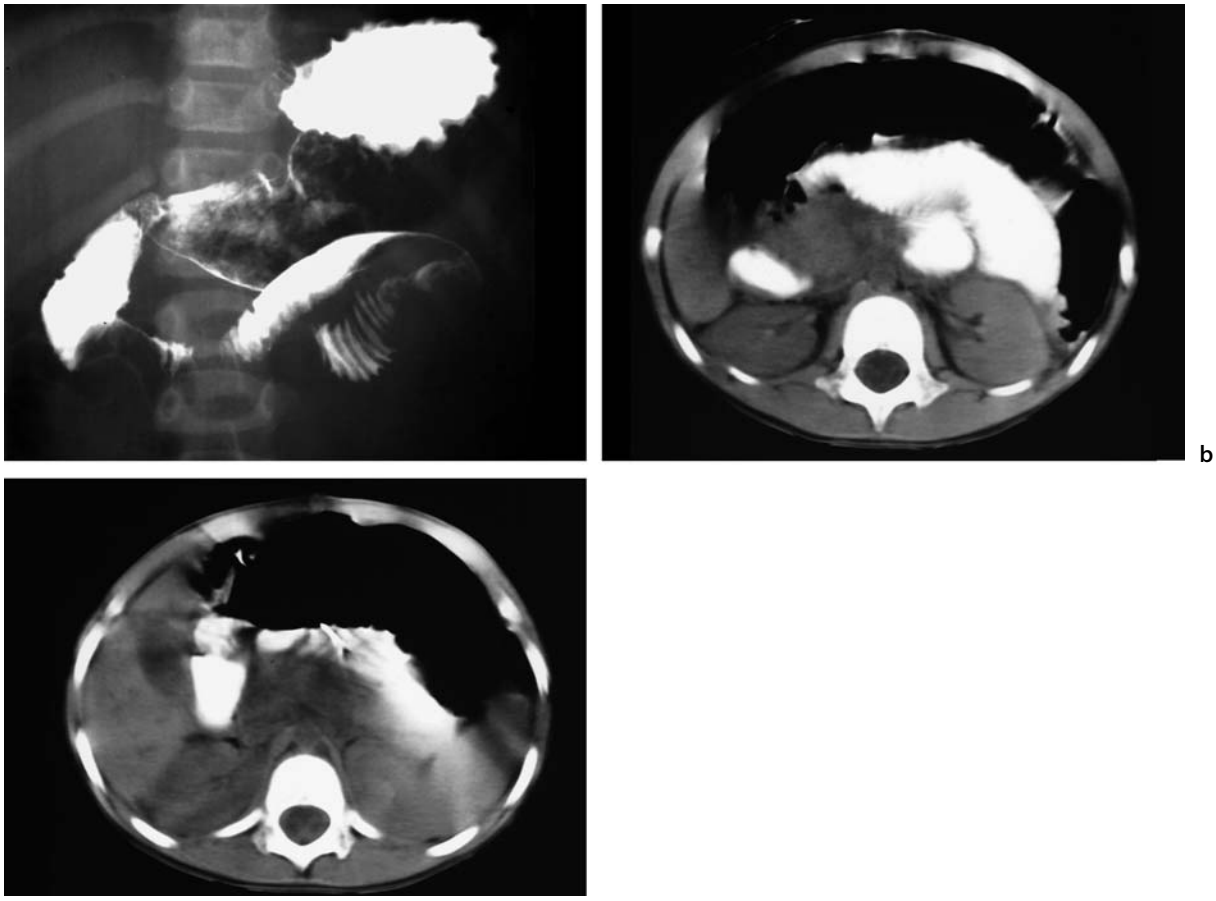

Fig. 5.21. An 8-year-old with right epigastric pain
a Upper gastrointestinal series shows a dilated second and third duodenum with the contrast (white) being squeezed and stretched over an intramural duodenal hematoma
b CT scan of the same child showing the large hematoma (gray) surrounded by contrast
c A third image of the CT slightly lower than **b** showing the contrast around the duodenal mass

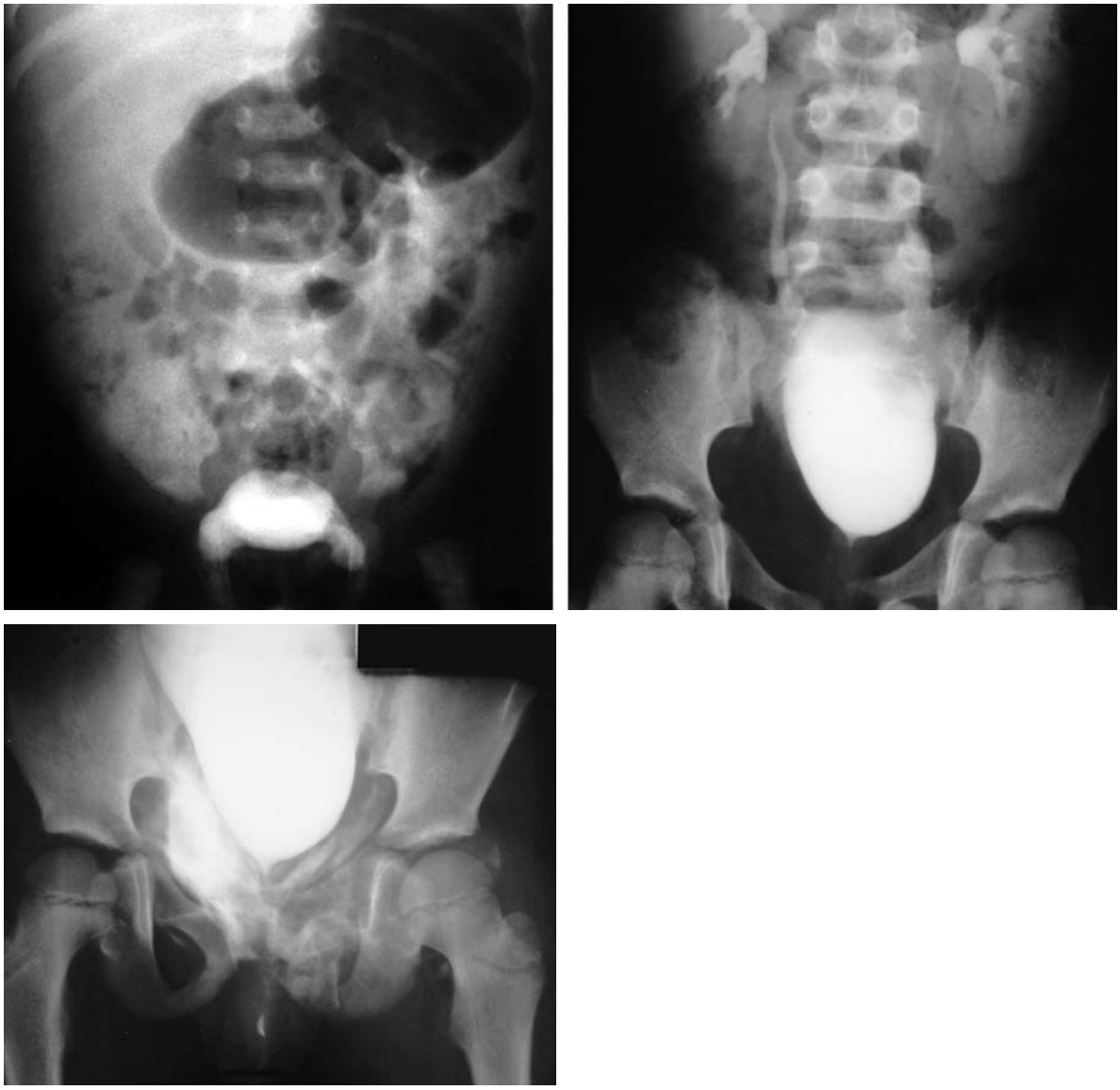

Fig. 5.37. What abnormalities do you see?
a VCU in a neonate with urinary tract infection. A portion of the bladder wall has herniated (laterally) into each patent processus vaginalis in the inguinal canal. These are called "bladder ears" and are of no clinical significance
b, c An excretory urogram in a 15-year-old who was in an automobile accident. The upper tracts appear normal, but the bladder is raised off the pelvic floor and pushed to the left. There is obvious disruption of the left pubic bone. In **c**, a retrograde urethrogram was performed, and the catheter was removed. There is contrast in the pelvis because of disruption of the posterior urethra. Faint contrast also in the left hip joint above the cartilage indicates disruption of the bones of the acetabulum as well

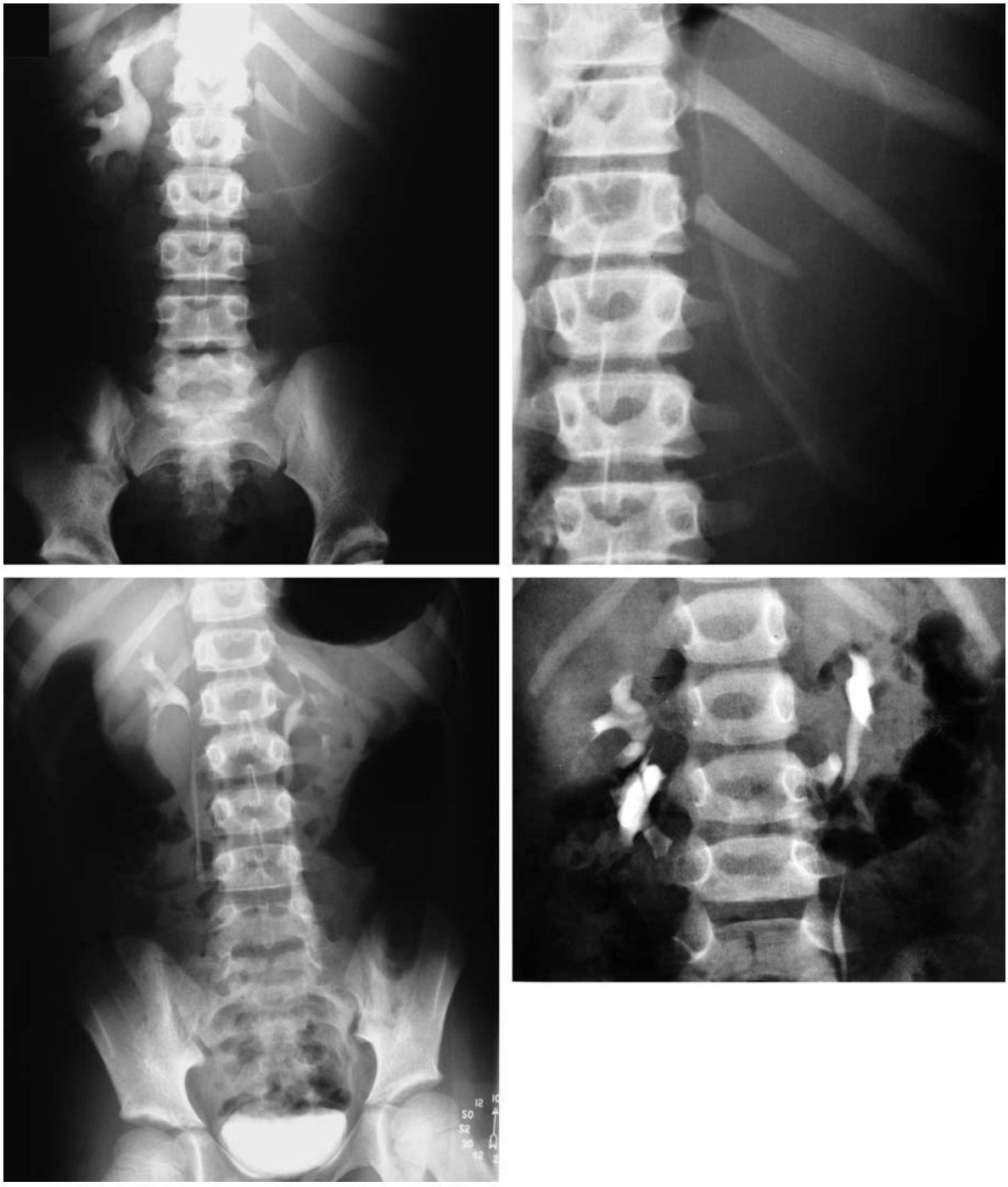

Fig. 5.41. Multiple abnormal excretory urograms
a, b Teenage female with a left flank mass. On the 10-min film (**a**) the right kidney appears normal, but on the left there is a large mass with linear opacities. These represent the parenchymal tubules being pushed in a vertical direction (parenchymal rims about a more lucent, dilated, urine-filled collecting system). A coned-down view of this kidney (**b**) shows the rims to better advantage. This patient had a ureteropelvic junction obstruction
c A 5-min film in a 10-year-old girl with multiple urinary tract infections. The left kidney is considerably smaller than the right and measures less than three vertebral bodies in height. The right kidney is larger than normal, measuring just about five vertebral bodies in height. Note how close the left upper pole calyx comes to the spine! This indicates loss of polar renal parenchyma
d A child with fever. The excretory urogram shows the lower pole calyces overlying the spine. This is a *horseshoe kidney,* perhaps unrelated to the fever

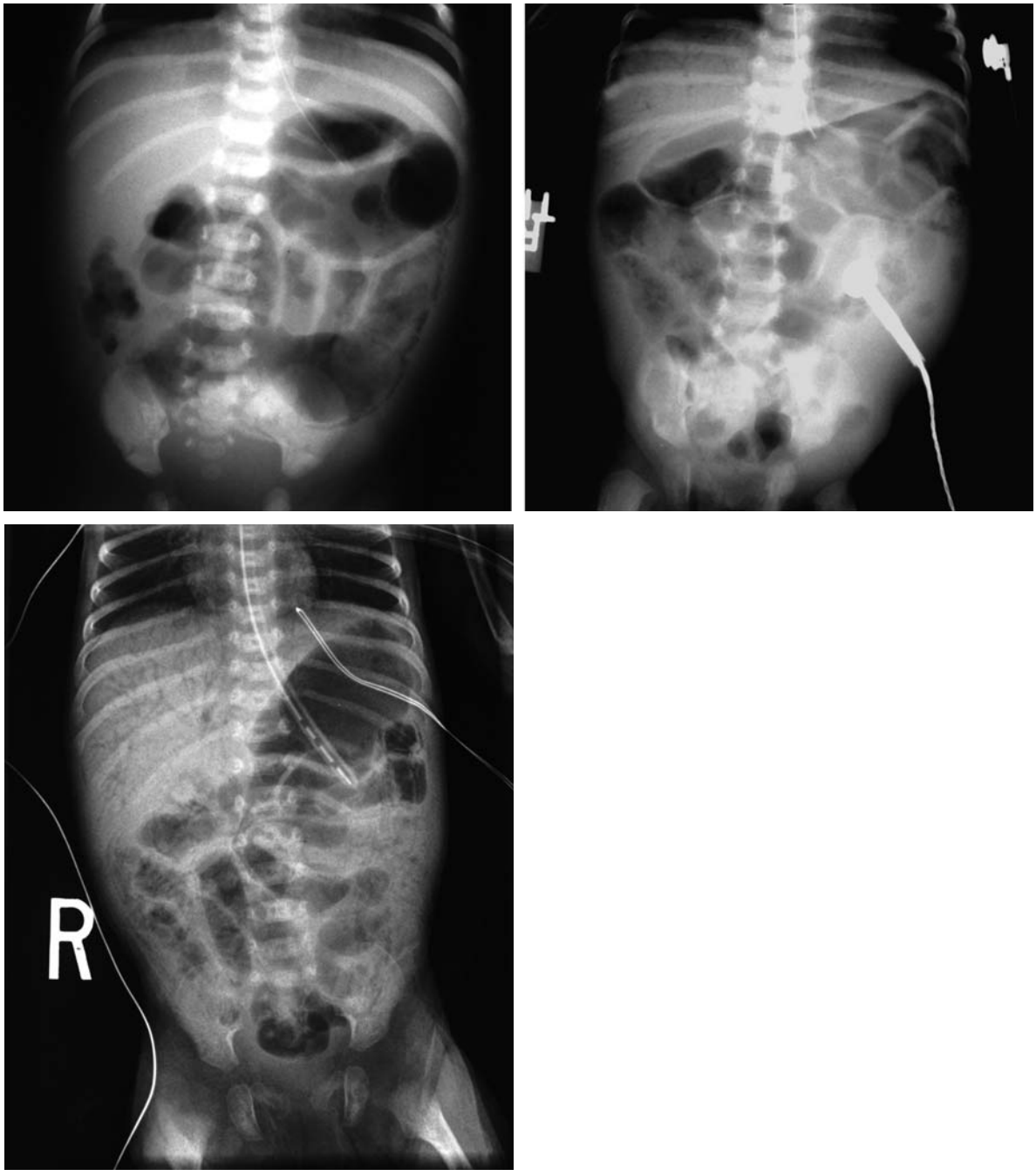

Fig. 5.57. Two neonates with abdominal distention
a, b There is extraluminal gas (pneumatosis intestinalis) in the descending colon (linear black streaks along left lateral abdominal cavity). This is pneumatosis intestinalis or air in the wall of the bowel. In **b**, one sees black streaks in the liver – portal venous gas. This baby has necrotizing enterocolitis
c Another infant with extreme pneumatosis intestinalis and portal venous gas

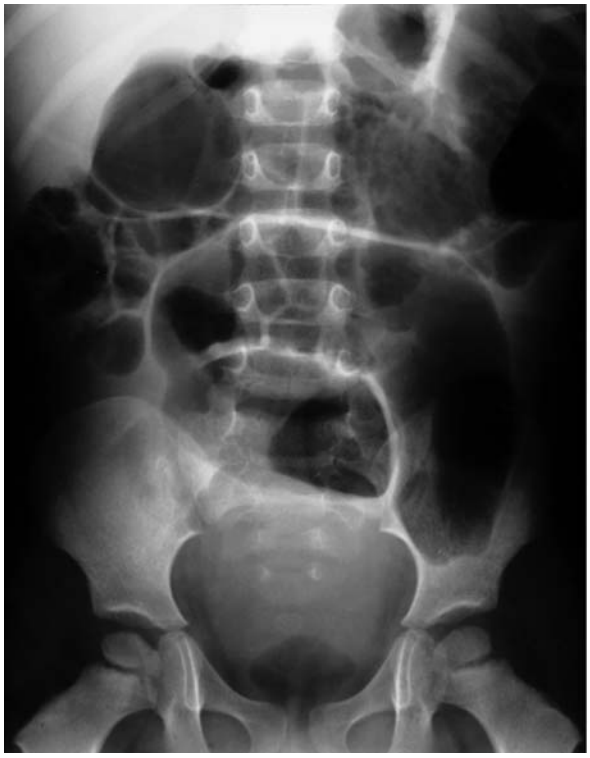

a

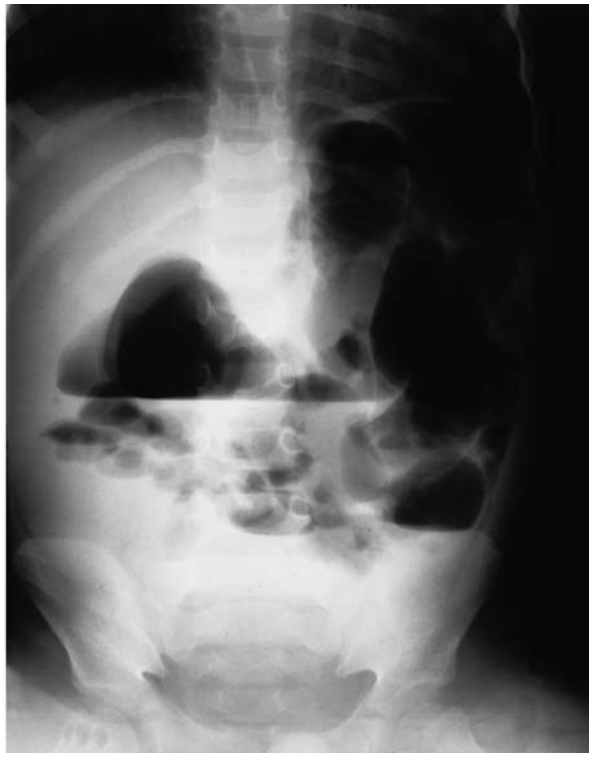

b

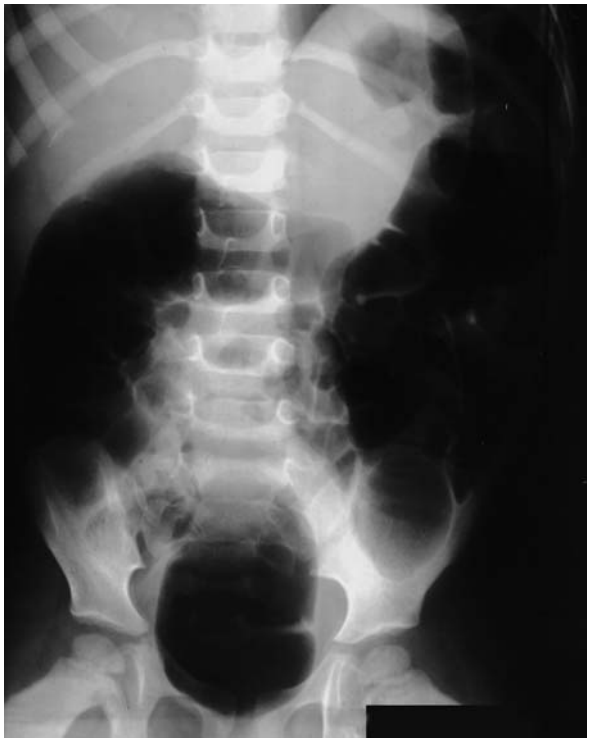

c

Fig. 5.58. A 1-year-old with abdominal pain and distention. Three views of the abdomen help us define the problem
a The supine view shows dilated bowel filled with air in the central abdomen
b, c The erect film (**b**) shows multiple air fluid levels. Does the baby have small bowel obstruction? The answer is on the prone film (**c**), where all the gas is seen to be in the colon and rectum
The patient does not have an intestinal obstruction. Use the prone film to move air with the help of gravity

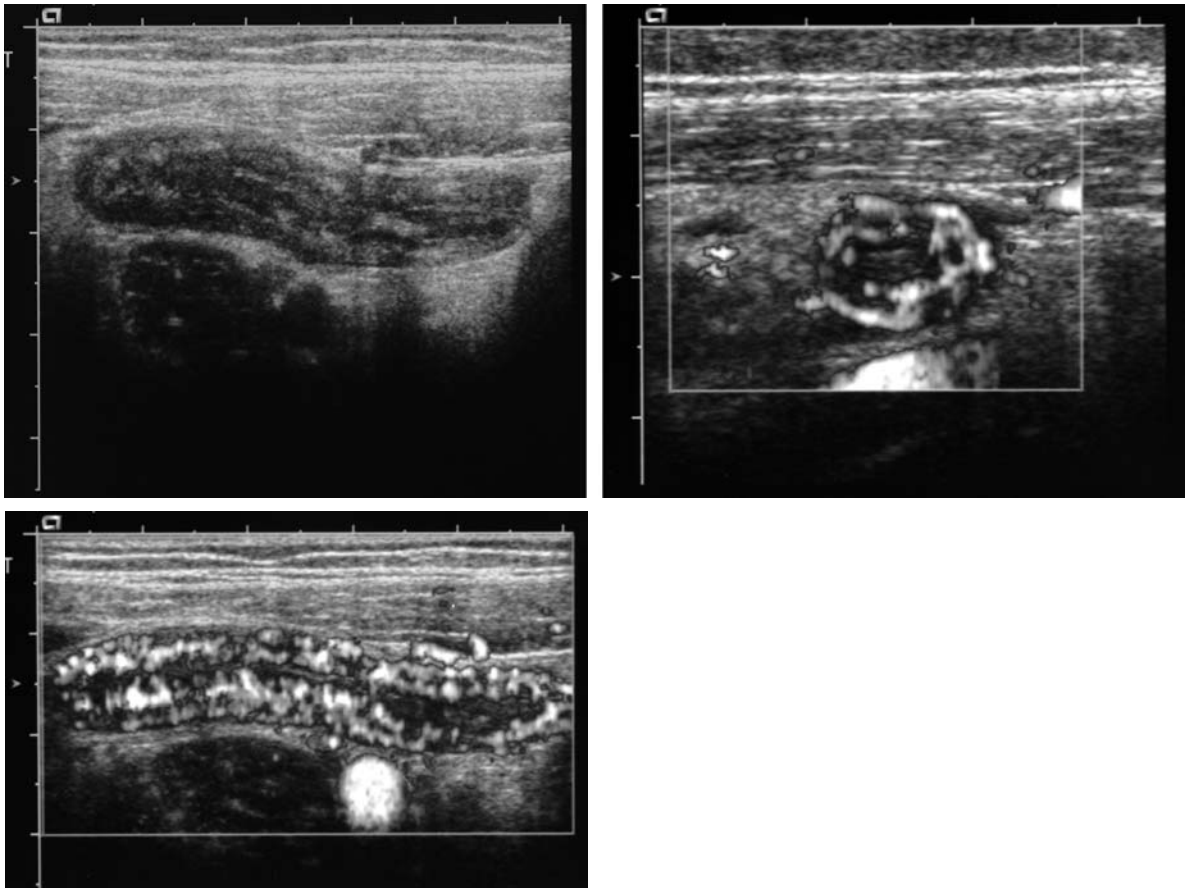

Fig. 5.59. Teenage boy with right lower quadrant pain – appendicitis
a Longitudinal ultrasound scan shows a large elliptical structure which has characteristics of bowel (hypoechoic muscle and hyperechoic lumen) and is not compressible. It measured almost a centimeter in diameter
b Similar scan with color flow Doppler shows perfuse flow to the muscle
c Transverse scan with Doppler confirms these findings. This was an inflamed appendix with appendicitis

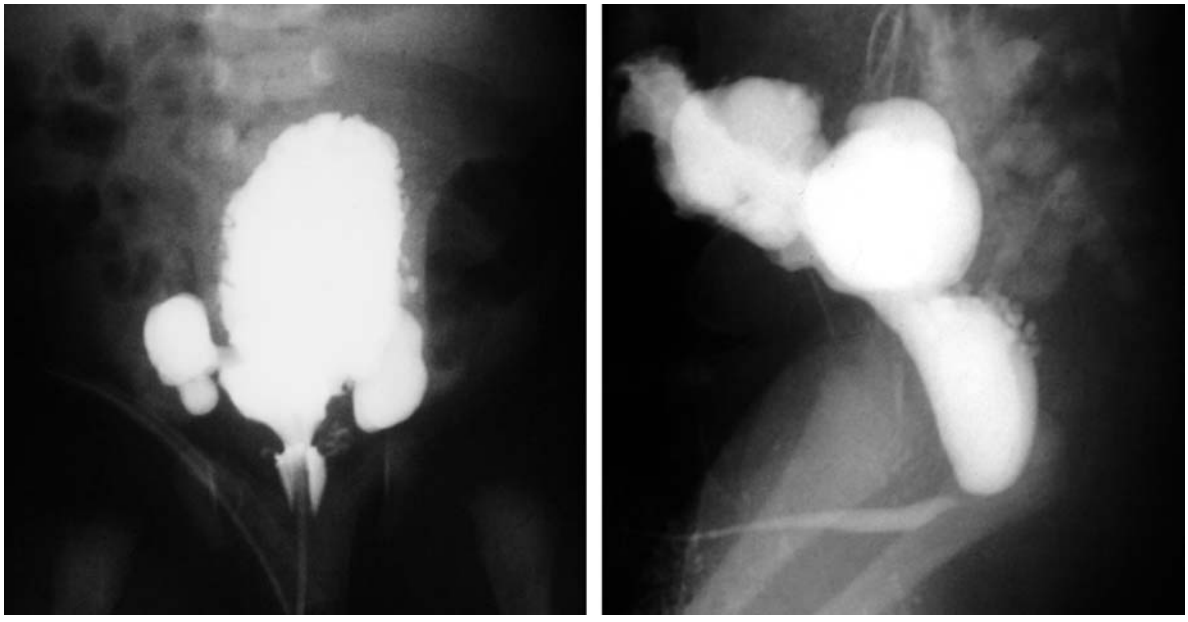

a b

Fig. 5.60. A cystogram on a 3-year-old with poor urinary stream – posterior urethral valves
a Frontal film shows an irregular trabeculated bladder with diverticulum laterally
b Lateral film during the voiding phase shows dilatation of the posterior urethra and a normal anterior urethra. There is contrast in an irregular configuration posterior to the posterior urethra – reflux into the prostate. The bladder is irregularly contracted. This patient has posterior urethral valves. It is most evident by the discrepancy between the size of the anterior and posterior urethra. On other images, the patient had significant vesicoureteral reflux

Chapter 7

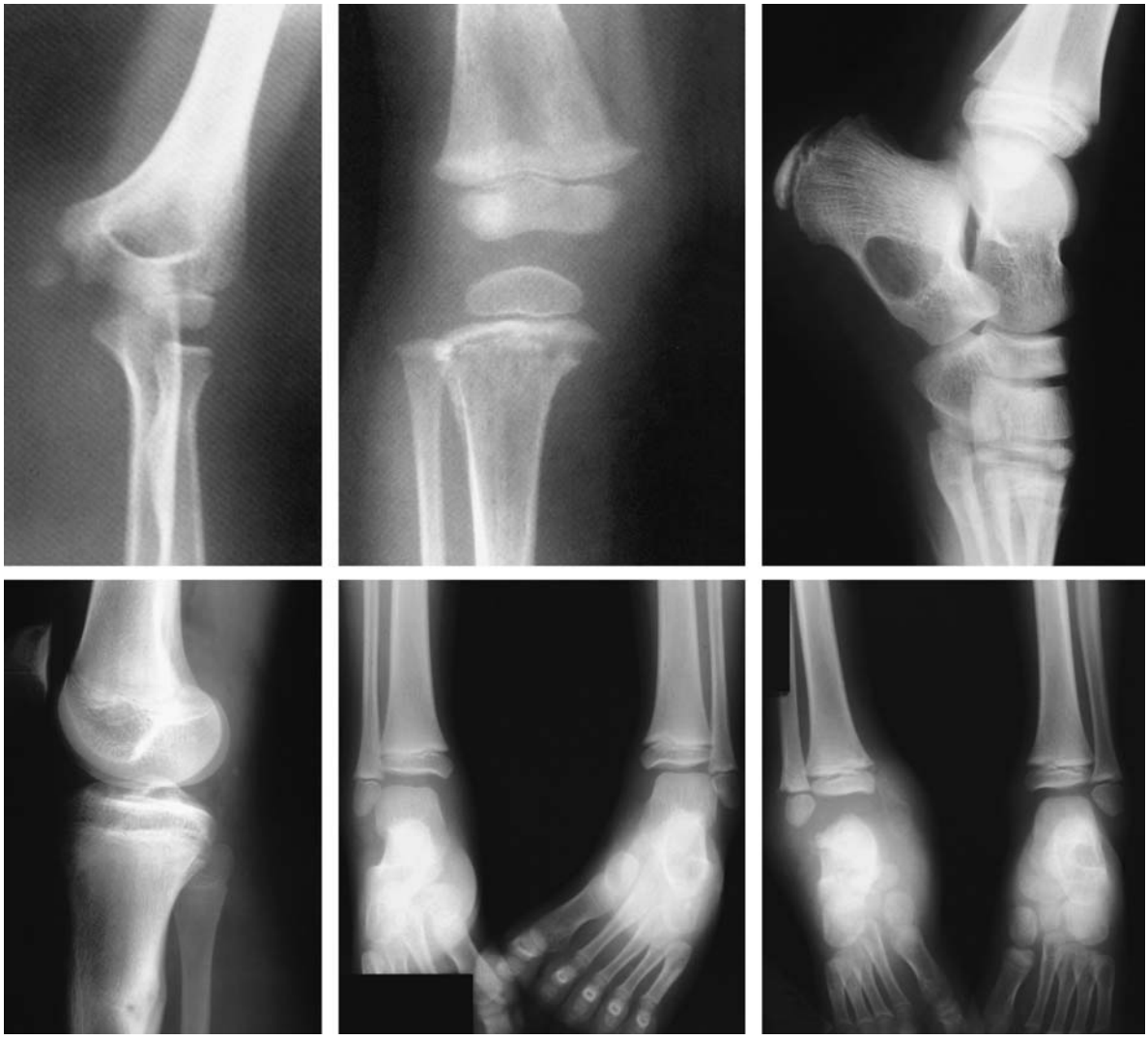

Fig. 7.46. Multiple bone and soft tissue abnormalities

a Ten-year-old with left elbow pain. The medial epicondyle is displaced inferiorly due to a fracture through the apophyseal growth-plate. There is marked soft tissue swelling. Sometimes subtle growth-plate injuries require comparison views of the other extremity. (Reproduced with permission from Yonatan Rosen)

b Two-year-old with knee pain. There is a lytic lesion in the proximal tibial metaphysis with an ill-defined zone of transition and associated periosteal reaction. You should guess from these features that this is an aggressive lesion; this patient has metastatic neuroblastoma

c Teenager with heel pain. Benign bone cyst of the calcaneus. It is a solitary lesion which has a clear zone of demarcation, no periosteal reaction, and a single lucency, typical of a cyst. You thought this was benign, didn't you?

d Teenager with leg pain. The sclerosis at the posterior aspect of the proximal tibia diaphysis is a clue. A lucency can be seen in the center, and the differential diagnosis include infections such as a chronic abscess, osteoid osteoma, and healing fracture. This was a bone abscess

e Eight-year-old with right ankle pain. There is a right ankle effusion. Did you notice the asymmetric widening of the distance between the right distal tibial epiphysis and the talar dome? There is soft tissue swelling

f Six-year-old with swollen right ankle. This is a classic example of a Charcot (neuropathic) joint. The typical findings, as seen in this case, include increased density of the bones, destructive changes (as in the talar dome), joint effusion, calcification, and soft tissue swelling. Such joint pathology is seen in patients with insensitivity to pain (e.g., from syringomyelia, diabetes, or congenital insensitivity to pain)

g–n see pp. 278, 279

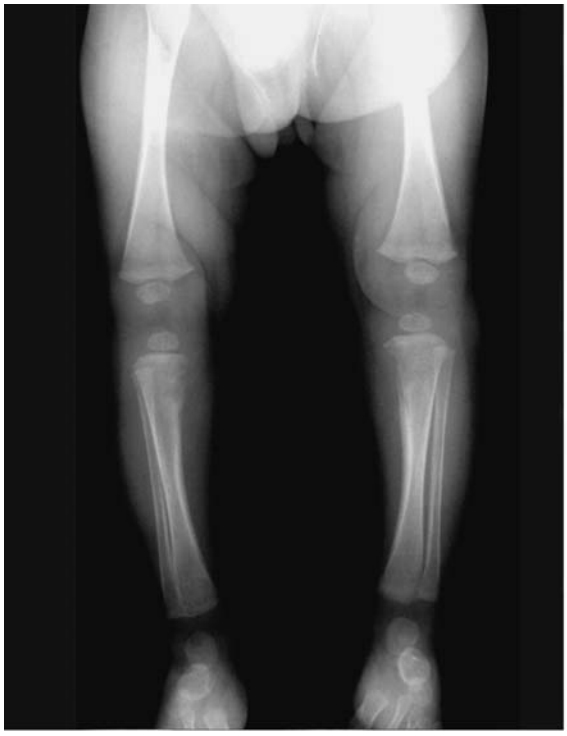

g, h

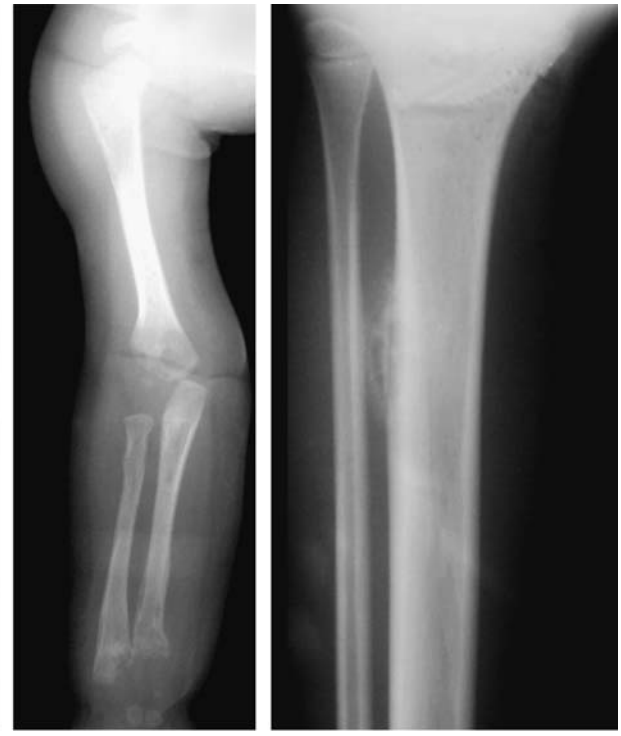

i

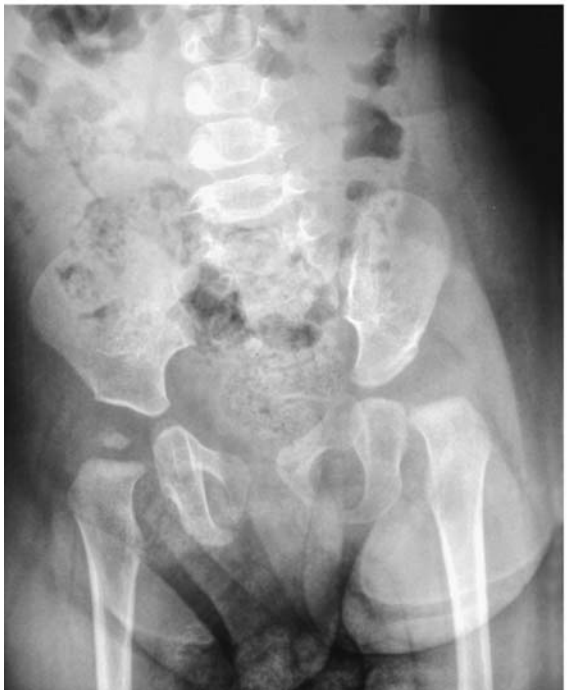

j

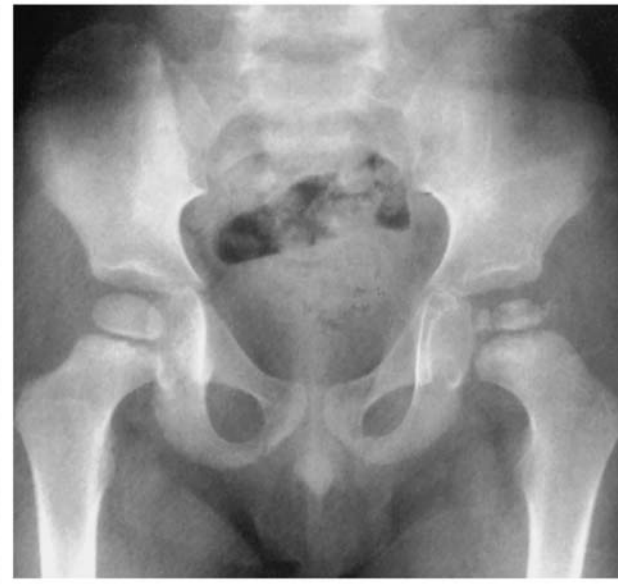

k

Fig. 5.46 (*continued*). Legend see p. 279

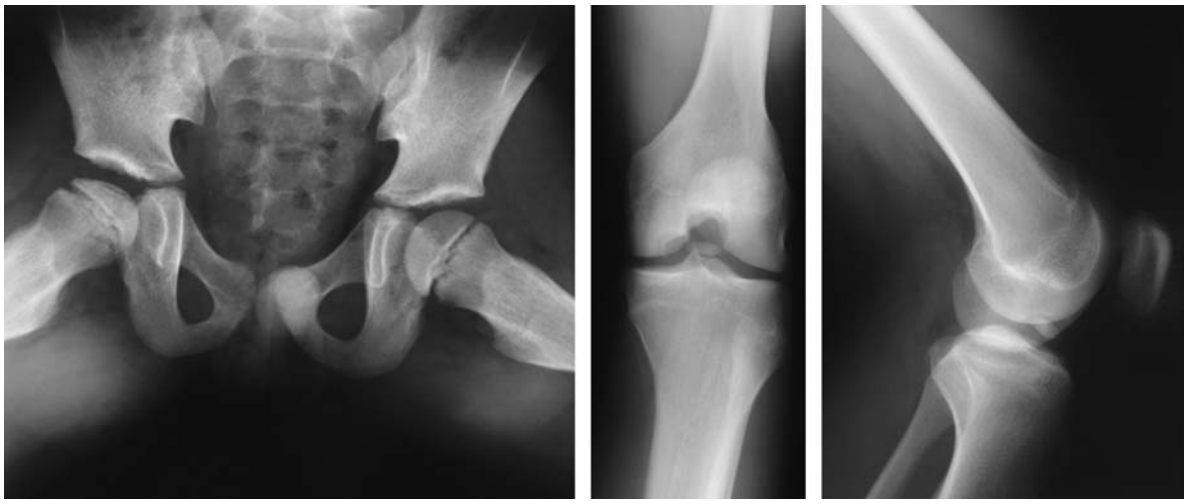

l, m n

Fig. 5.46 (*continued*)
g, h Newborn with swollen extremities. This infant has diaphysitis and metaphysitis from congenital syphilis. Notice the periosteal reaction along the shafts of both femora, both tibiae, the radius and the ulna. Also notice the bony erosions in the medial tibial metaphyses (Wimberger's sign) as well as in the distal radial and ulnar metaphyses
i Ten-year-old with bump on leg. Myositis ossificans. Did you see the soft tissue calcification at the lateral aspect of the proximal tibial diaphysis? There is a lucent (black) zone between the tibia and the calcification, which is characteristic of myositis ossificans
j Eight-month-old with asymmetric gluteal folds. Left hip developmental dysplasia. The left femur is displaced laterally and in contrast to the normal right hip, the femoral head is not yet ossified. The left acetabular roof is abnormally steep. The projected left femoral head would be outside the acetabulum
k Seven-year-old with left hip pain. Avascular necrosis of the left capital femoral epiphysis. The head is small and fragmented. This is Legg-Calvé-Perthes disease
l Five-year-old with right hip pain. Frog lateral view of the pelvis shows mild flattening and linear subchondral lucency in the right capital femoral epiphysis, consistent with early avascular necrosis of the right capital femoral epiphysis. Another case of Legg-Calvé-Perthes disease
m, n Teenager with left knee pain. Osteochondritis dissecans of the lateral aspect of the medial femoral condyle (lucent area) with resulting detachment of bony fragment, which is now loose in the knee joint. The loose body is seen just superior to the tibial spines on the frontal view and over the anterior aspect of the distal femur on the lateral view

Chapter 8

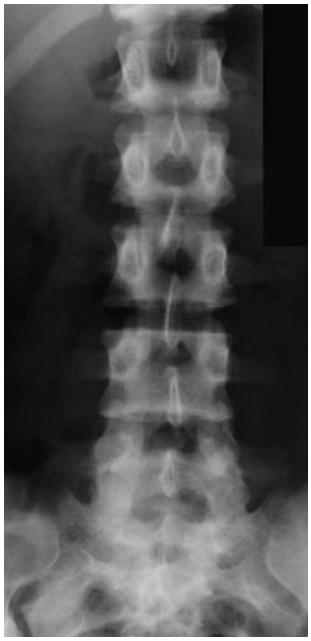

Fig. 8.21. Osteoid osteoma. Compare the pedicles on this X-ray. The left pedicle of L5 is dense compared to the right pedicle or to either pedicle of L4. This is a common location for an osteoid osteoma, which is a benign bone lesion causing pain

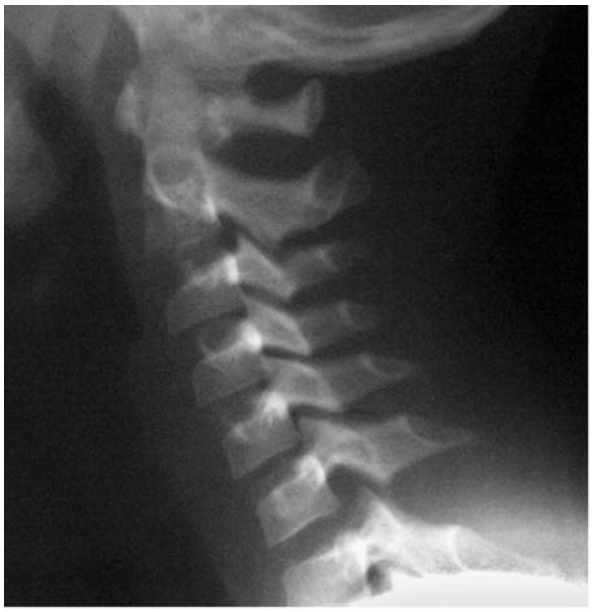

b

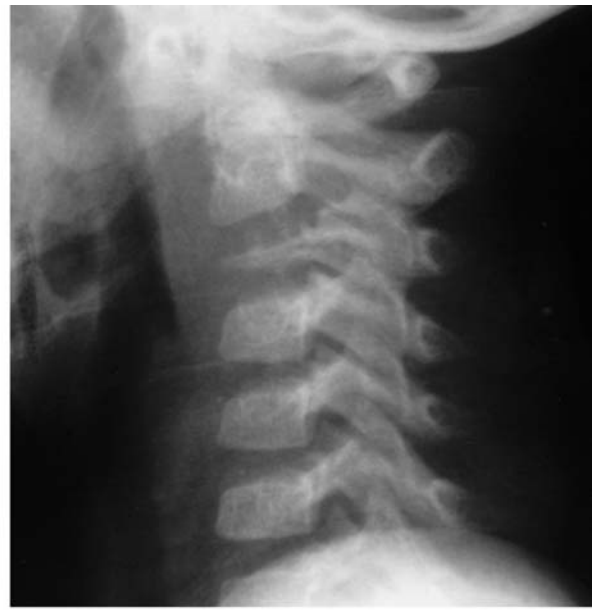

c

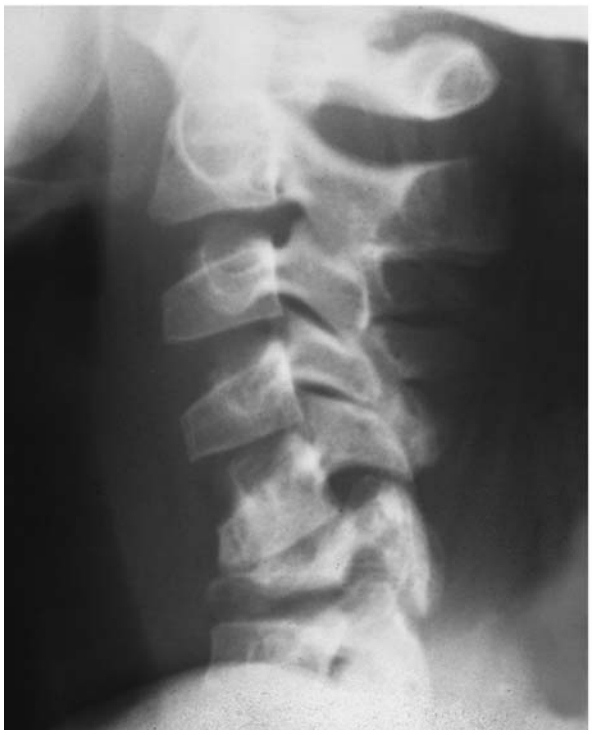

d

Fig. 8.22. Abnormalities of the spine
b Pay careful attention to the hypothetical vertical line along the posterior bodies of the vertebrae, which reveals that C7, the lowest cervical vertebra, is out of position. Look at the relationship of the articulating facets. This is a dislocation of C7
c Are all the vertebral bodies the same height? C3 is a "wafer" vertebra (vertebra plana). The joint space is intact, but the vertebral body is severely compressed. This is commonly found in eosinophilic granuloma of bone
d There is a compression fracture of C5 and C6. Trauma is a major cause of vertebral compression fractures and wedging

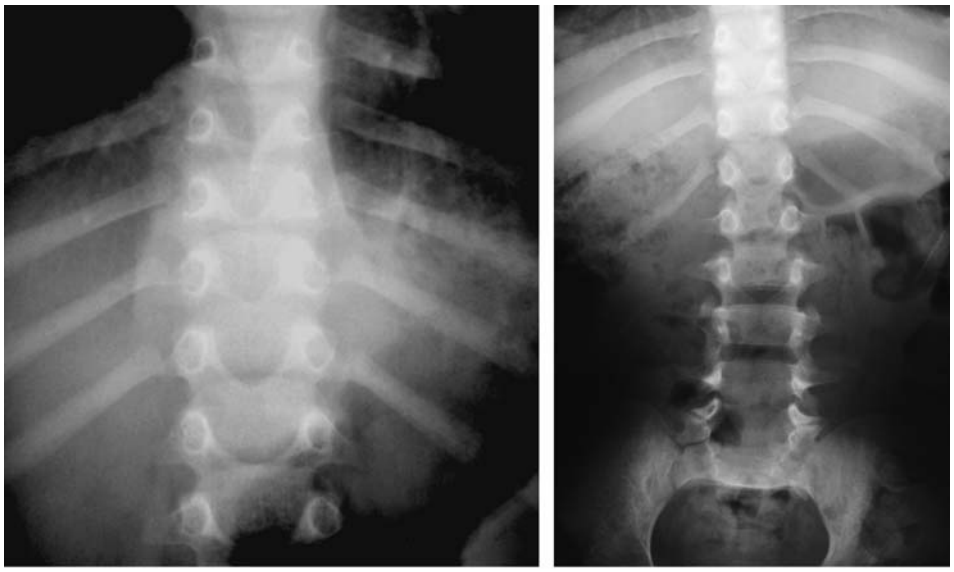

a

b

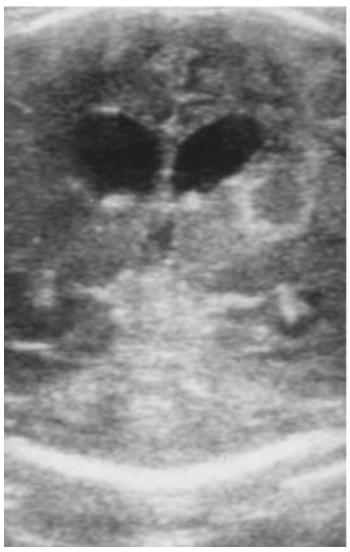

c

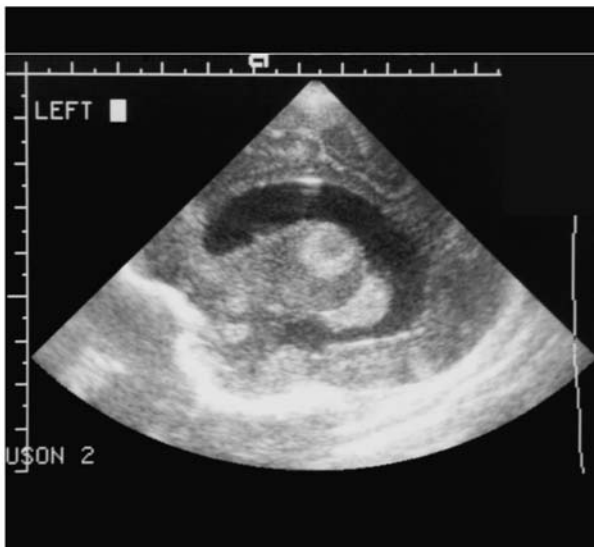

d

Fig. 8.25. Multiple patients
a A 2-year-old with back pain. This is tuberculosis – Pott's disease. Note the disc space narrowing of T10–12. There are bilateral paraspinal masses with wide paraspinal lines
b A 9.5-year-old with a congenital anomaly. You should detect the absence of the spinous processes of L2 through the sacrum. Did you notice that the pedicles have lost their convex inner margin? This patient had meningomyelocele at birth
c, d One-month-old female with a history of abdominal wall defects and now thrombocytopenia. On coronal (**c**) and sagittal (**d**) images, there are multiple lesions. These have an echogenic (white) rim with isoechoic (gray) center. Some are mostly echogenic. These are multiple sites of bleeding

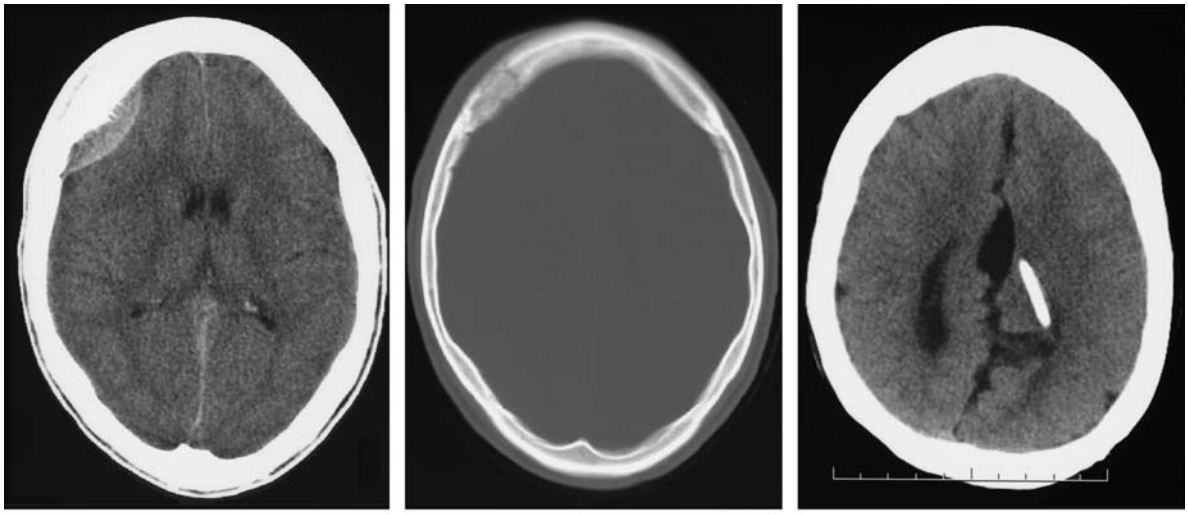

a, b c

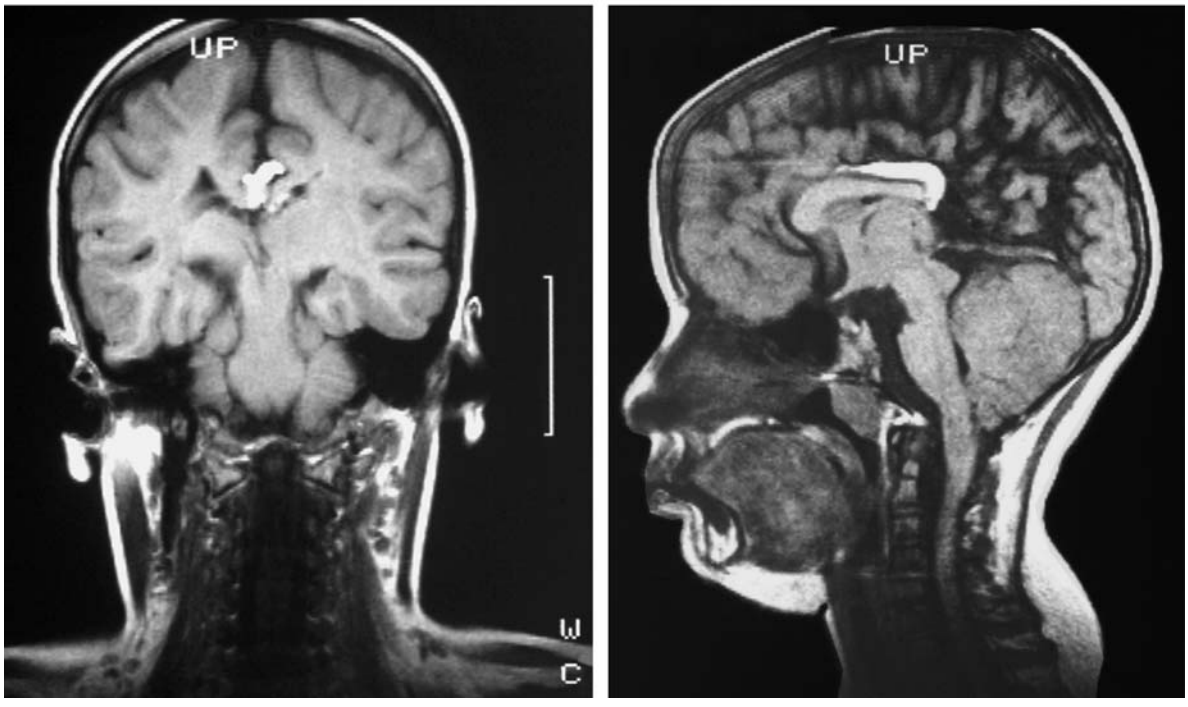

d e

Fig. 8.26. Multiple patients

a, b On enhanced brain window CT (**a**) there is an elliptical enhancing (white) mass (convex toward the brain) with abnormal spicules of the bone. Bone window (**b**) shows the bone destruction of the right frontal bone. This is an epidural metastasis with bone destruction secondary to neuroblastoma

c–e Teenage myelomeningocele patient. The CT (**c**) shows a shunt catheter on the left and mild dilatation of the right lateral ventricle. The falx is missing and the interhemispheric fissure is dysraphic (bent). What is the black central structure? It is blacker than fluid and represents fat – a congenital lipoma of the corpus callosum. Sagittal (**d**) and coronal (**e**) MR show the lipoma (white) over the anterior corpus callosum and absence of the posterior corpus callosum.

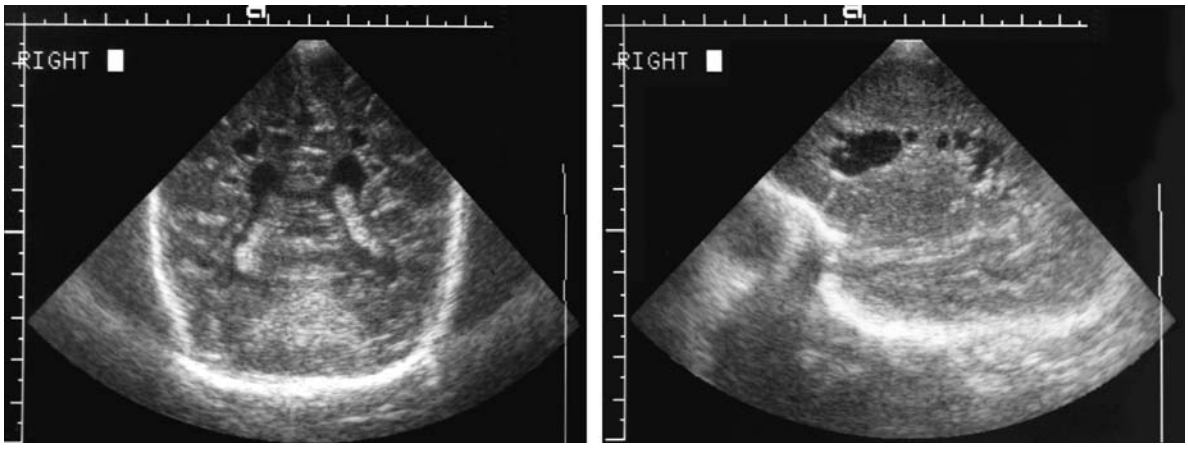

a b

Fig. 8.27. Ultrasound of a premature (26 weeks' gestation) infant at 4 weeks of age. Coronal (**a**) and sagittal (**b**) images of this neonate reveal multiple cavities (black holes) surrounding the ventricle. This represents ischemic disease called periventricular leukomalacia

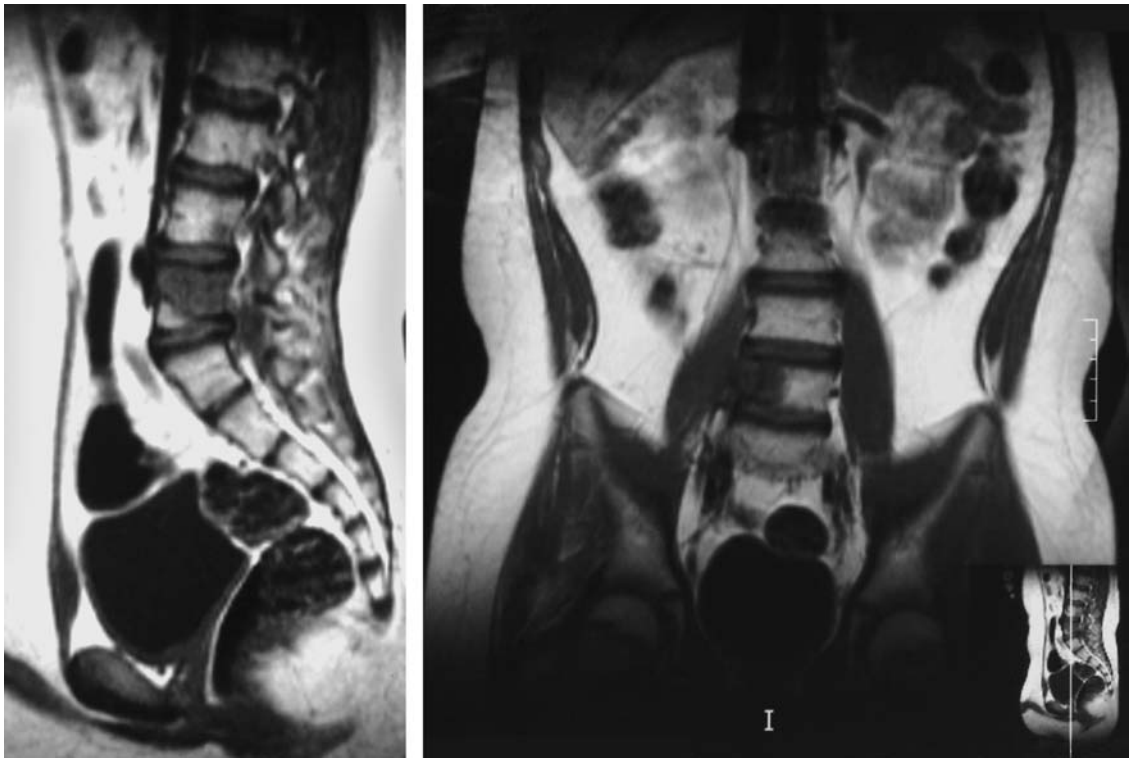

a b

Fig. 8.28. A 14-year-old with back pain. Sagittal (**a**) and coronal (**b**) T1-weighted images show abnormal signal (gray) in the 5th lumbar vertebral body. This represented a Ewing's tumor

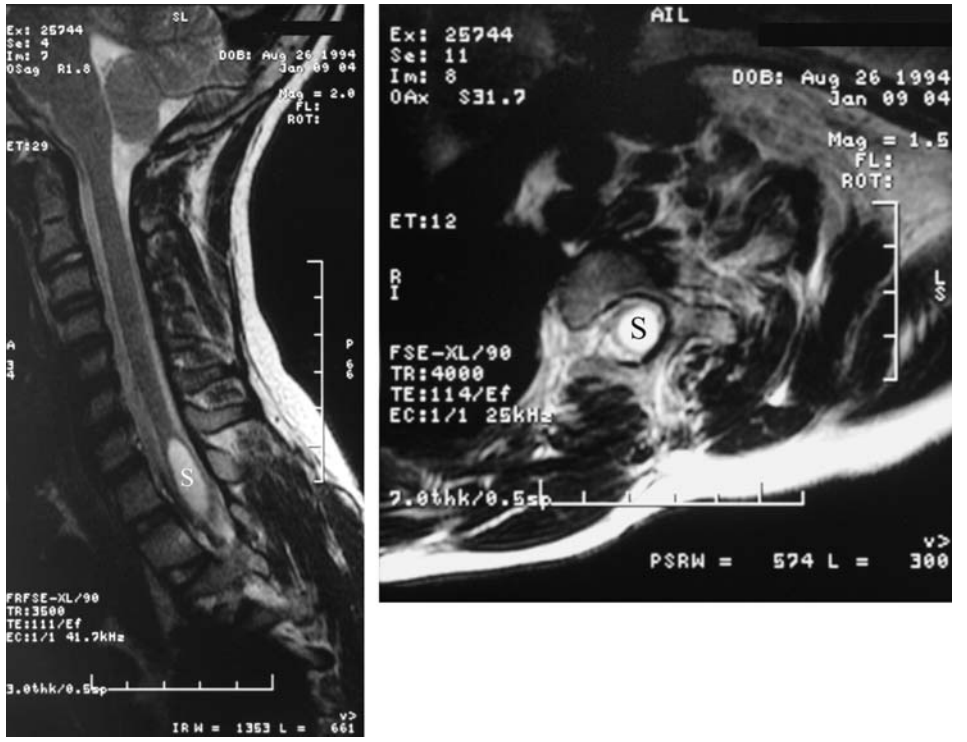

Fig. 8.29. A 10-year-old with weakness. Sagittal (**a**) and axial (**b**) T2-weighted images of the cervical spine show a large high signal lesion (*S*) within the spinal cord. It is a fluid collection called a syrinx. It thins the neural tissues

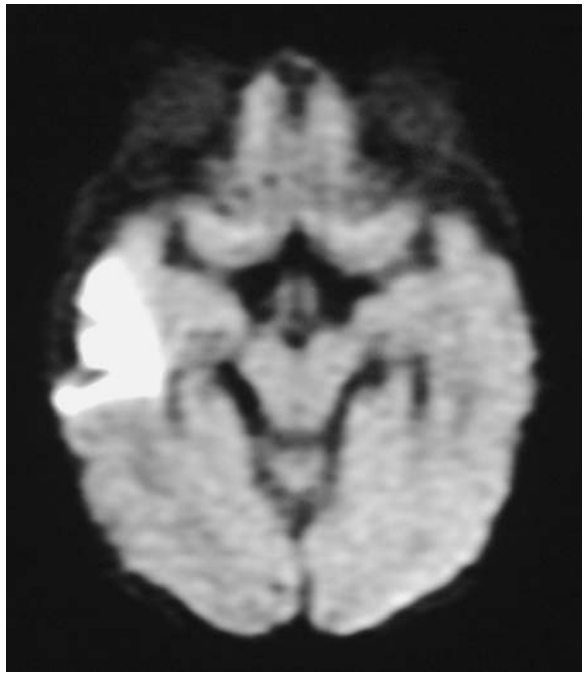

Fig. 8.30. One-month-old baby with encephalopathy. Axial diffusion weighted MR images show high signal in the right temporal region. This region was normal on T2-weighted sequences. This baby has a stroke, and diffusion images are the most sensitive sequence

Subject Index